Springer Series on Polymer and Composite Materials

Vijay Kumar
Susheel Kalia
Hendrik C. Swart *Editors*

Conducting Polymer Hybrids

Springer

Springer Series on Polymer and Composite Materials

Series editor

Susheel Kalia, Dehradun, India

More information about this series at http://www.springer.com/series/13173

Vijay Kumar · Susheel Kalia
Hendrik C. Swart
Editors

Conducting Polymer Hybrids

Springer

Editors
Vijay Kumar
Department of Applied Physics
Chandigarh University
Gharuan, Mohali, Punjab
India

Hendrik C. Swart
Department of Physics
University of the Free State
Bloemfontein
South Africa

Susheel Kalia
Department of Chemistry, Army Cadet College Wing
Indian Military Academy
Dehradun
India

ISSN 2364-1878 ISSN 2364-1886 (electronic)
Springer Series on Polymer and Composite Materials
ISBN 978-3-319-46456-5 ISBN 978-3-319-46458-9 (eBook)
DOI 10.1007/978-3-319-46458-9

Library of Congress Control Number: 2016952501

Printed on acid-free paper

This Springer imprint is published by Springer Nature
The registered company is Springer International Publishing AG
The registered company address is: Gewerbestrasse 11, 6330 Cham, Switzerland

Contents

Conducting Polymer Nanocomposites: Recent Developments and Future Prospects

Changyu Tang, Nanxi Chen and Xin Hu

Abstract Electrically conducting polymer nanocomposites (CPCs) consist of conductive nanofillers (e.g., metal nanoparticle, carbon nanotube, and graphene) and polymer matrices, which have become a greatly active field in the composite materials study. Due to their ease of processing, low density, tunable electrical properties, oxidation resistance, and flexibility, CPCs show versatile electrical applications such as antistatic protection, electromagnetic interference (EMI) shielding, energy storage electrode, sensors, flexible electronics, and thermoelectric devices. In this chapter, we review the recent progress and main challenges on CPCs and predict their development trend by several sections including the introduction, background, fabrication methods, the morphology control strategies, some application cases, and outlook. The key issues for successful fabrication of high-performance CPCs are discussed. Among them, the strategies on control of conductive network morphology and their effects on the electrical properties in CPCs are emphasized. Some interesting applications of CPCs based on the electroactive functions are described, and their property-related requirements are also proposed. We hope that the small review can provide a valuable reference for the researchers from academic and industry communities working on the CPCs and their functional devices.

Keywords Conducting polymer · Nanocomposites · Conductive nanofillers · Conductive network · Electrical properties

C. Tang (✉) · X. Hu
Chengdu Green Energy and Green Manufacturing Technology R&D Center, Chengdu Development Center of Science and Technology, China Academy of Engineering Physics, Chengdu 610207, China
e-mail: sugarchangyu@163.com

N. Chen
Sichuan Province Fiber Inspection Bureau, Chengdu 610015, China

V. Kumar et al. (eds.), *Conducting Polymer Hybrids*,
Springer Series on Polymer and Composite Materials,
DOI 10.1007/978-3-319-46458-9_1

1 Introduction

For a very long time, metal materials (e.g., silver, copper, and aluminum), which exhibit an extremely high electrical conductivity of over 10^6 S/m, have been used for various electrical applications such as conductor, heater, and electromagnetic interference (EMI) [1, 2]. However, these conducting materials are limited to their heavy weight and ease of chemical corrosion. Compared to metal materials, polymeric materials exhibit a very low density (1.0–1.3 g/cm^3) and can withstand various chemical corrosions, but they are generally insulating. Amazingly, the discovery of intrinsically conducting polymers in the 1970s brought people new recognition to the chemical structure and the electrical properties of polymeric materials [3]. The p electrons in the conjugated backbone from conducting polymers (CPs) can delocalize into a conduction band and thus give rise to the conductivity of metal materials [4]. The typical CPs with conjugated bonds include polypyrrole (PPy), polyaniline (PANI), polythiophene (PTh), and their derivatives (Fig. 1). However, neutral conjugated polymers show a low conductivity (from 10^{-10} to 10^{-5} S/cm), and their conductivities can be improved up by 10^4 S/cm through doping using a variety of molecules such as salt ions, hyaluronic acid, and peptides [5]. After doping, the CPs can deliver positive or negative charge carriers and show unique electronic properties. This kind of CPs combines the conducting behavior from metallic materials and many advantages from polymeric materials; thus they have attracted various researchers to explore their applications for conductors with lightweight, antistatic protection, electromagnetic interference (EMI) shielding, energy storage electrode, sensors, and flexible electronics. However, CPs need further chemical modification or compounding with other polymers and nanofillers to overcome their inherent drawbacks such as poor solubility, mechanical properties, biocompatibility, and high cost [4, 6].

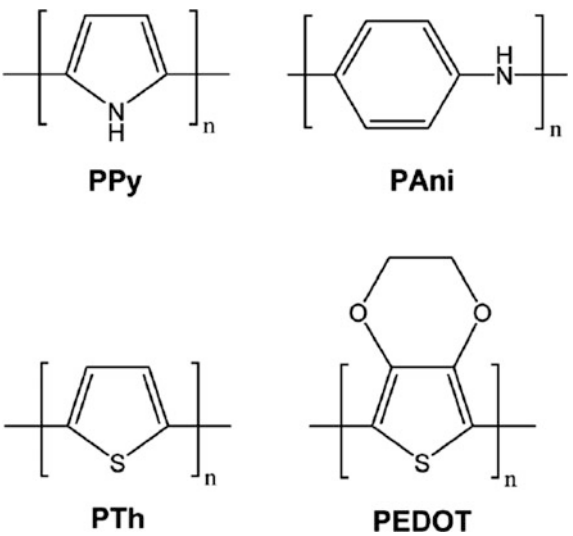

Fig. 1 Chemical structures of common CPs. Reproduced with permission [4], Copyright (2015) The Royal Society of Chemistry

Incorporating conductive fillers (e.g., a metal particle, carbon black, and graphite) into the nonconducting polymer matrix is another way to realize electrical conductivity in polymers [7–11]. The electrical properties of conductive polymer composites (CPCs) mainly rely on the percolated conductive network consisting of various conductive fillers. Furthermore, it is considered that most of the overall resistance arises from tunneling between nearby conductive fillers dispersed in the polymer matrix [9]. Due to the ease of processing, tunable electrical properties (10^{-8}–10^{6} S/m), good mechanical properties, and low cost, CPCs based on nonconducting polymers and conductive fillers attracted more attention from both the academic and industrial communities and have become a very active topic in the field of polymer composites.

In CPCs, a sharp change of several orders of magnitude in conductivity (i.e., an insulator/conductor transition) can be observed when filler content increases to a critical value in the polymer matrix (Fig. 2). The critical filler content is defined as the electrical percolation threshold (φ_c), which corresponds to the formation of the initially conducting pathway. For microsized conductive fillers (e.g., carbon black), filler content of over 15 wt% is often required to achieve electrical percolation in CPCs [12]. Such high filler consumption can lead to high production cost, processing difficulties, and loss of flexibility characteristics of polymeric materials. One of the current critical issues in the advancement of high-performance CPC applications is reducing the percolation threshold and increasing the conductivity. It is found that conductive nanofillers with high-aspect-ratio (e.g., carbon nanotubes, and graphene sheets) can support well-connected conductive filler network and result in much lower percolation threshold (0.01–4.0 vol%) in the CPCs [9, 12–15]. The percolation threshold of CPCs is theoretically predicted to decrease with increasing filler aspect ratio [16–18]. This expectation has been verified by a number of reported literatures [19, 20]. Low amounts of incorporated conductive nanofillers mean that the original physical properties of polymer matrix could be preserved or even improved [21]. Thus, there is no doubt that CPCs with nanofillers can exhibit better electrical and other physical properties than traditional CPCs with microsized fillers.

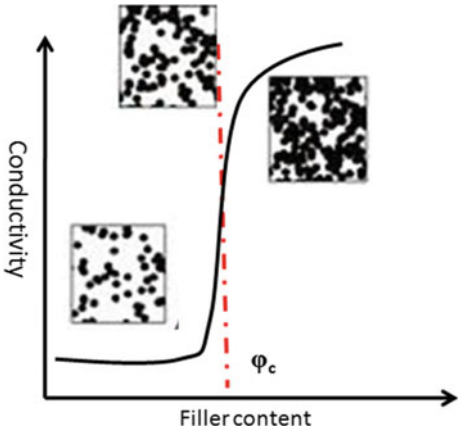

Fig. 2 Electrical percolation behavior of CPCs corresponding to different conductive filler morphologies as a function of filler content

Successful fabrication of high-performance nano-CPCs still faces three significant challenges [7, 22]. First, highly conductive nanofillers with controllable structure are needed to be synthesized for CPCs. For example, the intrinsic conductivity of carbon nanotubes (CNTs) depends on their types, defects, and purity. Second, nanoparticles readily aggregate and have reduced dispersion in polymer matrix due to their high-aspect-ratio, so surface modification of nanoparticles and special dispersion method are needed. Finally, controlling the conductive network morphology in the polymer matrix during compounding processing, which determines the final conductivity of CPCs, is still difficult. For example, Kovacs et al. [23] demonstrated that different processing parameters can significantly affect the conductive network morphology and percolation threshold of CPCs based on epoxy and carbon nanotubes (CNTs). The control of filler network morphology also can tune the conductivity value of CPCs for various electrical applications. For example, the CPC for electrostatic dissipation typically requires an electrical conductivity of 10^{-8} S/m, while EMI shielding requires conductivity values of 10^{2} S/m [9].

In the past years, the above challenging problems have always been resolving under researchers' great effort and result in the rapid development of CPCs and the emergence of exciting applications from tailored CPCs. Nevertheless, a detailed review of the recent extensive progress on CPCs remains absent. Here, we do a study in the present chapter to introduce the recent development and future prospect of conductive polymer nanocomposites by several sections including the introduction, background, fabrication methods, physical properties, the morphology control strategies, and some application cases and outlook.

2 Background

2.1 Percolation Theory

Electrically conductive polymers can be divided into two categories: (1) intrinsically conductive polymers [6, 24], in which the electronic structure of these polymers is responsible for electron transport, and (2) CPCs, in which the incorporation of conductive fillers to the insulating polymer matrix provides the conducting ability. Here, we mainly introduce the latter one.

An insulator–conductor transition (Fig. 2) could be observed with increasing conductive filler content in the CPCs. The electrical conductivity of CPCs dramatically increases by several orders of magnitude after the critical filler content (φ_c). The percolation theory usually describes this behavior. The percolation theory was developed based on an infinite dimensional lattice, and can be used to describe many physical properties of the materials. When conductivity is considered, each site of the lattice can be conductive or nonconductive. According to classical percolation theory, the conductivity of the composites as a function of conductive filler can be described by a scaling law [25, 26]:

$$\sigma = \sigma_0(\phi - \phi_c)^t, \tag{1}$$

where σ is the conductivity of composite, σ_0 is the proportionality constant related to the intrinsic conductivity of filler, ϕ is the volume fraction of filler, ϕ_c is the volume fraction of filler at percolation threshold, and t is the critical exponent reflecting the system dimensionality of composites. This theory is widely used to study the conductive network of CPCs, showing a good agreement with experimental results.

In a random conductive network, the exponent t does not depend on the lattice geometry details, but only depends on the dimensionality of the network [27]. This is called universal percolation behavior. Theory calculation shows that $t \approx 1$–1.3 and $t \approx 2.0$ correspond to two- and three-dimensional networks, respectively. However, many experimental studies reported a wide range of t value from 1 to 12 [19, 28]. Some studies claim that a lower t value is caused by a narrow tunneling distance distribution in the composite system and that a higher t value is caused by abroad tunneling distance distribution. Nevertheless, the difference between the theoretical prediction and the experimental results is still an unresolved issue.

2.2 Conduction Mechanism

CPCs are generally consist of insulating polymer and conductive fillers. In the CPCs, electrons do not only transport in the conductive fillers themselves, but also need to transport from one filler to another one. Hence, it is highly possible that energy barriers exist between conductive fillers, and the electrons need to go through these barriers by quantum mechanics tunneling, which are called "tunnelling resistance" [28]. The tunneling resistance is dependent on the temperature. Various models have been developed to describe the tunneling resistance in disordered solids such as Fluctuation Induced Tunneling (FIT) model and Variable Range Hopping (VRH) model [29–31]. Besides, tunneling resistance has an exponential dependence on the gap width (interfiller distance) [29]. In other words, the gap width varies linearly while the tunneling resistance changes exponentially. Conductive networks in CPCs cannot always be considered as ideal percolation networks because these conductive networks do not only consist of an infinite resistor (polymer matrix) and infinite conductors.

2.3 Characterization of Conductive Network in CPCs

For the study on CPCs, the control of the morphology of the conductive filler network is one of the key points, so it is crucial to characterize the detail information of these networks. Researchers have developed various direct and indirect

methods to describe the morphologies of conductive filler networks in CPCs, such as optical microscopy (OM) [32], scanning electron microscopy (SEM) [33–36], transmission electron microscopy (TEM) [37–39], scanning probe microscopy (SPM), and atomic force microscopy (AFM) [40–42]. These methods have been widely used as general microscopic methods to characterize the morphology of CPCs on different size scales.

OM is often employed to study morphology at a range of a few microns or above. For anything below this magnitude, SEM, TEM, and AFM are needed. However, all conventional microscopy techniques have their disadvantages in imaging the nanofiller dispersion within a polymer matrix. For instance, optical microscopy only observes enormous nanofiller agglomerates, while SEM and AFM only can characterize the surface or cross section of samples. Besides, it is hard to draw conclusions on the bulk organization of the composite by the TEM images of thin sections ($\sim$100 nm in thickness). Therefore, auxiliary methods are needed to provide more information on conductive networks, such as the orientation of the conductive fillers, and the formation of the conductive networks. Other measurements including wide-angle X-ray diffraction (WAXD), Raman spectroscopy, rheology, and electrical conductivity can be used to characterize further the morphology of conductive networks [43–47]. For example, the orientation degree of the filler and the polymer matrix, as well as the polymer–nanofiller and nanofiller–nanofiller interactions, can be estimated by WAXD, Rheology, and Raman spectroscopy. Also, a conductivity measurement is often used as a simple method for evaluating the formation of conductive networks and gives direct evidence of the conductive network in CPCs [48].

3 The Design for High-Performance CPCs

One of the important goals for fabricating high-performance CPCs applications is pursuing a lower percolation threshold and a higher the conductivity. In other words, we hope to obtain high-performance CPCs by adding conductive fillers as little as possible. These characteristics are strongly dependent on the conductive fillers, polymer matrix, and fabrication method, which can synergistically construct a conductive network with high quality and compromise other physical properties [9].

3.1 Conductive Fillers

According to percolation theory, the percolation threshold decreases with an increase of aspect ratio in the conductive fillers. Carbon black (CB) is one of the commonly used sphere-like fillers (0-dimension) for CPCs (Fig. 3a). For spherical particles (L/D = 1), high volume fraction of 16 vol% is needed to achieve a percolation network in the CPCs [49]. CNTs having much higher aspect ratios

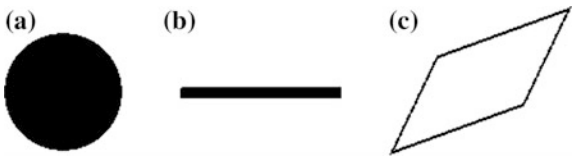

Fig. 3 Conductive nanofillers with different dimensions: **a** 1D, **b** 2D and **c** 3D

(L/D > 100) promise much lower percolation thresholds than CB. The critical concentration (percolation threshold) in CPCs could be less than 5 vol% if conductive fillers with aspect ratios over 100 are used. Due to the low percolation threshold, the original properties of the polymer matrix can be well preserved or even improved accompanying with the increasing conductivity. Thus, the conductive fillers with high-aspect-ratio (such as CNT, carbon nanofiber, silver nanowire, silver flakes, and graphene) are preferred for fabrication of CPCs with low percolation threshold. This prediction has been confirmed by the experimental results. For examples, Grunlan et al. [50] studied the percolation behaviors of the poly(vinyl acetate) (PVAc) CPCs filled with low-aspect-ratio CB and high-aspect-ratio Single-walled CNTs (SWNTs).The percolation threshold of the PVAc/SWNT CPCs reaches an ultralow value of 0.03 vol%, which is much lower than that of the ones with CB (2.39 vol%). Besides, the high-aspect-ratio conductive fillers always result in a higher conductivity. Kim et al. [51] found that the maximum conductivity ($\sim 10^3$ S/cm) of the PVAc/SWNT CPCs was approximately 3–4 times higher than that of CPCs with Multi-Walled CNTs (MWNTs). The geometry of the conductive fillers also affects the t value of the conductive networks. When using the two types of high-aspect-ratio fillers (2D graphene and 1D CNT) for fabrication of CPCs, the graphene networks often show a t value of below 1.3, implying a 2D percolated structure [52]. The CPCs with 1D CNTs exhibit a relatively high t value of over 2.0, indicating a 3D conductive network formed in the polymer matrix [53, 54].

Nevertheless, high-aspect-ratio conductive fillers easily aggregate. Mierczynska et al. [55] revealed that the high degree of SWNT agglomeration rendered the CPCs less conductive than the ones with MWNT. Therefore, effective dispersion methods are necessary to take full advantages of high-aspect-ratio conductive fillers for fabricating highly conductive CPCs. For this purpose, various strategies such as high-rate shear, filler surface modification, dispersants were often employed to realize the good dispersion of conductive nanofillers [9, 56–59].

3.2 Polymer Matrix

The polymer matrix is the scaffolds for the conductive filler networks, their chemical, and physical properties can affect the electrical performance of the s-CPCs. Polyethylene (PE) is a commonly used petroleum-based material with good chemical stability, which can bear acid- and oxidation corrosion. With the

help of PE, the conductivity of CPCs with metal and carbon nanofillers does not significantly degrade when CPCs work in a harsh environmental. This type of CPC has been used for the fuel cell electrode and vanadium battery electrodes [10, 60, 61], both of which require highly chemical stability.

The molecular weight and modulus of host polymeric matrix also affect the percolation behaviors of CPCs. The host polymers with high molecular weights and moduli are better able to plastic barrier deformation during hot compaction, resulting in a low percolation threshold. For example, Grunlan et al. [62] found that the carbon black emulsion-based CPCs with high moduli (640 MPa) generated a lowest percolation threshold (1.5 vol%) and the highest conductivity (10^{-1} S/cm). For the low modulus (6.5 MPa) matrix, percolation threshold appeared at approximately 4.93 vol% with a relatively low conductivity (10^{-2} S/cm). It should be attributed that the high-modulus polymer particles pushed the CB particles into the interstitial space more efficiently, facilitating the formation of the segregated conductive networks. The molecular weight distribution (MWD) of the polymer matrix also affects the electrical properties of CPCs. For example, Hermant et al. [63] found the percolation threshold for PMMA/MWNT CPCs decreased from 0.6 to 0.3 wt% after introducing PMMA with low-molecular weight ($\sim 80 \times 10^3$ g/mol). The reason is that the decrease of polymer melt viscosity by adding low-molecular weight PMMA facilitates the reorganization of conductive fillers to form additional conductive pathways.

Besides, the crystallization of polymer matrix also affects the electrical properties of CPCs. A better conductivity of CPCs could be obtained in a semi-crystalline polymer matrix against an amorphous one [64] because the conductive fillers are excluded from the crystalline region during polymer crystallization, achieving a relatively high concentration of conductive fillers in the amorphous phase.

3.3 *The Choice of Fabrication Methods*

In the CPCs, charge carriers (current) transport along the interconnected conductive filler network embedded in the polymer matrix. Thus, the constructing conductive network with high quality plays a crucial role in the fabrication of CPCs with superior electrical properties. Good conductive network often needs fillers to interconnect firmly and form 3D continuous distribution in the polymer matrix [7]. Figure 4a shows the randomly dispersed filler network, which contains a lot of unconnected sites and leads to a poor conductivity and a high percolation threshold in CPCs. In contrast, if the conductive fillers are confined to distribute in the polymer matrix and form a continuous and ordered network structure (Fig. 4b), the electrical properties would be much better than former structure [65]. In another word, only a few amounts of conductive fillers are needed for forming a percolated network. Thus, controlling the morphology of filler network is very critical to tailor the electrical properties of CPCs. The processing routes and parameters of the CPCs can significantly tune the morphology of the conductive network structures and greatly

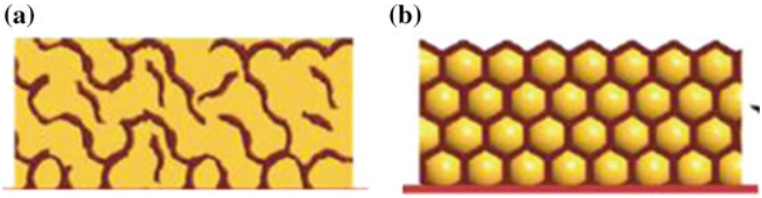

Fig. 4 Schematic illustrations for the **a** random and **b** ordered conductive filler network. Reproduced with permission [65] from Copyright (2011) The American Chemical Society

affect their percolation behaviors. There are three main types of methods for the preparation of CPCs: melt blending, in situ polymerization, and solution mixing.

3.3.1 Melting Blending

Melt blending method employs high temperature and high shear forces to disperse nanofillers into a melting polymer matrix by traditional melt processing equipment (e.g., extruder, internal mixer, and two-roll mill). During this process, the fillers are dispersed by mechanical shear force and are prevented from reaggregation by the viscous polymer matrix. Finally, these polymer composites can be formed in the final samples by various polymer processing techniques such as fiber spinning, hot compression, and injection molding [66–69].This method is cost-effective and environmental-friendly and quite fits the current industrial practices. Many studies have demonstrated the successful application of melt blending method to disperse conductive fillers into various polymer matrices [14, 19, 70]. Here, several recent studies on the effect of the processing parameters of the filler dispersion and other physical properties will be introduced.

Villmow et al. [32] studied the effect of melt processing parameters on the final properties of polymer/CNT composites. The processing conditions significantly influenced the residence time of the mixture and the CNT dispersion. The residence time decreased with increasing the shear speed, so suitable shearing speed and time should be controlled for filler dispersion. Besides the equipment parameters, the design of the screw profiles is also necessary for filler dispersion. For instance, the use of distributive screw configurations containing mixing elements can further improve the filler dispersion. With the control of processing parameter, the macroscopic agglomerates in the polymer matrix can be completely dispersed, this process which resulted in a very low electrical percolation threshold of 0.24 vol% CNTs.

Also, the interaction between the filler and the polymer matrix plays a significant role in the filler dispersion during melt blending. For example, CNTs easily aggregate in nonpolar polypropylene (PP) [71, 72] but can easily well disperse in a Polyamide 6 (PA6) matrix due to the high interaction between the PA6 polymer chains and the CNTs [73]. To overcome the difficulty of CNT dispersion in a

nonpolar polymer matrix, compatibilizers, or surfactants have often been used to improve the interaction between the filler and the nonpolar polymer matrix [74–76].

Overall, melt blending is a simple and cost-effective way to disperse conductive nanofillers in polymer matrices. The control of mixing time and shear stress during compounding is very critical for dispersing filler and avoiding the damage of filler and polymer themselves. Too high-shear stresses and excessive mixing time can lead to the reduction in the aspect ratio of filler during processing due to the filler breakage. Thus, shear mixing processes should be optimized to balance the filler breakage and dispersion states for achieving the desirable properties of the CPCs.

3.3.2 Solution Mixing

Melt blending can realize the macroscopic dispersion of nanofillers, but is generally less efficient at dispersing nanofillers in a polymer matrix at microscale and is limited to lower concentrations due to the high viscosities of the composites at higher filler concentration [22]. Solution mixing method can be considered to obtain better nanofiller dispersion in a diluted solution. This process involves three major steps: (1) dispersing nanofiller in a suitable solvent for a suspension, (2) mixing the resultant suspension with the polymer, and (3) forming the composite by precipitating or solvent evaporation. However, most of the conductive fillers, especially carbon-based nanofillers have poor dispersion in a common organic solvent due to their nonpolar surface and large surface area. Therefore, it is hard to disperse the pristine carbon-based nanofillers (e.g., CNT, graphene, and nano-graphite) in the solvent by a simple mechanical stirring. High-power ultrasonication is often needed to make a metastable suspension of nanofillers/polymer mixture. Besides, chemical functionalization or dispersant is always required to obtain more stable nanofiller suspension. Chemical modification of carbon nanofiller surface by oxidation in a rich acidic medium can introduce oxygenated groups on filler surface to promote the filler dispersion [56, 57, 70], but it usually degrades the electrical performance of the carbon nanofillers. In contrast, non-covalent functionalization of nanofillers by adsorption of dispersants (e.g., surfactants and other molecules) without surface structure damage is becoming a more promising method to disperse nanofiller for CPCs because it can preserve the original physical properties of nanofillers including the conductivity [77].

One of the most commonly used surfactants (Fig. 5) is sodium dodecylsulfate (SDS), in which the hydrophobic chain end has good affinity for carbon nanofiller surface [78]. Koning et al. used SDS to stabilize CNTs in water and then mixed CNT suspension with a polymer latex [59, 79]. After that the mixture is dried and hot pressed into film. Good conductivities can be achieved with CNT concentration of 1.5 wt% using this technique. In fact, nanofiller dispersion can be problematic because the residual surfactants on conductive fillers are electrically insulating and might degrade the electrical properties of the resulting CPCs. Solvent evaporation process usually lead to reaggregation of nanofiller. Koratkar et al. [80] proposed a coagulation method to overcome this issue by preventing it from reaggregation of

Fig. 5 Various surfactants for CNT dispersion. Reproduced with permission [78] from Copyrights (2003) The American Chemical Society

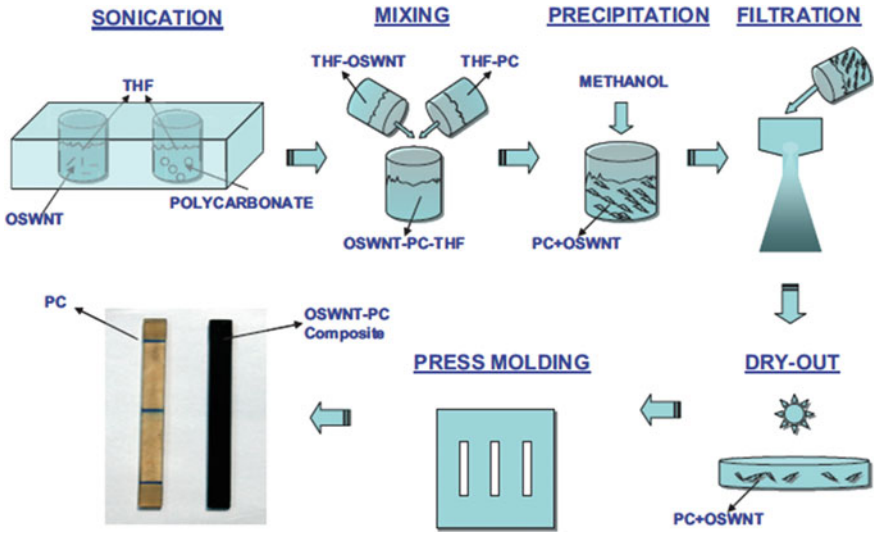

Fig. 6 The schematic for fabrication process of PC/CNT composites. Reproduced with permission [80] from Copyrights (2006) The John Wiley

dispersed CNTs (Fig. 6). In this method, a Polycarbonate (PC)/CNT suspension (tetrahydrofuran as solvent) was dropped into a bad solvent (water) bath to induce instant precipitation of the polymer chains. The precipitating polymer rapidly wraps the carbon nanostructures and prevented them from bundling again.

3.3.3 In Situ Polymerization

In fact, in situ polymerization is one of unique solution mixing techniques for dispersing conductive fillers in a polymer matrix, which involves a chemical reaction to form the final composites [81]. In this process, the conductive fillers

disperse into the polymer monomers. During polymerization, polymer chains can be grown on the filler surface and result in a good interfacial interaction between the filler and the polymer matrix. This method allows for fabricating CPCs with high filler weight fraction.

Early, in situ radical polymerization was used for the synthesis of poly(methyl methacrylate) (PMMA)–CNT composites [82]. In situ polymerization was performed using the radical initiator 2,2-azobisisobutyronitrile(AIBN). In this reaction, p-bonds in CNTs were initiated by AIBN, and therefore nanotubes could participate in PMMA polymerization to form a strong interface between the CNT and the PMMA matrix. PA6/CNT composites have been prepared by in situ polymerization of e-caprolactam in the presence of pristine and carboxylated CNTs. The e-caprolactam monomer was found to form an electron-transfer complex with CNTs and result in a homogeneous, polymerizable solution. The final composites can be spun into PA6/CNT fibers (Fig. 7) with excellent mechanical and electrical properties [83].This method is also suitable for the fabrication of thermosetting polymer composites with nanofillers. Bauhofer et al. [84] dispersed CNTs in an epoxy solution system based on a bisphenol-A epoxy resin and an amine hardener During nanocomposite curing, electric fields were used to induce the formation of aligned conductive nanotube networks. Recently, the in situ polymerization method

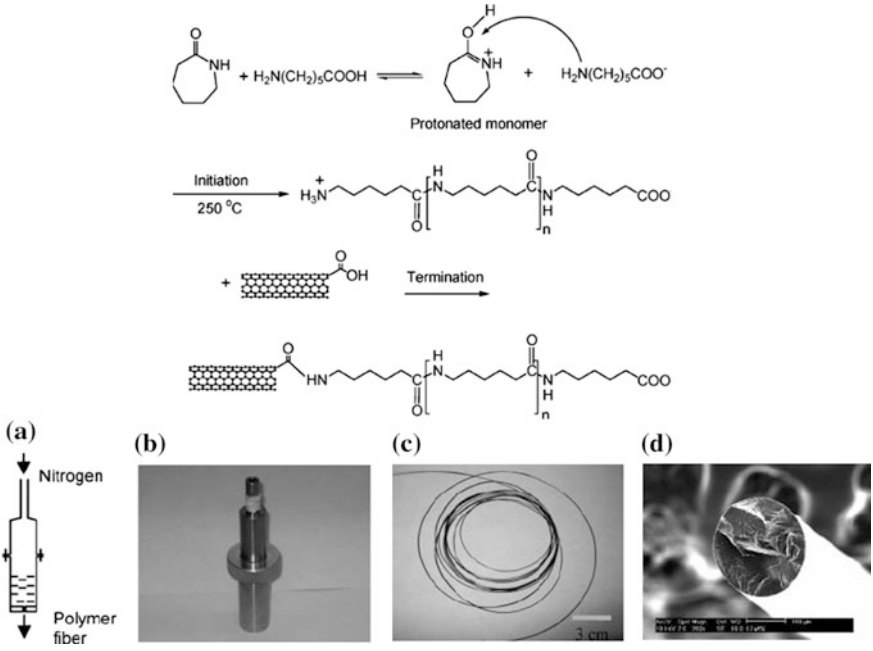

Fig. 7 *Top graph* Scheme for the preparation of PA6/CNT composites by ring-opening polymerization of caprolactam. *Bottom graph* **a** Schematic of the spinneret setup; **b** photograph of the setup; **c** photograph of the composite fiber; **d** SEM image of cross-sectional fracture of the composite fiber. Reproduced with permission [83] from Copyright (2005) American Chemical Society

was used to fabricate CPCs with graphene. A relatively high temperature during polymerisation was utilized to reduce graphene oxide into conductive graphene in the polymer matrix [85].

4 The Strategy for Controlling the Morphology of Conductive Filler Network in CPCs

4.1 Morphology Control by Polymer Blends

Blending two or above polymers together is an important way to create synergistically new physical properties of the composites in the polymer industry. Furthermore, the multiphase separation is produced by polymer blending, and thus, phase morphology of the polymer blends significantly affects the final properties of the composites. When conductive fillers are added to the immiscible polymer blends, the location of conductive fillers in polymer phases may be various and could lead to different electrical properties of CPCs. In another word, conductive fillers can be selectively located in one of the polymer phases or at the phase interfaces [86–88], which can be controlled to construct a desirable conductive network structure in CPCs.

In this multiphase system, the term "double percolation" is defined to describe the conductive mechanism of polymer nanocomposites with a percolated network of nanofiller in one phase, which enables the formation of the conductive network through the whole polymer matrix. It has been proved that addition of conductive nanofillers into an immiscible polymer blend allows for the formation of cocontinuous structure and efficiently decreases the percolation threshold of nanofillers due to the selective localization of the conductive networks. For example, Petra Poitschke et al. [89] introduced CNTs into Polycarbonate/Poly(styrene-acrylonitrile) (PC/SAN) to prepare CPCs. The percolation threshold of CNTs was less than 1 wt %, which is lower than those of CNTs in single PC matrix (1.2 wt%) and in single SAN phase (2.0 wt%).The localization of the conductive filler in polymer matrix depends on the interfacial energies of components and can be predicted by following Eq. (2) [86].

$$\omega_a = \frac{\gamma_{\text{filler}-\text{polymer1}} - \gamma_{\text{filler}-\text{polymer2}}}{\gamma_{\text{polymer1}-\text{polymer2}}} \tag{2}$$

In this equation, ω_a is the wetting coefficient used for judging the location of filler in different polymer phase in the term of thermodynamics. The symbols γ_x represented in the numerator are the different interfacial tensions between filler and polymers 1 and 2 and in the denominator the interfacial tensions between the two blend phases. If $\omega_a > 1$, fillers preferentially distribute in polymer 2; if $\omega_a < -1$, fillers preferentially distribute in polymer 1, and if $-1 < \omega_a < 1$, fillers distribute at

the interface between the two phases. The interfacial tension between fillers and polymers can be adjusted by different surface modifications of fillers and the choice of the polymer matrix.

Several research groups [90, 91] have shown that the choice of the polymer matrix can significantly influence the location of the conductive filler in polymer blends due to the different interactions between these polymers and the filler. Conductive nanofillers are often located in the polymer phase that has good affinity with them. Fu et al. [92] showed that the functionalization of filler can also change the distribution of the filler in polymer blends. Moreover, Potschke et al. [89] used a reactive component to tune the interaction between SAN and CNTs in a polymer blend based on PC and SAN. It is observed that CNTs transferred from the PC phase to the SAN phase after the addition of the reactive component due to an enhanced interaction.

Other than thermodynamic issues, kinetic factors such as the mixing sequence, blending time, and polymer viscosity, also play important roles in the distribution of the conductive filler [86, 91]. These factors can be utilized to enable the selective distribution of conductive nanofiller at the phase interface which is proposed to be the ideal way to achieve the lowest electrical percolation concentration. For example, Dai et al. [93] adopted a particular process to achieve to the selective location of CB particles at the interface between PET and PE phases although CB is predicted to preferentially distribute in PET phase from the CPC. In the fabrication process, CB particles were first mixed with unfavorable PE matrix, and then PET was added into CB/PE compound. During melting mixing, the CB tend to migrate from PE phase to PET phase, but slowly reach the interface between PET and PE due to the high viscosity of PE and suitable mixing time. Finally, the composite exhibits a low percolation threshold of 3.8 vol% CB and good conductivity.

Recently, Potschke et al. [94] studied the distribution state of CB and CNT in an SAN/PC blend. It is found that CNTs (the high-aspect-ratio filler) transferred from one phase to the other one more quickly than CB. It is demonstrated that the transfer dynamics, as well as the stability of different nanofillers at the interface of an immiscible polymer blend, strongly depend on the particle shape (aspect ratio).The larger the aspect ratio is the higher the migration rate of nanofillers across the interface between two phases. It was suggested that the spherical-like CB particles are more stable at the interface than CNTs (Fig. 8). Therefore, it is a big challenge to obtain a CPC where nanofillers with high-aspect-ratio selectively distribute at the interface between two polymer phases. Recently, Wang et al. reported that selective distribution of CNTs) at the interface of immiscible PC/ABS (Fig. 9) is achieved via a combination of adding maleic anhydride grafted ABS (ABS-g-MA) and used an appropriate processing procedure. The resultant CPC shows a much lower percolation threshold of 0.05 wt% [95].

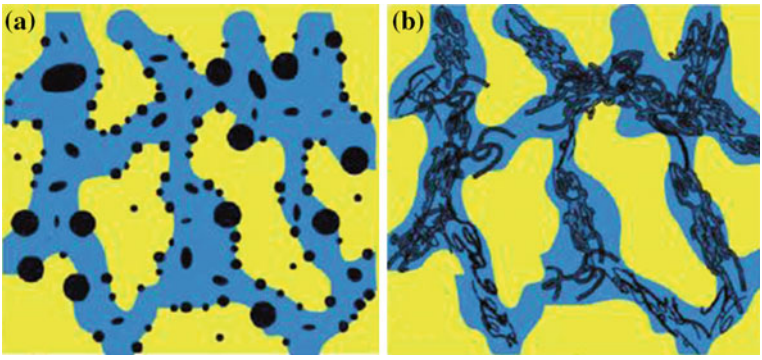

Fig. 8 Typical localization states for low (**a**) and high (**b**) aspect ratio nanofillers. Reproduced with permission [94] from Copyrights (2011) American Chemical Society

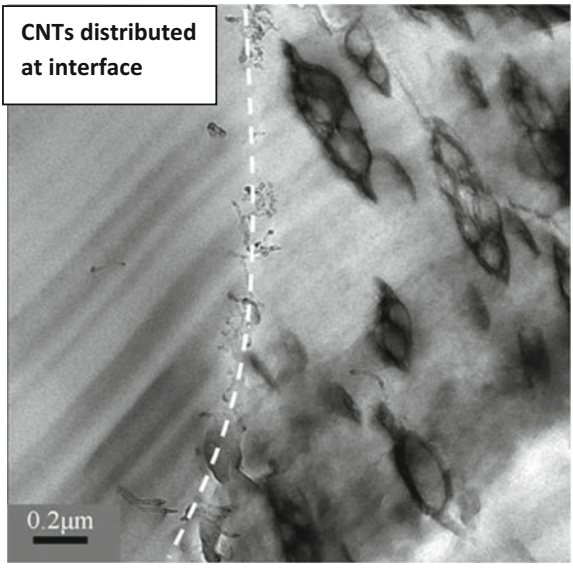

Fig. 9 TEM image of a CNT/PC/ABS/ABS-g-MA CPC showing the selective distribution of CNTs at the interface between the polymer phases. Reproduced with permission [95] from Copyrights (2012) Royal Society of Chemistry

4.2 Morphology Control by Thermal Annealing

Thermal annealing treatment involves the heating of CPCs at a temperature above their glass transition temperature or melting temperature. Through this process, conductive fillers in polymer matrix move with the motion of polymer chains and self-organize into conductive networks [48, 96–99]. For example, conductive networks that were destroyed by shearing can be repaired by reaggregation of CNTs arising from thermal annealing.

Many researchers studied the dynamic process of conductive network formation in CPCs by combining experimental observations and theoretical modeling

[43, 100–102]. A relaxation time or percolation time of conductive filler was obtained by time-dependent conductivity measurement. The percolation time can be characterized as the annealing time at which the conductivity starts to increase sharply during the dynamic percolation process. The results demonstrated that the percolation time is directly correlated to the zero shear rate viscosity of the polymer matrix, regardless of the filler concentrations [103, 104].

Recently, Deng et al. [43] described a new method to fabricate highly conductive CPC tapes with double-layer structure, in which one layer is CPCs filled with CNT based on a lower melting temperature polymer and another one is an unfilled polymer core with higher melting temperature. In such a system, the morphology of the conductive network changed from an isotropic to a highly oriented state during solid-state drawing. Subsequently, annealing process induced the relaxation of the highly oriented CNT and resulted in the formation of a conductive network consisting of relaxed oriented bundles with "hairy" local contacts. During annealing, the resistivity of these CPCs was significantly reduced due to the formation of these conductive networks (Fig. 10). The conductivity of these CPC tapes can be as high as 275 S/m with a high tensile strength of around 500 MPa.

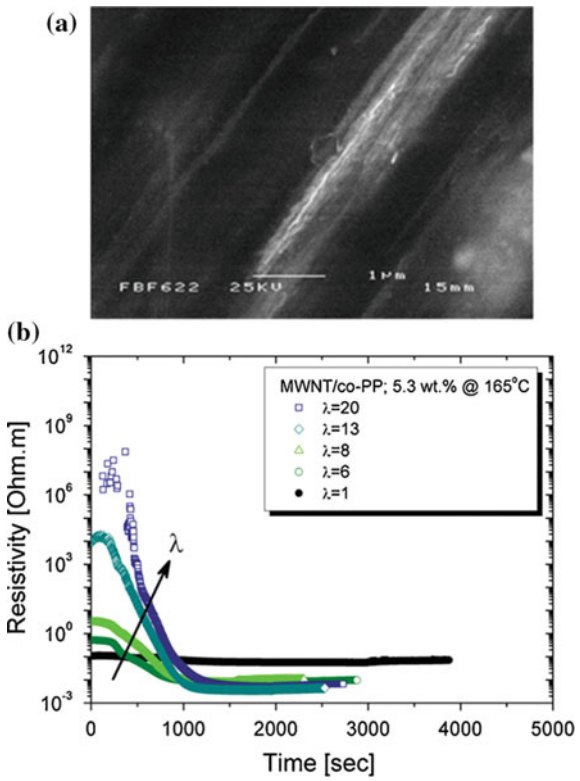

Fig. 10 **a** SEM image showing orientation of CNT in PP matrix after solid-state drawing; **b** in situ electrical measurement carried out at 165 °C on solid-state drawn tapes of different draw ratios containing 5.3 wt% MWNT. Reproduced with permission [43] from Copyrights (2010) John Wiley

4.3 Morphology Control by Shear Force

Shear forces exist in various polymer processing methods, including extrusion, injection molding, spinning, and solution stirring. The morphology control of the conductive filler networks in CPCs can also be operated by a shear force [23, 71]. Shear-induced orientation of fillers and polymer chain is often observed during shear process and can lead to electrical anisotropy due to the orientation in the conductive network. As shown in Fig. 10, solid-state drawing of CPCs tape can induce to orientation of CNT conductive network and results in anisotropic electrical resistivity of CPCs [43]. Eken et al. [105] studied the effect of shear on the microstructure and electrical properties of polymer/CNT composites. The rate of the shear flow influenced the composite conductivity by triggering the formation or destruction of conductive networks. It should be noted that conductive clusters formed and broke simultaneously at a low filler concentration in CPCs, which led to large conductivity fluctuations. For relatively high filler contents, the conductivity fluctuations decreased due to the persistence of these percolating clusters under shear. Furthermore, a CNT agglomerated structure is beneficial for network formation.

4.4 Morphology Control by Latex Technology

It is hard to mix well nanofillers with polymer matrix with high melt viscosity [e.g., polystyrene (PS)], but this type of polymer can be produced as stable polymer latex in an aqueous medium by emulsion polymerization. Fabrication of CPCs with nanofillers by latex technology is very environmental-friendly because this process mainly consumes water. In the emulsion, polymer latex exists as microscopic polymer particles with size from tens of nanometers to several micrometers. Thus, these solid particles can create excluded volume and push nanofillers into interstitial space between them and lead to the formation of the segregated conductive network when mixing nanofillers with polymer latex for CPCs. This method can reduce the space available for the conductive nanofillers to form a conductive network, which results in a significantly reduced percolation threshold. For example, Grunlan et al. [12] employed Gum Arabic as a surfactant to disperse SWNTs and mixing the resultant suspension with PVAc latex. After drying, a PVAc/SWNT film formed with a segregated network, which shows a percolation threshold as low as 0.1 wt%. However, traditional surfactants are usually insulating and can generate a negative effect on the conductivity of CPCs. To overcome this problem, Grunlan, and Koning et al. [21, 51] employed conductive polymer (PEDOT:PSS) as a stabilizer to enhance the dispersion of conductive fillers for latex mixing (Fig. 11). The conductive polymer can connect with adjacent CNT to reduce their contact resistance, so a PVAc/CNTCPC with ultrahigh electrical conductivity (up to $\sim$40,000 S/m) was successfully prepared.

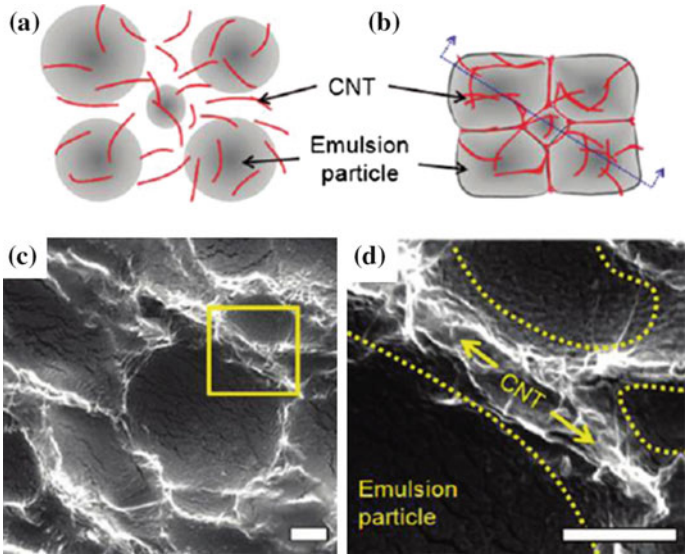

Fig. 11 **a**, **b** The scheme for the formation of PVAc/SWNTs with segregated network; **c**, **d** SEM images of the cross-section of CPCs at low and high magnifications. Reproduced with permission [51] from Copyrights (2010) American Chemical Society

Polymer latexes were also employed to fabricate polymer/graphene CPCs by using water-soluble graphene oxide (GO) [42].The traditional method for scale preparation of polymer/graphene CPCs often involves the chemical reduction of GO, which leads to the reaggregate of GO sheets aggregate due to loss of oxygenated groups. Thus, the dispersants were used to prevent the restacking of reduced GO (RGO) during chemical reduction with highly toxic hydrazine. As a result, the RGO sheets dispersed homogeneously in the polymer matrix and resulted in a CPC with a low percolation threshold of below 1.0 wt% and a maximum conductivity of 15 S/m. However, the presence of dispersant can hinder the conductivity enhancement of CPC. Recently, Tang et al. [54] developed an environmental-friendly method to fabricate highly conductive composites involving no dispersant by strengthening the interaction between polymer and filler (Fig. 12). In the water, GO sheets were self-assembly on PVP-grafted PS microspheres by hydrogen bonding and via π-π bonding. In the absence of dispersant, PS immobilizes the dispersed GO sheets to prevent them from undesirable self-aggregation during the transition from GO to RGO by chemical reduction with Vitamin C. During the formation of CPCs, micron-sized PS microspheres act as a template to induce the RGO sheets to form a three-dimensional segregated RGO structure with a long-range order. The formation of a compact percolated network and lack of dispersant enable composite a very low percolation threshold (0.08 vol%) and high-composite conductivity (20 S/m). The electrical property of this composite with the segregated filler network is much better than that with random filler network.

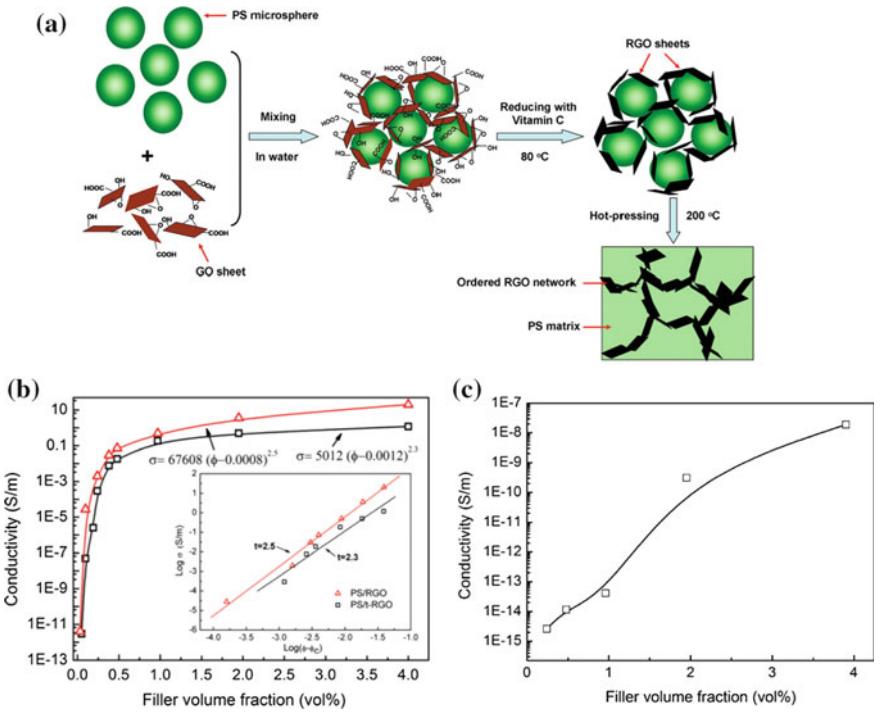

Fig. 12 **a** Schematic illustration of preparation of PS/RGO composite with an ordered three-dimensional segregated network; the electrical conductivities of PS/RGO composites with **b** the segregated network and **c** the random network. Reproduced with permission [54] from Copyrights (2013) The Royal Society of Chemistry

4.5 Morphology Control by Mixing Different Nanofillers

To achieve a lower percolation threshold and a high conductivity, more than one type of filler with different dimensions can be used to prepare CPCs, such as zero-dimensional atomic clusters (e.g., nano-carbon black, and silica), 1D rod-like nanofiller (e.g., carbon nanotubes, and silver nanowires), and 2D layered nanofiller (e.g., clay platelets, and graphene) [106–110]. In fact, because of their differences in shape and element component, each nanoparticle has its own unique ability. Positive synergistic effects of these nanoparticles on improving the electrical and other properties of polymer matrix are expected.

A theoretical study showed that it is not necessary to build a conductive network with a high-aspect-ratio filler alone [109] and that the percolation threshold of CPCs is sensitive to the part of high-aspect-ratio filler in a system that contains hybrid fillers with different dimensions [111]. A number of studies on CPCs with two mixed carbon-filler-filled have been reported. The percolation thresholds of these systems are often close or below the average value of the systems that are filled with

one kind of carbon filler alone, indicating that a considerable amount of a high-aspect-ratio and expensive filler can be replaced with a low-aspect-ratio filler. For example, a low-aspect-ratio filler (CB) can act as a bridge between the networks consisting of the high-aspect-ratio filler (CNTs) in the PP matrix [112]. This result means that the fabrication cost can be reduced by this method. However, in these systems, only a sum effect of two fillers in the electrical properties of CPCs was observed because the network morphologies do not change significantly.

Recently, Tang et al. [113] reported a simple and water-based method to construct a 3D foam-like hierarchical conductive network structure via self-assembly, with conductive carbon nanotubes (CNTs) and graphene sheets as the 1D and 2D nanoconstituents and latex–polystyrene (PS) microspheres (Fig. 13). The introduction of a second conductive filler (graphene) can significantly change the conductive network morphology of CPCs filled with CNT. The electrical properties of CPCs with such 3D hierarchical structures are much better than those of CPCs with RGO or CNTs alone. The enhanced properties are attributed to the synergy from graphene and CNTs in forming a 3D conducting network with high quality, which is produced by the following main key factors: (1) GO is used as an alternative stabilizer to insulating surfactants and can be reduced to conductive graphene to connect electrically with CNTs; (2) the resultant graphene sheets act as a "nano-wall" to prevent CNTs from randomly diffusing into the polymer

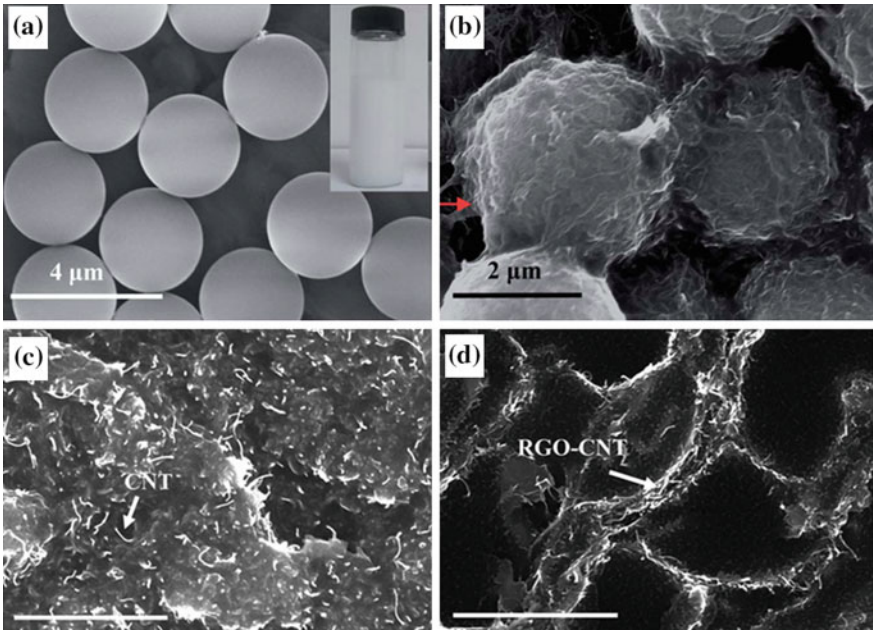

Fig. 13 SEM images of **a** PS microspheres, **b** RGO-CNT/PS microspheres, **c** PS/CNT, and **d** PS/RGO-CNT composites. Reproduced with permission [113] from Copyrights (2014) The Royal Society of Chemistry

microsphere and form a complete segregated conductive network; (3) CNTs on RGO serve as useful spacers to prevent graphene from re-stacking for producing available large surface area. Therefore, besides the polymer/filler interaction, understanding and controlling the interaction between different nanofillers can produce a new synergetic effect for improving the electrical properties of CPCs. The addition of nanofiller can also improve the electrical properties of CPCs-filled microsized conductive fillers. For example, Wong et al. [114] added diacids-functionalized silver nanoparticles into the polymer matrix with silver flakes as conductive fillers. The resistivity of the silver flakes and nanoparticles (molar ratio of silver flakes to nanoparticles is equal to 6:4) incorporated polymer composites was dramatically reduced to as low as 5×10^{-6} Ω cm due to the sintering of silver nanoparticles.

Both nonconductive and conductive filler have also been used to fabricate CPCs with improved electrical properties. Bilotti et al. [115] found that addition of nonconductive needle-like clay could accelerate the dynamic percolation behavior of the CNT conductive network. Grunlan et al. [108] observed that the addition of 0.5 wt% clay could increase the electrical conductivity of epoxy filled with SWNTs by more than four orders of magnitude. Furthermore, the percolation threshold of these nanocomposites was reduced from 0.05 to 0.01 wt% with the addition of clay. The enhanced electrical properties of CPCs are attributed to the good interaction between SWNTs and the clay helps the dispersion of CNT and the exclusive volume from clay clusters induced a formation of segregated SWNT network (as shown in Fig. 14). Kim et al. [116] found that introducing silica nanoparticles can increase the electrical conductivity of silver nanowire/polymer nanocomposites by up to about eight orders of magnitude and the electrical percolation threshold volume fraction of silver nanowires decreases from 0.12 to 0.02 vol%. Monte Carlo simulations show that van der Waals attractive interaction between silica nanoparticles and silver nanowires dominates over the depletion-induced interaction between silver nanowires and results in improving the dispersion of silver nanowires.

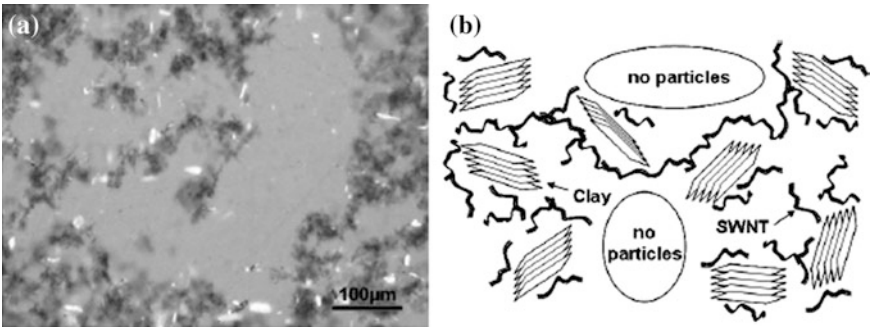

Fig. 14 **a** Optical microscope image for composites containing 0.05 wt% SWNT and 2 wt% clay under partial polarized light condition and **b** schematic illustration for clay assisted dispersion of SWNT. Reprinted with permission [108] from Copyrights (2007) The John Wiley

4.6 Morphology Control Through Other Methods

Besides above methods, other methods were developed for controlling the morphology of conductive networks. For example, the electric or magnetic field was employed to monitor the filler network. Some studies have demonstrated that conductive fillers can be oriented in an electric field [117–119] and that an electric field can accelerate the dynamic percolation process. The formation of a conductive network under an electric field can directly result in a very low electric percolation threshold. Similar to an electric field, a magnetic field can also be used to orient conductive filler and to trigger the formation of conductive networks. All these methods are based on controlling the dispersed filler in the polymer matrix. Recently, some researchers fabricated the CPCs by constructing the conductive filler network first and then infiltrating a polymer liquid into network [120]. For instance, Li et al. manufactured a graphene/CNT 3D conductive scaffold first and then filled it with poly(dimethylsiloxane) (PDMS) by the vacuum-assisted suction method to obtain a highly conductive and stretchable polymer composite [121].The electrical conductivity of this composite exhibits an improvement of more than four orders of magnitude compared to the composite prepared by solution blending method. Nevertheless, this method is not suitable for the scalable production of CPCs.

5 Applications of CPCs

CPCs can find many applications such as sensors, EMI shielding, stretchable conductor, and thermoelectric materials based on their excellent electrical properties and other unique physical characteristics. In this section, some application cases are presented and the property requirements of CPCs-based specific electrical application are discussed, most of which greatly associate with conductive network structure in CPCs.

5.1 Sensors

CPC sensors work based on conductivity change of CPCs under various external stimulus such as temperature shifts [122, 123], mechanical deformation [124–127], and contacting with organic vapor or solvent [128–131]. The conductivity of CPCs is associated with the tunneling between local conductive networks and the change of tunneling barrier under an external stimulus could lead to a significant change in the conductivity. These changes can be monitored as a signal for sensing purposes.

5.1.1 Temperature Sensors

CPCs are used as temperature sensors in multiple applications such as over-temperature protection devices, self-regulating heaters, and micro-switch sensors [132]. These applications are based on positive temperature coefficient (PTC) and negative temperature coefficient (NTC) effects which are often observed as a sharp increase and subsequent gradual decrease in resistivity of CPCs with increasing temperature [133]. This phenomenon arises from the thermal expansion or melting of the polymer matrix in CPCs which causes a change in the conductive network. The melting of the crystalline phase is accompanied by a significant volume expansion, which results in an increased interparticle distance between the conductive fillers and reduces the probability of electrons tunneling between conductive regions. The following reaggregation of the conductive fillers in the polymer melt caused a gradual recovery of the conductive network in CPCs. Li et al. reported that the NTC effect was observed in a PU foam containing CNTs [134]. The expanded gas squeezes the cell struts and cell walls. The reduction in the cell walls thickness causes the decrease in the distance between adjacent CNTs and creates more efficient conductive paths within the matrix. Thus, the NTC effect appears during heating. Kar and coworkers reported a highly repeatable PTC effect below the glass transition temperature of a polymer matrix for CPCs that are based on PMMA and Ag-coated glass beads [135]. The mismatch of the thermal expansion coefficients between PMMA and the glass beads causes a disruption in the continuous conductive network which is responsible for this phenomenon.

The temperature-resistivity intensity (I_{PTC} and I_{NTC}) of CPCs is essential for temperature sensing a property of CPCs. A desirable temperature sensor usually requires a low I_{NTC} value to maintain highly responsive toward temperature stimuli [136]. Many efforts have been made to eliminate the NTC effect, and the usual method is irradiation or chemical cross linking, which increase the viscosity of the polymeric matrices and produce a gel network that stabilizes the conductive fillers in the polymer melt [53, 137]. However, this approach leads to complex processing and expensive production. CPCs with segregated structure have superiority in monitoring the NTC effect than conventional CPCs because the conductive fillers are mostly located at the interfaces of polymer matrix instead of being randomly distributed throughout the whole CPC system. Thus, it is easier to control the aggregation of conductive fillers. Recently, Lu et al. demonstrated that the PTC effect can be enhanced and that the NTC effect can be eliminated by the selective distribution of CB at the interface of PA6/PS blends [138]. The conductive pathways are confined at the interface and are narrower than PA6/PS/CB composite prepared by the conventional melting blending method. Thus, this conductive path can be broken up by a slight volume expansion, resulting in an active PTC effect. To eliminate the NTC phenomenon in the CPC-based sensors, Zhang et al. [136] designed a segregated CB/UHMWPE s-CPC-based temperature sensor without the NTC behavior by combining the segregated structure with the ultrahigh melt viscosity of UHMWPE. In this material, the CB particles distribute around UHMWPE granules and form a stabilized isolated conductive network that remained

unchanged when UHMWPE crystallites are melted. Moreover, the ultrahigh melt viscosity of the UHMWPE matrix also hindered the arrangement of the CB particles in the polymer melt. Therefore, the fluctuated CB structure was stabilized at elevated temperatures, thus eliminated the NTC effect. More similar results were reported by different groups [139–141].

5.1.2 Strain Sensor

Strain sensing based on CPCs has been widely investigated for movement measurement, health monitoring, and wearable electronics. Figure 15 shows a class of wearable and stretchable sensor devices based on aligned SWNT films and PDMS, which can be incorporated into stockings, bandages, and gloves to detect different types of human motion [142]. For this application, the CPCs are required to change their resistivity (conductivity) with strain [104].

The electrical response of CPCs toward strain commonly occurs when the distance between the conductive fillers increases to exceed the tunneling distance under the applied load [143].The sensitivity of these strain sensors is a critical parameter for various applications. However, Zhang et al. [126] demonstrated that a universal logarithmic resistivity–strain relation is independent of the CNT concentration in thermoplastic polyurethane (TPU), indicating that adjusting conductive filler concentration is not an available way to modify the strain sensitivity. The processing conditions and material properties, such as the weight fraction, diameter, and conductivity of the conductive fillers, the processing temperature, and the tunneling barrier height of the polymer matrix, all play a role in determining the sensitivity

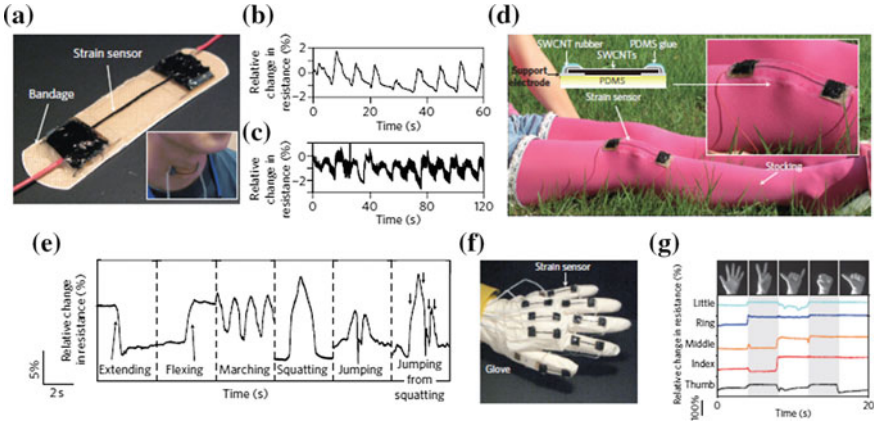

Fig. 15 Stretchable wearable devices. **a**, **d**, **f**, Photographs of a bandage strain sensor (**a**), a strain sensor fixed to a stocking (**d**) and a data glove (**f**). *Inset* **a** Photograph of the sensor adhered to the throat. *Inset* **d** close-up of the device. **b**, **c**, **e**, **g**, Relative changes in resistance versus time for breathing, phonation (speech), knee motion and data glove configurations, respectively. Reproduced with permission from Copyrights (2011) The Nature Publishing Group [142]

[144]. Several methods have been found to modify the strain sensitivity of CPCs. Murugaraj et al. [145] observed that a narrow distribution of tunnel gaps between overlapping nanochannels was beneficial for high sensitivity in their CPCs. Dang et al. [125] noted that a CNT with a higher aspect ratio was preferred for a higher sensitivity in silicone rubber/CNT nanocomposites. Fu et al. demonstrated that mixed fillers containing CNTs and metallic particles in different volume ratios could be used to modify the strain sensitivity of CPCs fibers, indicating that the strain sensitivity can be tuned by using mixed fillers with different compositions [146].

5.1.3 Chemical Sensor

One of the most studied chemical sensing properties of CPCs is vapor and liquid sensing. Many studies have reported that CPCs can detect and distinguish vapor or liquid chemicals [129, 130, 147, 148]. Sensing is achieved by the ability of the polymer matrix to swell when exposed to organic vapor or liquid. After vapor or solvent diffuse into the polymer matrix, the polymer expansion increased the distance between the conductive fillers, resulting in the change of resistivity [149]. The following removal of such stimuli led to the recovery of the resistivity back to its original value. Many potential liquid detection applications for the tank on a truck,

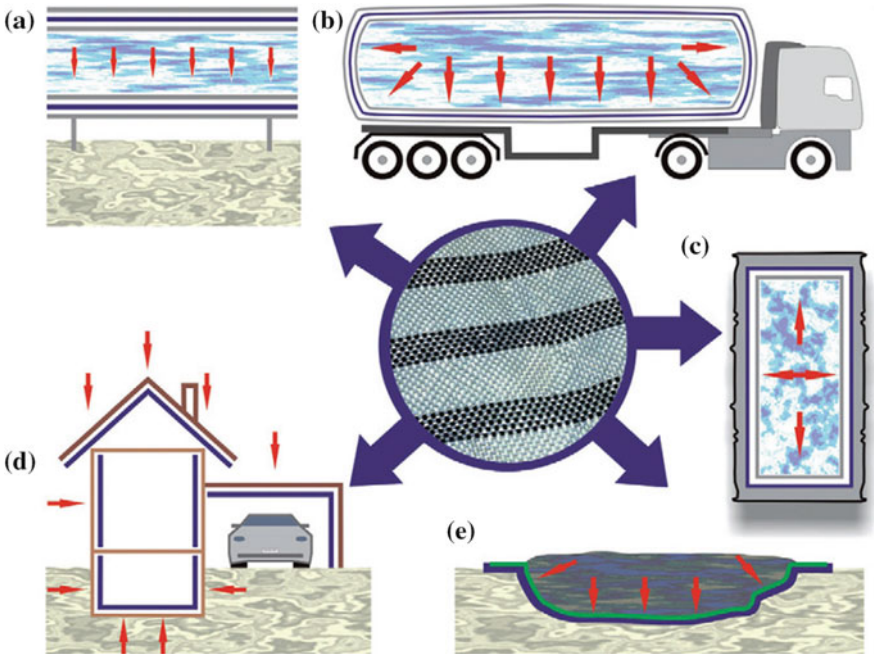

Fig. 16 Potential applications for CPC textiles with liquid sensing capability. **a** piping system, **b** tank on a truck, **c** barrel, **d** buildings, and **e** landfill waste disposal site. Reproduced with permission [150] from Copyrights (2011) Elsevier Science Ltd

barrel, buildings, and landfill waste disposal sit have been proposed as shown in Fig. 16 [150].

The sensitivity, selectivity, and recoverability of these sensors could be modified by various methods. Castro et al. [151] reported a poly(epsilon-caprolactone)/CNT composite vapor sensors. It is found that the sensor response amplitude could be enhanced by grafting PCL onto the surfaces of CNTs. Feller et al. [152] demonstrated that the chemical sensitivity of CPCs based on chitosan could be modified by controlling the conductive junction gap because the sensitivity of vapor sensors depends exponentially on the average gap between two conductive nanofillers at conductive junctions. This control was realized through the chemical modification of the MWNT surfaces. But there are still some problems in these applications. The swelling process is often very slow to separate the conductive fillers, causing a low response rate [153]. The disconnected conductive network microstructure often cannot recover during the subsequent drying process because of the disorder of conductive fillers and seriously depressing the repeatability. To address these issues, many researchers have focused vapor and liquid sensors based on CPCs with segregated network [154–156], because the segregated conductive networks located in the interfacial of the polymer matrix can accelerate the permeation of organic solvents or vapors by the capillary effect. Furthermore, the conductive fillers in CPCs with the segregated network are more ordinary and easy to recover in the drying process. Lu et al. [154] investigated this method by using poly (butyl acrylate) (PBA) latex filled with MWNTs to produce a novel vapor sensor with segregated structure. The MWNTs were confined in the interstitial between the latex nanoparticles and they were sprayed layer-by-layer. These CPC transducers detected different volatile organic vapors such as ethanol, chloroform, and toluene rapidly and reproducibly. Ion selective sensors are another kind of widely studied and developed chemical sensors in analytical chemistry. Ion sensing of CPCs is based on the catalytic activity of chemical groups on CPCs with special ions. Many studies have been reported for the detection of nitrite ion (NO_2) [157–160]. For instance, Liu et al. [160] reported a Poy(3,4-ethylenedioxythiophene)/GO modified Au electrode with the notable catalytic ability for NO_2.

5.1.4 Stretchable Conductor

Conventional materials used for electrical devices like electrodes are metals or other rigid materials which will be crack and broken when highly stretched. Here, stretchable conductors are the kind of materials which can remain conductive when highly stretched. They can render the fabrication of the material into novel geometries and can keep conductivity subjected to stretching. So this kind of materials has attracted extensive interest in recent years [161–163]. CPCs have superiority in this area because the polymer matrix has good extensibility. However, it is a big challenge to maintain a stable conductive network during stretching because the conductive network is easily broken with deformation.

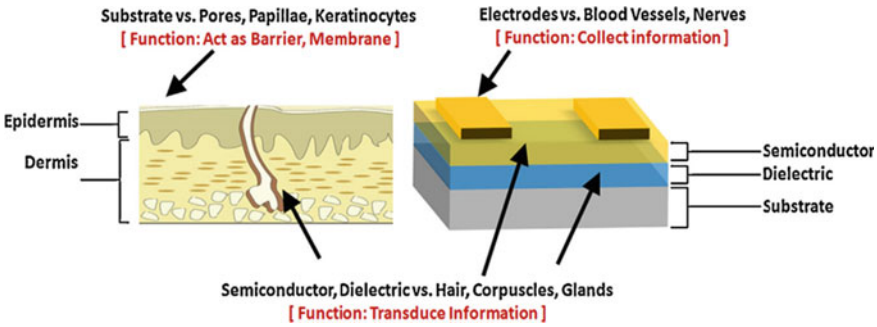

Fig. 17 Electronic skin and its various components are compared to human skin and its sublayers. Reproduced with permission [164] from Copyrights (2012) The American Chemical Society

This type of CPCs is desirable for applications in robot arm joints, wearable displays, health monitors, disease diagnostics and electronic skins. We take the electronic skin (E-skin) as an example. As E-skin, the material must have stretchability, flexibility, and dexterous electronic reaction. E-skin should be able to emulate the touch and pressure sensitivity of human skin [164, 165], as shown in Figs. 17 and 18.

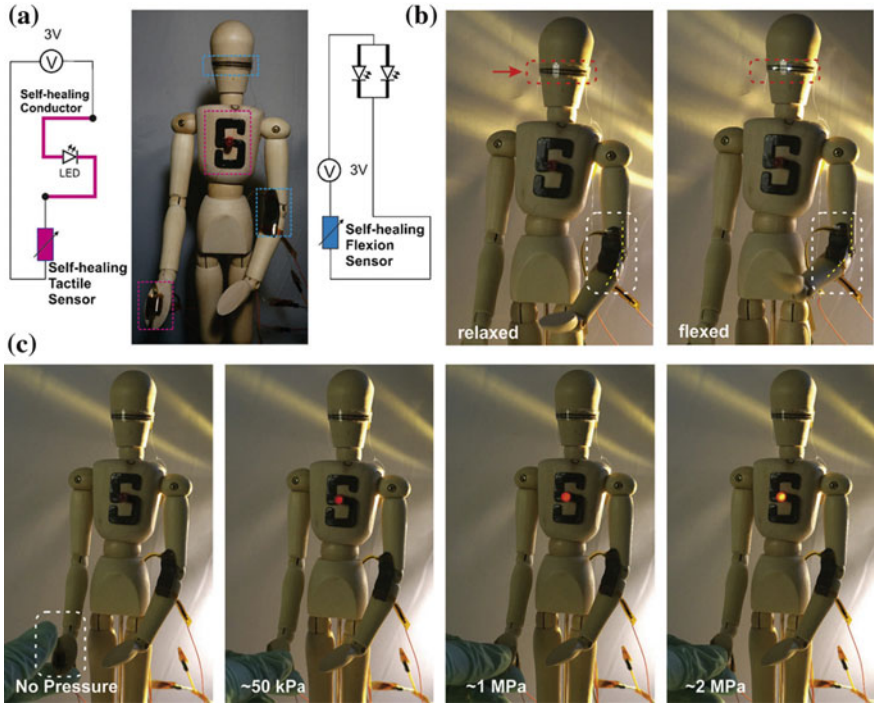

Fig. 18 Humanoid mannequin showing integration of E-skin. LEDs placed on the mannequin light up at varied intensities based on the movements and magnitude of the inflicted perturbations. Reproduced with permission [165] from Copyrights (2012) The Nature Publishing Group

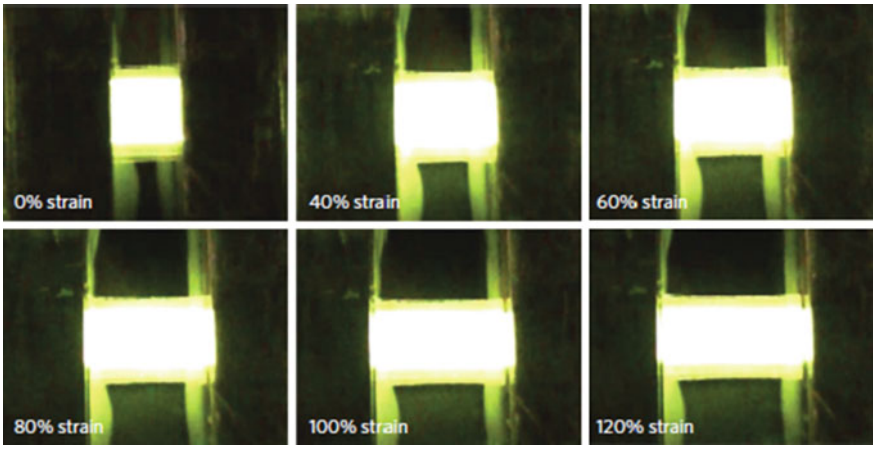

Fig. 19 Photographs of a stretchable polymer light-emitting device at different strains. Reproduced with permission from Copyrights (2013) The Nature Publishing Group [167]

Generally, stretchable conductors can be realized by the topography design of a new conducting structural configuration. For example, conducting material structures with 'wavy' layouts on an elastomeric polymer substrate are utilized [120]. When a compressive load is applied to an elastomeric polymer substrate that is bonded to a rigid thin film, the surface strain can be released by mechanical buckling, thereby significantly improving the stretchability [166]. Recently, Pei et al. [167] reported a stretchable polymer light-emitting device (Fig. 19) comprising an electroluminescent polymer layer sandwiched between a pair of new transparent elastomeric composite electrodes. The composite electrode is composed of a thin silver nanowire network in the surface layer of a rubbery poly(urethane acrylate) matrix, which could be stretched as large as 120 %.

Composites with a low content of conductive fillers can produce highly elastic conductors with a strain more than 100 %, yet the conductivity is typically too low for the flexible conductor. Composites with a high concentration can produce a high conductivity but with poor stretchability due to the agglomeration of the fillers. A mixture of SWNTs and ionic liquids (ILs) was ground in an agate mortar or strongly sonicated to produce stable bucky gels, which were then dispersed in the elastomeric matrices, such as a vinylidene fluoride-hexafluoropropylene copolymer [162], PDMS [168] and polyurethane (PU) [169]. The as-prepared composites exhibited very high conductivities under zero strain and excellent ultimate stretchability. These materials can be fabricated with stretchable electrodes with various patterns. However, the electrical conductivity of these composite decreased significantly with stretching. To overcome this issue, ultralight CNT aerogels [170], or pregrown graphene networks [120] were used to form an ordered structure that was proven to be electrically stable under an applied pressure.

5.1.5 Thermoelectric Material

A thermoelectric material can generate electricity under a temperature gradient because charges can diffuse from the high temperature side to the low temperature side, thus producing a current [171, 172]. This phenomenon is known as the Seebeck effect, which is the basis for thermoelectric power generation. The dimensionless TE figure of merit (ZT) for a certain material can be calculated using the following equation:

$$ZT = \frac{\sigma S^2 T}{k},$$

where S, σ, T, and k represent the Seebeck coefficient, electrical conductivity, temperature, and thermal conductivity, respectively. Such an effect can be used to generate electricity from waste heat or natural heat sources. Moreover, thermoelectric material can also be used for harvest energy on wearable electronics, on-chip electronic cooling, and automobiles.

Traditional inorganic thermoelectric, such as bismuth telluride (Bi_2Te_3) [173], which shows a figure of merit as high as 2 at room temperature have been reported widely. However, there are some drawbacks of this thermoelectrics including a high production cost, difficult processing, a toxic nature, and scarcity of materials. Due to these issues, CPCs based on insulating polymer matrices and conductive fillers have been investigated as inexpensive, lightweight, and environmentally friendly alternatives for inorganic thermoelectric materials [174–176].

High-performance thermoelectric materials based on CPCs require a high electrical conductivity and a low thermal conductivity. Grunlan et al. [176] used SWNTs and PVAc to fabricate thermoelectric composites. The thermal conductivity and thermopower of this composite remain relatively insensitive to the filler concentration. This behavior has resulted from thermally disconnected, but electrically connected, junctions in the CNT network. With a CNT concentration of 20 wt%, these composites exhibit a high electrical conductivity of 4800 S/m, a low thermal conductivity of 0.34 W/m K and a ZT of greater than 0.006 at room temperature. However, the ZT value is too low for real application. To further improve the ZT value, Grunlan et al. [177, 178] used SWNTs, and PVAc with a conductive poly(3,4-ethylenedioxythiophene):poly(styrene sulphonate) (PEDOT:PSS) with high Seebeck coefficient to fabricate composites. In this work, the SWNTs were successfully coated with PEDOT:PSS particles to facilitate electrical conduction but prevented thermal conduction between nanotubes. As a result, this composite exhibited a high ZT value of 0.02 at room temperature, which is, at least, one order of magnitude higher than most polymers and higher than that of bulk silicone materials.

Recently, Hewitt et al. [171], assemble a multilayer of MWNT/PVDF films into a felt fabric for thermoelectric devices, as shown in Fig. 20. The author demonstrated that the thermoelectric voltage generated by these fabrics was the sum of contributions from each layer, resulting in increased power output. And this kind of

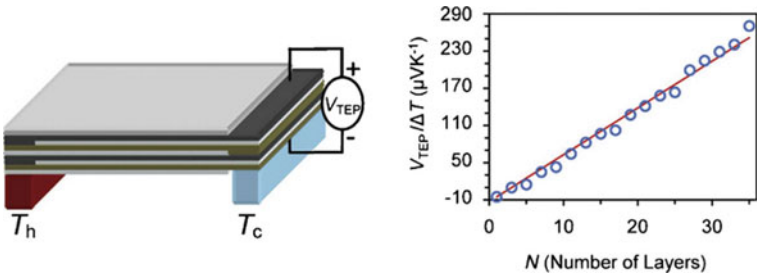

Fig. 20 Alternating PVDF and MWNT/PVDF film that are layered into a fabric (*Left*); the thermoelectric properties of such fabric at different number of layers (*Right*). Reproduced with permission [171] from Copyrights(2012) The American Chemical Society

fabric materials shows good promise as a realistic alternative to a number of applications such as lightweight, portable electronics for its lightweight and low cost.

5.1.6 Electrodes for Energy Storage

Energy storage devices such as fuel cells, supercapacitors, and lithium batteries, which are indispensable components of various electronics and mobile tool, have been extensively studied for the past decades. With the development of flexible electronic, inexpensive, flexible, and lightweight energy storage devices are strongly demanded [179, 180]. The elaboration of flexible electrodes based on CPCs could be a good way to realize above requirement. CPCs based on nano-sized structures are expected to show improved performance in energy storage because of the unique properties arising from their nanoscaled sizes such as high electrical conductivity, large surface area, short path lengths for the transport of ions, and high electrochemical activity. A typical electrode in a battery or supercapacitor is a composite of an electrochemically active material, conductive agents/additives, and a polymer matrix. The electrode must ideally form a mechanically and electrochemically robust unit that can withstand thousands of charge–discharge cycles with minimal chemical or physical changes, even with the dramatic volume change of the active particles. Conducting polymers (CPs), such as PPy, PANI, and PTh can be used to manufacture flexible batteries and supercapacitors. However, batteries and supercapacitors based on CPs show poor cycling stabilities, and high self-discharge rates, and low capacities. Some problems have been partly addressed by combining carbon nanofillers with CP materials. For example, Integrating PPy with CNTs has been proposed to improve the electrochemical properties and cycling performance of electrodes based on pseudocapacitance materials [181–183]. A PPy/SWNT composite has a specific capacitance of 265 F/g, which is higher than that of PPy alone (192 F/g). Besides, the PPy/CNT composite shows a better cycling stability than PPy alone. During the fabrication of electrodes, the CP can be used to disperse the active nanoparticles.

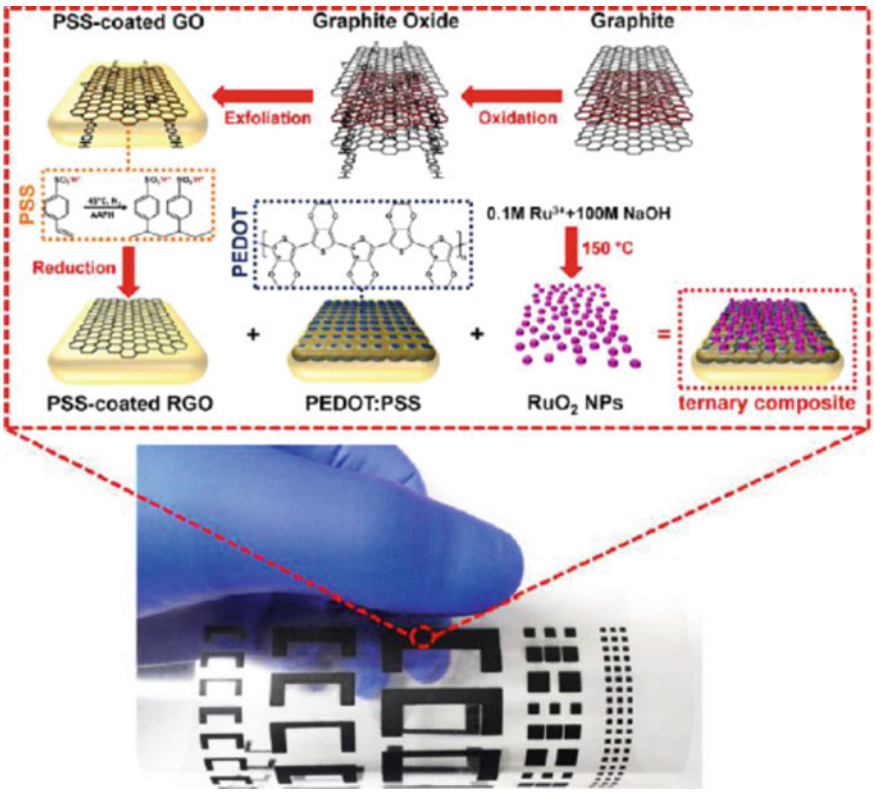

Fig. 21 Overall procedure for fabricating RuO2/PEDOT:PSS/graphene screen-printed electrode and photograph of screen-printed electrode. Reproduced with permission [184] from Copyrights (2015) The American Chemical Society

Recently, Jang prepared a water-dispersible RuO_2-graphene-based inks stabilized by PEDOT:PSS [184], which can be screen printed on the flexible substrate for high-performance electrochemical capacitors (Fig. 21). The resulting screen-printed electrode system exhibited significantly higher conductivity (1570 S cm^{-1}), a larger specific capacitance (820 F g^{-1}), and better cycling performance (81.5 % after 1000 cycles) compared with PEDOT:PSS.

5.1.7 Biomedical Application

In the past years, CPCs showed great potential for biomedical applications for tissue engineering scaffolds and biosensors [4, 185]. Engineering Scaffolds are used to stimulate native tissue activities for treating organ failures arising from injuries, aging, and diseases [186]. They should have the ability to mimic the complex tissue architecture and to control the formation of functional tissues by inducing the cell

growth [187]. For this case, CPCs can be used as functional scaffolds to modulate cellular activities such as cell-to-cell attachment, cell growth, cell migration, and cell differentiation because most biological cells are sensitive to electrical stimulus [188]. But their biocompatibility should be considered carefully. PANI and PPY are typical candidates for biomedical applications due to their ease of synthesis and rich redox chemistry. A recent in vitro study reported that PPy nanoparticles are cytotoxic at high concentrations and negatively affected the cell viability/proliferation [186]. Furthermore, this effect was dependent on the nanoparticle concentration. Integrating biocompatible polymers and conductive nanofillers into hydrogel is an important way to improve the biocompatibility of tissue scaffold. For examples, CNTs were embedded in a porous gelatin methacrylate (GelMA) network (Fig. 22) for a scaffold. It was found that cardiomyocytes seeded onto CNT-GelMA nanocomposite hydrogels had a threefold increase in their spontaneous beating frequency compared with pure GelMA hydrogels [189]. Besides, the external voltage for inducing beating in the cells was significantly decreased due to the high electrical conductivity of the CNTs in the nanocomposite hydrogels.

Besides, CPs have unique electrochemical properties and can show various electrical signal change interacting with chemical substances. Therefore, they could be used as biosensors for detecting the adsorption, catalytic, and redox, and transport behavior relating to biomedical application [185]. Incorporating

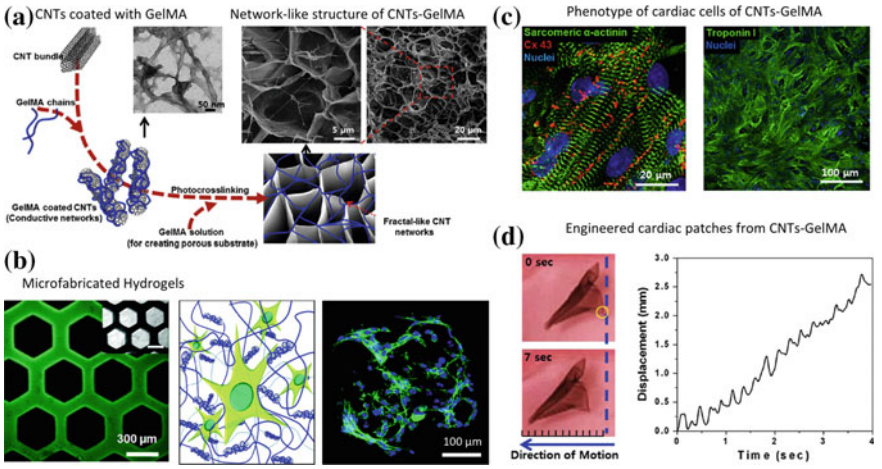

Fig. 22 Nanocomposite hydrogels from CNTs and GelMA. **a** Schematic showing synthesis of nanocomposite network. **b** Due to photocrosslinking ability of the nanocomposite network, microfabrication technologies can be used to control cellular interactions. **c** Cardiac cells that were seeded on CNTs-GelMA nanocomposites retained their phenotype as determined by the expression of sarcomeric α-actinin and troponin I. **d** The engineered cardiac patch obtained by seeding cardiac cells on CNTs-GelMA surface showed macroscopic mechanical displacement due to continuous contraction and relaxation of the patch. Reproduced with permission [187, 189] from Copyright (2013) American Chemical Society and Copyright (2013) John Wiley

nanofillers into intrinsically conducting polymers with high surface area for a CPC sensing materials results in an increased surface area, more numbers of analytical recognition sites, and low resistance, due to the synergetic properties from both components. For instance, sensing electrode based on PANI/graphene composite film can respond rapidly and a much lower LOD (limitation of detection) of 0.8×10^{-7} M of H_2O_2 [190].To further accelerate the electron transfer and enhance the electrocatalytic activity, metal nanoparicles can be added into the CPCs matrix for the enzyme immobilization. The sensor based on Pt/PANI/graphene shows a LOD of 50 nM for H_2O_2 and a LOD of 0.18 μM for glucose, respectively [191].

6 Conclusion and Outlook

In the past decades, CPCs underwent an exciting development under the drive of the requirement for the lightweight, low cost, and flexible conductor and had presented various electrical applications. The new emergence of different conductive nanofillers (e.g., CNT, graphene, and silver nanowire) significantly contributes to the improved electrical properties of CPCs. Compared to traditional CPCs with micron-sized fillers, the incorporation of a little conductive nanofillers can impart the desirable conductivity of CPCs. This characteristic can preserve some original physical properties of polymers (e.g., flexibility, and transparency) and can realize a "real" flexible conducting material based polymer materials, which could be used for strain-senor, flexible conductor, and flexible electrodes. Thus, pursuing the low percolation threshold and high conductivity is still an important subject for the future development of high-performance CPCs.

The maximum conductivity of CPC mainly depends on the conductivity of nanofiller. Although graphene and CNT (high-aspect-ratio fillers) have a lot of excellent properties (e.g., corrosion resistance, superior mechanical strength, and low density) beyond ordinary metal fillers, and their conductivities were theoretically predicted to be over 10^6 S/m, the conductivity of commercial carbon nanofillers (e.g., graphene and CNT) is often 2–3 orders of magnitude lower than that of metal filler (e.g., silver) due to some unresolved issues in the synthesis of carbon nanofillers (e.g., defects and purity). Therefore, in the electronic industry, carbon nanofillers cannot replace silver fillers for the fabrication of highly conductive adhesives. Recent years, with the progress in controllable synthesis and element doping of CNTs, the conductivity of CNTs have been mostly improved to match that of metal filler. It is believed that carbon nanofillers will be increasingly used for the high-performance CPCs in near future as long as their quality is improved continuously. As so far, the silver nanowire is reported to be 1D nanofiller available with superior high conductivity. But it is limited to its production yield and is very expensive. Silver nanowire is expected to use for a transparent electrode in touch screen instead of Indium Tin Oxides (ITO) material, which is less sensitive to cost. Mixing other cheap nanofillers with silver nanowire in CPCs could be a quick-fix way to overcome the cost problem. For examples, the addition of silica into CPC

filled with silver nanowire has been proven to reduce not only the cost but also improve the electrical properties of CPCs.

Controlling the conductive network morphology in the polymer matrix is emphasized in this review, determining if the excellent electrical of conductive nanofiller efficiently transfer to the final CPCs. Besides, other functional characteristics of CPCs such as the response of conductivity to the strain and the vapor and the thermoelectric behavior are determined by the design and construction of the specific conductive network. For network morphology control, the dispersion of nanofillers should be considered firstly. Filler surface modification with the chemical method or dispersant was often used to improve the nanofiller dispersion, but it often degrade the electrical connection between nanofillers. Recently, some researchers resolved above issue by using conductive polymers and graphene as a dispersant to disperse conductive nanofillers.

The majority of the resistance in CPC is generated from the tunneling resistance between local conductive networks, so the electrical properties of CPC can be tailored by the conductive network morphology. Various processing methods can confer distinct characteristics to the network. Currently, most of the processing methods are limited to precisely constructing high-quality 3D conducting networks using CNTs and graphene. It is noted that various elaborate 3D hierarchical structures built by tiny nanoscale blocks widely exist in biological organisms (e.g., bone, teeth, and hair) and these super architectures are precisely controlled by self-assembly processes. Thus, inspired by our nature, constructing an ordered 3D conductive network in CPCs by self-assembly could be a good example to prepare high-performance CPCs [113]. Among different network structure, the segregated network is considered as the best way to obtain ultralow percolation threshold, but the CPCs with this structure usually show a very poor mechanical strength due to the poor interface adhesion between polymer matrix and nanofillers. Thus, the mechanical properties of CPCs should be paid more attention, which determines their practical application. Moreover, new conductive network structure and formation mechanism should be further studied by computation simulation combining experimental data, to guide the fabrication of CPCs with better comprehensive properties.

The tunable properties of CPCs based on the control of network structure can meet the various electrical application requirements from strain–senor, liquid and vapor sensors and stretchable conductor, flexible electrodes, and thermoelectric. It is believed that more novel applications will be produced for CPCs. With the development of emerging applications (e.g., wearable electronics, and flexible energy storage device), fabrication of mechanically flexible CPCs will be a new trend. For this application, the CPCs are needed to bear various mechanical deformations (e.g., bending, stretching, and compression) and their mechanical failure issue should be considered. Constructing a stable and recovered conductive network during deformation is very critical to prepare such CPCs. Thus, the dynamic behavior of conductive network and electrical properties in CPCs under loading should be a detailed study in further study.

Acknowledgments We would like to express our sincere thanks to the financial supports from the National Natural Science Foundation of China (51103141 and 51573217), CAEP fund (2011B0302053) and advanced functional polymer coating program.

References

1. Callister WD, Rethwisch DG (2007) Materials science and engineering: an introduction, vol 7. Wiley, New York
2. Chaikin PM, Lubensky TC (2000) Principles of condensed matter physics, vol 1. Cambridge University Press, Cambridge
3. Shirakawa H (2001) The discovery of polyacetylene film: the dawning of an era of conducting polymers (Nobel lecture). Angew Chem Int Ed 40:2574
4. Kaur G, Adhikari R, Cass P, Bown M, Gunatillake P (2015) Electrically conductive polymers and composites for biomedical applications. RSC Advances 5:37553
5. Li C, Bai H, Shi G (2009) Conducting polymer nanomaterials: electrosynthesis and applications. Chem Soc Rev 38:2397
6. Oueiny C, Berlioz S, Perrin F-X (2014) Carbon nanotube–polyaniline composites. Prog Polym Sci 39:707
7. Deng H, Lin L, Ji M, Zhang S, Yang M, Fu Q (2014) Progress on the morphological control of conductive network in conductive polymer composites and the use as electroactive multifunctional materials. Prog Polym Sci 39:627
8. Sengupta R, Bhattacharya M, Bandyopadhyay S, Bhowmick AK (2011) A review on the mechanical and electrical properties of graphite and modified graphite reinforced polymer composites. Prog Polym Sci 36:638
9. Pang H, Xu L, Yan D-X, Li Z-M (2014) Conductive polymer composites with segregated structures. Prog Polym Sci 39:1908
10. Ding C, Zhang H, Li X, Liu T, Xing F (2013) vanadium flow battery for energy storage: prospects and challenges. J Phys Chem Lett 4:1281
11. Li JR, Xu JR, Zhang MQ, Rong MZ (2003) Carbon black/polystyrene composites as candidates for gas sensing materials. Carbon 41:2353
12. Grunlan JC, Mehrabi AR, Bannon MV, Bahr JL (2004) Water-based single-walled-nanotube-filled polymer composite with an exceptionally low percolation threshold. Adv Mater 16:150
13. Du J, Zhao L, Zeng Y, Zhang L, Li F, Liu P, Liu C (2011) Comparison of electrical properties between multi-walled carbon nanotube and graphene nanosheet/high density polyethylene composites with a segregated network structure. Carbon 49:1094
14. Kuilla T, Bhadra S, Yao D, Kim NH, Bose S, Lee JH (2010) Recent advances in graphene based polymer composites. Prog Polym Sci 35:1350
15. Kyrylyuk AV, Hermant MC, Schilling T, Klumperman B, Koning CE, van der Schoot P (2011) Controlling electrical percolation in multicomponent carbon nanotube dispersions. Nat Nano 6:364
16. Munson-McGee SH (1991) Estimation of the critical concentration in an anisotropic percolation network. Phys Rev B 43:3331
17. Schadler LS (2003) Polymer-based and polymer-filled nanocomposites. Wiley, London
18. Dalmas F, Dendievel R, Chazeau L, Cavaillé J-Y, Gauthier C (2006) Carbon nanotube-filled polymer composites. Numerical simulation of electrical conductivity in three-dimensional entangled fibrous networks. Acta Mater 54:2923
19. Bauhofer W, Kovacs JZ (2009) A review and analysis of electrical percolation in carbon nanotube polymer composites. Compos Sci Technol 69:1486
20. Cai D, Song M (2010) Recent advance in functionalized graphene/polymer nanocomposites. J Mater Chem 20:7906

21. Hermant MC, Klumperman B, Kyrylyuk AV, van der Schoot P, Koning CE (2009) Lowering the percolation threshold of single-walled carbon nanotubes using polystyrene/poly(3,4-ethylenedioxythiophene): poly(styrene sulfonate) blends. Soft Matter 5:878
22. Moniruzzaman M, Winey KI (2006) Polymer nanocomposites containing carbon nanotubes. Macromolecules 39:5194
23. Kovacs JZ, Velagala BS, Schulte K, Bauhofer W (2007) Two percolation thresholds in carbon nanotube epoxy composites. Compos Sci Technol 67:922
24. Gangopadhyay R, De A (2000) Conducting polymer nanocomposites: a brief overview. Chem Mater 12:608
25. Xu S, Rezvanian O, Peters K, Zikry M (2013) The viability and limitations of percolation theory in modeling the electrical behavior of carbon nanotube–polymer composites. Nanotechnology 24:155706
26. Stauffer D, Aharony A (1994) Introduction to percolation theory. CRC Press, Boca Raton
27. Kirkpatrick S (1973) Percolation and conduction. Rev Mod Phys 45:574
28. Vionnet-Menot S, Grimaldi C, Maeder T, Strässler S, Ryser P (2005) Tunneling-percolation origin of nonuniversality: theory and experiments. Phys Rev B 71:064201
29. Sheng P, Sichel E, Gittleman J (1978) Fluctuation-induced tunneling conduction in carbon-polyvinylchloride composites. Phys Rev Lett 40:1197
30. Yosida Y, Oguro I (1999) Variable range hopping conduction in bulk samples composed of single-walled carbon nanotubes. J Appl Phys 86:999
31. Benoit J, Corraze B, Chauvet O (2002) Localization, Coulomb interactions and electrical heating in single-wall carbon nanotubes/polymer composites. arXiv preprint cond-mat/0204520
32. Villmow T, Kretzschmar B, Pötschke P (2010) Influence of screw configuration, residence time, and specific mechanical energy in twin-screw extrusion of polycaprolactone/multi-walled carbon nanotube composites. Compos Sci Technol 70:2045
33. Kovacs JZ, Andresen K, Pauls JR, Garcia CP, Schossig M, Schulte K, Bauhofer W (2007) Analyzing the quality of carbon nanotube dispersions in polymers using scanning electron microscopy. Carbon 45:1279
34. Li W, Buschhorn ST, Schulte K, Bauhofer W (2011) The imaging mechanism, imaging depth, and parameters influencing the visibility of carbon nanotubes in a polymer matrix using an SEM. Carbon 49:1955
35. Li W, Bauhofer W (2011) Imaging of CNTs in a polymer matrix at low accelerating voltages using a SEM. Carbon 49:3891
36. Chang L, Friedrich K, Ye L, Toro P (2009) Evaluation and visualization of the percolating networks in multi-wall carbon nanotube/epoxy composites. J Mater Sc 44:4003
37. Loos J, Sourty E, Lu K, de With G, van Bavel S (2009) Imaging polymer systems with high-angle annular dark field scanning transmission electron microscopy (HAADF-STEM). Macromolecules 42:2581
38. Alig I, Skipa T, Engel M, Lellinger D, Pegel S, Pötschke P (2007) Electrical conductivity recovery in carbon nanotube–polymer composites after transient shear. Phys Status Solidi (b) 244:4223
39. Pegel S, Pötschke P, Petzold G, Alig I, Dudkin SM, Lellinger D (2008) Dispersion, agglomeration, and network formation of multiwalled carbon nanotubes in polycarbonate melts. Polymer 49:974
40. Desbief S, Hergué N, Douhéret O, Surin M, Dubois P, Geerts Y, Lazzaroni R, Leclère P (2012) Nanoscale investigation of the electrical properties in semiconductor polymer–carbon nanotube hybrid materials. Nanoscale 4:2705
41. Alekseev A, Chen D, Tkalya EE, Ghislandi MG, Syurik Y, Ageev O, Loos J, de With G (2012) Local organization of graphene network inside graphene/polymer composites. Adv Funct Mater 22:1311
42. Tkalya E, Ghislandi M, Alekseev A, Koning C, Loos J (2010) Latex-based concept for the preparation of graphene-based polymer nanocomposites. J Mater Chem 20:3035

43. Deng H, Skipa T, Bilotti E, Zhang R, Lellinger D, Mezzo L, Fu Q, Alig I, Peijs T (2010) Preparation of high-performance conductive polymer fibers through morphological control of networks formed by nanofillers. Adv Funct Mater 20:1424
44. Wang Z, Ciselli P, Peijs T (2007) The extraordinary reinforcing efficiency of single-walled carbon nanotubes in oriented poly (vinyl alcohol) tapes. Nanotechnology 18:455709
45. Abbasi S, Carreau PJ, Derdouri A (2010) Flow induced orientation of multiwalled carbon nanotubes in polycarbonate nanocomposites: rheology, conductivity and mechanical properties. Polymer 51:922
46. Abdalla M, Dean D, Theodore M, Fielding J, Nyairo E, Price G (2010) Magnetically processed carbon nanotube/epoxy nanocomposites: morphology, thermal, and mechanical properties. Polymer 51:1614
47. Alig I, Skipa T, Lellinger D, Pötschke P (2008) Destruction and formation of a carbon nanotube network in polymer melts: rheology and conductivity spectroscopy. Polymer 49:3524
48. Su C, Xu L, Zhang C, Zhu J (2011) Selective location and conductive network formation of multiwalled carbon nanotubes in polycarbonate/poly (vinylidene fluoride) blends. Compos Sci Technol 71:1016
49. Tang H, Chen X, Luo Y (1996) Electrical and dynamic mechanical behavior of carbon black filled polymer composites. Eur Polym J 32:963
50. Grunlan JC, Gerberich WW, Francis LF (2001) Lowering the percolation threshold of conductive composites using particulate polymer microstructure. J Appl Polym Sci 80:692
51. Kim D, Kim Y, Choi K, Grunlan JC, Yu C (2010) Improved thermoelectric behavior of nanotube-filled polymer composites with poly(3,4-ethylenedioxythiophene) poly(styrene-sulfonate). ACS Nano 4:513
52. Ren P-G, Di Y-Y, Zhang Q, Li L, Pang H, Li Z-M (2012) Composites of ultrahigh-molecular-weight polyethylene with graphene sheets and/or MWCNTs with segregated network structure: preparation and properties. Macromol Mater Eng 297:437
53. Regev O, ElKati PNB, Loos J, Koning CE (2004) Preparation of conductive nanotube–polymer composites using latex technology. Adv Mater 16:248
54. Long G, Tang C, Wong K-w, Man C, Fan M, Lau W-m, Xu T, Wang B (2013) Resolving the dilemma of gaining conductivity but losing environmental friendliness in producing polystyrene/graphene composites via optimizing the matrix-filler structure. Green Chem 15:821
55. Mierczynska A, Mayne-L'Hermite M, Boiteux G, Jeszka JK (2007) Electrical and mechanical properties of carbon nanotube/ultrahigh-molecular-weight polyethylene composites prepared by a filler prelocalization method. J Appl Polym Sci 105:158
56. Ajayan PM, Tour JM (2007) Materials science: nanotube composites. Nature 447:1066
57. Ausman KD, Piner R, Lourie O, Ruoff RS, Korobov M (2000) Organic solvent dispersions of single-walled carbon nanotubes: toward solutions of pristine nanotubes. J Phys Chem B 104:8911
58. Balasubramanian K, Burghard M (2005) Chemically functionalized carbon nanotubes. Small 1:180
59. Grossiord N, Loos J, Regev O, Koning CE (2006) Toolbox for dispersing carbon nanotubes into polymers to get conductive nanocomposites. Chem Mater 18:1089
60. Hermann A, Chaudhuri T, Spagnol P (2005) Bipolar plates for PEM fuel cells: a review. Int J Hydrog Energy 30:1297
61. Wu M, Shaw LL (2005) A novel concept of carbon-filled polymer blends for applications in PEM fuel cell bipolar plates. Int J Hydrog Energy 30:373
62. Kim YS, Wright JB, Grunlan JC (2008) Influence of polymer modulus on the percolation threshold of latex-based composites. Polymer 49:570
63. Hermant MC, Smeets N, van Hal RC, Meuldijk J, Heuts H, Klumperman B, Herk AMV, Koning CE (2009) Influence of the molecular weight distribution on the percolation threshold of carbon nanotube–polystyrene composites. e-Polymers 9:248

64. Feng J, Chan C-M (2000) Double positive temperature coefficient effects of carbon black-filled polymer blends containing two semicrystalline polymers. Polymer 41:4559
65. Jurewicz I, Worajittiphon P, King AA, Sellin PJ, Keddie JL, Dalton AB (2011) Locking carbon nanotubes in confined lattice geometries: a route to low percolation in conducting composites. J Phys Chem B 115:6395
66. Kumar S, Doshi H, Srinivasarao M, Park JO, Schiraldi DA (2002) Fibers from polypropylene/nano carbon fiber composites. Polymer 43:1701
67. Haggenmueller R, Gommans H, Rinzler A, Fischer JE, Winey K (2000) Aligned single-wall carbon nanotubes in composites by melt processing methods. Chem Phys Lett 330:219
68. Li S-N, Li B, Li Z-M, Fu Q, Shen K-Z (2006) Morphological manipulation of carbon nanotube/polycarbonate/polyethylene composites by dynamic injection packing molding. Polymer 47:4497
69. Andrews R, Jacques D, Minot M, Rantell T (2002) Fabrication of carbon multiwall nanotube/polymer composites by shear mixing. Macromol Mater Eng 287:395
70. Spitalsky Z, Tasis D, Papagelis K, Galiotis C (2010) Carbon nanotube–polymer composites: chemistry, processing, mechanical and electrical properties. Prog Polym Sci 35:357
71. Deng H, Zhang R, Bilotti E, Loos J, Peijs T (2009) Conductive polymer tape containing highly oriented carbon nanofillers. J Appl Polym Sci 113:742
72. Deng H, Bilotti E, Zhang R, Peijs T (2010) Effective reinforcement of carbon nanotubes in polypropylene matrices. J Appl Polym Sci 118:30
73. Gorrasi G, Bredeau S, Di Candia C, Patimo G, De Pasquale S, Dubois P (2011) Electroconductive polyamide 6/MWNT nanocomposites: effect of nanotube surface-coating by in situ catalyzed polymerization. Macromol Mater Eng 296:408
74. Ezat GS, Kelly AL, Mitchell SC, Youseffi M, Coates PD (2012) Effect of maleic anhydride grafted polypropylene compatibilizer on the morphology and properties of polypropylene/multiwalled carbon nanotube composite. Polym Compos 33:1376
75. Cheng HKF, Pan Y, Sahoo NG, Chong K, Li L, Hwa Chan S, Zhao J (2012) Improvement in properties of multiwalled carbon nanotube/polypropylene nanocomposites through homogeneous dispersion with the aid of surfactants. J Appl Polym Sci 124:1117
76. Khare RA, Bhattacharyya AR, Kulkarni AR (2011) Melt-mixed polypropylene/acrylonitrile-butadiene-styrene blends with multiwall carbon nanotubes: effect of compatibilizer and modifier on morphology and electrical conductivity. J Appl Polym Sci 120:2663
77. Tang C, Zhou T, Yang J, Zhang Q, Chen F, Fu Q, Yang L (2011) Wet-grinding assisted ultrasonic dispersion of pristine multi-walled carbon nanotubes (MWCNTs) in chitosan solution. Colloids Surf B 86:189
78. Islam MF, Rojas E, Bergey DM, Johnson AT, Yodh AG (2003) High weight fraction surfactant solubilization of single-wall carbon nanotubes in water. Nano Lett 3:269
79. Regev O, ElKati PN, Loos J, Koning CE (2004) Preparation of conductive nanotube-polymer composites using latex technology. Adv Mater 16:248
80. Zhang W, Suhr J, Koratkar NA (2006) Observation of high buckling stability in carbon nanotube polymer composites. Adv Mater 18:452
81. Coleman JN, Khan U, Gun'ko YK (2006) Mechanical reinforcement of polymers using carbon nanotubes. Adv Mater 18:689
82. Jia Z, Wang Z, Xu C, Liang J, Wei B, Wu D, Zhu S (1999) Study on poly (methyl methacrylate)/carbon nanotube composites. Mater Sci Eng, A 271:395
83. Gao J, Itkis ME, Yu A, Bekyarova E, Zhao B, Haddon RC (2005) Continuous spinning of a single-walled carbon nanotube-nylon composite fiber. J Am Chem Soc 127:3847
84. Martin C, Sandler J, Windle A, Schwarz M-K, Bauhofer W, Schulte K, Shaffer M (2005) Electric field-induced aligned multi-wall carbon nanotube networks in epoxy composites. Polymer 46:877
85. Liu K, Chen L, Chen Y, Wu J, Zhang W, Chen F, Fu Q (2011) Preparation of polyester/reduced graphene oxide composites via in situ melt polycondensation and simultaneous thermo-reduction of graphene oxide. J Mater Chem 21:8612

86. Baudouin A-C, Devaux J, Bailly C (2010) Localization of carbon nanotubes at the interface in blends of polyamide and ethylene–acrylate copolymer. Polymer 51:1341
87. Baudouin A-C, Auhl D, Tao F, Devaux J, Bailly C (2011) Polymer blend emulsion stabilization using carbon nanotubes interfacial confinement. Polymer 52:149
88. Baudouin A-C, Bailly C, Devaux J (2010) Interface localization of carbon nanotubes in blends of two copolymers. Polym Degrad Stab 95:389
89. Gültner M, Göldel A, Pötschke P (2011) Tuning the localization of functionalized MWCNTs in SAN/PC blends by a reactive component. Compos Sci Technol 72:41
90. Göldel A, Kasaliwal G, Pötschke P (2009) Selective localization and migration of multiwalled carbon nanotubes in blends of polycarbonate and poly (styrene-acrylonitrile). Macromol Rapid Commun 30:423
91. Zhang L, Wan C, Zhang Y (2009) Morphology and electrical properties of polyamide 6/polypropylene/multi-walled carbon nanotubes composites. Compos Sci Technol 69:2212
92. Li C, Zhao Q, Deng H, Chen C, Wang K, Zhang Q, Chen F, Fu Q (2011) Preparation, structure and properties of thermoplastic olefin nanocomposites containing functionalized carbon nanotubes. Polym Int 60:1629
93. Dai K, Xu X-B, Li Z-M (2007) Electrically conductive carbon black (CB) filled in situ microfibrillar poly (ethylene terephthalate)(PET)/polyethylene (PE) composite with a selective CB distribution. Polymer 48:849
94. Göldel A, Marmur A, Kasaliwal GR, Pötschke P, Heinrich G (2011) Shape-dependent localization of carbon nanotubes and carbon black in an immiscible polymer blend during melt mixing. Macromolecules 44:6094
95. Chen J, Shi Y-y, Yang J-h, Zhang N, Huang T, Chen C, Wang Y, Zhou Z-w (2012) A simple strategy to achieve very low percolation threshold via the selective distribution of carbon nanotubes at the interface of polymer blends. J Mater Chem 22:22398
96. Alig I, Pötschke P, Lellinger D, Skipa T, Pegel S, Kasaliwal GR, Villmow T (2012) Establishment, morphology and properties of carbon nanotube networks in polymer melts. Polymer 53:4
97. Jiang F, Zhang L, Jiang Y, Lu Y, Wang W (2012) Effect of annealing treatment on the structure and properties of polyurethane/multiwalled carbon nanotube nanocomposites. J Appl Polym Sci 126:845
98. Pan Y, Cheng HKF, Li L, Chan SH, Zhao J, Juay YK (2010) Annealing induced electrical conductivity jump of multi-walled carbon nanotube/polypropylene composites and influence of molecular weight of polypropylene. J Polym Sci, Part B: Polym Phys 48:2238
99. Zhang Y-C, Pang H, Dai K, Huang Y-F, Ren P-G, Chen C, Li Z-M (2012) Conductive network formation during annealing of an oriented polyethylene-based composite. J Mater Sci 47:3713
100. Cao Q, Song Y, Tan Y, Zheng Q (2009) Thermal-induced percolation in high-density polyethylene/carbon black composites. Polymer 50:6350
101. Zhang C, Zhu J, Ouyang M, Ma C-a (2009) Electric field controlled formation and dissociation of multiwalled carbon nanotube conductive pathways in a polymer melt. Appl Phys Lett 94:111915
102. Cao Q, Song Y, Tan Y, Zheng Q (2010) Conductive and viscoelastic behaviors of carbon black filled polystyrene during annealing. Carbon 48:4268
103. Zhang C, Wang L, Wang J, Ma C-a (2008) Self-assembly and conductive network formation of vapor-grown carbon fiber in a poly (vinylidene fluoride) melt. Carbon 46:2053
104. Bilotti E, Zhang R, Deng H, Baxendale M, Peijs T (2010) Fabrication and property prediction of conductive and strain sensing TPU/CNT nanocomposite fibres. J Mater Chem 20:9449
105. Eken A, Tozzi E, Klingenberg D, Bauhofer W (2011) A simulation study on the effects of shear flow on the microstructure and electrical properties of carbon nanotube/polymer composites. Polymer 52:5178

106. Etika KC, Liu L, Hess LA, Grunlan JC (2009) The influence of synergistic stabilization of carbon black and clay on the electrical and mechanical properties of epoxy composites. Carbon 47:3128
107. Hermant M-C, van der Schoot P, Klumperman B, Koning CE (2010) Probing the cooperative nature of the conductive components in polystyrene/poly (3, 4-ethylenedioxythiophene): poly (styrene sulfonate): single-walled carbon nanotube composites. ACS Nano 4:2242
108. Liu L, Grunlan JC (2007) Clay assisted dispersion of carbon nanotubes in conductive epoxy nanocomposites. Adv Funct Mater 17:2343
109. Sun Y, Bao H-D, Guo Z-X, Yu J (2008) Modeling of the electrical percolation of mixed carbon fillers in polymer-based composites. Macromolecules 42:459
110. Yu K, Zhang Z, Liu Y, Leng J (2011) Carbon nanotube chains in a shape memory polymer/carbon black composite: to significantly reduce the electrical resistivity. Appl Phys Lett 98:074102
111. Otten RH, van der Schoot P (2009) Continuum percolation of polydisperse nanofillers. Phys Rev Lett 103:225704
112. Sumfleth J, Adroher XC, Schulte K (2009) Synergistic effects in network formation and electrical properties of hybrid epoxy nanocomposites containing multi-wall carbon nanotubes and carbon black. J Mater Sci 44:3241
113. Tang C, Long G, Hu X, K-w Wong, W-m Lau, Fan M, Mei J, Xu T, Wang B, Hui D (2014) Conductive polymer nanocomposites with hierarchical multi-scale structures via self-assembly of carbon-nanotubes on graphene on polymer-microspheres. Nanoscale 6:7877
114. Jiang H, Moon K-s, Li Y, Wong CP (2006) Surface functionalized silver nanoparticles for ultrahigh conductive polymer composites. Chem Mater 18:2969
115. Bilotti E, Zhang H, Deng H, Zhang R, Fu Q, Peijs T (2013) Controlling the dynamic percolation of carbon nanotube based conductive polymer composites by addition of secondary nanofillers: the effect on electrical conductivity and tuneable sensing behaviour. Compos Sci Technol 74:85
116. Nam S, Cho HW, Lim S, Kim D, Kim H, Sung BJ (2013) Enhancement of electrical and thermomechanical properties of silver nanowire composites by the introduction of nonconductive nanoparticles: experiment and simulation. ACS Nano 7:851
117. Pang H, Chen C, Zhang Y-C, Ren P-G, Yan D-X, Li Z-M (2011) The effect of electric field, annealing temperature and filler loading on the percolation threshold of polystyrene containing carbon nanotubes and graphene nanosheets. Carbon 49:1980
118. Ma C, Zhang W, Zhu Y, Ji L, Zhang R, Koratkar N, Liang J (2008) Alignment and dispersion of functionalized carbon nanotubes in polymer composites induced by an electric field. Carbon 46:706
119. Knaapila M, Rømoen OT, Svåsand E, Pinheiro JP, Martinsen ØG, Buchanan M, Skjeltorp AT, Helgesen G (2011) Conductivity enhancement in carbon nanocone adhesive by electric field induced formation of aligned assemblies. ACS Appl Mater Interfaces 3:378
120. Chen Z, Ren W, Gao L, Liu B, Pei S, Cheng H-M (2011) Three-dimensional flexible and conductive interconnected graphene networks grown by chemical vapour deposition. Nat Mater 10:424
121. Chen M, Tao T, Zhang L, Gao W, Li C (2013) Highly conductive and stretchable polymer composites based on graphene/MWCNT network. Chem Commun 49:1612
122. Zhang YC, Dai K, Pang H, Luo QJ, Li ZM, Zhang WQ (2012) Temperature and time dependence of electrical resistivity in an anisotropically conductive polymer composite with in situ conductive microfibrils. J Appl Polym Sci 124:1808
123. Rybak A, Boiteux G, Melis F, Seytre G (2010) Conductive polymer composites based on metallic nanofiller as smart materials for current limiting devices. Compos Sci Technol 70:410
124. Bautista-Quijano J, Aviles F, Aguilar J, Tapia A (2010) Strain sensing capabilities of a piezoresistive MWCNT-polysulfone film. Sens Actuators, A 159:135

125. Dang Z-M, Jiang M-J, Xie D, Yao S-H, Zhang L-Q, Bai J (2008) Supersensitive linear piezoresistive property in carbon nanotubes/silicone rubber nanocomposites. J Appl Phys 104:024114
126. Zhang R, Baxendale M, Peijs T (2007) Universal resistivity–strain dependence of carbon nanotube/polymer composites. Phys Rev B 76:195433
127. Kollosche M, Stoyanov H, Laflamme S, Kofod G (2011) Strongly enhanced sensitivity in elastic capacitive strain sensors. J Mater Chem 21:8292
128. Castro M, Kumar B, Feller J-F, Haddi Z, Amari A, Bouchikhi B (2011) Novel e-nose for the discrimination of volatile organic biomarkers with an array of carbon nanotubes (CNT) conductive polymer nanocomposites (CPC) sensors. Sens and Actuators B: Chem 159:213
129. Cheng J, Wang L, Huo J, Yu H (2011) A novel polycaprolactone-grafted-carbon black nanocomposite-based sensor for detecting solvent vapors. J Appl Polym Sci 121:3277
130. Graham A, Laughlin P, Bloor D (2013) Metal–polymer composite sensors for volatile organic compounds: Part 2. Stand alone chemi-resistors. Sens Actuators B: Chem 177:507
131. Dong XM, Luo Y, Xie LN, Fu RW, Zhang MQ (2008) Conductive carbon black-filled polymethacrylate composites as gas sensing materials: effect of glass transition temperature. Thin Solid Films 516:7886
132. Xu H-P, Dang Z-M, Shi D-H, Bai J-B (2008) Remarkable selective localization of modified nanoscaled carbon black and positive temperature coefficient effect in binary-polymer matrix composites. J Mater Chem 18:2685
133. Zha J-W, Li W-K, Liao R-J, Bai J, Dang Z-M (2013) High performance hybrid carbon fillers/binary–polymer nanocomposites with remarkably enhanced positive temperature coefficient effect of resistance. J Mater Chem A 1:843
134. Xiang ZD, Chen T, Li ZM, Bian XC (2009) Negative temperature coefficient of resistivity in lightweight conductive carbon nanotube/polymer composites. Macromol Mater Eng 294:91
135. Kar P, Khatua BB (2011) Highly reversible and repeatable PTCR characteristics of PMMA/Ag-coated glass bead composites based on CTE mismatch phenomena. Polym Eng Sci 51:1780
136. Zhang C, Ma C-A, Wang P, Sumita M (2005) Temperature dependence of electrical resistivity for carbon black filled ultra-high molecular weight polyethylene composites prepared by hot compaction. Carbon 43:2544
137. Xi Y, Yamanaka A, Bin Y, Matsuo M (2007) Electrical properties of segregated ultrahigh molecular weight polyethylene/multiwalled carbon nanotube composites. J Appl Polym Sci 105:2868
138. Lu C, Hu X-n, He Y-x, Huang X, Liu J-c, Zhang Y-q (2012) Triple percolation behavior and positive temperature coefficient effect of conductive polymer composites with especial interface morphology. Polym Bull 68:2071
139. Gao J-F, Li Z-M, Peng S, Yan D-X (2009) Temperature-resistivity behaviour of CNTs/UHMWPE composites with a two-dimensional conductive network. Polym-Plast Technol Eng 48:478
140. Pang H, Zhang Y-C, Chen T, Zeng B-Q, Li Z-M (2010) Tunable positive temperature coefficient of resistivity in an electrically conducting polymer/graphene composite. Appl Phys Lett 96:251907
141. Sachdev V, Mehra N, Mehra R (2004) Study of pre-localized graphite/polyvinyl chloride electroconductive composites for sensors. Phys Status Solidi (a) 201:2089
142. Yamada T, Hayamizu Y, Yamamoto Y, Yomogida Y, Izadi-Najafabadi A, Futaba DN, Hata K (2011) A stretchable carbon nanotube strain sensor for human-motion detection. Nat Nanotechnol 6:296
143. Knite M, Ozols K, Zavickis J, Tupureina V, Klemenoks I, Orlovs R (2009) Elastomer–carbon nanotube composites as prospective multifunctional sensing materials. J Nanosci Nanotechnol 9:3587

144. Hu N, Karube Y, Arai M, Watanabe T, Yan C, Li Y, Liu Y, Fukunaga H (2010) Investigation on sensitivity of a polymer/carbon nanotube composite strain sensor. Carbon 48:680
145. Murugaraj P, Mainwaring D, Khelil NA, Peng JL, Siegele R, Sawant P (2010) The improved electromechanical sensitivity of polymer thin films containing carbon clusters produced in situ by irradiation with metal ions. Carbon 48:4230
146. Lin L, Deng H, Gao X, Zhang S, Bilotti E, Peijs T, Fu Q (2013) Modified resistivity–strain behavior through the incorporation of metallic particles in conductive polymer composite fibers containing carbon nanotubes. Polym Int 62:134
147. Kumar B, Park Y, Castro M, Grunlan J, Feller J-F (2012) Fine control of carbon nanotubes–polyelectrolyte sensors sensitivity by electrostatic layer by layer assembly (eLbL) for the detection of volatile organic compounds (VOC). Talanta 88:396
148. Pötschke P, Kobashi K, Villmow T, Andres T, Paiva MC, Covas JA (2011) Liquid sensing properties of melt processed polypropylene/poly (ε-caprolactone) blends containing multiwalled carbon nanotubes. Compos Sci Technol 71:1451
149. Shang S, Zeng W, Tao X-M (2012) Investigation on the electrical response behaviors of multiwalled carbon nanotube/polyurethane composite in organic solvent vapors. Sens Actuators B: Chem 166:330
150. Villmow T, Pegel S, John A, Rentenberger R, Pötschke P (2011) Liquid sensing: smart polymer/CNT composites. Mater Today 14:340
151. Castro M, Lu J, Bruzaud S, Kumar B, Feller J-F (2009) Carbon nanotubes/poly (ε-caprolactone) composite vapour sensors. Carbon 47:1930
152. Kumar B, Castro M, Feller J-F (2012) Controlled conductive junction gap for chitosan–carbon nanotube quantum resistive vapour sensors. J Mater Chem 22:10656
153. Pang H, Bao Y, Xu L, Yan D-X, Zhang W-Q, Wang J-H, Li Z-M (2013) Double-segregated carbon nanotube–polymer conductive composites as candidates for liquid sensing materials. J Mater Chem A 1:4177
154. Lu J, Feller J-F, Kumar B, Castro M, Kim Y, Park Y, Grunlan J (2011) Chemo-sensitivity of latex-based films containing segregated networks of carbon nanotubes. Sens Actuators B: Chem 155:28
155. Dai K, Zhao S, Zhai W, Zheng G, Liu C, Chen J, Shen C (2013) Tuning of liquid sensing performance of conductive carbon black (CB)/polypropylene (PP) composite utilizing a segregated structure. Compos A Appl Sci Manuf 55:11
156. Pang H, Piao Y-Y, Xu L, Bao Y, Cui C-H, Fu Q, Li Z-M (2013) Tunable liquid sensing performance of conducting carbon nanotube–polyethylene composites with a porous segregated structure. RSC Adv 3:19802
157. Nie T, Zhang O, Lu L, Xu J, Wen Y, Qiu X (2013) Facile synthesis of poly (3, 4-ethylenedioxythiophene)/graphene nanocomposite and its application for determination of nitrite. Int J Electrochem Sci 8:8708
158. Wang Q, Yun Y (2012) A nanomaterial composed of cobalt nanoparticles, poly (3, 4-ethylenedioxythiophene) and graphene with high electrocatalytic activity for nitrite oxidation. Microchim Acta 177:411
159. Ye D, Luo L, Ding Y, Chen Q, Liu X (2011) A novel nitrite sensor based on graphene/polypyrrole/chitosan nanocomposite modified glassy carbon electrode. Analyst 136:4563
160. Liu S, Tian J, Wang L, Luo Y, Sun X (2011) Production of stable aqueous dispersion of poly (3, 4-ethylenedioxythiophene) nanorods using graphene oxide as a stabilizing agent and their application for nitrite detection. Analyst 136:4898
161. Rogers JA, Someya T, Huang Y (2010) Materials and mechanics for stretchable electronics. Science 327:1603
162. Sekitani T, Noguchi Y, Hata K, Fukushima T, Aida T, Someya T (2008) A rubberlike stretchable active matrix using elastic conductors. Science 321:1468
163. Zhu Y, Xu F (2012) Buckling of aligned carbon nanotubes as stretchable conductors: a new manufacturing strategy. Adv Mater 24:1073

164. Sokolov AN, Tee BC, Bettinger CJ, Tok JB-H, Bao Z (2011) Chemical and engineering approaches to enable organic field-effect transistors for electronic skin applications. Acc Chem Res 45:361
165. Tee BC, Wang C, Allen R, Bao Z (2012) An electrically and mechanically self-healing composite with pressure-and flexion-sensitive properties for electronic skin applications. Nat Nanotechnol 7:825
166. Ahn J-H, Je JH (2012) Stretchable electronics: materials, architectures and integrations. J Phys D Appl Phys 45:103001
167. Liang J, Li L, Niu X, Yu Z, Pei Q (2013) Elastomeric polymer light-emitting devices and displays. Nat Photonics 7:817
168. Kujawski M, Pearse J, Smela E (2010) Elastomers filled with exfoliated graphite as compliant electrodes. Carbon 48:2409
169. Shang S, Zeng W, X-m Tao (2011) High stretchable MWNTs/polyurethane conductive nanocomposites. J Mater Chem 21:7274
170. Kim KH, Vural M, Islam MF (2011) Single-walled carbon nanotube aerogel-based elastic conductors. Adv Mater 23:2865
171. Hewitt CA, Kaiser AB, Roth S, Craps M, Czerw R, Carroll DL (2012) Multilayered carbon nanotube/polymer composite based thermoelectric fabrics. Nano Lett 12:1307
172. Du Y, Shen SZ, Cai K, Casey PS (2012) Research progress on polymer–inorganic thermoelectric nanocomposite materials. Prog Polym Sci 37:820
173. Yadav GG, Susoreny JA, Zhang G, Yang H, Wu Y (2011) Nanostructure-based thermoelectric conversion: an insight into the feasibility and sustainability for large-scale deployment. Nanoscale 3:3555
174. Tritt TM (2011) Thermoelectric phenomena, materials, and applications. Annu Rev Mater Res 41:433
175. Pang H, Piao Y-Y, Tan Y-Q, Jiang G-Y, Wang J-H, Li Z-M (2013) Thermoelectric behaviour of segregated conductive polymer composites with hybrid fillers of carbon nanotube and bismuth telluride. Mater Lett 107:150
176. Yu C, Kim YS, Kim D, Grunlan JC (2008) Thermoelectric behavior of segregated-network polymer nanocomposites. Nano Lett 8:4428
177. Yu C, Choi K, Yin L, Grunlan JC (2011) Light-weight flexible carbon nanotube based organic composites with large thermoelectric power factors. ACS Nano 5:7885
178. Kim D, Kim Y, Choi K, Grunlan JC, Yu C (2009) Improved thermoelectric behavior of nanotube-filled polymer composites with poly (3, 4-ethylenedioxythiophene) poly (styrenesulfonate). ACS Nano 4:513
179. Srivastava S, Schaefer JL, Yang Z, Tu Z, Archer LA (2014) 25th anniversary article: polymer-particle composites: phase stability and applications in electrochemical energy storage. Adv Mater 26:201
180. Nyholm L, Nyström G, Mihranyan A, Strømme M (2011) Toward flexible polymer and paper-based energy storage devices. Adv Mater 23:3751
181. Peng C, Jin J, Chen GZ (2007) A comparative study on electrochemical co-deposition and capacitance of composite films of conducting polymers and carbon nanotubes. Electrochim Acta 53:525
182. Frackowiak E, Jurewicz K, Delpeux S, Bertagna V, Bonnamy S, Béguin F (2002) Synergy of components in supercapacitors based on nanotube/polypyrrole composites. Mol Cryst Liq Cryst 387:73
183. An KH, Jeon KK, Heo JK, Lim SC, Bae DJ, Lee YH (2002) High-capacitance supercapacitor using a nanocomposite electrode of single-walled carbon nanotube and polypyrrole. J Electrochem Soc 149:A1058
184. Cho S, Kim M, Jang J (2015) Screen-printable and flexible RuO2 nanoparticle-decorated PEDOT:PSS/graphene nanocomposite with enhanced electrical and electrochemical performances for high-capacity supercapacitor. ACS Appl Mater Interfaces 7:10213
185. Lei W, Si W, Xu Y, Gu Z, Hao Q (2014) Conducting polymer composites with graphene for use in chemical sensors and biosensors. Microchim Acta 181:707

186. Vaitkuviene A, Kaseta V, Voronovic J, Ramanauskaite G, Biziuleviciene G, Ramanaviciene A, Ramanavicius A (2013) Evaluation of cytotoxicity of polypyrrole nanoparticles synthesized by oxidative polymerization. J Hazard Mater 250:167
187. Gaharwar AK, Peppas NA, Khademhosseini A (2014) Nanocomposite hydrogels for biomedical applications. Biotechnol Bioeng 111:441
188. Das TK, Prusty S (2012) Review on conducting polymers and their applications. Polym-Plast Technol Eng 51:1487
189. Shin SR, Jung SM, Zalabany M, Kim K, Zorlutuna P, Sb Kim, Nikkhah M, Khabiry M, Azize M, Kong J (2013) Carbon-nanotube-embedded hydrogel sheets for engineering cardiac constructs and bioactuators. ACS Nano 7:2369
190. Feng XM, Li RM, Ma YW, Chen RF, Shi NE, Fan QL, Huang W (2011) One-step electrochemical synthesis of graphene/polyaniline composite film and its applications. Adv Funct Mater 21:2989
191. Qiu JD, Shi L, Liang RP, Wang GC, Xia XH (2012) Controllable deposition of a platinum nanoparticle ensemble on a polyaniline/graphene hybrid as a novel electrode material for electrochemical sensing. Chem A Eur J 18:7950

Magnetic Nanoparticles-Based Conducting Polymer Nanocomposites

A. Muñoz-Bonilla, J. Sánchez-Marcos and P. Herrasti

Abstract This chapter reviews the state of art of nanocomposites based on conducting polymers and magnetic nanoparticles. The preparation of hybrid nanocomposites with both magnetic and electrical properties has emerging as attractive alternative in a wide number of applications especially as microwave absorbing material and electromagnetic shielding. An overview of the different synthetic routes of the hybrid nanocomposites is presented, which outlines the most development techniques to prepare homogenous matrix, core–shell nanoparticles, and thin films. This chapter also covers the discussion of both the magnetic and electrical properties of the nanocomposites that significantly vary from the individual components. Finally varies of the most relevant applications of the magnetic nanoparticles-based conducting polymer nanocomposites are highlighted.

Keywords Magnetic nanoparticles · Conducting polymers · Nanocomposites · Magnetic properties · Electrical properties

1 Introduction

Conducting polymers were first produced in the mid-1970s as a novel generation of organic materials that have both electrical and optical properties similar to those of metals and inorganic semiconductors, combined with attractive properties associated with conventional polymers, such as ease of synthesis and flexibility in processing.

Magnetic nanoparticles (NPs), in particular iron oxide magnetic nanoparticles exhibit remarkable magnetic properties particularly in radiofrequency region, physical flexibility, high electrical resistivity, mechanical hardness and chemical stability. They have found widespread applications in many fields covering

A. Muñoz-Bonilla · J. Sánchez-Marcos · P. Herrasti (✉)
Departamento de Química Física Aplicada, Facultad de Ciencias,
Universidad Autónoma de Madrid, UAM, C/Francisco Tomás y Valiente 7,
28049 Cantoblanco, Madrid, Spain
e-mail: pilar.herrasti@uam.es

V. Kumar et al. (eds.), *Conducting Polymer Hybrids*,
Springer Series on Polymer and Composite Materials,
DOI 10.1007/978-3-319-46458-9_2

catalysis, data storage, environmental remediation separation, purification, and biomedical uses [1–4]. For many of these applications, the synthesis of uniformly sized nanoparticles is of key importance, because their electrical, optical, and magnetic properties depend strongly on their dimensions.

In recent years the preparation of hybrid nanocomposites with both magnetic and electrical properties has received a great attention in industrial and academic fields. For instance, nanocomposites based on conducting polymers and magnetic nanoparticles are one of the most widely studied materials for microwave absorbing and electromagnetic shielding. The extensive development of electronic devices and the intensive usage of electromagnetic waves have created several problems of electromagnetic interferences (EMI) and the demand of adequate shielding is continuously growing. Besides, magnetoelectric polymeric nanocomposites find applications in many other fields such as in solar cells, sensors, memory devices, catalysis, among others. In general, the hybrid nanocomposites can be prepared, depending on their final use, by incorporating the magnetic nanoparticles in a conducting polymer matrix or by encapsulation of the nanoparticles leading to core–shell systems. Besides, the final properties of the hybrid materials depend not only on the properties of the individual components thus on the composition but also on the dispersibility of the nanoparticles, homogeneity of the nanocomposite and on the interfacial interactions between the components. Indeed, many attempts and synthetic strategies have been carried out with multiple nanocomposite systems to achieve highly uniform materials in order to attain the desirable electric and magnetic properties. Table 1 summarizes some of the most relevant magnetic nanoparticles-based conducting polymer nanocomposites reported in literature, with their respective properties and applications.

Table 1 Some of the most relevant examples of magnetic nanoparticles-based conducting polymer nanocomposites

Polymer	Magnetic Nps	Properties/applications	Refs
PPy	$CoZnFe_2O_3$	Ferrimagnetic behavior	[5, 6]
PPy	Fe_2O_3	Ferromagnetic/superparamagnetic	[7–14]
PPy	Fe_3O_4	Superparamagnetic/conductivity decreases with the NPs content	[15–18]
PPy	Fe_3O_4	Superparamagnetic/conductivity increases with the NPs content	[19]
PPy	Co	Induced resistive switching and magnetism (memory device application)	[20]
PANI	Fe_3O_4	Ferromagnetic/conductivity decreases with NPs content	[21–26]
PANI	Fe_3O_4	Superparamagnetic/conductivity decreases with the NPs content	[27–31]

(continued)

Table 1 (continued)

Polymer	Magnetic Nps	Properties/applications	Refs
PANI	$CoFe_2O_4$	Ferromagnetic/magnetization increases and coercivity decreases with NPs content	[32, 33]
PANI	$ZnFe_2O_4$	The conductivity decreases with the NPs content higher magnetoresistance	[34]
PANI	$NiFe_2O_4$	Ferromagnetic/conductivity decreases with NPs content	[35]
PANI	$BaFe_{12}O_{19}$ $Ba_xLaFe_{12-x}O_{19}$	Ferromagnetic/conductivity decreases with the NPs content	[36, 37]
PANI PAOABSA	γFe_2O_3	Superparamagnetic/conductivity decreases with the Nps content	[38–40]
PANI	Fe_2O_3 NiO	Superparamagnetic/conductivity decreases with the Nps content	[41]
PANI	$NiCrFe_xO_4$	Ferromagnetic/magnetization decreases with the NPs content	[42]
POEA	γFe_2O_3	Conductivity does not change with the content of NPs	[43]
SPAN	γFe_2O_3	Conductivity increases in the nanocomposite	[44]
PEDOT	Fe_3O_4 $CoFe_2O_4$ $NiFe_2O_4$	Superparamagnetic	[45–48]
PEDOT	Co_3O_4/GO	Electromagnetic absorption properties	[49]
PAN	Ni, Co, Ni–Co	Superparamagnetic/microwave absorption application	[50]

PPy polypyrrole, *PANI* polyaniline, *PAOABSA* poly(aniline-*co*-aminobenzenesulfonic acid), *POEA* poly(*o*-ethoxyaniline), *SPAN* sulfonated polyaniline, *PEDOT* poly(3,4-ethylenedioxythiophene), *PAN* polyacrylonitrile

As shown, a large number of investigations are focused on typical conducting polymers such as polypyrrole, polyaniline, polythiophene and their derivatives due to its good electrical properties and ease of synthesis. Relative to the magnetic component, iron oxide nanoparticles, i.e., magnetite and maghemite, are by far, the most preferred nanomaterials as a consequence of their strong magnetic and semiconducting properties together with their low cost. In addition, these ferromagnetic iron oxide nanoparticles can become superparamagnetic when they behave as single magnetic domains typically with small diameter. In general, the magnetic properties of the nanocomposites differ from the pure magnetic nanoparticle as a result of the nonmagnetic polymeric component, decreasing the magnetization saturation values and also affecting the anisotropy and the coercivity values [51, 52]. Regarding the electrical properties of the nanocomposites, the conductivity usually decreases with the content of magnetic nanoparticles due to the reduction of the electronic density of the polymer chains as a result of their interactions with the metal cations of the nanoparticles, among other factors. As commented the incorporation of magnetic

nanoparticles into a conducting polymer matrix introduces magnetic character, modifies the electrical behavior but also can vary other properties such as the processability, mechanical, and thermal properties, all of them highly important for the applicability of the materials. Hence, several aspects have to be taken into account and controlled to tune the desirable magneto-electrical behavior of the nanocomposites and suitable properties depending on their final application.

This chapter gives a brief overview of the hybrid magnetic nanoparticles-based conducting polymer nanocomposites and of their recent advances in the last decade. Also, it pretends to provide a complete background in the area, given a wide and insightful understanding of these kinds of materials, which have received a great attention in the last years due to the very promising potential in several applications. This chapter includes several sections that cover general topics, preparation methods, properties, and applications. The synthetic strategies employed to incorporate nanoparticles in the polymer matrix and to obtain core–shell materials and films will be addressed in detail. The magnetic and electrical properties of the hybrid nanocomposites will be presented second and compared with the pure components. The final section will be focused on the most important practical applications of the conductive and magnetic nanocomposites to end with the conclusion remarks and possible future research directions.

2 Synthetic Strategies

As described along the different chapters, most of the conducting polymers are typically synthesized by oxidative polymerization method induced chemically or electrochemically. Chemical oxidation (i.e., oxidation of aniline or pyrrole by iron salts [53] or peroxydisulfate [52]) is preferred when large amount of polymer is needed while the electrochemical oxidation [54] is more suitable to fabricate polymer films for electronic devices.

The polymerisation mechanism of conducting polymers is complex and number of explanations have been suggested by different researchers [54, 55].

Next, it is briefly described the accepted polymerisation mechanism of polypyrrole, probably the most used conducting polymers, in the electrochemical synthesis, although this mechanism can be extended to the chemical polymerisation.

Typically the monomer is oxidized losing an electron and forming different radical cation resonances (R^+) as shown in Scheme 1 of Fig. 1. If the oxidation of the monomer at the electrode surface is faster than the diffusion of the oxidized radicals from the electrode surface to the electrolyte solution the concentration of the radical cation increases and they can be involved in different coupling reactions. The monomer can react and generate nonconducting oligomers, which may deposit on the electrode, or diffuse into the solution and produce a soluble brown cloud if the radical cation is extremely active (unstable) or extremely inactive (stable). The stable radical cation can also undergo further coupling reactions to form dimers that lead to a proton release, as shown in Scheme 2 of Fig. 1.

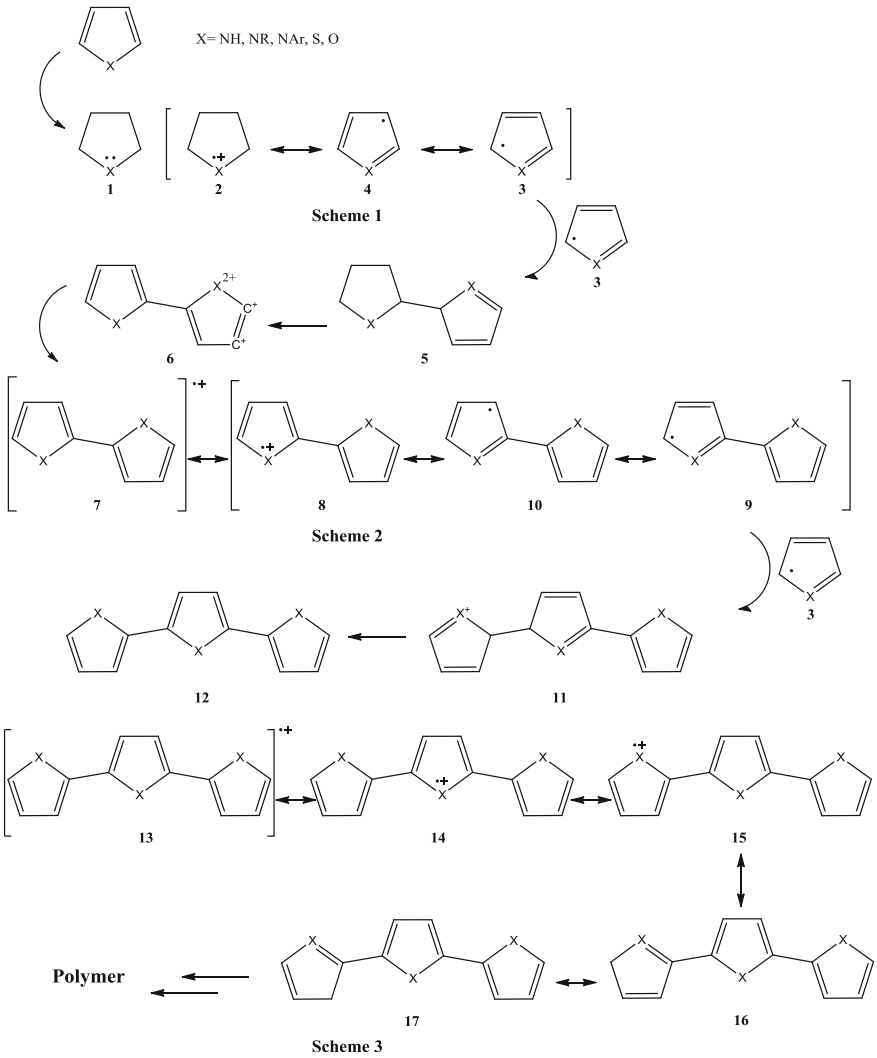

Fig. 1 Proposed mechanism for obtaining conducting polymers by polymerization of aromatic heterocyclic monomers [54]

The resonance form (3) with the α- α′ (2, 5) position having greatest density of unpaired electrons is predominant. The propagation of the polymer chain begins with the reaction between two stable radical cations at the α position to form a dication. This species loses two protons becoming neutral and stable (see Scheme 2). According to Genies et al. [55] the reaction coupling is between two π-radical cation monomers that leads to the formation of a dimer precursor which then deprotonates eliminating two protons to form a dimer radical, Scheme 2 of Fig. 1.

The dimer radical cation oxidizes easier than the monomer at the existing anode applied potential because of the delocalized unpaired electron over the heterocyclic rings. The predominant resonance form (9) is oxidized into a cation radical and undergoes further coupling reactions at β or β' with monomer radical cation 3 at α or α' positions, producing a trimer dication (11) (see Scheme 3, Fig. 1). The trimer dication then loses two protons to form the neutral trimer (12).

The neutral trimer (12) is oxidized to a trimer radical cation (13) (see Scheme 3 of Fig. 1), which reacts with the monomer to form a tetramer. The polymer chain continues growing via the same oxidation sequence, coupling and deprotonating until the chain growth terminates and the final polymer is obtained. Reaction with water could be one of the steps that end the polymerisation. Although, α position is the most active and predominant, the β position also reacts and increases the chain length and also the disorder. This disorder that forms the β coupling is responsible for the poor crystallinity of the conducting polymer but the crystallinity can be improved by blocking the two β positions with methyl groups or Cl atoms in order to form poly (β-β′-dimethylpyrrole) and the poly (β-β′-dichloropyrrole), respectively.

In relation with the magnetic nanoparticles component, a wide variety of magnetic nanoparticles with controlled size and shape have been synthetized including pure metal, such as Fe, Co, and Ni; iron oxides, such as Fe_3O_4 and Fe_2O_3; mixed ferrites as $MnFe_2O_4$ and $CoFe_2O_4$; as well as alloys, i.e., FePt. The magnetic properties of the nanoparticles are principally dominated by the chemical composition, phase, size effect, and surface effect and all of these aspects will be determined by the synthetic route. A large number of suitable methods have been developed to obtain magnetic nanoparticles which are mainly based on chemical approaches. The most popular and used methods include coprecipitation, thermal decomposition, microemulsion, hydrothermal synthesis, electrochemical route, and laser pyrolysis among other techniques [56]. The chemical coprecipitation is the preferred method to synthesize magnetic nanoparticles, especially iron oxides [57]. This general method consists in a solution containing Fe^{2+} and Fe^{3+} ions in water, to this solution is added NH_4OH and the system is stirred for a period of time. The precipitate is separated by magnetic decantation and washed with deionized water and ethanol to obtain the final magnetic nanoparticle iron oxide powder. Although, this is the most common method, some others have been used to generate magnetic nanoparticles to produce nanocomposites, for example, the electrochemical synthesis of magnetite and other ferrites nanoparticles [58–60]. The advantage of this method against conventional methods is the better nanoparticle size control by changing experimental parameters, such as oxidative potential or current. The control of size and the dispersion of the magnetic nanoparticles is a key parameter to obtain nanocomposites with homogeneous properties.

Therefore, the preparation of magnetic nanoparticles-based conducting polymer nanocomposites may successfully combine the strategies to synthesize both the magnetic nanoparticles and the conducting polymer in order to obtain a homogenous and appropriated material. The preparation method strongly affects the final properties of the nanocomposites and many investigations have been published regarding

the suitable incorporation of the nanoparticles into the conducting polymer matrix. As commented one of the major challenge is related to achieve a homogeneous dispersion because the aggregation of the nanoparticles generally demerits the properties of the materials and could limit the applications. In particular, the magnetic nanoparticles tend to the agglomeration due to magnetostatic interactions and this makes them difficult to be well dispersed into the polymer matrix. In the same way there are several synthetic methods to develop nanocomposites in stable colloidal form. A number of magnetic nanoparticles have been encapsulated by conducting polymer shells using a variety of strategies to overcome agglomeration problems and maintain the nanocomposite colloidally stable in the medium. Related to the preparation of thin film, much effort is dedicated to build homogeneous monolayer or multilayer usually by previously covering the nanoparticles with organic ligands to gain dispersibility in the used solvent [61].

In brief, the preparation methods of these nanocomposites can be classified in four main routes proposed in the literature that are graphically represented in Fig. 2 for the preparation of composites based on PPy. In the first strategy, both components, the polymer and the magnetic nanoparticles are synthesized separately and then mixed to produce the nanocomposite. This route presents as the main inconveniences that the conducting polymers, i.e., PPy, are not soluble in common solvent and also this method normally conducts to heterogeneous composites with

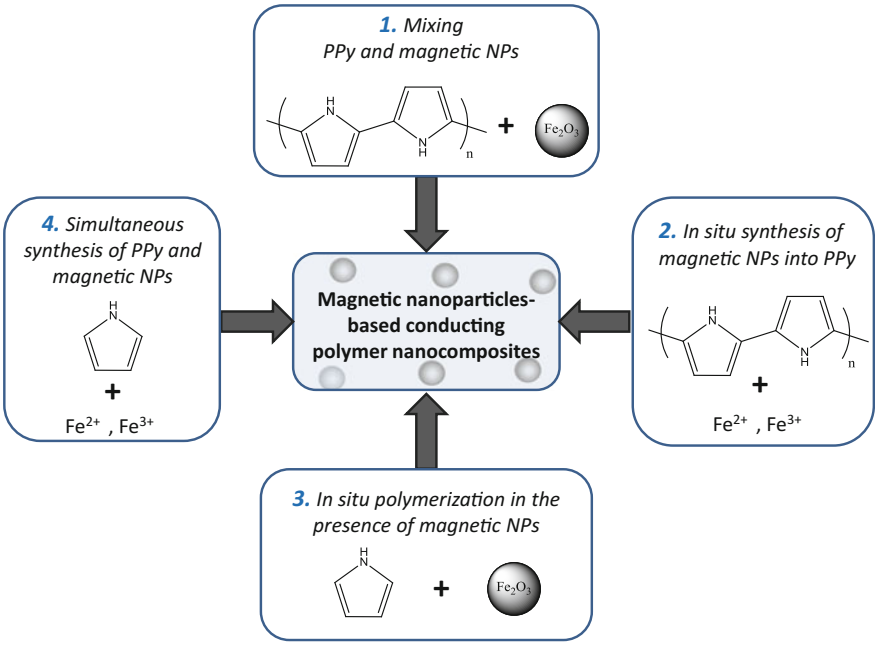

Fig. 2 Scheme of the different preparation methods of magnetic nanoparticles-based conducting nanocomposites

large aggregates of particles, and consequently it is not commonly used. Second route consists in the synthesis of the nanoparticles within the PPy previously synthesized, which provides nanocomposites more homogeneous. However, the control of the nanoparticle size is difficult and the solubilization of the polymer implies again an inconvenience. The third route is probably the most employed for the formation of magnetic nanoparticles-based conducting polymer nanocomposites. In this method, the nanoparticles are generated at first and then the polymerization is carried out in situ in the presence of the nanoparticles. Therefore, it is possible to synthesize nanoparticles in a controlled manner and at the same time, to produce homogeneous composites. At last the preparation of the nanocomposites by the in situ preparation of both the polymer and the nanoparticles is not yet very commonly used despite its simplicity and rapidity, as a result of its poor control over the polymer and the nanoparticles.

Next, the different strategies used to prepare magnetic nanoparticles-based conducting polymer nanocomposites employing both chemical and electrochemical routes are further discussed.

2.1 *Mixing or Blending Pre-synthesized Conducting Polymers and Magnetic NPs*

Hybrid nanoparticles–polymer nanocomposites are typically prepared by blending or mixing the different components in solution or in a melting process. However, these conventional strategies are not feasible in case of most of conjugated conducting polymers because they are generally insoluble in common solvents and present a very-high melting temperature. Only few examples are reported related to the preparation of nanocomposites based on conducting polymers using a solution method. In those cases the polymer has to be soluble or dispersible in the solvent and also the magnetic nanoparticles need to be colloidal stable in order to avoid the aggregation in the final nanocomposite (Fig. 3). For instance, water-soluble

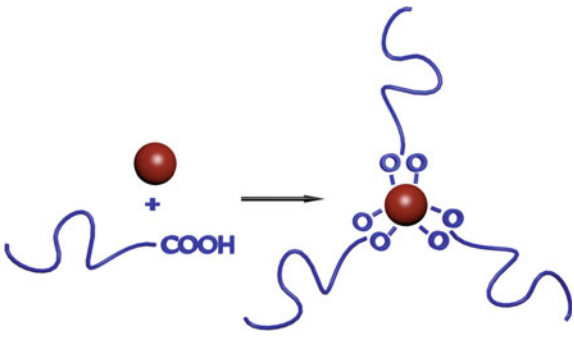

Fig. 3 Illustrative representation of the conducting nanocomposites prepared from pre-synthesized conducting polymers and magnetic NPs

polymers such as poly(1-vinyl-1,2,4-triazole) [62], as well as a polypyrrole derivative, poly(*N*-pyrrole phosphonic acid) [16, 17], were mixed with Fe_3O_4 nanoparticles in aqueous solution leading conducting and magnetic nanocomposites.

Other strategies employ polymer aqueous dispersion instead of solution, that is the case of the PEDOT:PSS (polystyrene sulfonate) system which is commercially available in aqueous dispersion and was blended with anionic coated iron oxide nanoparticles to prepare composite thin films [48]. Besides, layer by layer technique has been used to prepare several nanocomposite thin films from conducting polymer solution and ferrofluids for different applications [5, 43]. In these approaches layers of positively charged conducting polymer, such as PPy and poly(*o*-ethoxyaniline), in combination with positively charged magnetic nanoparticles were deposited alternatively with layers of negatively charged polymers such as polystyrene sulfonate.

On the other hand, cryomilling technique has been proposed as interesting alternative to the solvent method in order to obtain nanocomposites with magnetic nanoparticles homogenously dispersed in the polymer. This solid state method blends the components by milling under cryogenic temperature reducing the viscoelasticity of the polymer thus improving the compatibility between the polymer and the nanoparticles. Nanocomposites of PANI and iron nanoparticles were prepared by this technique using both micrometer and nanometer Fe particles as starting material [63, 64].

2.2 *In Situ Synthesis of Magnetic Nanoparticles into Conducting Polymers*

With the purpose of improving the nanoparticles dispersion into the conducting polymer, some investigations attempt to carry out the in situ synthesis of the magnetic nanoparticles into the polymer which again needs to be soluble in the used solvent. In a reported example, magnetite nanoparticles were synthesized by coprecipitation method in an aqueous solution containing a pre-synthetized poly (3-pyrrol-1-ylpropanoic acid) [16]. The incorporation of sulfonated groups into polyaniline also conducts to water-soluble conducting polymers and allows the preparation of the nanocomposites in aqueous solution by the in situ synthesis of iron oxide nanoparticles in the polymer solution [38]. Besides, the polymer chains can be chemically attached to the surface of the nanoparticles towards these functional groups enhancing the final properties of the nanocomposites. These particular kind of polymers with sulfonated groups, such as poly(pyrrole-*N*-propylsulfonate), when are prepared by reaction with $FeCl_3$ produce polymers with pendant SO_3^- and Fe^{2+} ions that provide overall charge neutrality in the material (Fig. 4). Further treatment with NH_4OH allows the synthesis of iron oxide

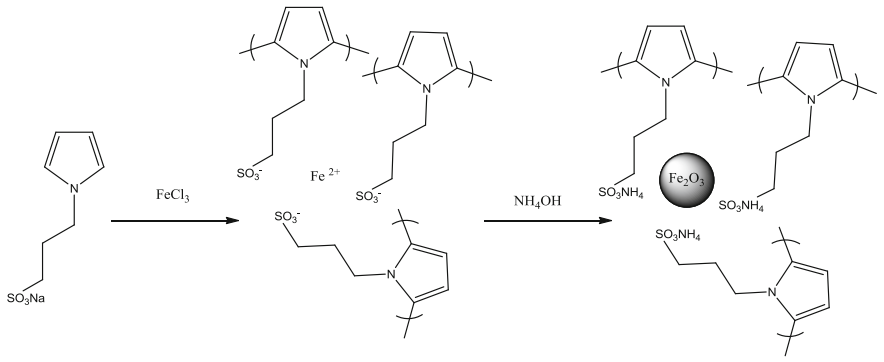

Fig. 4 Scheme of the synthetic procedure to obtain magnetic nanoparticles-based conducting polymer nanocomposites by in situ synthesis of Fe_2O_3 nanoparticles

nanoparticles in the polymer solution thus the in situ preparation of the magnetic polymer nanocomposite in aqueous solution [65].

A mixture of solvent can be also used to prepare the nanocomposite by in situ synthesis of the magnetic nanoparticles into the previously prepared polymer. A composite of PANI and Fe_3O_4 nanoparticles were prepared from *N*-methyl pyrrolidone polymeric solution by addition of an aqueous solution of iron(II) sulfate [66]. The magnetic properties of the final composites strongly depend on the preparation conditions, such as the reaction temperature and the $FeSO_4$ concentration.

Alternatively, the conducting polymers can be suspended in aqueous solution instead of be solubilized, and the magnetic nanoparticles created in the same medium, as reported for a nanocomposite consisting of PANI and magnetite [67].

Moreover, magnetic nanoparticles of Ni and Co have been also synthesized and directly incorporated into PANI fibers by electroless metal deposition [50]. However, by using this strategy only the surface of the fibers is functionalized with the magnetic nanoparticles.

2.3 *In Situ Polymerization in the Presence of Magnetic Nanoparticles*

However, and without any doubt, the in situ monomer polymerization in the presence of pre-prepared magnetic nanoparticles is the most common strategy to prepare nanocomposites based on conducting polymers. In this sense the polymerization can be carried out in either homogeneous medium or heterogeneous medium, i.e., in emulsion using surfactants, providing different types of nanocomposites, from films to core–shell particles.

The easiest strategy consists in the in situ polymerization of monomers, such as pyrrole or aniline, in solution and in the presence of magnetic nanoparticles. In this approach the selection of the solvent is of great importance to obtain a proper nanocomposite with the nanoparticles well dispersed into the polymeric matrix. The solvent should dissolve the monomer and the magnetic nanoparticles have to be colloidally stable in it to avoid their agglomeration. Nevertheless, vigorous stirring of the solution and/or sonication are normally required to suspend the nanoparticles and prevent their aggregation during the polymerization. Once the polymer is formed, thus the nanocomposite, a black precipitate is normally obtained in the reaction medium.

For instance, polyaniline is usually prepared by oxidative polymerization of aniline in acidic aqueous solution using oxidants such as ammonium persulfate. Under those conditions a wide number of magnetic nanocomposites based on PANI have been prepared by incorporation of magnetic nanoparticle into the polymerization mixture, Fe_3O_4 [44], $NiFe_2O_4$ [35], $CoFe_2O_4$ [32, 68], and $ZnFe_2O_4$ [34]. Similarly magnetic nanoparticles/polypyrrole nanocomposites are typically synthesized by in situ oxidative polymerization of pyrrole in a dispersion of magnetic nanoparticles [13, 69]. In this case, the pyrrole is directly soluble in distilled water and does not require the use of acidic conditions.

On the other hand, a wide number of core–shell particles nanocomposites have been obtained by in situ oxidative polymerization but using emulsion or microemulsion polymerization method instead. Surfactants are added to the aqueous solution forming micellar aggregates and stabilizing the magnetic nanoparticles in the medium to obtain a ferrofluid. Then, the monomer molecules are adsorbed at the surface of the magnetic nanoparticles and the polymerization takes place to generate core–shell structures (see Fig. 5). Presence of the surfactant enhances the dispersibility of nanoparticles, increases the polymerization rate and also acts as dopant improving the conductivity of the final nanocomposite. The use of surfactants offers other advantages to the nanocomposite such as better adhesion to the substrate and smoothness.

A large number of surfactants have been used in the preparation of conducting and magnetic composites principally based on PANI and PPy, such as dodecyl benzene sulphonic acid (DBSA) [39, 40, 45, 70, 71], sodium dodecylbenzene sulfonate (NaDS) [24, 72], sodium dodecyl sulfate (SDS) [18, 31, 73–75],

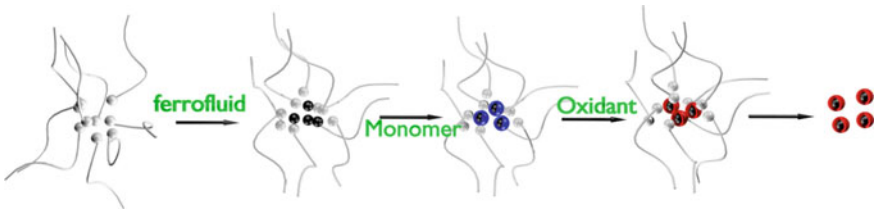

Fig. 5 Schematic representation of the formation of particle nanocomposites via in situ oxidative emulsion polymerization

p-toluenesulfonic (TSA) [8, 14, 21], cetyltrimethylammonium bromide (CTAB) [42], tetramethylammonium hydroxide [76], tetramethylammonium chloride [53], lignosulfonic acid (LSA) [46] sodium bis(2-ethylhexyl) sulfosuccianate (AOT) [19], polyvinyl alcohol [77], and so on. The addition of a cosurfactant, typically alkyl alcohols, is sometime required, especially in microemulsion polymerization.

In order to avoid the agglomeration of the nanoparticles and prepare composite core–shell particles an alternative process has been introduced in addition to the use of surfactant, the so-called common ion effects. This approach is based on the use of $FeCl_3$ as oxidant agent in the polymerization. Briefly, iron oxide nanoparticles are placed in a $FeCl_3$ solution and the Fe^{3+} ions are adsorbed onto the surface of the nanoparticles induced by the common ion effect principle forming a positively charged shell that prevents the aggregation. Besides, this shell became an active site to polymerize the monomer (see Fig. 6). This methodology has been employed for the polymerization of pyrrole [15, 78] and aniline [25] among others.

In addition to spherical particle nanocomposites, the preparation of nanotubes and nanowires composites with both magnetic and electrical properties is of great interest due to the enhancement of the conductivity. In general, the room temperature conductivity increases when the diameter decreases [79]. Conducting polymer nanotubes can be chemically or electrochemically synthesized by "hard" and "soft" template or template-free method in the presence of magnetic nanoparticles [8, 23, 27].

On the other hand, the in situ electropolymerization with magnetic nanoparticles in the medium generally conducts to the deposition of composite films. In this sense, the synthesis of conducting polymer layer containing magnetic nanoparticles on the surface of electrodes provides advanced properties interesting for instance, in electrocatalysis. For example, poly(3-thiophene-acetic-acid)/magnetite nanoparticles composite thin films were deposited onto a gold-covered quartz crystal electrode galvanostatically employing a current density of 3 mA/cm^2 and Bu_4NBF_4

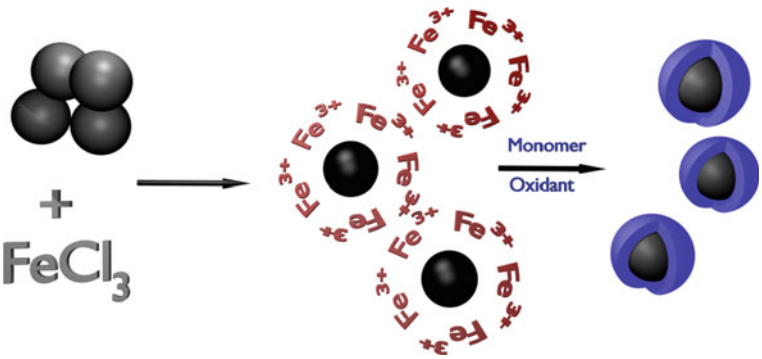

Fig. 6 Scheme of the mechanism for the synthesis of core–shell particle composites on the basis of the common ion effect

nitrobenzene solution [80]. In a previous step, the magnetic nanoparticles were stabilized in the medium by chemisorption of the 3-thiophene-acetic-acid monomer. In a similar way polypyrrole-magnetite composite films were electrodeposited via galvanostatic approach onto platinum electrodes and platinum-covered quartz crystal electrodes at a 3 mA/cm^2 current density in an aqueous solution containing potassium tetraoxalate [9]. In this particular case, the nanoparticles were functionalized with B12 biomolecules prior the polymerization. Potentiostatic electropolymerization has been also performed to deposit nanocomposite films. In particular PEDOT and PANI layers with embedded magnetite nanoparticles were formed onto a platinum electrode in presence of magnetite nanoparticles at a potential of 1.1 V and a charge density of 120 mC/cm^2 [81]. Smoother and more compact continuous films can be obtained by cyclic voltammetry (potential between 0.5 and 1.0 V at 250 mV/s) in comparison with the deposition under constant potentials [20]. In effect, high-quality electromagnetic composite films of PPy with different content of Co nanoparticles have been prepared onto $Si/SiO_2/Ti/Pt$ substrates from aqueous solution containing sodium sulfate and DBSA as electrolytes.

2.4 Simultaneous Polymerization and Synthesis of Magnetic Nanoparticles

In this methodology the synthesis of the nanoparticles and the monomer polymerization is carried out simultaneously in order to produce a homogenous nanocomposite. PANI/Fe_3O_4 nanocomposites have been obtained in one single step in aqueous solution as common solvent [26]. Typically, aniline monomer is added to a mixed solution of $FeCl_2$ and $FeCl_3$, which works as oxidant. The pH is controlled with NH_3 and after a certain time a black precipitate of PANI/Fe_3O_4 is formed.

Poly(*p*-phenylenediamine)(PpPD)/Fe_3O_4 composites were prepared by chemical oxidation polymerization of pPD monomer with APS and $Fe(NO_3)_3$ as oxidizing agents [82]. The Fe^{3+} was partly reduced to Fe^{2+} allowing the formation of the magnetite nanoparticles.

3 Magneto-Electrical Properties

3.1 Magnetic Nanoparticles

The magnetic nanoparticles are of great interest for numerous applications including separation systems, data storage, catalysis, and biomedical uses such as magnetic resonance imaging [83]. Each potential application requires different and

specific properties. While data storage applications need particles with switchable magnetic state being at the same time stable to temperature fluctuations, biomedical uses in general require superparamagnetic behavior, colloidal stability, and biocompatibility.

As described above a number of suitable methods have been developed for the synthesis of magnetic nanoparticles of various compositions, sizes, crystalline structures, shapes, and surfaces functionalities that will determine the magnetic properties of the nanoparticles and thus the final applications. In this sense the chemical composition is crucial for the magnetic behavior. There are a number of materials that exhibit magnetism, among other Fe, Co Ni, some rare earth, their oxides and alloys. The bulk ferromagnetic materials reduce its magnetostatic energy, created at the magnetic order, generating domains with random magnetic moments and making zero the net magnetic moment. In the presence of an external magnetic field the domain walls tend to move in order to the domains with the magnetic moment oriented in the direction of the field grow, at the expense of the rest domains. In other words, the magnetic moment of the domains tends to align with the field destroying the domain walls. When all the moments are aligned with field the materials reach the magnetic saturation (M_S), (Fig. 7a). Materials that retain the magnetization, remanence magnetization (M_r), in the absence of magnetic field are defined as hard magnet or permanent magnets and show a high coercivity field (H_c), the field required to bring the magnetization to zero, (Fig. 7a). Nevertheless, the materials that are easy to magnetize and demagnetize are known as soft magnetic materials and show a small remanence magnetization and coercivity field. In fact, not only the composition changes the magnetic behavior, the cation distribution is also important for the magnetic saturation. As an example, one of the most studied compounds is the ferrites, in which the iron cations are substituted by other 3d metals. Depending on the inverse degree of the ferrite, the relation between cations in the octahedral and tetrahedral sites of the spinel structure, the magnetic saturation moment could change drastically. The chemical composition also determines the magnetic transition temperature.

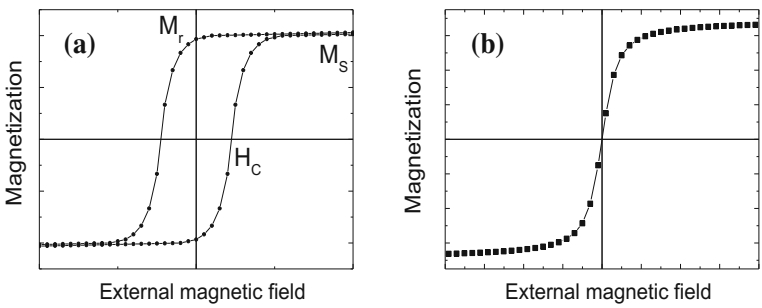

Fig. 7 Magnetic hysteresis loops of ferromagnetic material (**a**) and superparamagnetic material (**b**)

Besides, the size is crucial in all applications and its reduction induces new and exotic magnetic behaviors. In fact, the surface to volume ratio is the origin of these behaviors. The bulk ferromagnetic materials reduce its magnetostatic energy creating domain walls and regions with random magnetic moments, as it is described above. The magnetostatic energy is proportional to the volume, if volume increases the magnetostatic energy increases. On the other hand, the energy necessary to create the domain wall is proportional to the surface. Nevertheless, when the particle size decreases the volume decreases faster than surface area, thereby the magnetostatic energy decreases faster than domain wall energy. At certain size, the magnetostatic energy is less than domain wall energy and domains are not created, appearing nanoparticles with only one domain. It means that all atomic moments in the nanoparticles are aligned in one direction, showing a permanent magnetic in each nanoparticle. This critical size depends on the magnetic anisotropy of the material but is typically around 10–100 nm. Then, each nanoparticle becomes a single magnetic domain and shows supermagnetism [84]. In fact, the supermagnetism could be understood as a magnetism of super-magnetic-moments, one moment per nanoparticle. The different behaviors included in the supermagnetism are related with the interparticle interactions. For example, when the interaction is high, so the particle concentration is high, the superferromagnetism (SFM) appears as a ferromagnetism of super-magnetic-moments [85]. On the other side, when particle interactions are negligible the nanoparticle magnetic moments move randomly, as paramagnetic atoms, and superparamagnetic (SPM) behavior is expected. Undoubtedly, superparamagnetism depends on the temperature. There is a temperature called blocking temperature, below which the magnetic moments are frozen but above which the thermal energy is high enough to overcome the magnetic anisotropy. In this region the nanoparticle magnetic moments show a fast response to applied magnetic fields with negligible remanence magnetization (M_r) and coercivity field (H_c), Fig. 7b.

Due to the small surface to volume ratio, the surface plays an important role in the magnetic behavior. Usually the disorder in the surface reduces the magnetic saturation moment because the magnetic atoms at the surface do not contribute to the total magnetic moment. This surface is normally called dead layer. In other case, the surface could show another magnetic behavior creating a core–shell magnetic nanoparticle. In this sense the more interesting effect appears when the shell shows a high temperature antiferromagnetic order and the core a ferromagnetic one. The coupling each other produces the exchange bias effect which is a promising effect for storage data. The interaction between the AFM shell and FM core induces a shift in the magnetic hysteresis loop (exchange bias field; H_{eb}), Fig. 8, and an increase in the coercivity [56, 86].

In most of the applications the surface functionality of the magnetic nanoparticles needs to be controlled. The covering of the nanoparticles for instance with polymers protects the nanoparticles of degradation and oxidation that usually conduct to a loss of properties. The modification of the surface by the attachment of stabilizing molecules or compatibilizers is typically carried out to avoid the undesirable agglomeration of the particles and also favoring the stabilization and

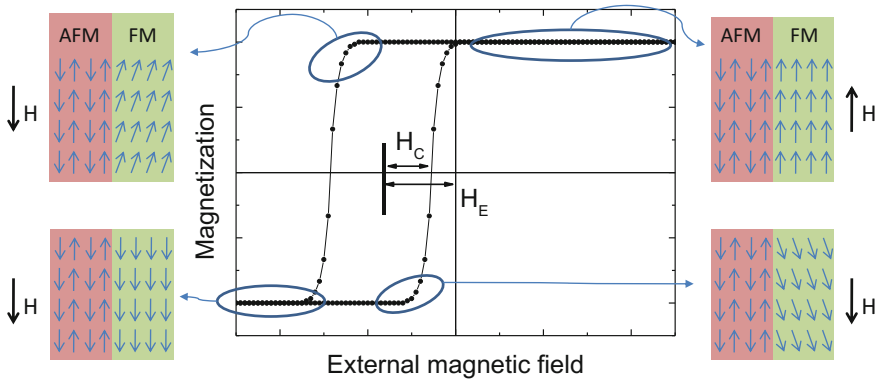

Fig. 8 Magnetic hysteresis loop showing the exchange bias effect with a schematic picture of magnetic moment behavior

dispersibility of the particles. In particular, coating the nanoparticles with a shell of conducting polymers not only stabilize the nanoparticles and enhance the dispersibility, but also confers to this system electrical conductivity.

3.2 Conducting Polymers

In the last decade, the discovery that is possible to control the electrical conductivity of polymers over the range from insulating to metallic had led to substantial efforts to prepare conducting polymers for technological applications.

The first major breakthrough in the field of electrically conducting polymers took place around 1978 when it was demonstrated by Shirakawa et al. [87, 88] that polyacetylene (PA) and intrinsically insulating organic conjugated polymer, exhibits a dramatic increase in electrical conductivity on treatment with oxidizing (electron-accepting) or reducing (electron-donating) agents. These processes are termed as p-doping, and n-doping, respectively.

The nature of the process responsible of inducing high conductivity in conducting polymers is different than that for inorganic semiconductors. In the doping of inorganic semiconductors the dopant species occupies positions within the lattice of the host materials thereby resulting in the presence of either electron-rich or electron-deficient sites with no charge transfer reaction occurring between the two sites. The doping reaction in organic conjugated polymers, on the other hand, is a charge transfer reaction, resulting in the partial oxidation, or reduction of the polymer.

The semiconductor properties of conjugated polymers are provided by the delocalised electrons of the aromatic or aliphatic carbon structures [89]. The conductivity can be improved by a doping process that in simple terms consists on

injecting charged species into the conjugated polymer backbone by chemical, electrochemical, or interfacial method [90]. The doping process is reversible and polymers can return to their original state with little or no degradation.

The increase in conductivity observed upon doping organic conjugated polymers are associated with formation of self-localized excitations such as solitons, polaron, and bipolarons [91]. These quasiparticles which arise from a strong interaction between the charge on the chain (electron or hole) acquired as a result of doping. In polymers such as polypyrrole, polythiophene, or poly(*p*-phenylene), initially polarons (positively charged, or negatively charged) are formed on doping. These polarons then combine to form spinless bipolarons which acts as the charge carriers.

The increase in the electrical conductivity is not without accompanying problems. The process of doping is often the source of chemical instability and poor processibility. In this sense the preparation of conducting polymer-based-hybrid composites is nowadays an interesting alternative and has been the focus of an intensive investigation. A variety of conjugated polymers has been combined with different nanoparticles leading nanocomposites with high electrical conductivity, in particular those including metal nanoparticles such as Ag, Au [92] and carbon nanotubes [93]. Related to the formation of hybrid nanocomposites the dispersion of the nanoparticles into the polymer matrix and the organic–inorganic interface are important issues in the achievement of the desirable electrical conductivity. Reddy et al. [93] reported the synthesis and the electrical conductivity studies of nanocomposites consisting in polyaniline functionalized multiwalled carbon nanotubes (MWCNTs) containing Au and Ag nanoparticles. It was demonstrated that the conductivity increases with the incorporation of MWCNTs, from 2.5×10^{-3} S/cm to 9.3×10^{-3} S/cm, for pristine PANI and after the incorporation of MWCNTs, respectively. The augment in the conductivity is, however, more significant when the MWCNTs are previously functionalized to improve the compatibility with the polymer matrix up to 0.18 S/cm. The additional incorporation of metal nanoparticles provokes a further increase in the conductivity, 5.04 S/cm in the case of the nanocomposites containing silver nanoparticles and functionalized MWCNTs.

3.2.1 Characteristics of the Most Common Conducting Polymers

Polyaniline

Discovered in 1862 during the oxidation of aniline, polyaniline (PANI) can be synthesized chemically and electrochemically in aqueous solutions [94]. PANI exists in the following species depending on its oxidation state: leucoemeraldine, emeraldine and pernigraniline but only protonated emeraldine is electrically conductive, while doped leucoemeraldine and pernigraniline have poor conductivity. PANI is thermally, electrochemically and environmentally stable in solution and air [95] and presents interesting electrochemical, electronic, optical and electro-optical properties resulting from the flexible—NH group in its backbone. PANI has been

used in different applications such as in corrosion protection, in OLED devices, electrochromic displays, electro-optic and smart windows for energy storage in secondary batteries [96, 97], and due to its biocompatibility PANI has extensively been used for biosensor [98, 99].

Polythiophene

This polymer has excellent environmental and thermal stability in their neutral and doped states [100, 101] exhibiting optical properties and conductivity values up to 600 S cm^{-1} in the doped form [102]. Polythiophene presents poor solubility in most organic solvents, except in mixtures such of arsenic trifluoride/pentafluoride which limits its applications. However, it has been reported that the incorporation of a long flexible alkyl side chain on the 3-position of the thiophene ring produces a soluble polymer in common organic solvents without altering the chemical and physical properties of the polymer [103].

In particular poly(3,4-ethylenedioxythiophene) (PEDOT) widely used can be synthesized by oxidative chemical or electrochemical polymerisation producing thin films that are optically transparent in the reduction state and light blue color in the oxidized state with high stability and conductivity. The most common dopant for PEDOT is polystyrene sulfonate (PSS) rendering a water-soluble compound [102].

Polypyrrole

Polypyrrole is probably the most common conducting polymer used due to its excellent properties. Pyrrole monomer is commercially available, easily oxidized, water-soluble that conducts to polymers with high electrical conductivity, redox properties and good environmental stability. Over the past three decades polypyrrole has attracted interest for a number of applications including supercapacitor for energy storage and secondary batteries [104], in dye-sensitized solar cells [105]. This polymer has been also used for metal protection [106] and to manufacture patterned arrays of nanoparticles for data storage or biosensors [107].

3.3 Magneto-Electrical Properties of the Composites

The formation of nanocomposites of conducting polymers and magnetic nanoparticles will lead to the combination of the electrical and magnetic properties from the individual components, described in the previous subsections, in one nanomaterial. The composites with both responses are of great interest because are suitable materials for a wide range of applications as will be exposed in following sections, especially as electromagnetic interference shielding and microwave absorbing,

actuators, solar cells, or sensors. The final properties of the nanocomposites will depend not only on the individual components but also on the proportion of both materials and on the microstructure, factors that are controlled by the preparation method. The electrical and the magnetic behavior in the nanocomposites will differ, in principle, from those in the polymer and in the magnetic nanoparticles, and, in general, both properties are deteriorated. Typically, magnetic parameters such as magnetization saturation and coercivity field values decrease with the content of the nonmagnetic polymeric component. Similarly, the electrical conductivity of the nanocomposites is normally reduced with the incorporation of magnetic nanoparticles. Nevertheless, this reduction in the properties is not progressive as a function of the percentage because the homogeneity and also the interface polymer-particle surface play an important role.

Typically the magnetization saturation (M_S) decreases with the content of the nonmagnetic polymer in the nanocomposites following the well-known equation $M_S = \phi \times m_S$, where ϕ is the mass fraction of the magnetic component and m_S is the saturation moment of a single nanoparticle. It is clear that M_S of the nanocomposite depends on the mass fraction of the magnetic nanoparticles and consequently on the mass fraction of the conducting polymers. This means that the total magnetic behavior of the nanocomposite can be tailored as a function of the percentage of both components (see Fig. 9) [23, 27, 51, 52].

However, in several described nanocomposites the magnetization saturation does not decrease progressively with the polymer content appearing some discrepancies. A series of nanocomposites based on PANI and $Ni_{0.5}Zn_{0.5}Fe_{1.5}Cr_{0.5}O_4$ (NZFCO) were prepared varying the proportion of PANI [108]. Although the incorporation of PANI reduces the M_S (referred to the nanocomposite mass) in comparison with the nanoparticles, the sample with the lower content of PANI exhibits an anomaly low value of M_S, the lowest of the series. This was attributed to

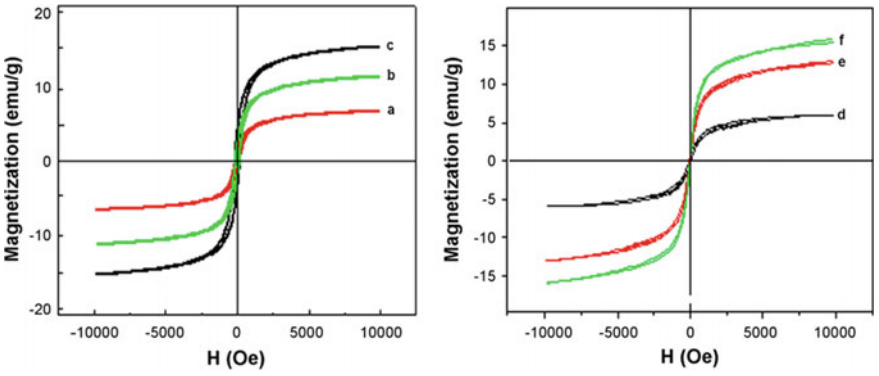

Fig. 9 Hysteresis loop of PANI/$Zn_{0.6}Cu_{0.4}Cr_{0.5}Fe_{1.46}Sm_{0.04}O_4$ nanocomposite at a nanoparticle content of **a** 20 wt%, **b** 40 wt% and **c** 60 wt%; and PPy/$Zn_{0.6}Cu_{0.4}Cr_{0.5}Fe_{1.46}Sm_{0.04}O_4$ at a nanoparticle content of **d** 20 wt%, **e** 40 wt% and **f** 60 wt%. Reprinted with the permission from Ref. [51]. Copyright (2010) Elsevier

the influence of the amorphous polymer–nanoparticles interactions. Concretely the polymeric molecules strongly interact electrostatically with the Fe^{3+} ions of the ferrite at the surface, leading to the creation of a dipole moment toward the PANI/nanoparticles interfaces. This reduces the free Fe^{3+} ions, which are the responsible of the magnetization. The surface modification effect of magnetite by conducting polymer, in the saturation magnetization was also observed in other studies. It was demonstrated that polypyrrole coating increases the saturation magnetization of magnetite nanoparticles, as a result of a charge transfer process from the polymers to the iron ions of the magnetite surface (Fig. 10) [70, 109]. Besides, the presence of the nanoparticle–polymer interactions can also explained the unexpected increase in the remanence magnetization and coercivity field with the polymer content that was recently observed in composites of PANI with ferromagnetic nanoparticles of cobalt ferrite [110].

Concerning the use of superparamagnetic nanoparticles, generally this superparamagnetism is retained in the nanocomposites [46, 74]. However, very different trend is observed in other systems. For instance, superparamagnetic $Mn_{0.68}Zn_{0.25}Fe_{2.07}O_3$ nanoparticles (with a blocking temperature of around 50 K) in the polypyrrole matrix present a significant increment in the blocking temperature and large hysteresis at 300 K, probably due to the clustering of the nanoparticles [6].

In contrast, it is reported in certain nanocomposites that the coercivity field and remanence magnetization decrease with increasing polymer concentration, becoming even negligible (Fig. 11) [111]. At low polymer content (PANI/Fe_2O_3 = 0.1/1) the nanocomposites show low values, 155–160 Oe of coercivity field and remanence magnetization of ~6–8 emu/g, while at composition of 2/1 H_c and M_r decrease down to 1.2 Oe and 0.03 emu/g, respectively. Therefore, the nanocomposite system changes from ferromagnetic to superparamagnetic for high polymer percentage. In addition, the systems became paramagnetic with higher content of polymer, fact that was confirmed through zero field cooled–field cooled magnetization measurements. This behavior can be explained as the interparticle distances increases as the polymer

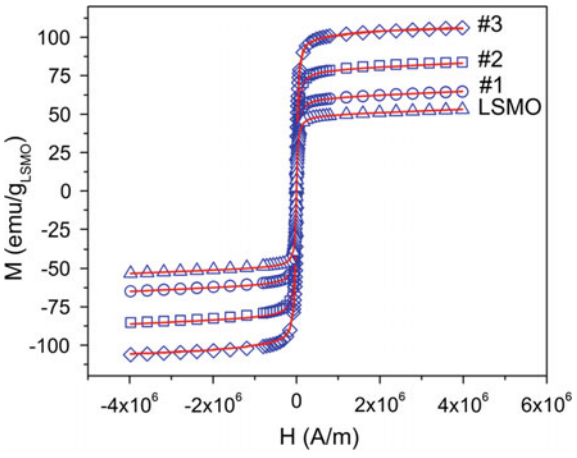

Fig. 10 Magnetic hysteresis loops of hybrid nanocomposites based on $La_{0.67}Sr_{0.33}MnO_3$ (LSMO) nanoparticles covered with different quantities of PPy: 14.3 wt% (#1), 56.3 wt% (#2) and 68.3 wt% (#3). Reprinted with the permission from Ref. [109]. Copyright (2012) AIP publishing

content augments and consequently the exchange and dipolar distances become weaker, diminishes the long range order in the nanocomposite and transforms the superferromagnetic material into a superparamagnetic one, as had been explained in the previous section. Similar results were obtained for composites formed by PPy and Fe_2O_3 in the same polymer concentration range [112].

Regarding the electrical properties of the nanocomposites, the electrical conductivity remarkably differs from the conducting polymers with the incorporation of magnetic nanoparticles as can be expected. The inherent conductivity of the conducting polymers arises from the presence of a conjugated electron system in their chain structures and the addition of nonconductive nanoparticles can disturb this conjugation and reduce the conductivity [21, 22, 40, 72]. Therefore the main reason of this decrease in conductivity lies in the partial blockage of conductivity path by the nanoparticles. Also the bonds between the particles and the polymers decrease the conjugated electron density in the polymer structure. In general, the total conductivity is the summation of the band and hopping parts that is the dc conductivity and the ac conductivity, respectively. Both terms have been studied more in detail in various publications related to magnetic nanoparticles-based conducting polymer nanocomposites. For instance, the ac conductivity of nanocomposites composed of PANI and ferrite nanoparticles, $Zn_{0.2}Mn_{0.8}Fe_2O_4$ [113] and $CoFe_2O_4$ nanoparticles [114] increases sharply at high frequency whereas in the neat PANI slowly increases with frequency even at high values. The augment in the frequency

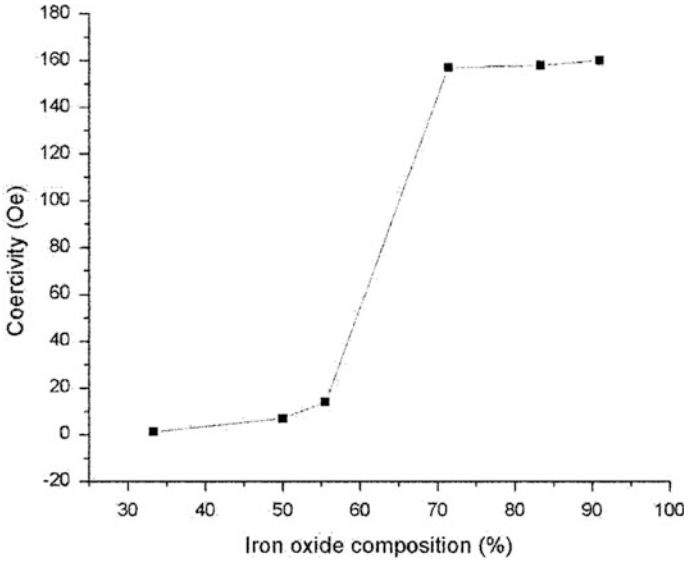

Fig. 11 Coercivity as a function of iron oxide composition in nanocomposites based on PANI. Reproduced with the permission from Ref. [111]. Copyright (2008) Springer

enhances electronic exchange occurring among the cations in the ferrite thus resulting in more ac conductivity. The ac conductivity usually increases with the content of ferrite nanoparticles in the nanocomposite probably due to the electron hopping processes. Other studies however, show nearly the same frequency dependent behavior in nanocomposites and in the pristine conducting polymer [16]. On the other hand, the direct current (dc) conductivity is strongly temperature dependent, decreasing with decrease in temperature following a semiconductor behavior. The incorporation of magnetic nanoparticles can modify this dependence. It is reported in PPy/Fe_3O_4 nanocomposites a first step at low temperatures where the conductivity decreases as the temperature rises [16]. As shown the nanoparticles modify the electrical conductivity processes, in general the conductivity in nanocomposites is usually lower than the pristine conducting polymers because the nanoparticles increase the charge carrier scattering and also the carrier charge trapping.

On the other hand it is reported a contrary effect, increasing the conductivity in the nanocomposites with the content of magnetic nanoparticles up to certain portion and then decreasing with further content of nanoparticles as displayed in Fig. 12. For instance in nanocomposites of PPy prepared by ultrasonication the maximum conductivity (11.3 S/cm) was reached with 40 wt% of Fe_3O_4 nanoparticles, 9 times higher than that of neat PPy [115]. Further content of nanoparticles conducts, however, to a decrease of conductivity. This behavior can be attributed to the doping level of the samples, which augments in the ultrasonication process thus becoming higher in the nanocomposites.

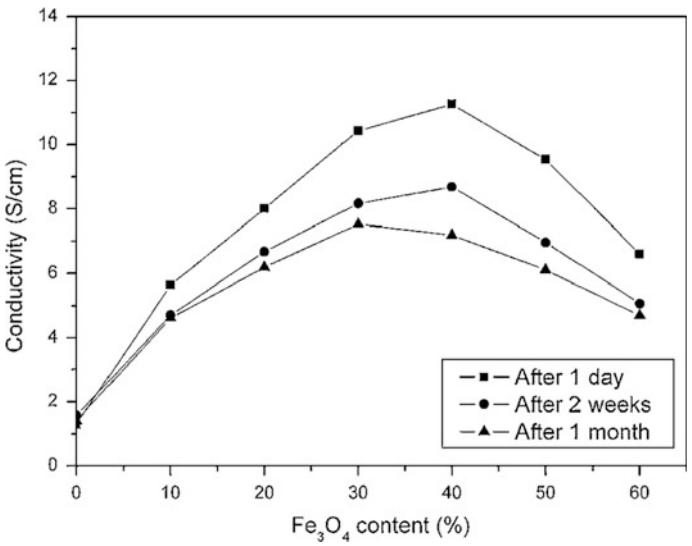

Fig. 12 Conductivity of Ppy/Fe_3O_4 nanocomposites at different magnetite content and at after different period of time. Reprinted with the permission from Ref. [115]. Copyright (2006) Wiley

In addition to the influence of dopant in the nanocomposites, the increase of conductivity associated with the incorporation of nanoparticles can be due to other factors. Core–shell structures were fabricated with Fe_3O_4 nanoparticles of 4 nm as core and PPy as shell [19]. The augment of the polymer content up to 36 % provokes a change of morphology from spherical to tubular, that could be the reason of the conductivity enhancement in comparison with the PPy without nanoparticles, from 10.1 to 59.4 S/cm. In the same way, nanocomposites of PPy functionalized with *p*-TSA and Fe_2O_3 nanoneedles show very high conductivity, ~65 S/cm [8].

4 Applications

The majority of conducting polymers offers several advantages over other polymeric systems in addition to their conductive properties, such as the ease of preparation and low cost, good environmental, and thermal stability. Therefore, they are extensively investigated as the polymeric component of many magnetic nanoparticles-based nanocomposites for a wide number of applications including remediation [31], catalysis [28], memory devices [20], magnetic resonance imaging [18], hyperthermia [77], photothermal therapy [116], etc. [117]. Nevertheless, the following section will be focused on the most important applications of magnetic nanoparticles-based conducting polymer nanocomposites derived from the conducting properties of the polymer in combination with the magnetic behavior provided by the magnetic nanoparticles component.

4.1 Electromagnetic Shielding and Microwave Absorbing Materials

Currently, there is a great interest in the development of microwave absorbing materials and electromagnetic shielding to avoid the interferences induced by electromagnetic signals in all the electronic devices and radiation sources. With the intensive growth of the telecommunication devices and electronic products, the development of these materials is necessary as the electromagnetic interferences (EMI) reduce the lifetime and efficiency of the equipment and affect the safety coexistence of all those instruments. The electromagnetic wave has essentially two components a magnetic field and an electric field perpendicular to each other. Therefore, these absorber materials should cancel both components for an effective absorption, by transforming the electromagnetic energy into other kinds of energy or simply dissipating the electromagnetic waves. The absorption basically relies on three main factors, dielectric loss, magnetic loss, and impedance matching, thus the combination of magnetic nanoparticles and polymers in a nanocomposite is

considered a proper strategy for this application with a reduced weight and cost, enhanced flexibility and corrosion resistance. Therefore, the electromagnetic interference can be diminished by positioning this kind of shielding material between the source and the component to be protected. The shielding can be defined as the reduction of the magnetic and electric fields and the effectiveness of a shield (SE), that is, its resulting attenuation can be expressed as

$$\mathrm{SE} = -10 \log \frac{P_t}{P_o} = \mathrm{SE_R} + \mathrm{SE_A} + \mathrm{SE_M} \tag{1}$$

where P_t and P_o are the transmitted and incident electromagnetic power, respectively, and $\mathrm{SE_R}$, $\mathrm{SE_A}$ and $\mathrm{SE_M}$ are the shielding effectiveness due to reflection, absorption and multiple reflections, respectively [118]. As described in the Eq. 1 there are three main mechanisms that contribute to the shielding effectiveness. On one hand, the incident wave is reflected from the surface of the shield, on second hand, the shield material absorbs part of the radiation and the third mechanism is based in multiple reflections which can either, support, or hider the effectiveness as shown in Fig. 13.

All the terms in the Eq. 1, $\mathrm{SE_R}$, $\mathrm{SE_A}$, and $\mathrm{SE_M}$, are expressed in decibels (dB). The multiple reflection factor $\mathrm{SE_M}$ is normally neglected in practical calculation due to the high value of $\mathrm{SE_A}$ (typically higher than 10 dB) [119]. The absorption loss is a function of the physical properties of the shield material then is expressed by the following equation:

$$\mathrm{SE_A} = 131t\sqrt{f\sigma\mu} \tag{2}$$

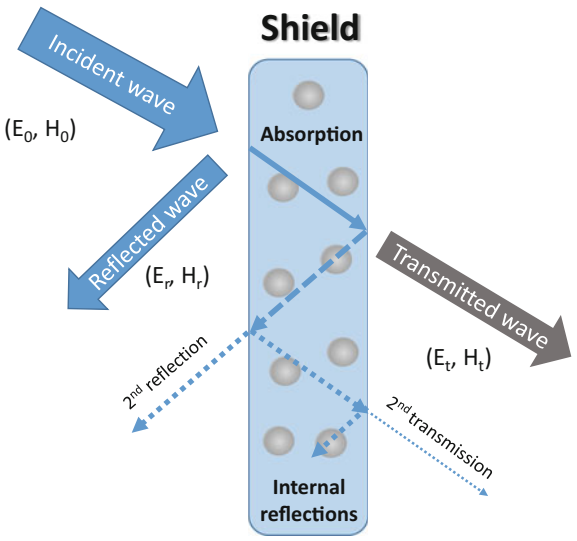

Fig. 13 Schematic representation of the EMI shielding

where t is the thickness, f is the frequency, σ is the electrical conductivity and μ is the magnetic permeability of the shield material. Related the SE_R component, this can be expressed as

$$SE_R = -10 \log\left(\frac{\sigma_T}{16\omega\varepsilon_0\mu}\right). \quad (3)$$

where σ_T is the total electrical conductivity, ω is the angular frequency, μ is the magnetic permeability of the shield material and ε_0 is the vacuum permittivity.

Experimentally, the shielding effectiveness of the nanocomposites is typically measured using network analyzer instruments. Scalar network analyzer (SNA) only measures the amplitude of signals whereas vector network analyzer (VNA) measures both amplitude and phase properties.

Several studies reported the preparation of nanocomposites composed on conducting polymers and iron oxide nanoparticles as magnetic components and their abilities as electromagnetic shielding. In all those investigations, the absorption properties of the nanocomposites also depend on their micro/nanostructure which is controlled by the synthesis method. A core–shell nanocomposite consisting of barium ferrite nanoparticles covered with a PEDOT polymeric layer was synthesized by in situ emulsion polymerization [120]. The barium ferrite contributes to the absorption properties due to its high magnetic losses and high resistivity whereas the PEDOT provides conductivity and dielectric properties. The EMI shielding effectiveness (SE) of the material was significantly higher as compared with that obtained by the PEDOT containing only the surfactant as control experiment, and the value increased with the content of ferrite nanoparticles in the measured frequency range between 12 and 18 GHz.

It was demonstrated that the main contribution to the SE comes from the absorption, 22.5 dB, as a result of the dielectric and magnetic losses. Similar study was carried out with a nanocomposite based on PANI also obtained by emulsion polymerization, with a SE_A value of 28.9 dB (99.9 %) in the same frequency range [121], The same group prepared a PPy/Fe_3O_4 nanocomposite by in situ oxidative polymerization which likewise demonstrates a strong microwave absorption properties in 12.4–18 GHz exhibiting a SE_A value of 20.4 dB [76]. Slightly higher values were obtained for polypyrrole nanocomposites decorated with Fe_2O_3 showing a total shielding effective of 28.4 dB and a SE_A of around 22.6 dB [122].

A recent study shows that electromagnetic wave absorbing properties can be controlled by tuning the proportion of both components in the composites based on PPy and Co nanoparticles [123]. It was demonstrated that reducing the Co NPs content could make the wave absorption performance of the nanocomposite moves to a lower wave absorbing frequency range, whereas a higher amount of Co could conducts to a higher frequency of wave absorption performance.

However, many investigations indicate that a shielding effectiveness value of 30 dB is required to protect electronic equipment in most of the cases [118]. In this regard, multicomponent nanocomposites containing also titanium dioxide nanoparticles have been evaluated as microwave absorbing material because the TiO_2 has

high dielectric constant and may contribute to the absorbing properties. PANI composites with ɣ-Fe_2O_3 and TiO_2 nanoparticles were synthesized via emulsion polymerization showing a SE_A value ~45 dB, in effect much higher than that obtained for PANI/ɣ-Fe_2O_3 and PANI/TiO_2 composites [124]. In a same way, PANI nanocomposites with TiO_2 and Fe_3O_4 show excellent microwave absorption, 99.950–99.999 %, when the magnetic nanoparticles are well dispersed in the polymer [25].

Besides, multifunctional nanocomposites consisting of conducting polymers, magnetic nanoparticles and graphene can be also applied as EMI shielding materials. Graphene mostly contributes to the electromagnetic absorption properties due to the dielectric loss. It has been described the development of nanocomposites by the incorporation of Fe_3O_4 NPs decorated-graphene oxide into PEDOT polymeric matrix. The loading of only 1 wt% of the Fe_3O_4 NPs decorated-graphene conducts to an EMI SE value of 22 dB and a surface resistivity of 80 Ω sq^{-1} [47]. Hybrid materials consisting of PEDOT and graphene but with Co_3O_4 [49] or $CoFe_2O_4$ [125] nanoparticles instead also show interesting shielding properties.

4.2 Polymer Solar Cells

In recent years, bulk heterojunction (BHJ) polymer solar cells (PSCs) have attracted a growing interest as a possible substitute to the inorganic-based cells due to their several advantages such as its light weight, flexibility, ease of fabrication, and promising capability for low-cost and large-scale production. Briefly, BHJ-PSCs consist on an active layer of conjugated polymer donor blended with fullerene derivative acceptor. In a typical design, both the donor and acceptor are sandwiched by a metal cathode, such as aluminum and an indium tin oxide (ITO) anode previously coated with a thin film of poly(3,4-ethylenedioxythiophene):poly(styrenesulfonate) (PEDOT:PSS) (Fig. 14). This layer smooths the ITO surface reducing the contact resistance with the BHJ layer, however, at the same time tends to degrade the BHJ component due to its acidic nature. In this sense magnetic nanoparticles, in particular magnetite, were incorporated into the PEDOT:PSS layer to improve the stability and enhance the efficiency as the nanoparticles may reduce the acidity of the PEDOT:PSS layer and also generate iron ions resulting in high conductivity [126]. Even the PEDOT:PSS layer was completely substituted by a magnetite nanoparticle layer in a success manner [127].

Magnetic nanoparticles have been also incorporated into the BHJ layer [128]. The composite was formed by mixing in a solution process poly(3-hexylthiophene-2,5-diyl) (P3HT) as conjugated polymer donor and [6,6]-phenyl-C61-butyricacidmethyl ester (PCBM) as acceptor, both soluble in chloroform. The addition of the nanoparticles significantly enhances the power conversion efficiency mainly attributed to the increase of short circuit currents as a consequence of the magnetic field effect from the superparamagnetic nanoparticles that increase the population of triplet excitons.

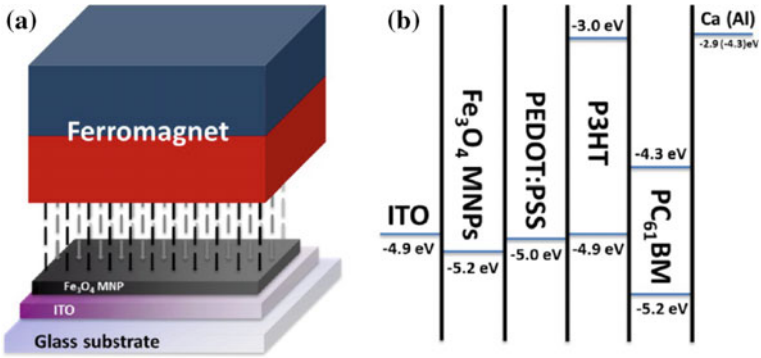

Fig. 14 **a** Schematic illustration of the fabrication procedure of a solution-processed Fe_3O_4 NP, followed by external magnetostatic field alignment, as a HEL for PSCs and **b** the LUMO and HOMO energy levels of P3HT and PCBM and work functions of PEDOT:PSS, Fe_3O_4, ITO, and Ca (Al). Reprinted with the permission from Ref. [127]. Copyright (2013) ACS

4.3 Sensors

Conducting polymer films and colloids have been widely investigated for sensor applications. Especially polypyrrole, which is one the most employed for the fabrication of biosensor because in addition to its good physical and electrical properties, this polymer is highly biocompatible. The association with magnetic nanoparticles to form a nanocomposite presents considerable progresses for their use as sensor. On one hand the nanostructuration created by the nanoparticles augments the surface area and provides new active sites. Second, they exhibit the capacity to promote faster electron transfer kinetics between electrodes. Moreover, their magnetic properties provide to the nanocomposites enhanced recovery ability and also the capacity of being oriented by external magnetic field. In this regard, the immobilization of magnetic nanoparticles on the surface of magnetic glassy carbon electrode (MGCE) is considered very promising approach for the fabrication of biosensors due to its high specific surface area and stability. Polypyrrole-$ZnFe_2O_4$ core–shell nanoparticles supported on the surface of MGCE were evaluated as enzymeless glucose sensor [129]. In the proposed electro-oxidation mechanism the glucose loses one proton in alkaline solution and forms the enediol structure that is able to complex with the Zn^{2+} ions of the nanoparticles to finally be oxidized. The presence of polypyrrole in the nanocomposites facilities the electron transfer rate due to its good electrical conductivity. Other core–shell nanocomposites based on polypyrrole and magnetite nanoparticles were also employed for the detection of glucose by immobilization, in this case, of the enzyme glucose oxidase [130]. The modified electrode presented significant sensibility and selectivity and short response time.

A biosensor based on magnetic Fe_2O_3-polypyrrole core–shell particles has been also prepared by immobilization of other biomolecules on their surface, such as

biotin with a strong affinity toward the protein avidin [11]. These core–shell particles were synthesized using a certain amount of pyrrole derivative containing *n*-carboxyl groups and through them were attached the biotin biomolecules.

Alternatively biotin molecules have been anchored directly to the magnetic nanoparticles component to create the biosensor [10]. Concretely, a nanocomposite was first obtained by immobilization of streptavidin labeled magnetic particles onto a thin PPy film. The covering of the nanoparticles was carried out by applying a magnetic field that conducts to a uniform assembly. Second, the nanoparticles were further functionalized with biotin-Fab fragment K47 antibody. This designed biosensor was successfully applied to measure very low concentration of atrazine.

Moreover, a photoelectrochemical bilirubin biosensor was fabricated by anchoring core–shell nanoparticles to the surface of MGCE [131]. Magnetite nanoparticles were first covered with a hydroxyapatite layer that exhibits photocatalyst activity and subsequently with polypyrrole in the presence of bilirubin molecules, thus employing the molecular imprinting approach (Fig. 15). Finally the nanocomposite particles were attached to the MGCE with the purpose of developing the biosensor which was highly sensitive to bilirubin in solutions and selective against very similar biomolecules such as biliverdin, cholesterol and testosterone. It was demonstrated that the PPy layer plays an important role in the transfer of the charges and thus enhancing the photoelectric conversion efficiency.

A biosensor based on hemoglobin (Hb) for hydrogen peroxide determination has been prepared by immobilization of hemoglobin into poly(*p*-phenylenediamine)/Fe_3O_4 nanocomposite previously deposited on the glassy carbon electrode [132]. This sensor works as an electrocatalytic process due to the reaction of HbFe(II) with H_2O_2. The cyclic voltammograms of the modified electrode in the presence of H_2O_2 shows an increase in the reduction peak current accompanied by a decrease of

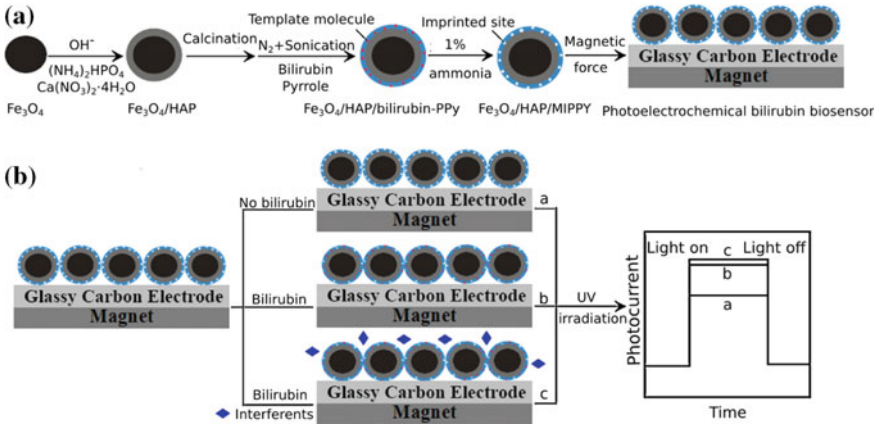

Fig. 15 Schematic illustration for **a** fabrication and **b** detection mechanism of the photoelectrochemical bilirubin biosensor. Reprinted with the permission from Ref. [131]. Copyright (2014) Elsevier

oxidation peak current. The nanocomposite acts in this case as an adequate platform.

Besides, nanocomposites of conducting polymers with iron oxide nanoparticles have been extensively used directly as sensor system. For example, core–shell particles of Fe_2O_3 covered with PANI were prepared by oxidative polymerization. In this case the sensing properties were investigated towards uric acid and those were attributed to the presence of both PANI and Fe_2O_3 electrocatalytic center [133].

The conducting polymer-based nanocomposites have also presented a great potential as humidity sensor and to monitor other gases. These sensors are based on changes in the resistance and capacitance when exposure to water vapor or other gases and, thus the microstructure of the nanocomposites is a crucial factor. Besides, the incorporation of semiconducting inorganic nanoparticles, e.g., Fe_3O_4, generally improves the stability of the sensor in those atmospheres. Tandon et al. [134, 135] have prepared different PPy/iron oxide nanocomposites with PPy contents up to 27 %. Then, they further studied their sensitivity to humidity as well as their gas sensing properties to CO_2, N_2, O_2, and CH_4.

An interesting system based on PEDOT:PSS with embedded iron oxide nanoparticles has been proposed as resistive humidity sensor due to the water adsorbing properties of this conducting polymer [48]. In particular a free standing nanocomposite films were prepared to be easily transferred onto different substrates which favor its applicability. Remarkably, the sensitivity to humidity increased with the nanoparticle concentration probably due to the augment of the surface roughness of the film that enlarges the exposed area to interact with water vapor.

5 Concluding Remarks and Future Perspectives

In the last decades, conducting polymers have evidenced much interest as they combine the properties of metal with the advantages of polymers. The preparation of magnetic nanoparticles-based conducting polymer nanocomposites goes one-step further with the addition of magnetic properties to the material. This emerging technology has attracted a great attention in many applications, especially as microwave absorbing materials and electromagnetic shielding. As commented, nowadays there is a great demand in the development of materials able to absorb or disperse electromagnetic radiation coming from telecommunication and electronic devices, and these magnetic and conductive materials seem to be appropriated for such a purpose. An intensive effort has been carried out in the preparation methods, many different nanocomposites have been prepared varying the type of polymers and magnetic nanoparticles, the percentage of each component and also using a large number of synthetic strategies. It is well known that the final properties of the nanocomposite depend on the type of polymer and magnetic nanoparticles but also on the dispersibility and homogeneity of the nanocomposites. Therefore, it is important to optimize the synthetic procedure to achieve more effective methods

and materials with enhanced properties. In general, the aim of all the investigations is the development of materials with high electrical conductivity and high magnetic properties, i.e., high magnetization saturation. However, these properties are typically diminished in the nanocomposite in comparison with the pristine component. Nevertheless, opposite results are also obtained in several works, in which the electrical conductivity increases with the incorporation of magnetic nanoparticles and magnetic parameters are enhanced in a particular concentration range. Most of these investigations seem to indicate that the interface polymer-magnetic nanoparticles plays a key role on the final properties and these interactions are probably the responsible of such contradictory results. However, these aspects and the complete mechanism of the process are still not well understood. The current directions in this field of research are mainly focused in addressing these features, establishing a clear relation between properties and structure, which is necessary for the development of materials with enhanced properties, especially for applications that will require a great improvement because of the more demand for new technologies and advancement of current technologies. This is the case of renewable energy, particularly solar energy, or the development of EMI shielding systems. Precisely in this last application, by the growth of the electronic industry in which the systems are getting lighter and faster, it is expected an important progress and the magnetic nanoparticles-based conducting polymer nanocomposites are a very promising candidate to fulfill these expectations. EMI shielding design should be optimized to meet the required efficiency while maintaining low cost and lightness, and presumable in the future flexibility and thinness will be also essential properties.

Acknowledgments The authors gratefully acknowledges the MINECO (Project MAT2012-37109-C02-02) for financial support. A. Muñoz-Bonilla also thanks the MINECO for her Ramon y Cajal contract.

References

1. Shylesh S, Schünemann V, Thiel WR (2010) Magnetically separable nanocatalysts: bridges between homogeneous and heterogeneous catalysis. Angew Chem Int Ed 49:3428–3459
2. Laurent S, Forge D, Port M et al (2008) Magnetic iron oxide nanoparticles: synthesis, stabilization, vectorization, physicochemical characterizations and biological applications. Chem Rev 108:2064–2110
3. Colombo M, Carregal-Romero S, Casula MF et al (2012) Biological applications of magnetic nanoparticles. Chem Soc Rev 41:4306
4. Tang SCN, Lo IMC (2013) Magnetic nanoparticles: essential factors for sustainable environmental applications. Water Res 47:2613–2632
5. Kim HSS, Sohn BHH, Lee W et al (2002) Multifunctional layer-by-layer self-assembly of conducting polymers and magnetic nanoparticles. Thin Solid Films 419:173–177
6. Poddar P, Wilson JL, Srikanth H et al (2004) Magnetic properties of conducting polymer doped with manganese–zinc ferrite nanoparticles. Nanotechnology 15:S570–S574
7. Jang J, Yoon H (2005) Multigram-scale fabrication of monodisperse conducting polymer and magnetic carbon nanoparticles. Small 1:1195–1199

8. Xiao HM, Zhang WD, Wan MX, Fu SY (2009) Novel electromagnetic functionalized γ-Fe_2O_3/polypyrrole composite nanostructures with high conductivity. J Polym Sci, Part A: Polym Chem 47:4446–4453
9. Janaky C, Endrodi B, Hajdu A, Visy C (2010) Synthesis and characterization of polypyrrole-magnetite-vitamin B12 hybrid composite electrodes. J Solid State Electrochem 14:339–346
10. Ben Fredj H, Helali S, Esseghaier C et al (2008) Labeled magnetic nanoparticles assembly on polypyrrole film for biosensor applications. Talanta 75:740–747
11. Mangeney C, Fertani M, Bousalem S et al (2007) Magnetic Fe_2O_3-polystyrene/PPy core/shell particles: bioreactivity and self-assembly. Langmuir 23:10940–10949
12. Esman N, Haviv A, Lellouche J-P (2011) Magnetically responsive polypyrrole nanotubes using Ce(III)-stabilized maghemite nanoparticles. Nanotechnology 22:285604
13. Azadmanjiri J, Hojati-Talemi P, Simon GP et al (2011) Synthesis and electromagnetic interference shielding properties of iron oxide/polypyrrole nanocomposites. Polym Eng Sci 51:247–253
14. Guo Z, Shin K, Karki AB et al (2008) Fabrication and characterization of iron oxide nanoparticles filled polypyrrole nanocomposites. J Nanopart Res 11:1441–1452
15. Luo YL, Fan LH, Xu F et al (2010) Synthesis and characterization of Fe_3O_4/PPy/P (MAA-co-AAm) trilayered composite microspheres with electric, magnetic and pH response characteristics. Mater Chem Phys 120:590–597
16. Karaoğlu E, Baykal A, Deligöz H et al (2011) Synthesis and characteristics of poly (3-pyrrol-1-ylpropanoic acid) (PPyAA)-Fe_3O_4 nanocomposite. J Alloys Compd 509:8460–8468
17. Temizel E, Ayan E, Senel M et al (2011) Synthesis, conductivity and magnetic properties of poly(N-pyrrole phosphonic acid)-Fe_3O_4 nanocomposite. Mater Chem Phys 131:284–291
18. Alves KGB, Andrade CAS, Campello SL et al (2013) Magnetite/polypyrrole hybrid nanocomposites as a promising magnetic resonance imaging contrast material. J Appl Polym Sci 128:3170–3176
19. Yen SJ, Chen EC, Chiang RK, Wu TM (2008) Preparation and characterization of polypyrrole/magnetite nanocomposites synthesized by in situ chemical oxidative polymerization. J Polym Sci, Part B: Polym Phys 46:1291–1300
20. Xu Z, Gao M, Yu L et al (2014) Co nanoparticles induced resistive switching and magnetism for the electrochemically deposited polypyrrole composite films. ACS Appl Mater Interfaces 6:17823–17830
21. Reddy KR, Lee KP, Gopalan AI (2008) Self-assembly approach for the synthesis of electro-magnetic functionalized Fe_3O_4/polyaniline nanocomposites: effect of dopant on the properties. Colloids Surf A Physicochem Eng Asp 320:49–56
22. Deng J (2002) Magnetic and conducting Fe_3O_4–cross-linked polyaniline nanoparticles with core–shell structure. Polymer (Guildf) 43:2179–2184
23. Long YY-Z, Chen Z, Duvail JL et al (2005) Micro- and nano-structured conducting polymeric materials. Prog Polym Sci 35:1673
24. Deng J, He C, Peng Y et al (2003) Magnetic and conductive Fe_3O_4-polyaniline nanoparticles with core–shell structure. Synth Met 139:295–301
25. Phang SW, Kuramoto N (2010) Microwave absorption property of polyaniline nanocomposites containing TiO_2 and Fe_3O_4 nanoparticles after FeCl $36H_2O$ treatment. Polym Compos 31:516–523
26. Jacobo SE, Aphesteguy JC, Lopez Anton R et al (2007) Influence of the preparation procedure on the properties of polyaniline based magnetic composites. Eur Polym J 43:1333–1346
27. Zhang Z, Wan M (2003) Nanostructures of polyaniline composites containing nano-magnet. Synth Met 132:205–212
28. Kong L, Lu X, Jin E et al (2009) Constructingmagneticpolyaniline metalhybridnanostructuresusing.pdf. J Solid State Chem 182:2081–2087

29. Della Pina C, Rossi M, Ferretti AM et al (2012) One-pot synthesis of polyaniline/Fe_3O_4 nanocomposites with magnetic and conductive behaviour. Catalytic effect of Fe_3O_4 nanoparticles. Synth Met 162:2250–2258
30. Park M, Cheng J, Choi J et al (2013) Electromagnetic nanocomposite of bacterial cellulose using magnetite nanoclusters and polyaniline. Colloids Surf B Biointerfaces 102:238–242
31. Mahto TK, Chowdhuri AR, Sahu SK (2014) Polyaniline-functionalized magnetic nanoparticles for the removal of toxic dye from wastewater. J Appl Polym Sci 131:40840
32. Prasanna GD, Jayanna HS, Lamani AR, Dash S (2011) Polyaniline/$CoFe_2O_4$ nanocomposites: a novel synthesis, characterization and magnetic properties. Synth Met 161:2306–2311
33. Della C, Maria A, Ponti A, Falletta E (2015) A green approach to magnetically-hard electrically-conducting polyaniline/ $CoFe_2O_4$ nanocomposites. Compos Sci Technol 110:138–144
34. Guo C, Zhou L, Lv J (2013) Effects of expandable graphite and modified ammonium polyphosphate on the flame-retardant and mechanical properties of wood flour-polypropylene composites. Polym Polym Compos 21:449–456
35. Khairy M (2014) Synthesis, characterization, magnetic and electrical properties of polyaniline/$NiFe_2O_4$ nanocomposite. Synth Met 189:34–41
36. Xie Y, Hong X, Wang X et al (2012) Preparation and electromagnetic properties of La-doped barium-ferrite/polythiophene composites. Synth Met 162:1643–1647
37. Jiang J, Ai LH, Bin Qin D et al (2009) Preparation and characterization of electromagnetic functionalized polyaniline/$BaFe_{12}O_{19}$ composites. Synth Met 159:695–699
38. Wan M, Fan J (1998) Synthesis and ferromagnetic properties of composites of a water-soluble polyaniline copolymer. J Polym Sci 36:13–16
39. Dhawan SK, Singh K, Bakhshi AK, Ohlan A (2009) Conducting polymer embedded with nanoferrite and titanium dioxide nanoparticles for microwave absorption. Synth Met 159:2259–2262
40. Singh K, Ohlan A, Kotnala RK et al (2008) Dielectric and magnetic properties of conducting ferromagnetic composite of polyaniline with γ-Fe_2O_3 nanoparticles. Mater Chem Phys 112:651–658
41. Nghia ND, Tung NT (2009) Study on synthesis and anticorrosion properties of polymer nanocomposites based on super paramagnetic $Fe_2O_3{\cdot}NiO$ nanoparticle and polyaniline. Synth Met 159:831–834
42. Ai LH, Jiang J (2009) Facile synthesis and characterization of magnetic NiCr ferrospinel embedded in conducting polymer. J Alloys Compd 487:735–738
43. Paterno LG, Fonseca FJ, Alcantara GB et al (2009) Fabrication and characterization of nanostructured conducting polymer films containing magnetic nanoparticles. Thin Solid Films 517:1753–1758
44. Reddy KR, Lee K-P, Gopalan AI et al (2007) Synthesis and properties of magnetite/poly (aniline-co-8-amino-2-naphthalenesulfonic acid) (SPAN) nanocomposites Kakarla. Polym Adv Technol 18:38–43
45. Nanocomposites P, Poddar A, Mukherjee S et al (2011) Electrical transport and magnetic properties of pedot-ferrite nanocomposites. Polym Compos 32:629–638
46. Reddy KR, Park W, Sin BC et al (2009) Synthesis of electrically conductive and superparamagnetic monodispersed iron oxide-conjugated polymer composite nanoparticles by in situ chemical oxidative polymerization. J Colloid Interface Sci 335:34–39
47. Tung TT, Feller JF, Kim T et al (2012) Electromagnetic properties of Fe 3O 4-functionalized graphene and its composites with a conducting polymer. J Polym Sci, Part A: Polym Chem 50:927–935
48. Taccola S, Greco F, Zucca A et al (2013) Characterization of free-standing PEDOT:PSS/iron oxide nanoparticle composite thin films and application as conformable humidity sensors. ACS Appl Mater Interfaces 5:6324–6332
49. Liu P-B, Huang Y, Sun X (2013) Excellent electromagnetic absorption properties of poly (3,4-ethylenedioxythiophene)-reduced graphene oxide-Co_3O_4 composites prepared by a hydrothermal method. ACS Appl Mater Interfaces 5:12355–12360

50. Akman O, Kavas H, Baykal A et al (2013) Magnetic metal nanoparticles coated polyacrylonitrile textiles as microwave absorber. J Magn Magn Mater 327:151–158
51. Li L, Xiang C, Liang X, Hao B (2010) Zn0.6Cu0.4Cr0.5Fe1.46Sm0.04O4 ferrite and its nanocomposites with polyaniline and polypyrrole: preparation and electromagnetic properties. Synth Met 160:28–34
52. Khafagy RM (2011) Synthesis, characterization, magnetic and electrical properties of the novel conductive and magnetic polyaniline/$MgFe_2O_4$ nanocomposite having the core–shell structure. J Alloys Compd 509:9849–9857
53. Cabrera L, Gutierrez S, Morales MP et al (2009) Magnetic conducting composites based on polypyrrol and iron oxide nanoparticles synthesized via electrochemistry. J Magn Magn Mater 321:2115–2120
54. Sadki S, Schottland P, Brodie N, Sabouraud G (2000) The mechanisms of pyrrole electropolymerization. Chem Soc Rev 29:283–293
55. Genies EM, Bidan G, Diaz AF (1983) Spectroelectrochemical study of polypyrrole films. J Electroanal Chem Interfacial Electrochem 149:101–113
56. Lu AH, Salabas EL, Schüth F (2007) Magnetic nanoparticles: synthesis, protection, functionalization, and application. Angew Chem Int Ed 46:1222–1244
57. Massart R (1981) Preparation of aqueous magnetic liquids in alkaline and acidic media. IEEE Trans Magn 17:1247–1248
58. Cabrera L, Gutierrez S, Menendez N et al (2008) Magnetite nanoparticles: electrochemical synthesis and characterization. Electrochim Acta 53:3436–3441
59. Mazarío E, Herrasti P, Morales MP, Menéndez N (2012) Synthesis and characterization of CoFe 2O 4 ferrite nanoparticles obtained by an electrochemical method. Nanotechnology 23:355708
60. Mazarío E, Sánchez-Marcos J, Menéndez N et al (2015) High specific absorption rate and transverse relaxivity effects in manganese ferrite nanoparticles obtained by an electrochemical route. J Phys Chem C 119:6828–6834
61. Basavaraja C, Jo EA, Huh DS (2010) Characterization and magnetic properties of conducting poly(N-vinylcarbazole)-capped magnetite nanocomposite Langmuir–Schaefer films. Mater Lett 64:762–764
62. Kavas H, Durmus Z, Baykal A et al (2010) Synthesis and conductivity evaluation of PVTri-Fe_3O_4 nanocomposite. J Non Cryst Solids 356:484–489
63. Zhu YG, Li ZQ, Gu JJ et al (2006) Polyaniline/iron nanocomposites prepared by cryomilling. J Polym Sci, Part B: Polym Phys 44:3157–3164
64. Zhu Y, Li Z, Zhang D (2008) Electromagnetic nanocomposites prepared by cryomilling of polyaniline and Fe nanoparticles. J Polym Sci, Part B: Polym Phys 46:1571–1576
65. Shiina I, Mukaiyama T (1994) A novel method for the preparation of macrolides. Chem Lett 6:677–680
66. Meixiang W, Wenguang L (1997) A composite of polyaniline with both conducting and ferromagnetic functions. J Polym Sci Part A 35:2129–2136
67. Barbosa EF, Molina FJ, Lopes FM et al (2012) Immobilization of Peroxidase onto magnetite modified polyaniline. Sci World J 2012:1–5
68. Jiang J, Ai LH, Liu AH (2010) A novel poly(o-anisidine)/$CoFe_2O_4$ multifunctional nanocomposite: preparation, characterization and properties. Synth Met 160:333–336
69. Dey A, De A, De SK (2005) Electrical transport and dielectric relaxation in Fe_3O_4–polypyrrole hybrid nanocomposites. J Phys: Condens Matter 17:5895–5910
70. Turcu R, Pana O, Nan A et al (2008) Polypyrrole coated magnetite nanoparticles from water based nanofluids. J Phys D Appl Phys 41:245002
71. Resta IM, Horwitz G, Elizalde MLM et al (2013) Magnetic and conducting properties of composites of conducting polymers and ferrite nanoparticles. IEEE Trans Magn 49:4598–4601
72. Xiaotun Y, Lingge X, Choon NS, Hardy CSO (2003) Magnetic and electrical properties of polypyrrole-coated -Fe_2O_3 nanocomposite particles. Nanotechnology 14:624–629

73. De Oliveira HP, Andrade CAS, de Melo CP (2008) Electrical impedance spectroscopy investigation of surfactant-magnetite-polypyrrole particles. J Colloid Interface Sci 319:441–449
74. Shen W, Shi M, Wang M, Chen H (2010) A simple synthesis of Fe_3O_4 nanoclusters and their electromagnetic nanocomposites with polyaniline. Mater Chem Phys 122:588–594
75. Ramesan MT (2013) Synthesis and characterization of magnetoelectric nanomaterial composed of Fe_3O_4 and polyindole. Adv Polym Technol 32:21362
76. Varshney S, Ohlan A, Jain VK et al (2014) Synthesis of ferrofluid based nanoarchitectured polypyrrole composites and its application for electromagnetic shielding. Mater Chem Phys 143:806–813
77. Wuang SC, Neoh KG, Kang E-T et al (2007) Synthesis and functionalization of polypyrrole-Fe_3O_4 nanoparticles for applications in biomedicine. J Mater Chem 17:3354
78. Chen A, Wang H, Zhao B, Li X (2003) The preparation of polypyrrole-Fe_3O_4 nanocomposites by the use of common ion effect. Synth Met 139:411–415
79. Long Y-Z, Li M-M, Gu C et al (2011) Recent advances in synthesis, physical properties and applications of conducting polymer nanotubes and nanofibers. Prog Polym Sci 36:1415–1442
80. Csaba J, Csaba V, Ottó B, Etelka T (2009) Conducting polymer-based electrode with magnetic behavior: electrochemical synthesis of poly(3-thiophene-acetic-acid)/magnetite nanocomposite thin layers. J Phys Chem C 113:1352–1358
81. Janáky C, Kormányos A, Visy C (2011) Magnetic hybrid modified electrodes, based on magnetite nanoparticle containing polyaniline and poly (3,4-ethylenedioxythiophene). J Solid State Electrochem 15:2351–2359
82. Yang S, Liu D, Liao F et al (2012) Synthesis, characterization, morphology control of poly (*p*-phenylenediamine)-Fe_3O_4 magnetic micro-composite and their application for the removal of Cr_2O_{72}—from water. Synth Met 162:2329–2336
83. Frey NA, Peng S, Cheng K, Sun S (2009) Magnetic nanoparticles: synthesis, functionalization, and applications in bioimaging and magnetic energy storage. Chem Soc Rev 38:2532–2542
84. Bedanta S, Kleemann W (2008) Supermagnetism. J Phys D Appl Phys 42:013001
85. Frey NA, Peng S, Cheng K, Sun S (2009) Magnetic nanoparticles: synthesis, functionalization, and applications in bioimaging and magnetic energy storage. Chem Soc Rev 38:2532–2542
86. Meiklejohn WH, Bean CP (1957) New magnetic anisotropy. Phys Rev 105:904–913
87. Chiang CK, Druy MA, Gau SC et al (1978) Synthesis of highly conducting films of derivatives of polyacetylene, (CH)x. J Am Chem Soc 100:1013–1015
88. Shirakawa H, Macdiarmaid AG, Chiang CK (1977) Electrical conductivity in doped polacetylene. Phys Rev Lett 39:1098–1101
89. Heeger AJ (2010) Semiconducting polymers: the third generation. Chem Soc Rev 39:2354–2371
90. Heeger AJ (2001) Nobel lecture: simuconducting and metallic polymers: the fourth generation of polymeric materials. Rev Mod Phys 73:681
91. Bredas J, Street G (1985) Polarons, bipolarons, and solitons in conducting polymers. Acc Chem Res 1305:309–315
92. Pillalamarri SK, Blum FD, Tokuhiro AT, Bertino MF (2005) One-pot synthesis of polyaniline-metal nanocomposites. Chem Mater 17:5941–5944
93. Reddy KR, Sin BC, Ryu KS et al (2009) Conducting polymer functionalized multi-walled carbon nanotubes with noble metal nanoparticles: synthesis, morphological characteristics and electrical properties. Synth Met 159:595–603
94. Negi YS, Adhyapak PV (2002) Development in polyaniline conducting polymers. J Macromol Sci Part C Polym Rev 42:35–53
95. Huang J (2006) Syntheses and applications of conducting polymer polyaniline nanofibers. Pure Appl Chem 78:15–27

96. Bhadra S, Khastgir D, Singha NK, Lee JH (2009) Progress in preparation, processing and applications of polyaniline. Prog Polym Sci 34:783–810
97. Li S, Zhang G, Jing G, Kan J (2008) Aqueous zinc–polyaniline secondary battery. Synth Met 158:242–245
98. Dhand C, Das M, Datta M, Malhotra BD (2011) Recent advances in polyaniline based biosensors. Biosens Bioelectron 26:2811–2821
99. Zhong H, Yuan R, Chai Y et al (2011) In situ chemo-synthesized multi-wall carbon nanotube-conductive polyaniline nanocomposites: characterization and application for a glucose amperometric biosensor. Talanta 85:104–111
100. Karim MR, Lee CJ, Lee MS (2006) Synthesis and characterization of conducting polythiophene/carbon nanotubes composites. J Polym Sci, Part A: Polym Chem 44:5283–5290
101. Green RA, Lovell NH, Wallace GG, Poole-Warren LA (2008) Conducting polymers for neural interfaces: challenges in developing an effective long-term implant. Biomaterials 29:3393–3399
102. Rozlosnik N (2009) New directions in medical biosensors employing poly (3,4-ethylenedioxy thiophene) derivative-based electrodes. Anal Bioanal Chem 395:637–645
103. Bertran O, Armelin E, Estrany F et al (2010) Poly(2-thiophen-3-yl-malonic acid), a polythiophene with two carboxylic acids per repeating unit. J Phys Chem B 114:6281–6290
104. Cao J, Hu G, Peng Z et al (2015) Polypyrrole-coated $LiCoO_2$ nanocomposite with enhanced electrochemical properties at high voltage for lithium-ion batteries. J Power Sources 281:49–55
105. Wang W-Y, Ting P-N, Luo S-H, Lin J-Y (2014) Pulse-reversal electropolymerization of polypyrrole on functionalized carbon nanotubes as composite counter electrodes in dye-sensitized solar cells. Electrochim Acta 137:721–727
106. Herrasti P, del Rio AI, Recio J (2007) Electrodeposition of homogeneous and adherent polypyrrole on copper for corrosion protection. Electrochim Acta 52:6496–6501
107. Ayenimo JG, Adeloju SB (2015) Inhibitive potentiometric detection of trace metals with ultrathin polypyrrole glucose oxidase biosensor. Talanta 137:62–70
108. Mohamed MB, Karimat EL-S (2014) Structural, magnetic and dielectric properties of (PANI)–Ni0.5Zn0.5Fe1.5Cr0.5O4 nanocomposite. Compos Part B Eng 56:270–278
109. Pana O, Soran ML, Leostean C et al (2012) Interface charge transfer in polypyrrole coated perovskite manganite magnetic nanoparticles. J Appl Phys 111:044309
110. Antonel PS, Berhó FM, Jorge G, Molina FV (2015) Magnetic composites of $CoFe_2O_4$ nanoparticles in a poly(aniline) matrix: enhancement of remanence ratio and coercivity. Synth Met 199:292–302
111. Sharma R, Malik R, Lamba S, Annapoorni S (2008) Metal oxide/polyaniline nanocomposites: cluster size and composition dependent structural and magnetic properties. Bull Mater Sci 31:409–413
112. Sharma R, Lamba S, Annapoorni S (2004) Magnetic properties of polypyrrole-coated iron oxide nanoparticles. J Phys D Appl Phys 38:11
113. Khairy M (2014) Polyaniline-Zn0.2Mn0.8 Fe_2O_4 ferrite core–shell composite: preparation, characterization and properties. J Alloys Compd 608:283–291
114. Khan JA, Qasim M, Singh BR et al (2013) Synthesis and characterization of structural, optical, thermal and dielectric properties of polyaniline/$CoFe_2O_4$ nanocomposites with special reference to photocatalytic activity. Spectrochim Acta Part A Mol Biomol Spectrosc 109:313–321
115. Qiu G, Wang Q, Nie M (2006) Polypyrrole-Fe_3O_4 magnetic nanocomposite prepared by ultrasonic irradiation. Macromol Mater Eng 291:68–74
116. Song X, Gong H, Yin S et al (2014) Ultra-small iron oxide doped polypyrrole nanoparticles for in vivo multimodal imaging guided Photothermal therapy. Adv Funct Mater 24:1194–1201

117. Xiao H-M, Fu S-Y (2014) Synthesis and physical properties of electromagnetic polypyrrole composites via addition of magnetic crystals. CrystEngComm 16:2097–2112
118. Zhang CS, Ni QQ, Fu SY, Kurashiki K (2007) Electromagnetic interference shielding effect of nanocomposites with carbon nanotube and shape memory polymer. Compos Sci Technol 67:2973–2980
119. Saini P, Choudhary V, Singh BP et al (2011) Enhanced microwave absorption behavior of polyaniline-CNT/polystyrene blend. Synth Met 161:1522–1526
120. Ohlan A, Singh K, Chandra A, Dhawan SK (2010) Microwave absorption behavior of core–Shell structured poly (3,4-ethylenedioxy thiophene)–barium ferrite nanocomposites. ACS Appl Mater Interfaces 2:927–933
121. Ohlan A, Singh K, Chandra A, Dhawan SK (2008) Microwave absorption properties of conducting polymer composite with barium ferrite nanoparticles in 12.4–18 GHz. Appl Phys Lett 93:053114
122. Varshney S, Singh K, Ohlan A et al (2012) Synthesis, characterization and surface properties of Fe_2O_3 decorated ferromagnetic polypyrrole nanocomposites. J Alloys Compd 538:107–114
123. Wang H, Ma N, Yan Z et al (2015) Cobalt/polypyrrole nanocomposites with controllable electromagnetic properties. Nanoscale 7:7189–7196
124. Singh K, Ohlan A, Bakhshi AK, Dhawan SK (2010) Synthesis of conducting ferromagnetic nanocomposite with improved microwave absorption properties. Mater Chem Phys 119:201–207
125. Liu P, Huang Y, Zhang X (2015) Preparation and excellent microwave absorption properties of ferromagnetic graphene/poly(3, 4-ethylenedioxythiophene)/$CoFe_2O_4$ nanocomposites. Powder Technol 276:112–117
126. Wang K, Yi C, Hu X et al (2014) Enhanced performance of polymer solar cells using PEDOT:PSS doped with Fe_3O_4 magnetic nanoparticles aligned by an external magnetostatic field as an anode buffer layer. ACS Appl Mater Interfaces 6:13201–13208
127. Wang K, Ren H, Yi C et al (2013) Solution-processed Fe_3O_4 magnetic nanoparticle thin film aligned by an external magnetostatic field as a hole extraction layer for polymer solar cells. ACS Appl Mater Interfaces 5:10325–10330
128. Zhang W, Xu Y, Wang H et al (2011) Fe_3O_4 nanoparticles induced magnetic field effect on efficiency enhancement of P3HT:PCBM bulk heterojunction polymer solar cells. Sol Energy Mater Sol Cells 95:2880–2885
129. Shahnavaz Z, Lorestani F, Alias Y, Woi PM (2014) Polypyrrole–$ZnFe_2O_4$ magnetic nano-composite with core–shell structure for glucose sensing. Appl Surf Sci 317:622–629
130. Yang Z, Zhang C, Zhang J, Bai W (2014) Potentiometric glucose biosensor based on core–shell Fe_3O_4-enzyme-polypyrrole nanoparticles. Biosens Bioelectron 51:268–273
131. Yang Z, Shang X, Zhang C, Zhu J (2014) Photoelectrochemical bilirubin biosensor based on Fe3O 4/hydroxyapatite/molecularly imprinted polypyrrole nanoparticles. Sens Actuators, B Chem 201:167–172
132. Baghayeri M, Nazarzadeh Zare E, Mansour Lakouraj M (2014) A simple hydrogen peroxide biosensor based on a novel electro-magnetic poly(*p*-phenylenediamine)@Fe_3O_4 nanocomposite. Biosens Bioelectron 55:259–265
133. Suresh R, Giribabu K, Manigandan R et al (2014) Fe_2O_3@polyaniline nanocomposite: characterization and unusual sensing property. Mater Lett 128:369–372
134. Suri K, Annapoorni S, Sarkar AK, Tandon RP (2002) Gas and humidity sensors based on iron oxide-polypyrrole nanocomposites. Sens Actuators B Chem 81:277–282
135. Tandon RP, Tripathy MR, Arora AK, Hotchandani S (2006) Gas and humidity response of iron oxide—Polypyrrole nanocomposites. Sens Actuators B Chem 114:768–773

Polypyrrole Nanotubes-Silver Nanoparticles Hybrid Nanocomposites: Dielectric, Optical, Antimicrobial and Haemolysis Activity Study

J. Upadhyay and A. Kumar

Abstract In recent times, organic conducting polymers such as polypyrrole (PPy), polyaniline (PAni) and polythiophene (PTh) based hybrid nanocomposites have attracted the immense attention of the researchers worldwide due to their potential technological applications. Owing to their high thermal stability, redox activity, and electrical conductivity, conducting polymer nanostructures are used to entrap metal or metal oxide nanoparticles and carbon-based nanostructured materials. The hybrid nanocomposites overcome the poor processability of the metal or metal oxide nanoparticles. By combining the excellent electrical, optical and biological properties of different nanostructures with good thermal stability, biocompatibility and dielectric properties of conducting polymer nanostructures, the hybrid nanocomposites are unique multifunctional materials for varied applications in microelectronics, sensing, biotechnology, energy storage, etc. Among the conducting polymers, PPy nanostructures are gaining intensive attention due to their remarkable properties such as good environmental stability, redox activity and low toxicity and are excellent host material for metal/metal-oxide nanoparticles. Similarly, silver nanoparticles are of immense interest because of their excellent electrical, surface plasmon absorption and biocidal activity. The present chapter deals with synthesis, characterization, properties and applications of the conducting polymer nanostructures with metal/metal-oxide nanoparticles, carbon nanomaterial and ternary nanocomposites in general and polypyrrole nanotubes-silver nanoparticles hybrid nanocomposites, in particular. The different synthesis approaches of these hybrid nanomaterials with their application on the diverse field have been presented. Moreover, the chapter gives a glimpse of possible future work in this particular area. In the second part of this chapter, the dielectric, optical, antimicrobial and haemolysis activity of polypyrrole nanotubes (PPy-NTs): silver nanoparticles (Ag-NPs) hybrid nanocomposites synthesized by in situ reduction method in our laboratory will be discussed. PPy-NTs synthesized by reactive template method are used as the matrix as well as a capping agent for Ag-NPs synthesized by in situ reduction of silver nitrate. The formation of hybrid nanocomposites is revealed by

J. Upadhyay · A. Kumar (✉)
Department of Physics, Tezpur University, Napaam, Tezpur, Assam 784028, India
e-mail: ask@tezu.ernet.in

V. Kumar et al. (eds.), *Conducting Polymer Hybrids*,
Springer Series on Polymer and Composite Materials,
DOI 10.1007/978-3-319-46458-9_3

X-ray diffraction (XRD), scanning electron microscopy (SEM) and high-resolution transmission electron microscopy (HRTEM). The dielectric properties and ac conductivity with varying Ag-NPs loading is analyzed. Maximum conductivity of the order of 1.6×10^{-3} S/cm has been achieved with 15 wt% of Ag-NPs. The effect of Ag-NPs concentration on antimicrobial activity of the nanocomposites is investigated by Kirby–Bauer method. It is observed that the bactericidal performance of the nanocomposites increases with the concentration of Ag-NPs in the nanocomposites. Maximum zone of inhibition is measured around 23 mm with 15 wt% of Ag-NPs against gram negative (*Escherichia coli*) and gram-positive (*Staphylococcus aureus*) bacteria. The lowest minimum inhibitory concentration (MIC) values are determined as 0.078 and 0.15625 mg/ml for the nanocomposites having 15 wt% of Ag-NPs against *E. coli* and *S. aureus*, respectively. Haemolysis activity of the nanocomposites is carried out with mammalian red blood cell (RBC). All the nanocomposites exhibit haemolysis below the permissible limit of 5 % up to a concentration of 2.5 mg/mL.

Keywords Conducting polymers · Hybrid nanocomposites · Polypyrrole nanotubes-silver nanoparticles nanocomposites · Dielectric spectra · Antimicrobial activity · Haemolysis activity

1 Introduction

Hybrid nanocomposites involve a combination of two or more different functional components at the nano level, which results in material attaining unique properties, outperforming mere addition of the properties of individual components. In recent times, fabrication of inorganic–organic hybrid nanomaterials have been receiving significant importance due to their combined physicochemical properties and potential applications in the areas of supercapacitors, biotechnology, photonics, nanotechnology, etc. [1–3]. The favorable combination of properties of a nanocomposite mainly depends on their structures, compositions, synthesis conditions and dispersity [3]. The dispersed phase plays a critical role to enhance the different properties of the hybrid nanocomposites.

Conducting polymers are unique materials having alternating double and single conjugated sp^2 hybridized carbon atoms along their backbone. Among the conducting polymer based systems polypyrrole (PPy), polyaniline (PAni), polythiophene (PTh) and their derivatives based hybrid nanocomposites are of primary research interest because of the unique properties. Intrinsic conducting polymers which are also known as "synthetic metals" have been subjected to intensive investigation due to their dielectric, electrical, electronic, magnetic and optical properties analogous to that of metals or semiconductors while retaining advantages of polymer-like properties such as flexibility, ease of processing and low toxicity in biological environments [4]. These features along with chemical sensitivity, room temperature operation, and tuneable charge transport property have launched

conducting polymers as transducers in different applications. The modifiable redox activity, high electrical conductivity, and biocompatibility of conducting polymers established these materials in biosensing, tissue engineering and also in antioxidant and antimicrobial applications [5, 6]. Also, the controlled incorporation of nanostructures (mainly nanoparticles) of metal or metal oxides and carbon nanomaterials within conducting polymer matrix has become the high priority field of scientific research to develop novel multifunctional hybrid nanomaterials possessing serendipitous properties. The integration of these nano counterparts within conducting polymers not only improves the properties like thermal stability, mechanical strength, electrical conductivity, optical property, bioactivity and charge storing capability of the nanocomposites but also conducting polymers provide stability to the incorporated metal or metal oxides nanoparticles enhancing their reusability and functionality [7, 8]. Moreover, conducting polymers shield metal or metal oxide nanoparticles from their air or moisture sensitivity as bare nanoparticles are chemically highly active. Conducting polymers also prevent the agglomeration of these nanostructures as they are likely to agglomerate owing to their high surface energy [9]. The incorporation of magnetic or metal (like silver) nanoparticles increases the bioactivity of conducting polymer-based hybrid nanocomposites. For instance, conducting polymer silver nanocomposites have shown potential in biosensing due to their improved electron activity and high electron transfer kinetics and also exhibit enhanced antimicrobial activity because of the excellent bactericidal activity of nanosilver [10]. Integration of bio-functionalized magnetic nanoparticles within conducting polymer matrix yields the biocomposites with relevant features for biomedical applications. Nanocomposites of conducting polymers with carbon nanotubes and graphene have also been recently explored for possible applications in supercapacitors, biosensing and light emitting diodes [11–13].

Among the conducting polymers, polypyrrole is one of the most promising owing to its attractive properties such as high conductivity, excellent redox activity, easy processability, good thermal and electrochemical stability, low toxicity to the biological ambience, etc. The molecular structure of PPy in neutral, polaron and bipolaron states is presented in Fig. 1. The non-conducting state of PPy is an aromatic structure in the reduced state. During oxidative doping of PPy, it exhibits polaron and bipolaron states depending upon doping concentration. The formation of polaron creates new energy levels within the bandgap located about 0.5 eV away from the band edge in case of PPy while the bipolaron levels are found at 0.75 eV from the band edge in PPy [14, 15]. Upon continuous doping, the merging of bipolaron levels results in the formation of bipolaron bands. Upon heavy doping, upper and lower bipolaron bands merge with conduction and valence bands, respectively giving metal-like conductivity in PPy. Both the polaron and bipolaron states of PPy are in oxidized form with the bipolaron state having better conductivity than that of the polaron state. The existence of both the polaron and bipolaron states simultaneously is also possible, and the conductivity of PPy depends on the percentage of the polaron and bipolaron states [16] (Fig. 2).

PPy can be synthesized from pyrrole monomer by using chemical and electrochemical techniques. The chemical approaches that are used to synthesis PPy are

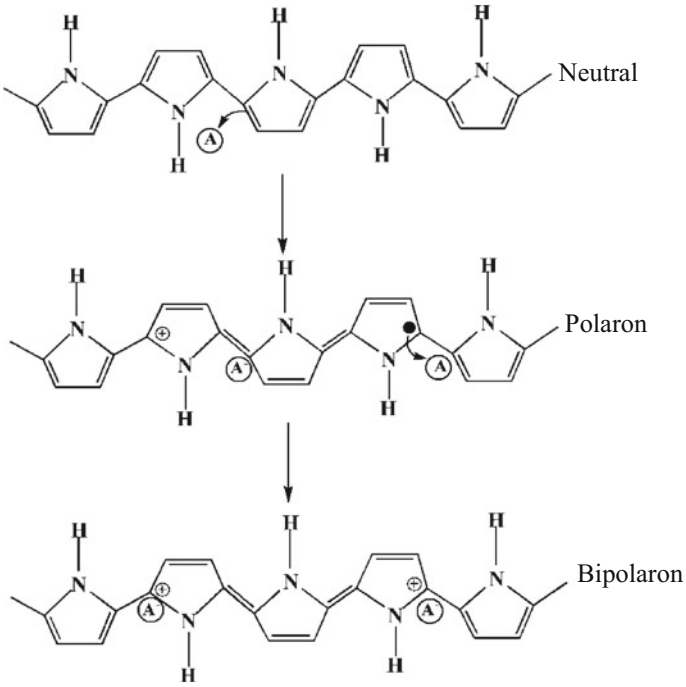

Fig. 1 Neutral, polaron and bipolaron states of Polypyrrole (Reprinted from Ref. [14] with permission from RSC)

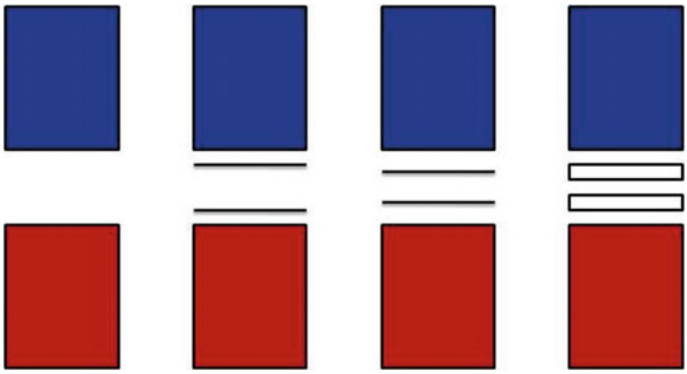

Fig. 2 Band diagram of (i) neutral, (ii) polaron, (iii) bipolaron and (iv) bipolaron band formation in PPy (Reprinted from Ref. [14] with permission from RSC)

hard chemical template method [17], soft chemical template method [18], reactive template method, etc. [19]. The hard chemical template is an effective way to synthesize polymer micro/nanotubes and wires with controlled diameter and length

by using a template membrane to guide the growth. A post-synthesis step is required to remove the template, which may drastically alter or even destroy the synthesized nanostructures. Soft template method is relatively simple and cheap method to synthesize conducting polymer nanostructures and also known as the template free or self-assembly method. This method employs some structure directing molecule such as a surfactant, which forms micelles and confines the polymerization of monomer into low dimensions. In reactive template method, the template not only directs the growth of conducting polymer nanostructures but also initiates the polymerization process of monomers by the oxidative reaction. This is a simple and one step method as most of the reactive template can be converted to soluble ions in the redox reaction. On the other hand, electrochemical synthesis of PPy is usually done in an electrochemical cell having three electrodes viz.; working, reference, and counter electrodes. In this process, the monomer is dissolved in an appropriate solvent and is polymerized on the surface of the electrode. Polymerization can be carried out in a different way for instance (i) constant current, i.e., galvanostatic, (ii) constant potential, i.e., potentiostat or (iii) potential scanning/cycling and sweeping methods, where the deposition is done by continuous cycling between the predetermined potential [20]. In addition to the above-mentioned processes, PPy nano or microfibers can be synthesized by using electrospinning technique [21]. In addition to different nanostructures of PPy, nanocomposites of PPy with various materials such as metal or metal oxide nanoparticles, carbon nanotubes, graphene and ternary nanocomposites have also been reported, where some specific nature of the association between the two or more components has been observed. These nanocomposites of PPy have been synthesized using different processes such as one-pot synthesis, in situ synthesis, interfacial polymerization, electrochemical polymerization, vapour phase polymerization, etc. discussed in Sect. 2. The schematic of the synthesis of PPy nanostructures by different procedures is presented in Fig. 3.

PPy has been considered for different applications in several fields. The nanostructures of PPy have been used in chemical and electrochemical sensors because the electrical property of PPy can be tuned by the doping–dedoping process [22]. Doped PPy has been found to exhibit microwave absorption property. Nanostructures of PPy have interesting applications in solar cell, electromagnetic interferences shielding devices [23]. PPy is also beneficial in energy storage devices such as supercapacitors due to its high specific capacitance [24]. Recently lots of biomedical applications such as tissue engineering, drug delivery, biosensor, the antioxidant and antimicrobial property of conducting PPy have been explored because of its low toxicity, high conductivity and excellent redox active property [25–27].

This chapter presents an overview of synthesis of conducting polymer-based hybrid nanocomposites with their properties and applications in different fields mainly emphasizing on PPy based materials. Band structure of PPy with various synthesis process of PPy based nanostructures and nanocomposites have been highlighted. Different approaches involving incorporation of metal or metal oxide nanoparticles and carbon-based nanostructures within conducting polymer matrix

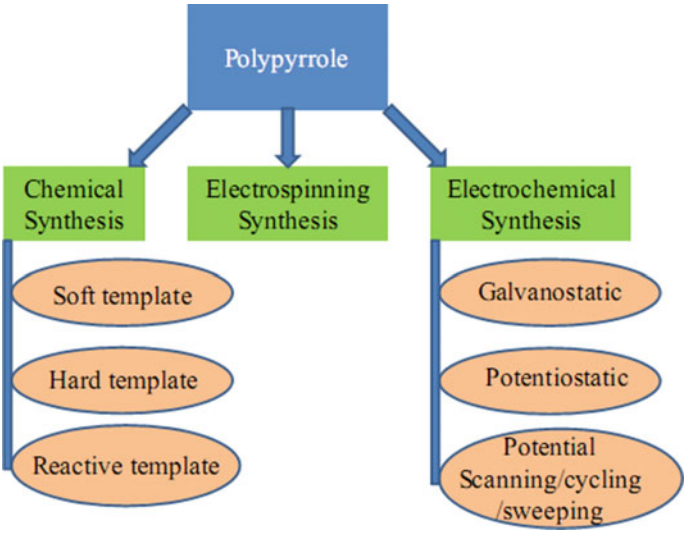

Fig. 3 Schematic of different synthesis processes of PPy

with their advantages and disadvantages have also been presented. The current status and possible future work in the field of conducting polymer based hybrids have also been included in this chapter. Further, this chapter deals with polypyrrole nanotubes (PPy-NTs)-silver nanoparticles (Ag-NPs) hybrid nanocomposites synthesized by in situ reduction method in our laboratory. The dielectric, optical, antimicrobial and haemolysis activity characterizations of the hybrid nanocomposites have been discussed in detail.

2 Present Status and Future Prospects of Conducting Polymer-based Hybrid Nanocomposites

Nanocomposites of conducting polymers exhibit improved physicochemical and biological properties as compared to their individual counterparts. The integration of secondary component within conducting polymer leads to dramatic increase in different properties that are useful from an application point of view. Size, shape and controlled distribution of the dispersed phase are the critical factors to control the desired properties of a nanocomposite. Different approaches such as in situ synthesis, one-pot synthesis, electrochemical polymerization and vapor-phase polymerization have been employed to synthesize the nanocomposites of conducting polymers with metal or metal oxide nanoparticles, carbon-based materials, ternary nanocomposites, etc. All of these methods have certain advantages and drawbacks. Functional nanocomposites synthesized by these methods display many

intriguing properties that have been extensively explored for their application in electronic nanodevices, chemical, and biological sensors, energy devices, microwave absorption, EMI shielding, and biomedicine.

Though a lot of development in the field of conducting polymer based nanocomposites is going on and different synthesis approaches have been developed, still the primary challenge is to control the morphology (shape, size, and distribution) of nanocomposites. By controlling the morphology of nanocomposites, we can control different properties and reach up to desired application of nanocomposites. Therefore, future work should concentrate on the development of synthesis method for conducting polymer-based hybrid nanocomposites with control parameters and morphology. Furthermore, a lot of work is going on to increase the charge storage capacity, power density and cycle life of conducting polymer based nanocomposites but is not up to the mark of practical application. So, work could be done in this particular field to improve the different deciding factors of supercapacitors by synthesizing nanocomposites of conducting polymers with different materials. Another exciting field of conducting polymer based nanocomposites is sensors, where a lot of possible future work could be done to improve the sensitivity, selectivity and reduce the toxicity against biomolecules. In biomedical applications, conducting polymer-based nanocomposites provide an excellent opportunity for the neural probe, nerve regeneration, artificial muscle and antimicrobial applications. Many efforts are, however, required to commercialize these exotic nanocomposite materials and to bring them to the market.

3 Conducting Polymer-Based Hybrid Nanocomposites

Incorporation of an inorganic secondary component into the matrix of conducting polymers is a useful approach to improve the functionality of conducting polymer-based nanocomposites. Nanoparticles of metal or metal oxide and other nanostructures such as graphene, carbon nanotubes (CNT) are used as dispersoid within conducting polymer matrix depending on the requirements. The shape, size, aspect ratio and the interfacial adhesion between the matrix and dispersoid affect the properties of the hybrid nanocomposites [28]. The synthesis, properties, and applications of different conducting polymer-based hybrid nanocomposites are discussed below.

3.1 Nanocomposites with Metal Nanoparticles

Metal nanoparticles are found to exhibit novel electronic, optical, chemical and biological properties differing from bulk form due to the quantum size effects.

These properties can be generated by controlling the shape, size and inter-particle spacing of metal nanoparticles [29]. Conducting polymers such as PAni, PPy, PTh and their derivatives have been employed to synthesize hybrid nanocomposites with different metal nanoparticles such as silver (Ag), gold (Au), and platinum (Pt) and the effects on optical, electronic, dielectric and biological properties have been investigated. Some of the developments in the field of conducting polymer–metal nanoparticles hybrid nanocomposites are summarized below.

Several chemical and electrochemical approaches have been employed to synthesize hybrid nanocomposites of conducting polymers with metal nanoparticles. In a one-pot approach, the monomer or polymer reduces the metal salts to form metal nanoparticles and intermediate purification is not required. In another method the metal nanoparticles are grown within the conducting polymer matrix or monomer is polymerized around metal nanoparticles [29]. In both the processes, the metal nanoparticles are capped by conducting polymers ensuring their enhanced stability and processability. Moreover, the interface of conducting polymer and metal nanostructures plays a critical role in determining the properties by the nanocomposites. Balamurugan et al. [30] have reported the synthesis of highly stable PEDOT silver nanoparticles–nanocomposites by the one-pot process. They used 3,4-ethylenedioxythiophene (EDOT) as a reducing agent and polystyrene sulfonate (PSS^-) as a dopant for PEDOT as well as particle stabilizer for silver nanoparticles (Ag-NPs). PPy-silver nanocomposites on cotton fabric using one-pot synthesis approach have been reported for antimicrobial applications. In the redox reaction between pyrrole and silver nitrate, silver ions oxidize pyrrole monomers, and at the same time, they get reduced and deposited as Ag-NPs resulting in PPy-silver nanocomposites [31]. Liu et al. [32] have reported the synthesis of PPy nanofiber network with a high loading of Cu and Ag nanoparticles by the one-pot method. One-pot fabrication of uniform PPy-gold nanocomposites has been reported for ammonia gas sensing [33]. In this method pyrrole was oxidized by ferric chloride and then $HAuCl_4$ was reduced in the same solution to ensure the formation of PPy-gold nanocomposites. Jiang et al. [34] reported the green one-pot synthesis of palladium-decorated PEDOT nanosphere and investigated them for biosensing applications [34].

As mentioned earlier in situ approach has also been used for the synthesis of conducting polymer–metal hybrid nanocomposites. Xu et al. [35] have reported the decoration of PPy nanotubes with gold nanoparticles by an in situ reduction process. They prepared PPy nanotubes by MO-$FeCl_3$ self-degrade template method and then reduced $HAuCl_4$ within PPy nanotubes in the presence of different surfactants such as sodium dodecyl sulfate (SDS), cetyltrimethylammonium bromide (CTAB) and Tween-80. Nanowires of silver PAni nanocomposites have been reported via in situ polymerization method [36]. In this method aniline is oxidized by ammonium persulfate (APS) in the presence of dodecylbenzene sulfonic acid (DBSA) and silver nitrate ($AgNO_3$). In another approach gold-PAni core–shell

nanocomposites have been synthesized by reducing aniline monomer on the surface of gold nanoparticles [37]. Silver nanoparticles embedded in PAni nanocomposites have been synthesized by in situ polymerization of aniline in the presence of silver nitrate as precursor [38]. The PEDOT:PSS-platinum nanoparticles films have been prepared for low-cost dye-sensitized solar cells by in situ generation of platinum (Pt) nanoparticles in the poly(3,4-ethylene dioxythiophene):poly(styrenesulfonate) (PEDOT:PSS) solution at room temperature [39]. They reported the formation of 20–40 nm diameter Pt-nanoparticles evenly dispersed in the conducting polymer matrix.

In addition to the chemical approaches, electrochemical methods have also been employed to synthesize conducting polymer–metal hybrid nanocomposites. Electrochemical methods are versatile for the synthesis of conducting polymer films and exhibit higher controllability as compared to the chemical methods. However, the quantity of the product is limited by the size of working electrode. A hybrid nanocomposite consisting of PEDOT and gold nanoparticles using electrochemical method has been reported by Hsiao et al. [40]. A thin layer of PEDOT is coated electrochemically on a bare screen-printed carbon electrode, and the nanosized gold nanoparticles are coated over it by electrochemical method resulting in PEDOT-gold nanoparticles nanocomposite film. Selective deposition of gold nanoparticles on top or inside thin conducting polymer film by a combination of electroless deposition and electrochemical reduction has been reported [41]. In situ homogeneously dispersed gold-PAni core–shell nanocomposite particles with controlled size on the highly oriented pyrolytic graphite (HOPG) are reported by Li et al. [42]. In this method, the HOPG surface is modified preferentially by covalent bonding of a two-dimensional 4-aminophenyl monolayer employing diazonium chemistry. $AuCl_4^-$ ions are attached to the Ar-NH_2 termination and reduced electrochemically and grown into gold nanoparticles. The formation of PAni as the shell wrap of Au nanoparticle has been carried out by localized electropolymerization method.

3.2 Nanocomposites with Metal–Oxide Nanoparticles

The fabrication of conducting polymer–metal oxide hybrid nanocomposites is an alluring aspect for the possible applications in sensors and energy storage devices. For intrinsic conducting polymers-metal oxides hybrid nanocomposites interface forms a heterojunction that can be very sensitive to analytes and is effective for sensor applications [43]. There are different chemical approaches used for the synthesis of conducting polymer–metal oxide nanocomposites. The synthesis of nanocomposites of PAni with TiO_2, Fe_2O_3, and Fe_3O_4, has been reported by an in situ process wherein the polymer is grown in the presence of pre-synthesized nanoparticles. Different properties of the nanocomposites such as morphology,

electrical and magnetic properties, hydrophobicity, etc. have been affected by the nanoparticles content [28]. The synthesis of PPy based nanocomposites with TiO_2, SnO_2, Fe_2O_3 Fe_3O_4 have also been reported by different groups using the in situ method. In this process pyrrole is polymerized in the presence of the pre-synthesized metal–oxide nanoparticles resulting in the synthesis of polypyrrole-metal oxide hybrid nanocomposites [44–47].

Analogous to that of conducting polymer–metal nanocomposites one-pot synthesis process is also followed for conducting polymer–metal oxide nanocomposites. Zeng et al. followed a simultaneous reaction process in which the generation of metal oxide layers, the oxidation polymerization of monomers, and the in situ formation of polymer–metal oxides sandwich structure is successfully realized which results in the formation of polyaniline-intercalated molybdenum oxide nanocomposites [48]. PAni based Fe_3O_4 nanocomposites have been reported by a facile one-pot synthesis method. In this method, Fe_3O_4 nanoparticles have been grown within PAni nanorods in the presence of dodecylbenzene sulfonic acid (DBSA) as surfactant via in situ self-assembly method [49]. In another approach, the fabrication of PAni-V_2O_5 nanobelts have been reported by one-pot method [50]. The final morphology of the nanocomposites depends on the pH of the solution and the initiator used. Hybrid core–shell nanobelts or nanoribbons of MoO_3, VO_2, and SnO_2 with PAni and PPy have been developed via solution based in situ polymerization approach [51].

Besides the in situ and one-pot synthesis, other approaches have also been followed for conducting polymer–metal oxide hybrid nanocomposites. Co-axial nanocables of PPy-TiO_2 have been obtained by a vapour phase polymerization method. The synthesis strategy involves three steps (i) synthesis of TiO_2 nanofiber by an electrospinning method, (ii) adsorption of Fe^{3+} ion on TiO_2 nanofibers and (iii) polymerization of pyrrole (vapour) on TiO_2 surface [52]. Electrochemical co-deposition is an efficient way for the synthesis of conducting polymer–metal oxide hybrids which require surface negatively charged nanoparticles. Yoneyama et al. [53] successfully incorporated the negatively charged WO_3, SiO_2, SnO_2 and Ta_2O_5 particles into PPy film employing electropolymerization method by adjusting the pH values of the electrolyte above the isoelectric point of the respective oxides to build negative charges on its particle surfaces [53].

3.3 Nanocomposites with Carbon Materials

Nanocomposites of conducting polymers with carbon materials such as carbon nanotubes (CNT), graphene, graphene oxide, etc. have been receiving much attention for their potential applications such as in nanoelectronic and photovoltaic

devices, superconductors, electromechanical actuators, electrochemical capacitors, nanowires and nanocomposite materials. On account of their excellent properties, CNTs can be used as ideal reinforcing agents for high-performance polymeric nanocomposites [54]. However, it is difficult to process CNTs as they are insoluble in most solvents. Therefore, chemical functionalization of CNTs has been carried out to increase their solubility that facilitates their processing. To synthesize conducting polymer nanocomposites with carbon materials interfacial polymerization has been employed. As an example, PPy-CNT nanocomposites have been synthesized by dispersing organically modified multiwall carbon nanotubes (MWCNTs) during interfacial polymerization of pyrrole. This process involved the polymerization of pyrrole in water-chloroform interface with pyrrole and functionalized MWCNT in the organic phase while oxidant $Fe(NO_3)\cdot 9H_2O$ is in water phase [55]. In another approach nanocomposites of carboxylated-CNT and PPy have been synthesized using interfacial polymerization [56]. Fabrication of PPy/graphene oxide nanocomposites by liquid/liquid interfacial polymerization have been reported by Bora et al. [57]. In this method graphene oxide and $FeCl_3\cdot 6H_2O$ are dispersed in water phase while pyrrole is mixed in chloroform. The water phase is added to the organic phase dropwise and kept undisturbed for 24 h. Jin et al. [58] have reported the preparation of PAni nanofiber-graphene oxide hybrids by an oil–water interfacial polymerization method. In this method aniline is mixed in oil phase while graphene oxide is dispersed in the water phase and the reaction is carried out at room temperature.

Nanocomposites of Surface functionalized MWCNTs and PAni have also been reported by an in situ approach where the surface functionalized MWCNTs are mixed in aniline cation solution at 0 °C. Subsequently, ammonium persulfate (APS), which acts as an oxidizing agent is added drop-wise to the reaction mixture which results in PAni-MWCNT hybrid nanocomposites [59]. In situ synthesis of PAni-CNT nanocomposites is also reported by several groups [60–62]. Liu et al. reported the in situ synthesis of graphene-PPy intercalating nanocomposites where PPy layers are intercalated between the chemically modified graphene nanosheets [63]. The synthesis of PPy-graphene oxide nanocomposites have also been reported by in situ polymerization. The polymerization reaction of pyrrole is carried out in a water–ethanol mixture solution having graphene oxide using ferric chloride as oxidant [64]. In situ synthesis of PAni-graphene nanocomposites have also been reported by several groups [65–68].

Besides chemical approaches, electrochemical polymerization has also been used for the preparation of conducting polymer-carbon material nanocomposites. Zhou et al. [69] have used electrochemical co-deposition method to fabricate graphene oxide-PPy nanocomposites. Graphene oxide synthesized from natural graphene is dispersed in pyrrole solution and electrodeposited onto the FTO conducting glasses in a galvanostatic mode. Electrochemical deposition of PPy with

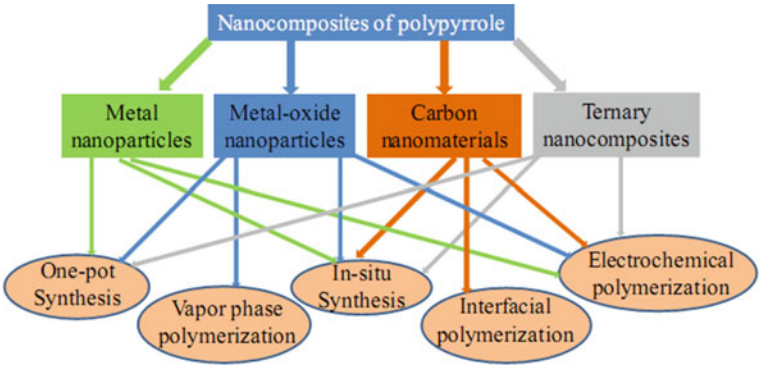

Fig. 4 Schematic of different synthesis processes of PPy based nanocomposites

graphene oxide and CNTs has been reported by other groups [70–72]. Electrochemical deposition of MWCNT-PAni nanocomposites have been reported by an in situ method of an aniline solution having different MWCNT contents [73].

3.4 Conducting Polymer Based Ternary Nanocomposites

In addition to the binary nanocomposites, conducting polymers based ternary nanocomposites have attracted a lot. Research is going on in the field of conducting polymer based ternary nanocomposites. Lu et al. [74] have developed graphene/PPy/CNT-based ternary nanocomposites via in situ polymerization method. Poly(sodium 4-styrene sulfonate) functionalize graphene and CNT dispersed solution have used to facilitate the polymerization of pyrrole. Ternary nanocomposites consisting of graphene, poly(3,4-ethylenedioxythiophene), $CoFe_2O_4$ nanoparticles and graphene, PPy, Fe_3O_4 have been prepared by a facile two-step method [75, 76]. A ternary electrode material, based on graphene, tin oxide (SnO_2) and polypyrrole (PPy) is obtained via one-pot synthesis method, which involves the addition of SnO_2 nanoparticles to the graphene suspension and subsequently pyrrole is polymerized in the graphene-SnO_2 dispersed solution [77]. In another approach, the synthesis of gold-PAni-MWCNT hybrid nanocomposites has been reported by one-pot synthesis approach [78]. PAni coated Fe_3O_4 nanoparticle-CNT nanocomposites have also been reported by co-precipitation of Fe^{2+} and Fe^{3+} and in situ polymerization of aniline [79]. Synthesis processes of PPy based nanocomposites have been presented in the schematic diagram (Fig. 4). The different synthesis methods of conducting polymer hybrid nanocomposites with their advantages and disadvantages are summarized in Table 1.

Table 1 Advantages and disadvantages of different synthesis processes of conducting polymer based nanocomposites

Conducting polymer nano-composite with	Synthesis method	Advantage/disadvantage of different synthesis process
Metal nanoparticles	one-pot/in situ/ electrochemical	**One-pot synthesis** Advantage: (1) In this method monomer or polymer reduces the metal salts to form metal nanoparticles therefore intermediate purification is not required (2) It is a single step and direct process and purification in the intermediate state is not required (3) This method produces material with relatively uniform distribution of functional groups with fewer synthesis steps and functional groups **In situ synthesis** Advantage: (1) This method offers the possibility of good dispersion of dispersed phase as it is grown inside the matrix phase Disadvantage: (1) It may be a multistep process, which requires the intermediate purification step **Electrochemical synthesis** Advantage: (1) In electrochemical synthesis morphology and properties of the nanocomposites can be controlled by the electropolymerization conditions, such as the applied potential or current density Disadvantage: (1) This synthesis method is not favourable for large scale production **Interfacial polymerization** Advantage: (1) In this method, growth of nanostructures takes place at the interface of two liquids and controlled growth is possible (2) It is a simple and direct process Disadvantage: (1) This process also suffers from the drawback of large scale production as the polymerization takes place at the interface only **Vapor phase polymerization** Advantage: (1) Vapor phase polymerization is a solvent-free process and polymers are synthesized by delivering monomers to a surface through the vapor phase (2) This method can also form chemically well-defined films directly on different surface or template, and represents a facile way to prepare conducting polymers and their nanocomposites on special substrates such as porous structures Disadvantage: (1) The evenness of the final polymer film is dependent on the evenness of oxidant layer on which the polymer is deposited (2) The vapor of monomer is harmful and require special sealed environment
Metal-oxides nanoparticles	one-pot/in situ/vapor phase polymerization/electrochemical	
Carbon materials	Interfacial polymerzation/in situ/electrochemical	
Ternary nano-composites	one-pot/in situ/electrochemical	

4 Properties and Applications of Conducting Polymer Based Hybrids

Conducting polymer based hybrids have raised a great deal of scientific and technological interest from the point of versatility of synthesis techniques, properties and broadness of scope of applications. Lots of applications including nanoelectronics, energy storage, sensors, microwave and EMI shielding and biomedical applications of conducting polymer based hybrids have been reported. In this section selected applications of conducting polymer hybrid nanocomposite materials have been discussed.

4.1 Nanoelectronics

Nanostructures of different conducting polymers have been explored for different electronic nanodevices because of their high electrical conductivity, mechanical flexibility, and low cost. Incorporating metals, metal oxides, semiconductors and carbon nanomaterials into conducting polymers matrix to form hybrid nanocomposites affect the conductivity of conducting polymers, which is potentially applicable in the light emitting diodes, transistors, memory and photovoltaic devices [80]. Li et al. [81] have developed flexible white phosphorescent organic light emitting diodes based on bilayer graphene/PEDOT:PSS transparent conducting film formed by CVD and spray-coating technique. Single-wall carbon nanotube/PEDOT nanocomposite film synthesized by in situ polymerization has been investigated for flexible organic light emitting diodes [82]. The nanocomposite film exhibits much lower sheet resistance (160 Ohm/sq) with a high transmittance (86 % at 550 nm) as compared to that of the neat PEDOT film of the same thickness. The current–voltage characteristics of Al/PTh-SiO_2/p-Si Schottky diode have been analyzed at room temperature. The barrier height and ideality factor of the diode are determined by using the conventional current–voltage method as 0.729 eV and 2.12, respectively [83]. Field effect transistor and diodes have also been reported by using conducting polymer–metal nanocomposites [28]. An electric bistable memory device by using an electro-synthesized P3HT/gold nanoparticle composite film as the active layer has been synthesized by Li et al. [53]. It is reported that gold nanoparticles are distributed uniformly without phase separation and aggregation within the conducting polymer film and device exhibited a good on-off switching ratio and high stability.

4.2 Energy Storage Devices

Conducting polymer hybrid nanocomposites are relevant electrode materials for electrochemical energy storage devices. CuO-PPy core–shell nanocomposites have

been investigated as anode material for Li-ion battery. It is observed that the CuO-PPy core–shell nanocomposites exhibit a high initial capacity of 991 mAh g^{-1} and retain an excellent reversible value of 613 mAh g^{-1} over 80 cycles [84]. Graphene-PEDOT conducting polymer nanocomposites synthesized by in situ chemical polymerization method have been reported for supercapacitor applications [85]. The electrochemical charge/discharge characteristics of G-PEDOT nanocomposites are investigated in different electrolytic media, and the specific discharge capacitance is estimated to be 374 F/g. Other groups have also reported supercapacitors based on conducting polymer-based hybrid nanocomposites [86–89]. In addition to these applications conducting polymer based hybrids have also been investigated for photovoltaic applications [90, 91]. The optical properties and photocurrent response of hybrid nanocomposites of poly (2-methoxy-5-(2-ethyhexyl-oxy)-*p*-phenylenevinylene) (MEH-PPV) and silicon nanowires deposited onto ITO substrate by spin coating method have been investigated. The photocurrent density of ITO/MEH-PPV:Si NWs/Al structures have been obtained by J-V characteristics. The J_{sc} value is measured to be 0.39 μA/cm^2 [91]. Graphene-SnO_2-PPy based ternary nanocomposites have been investigated as supercapacitor electrode material [77]. An enhanced specific capacitance (616 F g^{-1}) of the nanocomposites has been obtained at 1 mV S^{-1} in 1 M H_2SO_4 as compared to the graphene-SnO_2 (80.2 F g^{-1}) and PPy (523 F g^{-1}). $BaTiO_3$ nanoparticles are incorporated poly(3-hexylthiophene):[6,6]-phenyl-C-61-butyric acid methyl ester (P3HT:PCBM) nanocomposite has been used for flexible polymer solar cell, where the nanoparticles avoid the electric shorting without any deleterious effect on the power conversion process [92]. The power conversion efficiency without nanoparticles is 3.81 under AM 1.5 G irradiation while it is around 3.79 with nanoparticles. Therefore, the incorporation of nanoparticles has a negligible effect on the power conversion efficiency of the device. The schematic of formation of laminated polymer solar cell with and without incorporation of $BaTiO_3$ nanoparticles is shown in Fig. 5a and b, respectively. The device structure and laminated process to form polymer solar cell is presented in Fig. 5c.

4.3 Sensors

The unusual synergic activity of organic and inorganic material that is unavailable from their single components can provide novel or enhanced functionalities for different sensor applications. PPy-gold nanocomposites by one-pot synthesis method have demonstrated great potential for detecting ammonia gas at room temperature, showing enhanced sensor performances in comparison to pure PPy as a result of functionalization of Au nanoparticles on PPy [29]. Poly(styrene-co-butylacrylate)/PPy-expanded graphite core–shell nanocomposites synthesized by mini-emulsion polymerization have investigated for methanol sensing. The core–shell particles show

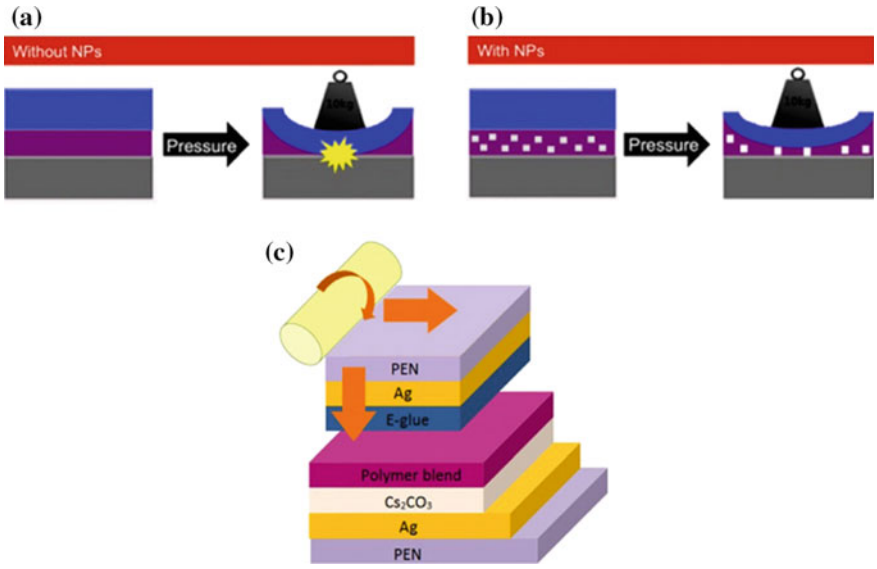

Fig. 5 **a**, **b** The illustration of the formation of a laminated polymer solar cell with and without incorporation of NPs as a spacer. Concentrated stress can deform the soft active layer causing the shorting of cathode and anode, and the incorporated hard NPs can prevent the shorting of cathode and anode; **c** the device structure and lamination process to form the polymer solar cells (Reprinted from Ref. [92] with permission from IOP)

good response towards methanol vapour of concentration as low as 50 ppm and the response time of the sensor is around 60 s. The response of the composite particles remains intact beyond 10 days in the open ambient air [93]. The electrochemical sensing of ascorbic acid has been reported by hybrid graphene-copper phthalocyanine-PAni nanocomposites [94]. The performance of the sensor exhibited a linear range from 5×10^{-7} to 1.2×10^{-5} M with a low limit of detection of 6.3×10^{-8} M (S/N = 3) and the sensitivity of the sensor has been found to be 24.46 μA mM^{-1}. In addition to the chemical sensors conducting polymer hybrid nanocomposites are also applied for biosensors to detect different analytes such as DNA, glucose, urea, etc. Large numbers of DNA sensors have been reported by the various groups using different conducting polymer based nanocomposites [95]. Glucose sensor based on gold nanoparticles-PAni nanocomposites have been reported by Mazeiko et al. [96]. It has been observed that Au-NPs included in GO_x/Au-NPs/PAni nanocomposites significantly increases the amperometric signal as compared to that of GO_x/PAni. Amperometric urea biosensor based on covalently immobilized urease on an electrochemically polymerized film of PAni containing MWCNTs have also been reported [97]. The value of the apparent Michaelis–Menten constant, I_{max} and sensitivity (I_{max}/K_m) experimentally determined to be 2.02 mM,

2.5×10^{-5} A cm^{-2} and 12×10^{-5} A mM^{-1} cm^{-2}, respectively. The optimized urea biosensor shows a good sensitivity from 10^{-2} to 10^{-5} M urea concentration range and a response time of about 50 s with a detection limit of 0.04 mM. PEDOT-reduced graphene oxide nanocomposite based reusable aptasensor for determination of dopamine in human blood has been developed by Wang et al. [98]. The schematic illustration of preparation and sensing of the aptasensor is presented in the Fig. 6. The sensor shows linear response within the range of 0.001–160 nM, with a linear regression equation as ΔI (μA) = 1.52 + 0.854C (nM) and regression coefficient of 0.9988.

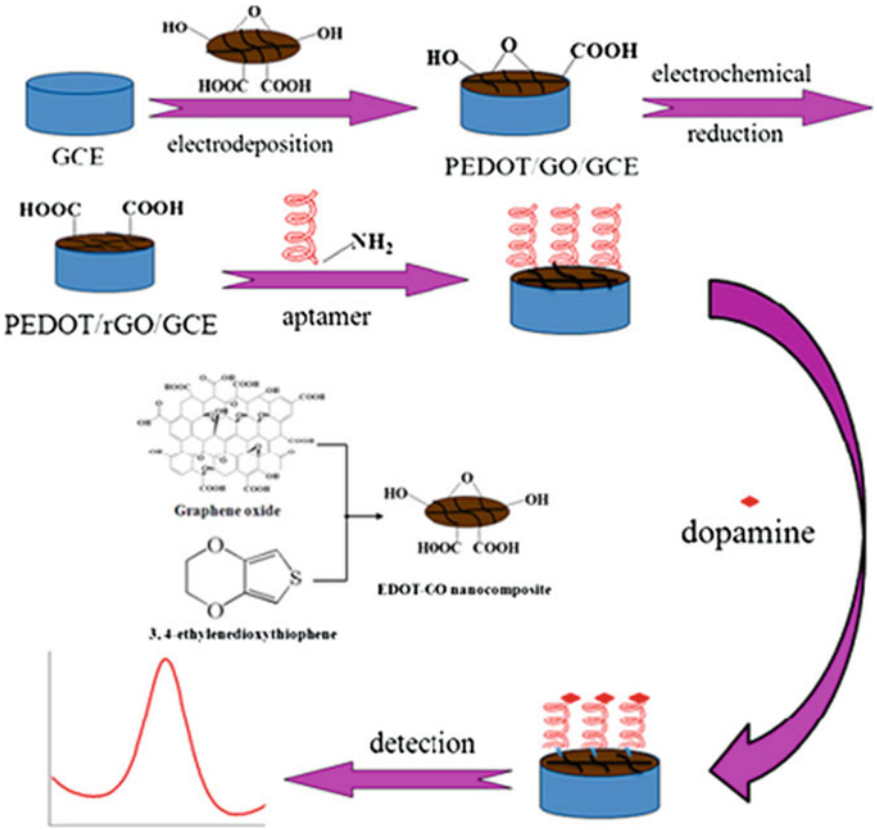

Fig. 6 Schematic illustration of the preparation and sensing of the aptasensor. Graphene oxide and EDOT was electrochemically deposited onto a glassy carbon electrode to form a composite of PEDOT/GO, and it was further electrochemically reduced to PEDOT/rGO (carboxyl group of rGO was retained); Aptamer functionalized with amine group was attached to the PEDOT/rGO nanocomposite film through the reaction between the amine and carboxyl groups; Dopamine was selectively captured by the aptamer, and the collected dopamine was then electrochemically detected (Reprinted from Ref. [98] with permission from Springer)

4.4 Microwave Absorption and EMI Shielding

The proliferation of electronics and instrumentation in commercial, industrial, healthcare and defense sectors has led to a new kind of pollution known as electromagnetic interference. Recently, conducting polymer nanocomposites with other materials have been developed for microwave absorption and electromagnetic shielding. As an example, PAni-MWCNT nanocomposites prepared by in situ polymerization method have been investigated for microwave absorption and EMI shielding [99]. The absorption dominated total shielding effectiveness in a range of −27.5 to −39.2 dB indicates that these materials could be utilized effectively for shielding purposes in the Ku-band (12.4–18.0 GHz). Conducting PAni nanocomposites with γ-Fe_2O_3, TiO_2 and barium ferrite nanoparticles have also been reported for the same purpose [100–102]. Hybrid nanocomposites of PPy and iron oxide have also been investigated for electromagnetic interference shielding application [103]. Microwave absorption properties of core shell type PEDOT nanocomposite with barium ferrite, synthesized by in situ emulsion polymerization, in the 12.4–18 GHz frequency range have been investigated [104]. The nanocomposite demonstrates strong microwave absorption properties in 12.4–18 GHz with SE_A value of 22.5 dB at 15 GHz with minimal reflection loss of 2 dB. Microwave absorption of ternary nanocomposite of graphene, poly(3,4-ethylenedioxythiophene) and $CoFe_2O_4$ nanoparticles have been reported. The investigation indicated that graphene/PEDOT/$CoFe_2O_4$ nanocomposites exhibit enhanced microwave absorption properties compared with graphene/PEDOT and graphene/$CoFe_2O_4$ [75]. The maximum reflection loss of the ternary nanocomposites has been measured up to −43.2 dB at 9.4 GHz and the absorption bandwidths exceeding −10 dB reported at 3.1 GHz with a coating layer thickness of 2.4 mm.

4.5 Biomedical Applications

In addition to the biosensing applications, conducting polymer based hybrids are also used in different biomedical applications such as neural probe [105], nerve regeneration [106], artificial muscle [107], antimicrobial [108], etc. Xiao et al. [109] have reported the use of PPy/carbon nanotubes composite film electrode for neural interfaces. The PPy/SWCNT microelectrodes exhibited an unusually high safe charge injection limit of $\sim$7.5 mC/cm^2 and low electrode impedance at 1 kHz. They have also performed the cell attachment and neurite outgrowth test of rat pheochromocytoma (PC12) cells on the nanocomposites. Furthermore, the PPy/SWCNT film showed excellent biocompatibility both in vitro and in vivo [110]. Antibacterial activity of a novel nanocomposite based on PAni/polyvinyl alcohol/Ag has been reported [111]. Aregueta-Robles et al. [112] developed platinum electrode coated with conducting polymer-CNT hydrogel to enhance electrical properties and also increase the tissue integration as shown in Fig. 7.

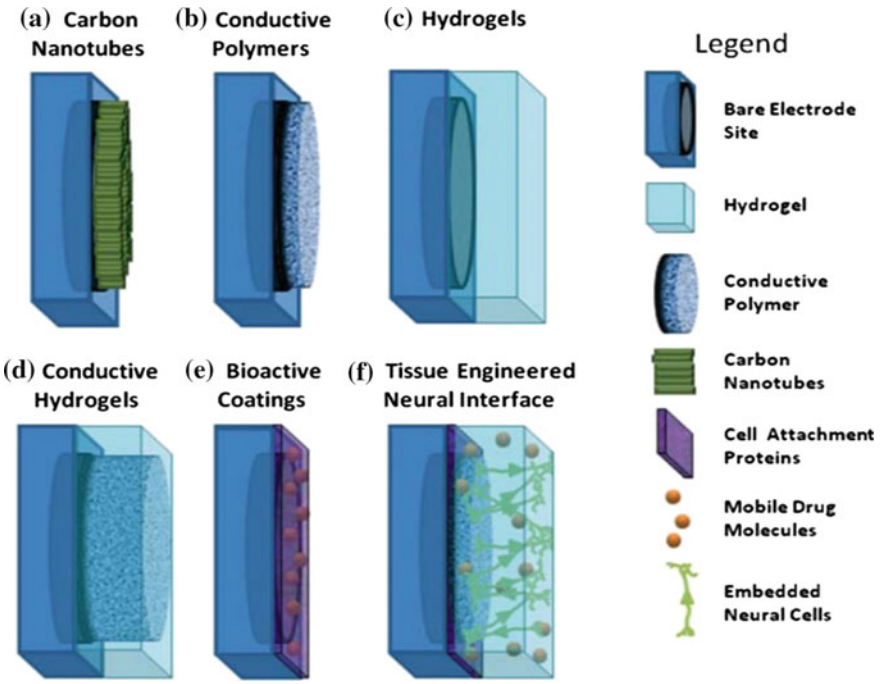

Fig. 7 Schematic of coating approaches used for addressing the limitations of metallic electrodes. **a** Aligned carbon nanotubes on metallic electrodes; **b** conductive polymers electrodeposited on metallic electrodes; **c** hydrogels polymerised to coat electrode site and device; **d** interpenetrating network of conductive polymer grown through hydrogel coating to form conductive hydrogel over electrodes sites; **e** electrodes sites coated with biological active molecules; **f** schematic of ideal tissue engineering interface incorporating combined coating approaches of conductive polymers, hydrogel and attachment factors with neural cells (Reprinted from Ref. [112] with permission from www.frontiersin.org)

Park et al. have also investigated the antimicrobial activity of silver nanoparticles decorated PPy nanotubes by vapor deposition polymerization (VDP)-mediated hard-template method [113]. GO/PPy films have been electrochemically synthesized for drug delivery applications wherein incorporated anti-inflammatory drug dexamethasone released in the response to electrical stimulation without passive diffusion [114]. Graphene oxide (GO) enhanced conducting polymer composite coating has been developed by the electrochemical method by Tian et al. [115] for the electrode-tissue interface. As compared to the bare gold electrode, the impedance of PEDOT/GO film modified electrode decreases nearly two orders of magnitude at 1 kHz, and the charge storage capacity increases. Furthermore, PEDOT/GO modified microelectrodes exhibit the outstanding capacity to perform electrical stimulation for the high charge injection limit. Besides, nontoxic PEDOT/GO film induces little cell response as compared to gold and promoted cell adhesion as confirmed by cell attachment, viability, and proliferation tests.

Similarly, biocompatible pure GO doped PEDOT nanocomposites synthesized by electrochemical polymerization method found to exhibit minimal cytotoxicity after 24 h and supported neuron growth with significantly longer neurites than a control PEDOT/PSS film [116]. Moreover, it is found that functional laminin peptide covalently binds to the surface of the PEDOT/GO film due to the existence of functional carboxyl group without losing its bioactivity which increases the possibility of using this material in biosensing.

5 Surface-Enhanced Raman Spectroscopy Studies of Metal-Polypyrrole Nanocomposites

Surface-enhanced Raman spectroscopy (SERS) is a Raman spectroscopic technique that provides greatly enhanced Raman signal from Raman-active analyte molecule that have been prepared onto the certain specially prepared metal surface. SERS combines molecular fingerprint specificity with potential single-molecule sensitivity. The increase in the intensity of the Raman signal has been observed on the order of 104–106 and can be high as 108 and 1014 for some systems. SERS additionally requires the presence of metal nanostructures as an integral component. SERS is very much surface sensitive as the selectivity of the surface signal results from the presence of surface enhancement mechanism only at the surface in comparison to the standard Raman spectroscopy. SERS is a rapid and non-destructive method, offers extremely high sensitivity, high specific molecular fingerprint information, and high multiplexing possibilities and can be applied for quantitative and qualitative measurements. Lots of applications of SERS have been considered recently especially in bio-analysis for investigation of DNA and RNA, peptides, proteins, whole cell and tissues and also in single molecule detection [117]. Study of conducting polymer–metal nanocomposites by different groups has also been reported using SERS. Ye et al. [118] studied surface-enhanced Raman scattering study of Ag@PPy nanoparticles. They have reported the enhancement of C–H bending vibration peak at 1384 cm^{-1} in the SERC spectra of Ag@PPy nanoparticles. Enhancement of SERC spectra of Ag/polypyrrole coaxial nanocables synthesized via ion adsorption method has been reported by Qiu et al. [119]. The enhanced intensities and high resolution of the spectra signify the powerful enhancing effect on the Raman signals provided by the specialties of the surface of Ag nanowires. Liu et al. [120] used SERS spectra to confirm the polymerization of pyrrole on the surface of Ag nanoparticles deposited on the gold substrate. In this work, a 632.8 nm laser was used to investigate the SERS spectrum of PPy on Ag to avoid the decomposition of PPy and the interference of fluorescence. In other work, the conductivity of gold/PPy core–shell nanocomposites has been estimated with the help of SERC result of C=C backbone stretching at 1590 cm^{-1} [121] (Table 2).

Table 2 Some of the most relevant examples of polypyrrole based nanocomposites

Nanocomposites of PPy with		Synthesis process
Metal nanoparticles	PPy-silver nanocomposite	One-pot synthesis [31]
	PPy-nanofiber nanocomposites with Cu and Ag nanoparticles	One-pot synthesis [32]
	PPy-gold nanocomposite	One-pot synthesis [33]
	Polypyrrole nanotubes-gold nanoparticles nanocomposite	In situ reduction [35]
Metal-oxide nanoparticles	PPy based nanocomposites with TiO_2, SnO_2, Fe_2O_3 and Fe_3O_4	In situ [44–47]
	Co-axial nanoscales of PPy-TiO_2 nanocomposite	Vapour phase polymerization method [52]
	PPy nanocomposites with WO_3, SiO_2, SnO_2 and Ta_2O_5	Electropolymerization method [53]
Carbon nanomaterials	PPy-CNT nanocomposite	Interfacial polymerization [55]
	Carboxilated CNT-PPy nanocomposite	Interfacial polymerization [56]
	PPy-graphene oxide nanocomposite	Interfacial polymerization [57]
	PPy-graphene oxide nanocomposite	In situ [64]
	Nanocomposites of PPy with graphene oxide and CNTs	Electrodeposition [70–72]
Ternary nanocomposites	Graphene-PPy-CNT based ternary nanocomposite	In situ [74]
	Graphene-tin oxide (SnO_2)-PPy nanocomposite	One-pot [77]

6 Polypyrrole Nanotubes-Silver Nanoparticles Hybrid Nanocomposites

6.1 Synthesis

6.1.1 Synthesis of Polypyrrole Nanotubes

Polypyrrole nanotubes (PPy-NTs) were synthesized using self-degraded MO-$FeCl_3$ template method which is as follows: 0.243 g (1.5 mmol) of $FeCl_3$ was dissolved in 30 mL of 5 mM Methyl orange (MO) deionized water solution (0.15 m mol). The appearance of flocculent precipitate is observed immediately. 105 μL (1.5 m mol) pyrrole was added to the reaction solution. After some time, the solution appeared black indicating the polymerization of pyrrole. The mixture was stirred at room temperature for 24 h. The precipitate was washed with deionized water and ethanol

several times until the filtrate was colorless and separated by centrifugation. Subsequently, the PPy-NTs were dried in a desiccator overnight.

It is well known that MO itself does not act as a surfactant due to the absence of critical micelle concentration (CMC). In aqueous solution MO has a planar hydrophobic part and anionic SO_3^{2-} hydrophilic group. On the other hand, $FeCl_3$ (oxidant) acts as flocculant that suppresses the electrostatic repulsive force between negatively charged MO aggregates in solution leading to the formation of MO-$FeCl_3$ template [122]. This template directs the growth of PPy-NTs and degrades automatically due to the reduction of oxidizing cations.

6.1.2 Preparation of Polypyrrole Nanotubes-Silver Nanoparticles Nanocomposites

PPy-NTs:Ag-NPs nanocomposites have been prepared by in situ reduction method. 70 mg of PPy-NTs were dispersed in 25 ml DD water and ultrasonicated for 20 min. An appropriate amount of metal salt ($AgNO_3$) was mixed with PPy-NTs solution by stirring. The sodium borohydride ($NaBH_4$) solution was prepared separately by dissolving in 75 ml of DD water by maintaining the molar ratio of silver nitrate to sodium borohydride at 1:2. The silver nitrate solution was mixed with sodium borohydride solution drop-wise and magnetically stirred for 24 h at room temperature. Finally, the filtrate was thoroughly washed in ethanol and DD water and dried. Four different compositions with different Ag-NPs concentration were prepared by varying $AgNO_3$ concentration as 6, 9, 12 and 15 wt% with respect to PPy-NTs and presented in Table 3.

6.2 Morphological Analysis

Morphology of the nanocomposites has been analyzed by Scanning electron microscopy (SEM) and high-resolution transmission electron microscopy (HRTEM) and is presented in the Figs. 8 and 9, respectively. The nanotubular morphology of PPy and nanoparticle nature of Ag is established from the electron microscopy images. The average diameter of PPy-NTs and Ag-NPs is measured to be 130 ± 5 and 25 ± 3 nm, respectively. It is observed that the concentration of

Table 3 Sample compositions of PPy-NTs:Ag-NPs nanocomposites with varying silver nitrate concentrations

Sample	PPy-NTs (mg)	$AgNO_3$ (wt% w.r.t PPy-NTs)
6 wt% Ag-NPs	70	6
9 wt% Ag-NPs	70	9
12 wt% Ag-NPs	70	12
15 wt% Ag-NPs	70	15

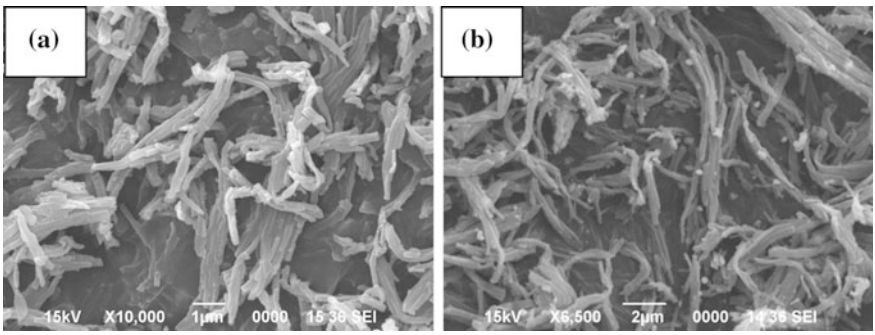

Fig. 8 SEM images of PPy-NTs:Ag-NPs nanocomposites with **a** 6 wt% and **b** 15 wt% of Ag-NPs

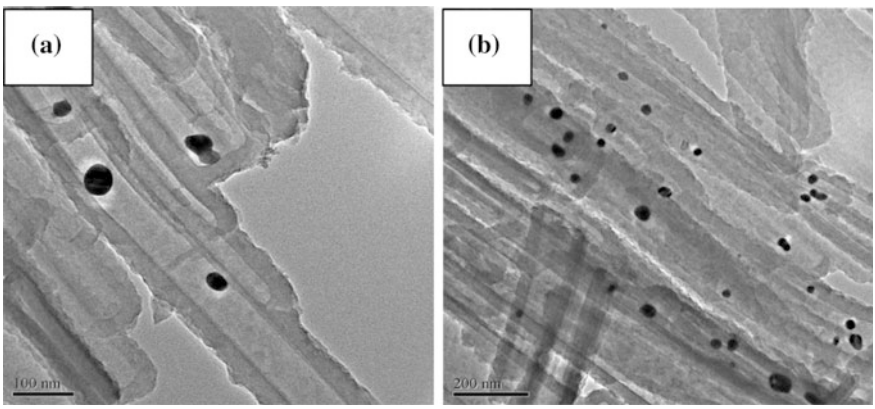

Fig. 9 HRTEM micrographs of PPy-NTs:Ag-NPs nanocomposites with **a** 6 wt% and **b** 15 wt% of Ag-NPs

Ag-NPs in the nanocomposites increases with the increase amounting to $AgNO_3$. SEM micrographs displayed the uniform distribution of Ag-NPs within the polymeric matrix. Metal nanoparticles have very high surface energy and tend to agglomerate which reduces their stability and activity. In this synthesis process, the aggregation of Ag-NPs is suppressed by PPy-NTs by capping the Ag-NPs, which in turn improves the stability of the metal nanoparticles.

6.3 X-Ray Diffraction Study

We further performed the X-ray diffraction measurements to confirm the formation of PPy-NTs:Ag-NPs nanocomposites. The XRD patterns (Fig. 10) exhibit the

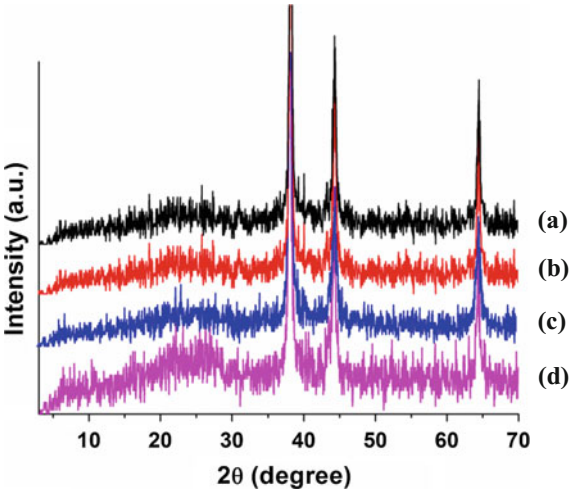

Fig. 10 X-ray diffractogram of PPy-NTs:Ag-NPs nanocomposites with **a** 15 wt %, **b** 12 wt%, **c** 9 wt% and **d** 6 wt% of Ag-NPs

diffraction peaks at 2θ values of 38.3°, 44.6° and 64.4° corresponding to the (111), (200) and (220) planes of face-centred cubic silver, respectively [123]. A broad hump of PPy-NTs is observed in the 2θ range of 20°–30°, which can be attributed to the semi-crystalline nature of the PPy that arises due to π–π interaction of polypyrrole chain. Normally conducting polymers are semicrystalline in nature and crystallinity arises within the polymer due to periodic chain folding. The diffraction peaks assigned to the Ag-NPs appear with a higher intensity than that of the band of PPy due to higher scattering intensity of the particles. The crystallite size (D) and microstrain (ε) of the silver nanoparticles have been calculated from the Williamson–Hall (W–H) equation given by

$$\beta \cos\theta = \frac{0.9\lambda}{D} + 4\varepsilon \sin\theta \tag{1}$$

where β is full width at half maximum (FWHM) at Bragg angle 2θ and λ is the wavelength of Cu K_α radiation ($\sim$1.5406 Å). Williamson–Hall equation is a straight line. The microstrain and crystallite size can be obtained from the slope and intercept, respectively of Eq. 1. The Williamson–Hall plot for the sample with 15 wt% of Ag-NPs is presented in Fig. 11. Calculated values of the crystallite size and microstrain of Ag-NPs with different compositions are given in the Table 4.

6.4 UV–Vis Spectroscopy Study

The UV–Vis absorption spectrum of PPy-NTs:Ag-NPs nanocomposites are depicted in Fig. 12. Pristine PPy-NTs exhibit π–π^* absorption band centred at 485 nm (inset of Fig. 12) and Ag-NPs exhibit characteristic surface plasmon

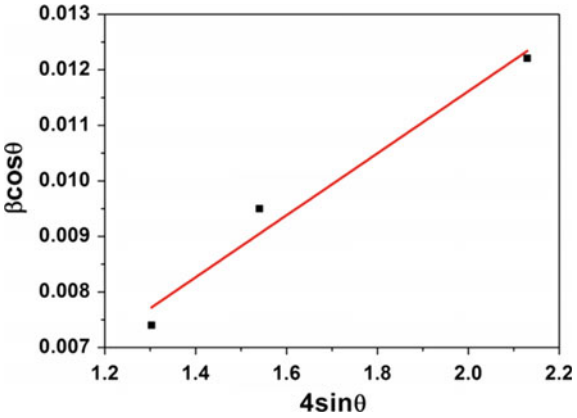

Fig. 11 Williamson–Hall plot of PPy-NTs:Ag-NPs nanocomposites with 15 wt% of Ag-NPs

Table 4 Calculated values of crystallite size and microstrain of silver nanoparticles from Williamson–Hall plot

Sample	Crystallite size (nm)	Microstrain (%)
6 wt%	22.8	0.92
9 wt%	24.1	0.25
12 wt%	23.1	0.28
15 wt%	23.3	0.14

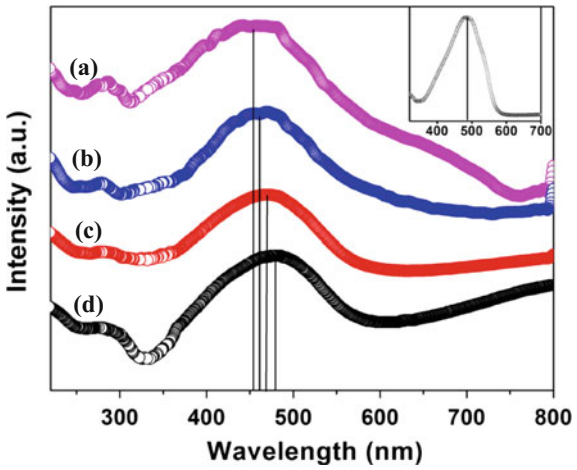

Fig. 12 UV–Vis spectra of PPy-NTs:Ag-NPs nanocomposites with **a** 15 wt%, **b** 12 wt%, **c** 9 wt% and **d** 6 wt% of Ag-NPs. *Inset* UV–Vis spectra of PPy-NTs

resonance absorption within 400–440 nm depending on the particles size [124]. Surface plasmon represents the quantized oscillations of surface charge produced by an external applied electric field on the boundary of a metal. From the figure it is observed that the PPy-NTs:Ag-NPs nanocomposites exhibit single broad absorbance band in the range of 310–550 nm, which can be attributed to the overlapping of the π–π^* transition of PPy and surface plasmon resonance absorption of Ag-NPs.

With the increase in concentration of Ag-NPs in the nanocomposites, blue shifting of the absorption band peak to 460 nm is observed which is attributed to the increased absorption of Ag-NPs.

6.5 *Dielectric Spectroscopy*

The dielectric relaxation spectroscopy has been used to investigate the molecular dynamics by studying the effect of applied ac field. Under the application of electric field electrical charges of dielectric material get displaced from their equilibrium position which results in dielectric polarization. To investigate the transport and polarization characteristics of PPy-NTs:Ag-NPs nanocomposites we examined the dielectric relaxation spectra in the frequency range 42 Hz–5 MHz.

6.5.1 Permittivity Formalism

Figure 13 shows the behavior of both real and imaginary parts of dielectric constant of PPy-NTs:Ag-NPs nanocomposites. The spectra present a high-frequency dependence of dielectric constant in the low-frequency region followed by a nearly frequency independent behaviour above 106 Hz. The electrode polarization and interfacial polarization effects are responsible for the high value of dielectric constant in the low-frequency region [125]. Moreover, with the increase in Ag-NPs concentration, the value of dielectric constant also increases, which demonstrates that the incorporation of Ag-NPs in the polymer matrix delivers an enormous impact on the dielectric constant value. This enhancement in dielectric constant is attributed to the space charge polarization and interfacial effects [126]. When the concentration of Ag-NPs in the nanocomposites increases, the Ag-NPs come closer increasing the heterogeneity and the Ag-PPy interfacial area. This gives rise to an

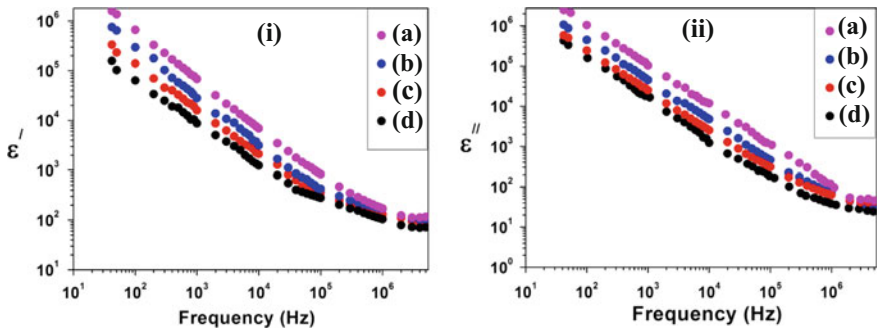

Fig. 13 **i** Real and **ii** Imaginary parts of dielectric constant of PPy-NTs:Ag-NPs nanocomposites with (*a*) 15 wt%, (*b*) 12 wt%, (*c*) 9 wt% and (*d*) 6 wt% of Ag-NPs

increase in the intensity of local electric field that promotes the migration and accumulation of charge carriers at the Ag-PPy interfaces, which contributes to the dielectric permittivity at low frequency. However, as the frequency increases the value of dielectric constant is decreased continuously which is ascribed to the inability of relaxation of charges accumulated at Ag-PPy interface as the charges lag behind the reversing field.

6.5.2 Modulus Formalism

In the case of dielectric materials, the dielectric permittivity formalism cannot explain the relaxation process completely because of the significant contribution of dc conductivity in the low frequency region. Therefore modulus formalism has been considered as a useful tool to explain the electrical transport mechanism and conductivity relaxation process. The electrical modulus can be expressed as,

$$M' = \frac{\varepsilon'}{\varepsilon'^2 + \varepsilon''^2} \tag{2}$$

$$M'' = \frac{\varepsilon''}{\varepsilon'^2 + \varepsilon''^2} \tag{3}$$

$$M = M' + iM'' \tag{4}$$

Figure 14i exhibits the M′ spectra of the nanocomposites which approaches to zero at low frequencies suggesting that the effect of electrode polarization gives a negligible contribution. The frequency dependence of M″ at room temperature is presented in the Fig. 14ii. A relaxation peak appears at high frequency which is attributed to Ag-PPy interfacial polarization effects. Accumulation of charges at the Ag-PPy interface takes place due to difference between the dielectric permittivity of silver and PPy phases in the nanocomposite giving rise to interfacial polarization.

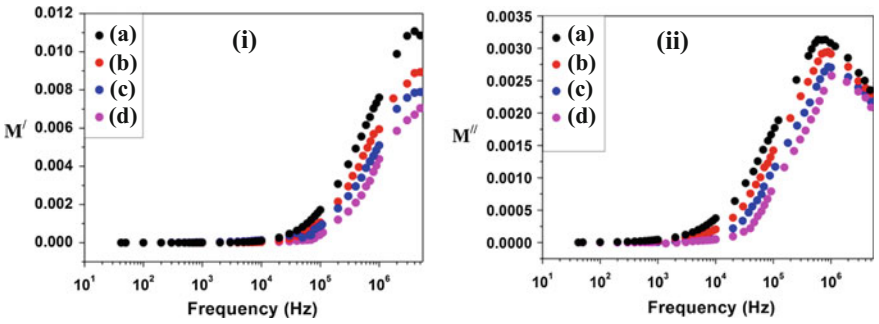

Fig. 14 i Real and ii Imaginary parts of modulus of PPy-NTs:Ag-NPs nanocomposites with (*a*) 6 wt%, (*b*) 9 wt%, (*c*) 12 wt% and (*d*) 15 wt% of Ag-NPs

The appearance of relaxation peak indicates the transition of the motion of charge carriers from long range to the short range with increasing frequency. The low frequency side of M″ spectra represents the range of frequency where the charge carriers undergo successful hopping from one site to the other neighbouring site. On the other hand the charge carriers are confined and performing localized displacement motion within potential well in the high frequency region [125].

6.6 Ac Conductivity Study

The frequency dependent room temperature conductivity of the nanocomposites in the frequency range 42 Hz–5 MHz is displayed in the Fig. 15. The red lines are the best fit curves to the Eq. (5) expressing the total conductivity (σ)

$$\sigma = \sigma_{dc} + A\omega^s \tag{5}$$

where, σ_{dc} is the frequency independent conductivity part, A is a temperature dependent constant and s is an exponent having value between 0 and 1. The conductivity plot exhibits two distinct regions. The first one is plateau region exits in the lower frequency region and is known as dc conductivity region which is attributed to the long range motion of the charge carriers. But on the high frequency side the value of conductivity increases with the applied frequency and is attributed to the activation of trapped charges which undergoes short range back and forth motion. From the plot it is observed that conductivity increases with the increase in concentration of Ag-NPs in the nanocomposites (Table 5). At the low concentration of Ag-NPs, the inter-particle distance between the Ag-NPs is sufficiently large and the conduction is restricted by the presence of dielectric matrix. However, as the concentration of Ag-NPs in the nanocomposites increases the metal nanoparticles get closer

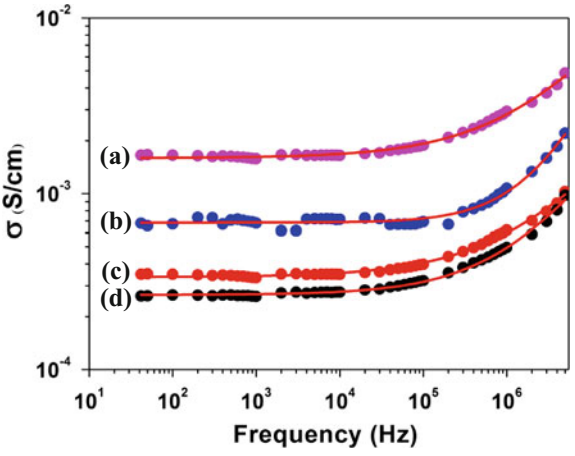

Fig. 15 Ac conductivity spectra of PPy-NTs:Ag-NPs nanocomposites with *a* 15 wt%, *b* 12 wt%, *c* 9 wt% and *d* 6 wt% of Ag-NPs

Table 5 Ac conductivity of PPy-NTs:Ag-NPs nanocomposites with different Ag-NPs concentrations

Sample	Conductivity (S/cm)
6 wt%	2.6×10^{-4}
9 wt%	3.4×10^{-4}
12 wt%	6.6×10^{-4}
15 wt%	1.6×10^{-3}

to each other and form a 'conducting network' through which the charge carriers move easily causing enhancement in the conductivity value.

6.7 *Antimicrobial Activity of the Nanocomposites*

The antibacterial activity of the nanocomposites was investigated by modified Kirby–Bauer diffusion plate method against gram negative *Escherichia coli* (*E. coli*) and gram positive *Staphylococcus aureus* (*S. aureus*). An equal quantity of the nanocomposites with different Ag-NPs concentrations was pressed into pellets of diameters about 13 mm and thickness of 1–2 mm and incubated with the bacteria at 37 °C. Zone of inhibition was measured after 24 h of incubation. Broth dilution method was employed to determine the values of MIC (Minimum Inhibitory Concentration) of PPy-NTs:Ag-NPs nanocomposites against *E. coli* and *S. aureus*.

The antibacterial activity of PPy-NTs:Ag-NPs nanocomposites with different Ag-NPs concentrations investigated by Kirby–Bauer test have been presented in the Fig. 16. It has been observed that the antibacterial activity increases with the increase in Ag-NPs concentrations in the nanocomposites. Nanocomposites with 6 wt% of Ag-NPs exhibit zone of 18 and 21 mm against *E. coli* and *S. aureus*, respectively and increases up to 23 mm for 15 wt% of Ag-NPs against both the microorganisms (Table 6). In contrast, the antibacterial activity of pristine PPy-NTs

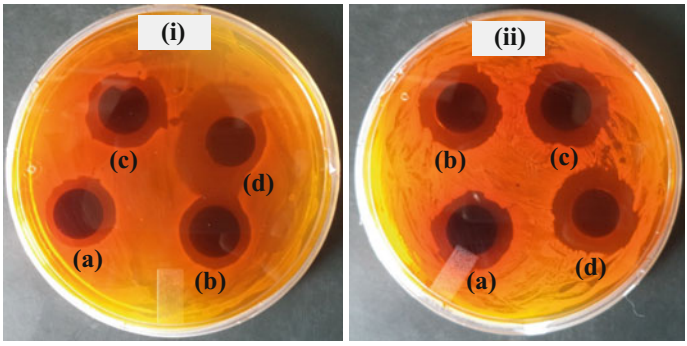

Fig. 16 Photograph images of the zone of inhibitions of PPy-NTs:Ag-NPs nanocomposites with (*a*) 6 wt%, (*b*) 9 wt%, (*c*) 12 wt% and (*d*) 15 wt% of Ag-NPs by Kirby–Bauer test against i *E. coli* and ii *S. aureus* bacteria

Table 6 Diameters of zone of inhibitions of PPy-NTs: Ag-NPs nanocomposites against (i) *E. coli* and (ii) *S. aureus* bacteria

Sample	Diameter of zone of inhibition (mm)	
	E. coli	*S. aureus*
6 wt%	18	21
9 wt%	19	21
12 wt%	20	22
15 wt%	23	23

cannot be estimated by the diffusion plate method as it does not produce any clear zone of inhibition when in contact with *E. coli* and *S. aureus* bacteria. Therefore it is considered that the bacteria killing efficiency of the nanocomposites is mainly influenced by the presence of Ag-NPs and depends on the concentration of Ag-NPs in the nanocomposites. The antibacterial activity of Ag-NPs is due to the formation of 'pitch' on the bacterial membrane or due to the interactions of Ag^+ ions originating from Ag-NPs with the thiol groups of bacteria [127]. There may also electrostatic interaction in between the positively charged pyrrole molecules and negatively charged bacterial cell membrane which may affect the membrane permeability of bacteria and lead to bacteria death [128].

The MIC value which is defined as the minimum concentration of an antimicrobial that is able to restrict the growth of microbial after whole night incubation have been determined by broth dilution method. Initial concentration of the nanocomposites for the test is taken as 10 mg/ml and diluted twice in each time up to a concentration of 0.0195 mg/ml. Nanocomposites with different concentrations have been subjected to *E. coli* and *S. aureus* to investigate the value of MIC. MTT (3-(4,5-dimethylthiazol-2-yl)-2,5-diphenyltetrazolium bromide) is added to the solution after 16 h incubation in Luria Berteni media in 96 well microtiter plate and incubated for 45 min in dark. Live bacterial cells which are capable to produce succinate dehydrogenase (enzyme) which reacts with MTT and forms formazan complexes with purple appearance. So the well having minimum concentration of sample where the complex does not form i.e. which does not appear purple is considered as the MIC value of the compound and is presented in the Table 7. It is observed that the MIC value of the nanocomposites decreases with the increase in Ag-NPs concentration in the nanocomposites and is minimum in the case of nanocomposites with 15 wt% of Ag-NPs.

Table 7 MIC values of PPy-NTs:Ag-NPs nanocomposites against *E. coli* and *S. aureus* with different loading concentrations of Ag-NPs

Sample	MIC value (mg/ml)	
	E. coli	*S. aureus*
6 wt%	0.625	0.625
9 wt%	0.3125	0.625
12 wt%	0.156	0.3125
15 wt%	0.078	0.156

6.8 Haemolysis Activity Study

Haemolysis is a phenomenon by which the destruction of red blood cells (RBC) takes place so that the contained haemoglobin is freed into surrounding medium. The in vitro haemolysis activity test of PPy-NTs:Ag-NPs nanocomposites with different weight concentrations has been investigated by using mammalian red blood cells by following the procedure of Zhu et al. [129]. The percentage of haemolysis caused by the nanocomposites with different Ag-NPs loading is calculated using Eq. 6 and depicted in Fig. 17.

$$\%\text{Haemolysis} = \frac{A_s - A_N}{A_P - A_N} \times 100 \tag{6}$$

where, A_S, A_P and A_N are the absorbance of the sample, positive control and negative control, respectively.

Triton X-100 is used to define 100 % haemolysis while (positive control), phosphate buffer (PBS) is used as negative controlled. It is observed that the percent haemolysis increases with increase in sample concentration as well as the amount of Ag-NPs in the nanocomposites. Therefore the haemolysis activity of the nanocomposites is influenced by the concentration and surface to volume ratio of silver nanoparticles. It has been reported that Ag-NPs are capable of damaging RBC because of its toxic effects. Ag-NPs are capable of forming depressions and pits on the RBC membrane that could ultimately result in haemolysis by forming pores on the membrane and osmotic lysis [130]. Moreover, PPy-NTs are also inducing haemolysis because of its toxic nature though it is less toxic toward RBC as compared to that of Ag-NPs. All the nanocomposites exhibit haemolysis below 5 % up to a concentration of 2.5 mg/ml which is permissible for biomaterials.

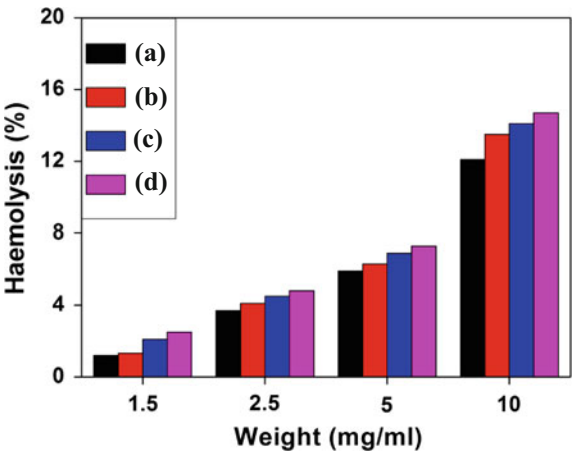

Fig. 17 Haemolysis activity of PPy-NTs:Ag-NPs nanocomposites with *a* 6 wt %, *b* 9 wt%, *c* 12 wt% and *d* 15 wt% of Ag-NPs

7 Conclusions

In the present chapter, we have reviewed conducting polymer-based hybrid nanocomposites with metal or metal oxide nanoparticles, carbon nanomaterials, and ternary nanocomposites. Different approaches for the synthesis of conducting polymer-based hybrid nanocomposites viz., one-pot synthesis, in situ synthesis, interfacial polymerization, vapour phase synthesis and electrochemical synthesis have been reviewed with their pros and cons. These different synthesis processes have been adopted to control various properties like shape, size and dispersion of the secondary phase within the conducting polymer matrix. These hybrids have been investigated in different possible fields, for instance, in sensing of chemical and biological analytes, energy storage devices, nanoelectronics, microwave and electromagnetic shielding and biomedical applications. For sensor application the incorporation of secondary phase within conducting polymer enhance the response time and selectivity of the nanocomposites. Conducting polymer hybrids have been investigated for different biomedical applications such as neural interface, tissue engineering, drug delivery, etc. owing to their low toxicity in biological media. Hybrids of conducting polymers are the most attractive materials for supercapacitor electrode also due to their moderate conductivity, charge–discharge kinetics, good thermal stability and doping–undoping processes, where the incorporation of secondary phase enhanced the cyclic stability of conducting polymers. Moreover, these hybrids have also been applied in microwave absorption and EMI shielding. In spite of this exciting development in the field of conducting polymer based hybrids, there is still a lot of possible work remains. For example, control synthesis of conducting polymer-based nanostructures and hybrids are still a challenge. In the case of sensors, we still need a sensor with enhanced selectivity and sensitivity for practical application. For supercapacitors, a lot of future works are required to improve the life cycle stability and power density of supercapacitors. Similarly for most of the biological applications, improving the biocompatibility of conducting polymer based hybrids is the primary challenge. In the case of electromagnetic wave absorption, future efforts are needed to develop conducting polymer based efficient electromagnetic absorber.

In addition to these, hybrid nanocomposites of PPy-NTs and Ag-NPs synthesized by in situ reduction method have also been discussed. Formation of the nanocomposites has been confirmed by using XRD, SEM, and HRTEM. UV–Vis spectra exhibit single absorption band in the wavelength range of 310–550 nm which is attributed the overlapping of both the absorption band of Ag-NPs and PPy-NTs. Dielectric spectra show an increase in both of $\varepsilon^{\wedge\prime}$ and $\varepsilon^{\wedge\prime\prime}$ values with increase in Ag-NPs concentration in the nanocomposites. This enhancement is attributed to the increase in silver PPy interfacial area which leads to an increase in interfacial polarization within the nanocomposites. In the modulus spectra, a relaxation peak is observed in the high-frequency range and is attributed to the interfacial polarization at the Ag-PPy interface. The AC conductivity is increased with increase in Ag-NPs concentration in the nanocomposites which can be

explained by the concentration of Ag-NPs increases the metal nanoparticles get closer to each other and form a 'conducting network' which eases the motion of the charge carriers within the nanocomposites. It is observed that the antibacterial activity of the nanocomposites against *E. coli* and *S. aureus* bacteria increases with increase in Ag-NPs concentration in the nanocomposites. The antibacterial activity of the PPy-NTs:Ag-NPs nanocomposites may be attributed to the interaction of Ag-NPs and/or Ag^+ ions originating at Ag-NPs with the bacteria and also due to the electrostatic interactions between positively charged pyrrole molecule and negatively charged bacterial cell membranes. The lowest MIC values are calculated as 0.078 and 0.15625 mg/ml for the nanocomposites having 15 wt% of Ag-NPs against *E. coli* and *S. aureus*, respectively. It is observed that the haemolysis activity of the nanocomposites increases with the concentration of Ag-NPs, which is attributed to the increased toxic effects of Ag-NPs towards RBC.

References

1. Jaidev, Jafri RI, Mishra AK et al (2011) J Mater Chem 21:17601–17605
2. Mostafaeia A, Zolriasatein A et al (2012) Prog Nat Sci Mater Int 22:273–280
3. Leung KC-F, Xuan S, Zhu X et al (2012) Chem Soc Rev 41:1911–1928
4. Ramanathan K, Bangar MA, Yun M et al (2004) Nano Lett 4:1237–1239
5. Ignatova M, Labaye D, Lenoir S et al (2003) Langmuir 19:8971–8979
6. Gizdavic-Nikolaidis MR, Stanisavljev DR, Easteal AJ et al (2010) J Phys Chem C 114:18790–18796
7. Kulesza PJ, Chojak M, Karnicka K et al (2004) Chem Mater 16:4128–4134
8. Zhou X, Huang X, Qi X et al (2009) J Phys Chem C 113:10842–10846
9. Lu A-H, Salabas EL, Schuth F (2007) Angew Chem Int Ed 46:1222–1244
10. Kaushik A, Vasudev A, Arya SK et al (2013) Biosens Bioelectron 50:35–41
11. Peng C, Zhang S, Jewel D et al (2008) Prog Nat Sci 18:777–788
12. Wang W, Xu G, Cui XT et al (2014) Biosens Bioelectron 58:153–156
13. Lin C-H, Chen K-T, Ho J-R et al (2012). doi:10.1155/2012/942629
14. Camurlu P (2014) RSC Adv 4:55832–55845
15. Bredas JL, Scott JC, Yakushi K, Street GB (1984) Phys Rev B 30(2):1023–1025
16. Zhong CJ, Tian ZQ, Tian ZW (1990) J Phys Chem 94(5):2171–2175
17. Martin CR (1994) Science 266:1961–1966
18. Deepshikha, Basu T (2011) Anal Lett 44(6):1126–1171
19. Wang J-G, Yang Y, Huang Z-H, Kang F (2014) Electrochim Acta 130:642–649
20. Gerard M, Chaubey A, Malhotra BD (2002) Biosens Bioelectron 17:345–359
21. Chen H, Elabd YA (2009) Macromolecules 42(9):3368–3373
22. Sulka GD, Hnida K, Brzózka A (2013) Electrochim Acta 104:536–541
23. Yang C, Mo H, Zang L, Qiu J, Sakai E, Wu X (2014) Phys B 449:181–185
24. Fan L-Z, Maier J (2006) Electrochem Commun 8(6):937–940
25. Shi G, Rouabhia M, Wang Z, Dao LH, Zhang Z (2004) Biomaterials 25(13):2477–2488
26. Runge MB, Dadsetan M, Baltrusaitis J, Knight AM, Ruesink T, Lazcano EA, Lu L, Windebank AJ, Yaszemski MJ (2010) Biomaterials 31:5916–5926
27. Lee R-J, Temmer R, Tamm T, Aabloo A, Kiefer R (2013) React Funct Polym 73:1072–1077
28. Lu X, Zhang W, Wang C et al (2011) Prog Polym Sci 36:671–712
29. Sih BC, Wolf MO (2005) Chem Commun 27:3375–3384
30. Balamurugan A, Ho K-C, Chen S-M (2009) Synth Met 159:2544–2549

31. Babu KF, Dhandapani P, Maruthamuthu S et al (2012) Carbohydr Polym 90:1557–1563
32. Liu Z, Liu Y, Zhang L et al (2012) Nanotechnology 23:335603
33. Zhang J, Liu X, Wu S et al (2013) Sens Actuators, B 186:695–700
34. Jiang F, Yue R, Du Y et al (2013) Biosens Bioelectron 44:127–131
35. Xu J, Hu J, Quan B et al (2009) Macromol Rapid Commun 30:936–940
36. Tamboli MS, Kulkarni MV, Patil RH et al (2012) Colloids Surf B 92:35–41
37. Eisa WH, Zayed MF, Abdel-Moneam YK et al (2014) Synth Met 195:23–28
38. Wankhede YB, Kondawar SB, Thakare SR et al (2013) Adv Mat Lett 4:89–93
39. Woo S, Lee S-J, Kim D-H et al (2014) Electrochim Acta 116:518–523
40. Hsiao Y-P, Su W-Y, Cheng J-R et al (2011) Electrochim Acta 56:6887–6895
41. Fedorczyk A, Ratajczak J, Czerwinski A et al (2014) Electrochim Acta 122:267–274
42. Li N-F, Lei T, Liu Y et al (2010) Trans Nonferrous Met Soc China 20:2314–2319
43. Hangarter CM, Chartuprayoon N, Hernández SC et al (2013) Nano Today 8:39–55
44. Zhang J, Wang S, Xu M et al (2009) J Phys Chem C 113:1662–1665
45. Dutta K, De SK (2007) J Phys D Appl Phys 40:734–739
46. Mallouki M, Tran-Van F (2009) Electrochim Acta 54:2992–2997
47. Qiu G, Wang Q, Nie M (2006) Macromol Mater Eng 291:68–74
48. Zheng L, Xu Y, Jin D et al (2011) Chem Asian J 6:1505–1514
49. Basavaiah K, Pavan Kumar Y, Prasada Rao AV (2013) Appl Nanosci 3:409–415
50. Li G, Zhang C, Peng H et al (2009) Macromol Rapid Commun 30:1841–1845
51. Xu J, Li X, Liu J et al (2005) Polym Sci A 43:2892–2900
52. Lu X, Zhao Q, Liu X et al (2006) Macromol Rapid Commun 27:430–434
53. Li C, Bai H, Shi G (2009) Chem Soc Rev 38:2397–2409
54. Sahoo NG, Rana S, Cho JW et al (2010) Progr Polym Sci 35:837–867
55. Georgakilas V, Dallas P, Niarchos D et al (2009) Synth Met 159:632–636
56. Liu P, Wang X, Li H (2013) Synth Met 181:72–78
57. Bora C, Dolui SK (2012) Polymer 53:923–932
58. Jin Y, Jia M (2014) Synth Met 189:47–52
59. Mekki A, Samanta S, Singh A et al (2014) J Colloid Interface Sci 418:185–192
60. Zhong H, Yuan R, Zhang CY et al (2011) Talanta 85:104–111
61. Guo H, Zhu H, Lin H et al (2008) Mater Lett 62:3919–3921
62. Ansari MO, Ansari SP, Yadav SK (2014) J Ind Eng Chem 20:2010–2017
63. Liu Y, Wang H, Zhou J et al (2013) Electrochim Acta 112:44–52
64. Bose S, Kuila T, Uddin ME et al (2010) Polymer 51:5921–5928
65. Baniasadi H, Ahmad RSA, Mashayekhan S et al (2014) Synth Met 196:199–205
66. Kumar M, Singh K, Dhawan SK et al (2013) Chem Eng J 231:397–405
67. Ameen S, Seo H-K, Akhtar MS et al (2012) Chem Eng J 210:220–228
68. Huang YF, Lin CW (2012) Polymer 53:2574–2582
69. Zhou H, Han G, Xiao Y et al (2014) J Power Sources 263:259–267
70. Deng M, Yang X, Silke M et al (2011) Sens Actuators, B 158:176–184
71. Wang J, Dai J, Yarlagadda T (2005) Langmuir 21:9–12
72. Lim YS, Tan YP, Lim HN et al (2014) Ceram Int 40:3855–3864
73. Zhang J, Kong L-B, Wang B et al (2009) Synth Met 159:260–266
74. Lu X, Zhang F, Dou H et al (2012) Electrochim Acta 69:160–166
75. Liu P, Huang Y, Zhang X (2014) Powder Technol 276:112–117
76. Liu P, Huang Y, Zhang X et al (2014) Mater Lett 129:35–38
77. Wang W, Hao Q, Lei W et al (2012) RSC Adv 2:10268–10274
78. Chang Q, Zhao K, Chen X et al (2008) J Mater Sci 43:5861–5866
79. Liu Z, Wang J, Xie D et al (2008) Small 4:462–466
80. Das TK, Prusty S (2012) Polym Plast Technol 51:1487–1500
81. Wu X, Li F, Wu W (2014) Appl Surf Sci 295:214–218
82. Kim M, Kim YC (2014) Synth Met 198:31–35
83. Aldemir DA, Esen M, Kökce A et al (2011) Thin Solid Films 519:6004–6009
84. Yin Z, Ding Y, Zheng Q et al (2012) Electrochem Commun 20:40–43

85. Alvi F, Ramc MK, Basnayaka PA et al (2011) Electrochim Acta 56:9406–9412
86. Sen P, De A, Chowdhury AD (2013) Electrochim Acta 108:265–273
87. Xiao Q, Zhou X (2003) Electrochim Acta 48:575–580
88. Zhang F, Xiao F, Dong ZH et al (2013) Electrochim Acta 114:125–132
89. Wang J, Wu Z, Hu K et al (2015) J Alloys Compd 619:38–43
90. He J, Duffy NW, Pringle JM et al (2013) Electrochim Acta 105:275–281
91. Chehata N, Ltaief A, Ilahi B et al (2014) Lumin 156:30–35
92. Lu Y, Alexander C, Xiao Z et al (2012) Nanotechnology 23:344007
93. Das D, Choudhury P, Borthakur LJ (2014) Sens Actuators, B 199:320–329
94. Pakapongpan S, Mensing JP, Phokharatkul D et al (2014) Electrochim Acta 133:294–301
95. Peng H, Zhang L, Soeller C et al (2009) Biomaterials 30:2132–2148
96. Mazeiko V, Kausaite-Minkstimiene A, Ramanaviciene A et al (2013) Sens Actuators, B 189:187–193
97. Meibodi ASE, Haghjoo S (2014) Synth Met 194:1–6
98. Wang W, Wang W, Davis JJ et al (2015) Microchim Acta 182:1123–1129
99. Saini P, Choudhary V, Singh BP et al (2009) Mater Chem Phys 113:919–926
100. Dhawan SK, Singh K, Bakhshi AK et al (2009) Synth Met 159:2259–2262
101. Phang SW, Tadokoro M, Watanabe J et al (2008) Curr Appl Phys 8:391–394
102. Ohlan A, Singh K (2008) Appl Phys Lett 93:053114-1–0531143-3
103. Azadmanjiri J, Hojati-Talemi P, Simon GP et al (2011) Polym Eng Sci 51:247–253
104. Ohlan A, Singh K, Chandra A et al (2010) ACS Appl Mater Interfaces 2:927–933
105. Depan D, Misra RDK (2014) Biomater Sci 2:1729–1739
106. Ghasemi-Mobarakeh L, Prabhakaran MP, Morshed M et al (2011) J Tissue Eng Regen Med 5:17–35
107. Ismail YA, Martinez JG, Harrasi ASA et al (2011) Sens Actuators 160:1180–1190
108. Kelly FM, Johnston JH, Borrmann T et al (2007) J Nanosci Nanotechnol 35:5571–5577
109. Xiao H, Zhang M, Xiao Y et al (2014) Colloids Surf B Biointerfaces 126:138–145
110. Lu Y, Li T, Zhao X et al (2010) Biomaterials 31:5169–5181
111. Ghaffari-Moghaddam M, Eslahi H (2014) Arab J Chem 7:846–855
112. Aregueta-Robles UA, Woolley AJ, Poole-Warren LA et al (2014) Front Neuroeng 7(15):1–18
113. Park E, Kim H, Song J et al (2012) Macromol Res 20:1096–1101
114. Weaver CL, LaRosa JM, Luo X et al (2014) ACS Nano 8:1834–1843
115. Tian HC, Liu J-Q, Wei D-X et al (2014) Biomaterials 35:2120–2129
116. Luo X, Weaver CL, Tand S et al (2013) J Mater Chem B 1:1340–1348
117. Cialla D, Marz A, Bohme R et al (2012) Anal Bioanal Chem 403:27–54
118. Ye S, Fang L, Qing X et al (2010) J Raman Spectrosc 41:1119–1123
119. Qiu T, Xie H, Zhang J et al (2011) J Nanopart Res 13:1175–1182
120. Liu Y-C, Lee H-T, Yang S-J (2006) Electrochim Acta 51:3441–3445
121. Liu Y-C, Chuang TC (2003) J Phys Chem B 107:12383–12386
122. Yang X, Zhu Z, Dai T et al (2005) Macromol Rapid Commun 26:1736–1740
123. Sun Y, Xia Y (2002) Science 298:2176–2179
124. De G, Tapfer L, Catalano M (1996) J Appl Phys Lett 68:3820–3822
125. Hazarika J, Kumar A (2014) NIMB 333:73–79
126. Singh K, Ohlan A, Kotnala RK et al (2008) Mater Chem Phys 112:651–658
127. Morones JR, Elechiguerra JL, Camacho A et al (2005) Nanotechnology 16:2346–2353
128. Varesano A, Vineis C, Aluigi A et al (2013) Fiber Polym 14:36–42
129. Zhu QY, Holt RR, Lazarus SA et al (2002) Exp Biol Med 227:321–329
130. Krajewski S, Prucek R, Panacek A et al (2013) Acta Biomater 9:7460–7468

Conductive Polymer Composites Based on Carbon Nanomaterials

Santosh Kr. Tiwari, Jawahar Mishra, Goutam Hatui and G.C. Nayak

Abstract In this chapter, authors have focused on various aspects of conducting polymers and their potential applications. Conducting polymers (CPs) are the very exciting class of electronic materials, which have attracted huge interest around the world since their discovery in past three decades. Conducting polymers (CPs) have several excellent reinforced properties, as compared to the non-conducting polymeric resins. In the recent years, many CPs have been used for fabrication of the electronic device, rechargeable batteries, artificial muscles, solar energy conversion, and sensors. This book chapter complies two main parts of the investigation. The first focuses most common conducting polymers. And the second is regarding their potential applications. In addition, to this authors have also added several very recent citations for further reading.

Keywords Carbon nanomaterials · Conducting polymers · Nanocomposites and electronic devices

1 Introduction

Carbon materials always play a vital role in our lives mainly via innovative applications and origination of new materials [1–6] without which it is impossible to imagine our modern lives. All the most significant milestones in the progression of our society are closely associated with advancement in the materials throughout the history [1, 2, 6]. For example, the Stone Age, Bronze Age, Iron Age, steel age (industrial revolution), silicon, and silica age (communication revolution). All these reflect that our modern civilization and daily life in the twenty-first century depends on an unlimited variety of materials of varying degrees of sophistication [2–6]. Thus, materials science plays a central role in our daily life. Therefore, materials are

S.Kr. Tiwari · J. Mishra · G. Hatui · G.C. Nayak (✉)
Department of Applied Chemistry, Indian Institute of Technology (Indian School of Mines), Dhanbad, Jharkhand 826004, India
e-mail: ismgraphene@gmail.com

V. Kumar et al. (eds.), *Conducting Polymer Hybrids*,
Springer Series on Polymer and Composite Materials,
DOI 10.1007/978-3-319-46458-9_4

fundamental to the new technology that makes our lives full of convenience, for instance, various electronic gazettes, viz., laptop, cell phones, etc. [1, 4, 5]. Invention and discovery of a new material always bring with it some of the most exciting and fruitful periods of scientific and technological research both in the theoretical and experimental field [1–5]. So, materials are cardinal of the technology that makes our lives full of convenience, for instance, the introduction of the laptop, digital cell phones, touch screens, and so on [3, 5, 6]. Therefore, the challenge of creating new, more functional and diverse materials grows with the needs of society [1, 2, 6]. And the shortcomings for covering essential needs such as sustainable energy, cost effective, personal protection, etc., are intimately associated with constraints on the properties of materials [3, 4, 6]. The most critical aspect of achieving an advanced material with desired and improved properties is imaginative molecular design and synthesis of new material [6]. Presently, at the frontiers of materials science and technology, the concept of conflating various types of materials synergically in suitable experimental conditions is one of the most accessible approaches to achieving specific goals with the greatest efficiency in properties and cost-effectiveness [6, 7]. It is well known that polymers are used in numerous applications and fields, and it is very common to tuning the properties or upgrades the performance of the polymer system to obtain an accurate processing and applications [5]. Thus, specific additives are frequently used to alter the polymer properties or to improve or change the performance of polymer systems. This is reason mixing of two or more different material (polymer as the matrix and additive as filler) in a suitable manner for the creation of improved quality desired materials adorably accepted by the scientific community [6]. In this regard, polymers are one of the most affordable and successfully exploited classes of materials due to the incredible variety of chemical structures available and their subsequent compendium of properties, along with their affordable cost, simple processing, amenable and their easy recyclability and applicability as sustainable materials [5, 7, 8]. The nature of various polymers to function as electrical insulators is fundamental for their full range applications in the electronic and electrical fields [8–10]. And the resistivity of these materials is generally ranging between 950 and 1015 W m [9, 10]. But many polymers also have an ability to conduct electricity in their native state [9]. In addition to this, material chemists have sought to impart conduction to polymers by blending insulating polymers with conductive ingredients such as carbon fibers, carbon blacks, CNTs, metal particles [9]. As a result a wide range of so-called conductive polymer composite has come into existence since the 1950s [9, 10] with the resistivity of metallic conductor (10–7 W m) and insulating materials (1015 W m) [8–10] which can find their applications in many fields such as floor heating elements, electronic equipment [4, 5] critical strategic materials such as electromagnetic interference (EMI) shielding apart from the conventional application of semi-conducting materials for dissipation of static electricity [3–5, 7]. More recently, conductive composites have been used for sensing purposes [8, 9]. Compared to the metallic conductor, conductive polymer composites (CPC) have the advantages of low density, ease of shaping, and a wide range of electrical conductivities along with the high corrosion resistance [5, 9, 10]. In the past decade,

carbon black particles and carbon fibers are the most commonly used conductive components to incorporate conduction polymer composite because of their high surface area and high charge transfer capabilities [9, 10]. Due to the rapid progress in the materials science and engineering has taken a new lead since the advent of the nano cluster-based materials or nanocomposites [11]. The nanocluster are the ultra-fine particles of nanometer dimensions (20–200 nm) and whose characteristics are size dependent and are different from those of the atomic and bulk similitude [11, 12]. Thus, nanocomposites are a special class of hybrid materials obtained from suitable combinations of two or more nano-sized objects using proper technique and optimum experimental conditions [11–13]. The resulting materials are having many unique physical properties and a wide range of application in the various fields of science and technology [5–7, 10–13]. Such novel properties of nanocomposites can be obtained only on the basis of a suitable and specific combination of matrix and filler [12, 13]. For the specific Conductive polymer composites based on carbon nanomaterials; materials chemists very often handle this by the effective combination of two or more carbon nanofillers with conductive polymer matrix [11, 14] the full potential for the technological purpose of the nanomaterials, it is very essential to endow them with good processability, which has ultimately guided scientists toward using conventional polymers as one component of the nanocomposites, resulting in a particular class of hybrid materials termed “polymeric nanocomposites.” These composite materials are also intimate combine with ions of one or more inorganic nanoparticles or organic fillers with a typical polymer so that newly induced unique properties of the former can be taken together with the existing qualities of the parental components [14]. Many excellent works regarding the development of such polymer nanocomposites have been published [13–16]. In most of the cases, such combinations for the synthesis of new materials require blending or mixing of the components in a specific manner [14–16]. Resulting nanocomposites have found successful applications in varied fields, viz., battery cathodes, microelectronics, nonlinear optics sensors, [6, 8, 9, 15, 16], etc. So, the main perspective is somewhat different from the conventional and inherently conducting polymers (ICP). Since the conventional conducting polymers are infusible in nature and are generally insoluble in common organic solvents [17]. This is a great limitation and has prevented the ICPs from combining with the foreign materials (nanofillers) to form nanocomposites [13–15]. Therefore, synthesis approaches had to be found and optimized to incorporate the inorganic component and organic components (fillers) into the conducting polymer (matrix) [18]. So that in the case of conventional nanocomposites, the polymer adds flexibility to the molecular system and improves processability to a vast extent. But in conducting polymer nanocomposites, on the other hand, the nanoparticles generally provide the system with some kind of processabilities like colloidal stability or mechanical strength although the specific properties of the latter are also utilized in some respects [16–18].

2 Brief History of Conductive Polymer and Their Composites

Polyaniline (PA) is treated as a first organic conductive polymer. It was first discovered by Henry Letheby in the mid-nineteenth century [19]. He observed that reduced form of PA is colorless, but the oxidized forms is showing deep blue color during an electrochemical study of aniline in acidic the media [19, 20]. The first highly conductive organic compounds were the charge transfer complexes [20, 21]. In the same line around the 1950s, some organic chemist reported that some polycyclic aromatic systems formed semi-conducting charge transfer complex salts with halogens elements [21]. In 1977, Alan J. Heeger, Alan MacDiarmid, and Hideki Shirakawa reported similar high conductivity in oxidized iodine-doped polyacetylene [21, 22]. For this research, they were awarded the 2000 Nobel Prize in Chemistry for the discovery and development of conductive polymers [23]. Polyacetylene itself did not find practical applications, but drew the attention of the scientific community and encouraged the rapid growth of the field. After the arrival of CNTs and the vast amount of research on other carbon nanomaterials around 1980 open a very dynamic and productive field for the real-time application of conductive polymers [23, 24].

3 Some Important Terms Related to Conductive Polymers and Their Definitions

3.1 Some Most Studied Conductive Polymers

Polymers have the ability to conduct electricity known as conducting polymer. Sometimes they also are known as intrinsically conducting polymers (ICPs). The intrinsically conducting polymers may have metallic conductivity or can be semiconductors; it depends on the nature of molecular systems [24]. These polymers are mostly not thermoformable though they possess organic constituent like other organic polymers (Insulator polymers, plastics). Conduction polymers offer high electrical conductivity but do not show similar mechanical properties to other commercially available polymers [25]. The electrical conductivity of such polymers can be tuned according to need using the methods of organic synthesis. The main advantage of using conductive polymers is their easy processability and very smooth dispersion in a broad range of organic solvents [24, 25]. Some most common examples of conducting polymers are given below with brief descriptions (Fig. 1).

3.2 Composites

Composites are also called composition materials or shortened to composites are materials made from two or more constituent materials with significantly different

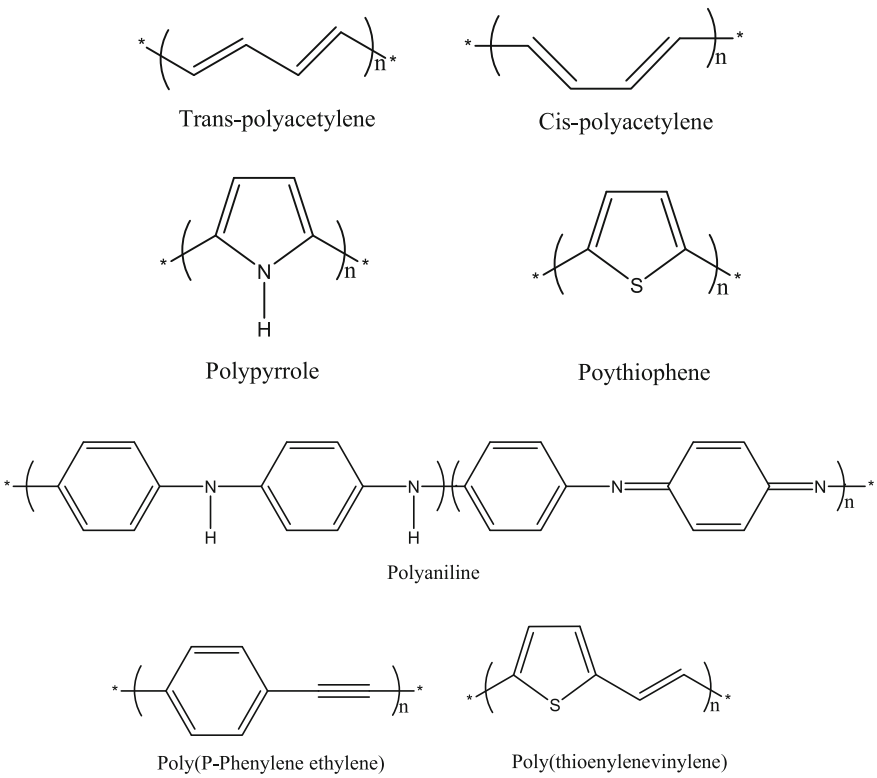

Fig. 1 Most frequently used conductive polymers in the past few decades

physical or chemical properties, that when combined, produce a material with characteristics different from the individual components [27, 28]. So that if the polymers mentioned above mixed with some other materials like nanoclays, a metal particle, or with the copolymer [29] to reinforce the properties of conducting polymers then called as Conductive polymer composites. Nowadays such polymer materials have a wide range of applications in the almost all field of science and technology [26–28]. The composite materials can be classified into two category: (1) Bulk composites or Microcomposites, (2) Nanocomposites (Fig. 2).

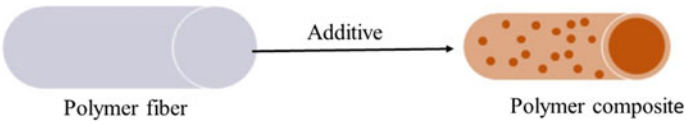

Fig. 2 Schematic diagram for synthesis of polymer composites

3.3 Nanomaterials and Conducting Polymer Composites

Nanomaterials are the materials which have at least one dimension in the size range of 1–100 nm [30]. Such materials possess many unique properties which are not possible in the bulk counterpart [29]. It is because at the nanoscale the laws of quantum mechanics are critical, and most of these peculiar behaviors of nanomaterials originate from quantum phenomena [30, 31]. So that such materials intentionally engineered to produce very specific properties related to size, shape, and surface properties [31]. These properties of powders and colloid materials mostly depend on the surface area and particle composition [31]. So conducting polymer composites are mixture or blends of conductive nanoparticles and polymers (may be conductive or not) [29, 30]. Several conductors, i.e., nanomaterials have been used in different forms together with a wide range of engineering plastics [30, 32]. A series of conductive nanofillers have been tried such as Nanoclays, carbon blacks, CNTs graphite flakes, fibers, metal powders, etc. [33]. During the synthesis of such engineered materials, a transition from insulating to non-insulating behavior is generally taken into the consideration [32, 33]. The various polymers, which have been used as the matrix, are PP, Nylon, and PVC and at present these nanomaterials offering a broad range of potential applications [33, 34]. Most of the modern synthetic conductive polymer nanocomposites are using CNTs, Fullerenes, Graphene, Nanoclays, ZnO, etc., as a nanofillers [30–35]. That is why? Nowadays nanotechnology is not limited to laboratory curiosity, and it became a multi-billion dollar industry [35]. And it has been the most remarkable transformation seen by the technology industries in the past two decades. The prime aim to fabricate such nanomaterials is to obtain desired properties according to the specific application. It may improve electronic, mechanical chemical properties, etc., of materials for the various applications [33, 34]. Some most frequently used nanomaterials for conductive polymer composites based on carbon nanomaterials are given below (Fig. 3).

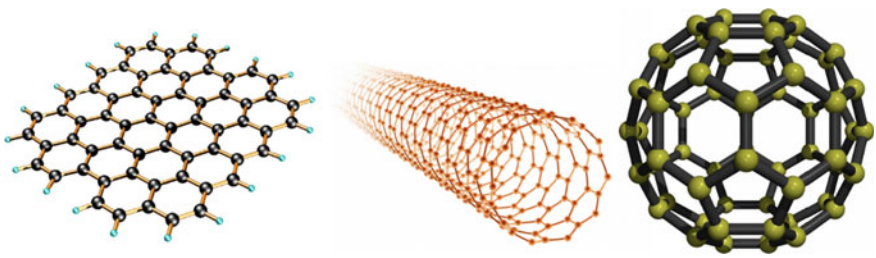

Fig. 3 Most studied nanomaterials in past two decades conductive polymer composites based on carbon nanomaterials (Graphene, SWCNT, and Fullerene from L-R: Figs. taken from Refs. [85–87])

4 Carbon Nanotube (CNT)-Based Conductive Polymer Composites

CNTs are the common allotropes of carbon element and possess cylindrical nanostructure [36, 37]. Nanotubes are members of the fullerene structural family, and its name is derived from their hollow, long structure with the walls formed by one-atom-thick sheets of carbon [36, 37]. CNTs have many exceptional properties, which are precious for modern science and technology [37]. And they have proven potential application in the field of electronics, optics, and other fields of materials science and technology [38]. In specific, owing to their outstanding thermal, mechanical and electrical properties and find significant applications in all field of science so, the area of the conductive polymer is not an exception [37, 38]. Some important properties of CNTs are tabulated below (Fig. 4; Table 1).

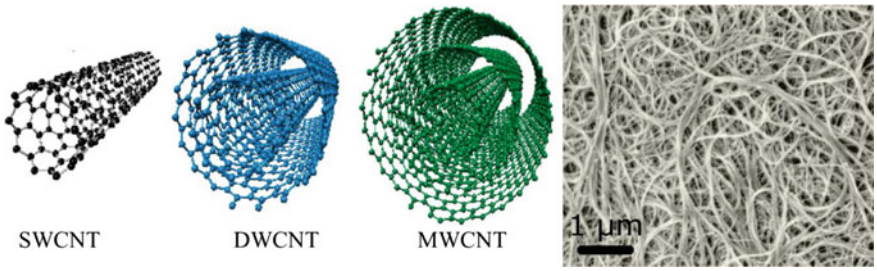

Fig. 4 Different types of carbon nanotubes on the basis of carbon atom layers and SEM image of CNTs Figs. taken from the Refs. [85–87], From L-R)

Table 1 First and second (top to bottom) showing important physical properties of carbon nanotubes (data collected from Refs. [3, 25–28, 32, 84–87])

Properties	SWCNTs	DWCNTs	MWCNTs
Surface area (m^2/g)	300–600	300–400	40–300
Geometric aspect ratio (length/diameter)	~10,000	~5000	100–1000
DC resistivity (Ω-cm)	2×10^{-4}	1.56×10^{-6}	2.45×10^{-6}

Properties	SWNTs	MWNTs
Specific gravity	0.8 g/cm^3	1.8 g/cm^3
Elastic modulus	~1 TPa	~0.3–1 TPa
Strength	50–500 GPa	10–60 GPa
Resistivity	5–50 μΩ cm	5–50 μΩ cm
Thermal conductivity	3000 W m^{-1} K^{-1}	3000 W m^{-1} K^{-1}
Thermal stability	>700 °C (in air)	>700 °C (in air)
	2800 °C (in vacuum)	2800 °C (in vacuum)
Specific surface area	~400–900 m^2/g	~200–400 m^2/g

A suitable combination of carbon nanotubes with conducting or non-conducting polymers offer a very attractive route to reinforce macromolecular compounds, as well as to introduce new electronic properties in the polymer system by modifications or electronic interactions between the two constituents (matrix and nanofillers) [38, 39]. Several conductive polymer based on CNTs have been developed, and they possess excellent conducting properties [39]. But the use of CNTs as a rough nanomaterial in different applications has been largely limited due to their poor processability, insolubility, and infusibility [40]. However, selective functionalization of CNTs can minimize the above difficulties during polymer nanocomposites synthesis [40, 41]. Materials science have been focusing on two types of materials for the conducting polymer composites (1) conductive composites based on insulating polymers such as polystyrene or poly (methyl methacrylate), etc., and (2) those made with conducting polymers such as polyaniline, Polypyrrole, poly (3,4-ethylenedioxy thiophene), polythiophene, 2,2-polybithiophene (PBTh), polyacetylene, etc. [42, 43]. The most often used process for the synthesis of CNT-based polymer composites is direct mixing of nanofillers in the melt or solution or via situ polymerization approach [43, 44]. The quality of formed nanocomposites mostly depends on the interfacial interaction between nanotube and polymer, which ultimately depends on the synthetic process [44]. Thus, in situ method of nanocomposites synthesis leads the most effective interfacial contact compared to the other reported method for the conducting polymer composites [44, 45].

4.1 Methods of Synthesis for CNTs-Based Conducting Polymers

Different methods have been reported to synthesize CNTs-based nanocomposites [46, 47]. However, the most effective, and common method for synthesis of conducting PANI/CNT composite is based on work published by Sivakkumar and coworkers [46–48]. They had prepared PA-based CNT nanocomposites by in situ approach, which is treated as the best for the preparation of polymer nanocomposites. For the development of nanocomposites, they have prepared a suspension of CNT in 1.0 M $HClO_4$ solution containing aniline monomer [46]. For the proper mixing 3–4 h sonication is very necessary after which the solution should be transferred to a polymerization reactor and the polymerization was initiated by maintaining a temperature of around 0–50 and by the addition of 1.0 M $HClO_4$ solution containing ammonium persulfate (APS) with mechanically stirring the monomer solution at around 400–500 rpm. After 3 h, the temperature was increased to 20 °C and the stirring was continued for 15 h [21]. The obtained polymer nanocomposites filtered and washed with water and acetonitrile, and then vacuum dried for 24 h. The effect of sonication on the quality of composite obtained can be checked quickly via similar synthesis without sonication. Figure 5 showing FESEM images of composite materials obtained with and without sonication [46]. After the

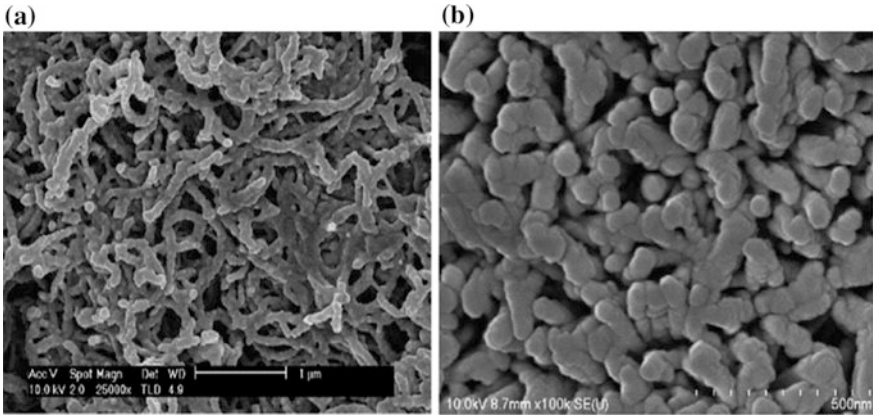

Fig. 5 FESEM images of **a** CNT/PANI nanocomposites prepared with sonication, **b** CNT/PANI nanocomposites prepared without sonication. It is crystal clear that in the case of sonication coating of PANI on CNTs is much better than without sonication (Reproduced with permission from Ref. [46])

completion of synthesis and drying of CNT-PANI composite electrode for supercapacitor can be designed using the procedure adopted in the research article published by Sivakkumar and coworkers.

Sivakkumar and coworker have investigated that electrochemical behavior (especially conducting behavior) CNT/PANI nanocomposites-based cell much better than of that pure polyaniline nanofiber-based cell [46–48]. It is ultimate because of very effective electric double-layer capacitance in the CNT-based electrode. During the study, it has been found that the current passed by the PANI/CNT composite-based device is higher than that of pure PANI nanofiber, which means that the capacitance of the nanocomposites is larger than that of the pure PANI nanofiber. This indicates a synergistic effect from the combined contributions from PANI and CNT [46] (Fig. 6).

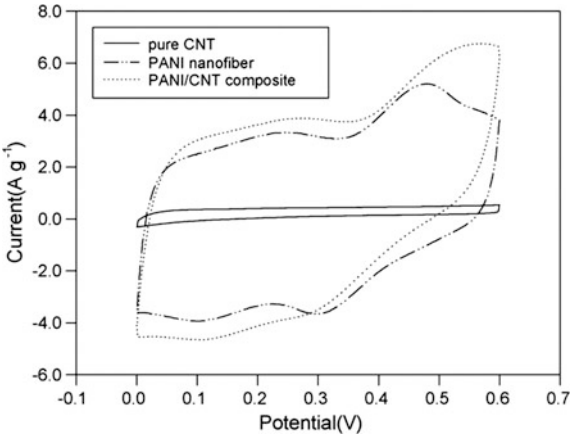

Fig. 6 Cyclic voltammograms for pure PANI nanofiber, pure CNT and PANI/CNT nanocomposites. At the scan rate is 10 mVs^{-1} (Reproduced with permission from Ref. [46])

So, that using similar polymerization approach several conducting polymer nanocomposites (with different polymers like polypyrrole (PPy), poly(phenylene-diamine) (PPD), and poly(3,4-ethylene dioxythiophene) (PEDOT, etc.) have been developed using CNT as nanofillers and various conductive polymer as a matrix. Some of them are reported in other literature [46, 49–51]. Ramesh and coworker [51] synthesized very useful nanoclays and conducting carbon-based nanocomposites for supercapacitor application. The procedure is briefly discussed below.

Nanoclays-based graphene-PANI hybrid nanocomposites were prepared by chemical oxidative polymerization of aniline via in situ and ex situ approaches using APS as an oxidant as follows. Equal quantities of graphene and nanoclays (50 % each) were dispersed in 50 ml of distilled water in a 250 ml beaker. To get a uniform graphene–nanoclays dispersion, the mixture was well sonicated for 30 min in an ultrasonic bath. To this, 1 ml of aniline was added dropwise under continuous stirring in an ice bath. The polymerization was initiated by the dropwise addition of APS (2.5 g dissolved in 50 ml of distilled water). Afer the addition of the APS solution, the entire solution became a deep and dusty greenish color with the progression of time. The entire solution was then stirred continuously for 5 h at room temperature. The prepared hybrid nanocomposites were filtered and washed several times with distilled water until the yellow color of sulfur had vanished. The as obtained composite was dried under vacuum at 60 °C for 12 h. The obtained nanocomposites were marked as GNA (the abbreviation represents the chronological order of the addition of all the components, i.e., graphene, nanoclays, and aniline). The ex situ composite was prepared by following the same process as that of the in situ composite, except that the nanoclays was added after the completion of the polymerization of aniline in the presence of graphene and was coded as GAN (the abbreviation represents the chronological order of the addition of all the components, i.e., graphene, aniline, and nanoclays). One set of graphene–PANI samples was also prepared with the same graphene–aniline ratio for comparison (coded as GA). The synthesis process is schematically shown in Fig. 7.

4.2 Characterization Techniques

To obtain characteristic features of prepared conducting nanocomposites, the following main instrumental techniques frequently used by materials scientists. It is tough to explain all the instrumental methods in a single chapter, so some magnificent references have been added for the readers. And in very short the utility and importance of these characterization techniques discussed below, Atomic Force Microscopy: AFM (To obtain information about topographic images, advanced coating, thickness and for investigation of some mechanical properties), Field Emission Scanning Electron Microscopy: FESEM (To get information about surface morphology, advanced coating, thickness, structure uniformity determination, contamination in samples and elemental composition measurement), Fourier Transform Infrared spectroscopy: FTIR (To obtain information about the various

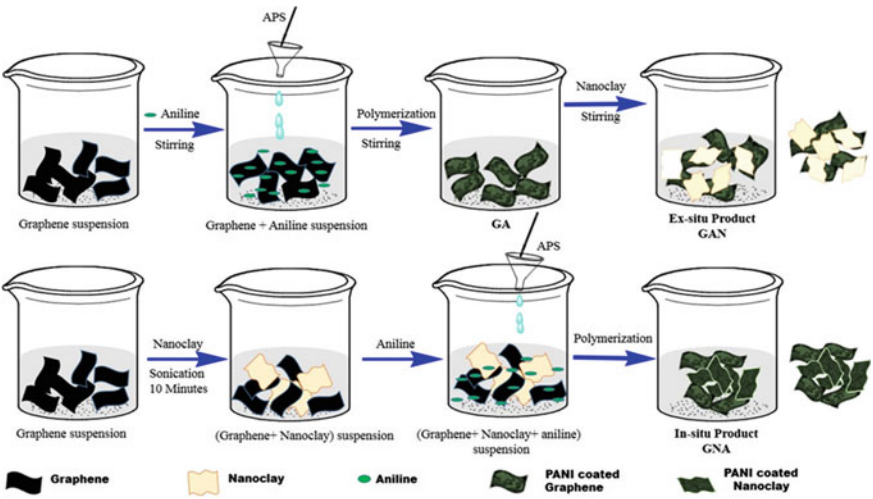

Fig. 7 Schematic diagram for the synthesis of carbon-based conducting polymer nanocomposites for super capacitor applications (Reproduced from authors own paper Ref. [51])

functional groups present in composites), Raman spectroscopy (To obtain information about the nature of materials and for the characterization carbon-based nanofillers) X-ray Powder Diffraction: XRD (to get information about crystallinity of material and also for the information about the unit cell dimensions), Rheometer (It used to measure the viscous-elastic properties of composite with response to applied forces), Thermogravimetric Analysis: TGA (To obtain information about physical phenomena, like as second-order phase transitions, including vaporization, absorption, sublimation, desorption, and adsorption thus it is used measure thermal stability of composites), Differential Scanning Calorimetry: DSC (It is used widely for examining polymeric materials or composites to determine their thermal transitions. And this thermal transitions can be utilized to compare stability of materials), Cyclic Voltammetry: CV (To obtain information about a variety of redox processes, to determine the stability of reaction products, the presence of intermediates in redox reactions, reaction and electron transfer kinetics, and the reversibility of a reaction), LCR meter: (It is used to measure the inductance, capacitance, and resistance of a conducting materials. The simpler versions of this instrument the impedance is measured internally and converted for display to the corresponding capacitance or inductance value), BET surface area: BET analysis (To obtain information about physical adsorption of gas molecules on a solid surface and serves as the basis for an important analysis technique for the measurement of the specific surface area of a material).

4.3 Application of CNT-Based Conducting Polymer Nanocomposites

CNT-based polymer nanocomposites have proven very good electrode materials. This is why it has been widely used in the fields of electroanalysis, electrochemistry, batteries, and capacitors, etc. [40, 46, 49–51]. In these applications, both conductivity and electrochemical activity play vital role in nanocomposites [42, 43]. Moreover, molecules and small ions can readily diffuse into the CNT-based polymer nanocomposites, providing an additional advantage of the conventional materials [45, 46]. Due to the intrinsic property of CNT-based polymer nanocomposites allows electrochemical reactions to take place throughout the matrices of nanocomposites, and thus greatly increasing the active sites for electrochemical processes by using a 3D electrode [46]. However, to efficiently utilize all the active sites on the electrode matrix and to enhance mass transportation during the electrode process, the thickness of the CNT-based polymer nanocomposites should be reduced to facilitate the ion diffusion in the matrices [45, 46]. Considering these important facts, these nanomaterials show superior advantages, due to their small dimension and very larger specific surface areas.

4.3.1 Supercapacitors

Conducting polymers have been widely studied as an energy storing materials for the various kinds of capacitors due to their large pseudo capacitances. Since charges are stored in its whole volume, conducting polymer-based capacitors can achieve a much higher specific charge density in comparison with other carbon materials [46, 52, 53]. But the CNT-based conducting polymers are of particular importance in the fabrication of capacitors because they have very high specific surface areas and small dimensions. It allows simple diffusion of electrolytes in the polymer matrices and more available active sites for redox reactions [37, 38, 46]. Moreover, being directly related to the surface area, the double-layer capacitance of a nanostructured composite film is also much larger than other known similar materials [45, 46]. For example, CP/carbon nanocomposites are regarded as good candidates for capacitors [46]. In these nanocomposites, i.e., CNT act as the templates for the electro synthesis of CPs, and they also increase the conductivity of the composite electrode and facilitate the electron transportation in the device. Some electro chemically active inorganic materials can also be incorporated into CP matrices to prepare capacitors. Electro-synthesized PANI/polyoxometalates nanocomposites were tested to have high specific capacitances, resulting from the combination of the capacitances of both components [46, 50–52] (Fig. 8).

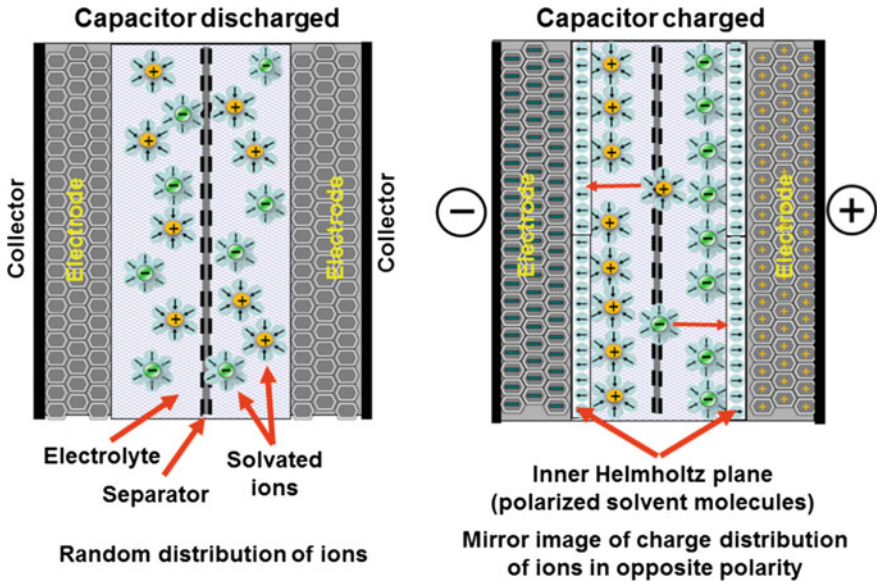

Fig. 8 Diagrammatic representation of functioning of super capacitors (Available online for the non-commercial use)

4.3.2 Fuel Cell Electrode

Methanol fuel cell is treated as one of the most significant fuel cells because of its low cost and very high energy density [53, 54]. Usually, oxidation of precursor (methanol) is rather difficult, and catalysts are needed [53, 54]. So far as we know, the best catalysts for the methanol oxidation are noble metal nanoparticles [55]. To achieve a uniform dispersion, high utilization, and good stability of catalyst, metal nanoparticles need to be properly deposited on a supporting substrate [56]. The widely used catalyst supports for fuel cell electrodes are various carbon materials. However, fabrication and processing of carbon materials electrodes are difficult [56, 57]. Therefore, conductive polymers were developed as alternative supports for dispersing metal particle catalysts [57]. Since the metal particles can be trapped in the matrices of conductive polymers, forming a 3D catalyst array, the conductive polymers/metal nanoparticle composite electrodes can load more catalysts without an apparent increase in thickness of the modification layers [57, 58]. Thus it is very successfully resolves contravenes of the catalyst amount and the chemical reagent diffusion rate. However, there is plenty of work focused on developing metal nanoparticle/conductive polymers electrodes, and only a few of them were prepared for electrochemical approaches [58, 59], but the electrodeposition of such electrodes has it over advantages [58, 60]. The use of PANI/Pt and PPy/Pt conducting polymer nanocomposites as the catalytic electrodes for electro-oxidation of methanol has been well studied around the 1990s, and in recent years, research

work has focused on shaping the conducting polymer matrices into a nanostructured morphology [61–63]. For the instance, in an electrodeposited PPy nanowires matrix, Pt nanoparticles were electrochemically deposited, forming a PPy/Pt conducting polymer composite [62]. The PPy/Pt conducting polymer composite modified electrode showed excellent catalytic action toward both the methanol oxidation reaction and oxygen reduction reaction the in comparison with the pure Pt-modified electrode [58–63]. So, that it is crystal clear that fabrication and application electrode based on PPy/Pt (or other metal nanoparticles) and like conducting polymer composite is expensive and requires great care. To resolve all the critical issues CNTs-based conducting polymer composites are the best alternative to much superior efficiency [64–67] (Fig. 9).

4.3.3 Electrochemical Actuators

The ability of gels to reversibly swell and de-swell under controllable conditions has made them an attractive for use in electrochemical actuators [68]. However, their applications present several issues. They usually swell isotropically, which is a bad thing for the actuation technologies because it requires of linear response. Swelling is slow due to poor solvent and ionic diffusion of the material. The swelling of such materials can be controlled by the optimizing a broad range of external factors [68]. Electrochemical polymerization (of conducting polymers) is an efficient method to fabricate conducting soft polymer actuators because this approach can produce very high-quality conducting polymer films [46, 69] with actuator characteristics [46, 68, 69]. In the case of bending-type conducting polymer actuator, an asymmetric double layered or multilayered conducting polymer

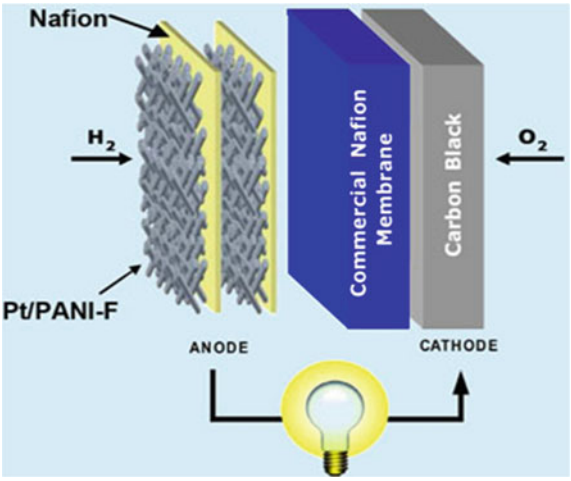

Fig. 9 Schematic diagram of fuel cell and their electrodes based on conducting polymers (Available online for the non-commercial use)

film is needed. And it could be easily obtained via successive Electrochemical Deposition (ECD) in different electrolytes [46, 70, 71]. Moreover, a nanostructured conducting polymer layer can also be combined into a conducting polymer actuator via an electrochemical route [70, 71]. Actuators made of conducting polymer composites not only have modified and improved actuation performances but also may have many new functions based on their nanostructure [72]. For the example, an actuator fabricated from a monolithic PPy film (PPy-CNT-based conducting polymer composites) exhibited a enormous bending angle, rate and a long lifetime, being related to the asymmetric structure, non-delamination and high conductivity of the PPy-CNT-based nanocomposites film [72, 73]. An actuator consisting of a PPy/nanotube layer and a compact PPy film layer can capture PS microparticles from a diluted aqueous dispersion) and transfer the particles to a new medium by sonication or electrochemical control. Thus, CNT/conducting polymer-based are much-2 efficient than the conventional polymer and conventional nanocomposites [70–76].

4.3.4 Memory Devices

Conducting polymers and their nanocomposites can be used to fabricate stable, economical and non-volatile memory devices by modifying their conductivity, to encode '0' and '1' signals [77, 78]. It was reported that conducting polymer/gold nanocomposites showed an apparent electric bi-stability response to an applied voltage [79, 80]. That is, the conductivity of the composite materials increases sharply by several times of magnitude when a fixed potential is applied to it, and this high conductivity can be maintained until a proper reverse potential is applied [81]. During the turn-on process, an electric field driven electron transfer from conducting polymer to gold/CNTs nanoparticles occurs [81, 82]. Recently, it has been reported the fabrication of an electric bi-stable memory device by using an electro-synthesized conducting polymer/CNTs-based composite film as the active layer [83]. It was found that CNTs were very successfully incorporated and uniformly dispersed in the active layer without phase separation and aggregation, and the device exhibited an excellent on/off switching ratio and very high stability [81, 82]. These results indicated that electrochemical co-deposition provides a direct and convenient method for fabricating the active layer of memory devices using CNTs nanofillers and various conducting polymers as matrix [84].

4.3.5 Field Emission Devices

The field emission devices are based the organic light-emitting transistor (OLET) technology. An OLET is a form of transistor that emits light. These transistors (OLETs) have been claimed to have the potential for digital displays, and on-chip

optical interconnects [85]. So, that OLET is a new light-emission concept, providing planar light sources that can be easily integrated into substrates like glass, silicon, paper using standard microelectronic techniques [85–87]. Recently it has been reported that conducting polymer nanowires and CNTs arrays are excellent candidates for fabricating organic field emitters. Template-guided electrochemical polymerization usually prepares these materials. Joe and coworkers have studied the field emission performances of PANI, PPy, and PEDOT nanotube and nanowires arrays. The devices showed turn-on voltages of 3.5–5.5 V mm^{-1} and field enhancement factors of 700–900 [88]. To enhance the functioning of the conducting polymer field emitter, a highly conductive PPy nanowires array was electro-synthesized in the mixed solvent of isopropyl alcohol. Similarly, BFEE and poly (ethylene glycol), nanomaterials device exhibited a lower turn-on voltage of 1.2 V mm^{-1} and a higher b of 10,000 [87–90].

4.3.6 Lithium Batteries

As previously mentioned, CNTs-based nanocomposites material electrodes are one the best candidate for the supercapacitors application [46–52]. Similarly, CNTs open up different ways of interaction with various molecules or atoms specifically, the intercalation between the pseudo-graphitic layers or insertion of the central tube [91]. Such a doping, by intercalation of donor or acceptor species between the carbon shells, could allow for control of the properties of CNTs (especially electronic properties), and allow to the exchange of electrons via a redox reaction [40, 45, 83, 91–93]. Very recently, CNTs-based conducting polymers have also been used for the storage of adsorbed molecules [94–96]. The fundamental principle of rechargeable lithium-based batteries is electrochemical intercalation and deintercalation of a lithium atom in both electrodes (CNTs conducting polymer-based electrode) [40, 45, 83, 91–93]. A simple battery has a less charging time, high energy capacity, and a long cycle time and all these features can be obtained using CNTs conducting polymer-based electrode [97]. The efficiency of such battery determined by the lithium saturation concentration of the electrode materials. And it has been reported that efficiency is very high in the case CNTs/conducting polymer-based electrode which is ultimate because of very good interaction between the CNTs/conducting polymer-based electrode and lithium [91, 93, 95–97]. It has also been reported the reason for highest efficiency is all the interstitial sites of CNTS are accessible for Li-intercalation [98]. SWCNTs have shown to possess both highly reversible and irreversible capacities. Because of the large observed voltage hysteresis, Li-intercalation in nanotubes is still unsuitable for battery application [92, 93, 95–98]. Similar observations have also been reported using CNTs-based polyaniline (PANI), polypyrrole (PPy), poly(phenylenediamine) (PPD), and poly(3,4-ethylenedioxythiophene) (PEDOT).

5 Graphene-Based Conductive Polymer Composites

5.1 Graphene

Graphene is newly discovered carbon allotrope [99]. It is magical; mother of all graphitic carbon, one-atom-thick, two-dimensional carbon material graphene has emerged as a new hope for the entire scientific fraternity [99, 100]. It has ultra-high intrinsic carrier mobility (200,000 cm^2/V^3 s and exhibits a thermal conductivity of several times higher than that of Cu metal). It also has a very large surface area which is even much greater than SWCNTs (2630 mg^{-1}), excellent thermal, mechanical and elastic properties, etc. In the whole scientific community initially the uniqueness of GR created hype due to following unbelievable physical properties as given below [99–102].

i. It is purest form of carbon.
ii. Very large theoretical specific area which is about 2360 m^2/g.
iii. Highest intrinsic mobility 200,000 $cm^2\ v^{-1}\ s^{-1}$.
iv. Extremely high Young's modulus is about 1.0 TPA.
v. Exceptional thermal conductivity is about 5000 $Wm^{-1}\ k^{-1}$.
vi. Optical transmittance is more than 98 %.
vii. Lightest and thinnest known material in the universe.
viii. Zero band gaps.
ix. Outstanding elasticity.

The discovery of graphene has been entirely changed the face of material science [99–102]. Its development started when Kaleb a six-year-old child, look out his pencil and began writing letters on a piece of paper [102, 103]. He did not know that he was just going to open a significant research topic that caught a great attention of all scientific community that same day [103, 104]. For outstanding contribution to the field of GR (Andre Geim and Konstantin Novoselov) of MIT, UK awarded Nobel Prize in physics in 2010 [104] (Fig. 10).

5.2 Graphene and Derivatives-Based Conducting Polymers

At present, graphene-based conducting polymer composite materials have been attracting much attention because of the high performance of graphene as a nanofillers, giving these materials enhanced mechanical and electrical properties [35, 105–108]. The synthetic procedure of these nanomaterials is very similar to the CNTs-based conducting polymer nanocomposites. A number of graphene-based (polyaniline (PANI), polypyrrole (PPy), poly(phenylenediamine) (PPD), and poly (3,4-ethylenedioxythiophene) (PEDOT)) conducting polymer composites have been reported for the various application [35, 105–110]. These composites are showing very high efficiency in super capacitors, solar cells, sensors and other

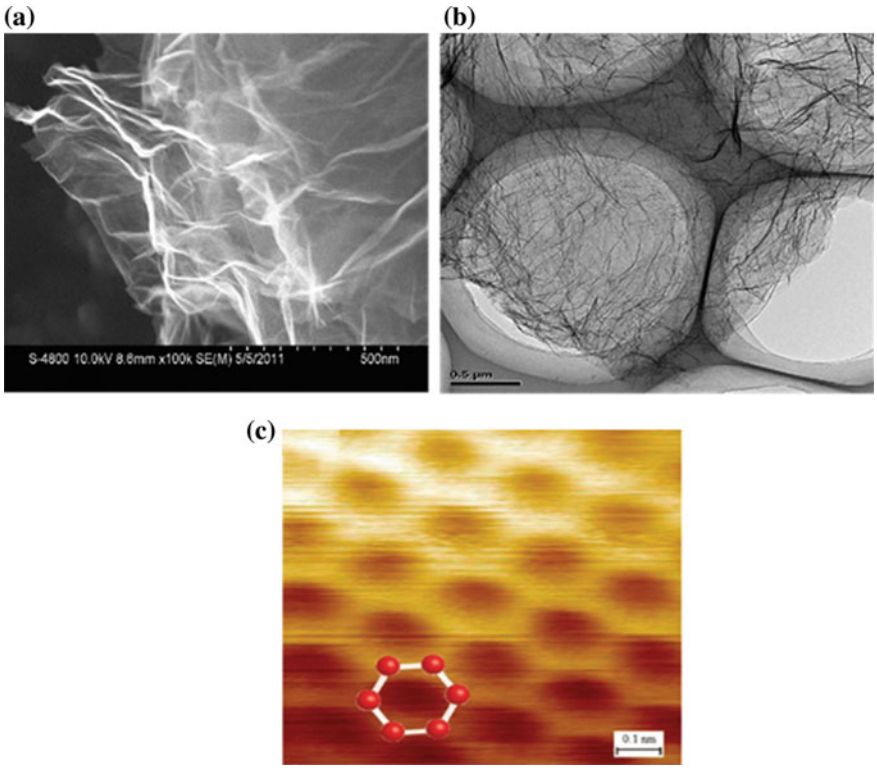

Fig. 10 FESEM-A and TEM-B image of ACS Material-Industrial-Quality Graphene and STM-C image of single layers graphene (Reproduced with permission from ACS materials wave page)

devices. The bottleneck in the path of these nanomaterials synthesis is aggregating the nature of graphene [35, 110, 111]. To remove this lacuna, various very good efforts and several approaches have been made to prepare graphene-dispersed composites in which graphene is homogeneously dispersed into polymer matrices [35, 111, 112].

Most of the scalable approaches to graphene-based conducting polymer composite materials (few-layer platelets or monolayer carbon sheets with heteroatoms and topological defects) mostly use graphite as the precursor material for the graphite oxide, graphene oxide, reduced graphene oxide, and graphene. Graphite oxide has been investigated as far back as the 1840s [35]. A variety of uses have been studied and demonstrated for the graphene-based conducting polymer composite and also for other graphene-based materials. And their use as a composite filler has attracted the considerable interest of the whole scientific community, especially of polymer chemist [35, 105, 106, 110–113]. While polymer composites incorporating these fillers continue to be a significant research focus, recently many groups have primarily focused on the use of graphene-based filler materials derived from

graphene or reduced graphene oxide mainly to develop graphene-based efficient polymer nanocomposites [35, 106, 110–113]. Recently, it has a been reported that graphene oxide fillers-based conducting polymer could exhibit very high electrical conductivities (on the order of thousands of S/m) high moduli (reported values ranging from 200 GPa to over 650 GPa), and can be easily functionalized to tailor their compatibility with the host polymer [105, 112, 113]. The reported values of stiff ness and electrical conductivity of graphene oxide fillers-based conducting polymer could be higher than those reported for nanoclays and many other fillers [35, 105, 112, 113]. However, generally lower than those reported for single-walled carbon nanotubes (SWNTs) [114]. However, the intrinsic mechanical properties and electrical and thermal conductivities of SWNTs may be comparable to those of pristine graphene but in the both case mechanism of electrical conduction is a matter of deep consideration [113, 114]. Moreover, the 2D flat geometry of graphene and graphene-based materials may offer certain property improvements that SWNTs cannot provide when dispersed in a polymer composite, such as improved gas permeation resistance of the composite [105, 112–114].

5.3 Various Approaches for the Synthesis of Graphene-Based Conducting Polymer

5.3.1 Solution and Melt Mixing Without Covalent Bonding

Solution mixing synthetic approaches generally involve the mixing of colloidal suspensions of graphene oxide or other graphene-based materials with the selected polymer matrix, either itself already in solution or by dissolving in the polymer in the suspension of graphene derivate by simple stirring or shear mixing [90, 91]. The resulting suspension now can then be precipitated using a particular non-solvent for the polymer, causing the polymer chains to encapsulate the filler upon precipitation [90, 115]. The precipitated composite materials can then be extracted, dried, and further processed for testing and application [90, 115]. By another route, the suspension can be directly cast into a mold and the solvent removed. But a problem with this route is the aggregation of the filler (graphene, graphene oxide, etc.) in the nanocomposites, which may affect the properties composite materials [95, 115, 116]. This approach of mixing has been widely reported in the literature, as Chemically Modified Graphene (CMG) can often be processed in either water or organic solvents [115, 116]. The solution mixing method has been used for incorporating graphene oxide derived fillers into a variety of polymers, including polycarbonate [97, 116], polyacrylamide [98], polyimides [99], and poly (methyl methacrylate) (PMMA) [100, 117]. The facile synthesis of aqueous graphene oxide platelet suspensions via sonication makes this technique particularly very applicable for water-soluble polymers such as polyvinyl alcohol (PVA) and poly (allylamine), nanocomposites of which can be produced by the simple filtration [104, 106, 115–117]. In addition,

vacuum filtration of graphene oxide/PVA and graphene oxide/PMMA solutions has been used to make composite films across a broad range of loadings which have a layered external appearance similar to the graphene oxide paper. The restacking of the some platelets may be possible, for solution mixing methods the dispersion of platelets in the composite is largely governed by the level of exfoliation of the platelets achieved prior to, or during, mixing [100–115]. Thus, solution mixing offers a potentially simple route to dispersing single-layer CMG platelets into a polymer matrix [115]. As above mentioned, a fictionalization of small molecule and grafting have been reported to achieve stable CMG platelet suspensions of highly exfoliated platelets before mixing with the polymer host. Lyophilization methods [116], the phase transfer methods and surfactants have all been used to facilitate solution mixing of graphene-based composites. But, it has also been reported that use of surfactants could affect the properties of prepared composite. For example, surfactants have been reported to increase the matrix-filler interfacial thermal resistance in CNTs-based polymer composites, attenuating the thermal conductivity enhancement about CNTs that were processed without surfactants [116, 117].

In the case of melt mixing (also known as melt compounding methods), a polymer melt and filler (in a complete dried powder form) are mixed under suitable temperature/pressure conditions [118]. In comparison to solution mixing technique, melt mixing is often considered more economical and environmentally friendly (because in this case there is no need for solvent) and is much more compatible with the industrial applications [118, 119]. But one of the most important drawbacks of this method is a heterogeneous dispersion of the filler in the polymer matrix unlike the solvent mixing or in situ polymerization methods [104, 106, 115–117]. But the dispersion of single or few-layer graphene/graphene oxide and derived fillers via melt compounding is tough because a greater probability of aggregation of the sheet during the mixing [118]. However, many studies report melt mixing using TEGO matrix and graphene derivatives as nanofillers, where these nanomaterials could be fed directly into the extruder machine and dispersed in a polymer matrix without the utilization of any surfactants or solvents. But in this case, the very low bulk density of TEGO makes handling of the dry powders difficult and poses a processing challenge (feeding into the extruder machine). In the same line, it is reported that mixing of conducting polymer and nanofillers is possible without the use of any surfactants or solvents by optimization of shear pressure, rpm, and temperature of extruder [118, 119]. In a different method to ‘premix’ the matrix and filler before mixing, graphene derivatives were sonicated in a non-solvent, such that polymer particles were uniformly coated with graphene derivatives before melt mixing, which was reported to lower the electrical percolation three should of a graphene derivatives/polypropylene composite. Notably, for composites incorporating graphene oxide as filler, melt processing, and molding operations may cause substantial reduction of the graphene oxide due to their thermal instability [120].

5.3.2 In Situ Polymerization Without Covalent Bonding

In situ polymerization approach for the preparation of polymer composites generally involve mixing of filler in neat monomer/with different monomers of the polymer or a solution of the monomer in the polymer, followed by a polymerization reaction in the presence of the nanofillers [121]. These efforts are very commonly used with extraction or solution casting methods to generate samples for testing. Many researchers reported that in situ polymerization processes is a very important way to produce conducting polymer nanocomposites with covalent linkages between the polymer matrix and nanofillers [121, 122]. Moreover, it also been reported that in situ polymerization has also been used to produce conducting polymer nanocomposites without covalent interactions with the variety of polymers. For example, poly (pyrrole), poly (ethylene), PMMA [122–124]. So, it should be very clear to the reader that method of preparations (of conducting polymer composites based of carbon nanomaterial) not the determined type of interactions between the matrix and filler and it only depends on the nature of monomer and nanofillers [121–123]. In several cases monomer of the matrix is intercalated between the layers of graphite oxide or few layers graphene, followed by polymerization reaction to separate the layers. This technique of polymerization is commonly known as intercalation polymerization. This technique has widely been investigated for Nanoclays-based polymer composites and has also been applied to graphene and CNTs-based polymer nanocomposites [124].

Very recently, our group reported a unique graphene-based polymer nanocomposite (via in situ polymerization) using waste paper for the supercapacitors application [125]. The method of synthesis of this new graphene-based polymer nanocomposites mentioned below; this specific example will be very useful to understand the inside the graphene-based polymer nanocomposites. First, 50 mg of the prepared graphene was dispersed in 50 ml of distilled water and sonicated for about 15 min. After the proper dispersion of graphene, 1 ml pyrrole was slowly added to it with constant stirring (400 rpm). The solution was further sonicated for 15 min for the homogeneous dispersion. To the above homogeneous solution, 2.5 g Ammonium Persulphate (APS) in 50 ml distilled water was gradually and very slowly added. Then it was stirred for 30 min with the help of magnetic stirrer and followed by 15 min sonication. The beaker was covered and refrigerated overnight for complete polymerization. The resulted solution was filtered, washed and dried to obtain the product composite. Now 50 mg of extracted cellulose [125] was sonicated for 15 min in 50 ml of distilled water followed by very controlled addition of 1 ml pyrrole. The solution was again sonicated for 15 min. To the above solution, 2.5 g APS in 50 ml distilled water was gradually added. It was then kept under magnetic stirring for 30 min followed by 15 min of sonication. The beaker was covered and refrigerated overnight for the proper polymerization of pyrrole in the presence of added additives. The solution was then filtered, washed and dried to obtain the composite. Finally, Cellulose- and graphene-based PPy composite was prepared by using the same process as in CP in the presence of Graphene. In brief [125], 50 mg of extracted cellulose was sonicated in 50 ml of distilled water followed by addition

of 50 mg of dispersed graphene. The whole solution was sonicated for 15 min to obtained homogeneous solution. 1 ml of pyrrole monomer was very slowly added to this dispersion with stirring (400 rpm) followed by slow addition of 50 ml of APS solution. The whole solution was stirred for 30 min and finally sonicated for 15 min. The beaker was covered and refrigerated overnight. The solution was then filtered, washed and dried to obtain the final graphene-based composite [124, 125]. In this way, waste papers (Since cellulose, is an essential constituent of paper, and can be extracted very easily from the papers) can be utilized for bio-composites and energy storage applications using the approach as mentioned earlier. Even though cellulose itself is a non-electro-active material, its application in the supercapacitor field has been created enormous interest for further studies.

5.3.3 Characterization Techniques

Almost all characterization techniques which have been described in Sect. 4.2 of CNTs-based conducting nanocomposites equally applicable for the graphene-based conducting polymers nanocomposites. So, there is no need to discuss it again. For the further study of the characterization of these materials reader may review an excellent book by P. Mukhopadhyay and R.K Gupta, CRC Press, ISBN: 978-1-4398-2779-6.

5.3.4 Application of Graphene-Based Conducting Polymers

Graphene-based conducting polymer composites are much better and very efficient substituent of CNTs-based conducting polymers as mentioned in brief in the CNTs-based conducting polymer sanction [40–56]. So that graphene-based conducting polymer composites equally applicable to the supercapacitors, lithium ions batteries, various kinds of sensors, memory devices, fuel cells electrodes, electrochemical actuators, field emission devices, and as coating materials [35, 105–108, 111–115, 120–125]. However, an instance research will be necessary to investigate the suitable mechanism of interactions between components (between the matrix and nanofillers) in these conducting composites. We have a firm belief that graphene-based conducting polymers with a broad range of functions are promising materials for future research and applications in electrical soft materials.

6 Conclusion and Future Prospects

The conductive polymer composites based on carbon nanomaterials have a significant and unique place in the list of advanced materials so far invented and discovered by materials scientists. The history of these new materials is not older than 3–5 decade. Conducting polymers represent new advanced materials as a critical issue for

the development of different kind of devices and structures offering the association of the various properties required for the efficient technological applications. Supercapacitors, due to their ability to perform during long momentary periods, are nowadays using as the electrical energy storage devices. They have technical and economic advantages of electrical appliances. For example as power supplies, protection of computer memory, microchip, fuel cells, and batteries. Moreover, these nanomaterials are rising very rapidly because of massive scientific and technological interest for the real-time applications, and these materials have led the research in materials science in a new direction. Such sensational growth of these materials ultimately due to the versatility of synthesis techniques, properties, and very broad scope of application. This book chapter provides a brief and an up to date account about the conductive polymer composites based on carbon nanomaterials including historical development, fundamental terms, an important method of synthesis and widespread application. To explore the versatility, processability, uniqueness, and implementation potential of these conducting nanomaterials, some very new and important conducting composites based on CNTs and graphene are taken as the example and have been discussed in proper context. By varying the nature of the carbon-based nanofillers and the reaction conditions, many of the physical and chemical properties namely magnetic susceptibility, colloidal stability, and electrical properties have been improved which never possible by a standard mixing or by simple blending. So, all these aspects of conductive polymer composites based on carbon nanomaterials have explored with the suitable examples. Keeping the rapid progress of research in this field of conducting nanomaterials up to date, it can be stated that these materials will be commercially available in near future, and their suitable applications will give a high boost to material science and technology.

Due to their tedious processability, these nanomaterials have very small commercial production. They have promised in antistatic materials, and they have been incorporated into commercial displays and batteries, but there have had limitations due to the production costs, toxicity and due to inhomogeneous solubility in solvents. Many workers reported its promising utilization in printing electronic circuits, organic solar cells electrochromism, chemical sensors, supercapacitors and biosensors, transparent flexible displays, electromagnetic shielding. Moreover, its use is for microwave-absorbent coatings, particularly radar-absorptive coatings on stealth aircraft. So, that author believes that shortly carbon-based conducting polymer nanocomposites-based technologies would be cheap, reliable and industrially available.

References

1. Yaghi OM, Keeffe M, Ockwig NW, Chae HK, Eddaoudi M, Kim J (2003) Nature 423:6941
2. Wei BQ, Vajtai R, Jung Y, Ward J, Zhang R, Ramanath G, Ajayan PM (2002) Nature 416:495
3. Mestl G, Maksimova NI, Keller N, Roddatis VV, Schlögl R (2001) Angew Chem Int Ed 40:11
4. Geim AK (2009) Science 324:1530–1534

5. Li D, Kaner RB (2008) Graphene-Based Mater Nat Nanotechnol 3:101
6. Nolas GS, Sharp J, Goldsmid J (2001) Thermoelectrics, vol 45. Springer, Berlin
7. Budinski KG (1997) Wear 203:302
8. Cantwell WJ, Morton J (1991) Composites 22:347
9. Huang WS, Humphrey BD, MacDiarmid AG (1986) Faraday Trans 1(82):2385
10. McCullough RD, Lowe RD, Jayaraman M, Anderson DL (1993) J Org Chem 58:904
11. De Gangopadhyay R (2000) Chem Mater 12:608
12. McCarthy PA, Huang J, Yang SC, Wang HL (2002) Langmuir 18:259
13. Freund MS, Lewis NS (1995) Proc Natl Acad Sci 92:2652
14. Jannasch P (2003) Curr Opin Colloid Interface Sci 8:96
15. Miasik JJ, Hooper A, Tofield BC (1986) Faraday Trans 1(82):1117
16. Marsella MJ, Swager TM (1993) J Am Chem Soc 115:12214
17. Pan YX, Yu ZZ, Ou YC, Hu GH (2000) J Polym Sci Part B: Polym Phys 38:1626
18. Sumita M, Sakata K, Asai S, Miyasaka K, Nakagawa H (1991) Polym Bull 25:265
19. Inzelt G (2012) Conducting polymers: a new era in electrochemistry. Springer Science & Business Media, Mar 23
20. HushNoel S (2003) Ann N Y Acad Sci 1006:20
21. Akamatu H, Inokuchi H, Matsunaga Y (1954) Nature 173:168
22. Shirakawa H, Louis EJ, Alan G, Chwan K, Heeger V, Alan J (1977) Chem Commun 16:578
23. De Surville R, Jozefowicz M, Yu M, Pepichon LT, Buvet JR (1968) Electrochim Acta 13:1451
24. Joo J, Epstein A (1994) J Appl Phys Lett 65:2278
25. Hatchett DW, Josowicz M (2008) Chem Rev 108:746
26. Huo Q, Margolese DI, Feng P, Gier TE, Sieger P (1994) Generalized syntheses of periodic surfactant/inorganic composite materials. California University, Santa Barbara Dept. Chemistry
27. Hashin Z (1983) Analysis of composite materials—a survey. J Appl Mech 50:481
28. Michel JC, Moulinec H, Suquet P (1999) Comput Methods Appl Mech Eng 172:109
29. Buzea C, Pacheco I, Robbie K (2007) Biointerphases 2:MR17
30. Cuenot S, Frétigny C, Demoustier-Champagne S, Nysten B (2004) Phys Rev B 69:165410
31. Li H, Xu C, Srivastava N, Banerjee K (2009) IEEE Trans 56:1799
32. Gojny FH, Wichmann MH, Fiedler B, Bauhofer W, Schulte K (2005) Compos A Appl Sci Manuf 36:1525
33. Luo X, Morrin A, Killard AJ, Smyth MR (2006) Electroanalysis 18:319
34. Camargo PHC, Satyanarayana KG, Wypych F (2009) Mater Res 12:1
35. Kuilla T, Bhadra S, Yao D, Kim NH, Bose S, Lee JH (2010) Prog Polym Sci 35:1350
36. Monthioux M, Kuznetsov VL (2006) Who should be given the credit for the discovery of carbon nanotubes? Carbon 44:1623
37. Qin LC, Zhao X, Hirahara K, Miyamoto Y, Ando Y, Iijima S (2000) Nature 408:50
38. Baughman RH, Zakhidov AA, Heer WA (2002) Science 297:787
39. Xiao Q, Zhou X (2003) The study of multiwalled carbon nanotube deposited with conducting polymer for supercapacitor. Electrochim Acta 48:575
40. Du Y, Shen SZ, Cai K, Casey PS (2008) Prog Polym Sci 37:820
41. Huang G, Wang B, Lu H, Mamedov A, Gupta S (2006) Material characterization and modeling of single-wall carbon nanotube/polyelectrolyte multilayer nanocomposites. J Appl Mech 73:5
42. Meng C, Liu C, Fan S (2009) Electrochem Commun 11:186
43. Zhang X, Zhang J, Wang R, Zhu T, Liu Z (2004) ChemPhysChem 5:998
44. Wang F, Gu H, Swager TM (2008) J Am Chem Soc 130:5392
45. Hussain ST, Abbas F, Kausar A, Khan MR (2013) High Perform Polym 25:70
46. Sivakkumar SR, Kim WJ, Choi JA, MacFarlane DR, Forsyth M, Kim DW (2007) J Power Sources 171:1062
47. Gajendran P, Saraswathi R (2008) Pure Appl Chem 80:2377
48. Xu J, Yao P, Wang Y, He F, Wu Y (2009) J Mater Sci: Mater Electron 20:517

49. Frackowiak E, Khomenko V, Jurewicz K, Lota K, Beguin F (2006) J Power Sources 153:413
50. Sahoo NG, Rana S, Cho JW, Li L, Chan SH (2010) Prog Polym Sci 35:837
51. Oraon R, De Adhikari A, Tiwari SK, Nayak GC (2015) RSC Adv 5:68334
52. Snook GA, Kao P, Best AS (2011) J Power Sources 196:1
53. Hamnett A (1997) Catal Today 38:445
54. Liu H, Song C, Zhang L, Zhang J, Wang H, Wilkinson DP (2006) J Power Sources 155:95
55. Iwasita T (2002) Electrochim Acta 47:3663
56. Wang M, Guo DJ, Li HL (2005) J Solid State Chem 178:1996
57. Tripković AV, Popović KD, Grgur BN, Blizanac B, Ross PN, Marković NM (2002) Electrochim Acta 47:3787
58. Guo DJ, Li HL (2005) Carbon 43:1259
59. Feng X, Huang H, Ye Q, Zhu JJ, Hou W (2007) J Phys Chem C 111:8463
60. Choudhury A (2009) Sens Actuators B: Chem 138:318
61. Lemos HG, Santos SF, Venancio EC (2015) Synth Met 203:22
62. Li C, Bai H, Shi G (2009) Chem Soc Rev 38:2397
63. Zhai D, Liu B, Shi Y, Pan L, Wang Y, Li W, Yu G (2013) ACS Nano 7:3540
64. Hou Y, Cheng Y, Hobson T, Liu J (2010) Nano Lett 10:2342
65. Spitalsky Z, Tasis D, Papagelis K, Galiotis C (2010) Prog Polym Sci 35:357
66. Breuer O, Sundararaj U (2004) Polym Compos 25:630
67. Bhambi M, Sumana G, Malhotra BD, Pundir CS (2010) Artif Cells Blood Substit Biotechnol 38:178
68. Goswami SK, McAdam CJ, Lee AM, Hanton LR, Moratti SC (2013) J Mater Chem A 1:212
69. Suckeveriene RY, Zelikman E, Mechrez G, Narkis M (2011) Rev Chem Eng 27:15
70. Paunovic M, Schlesinger M (2006) Fundamentals of electrochemical deposition. John Wiley & Sons
71. Simon P, Gogotsi Y (2008) Materials for electrochemical capacitors. Nat Mater 7:11
72. Li C, Bai H, Shi G (2009) Chem Soc Rev 38:2397
73. Koerner H, Price G, Pearce NA, Alexander M, Vaia RA (2004) Remotely actuated polymer nanocomposites—stress-recovery of carbon-nanotube-filled thermoplastic elastomers. Nat Mater 3:115
74. Yang L, Setyowati K, Li A, Gong S, Chen J (2008) Adv Mater 20:2271
75. Yang L, Setyowati K, Li A, Gong S, Chen J (2008) Reversible infrared actuation of carbon nanotube–liquid crystalline elastomer nanocomposites. Adv Mater 20:2271
76. Liu S, Liu Y, Cebeci H, de Villoria RG, Lin JH, Wardle BL, Zhang QM (2010) High electromechanical response of ionic polymer actuators with controlled-morphology aligned carbon nanotube/nafion nanocomposites electrodes. Adv Funct Mater 20:3266
77. Scott JC, Bozano LD (2007) Adv Mater 19:1452
78. Prakash A, Ouyang J, Lin JL, Yang Y (2006) J Appl Phys 100:054309
79. Park JH, Lim YT, Park OO, Kim JK, Yu JW, Kim YC (2004) Chem Mater 16:688
80. He JA, Valluzzi R, Yang K, Dolukhanyan T, Sung C, Kumar J, Tomalia DA (1999) Chem Mater 11:3268
81. Meng Q, Hu J (2009) Compos A 40:1661
82. Yu G, Hu L, Liu N, Wang H, Vosgueritchian M, Yang Y, Bao Z (2011) Nano Lett 11:4462
83. Mather PT, Luo X, Rousseau IA (2009) Annu Rev Mater Res 39:445
84. Sahoo NG, Jung YC, Yoo HJ, Cho JW (2007) Compos Sci Technol 67:1920
85. http://en.wikipedia.org/wiki/Organic_light-emitting_transistor
86. http://spectrum.ieee.org/semiconductors/optoelectronics/organic-transistor-could-outshine-oleds/0
87. Tiwari SK, Kumar V, Huczko A, Oraon R, De Adhikari A, Nayak GC (2016) Magical allotropes of carbon: prospects and applications. Crit Rev Solid State Mater Sci 3:1–61
88. Long YZ, Li MM, Gu C, Wan M, Duvail JL, Liu Z, Fan Z (2011) Prog Polym Sci 36:1415
89. Li C, Bai H, Shi G (2009) Chem Soc Rev 38:2397

90. Zhao Y, Tong T, Delzeit L, Kashani A, Meyyappan M, Majumdar A (2006) J Vac Sci Technol B 24:331
91. Potts JR, Dreyer DR, Bielawski CW, Ruoff RS (2011) Polymer 52:5
92. Lee SW, Yabuuchi N, Gallant BM, Chen S, Kim BS, Hammond PT, Shao-Horn Y (2010) Nat Nanotechnol 5:531
93. Reddy ALM, Shaijumon MM, Gowda SR, Ajayan PM (2009) Nano Lett 9:1002
94. Wang Q, Johnson JK (1999) J Chem Phys 110:577
95. Lee SM, Lee YH (2000) Appl Phys Lett 76:2877
96. Darkrim FL, Malbrunot P, Tartaglia GP (2002) Int J Hydrogen Energy 27:193
97. Chen J, Liu Y, Minett AI, Lynam C, Wang J, Wallace GG (2007) Chem Mater 19:3595
98. Malinauskas A, Malinauskiene J, Ramanavičius A (2005) Nanotechnology 16:R51
99. Geim AK, Novoselov KS (2007) Nat Mater 6:183
100. Geim AK (2009) Graphene: status and prospects. Science 324:1530
101. Schwierz F (2010) Nat Nanotechnol 5:487
102. Khot MB, Gadekar AS, Kahane MJ, Potnis VV, Baghwan DB, Dhamane SP, Kulkarni AS (2011) Int J Pharm Phytopharmacol Res 3:55
103. Allen MJ, Tung VC, Kaner RB (2009) Chem Rev 110:132
104. Novoselov KS (2011) Rev Mod Phys 83:837
105. Potts JR, Dreyer DR, Bielawski CW, Ruoff RS (2011) Polymer 52:5
106. Li D, Müller MB, Gilje S, Kaner RB, Wallace GG (2008) Nat Nanotechnol 3:101
107. Stankovich S, Dikin DA, Dommett GH, Kohlhaas KM, Zimney EJ, Stach EA, Ruoff RS (2006) Nature 442:282
108. Gómez H, Ram MK, Alvi F, Villalba P, Stefanakos EL, Kumar A (2011) J Power Sources 196:4102
109. Zhang LL, Zhao S, Tian XN, Zhao XS (2010) Langmuir 26:17624
110. Jo K, Lee T, Choi HJ, Park JH, Lee DJ, Lee DW, Kim BS (2011) Langmuir 27:2014
111. Yan J, Wei T, Shao B, Fan Z, Qian W, Zhang M, Wei F (2010) Carbon 48:487
112. Suk JW, Piner RD, An J, Ruoff RS (2010) ACS Nano 4:6557–6564
113. Liu WJ, Tran XA, Liu XB, Wei J, Yu HY, Sun XW (2013) ECS Solid State Lett 2:M1
114. Thostenson ET, Li CY, Chou TW (2005) Compos Sci Technol 65:491
115. Luo J, Kim J, Huang J (2013) Acc Chem Res 46:2225
116. Modaress MP, Mirzadeh H, Zandi M (2012) Iran Polym J 21:191
117. Fang M, Wang K, Lu H, Yang Y, Nutt S (2009) J Mater Chem 19:7098
118. Pötschke P, Bhattacharyya AR, Janke A (2004) Eur Polym J 40:137
119. Akamatu Y, Tomori M, inventors; Nippon Gohsei Kagaku Kogyo Kabushiki Kaisha, assignee (1994) Process for preparing biodegradable resin foam. United States patent US 5,308,879
120. Zhang HB, Zheng WG, Yan Q, Yang Y, Wang JW, Lu ZH, Yu ZZ (2010) Polymer 51:1191
121. Steurer P, Wissert R, Thomann R, Mülhaupt R (2009) Macromol Rapid Commun 30:316
122. Kim H, Abdala AA, Macosko CW (2010) Macromolecules 43:6515
123. Li W, Tang XZ, Zhang HB, Jiang ZG, Yu ZZ, Du XS, Mai YW (2011) Carbon 49:4724
124. Shen Y, Jing T, Ren W, Zhang J, Jiang ZG, Yu ZZ, Dasari A (2012) Compos Sci Technol 72:121
125. De Adhikari A, Oraon R, Tiwari SK, Lee JH, Nayak GC (2015) RSC Adv 5:27347

Clay-Based Conducting Polymer Nanocomposites

Alessandra F. Baldissera and Carlos A. Ferreira

Abstract Nanomaterials have been regarded as most gifted materials for large number of scientific and technological applications. In engineering, polymer nanocomposites are a novel class of composite materials, where a clay or filler with nano size dimensions is added in a polymer matrix at a very small ratio or volume. When dispersed in contents less than 5 % in the nanocomposites, clay cause a noteworthy enhancement in various properties, such as mechanical, optical, magnetic barrier, and especially permeability and flammability resistance. In this perspective, the major goal of the present chapter is to give a brief summary about polymeric nanocomposites, their preparation and some nanocomposites based on conducting polymers. At the end, different polymeric nanocomposites obtained from the synthesis of polyaniline (PAni) with different commercial clays (Cloisite Na^+, 10A, 15A, 20A and 30B) are described. The synthesis of PAni and montmorillonite (PAni–MMT) nanocomposites was carried out by in situ polymerization of aniline in acidic media (HCl). Electrical conductivity measurements, FT-IR, TGA and X-ray diffraction were some of the tools employed to characterize the nanocomposites. The results confirmed that it is feasible to get PAni–MMT nanocomposites by chemical synthesis method and the X-ray diffraction patterns and photomicrographs confirmed the better exfoliation of the clay by the PAni chains and the development of PAni–MMT nanocomposite.

Keywords Nanocomposite · Clay · Montmorillonite · Conductive polymers · Polyaniline

A.F. Baldissera (✉) · C.A. Ferreira
Programa de Pós Graduação em Engenharia de Minas, Metalúrgica e de Materiais (PPGE3M), Universidade Federal do Rio Grande do Sul, Porto Alegre, RS, Brazil
e-mail: alebaldissera@hotmail.com

C.A. Ferreira
e-mail: ferreira.carlos@ufrgs.br

V. Kumar et al. (eds.), *Conducting Polymer Hybrids*,
Springer Series on Polymer and Composite Materials,
DOI 10.1007/978-3-319-46458-9_5

1 Introduction

In the last years, the development of inorganic–organic hybrid materials has become a subject of great scientific interest. This is attested by the ever-growing number of symposia, books, and specialized journals that are devoted to this subject.

By definition, composite materials are solids resulting from the combination of two or more simple materials that develop a continuous phase (polymer, metal, ceramic, etc.), and a dispersed phase such as glass fibers, carbon particles, silica powder, clay minerals, etc. In addition, they have properties that are essentially different from the components taken separately. Within the large amount of inorganic–organic hybrid materials, nanocomposites are an emerging group that established a vast attention mainly due to their potential in industrial applications [1].

In the literature, terms like 'nanoparticles' and 'nanocomposites' seem to be very usual and are often misused for systems that do not properly fall under the label 'nano' in the sense of advertising. There is a strong requirement to understand the mechanism of the formation of such materials, in order to avoid the inappropriate use of these terms. Aspects important of chemistry involved in the formation of these systems are uniformity, phase continuity, domain sizes, and molecular mixing at the phase boundaries, all of which have a direct influence on optical, physical, and mechanical properties [2].

A field of growing attention is the development of polymer–clay nanocomposites due to the significant technological applications of these materials. Therefore, composite systems produced by organic polymers and clay minerals prepared at the nanoscale level, which typically present a unique layered structure, rich intercalation chemistry and availability at low cost, have been used to develop plastic materials with superior mechanical properties, molecular barrier behavior, fire retardant abilities, enhanced thermal stability, among other properties, compared to the individual polymeric materials [3–5].

Conversely, electrically conducting polymers have also gained a large amount of consideration due to their many promising technological applications, for example microelectronic devices, electroluminescence devices, corrosion inhibitors, electrochemomechanical devices, and chemical sensors [6]. Among conducting polymers, polyaniline (PAni) and polypyrrole (PPy) are mainly attractive for their simple synthesis, high conductivity, and superb environment stability. As a consequence, many PAni–clay [7–11] and PPy–clay [11–14] nanocomposites have been prepared and analyzed in the last years. The main effect induced by the incorporation of the clay was the improvement of the thermal stability, which was found to be higher for the nanocomposites than for the conducting polymers.

The aim of this contribution is to establish a base for further studies, rationalize and comment on the processes used to prepare those compounds, and finally to illustrate some properties of these materials such as thermal, mechanical, and conductivity and to call the attention of clay scientists and engineers to the numerous opportunities that this type of new materials offer.

2 Nanocomposites

The use of the prefix 'nano' to the title of various materials means that they have at least one dimension in the nanometer range, which is less than 100 nm [15]. Nanomaterials have been considered as highly promising materials for various technological applications. Therefore, the development of these materials is a multidisciplinary field where professionals from different areas work collectively with the goal of discover superior materials that have range of potential end-use applications [16].

Nanocomposites must have at least one ultrafine phase dimension, typically less than 100 nm, and exhibit improved properties when compared to other composites. They are in particular attractive because this arrangement offers for the inclusion of broad functionalities and, in certain cases, to confer new properties as a consequence of synergistic effects [11].

Organic–inorganic hybrid materials can be formed with the appropriate combination of two chemically distinct components, providing materials with different properties from those that created and compose of a substitute for the fabrication of new multifunctional materials with extensive application. In Engineering, polymer nanocomposites are a new class of composite materials, where a **clay** or **filler** with nanometric dimensions is dispersed in a polymer matrix at low concentration or volume [17, 18]. These nanocomposites correspond to the latest progression in science and technology and have established huge attention in academic and industrial areas. The interest in the field of nanotechnology is the unusual properties revealed by these materials, not only because they make possible to attain properties comparable to the conventional composites, but also demonstrate special unique characteristics.

Currently, a great research effort is devoted to hybrid inorganic–organic materials based on conducting polymers and inorganic components. The combination of conducting polymers with amorphous mineral phase or metal particles leads new hybrid materials with different characteristics [19]. The conducting polymer–clay [20, 21] and composites of conducting polymer with inorganic nanocrystals [22, 23] are the mostly investigated systems.

2.1 Clays

The most common inorganic particles belong to the family of 2:1 phyllosilicates (also referred to as clay minerals or smectites), where the crystal structure is (Fig. 1) [24] made up of an aluminium or magnesium hydroxide octahedral sheet squeezed among two silicon oxide tetrahedral sheets. The layer thickness of each platelet is around 1 nm, and their lateral dimensions may vary from 30 nm to several microns.

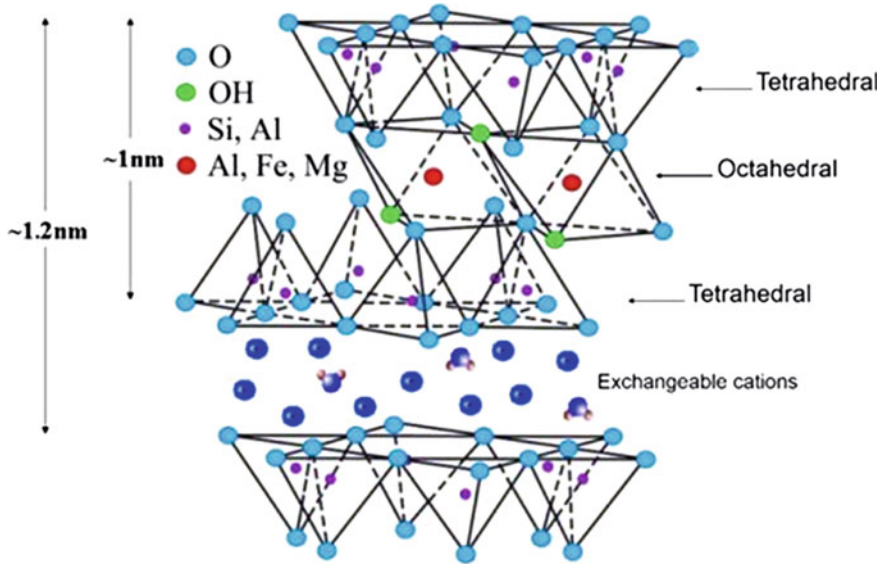

Fig. 1 The crystal structure of the phylosilicates, adapted from [24]

The layers are placed on top of each other similar to the pages of a book and Van der Waals gaps are produced between these layers, called galleries. The isomorphic substitution of the tetrahedral or octahedral cations, for example the substitution of Al^{3+} with Mg^{2+} or Fe^{2+} with Li^{+}, creates negative charges that are compensated by alkali and alkaline earth cations situated within the galleries. In the case of tetrahedral substitution, the negative charge is located on the surface of the silicate layers and, as a result, the polymer matrices can interact more readily with tetrahedral than with octahedral substituted material [25].

Layered aluminosilicates and their organic alterations are an essential part of industrial materials and are increasingly employed as absorbents to purify and decolorize liquids, as fillers in paper and rubber materials, as rheology modifiers in paints, greases, and drilling muds, and as a base in cosmetics and medicines. Most recently, they have been a successful for their performance-enhancing properties when used as a nanoscale additive in plastics to generate polymer nanocomposites [26].

Because the clays are naturally hydrophilic, it is very tough to interact and get a uniform mixture with the polymeric matrices. Therefore, it is required to make it organophilic via cation exchange, normally with alkylammonium, imidazonium, or phosphonium cations, functionalizing the aluminosilicate surface and lowering interfacial free energy [27]. The compatibility of these organically modified layered aluminosilicates with polymers, resins, or organic solvents can be manipulated depending on the composition, packing density, and length of these modifiers. The use of organically modified montmorillonites (MMTs) as nanofillers for polymers

has motivated extensive recent efforts to elucidate the factors that dictate the structure of organic surfactant within the interlayer gallery and thus to understand better the underlying factors determining their compatibility and interfacial properties with various polymers [28, 29].

The ability of silicate sheets to disperse into individual layers, and the possibility to modify their surface chemistry through ion exchange reactions with organic and inorganic cations are two important characteristics of layered silicates in the successfully creation of nanocomposites. The simple mixing of polymer and layered silicates does not always result in the generation of a nanocomposite, as this usually leads to dispersion of stacked sheets. This failure is due to the weak interactions between the polymer and the inorganic component. However, if these interactions become stronger, then the inorganic phase can be dispersed in the organic matrix in nanometer scale [25].

When the clays are added in quantities below 5 % in nanocomposites, they impart a significant increase in material properties, such as mechanical, optical, magnetic, barrier, and especially permeability and flammability resistance [30, 31].

2.2 Polymeric Nanocomposites

Polymer composites formed by micron-sized particulates and long fibers are widely used in automotive, aerospace, construction, and electronic industries because they provide improved mechanical properties (for example, stiffness, strength) and physical properties over pure polymers. When compared to their microcomposite counterparts, the nanocomposites, a new class of materials, provide superior properties to the materials. An addition of a small amount of nanoparticles can significantly improve a variety of properties without sacrificing the lightweight of polymer matrices [15].

Though the clay polymer nanocomposites have a historical background, the era of clay polymer nanotechnology can truly be said to have begun with Toyota's work on the exfoliation of clay in nylon-6 for manufacturing long lasting timing belts of its vehicles in the latter part of the 1980s and the beginning of the 1990s [32, 33]. This work demonstrated a significant improvement in a wide range of engineering properties by reinforcing polymers with clay on the nanometer scale [34, 35].

The interaction between the matrix and the filler is the key to the optimization of the properties of polymer nanocomposites. Therefore, the performance of the nanocomposite is compromised by the state of dispersion of the filler and the nature of the interface/interphase with the host matrix. The aspect ratio and orientation of the filler or the changes triggered in the matrix morphology upon addition of the reinforcement are other important parameters that can significantly influence the composite properties [36].

The principal used in polymer–clay nanocomposites leads the individual clay layers as well as the polymer chains to function more effectively with numerous improved properties such as high moduli, increased strength and heat resistance, decreased gas permeability and flammability, increased biodegradability of biodegradable polymers, and attractive electrical properties when compared to virgin polymers or conventional micro- and macrocomposites [37]. These properties make them ideal materials for applications in food packaging, structural automotive components, and electronics among others.

Therefore, the nanocomposites have become an area of intensive research activity and their high mechanical properties are the most important reason for this development. The complete dispersion of clay nanolayers in a polymer optimizes the number of available reinforcing elements that carry an applied load and deflect the evolving cracks. The coupling between the large surface area of the clay and the polymer matrix facilitates the stress transfer to the reinforcing phase allowing for the improvement of the tensile stress and toughness [38, 39]. Regarding the mechanical performance of polymer/layered silicate nanocomposites, very low clay concentrations (2–5 %) impart a significant improvement in Young's modulus and tensile strength [40]. Many parameters such as preparation method, the nature of the matrix and the content and degree of dispersion of the filler, surface treatment of the clay, orientation of the dispersed platelets ,or the influence of the nanofiller on the development of crystallinity in thermoplastic based polymer/layered silicate nanocomposites are considered when analyzing the mechanical properties of these nanomaterials [36].

The enhanced barrier properties is the second major advantage of the nanocomposites once the impermeable clay layers force a tortuous pathway for a permeant traversing the material. It is reported that even with small quantities of nanoclays the gas permeability can be reduced by 50–500 times through polymer films [25].

The phyllosilicate particles present a very high aspect ratio of width/thickness, in the order of 10–1000 and the complete exfoliation of the layered silicate in the polymer matrix is the main goal for the successful development of clay-based nanocomposites. For very low concentrations of particles, the total interface between polymer and layered silicates is much greater than that in conventional composites. Depending on the strength of the interfacial interaction, four types of morphology are possible in nanocomposites (Fig. 2) [24]:

- *Aggregated*: the insertion of a polymer matrix into the layered silicate structure is small.
- *Intercalated*: the insertion of a polymer matrix into the layered silicate structure occurs in a crystallographically regular fashion, regardless of the clay-to-polymer ratio. Intercalated nanocomposites are normally interlayered by a few molecular layers of polymer. The properties of these nanocomposites typically resemble those of ceramic materials.

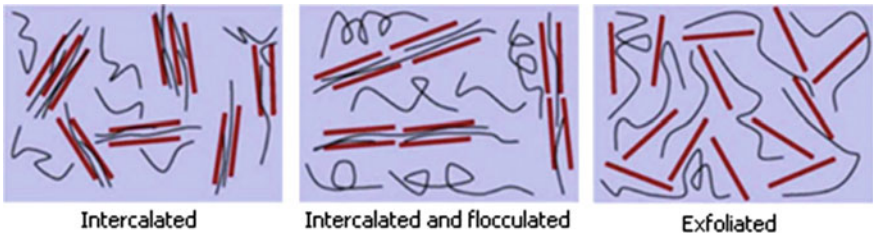

Fig. 2 Schematic representation of three types of polymer/clay nanocomposites, adapted from [25]

- *Flocculated*: these materials have the same concept of the intercalated nanocomposites. However, silicate layers are sometimes flocculated due to hydroxylated edge–edge interactions of the silicate layers.
- *Exfoliated*: the individual clay layers are separated in a continuous polymer matrix by an average distance that depends on clay loading. Usually, the clay content of an exfoliated nanocomposite is much lower than that of an intercalated nanocomposite [41].

The organically modified clay is more compatible with organic solutions or polymers, being one of the alternatives to improve the connectivity between these materials. The other alternative is mechanochemical grinding. Ogawa and coworkers [42] have reported that mechanochemical reactions help to introduce organic guest species into the interlayer spaces of clay minerals. They succeeded in the solid-state intercalation of organic compounds into MMT by both cation exchange reaction and adsorption of polar molecules.

The most intense research devoted to clay–polymer nanocomposites concerns natural (montmorillonite, hectorite, saponite) or synthetic (laponite, fluorohectorites) smectites because these 1D nanofillers have a layer thickness of the order of one nanometer. The other dimensions of the clay mineral are about 1000 times larger than the thickness, i.e., they are at the micrometer scale. Figure 3 shows the different structures that can be formed by the association of these clay minerals with polymers.

Conventional filler-polymer microcomposites are formed by the dispersion of clay aggregates in the polymer. In the nanocomposites, the single clay mineral layers or nanometer particles are dispersed in the polymer. Nanocomposites are denominated ‘intercalated’ when the layers are regularly intercalated with polymeric chains and denominated ‘delaminated’ or ‘exfoliated’ when the clay mineral layers or the particles are irregularly dispersed in the polymer. Information about the degree of orientation and distribution of the nanofillers and the matrix-filler interactions can be obtained with microscopic techniques such as scanning and transmission electron microscopies (SEM and TEM). Techniques such as wide angle X-ray scattering (WAXS) and differential scanning calorimetry (DSC) are frequently used to assess the crystalline structure, degree of crystallinity, and crystal orientation of the matrix in the composite [36, 44].

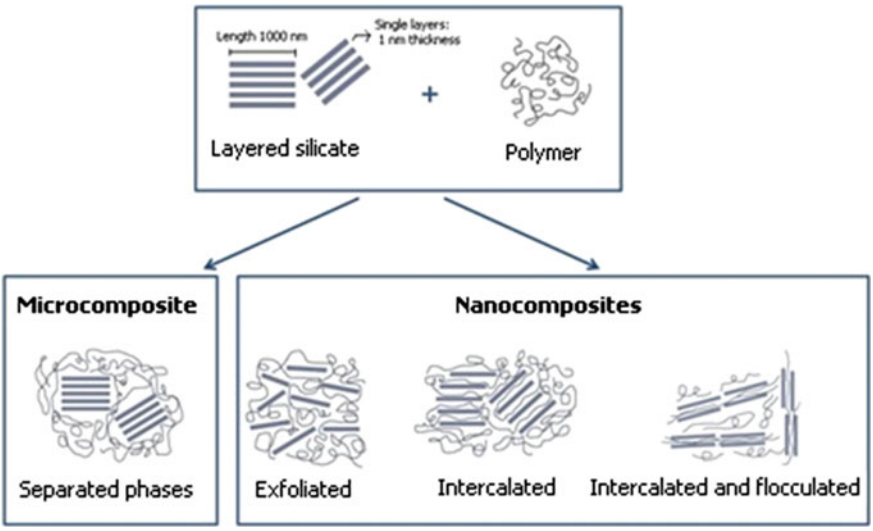

Fig. 3 Different structures proposed for clay–polymer materials arranged as nano- and microstructured solids, adapted from [43]

The research around the use of montmorillonite to obtaining nanocomposites polymer–MMT has become even more intense. In a review, Biswas and Ray [45] described several features of polymer–MMT nanocomposite materials. Ray and Okamoto [24] reported various characteristics of polymer–layered silicate nanocomposite materials, some of these materials exhibited distinctive properties like biodegradability. Ahmadi et al. [46] reviewed synthetic routes, properties, and future applications of polymer–layered nanocomposites. Significantly, nanocomposites of PAni and PPY with MMT clay via emulsion polymerization technique [47, 48] were found to act as electrorehological fluids, sometimes denominated 'smart fluids.' In this context, Ballav and Biswas [49, 50] reported high yield oxidative polymerization of thiophene, aniline, pyrrole, and furan by MMT—without extraneous oxidant—vis-à-vis nanocomposites formation of the corresponding polymers with MMT.

Some representative examples of polymeric nanocomposites and their properties are reported in Table 1.

2.2.1 Preparation of Nanocomposites

The main target of the preparation of nanocomposites is to attain controlled nanoparticle dispersion and distribution in a polymer matrix. As previously described, every individual clay platelet presents a huge surface area and high aspect ratio, and both are critical for enhancing mechanical properties, thermal stability, and barrier properties of the nanocomposite. To separate and distribute the

Table 1 Representative examples of polymeric nanocomposites

Reference	Nanocomposite	Properties
Lal et al. [51]	Montmorillonite-poly lactic-co-glycolic acid (MMT–PLGA)	MMT has promising probability of providing gastro retentive sustained release characteristic properties to the nanocomposites for oral drug delivery
Sahoo et al. [52]	DGEBA epoxy-EMS bioresin-C30B clay (Epoxy-EMS-C30)	Addition of clay improved the thermal stability of epoxy blend that restricted the mobility of chain and hindered the decomposition process
Deka et al. [53]	Poly(vinylidene fluoride)-montmorillonite modified (PVdF–MMT)	The presence of MMT in the nanocomposite reduces the interfacial resistance with lithium electrode and provides a better electrochemical stability window
Yi et al. [54]	Polypropylene/ammonium polyphosphate/montmorillonite (PP/APPMMT)	The clay plays an important role of controlling the viscosity during char formation and enhanced flame retardancy
Hu et al. [55]	Polyaniline/decavanadate-intercalated LDH modified (PAni/AD–LDH)	The coating containing the nanocomposite offered better protection against corrosion than the polymer and clay coating did
Pongprayoon et al. [56]	Na^+-bentonite with poly (diallyldimethyl ammonium chloride) or poly(methylmethacrylate) or poly (vinylidene chloride) (Na^+-Bent-PDADMAC, Na^+-Bent-PMMA and Na^+-Bent-PVDC)	The presence of clay in these polymer nanocomposites exhibited efficacy in the inhibition of bacterial growth in inoculated samples
Zapata et al. [57]	Polyethylene-montmorillonite (PE–MMT)	The polymer particle morphology improved with the presence of the clay in the polymerization and the molecular weight for support systems presented an increasing ca. 40 % compared to neat PE

layers throughout polymer matrices it is required the development of special surface chemistry and specific synthesis and processing technologies, because a distinctive clay particle may contain several thousand individual layers in their crystallites [58]. As mentioned, the most widely used strategy to increase the hydrophobicity and compatibility through ion exchange reactions with the polymer matrices is to bind surfactants onto the clay surface.

Preparation of nanocomposite polymer can be done by three important methods: intercalation of the polymer from a solution, intercalation in the melt state, and in situ polymerization [59].

- *Solution process*: in this method, a solvent or solvent mixture is employed to dissolve the polymer matrix and disperse the nanoparticles. Depending on the interactions of the solvent and the clay, the nanoparticle aggregates can be breakdown due to the weak Van der Waals force that stacks the layers collectively. Polymer chains can then be adsorbed onto the nanoparticles (Fig. 4). However, the nanoparticles tend to re-agglomerate upon solvent removal. Few exfoliated nanocomposites were prepared via this method and a large amount of solvent is needed, resulting in a high product cost. Limitations of the applicability of this method are the types of polymers that can be used to synthesize the nanocomposites, once depend of the selection of proper solvent to be solubilized. Nevertheless, this is an attractive route to prepare nanocomposites based on water-soluble polymer and layered silicate nanocomposites. Almost all water-soluble polymers are polar and hydrophilic enough to interact with the silicate surface without the need of cation exchange modification on the silicate surface. Inorganic layered silicates are able to exfoliate in water and form colloidal particles [15]. Several polymer nanocomposites, including polyethylene oxide (PEO) [60], polyvinyl alcohol (PVA) [61] and polyacrylic acid (PAA) [62] were prepared via this method. It was observed that an ultrasound-assisted solution processing technique was used for the better dispersion, because the intense sharing due to ultrasound helps in the dispersion of nanofillers in polymer matrix. This uniform dispersion of nanofiller due to sonication significantly improves the mechanical and electrical properties of polymer nanocomposite, which are always better than conventional methods [63].
- *Melt state:* this method consists in mixing the clay directly with a molten polymer and then polymer inorganic nanocomposites are obtained by extrusion (Fig. 5). This process is not necessary to use solvent and is compatible with industrial polymer extrusion and blending processes, providing an economically viable route to obtain polymeric nanocomposites [15]. A wide variety of

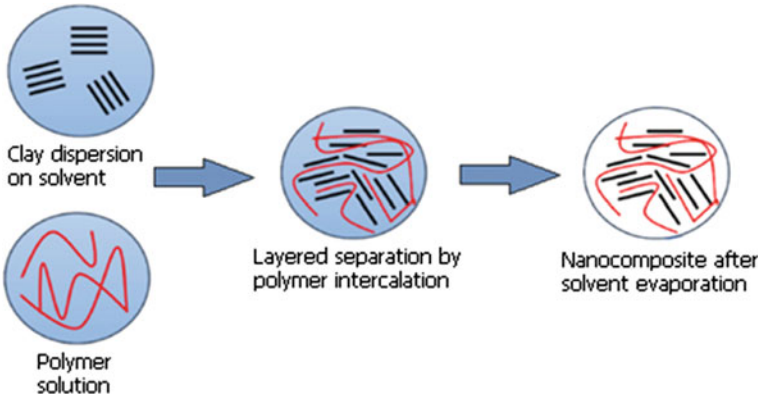

Fig. 4 Schematic representation of nanocomposite obtained by solution process, adapted from [40]

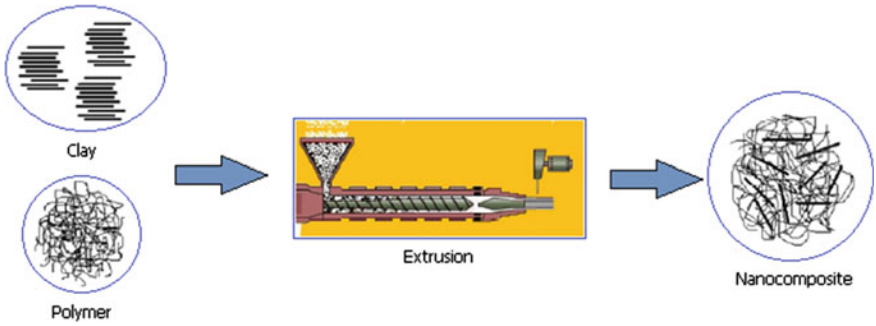

Fig. 5 Schematic representation of nanocomposite obtained by melt state

polymer/clay nanocomposites have been prepared via this method, i.e., nylon 6 [64, 65], polystyrene (PS) [66, 67], and polypropylene (PP) [68, 69]. Although it is a simple way to prepare the nanocomposites, care has to be taken with the compatibility between the polymer matrix and the silicate. Many studies have shown that the polar interactions of polymer and clay surface play a critical role in achieving particle delamination/dispersion. For nonpolar polymers, the addition of compatibilizing agents is required. In the case of PP processing, for example, a polar compatibilizer such as maleic anhydride modified PP (PP–MA) is commonly added to improve the compatibility of the polymer and clay and thus the clay nanoparticle dispersion [70, 71]. Although the melt mixing is an effective method, it has some disadvantages: in this process the bond formed between the polymer and the nanoparticles is relatively weak; due to high surface energy, the nanoparticles have a strong tendency to aggregate; for some polymers a rapid increase of the viscosity with the addition of a few volume fractions of nanoparticles can occur, limiting the processing method [63]. The limitation of agglomeration and dispersion of nanofiller during melt mixing has been overcome up to some extent, if the polymer melt and the nanoparticles are dispersed in solution. The presence of solution allows surface modification of nanoparticle without drying, reducing particle agglomeration. After the dispersion, the polymer nanoparticle solution can then be sonicated by high intensity ultrasound for fine dispersion of nanoparticles or exfoliation of clay platelets into polymer melt [63, 72, 73].

- In situ *polimerization* is an effective way for the synthesis of polymer nanocomposite material. This polymerization is based on the nanocomposite synthesis by growth of polymer chains inside the galleries of a silicate, where is anchored the catalyst (or monomer) (Fig. 6). Because of the low monomer viscosity (comparing to melt viscosity), it is much easier to achieve uniform mixing of particles in the monomer using a high shear mixer. In addition, the low viscosity and high diffusivity result in a higher rate of monomer diffusion into the interlayer region. Through the combination of reaction conditions and clay surface modification, it is possible to control nanocomposite morphology.

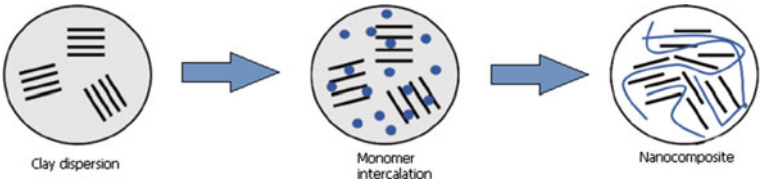

Fig. 6 Schematic representation of nanocomposite obtained by in situ polymerization, adapted from [24]

This method is the only viable route to prepare nanocomposites for most thermoset polymers [15]. Linking interactions between the monomer, the surfactant, and the clay surface, exfoliated nanocomposites have been successfully synthesized via the ring-opening polymerization, for example epoxy, nylon-6 and polycarbonate. The functional group in the organic cation can catalyze the intralayer polymerization and facilitate layer separation. Many thermoplastic nanocomposites have been synthesized by free radical polymerization. Efforts have been made to anchor initiators in the interlayer region to improve the intralayer polymerization rate for exfoliated nanocomposites [15, 74].

Among the most widely used methods for the preparation of nanocomposite with fine dispersion of the inorganic particles by surface encapsulation, the emulsion polymerization has the significant advantage of generating monodispersed polymer nanoparticles with controlled molecular weight and employment of water as a dispersion medium. Further, it is a convenient route for the encapsulation and preparation of polymer/inorganic composite particles on large scale [75, 76]. In emulsion polymerization, dispersed monomer droplet acts as nanoreactor for growth of polymer and prevents agglomeration [77].

Among the methods used for the addition of such fillers, only a small number of studies in the literature describe the preparation of these materials by in situ polymerization. Cho and coworkers [78] first utilized the in situ intercalative polymerization method for the preparation of polymer–clay nanocomposite consisting of conducting PAni and MMT.

2.3 Conducting Polymer Nanocomposites

Conducting polymer nanostructures (i.e., nanorods, -tubes, -wires, and -fibers) have received increased interest both academically and commercially because they combine the advantages of organic conductors with low-dimensional systems and, therefore, create interesting physicochemical properties and potentially useful applications [79–82].

Conducting polymer/inorganic nanoparticle composites have been attracted more attention, since they have interesting physical properties and many potential

applications. However, it is difficult to synthesize these nanocomposites by conventional blending or mixing in solution or melt form because the conducting polymer is not dissolved in nature and usually is insoluble in common solvents [63]. Therefore, the most widely used method to obtain these materials is the in situ polymerization.

Conducting polymer/inorganic clay nanocomposites provide the new synergistic properties, which cannot attain from individual materials, such that the conductivity is more easily controlled, and the mechanical or thermal stability is improved through the synthesis of the nanocomposites [48]. Emulsion polymerization has been used to produce various nanocomposites consisting of PAni [83], PS [84], or styrene/acrylonitrile copolymer [85] and MMT–Na^+. Interlayers of MMT–Na^+ are filled with sodium cations, therefore the hydrophilic properties are enhanced and lead to a high degree of swelling in water. In this case, if aqueous systems are used during the intercalation procedure, this method can be very effective for the preparation of intercalated nanocomposites.

PAni–clay nanocomposites are employed in the areas of corrosion protection and enhanced electrical conductivity [48, 86]. Great efforts have also been focused on the development of energy storage devices that can be fabricated easily with a low cost using such clay–polymer nanocomposite electrodes or electrolytes. Among them, the solid-state batteries with conducting polymer electrolytes or electrodes can be used for a wide range of products ranging from smart credit cards to standby power supply in telecommunications [87]. However, the improvement of the thermal stability was the main effect induced by the incorporation of the clay in the polymeric matrix and remained higher for nanocomposites than for conductive polymers [6].

2.3.1 Conducting Polymer

Conducting polymers have been extensively studied in recent years due to a great variety of possible applications in several fields, such as in energy storage systems, electrocatalysis [88, 89], electrodialysis membranes [90, 91], sensors [92, 93], biomedical applications [94, 95], and anticorrosion coatings [96–100]. They exhibit different oxidation states and behave as electronic or mixed conductors [101]. These new materials, also known as synthetic metals, can reach high electrical conductivity, very close to the value of some metals.

Conducting polymers are formed by molecules that contain alternating double bonds, forming a resonant structure with relocation of the π bond electrons that can move freely when free sites are generated in the polymer molecule. These materials do not depend on the addition of conductive materials in its matrix to conduct electricity. Conduction occurs along the polymer chain itself and is an intrinsic property thereof [102]. The properties of these polymers are focused on the ability to suffer oxidation–reduction, with the reversibility between an oxidized state, conductor, and a reduced state, insulating.

Obtaining processes of conducting polymers are divided into:

- *Electrochemical synthesis*: the polymer is generally obtained in the form of a continuous film on a metallic or semiconducting electrode by passing electric current in a solution containing the monomer. The most commonly used electrodes are the noble metals (Pt, Au), semiconductors (ITO, AsGa), or oxidizable metals (Fe, Al).
- *Chemical synthesis*: the polymer, generally in powder form, is obtained by reaction of the monomer with an oxidizing agent in solution. The polymer is then purified by filtration and washing powder to remove the excess oxidizing agent.

One of the most important areas of research in conducting polymers concerns with the methods for making them processable. The main approaches can be divided into three groups:

(a) preparation of composites with other polymers,
(b) synthesis of soluble derivatives, and
(c) synthesis of dispersions of insoluble conducting polymers.

Among the large number of conducting polymers, polypyrrole (PPy) and polyaniline (PAni) are the most promising polymers for corrosion protection and the most frequently used polymers for clay included nanocomposites [103]. These polymers exhibit poor dispersion in water and tendency to agglomerate in irregular morphology, which occasionally reduces the surface area. Therefore, several researchers have focused on the fabrication of nanostructured PPy and PAni or PPy/PAni based nanocomposites with large surface area, these materials also exhibit highly efficient removal of contaminants from water [104, 105].

Soundararajah et al. [10] studies indicated that the mechanical properties of the PAni–MMT nanocomposite, Young's modulus, fracture toughness, hardness, and impact energy of polyaniline significantly increased by the presence of MMT clay in the nanocomposite of PAni and MMT up to 23 wt% of MMT and decreased at higher clay contents. The degree of exfoliation and the bond strength of the MMT clay attribute to the better mechanical properties.

Polyaniline (PAni) is one of the most intensively studied conducting polymers during the last decade. This polymer offers the following advantages: it can be synthesized easily; it is comparatively stable in air; it has high conductivity; it is stable and easy to fabricate; it has many prospective applications in electrochromic devices, light-emitting diodes, chromatography, secondary batteries, electrostatic discharge protection, and corrosion-resistant paint [88, 106].

PAni is used as a model material to systematically investigate the syntheses, properties, and applications of nanocomposites of conjugated polymers. Its doping level can be readily controlled through an acid–base doping/dedoping process making it a unique material among the family of conducting polymers [107].

Other conducting polymers that have paying attention in composite preparation due to their remarkable physical and chemical properties are polypyrrole (PPy), polyvinylcarbazole (PNVCz), polythiophene (PTh), and their derivatives.

Polyaniline

PAni is regarded as the most prominent conductive polymer of the upcoming era. Aniline can be polymerized electrochemically or chemically by using an oxidant in different types of acids. The chemical method has an immense significance since it is more practicable for the synthesis of PAni in high quantities. The majority of acids employed during the synthesis are hydrochloric acid, sulfuric acid, carboxylic acid, dicarboxylic acid, sulfonic acid, etc. [108, 109]. $(NH_4)_2S_2O_8$, $K_2Cr_2O_7$, KIO_3, $FeCl_3$, H_2O_2, and $KBrO_3$/KBr are recommended oxidants [108, 110–112]. The acid used in the synthesis of PAni directly affects yield and conductivity of the polymer [88].

The polyanilines are a class of polymers having the general formula represented in Fig. 7.

The value y represents the repeating units in the reduced form and the $1-y$ repeating units in the oxidized form, and y can range from 0 to 1. The fully oxidized state ($y = 0$) is called pernigraniline, the partially oxidized and partially reduced state ($y = 0.5$) is called esmeraldine and the fully reduced state ($y = 1$) is called leucoesmeraldine [113].

PAni itself is not easy to process, for the reason that it decomposes prior to melting and is insoluble in ordinary solvents apart from strong acids and *n*-methylpyrrolidone (NMP). This behavior hampers production in the normal way, i.e., via polymer solution or melt. Therefore, various PAni derivatives possessing substituent groups ($–CH_3$, $–OCH_3$ or $–OC_2H_5$) have been investigated in order to improve the solubility [114, 115]. This change provides an excellent solubility of the polymer in organic solvents although derivative conductivity becomes lower than that of PAni within the whole doping range due to the presence of side groups disturbing the electronic conjugation in polymer backbone.

Production of nanocomposites with layered compounds can significantly improve the mechanical properties, stability of interface, thermal stability, and processability of PAni. For example, electronically conductive polymer nanocomposites can have electronic conductivities of several orders of magnitude higher than that of the conventional forms (for example powders or thin films) of the same polymer. Besides good conductivity and excellent application perspective in rechargeable cell, this kind of nanocomposites may show many novel properties, such as photoelectric display, photoelectric transition, thermoelectricity,

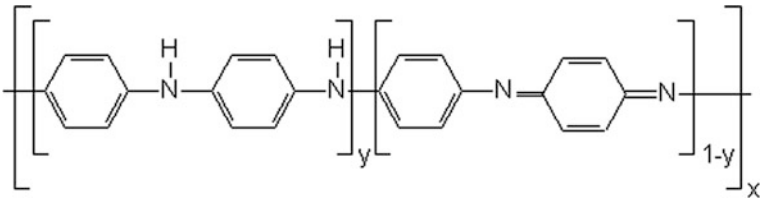

Fig. 7 General structure polyaniline

electromagnetism, and electrorheology, through synergic interaction of PAni with layered compounds [41].

MMT is a clay naturally abundant and inexpensive, and due to its capacity to swell and exchange cations it is the most common inorganic matrix used for PAni composites [116–118]. Using anilinium intercalated clay (Ani–MMT) as precursor, it is possible to obtain a special type of nanocomposite when anilinium (Ani) polymerization is carried out mainly between the interlayer regions [119, 120].

The formation of intercalated and/or exfoliated nanocomposite is dependent on the monomer/clay ratio when aniline polymerization is performed in an acidic aqueous suspension of MMT in the presence of an oxidizing agent. If a small amount of PAni is present in the composite, conductivity of the material is still very close to that of pure MMT clay. In a critical amount of polymer and denominated percolation threshold [121], conductivity increases by several orders of magnitude with a small increase in the PAni amount. After reaching the optimum values, the value of conductivity starts decreasing and found very close to that of free PAni. On the other hand, nanocomposites of PAni–MMT [116, 118, 119] obtained by Ani–MMT polymerization show lower conductivity than free PAni [117] and this fact can be attributed to the lack of connectivity between intercalated PAni chains [116, 118, 119] or a change in the nature of polymeric chains.

3 Applied Study: PAni and MMT

In this context, a study that evaluated obtaining and characterization of polymeric nanocomposites of polyaniline (PAni) with a variety of montmorillonite (MMT) clays (Cloisite Na^+, 10A, 15A, 20A and 30B) was developed by Baldissera and coworkers [122]. The aim of obtaining these nanocomposites is to link the features provided by nanofiller with the characteristics of conducting polymers.

PAni–MMT nanocomposites were prepared as described by Baldissera et al. [122]. First, the clay was added to a 1 M HCl solution and sonicated for 30 min with the help of an ultrasound probe. After that the monomer was added and the solution was sonicated for an extra 30 min to support the substitution of inorganic ions by molecules of aniline between the lamellae of the clay. A solution containing the oxidizing agent was added dropwise to the solution comprising the monomer and clay under constant stirring. The polymerization of aniline was carried out at temperatures between −4 and 0 °C, for 6 h. The PAni–MMT acquired was filtered under low pressure and the green powder was washed with distilled water and dried in oven at 60 °C for 24 h.

The synthesized polymers were characterized by FTIR analysis, whose characteristics bands showed the formation of conductive polymers. Thermogravimetric analysis (TGA) was carried out to evaluate thermal performance of the polymers. It was observed that the synthesized nanocomposites can be practically applied in

areas where the temperature is less than 200 °C, which is the degradation onset temperature of the polymers.

The electrical conductivity of the polymer pure and the nanocomposites was measured by four-point probe method [123]. The conductivity of the PAni/HCl was 83 S cm^{-1} and for the nanocomposites was about 62 S cm^{-1}. It has been noted the addition of clay directed to a little reduction in conductivity, unsurprisingly, owing to the presence of insulating charges between the polymer chains. However, the synthesized nanocomposite materials still present an excellent electrical conductivity.

X-ray diffraction analysis and photomicrographs obtained by transmission electron microscopy (TEM) indicated that the clay was intercalated by the polymer and almost completely exfoliated. Photomicrographs obtained by TEM shows the morphology of some nanocomposites (Fig. 8). It is obviously possible to visualize

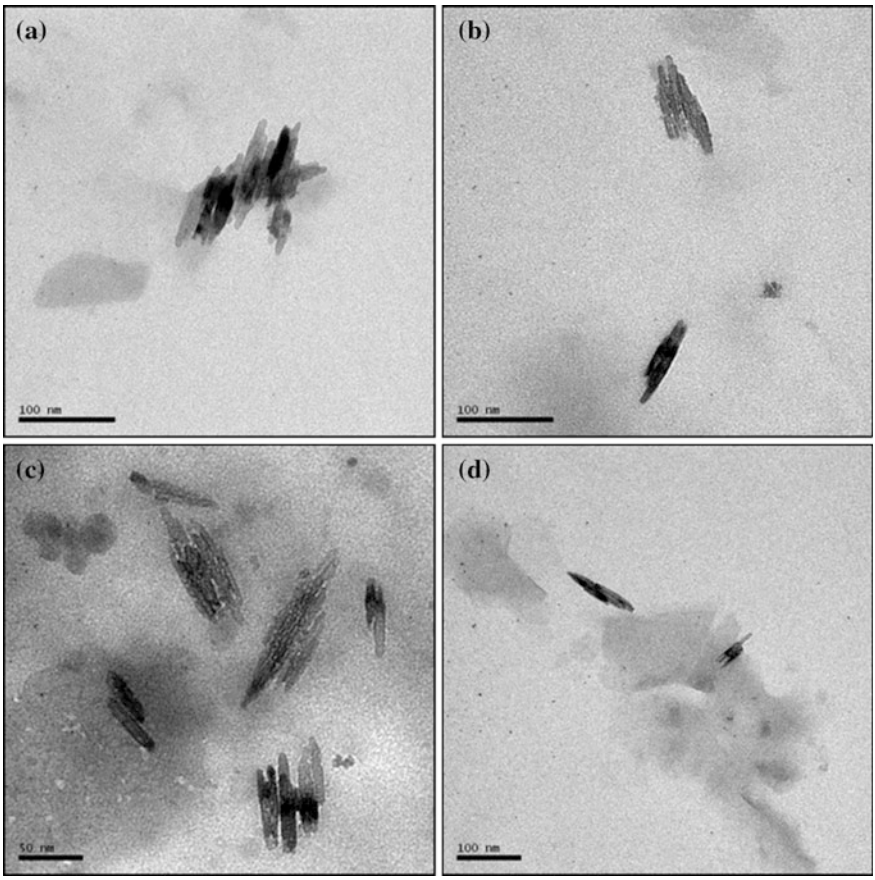

Fig. 8 Micrographs nanocomposites **a** PAni–MMT Na^+; **b** PAni–MMT 15A; **c** PAni–MMT 20A; **d** PAni–MMT 30B [122]

the polymer around of the lamellae of clays. More or less all the clays were exfoliated, except the PAni–MMT Na^+ nanocomposite. This can be explained by the fact that MMT clays 10A, 15A, 20A, and 30B are already organically modified, which make possible interaction with the aniline ion. The MMT–Na^+ clay is the only one that does not have the ammonium salt employed as a modifier, hindering the entry of the monomer ion among the layers of clay.

4 Conclusions

Clay minerals and polymers can be used to prepare polymer nanocomposites, having interesting physical properties and, in some instances, commercial applications. Even if the vast majority of people involved in clay mineral–polymer nanocomposite research rightfully believe in the future of these new materials, few products reached industrial application. Mass production of polymer nanocomposites depends on consistent and reasonable preparation and processing techniques. The existing literature is packed of new nanocomposite materials. However, in order to use these materials in commercial applications, a number of issues must be resolved. There must be healthy methods to prepare exfoliated nanocomposites with required mechanical properties in large scale and at a cheaper rate.

The study performed by the authors showed that it is feasible to get PAni–MMT nanocomposites by chemical synthesis route. It has been found that the conductivities of the nanocomposites are lesser than the PAni doped with HCl, which is due to the fact that clay is an insulating medium; however the nanocomposites still have an excellent electrical conductivity. The X-ray diffraction patterns and photomicrographs evidenced the efficient exfoliation of the clay by the PAni chains and the formation of PAni–MMT nanocomposite.

It is evident from the above studies that the field of polymer nanocomposites will go on increasing with the inclusion of new nanofillers and the development of complex hybrid and hierarchical materials to be useful as thin films, coatings, multilayers, or bulk. We hope this overview will be a step in this long journey.

References

1. Ruiz-Hitzky E (2004) Organic–inorganic materials: from intercalation chemistry to devices. In: Gómez-Romero P, Sánchez C (eds) Functional hybrid materials, chapter 2. Wiley-VCH Verlag, Weinheim
2. Kickelbick G (2003) Prog Polym Sci 28:83
3. Zheng QH, Yu AB, Lu GQ, Paul DRJ (2005) Nanosci Nano Technol 5:1574
4. Chen B, Evans JRG (2008) Polymer 49:5113
5. Paul DR, Robeson LM (2008) Polymer 49:3187
6. Aradilla D, Estrany F, Azambuja DS, Casas MT, Puiggali J, Ferreira CA, Alemán C (2010) Eur Polym J 46:977

7. Bekri-Abbes I, Srasra E (2015) Mater Sci Semicond Process 40:543
8. Wang J, Iroh JO, Hall S (2014) Appl Clay Sci 99:215
9. Singhal R, Datta MJ (2007) Appl Polym Sci 103:3299
10. Soundararajah QY, Karunaratne BSB, Rajapakse RMG (2009) Mater Chem Phys 113:850
11. Aranda P, Darder M, Fernández-Saavedra R, López-Blanco M, Ruiz-Hitzky E (2006) Thin Solid Films 495:104
12. Ramôa SDAS, Barra GMO, Merlini C, Schreiner WH, Livi S, Soares BG (2015) Appl Clay Sci 104:160
13. Kassim A, Mahmud HNME, Adzmi F (2007) Mater Sci Semicond Process 10:246
14. Boukerma K, Piquemal J-Y, Chehimi MM, Mravcakova M, Omastova M, Beaunier P (2006) Polymer 47:569
15. Lee LJ, Zeng C, Cao X, Han X, Shen J, Xu G (2005) Compos Sci Technol 65:2344
16. Pomogailo AD (2000) Russ Chem Rev 69:53
17. Koo JH (2006) Polymer nanomaterials, introduction chapter. In: Polymer nanocomposites: processing, characterization, and applications. McGraw-Hill Professional, AccessEngineering, New York
18. Utracki LA (2004) NCs with polymeric matrix. In: Clay—containing polymeric nanocomposites, vol 1. Rapra Technology Limited
19. Kryszewski M, Jeszka J (2003) Macromol Symp 194:75
20. Goddard YA, Vold RL, Hoatson GL (2003) Macromolecules 36:1162
21. Kuila AB, Nandi KK (2006) J Phys Chem B 110:1621
22. Liu YC, Chuang TC (2003) J Phys Chem B 107:12383
23. Khanna PK, Singh N, Charan S, Viswanath AK (2005) Mater Chem Phys 92:214
24. Ray SS, Okamoto M (2003) Prog Polym Sci 28:1539
25. Choudalakis G, Gotsis AD (2009) Eur Polym J 45:967
26. Jacobs JD, Koerner H, Heinz H, Farmer BL, Mirau P, Garrett PH, Vaia RA (2006) J Phys Chem B 110:20143
27. Biswas M, Ray SS (2001) Recent progress in synthesis and evaluation of polymer–montmorillonite nanocomposites. In: Advances in polymer science, vol 155. New polymerization techniques and synthetic methodologies. Springer, Heidelberg
28. Vaia RA, Giannelis EP (1997) Macromolecules 30:7990
29. Brown JM, Curliss D, Vaia RA (2000) Chem Mater 12:3376
30. Konta J (1995) Appl Clay Sci 10(4):275
31. Vaia RA, Price G, Ruth PN, Nguyen HT, Lichtenhan J (1999) Appl Clay Sci 15:67
32. Maiti P, Okamoto M (2003) J Macromol Mater Eng 288:440
33. Okada A, Kawasumi M, Tajima I, Kurauchi T, Kamigaito O (2003) J Appl Polym Sci 37:1363
34. Wang S, Hu Y, Li Z, Wang Z, Zhuang Y, Chen Z, Fan W (2003) J Colloid Polym Sci 281:951
35. Gao F (2004) Mater Today 7:50
36. Díez-Pascual AM, Gómez-Fatou MA, Ania F, Flores A (2015) Prog Mater Sci 67:1
37. Chen B, Evans JRG, Greenwell HC, Boulet P, Coveney PV, Bowden AA, Whiting A (2008) Chem Soc Rev 37:568
38. Powell CE, Beall GW (2006) Curr Opin Solid State Mater Sci 10:73
39. Jordan J, Jacob KI, Tannenbaum R, Sharaf MA, Jasiuk I (2005) Mater Sci Eng, A 393:1
40. Pavlidou S, Papaspyrides CD (2008) Prog Polym Sci 33:1119
41. Sezer E (2008) Conducting nanocomposites systems. In: The new frontiers of organic and composite nanotechnology. Elsevier, Amsterdam
42. Ogawa M, Shirai H, Kuroda K, Kato C (1992) Clays Clay Miner 40:485
43. Kiliaris P, Papaspyrides CD (2010) Prog Polym Sci 35:902
44. Ruiz-Hitzky E, Meerbeek AV (2006) Clay mineral—and organoclay–polymer nanocomposite. Developments in clay science, vol 1. Handbook of clay science. Elsevier, Amsterdam
45. Biswas M, Ray SS (2001) Adv Polym Sci 155:167
46. Ahmadi SJ, Huang YD, Li W (2004) J Mater Sci 39:1919

47. Kim BH, Jung JH, Hong SH, Joo J, Epstein AJ, Mizoguchi K, Kim JW, Choi HJ (2002) Macromolecules 35:1419
48. Kim JW, Liu F, Choi HJ, Hong SH, Joo J (2003) Polymer 44:289
49. Ballav N, Biswas M (2004) Synth Met 142:309
50. Ballav N, Biswas M (2004) Polym Int 53:1467
51. Lal S, Datta M (2015) Appl Clay Sci 114:412
52. Sahoo SK, Mohanty S, Nayak SK (2015) Thermochim Acta 614:163
53. Deka M, Kumar A (2015) J Power Sources 196:1358
54. Yi D, Yang R, Wilkie CA (2014) Polym Degrad Stabil 105:31
55. Hu J, Gan M, Ma L, Li Z, Yan J, Zhang J (2014) Surf Coat Technol 240:55
56. Pongprayoon T, Nuangchamnong R, Yanumet N (2013) Appl Clay Sci 86:179
57. Zapata PA, Belver C, Quijada R, Aranda P, Ruiz-Hitzky E (2013) Appl Catal A Gen 453:142
58. Alexandre M, Dubois P (2000) Mater Sci Eng R Rep R28:1
59. Park SJ, Seo DI, Lee JR (2002) J Colloid Interface Sci 251:160
60. Vaia RA, Sauer BB, Tse OK, Giannelis EP (1997) J Polym Sci Part B Polym Phys 35:59
61. Ogata N, Kawakage S, Ogihara T (1997) J Appl Polym Sci 66:573
62. Billingham J, Breen C, Yarwood J (1997) Vib Spectrosc 14:19
63. Bhanvase BA, Sonawane SH (2014) Chem Eng Process 85:86
64. Lincoln DM, Vaia RA, Wang ZG, Hsiao BS (2001) Polymer 42:1621
65. Cho JW, Paul DR (2001) Polymer 42:1083
66. Vaia RA, Giannelis EP (1997) Macromolecules 30:8000
67. Manias E, Chen H, Krishanmoorti R, Genzer J, Kramer EJ, Giannelis EP (2000) Macromolecules 22:7955
68. Svoboda P, Zeng C, Wang H, Lee LJ, Tomasko DL (2002) J Appl Polym Sci 85:1562
69. Nam PH, Maiti P, Okamoto M, Kotaka T, Hasegawa N, Usuki A (2001) Polymer 42:9633
70. Ginzburg VV, Balazs AC (2002) Polym Nanocompos 804:57
71. Zhulina E, Singh C, Balazs AC (1999) Langmuir 15:3935
72. Swain SK, Isayev AI (2007) Polymer 48:281
73. Ryu JG, Kim H, Lee JW (2004) Polym Eng Sci 44:1198
74. Weimer MW, Chen H, Giannelis EP, Sogah DY (1999) J Am Chem Soc 121:1615
75. Soares BG, Amorim GS, Souza FG, Oliveira MG, Pereira da Silva JE (2006) Synth Met 156:91
76. Qi DM, Bao YZ, Weng ZX, Huang ZM (2006) Polymer 47:4622
77. Borthakur LJ, Das D, Dolui SK (2010) Mater Chem Phys 124:1182
78. Cho MS, Choi HJ, To K (1998) Macromol Rapid Commun 19:271
79. Sailor MJ, Curtis CL (1994) Adv Mater 6:688
80. Epstein AJ (2001) Organic electronic materials: conjugated polymers and low molecular weight organic solids, vol 41. Springer, Berlin
81. Neves S, Gazzotti WA, De Paoli MA (2004) In: Nalwa HS (ed) Encyclopedia of nanoscience and nanotechnology, vol 2. American Scientific Publishers, New York
82. Huang J (2006) Pure Appl Chem 78:15
83. Kim JW, Kim SG, Choi HJ, Suh MS, Shin MJ, Jhon MS (2001) Int J Mod Phys B 15:657
84. Kim TH, Jang LW, Lee DC, Choi HJ, Jhon MS (2002) Macromol Rapid Commun 23:191
85. Kim JW, Noh MH, Choi HJ, Lee DC, Jhon MS (2000) Polymer 41:1229
86. Bober P, Stejskal J, Spírková M, Trchová M, Varga M, Prokes J (2010) Synth Met 160:2596
87. Rajapakse RMG, Rajapakse RMMY, Bandara HMN, Karunarathne BSB (2008) Electrochim Acta 53:2946
88. Gospodinova N, Terlemezyan L (1998) Prog Polym Sci 23:1443
89. Su YZ, Dong W, Zhang JH, Song JH, Zhang YH, Gong KC (2007) Polymer 48:165
90. Amado FDR, Gondran E, Rodrigues MAS, Ferreira JZ, Ferreira CA (2004) J Membr Sci 234:139
91. Chen G, Wang ZY, Xia DG, Zhang L, Hui R, Zhang JJ (2007) Adv Funct Mater 17:1844

92. Amado FDR, Rodrigues LF Jr, Rodrigues MAS, Bernardes AM, Ferreira JZ, Ferreira CA (2005) Desalination 186:199
93. Amado FDR, Rodrigues LF Jr, Forte MMC, Ferreira CA (2006) Polym Eng Sci 46:1485
94. Greco F, Fujie T, Ricotti L, Taccola S, Mazzolai B, Mattoli V (2013) ACS Appl Mater Interface 5:573
95. Kanik FE, Rende E, Timur S, Toppare L (2012) J Mater Chem 22:22517
96. Ferreira CA, Aeiyach S, Aaron JJ, Lacaze PC (1996) Electrochim Acta 41:1801
97. Meneguzzi A, Ferreira CA, Pham MC, Delamar M, Lacaze PC (1999) Electrochim Acta 44:2149
98. Baldissera AF, Freitas DB, Ferreira CA (2010) Mater Corros 61:790
99. Gonçalves GS, Baldissera AF, Rodrigues LF Jr, Martini EMA, Ferreira CA (2011) Synth Met 161:313
100. Baldissera AF, Ferreira CA (2012) Prog Org Coat 75:241
101. Meneguzzi AM, Pham C, Lacroix JC, Ferreira CA (2001) J Electrochem Soc 148:B121
102. Baldissera AF (2008) Development of non-conventional antifouling paint for ships and protection of metallic structures. Doctoral Thesis, Federal University of Rio Grande do Sul
103. Hosseini MG, Raghibi-Boroujeni M, Ahadzadeh I, Najjar R, Dorraji MSS (2009) Prog Org Coat 66:321
104. Bhaumik M, Maity A, Srinivasu VV, Onyango MS (2011) J Hazard Mater 190:381
105. Guo X, Fei GT, Su H, Zhang LD (2011) J Phys Chem C 115:1608
106. Zhang L, Wan M (2003) J Phys Chem B 107:6748
107. Huang J, Kaner RB (2004) J Am Chem Soc 126:851
108. Erdem E, Karakisla M, Saçak M (2004) Eur Polym J 40:785
109. Gok A, Sari B (2002) J Appl Polym Sci 84:1993
110. Prokes J, Trchová M, Hlavatá D, Stejskal J (2002) Polym Degrad Stab 78:393
111. Sarma TK, Chowdhury D, Paul A, Chattopadhyay A (2002) Chem Commun 10:1048
112. Chowdhury D, Paul A, Chattopadyay A (2002) J Phys Chem B 106:4343
113. Chiang J, MacDiarmid AG (1986) Synth Met 13:193
114. Sung JH, Choi JH (2005) J Macromol Sci, Phys 44:365
115. Mello SV, Mattoso LHC, Faria RM, Oliveria ON Jr (1995) Synth Met 71:2039
116. Lee D, Char K, Lee SW, Park YW (2003) J Mater Chem 13:2942
117. Kim BH, Jung JH, Kim JW, Choi HJ, Joo J (2001) Synth Met 121:1311
118. Nascimento GM, Constantino VRL, Temperini MLA (2004) J Phys Chem B 108:5564
119. Okamoto K, Ray SS, Okamoto M (2003) J Polym Sci, Part B: Polym Phys 41:3160
120. Nascimento GM, Constantino VRL, Landers R, Temperini MLA (2004) Macromolecules 37:9373
121. Clingerman ML, King JA, Schulz KH, Meyers JD (2002) J Appl Polym Sci 83:1341
122. Baldissera AF, Souza JF, Ferreira CA (2013) Synth Met 183:69
123. Smits FM (1958) Measurement of sheet resistivities with the four-point probe. The Bell Syst Tech J 37:711

A Review of Supercapacitor Energy Storage Using Nanohybrid Conducting Polymers and Carbon Electrode Materials

Punya A. Basnayaka and Manoj K. Ram

Abstract With the advancement of electronics and mobile technologies, supercapacitors are becoming the significant energy storage device. The properties of supercapacitor depend on electrochemical properties, electrochemical stability, surface area, and electrical conductivity of advanced electrode materials. Nanohybrid materials based on conducting polymers and carbon has been substantially explored over the preceding years. Strong hybridization with carbon materials, especially with graphene has been found in effectively improving the enactment of a supercapacitor with the control of size and morphology of nanoparticles, enrichment of the electron transport by adding nanocarbons, and modification of the electronic structures through charge transfer process. We have presented an overview of supercapacitor characteristics of hybrid nanostructures with conducting polymers, and carbon materials as electrode materials and extensively discusses their future trend for practical supercapacitor applications.

Keywords Electrochemistry · Graphene · Electrolytes · Energy density · Capacitance

P.A. Basnayaka
Department of Engineering and Engineering Technology,
Cuyahoga Community College, 2900, Community College Ave.,
Cleveland, OH 44115, USA

M.K. Ram (✉)
Nanotechnology Research and Education Center,
University of South Florida, 4202 E Fowler Avenue, ENB 118, Tampa,
FL 33620, USA
e-mail: mkram@usf.edu

M.K. Ram
Clean Energy Research Center, University of South Florida,
4202 E Fowler Avenue, ENB 118, Tampa, FL 33620, USA

V. Kumar et al. (eds.), *Conducting Polymer Hybrids*,
Springer Series on Polymer and Composite Materials,
DOI 10.1007/978-3-319-46458-9_6

1 Introduction

The rapid industrial growth and growing demand for energy consumption have caused to find the solution for secure and sustainable energy storage [1–3]. There is an urgent need for the production of energy from fossil fuels to renewable energy resources (solar, the wind, and geothermal) [4]. Some of the renewable energy sources are intermittent and confined locally to make the production difficult in competing for the energy demand of the world. Therefore, reliable and safe energy storage devices are desired to encounter the energy demand. The fuel cells, supercapacitors, photoelectrochemical cells, and batteries are considered as major energy storage devices. Among, supercapacitors has been found to be the most interesting device due to quick bursts of power, extended cycle life, lowcost, and ease of fabrication processes, than other energy storage devices. The supercapacitors have also been named as ultracapacitor and electrochemical capacitors (ECs) [4–8].

In the past two decades, nanoscale research has opened revolutionary opportunities for improving the performance of supercapacitors by fabricating nanoarchitecture electrodes which can easily facilitate mass transport of electrolytes ions in electrochemical processes, creating electroactive large-area surfaces and electrode/electrolyte interfaces, thus improves capacitance, cell voltage, and power density [9, 10]. Further, electrodes are devised by three-dimensional (3-D) architecture and nanohybrids or nanocomposites and are designed to exert the synergetic effect of individual materials. Conducting polymers (CPs), metal oxides, and carbon materials are three major material categories used in supercapacitor electrodes [11]. Hybrids or nanocomposites of CPs and carbon materials find a promising candidate for supercapacitors due to cost effectiveness, ability to meet the energy demand for future applications, and ease of synthesis in the fabrication of electrodes [4, 11–15]. Under this review, basic energy storage principles of supercapacitors and their prototypes have been discussed at length. Then, the nanoscale research progress based on hybrid nanostructures of CPs and carbon materials toward the development of supercapacitor performance have been discussed. The practical applications of nanohybrid materials have also been reviewed.

2 Supercapacitor Energy Storage Mechanisms

There are three types of widely discussed energy storage principles of supercapacitors found in the literature: the electric double-layer (EDL) principle, surface redox reaction-based pseudocapacitive charge storage mechanism, and the hybrid type formed by combining the EDL and pseudocapacitive charge storage mechanisms [5, 7, 16].

The first working principle of the supercapacitor is the EDL mechanism, and which was first described in a US patent in the 1950s [16]. The high surface area containing carbon electrode was immersed in sulfuric acid electrolytes to collect the polarized charge. Later, a wide usage of commercialized aqueous-electrolyte

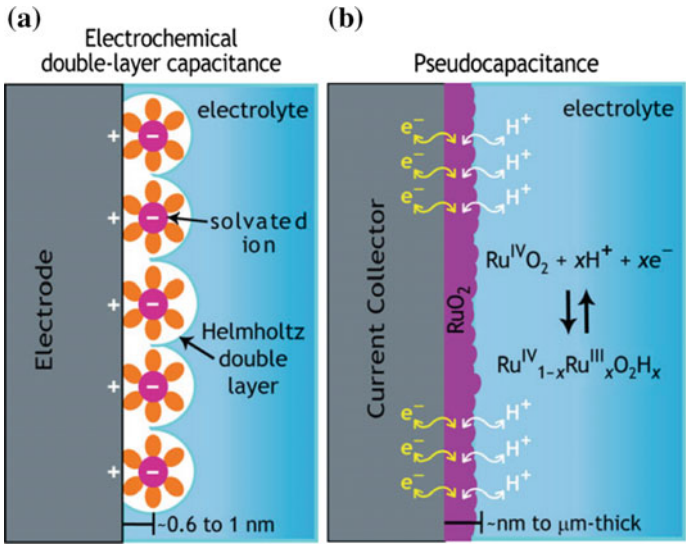

Fig. 1 Schematic of charge storage via the process of either **a** electrochemical double-layer capacitance or **b** pseudocapacitance [17] (Reprinted with permission from Ref. [17] Copyright (2011) by Cambridge University Press)

capacitors were introduced by NEC (Japan) in the 1970s [16]. The EDL design does not have the solid dielectric layer nor the chemical reactions found in batteries during charging and discarding. This technology is extremely clean energy in terms of environmental friendliness as shown in Fig. 1. The EDL type storage device has been based on charge separation at electrolyte and electrode interface. In contrast, pseudocapacitive mechanism involves faradaic oxidation-reduction reactions at electrode surfaces. Figure 1b shows the oxidation-reduction mechanism for RuO_2 electrode/electrolyte interface. These faradaic reactions-based resources are metal oxides, CPs, and doped carbons which offer high energy density. As a result, of Faradaic reactions at electrode surfaces, this type of supercapacitors is short in life cycle than EDL capacitors. As the name suggested, hybrid type supercapacitors incorporate mechanisms of both EDLCs and pseudocapacitors.

Basic supercapacitor device is consisting of two working electrodes (anode and cathode) with separator in between and filled with electrolytes which enable the movements of ions as illustrated by Fig. 2. The current collectors are connected with both electrodes which conduct electrical current from working electrodes.

The specific energy is calculated according to the relationship [16],

$$E_{\text{cell}} = 1/2\, CV^2$$

where C is the total capacitance, and the, V is the voltage of the cell. The power (P) of supercapacitor can be expressed by equation [16],

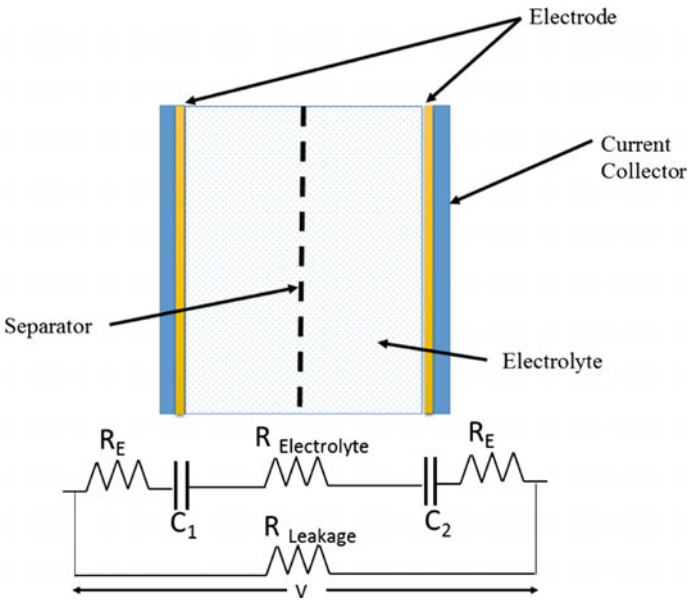

Fig. 2 Basic configuration of supercapacitor cell and the simplified equivalent DC circuit (with permission)

$$P = \frac{V^2}{4R}$$

R is the equivalent resistance of the capacitor. Each parameter is vital for the performance of the supercapacitors. The specific capacitance is dependent on the electrode materials and for EDL, the materials with the high surface area are desirable for high capacitance. On the other hand, the electrolytes are chosen carefully to increase operating voltage. There are various parameters which determine the performance of supercapacitors such as voltage window, electrolyte/electrode interface, porosity, the stability of electrodes in the electrolyte, temperature, self-discharge, and the internal resistance. Figure 3 shows the important parameters which control the supercapacitors [18]. However, the electrolytes are the influential items in the performance of the supercapacitors which is clearly illustrated in Fig. 3.

Nonaqueous acetonitrile-based electrolytes are capable of up to 2.7 V operating voltage and ionic electrolytes have been used to achieve 3.5–4 V operating voltages [16, 18]. The performances of supercapacitor cells in laboratories are carried by electrochemical measurement techniques such as galvanostatic charge–discharge technique, cyclic voltammetry (CV), and electrochemical impedance spectroscopy (EIS), techniques, respectively.

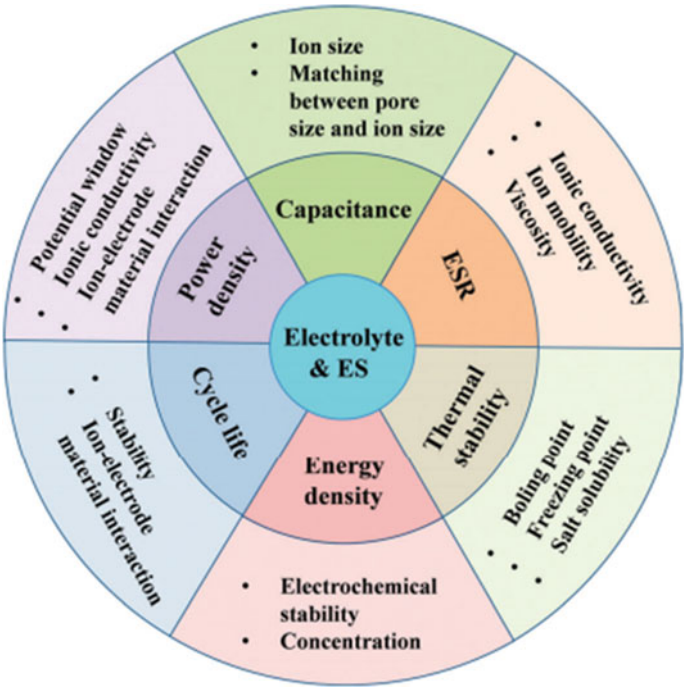

Fig. 3 Effect of electrolytes on supercapacitor performance [18] (Reprinted with permission from Ref. [18] Copyright (2015) by Royal Society of Chemistry)

3 CPs and Carbon Materials in Energy Storage

CPs, polyaniline (PANI), polythiophene (PTH), polypyrrole (PPy) have been found to be suitable electrode materials similar to other energy storage devices (fuel cells, photoelectrochemical, and batteries) [19–21]. Table 1 shows the theoretical and experimental capacitance data of few selected conducting polymers. With the nano-engineered techniques, 3-D structures of CPs gain many interests toward

Table 1 Theoretical and experimental capacitance data [10] (Reprinted with permission from Ref. [10] Copyright (2011) by Elsevier)

CP	Molecular weight of repeat unit (g)	Dopant level	Theoretical capacitance (Fg^{-1})	Experimental capacitance (Fg^{-1})
PANI	93	0.5	750	240
PPy	67	0.33	620	530
PTh	84	0.33	485	–
PEDOT	142	0.33	210	92

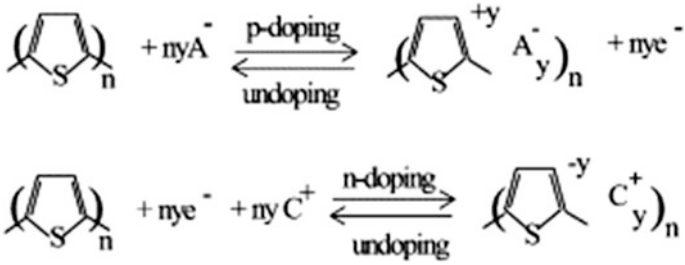

Fig. 4 Doping of polythiophene conducting polymer [20] (Reprinted with permission from Ref. [20] Copyright (2001) by Elsevier)

energy application due to the enlarged area in 3-D structures than bulk polymers, which enhances pseudocapacitance and the double-layer capacitance (DLC) as well as due to multiple redox processes in CV and EIS. CPs change its electronic conductance as a function of electrode potential, i.e., degree of oxidation. Khosrozadeh et al. have studied H_2SO_4/PVA-based gel electrolyte supercapacitor based on a composite of polyaniline and carbon particles electrodes which is dependent on charging and discharging properties of the supercapacitor [22].

Energy storage in electrochemical supercapacitors is largely due to the Faradaic reaction which takes place between electrode/electrolyte interface [20]. The doping in conducting polymer is also the charge-transfer process. The doped conducting polymer becomes conductive electronically. Figure 4 shows the doping of polythiophene which can also be understood by reversibly doping–undoping processes [2].

The equations have been simplified for both charging processes as indicated below [10]

$$\mathrm{Cp} \rightarrow \mathrm{Cp}^{n+(A^-)_n} + ne^- (\text{p-doping})$$

$$\mathrm{Cp} + \mathrm{ne}^- \rightarrow (C^+)_n \mathrm{CP}^{n-} (\text{n-doping})$$

Limited chemical stability (in particular of the n-doped state) has so far hindered the success of the application of supercapacitors. There are few short comings in conducting polymer such as swelling, contraction during charging and discharging processes [23]. The Faradaic process makes the conducting polymer-based supercapacitors less stable than carbon-based supercapacitors [23]. The carbon-based charging and discharging processes are due to EDL effect which brings the life cycle to >500 000 cycles. The hybrids of CP and carbon materials have been designed to enhance the chemical stability. Activated carbon (AC) [24, 25], carbon fibers, aerogels [26], carbon fiber fabrics [27], carbon nanotubes (CNTs) [12, 28–31], and graphene [32, 33] have utilized to design nanostructured 3-D CP-Carbon hybrids to improve the surface area and chemical stability of supercapacitor cells.

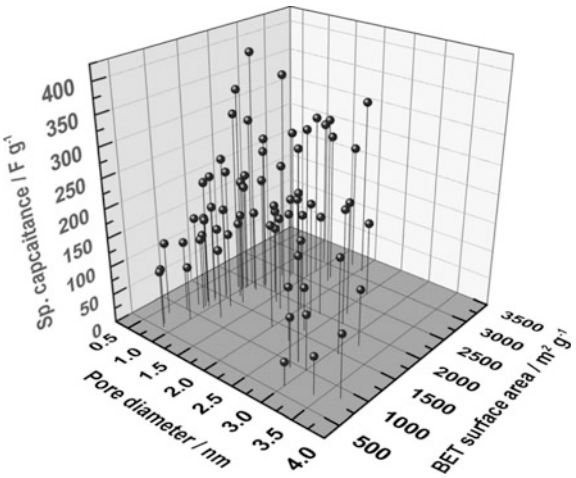

Fig. 5 3-D graphical representation of the dependence of specific capacitance on pore diameter and BET surface area [34] (Reprinted with permission from Ref. [33] Copyright (2012) by John Wiley and Sons)

The activated carbon (AC) reveals EDL capacitor. The capacitance of AC-based supercapacitors is dependent on specific conductivity, surface area, and porosity of the electrode. The porosity of the electrode material is estimated by Brunauer–Emmet–Teller (BET) [34]. The porosity in the material has been understood by measuring the diameters of the surface pores of the material. The diameter of microparticles has been categorized as less than 2 nm whereas meso lies between 2 and 50 nm and macropores are greater than 50 nm. The capacitance varies depending on the size of the ions interacting with the surfaces as shown in the Fig. 5.

CNTs is another promising EDL type material that has been utilized to increase the performance of the supercapacitors. The commercialization of CNT has been heralded due to poor energy density, Therefore attempts are put forward to increase the energy density through inexpensive and noncomplex purification process. The graphene is replacing the research of CNTs for supercapacitor applications due to cost effectiveness and enhanced supercapacitive performance [32, 33, 35].

The structure of graphene is the one layer of sp^2 hybridized carbon atoms, and Fig. 6 shows the Transmission Electron Microscope (TEM) image of graphene [36]. The large surface area ($\sim$2600 m^2 g^{-1}), high electrical and thermal conductivity, flexible, light weight, and high mechanical strength (Young's modulus $\sim$1100 GPa) properties have made graphene to use in electrochemical devices [37]. The graphene has been found to be of the ideal material to study in supercapacitor similar to activated carbon electrode. Table 2 shows the experimental capacitance values of different carbon materials.

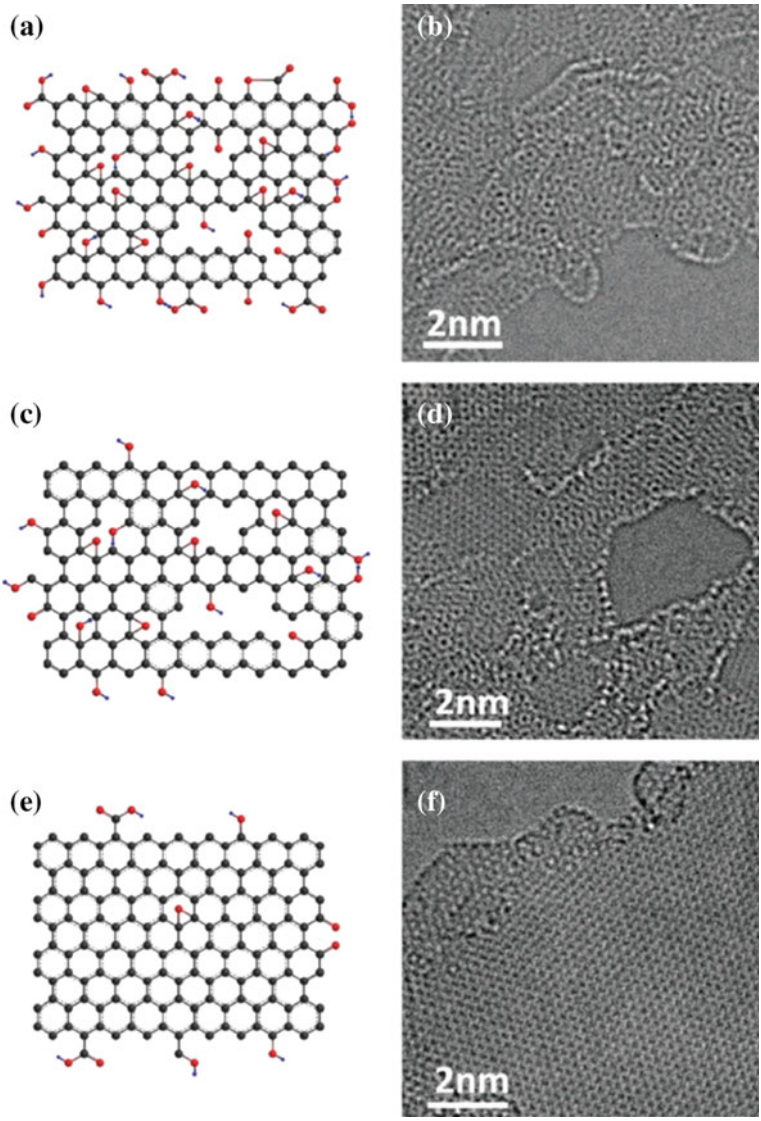

Fig. 6 Schematic chemical structures and TEM images of (**a**, **b**) graphene oxide (GO), (**c**, **d**) reduced GO and (**e**, **f**) chemically exfoliated graphene sheets. *Dark grey balls* carbon atoms; *red balls* oxygen atoms; *blue balls* hydrogen atoms. Hydrogen atoms on carbon atoms were omitted [38] (Reprinted with permission from Ref. [37] Copyright (2013) by Royal Society of Chemistry)

Table 2 Experimental capacitance data of different carbon materials

CP	Surface area (m^2g)	Electrical conductivity (S/cm^{-1})	Experimental capacitance (Fg^{-1})
ACs	1000–3500	0.1–1	75–200
Carbon aerogels	400–1000	1–10	75–120
CNTs	150–500	10^4	50–175
Graphene	~2600	10^6	100–225

4 CP/Carbon Hybrids as Electrodes for Supercapacitor

4.1 CP/Activated Carbon Hybrids

AC, carbon black and aerogel are the first carbon allotropes tested on supercapacitors and used in industrial type supercapacitor cells. To improve capacitive properties of EDLCs, their carbon-like nanostructure electrodes are modified with electroactive materials. This modification leads to accumulation of additional charge on the electrode surface and improved the capacitance. The carbon materials have been used as additives, catalyst for electron transfer, hosts for intercalation of ions, substrates for electrode materials, and electrodes for energy storage devices [39–41]. ACs have been used with PEDOT as composite for the enhancement of capacitance of supercapacitor cells. Activated carbon/CPs are also used in asymmetric supercapacitors [42–44].

4.2 CP/Carbon Nanotube Hybrids

A greater capacitance has been observed for the CP/CNT hybrid electrode than pristine CP or CNTs. PANI/CNT, PPy/CNT, and PEDOT/CNT have been widely explored as supercapacitor electrode materials [23, 43–51]. The pristine CPs are unstable to be used in supercapacitor applications. The carbon nanotubes help in retaining mechanical stability in hybrid structure and cycle stability where the occurrence of shrinkage and expansion of the nanostructure occurs for each cycle due to conducting polymer [23]. The increased capacitance have been described by two types of interaction between CNT and CPs. There exits the electrostatic interaction between the positive charges in the polymer chains whereas, the negative charges occur due to functional groups (e.g., carboxylic groups) present on the surface of CNTs. The second type of the interaction is the $\pi - \pi^*$ stacking interactions [1]. The highly unsaturated conjugated π-bonds are included in both CPs and CNTs which are highly susceptible to further bonding. The importance of random stacking of CNT in CP matrix has also been studied, and the advantage of aligned stacking is discussed by some researchers. Increased electrolyte accessibility in aligned structure and providing short diffusion paths for charging and discharging of supercapacitors are

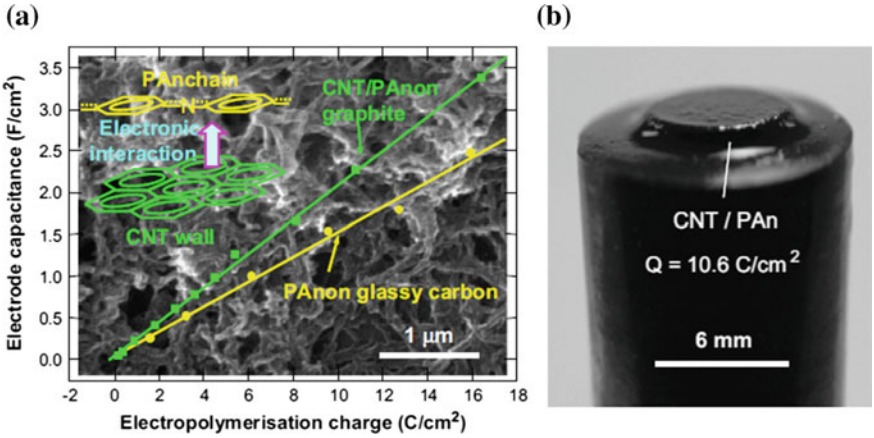

Fig. 7 **a** SEM picture of microstructure of the surface of an electro-deposited CNT/PAn film [1]. The superimposed plotting shows electrode capacitance varies proportionally to the deposition charge for CNT/Pan (*green marks* and *line*) and Pan (*yellow marks* and *line*). **b** Photograph of an epoxy-sheathed graphite electrode with a thick electro-deposited CNT/Pan coating [50] (Reprinted with permission from Ref. [50] Copyright (2013) by Elsevier)

explained. Figure 7 a is the Scanning Electron Microscope image of electro-deposited CNT/PANI composite, and the increase capacitance has been observed with the deposition current of the electrochemical deposition experiment. Figure 7 b is the illustration of fabricated supercapacitor cell using the electro-deposited electrodes.

CP/metal oxide: The PEDOT–MoO_3 nanocomposite material was made using a soft chemistry route and the fabricated PEDOT–MoO_3 electrode showed specific capacitance of 300 F/g [52]. The manganese dioxide (MnO_2), carbon nanotube (CNT), and conducting polymer (CP) based tertianary electrode have shown specific capacitance to be 427 F/g. The 60 % of MnO_2 loading could still be found to show the specific capacitance of 200 F/g [53]. The MnO_2/poly (aniline-co-o-anisidine) nanocomposite-based electrode were synthesized by delamination and reassembly technique which shows the specific capacitance of 262 F/g in 1 M Na_2SO_4 based electrolyte at current density of 1.0 F/g [54]. Mahore et al. [55] fabricated nanocomposite based on CNT and PPY and estimated the surface areal capacitance of 1.0619 F/cm^{-2} for PPy/CNT nanocomposite material.

4.3 CP/Graphene Hybrids

In recent years, much intensive efforts have been made to produce graphene hybrid materials as electrodes for innovative electrochemical energy storage and conversion devices. A sequence of such materials was developed by hybridizing graphene with

Table 3 Capacitive properties of graphene/PANI different morphological structures

Material	Synthesis method	Capacitance	Other performances	Reference
G-PANI	In situ polymerization	480 at 0.1 A/g/2 M H_2SO_4	–	[61]
G-PANI-nanofiber	Vacuum filtration	210 F/g at 0.3 A/g	–	[60]
G-PANI-hollow spheres	–	614 F/g at 1 A/g	–	[57]
G-PANI-vertically align nanorods	Interfacial polymerization	497 F/g at 0.2 A/g	5.7 % capacitance loss after 2000 cycle	[59]
G-PANI-flake	–	764 F/g at 0.1 A/g	–	[56]

CPs or metal/metal oxide. Incorporation of graphene sheets into CPs, such as, PANI, PEDOT, and PPy polymers have been aimed to improve rate capability, specific capacitance, and life cycle over other carbon/CP hybrid type supercapacitors. Graphene/PANI is the most studied hybrid materials as supercapacitor electrode due to its wide potential voltage window, high capacity, ease of synthesis, and stability among other CPs hybrids [56–61]. Different morphological structures, such as nanowires, nanorods, nanospheres of PANI have been considered to hybridize with graphene and observed promising supercapacitor performances with different synthesis methods as shown in Table 3. Further, the fibrillar polyaniline (PANI) doped using the in situ synthesis with graphene oxide showed the conductivity of 10 S/cm and electrode shows the specific capacitance of 531 F/g for the voltage in the range of 0.45 V at 0.2 A/g. The performance of supercapacitor with the different ratios of graphene to polyaniline present in the electrode material has been found in fibrillar polyaniline in graphene nanohybrids electrodes. [62].

The PANI hybrid electrodes reveals pseudocapacitive characteristic showing the pair of redox potential similar to pristine PANI as shown in Fig. 8. The

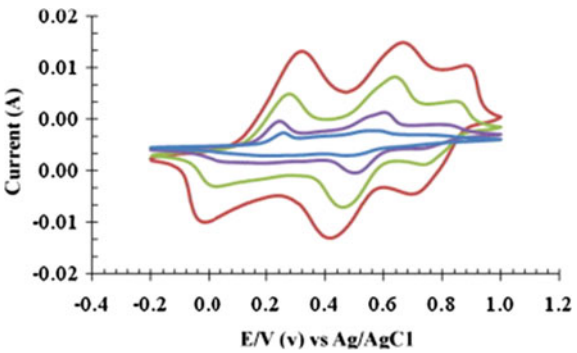

Fig. 8 Cyclic voltammetry of G-PANI in 0.2 M HCl [53] (Reprinted with permission from Ref. [53] Copyright (2011) by Elsevier)

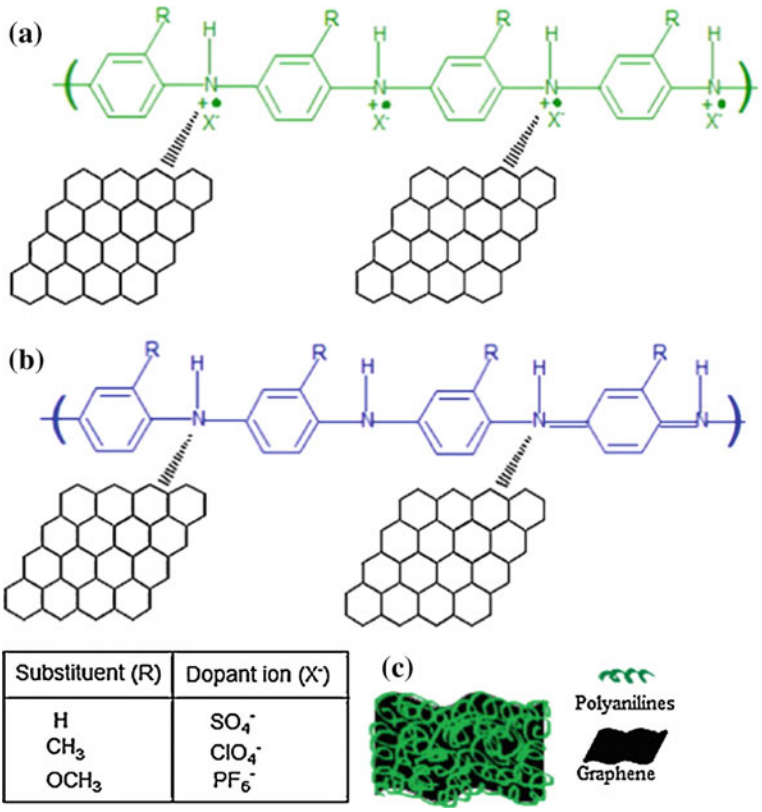

Fig. 9 **a** Emeraldine salt form of graphene–polyanilines nanocomposite, **b** emeraldine base form of graphene–polyaniline nanocomposites, **c** formation of CPs wrapping around graphene [63] (Reprinted with permission from Ref. [63] Copyright (2013) by Elsevier)

leucoemeraldine (semiconductor)/polaronic emeraldine salt (conductor) and Faradaic transformation of emeraldine base/pernigraniline are clearly visible in cyclic voltametry studies [57, 58].

We have recently studied the Graphene-PANI derivative nanocomposites, such as poly (o-methoxy aniline) [poly (o-anisidine) (POA)] and G-poly (o-methyl aniline) [poly (o-toluidine) (POT) electrodes for supercapacitors (Fig. 9). The specific capacitances (Cp) of supercapacitors based on G-PANI, G-POA, and G-POT in 2 M H_2SO_4 electrolyte has been estimated to be 400, 380, and 425 F/g, respectively [63].

The second most researched graphene-conducting polymer hybrid is the graphene-PPy. The capacitances of G-PPy have been reported as 267, 360, 200, and 270 F/g [64–67]. In addition to G-PANI and G-PPy, G-PEDOT, and G-PTh has also been studied. G-PEDOT found to be more promising than G-PTh in enhancing capacitance and stability than G-PTh-based supercapacitor cells [68–70].

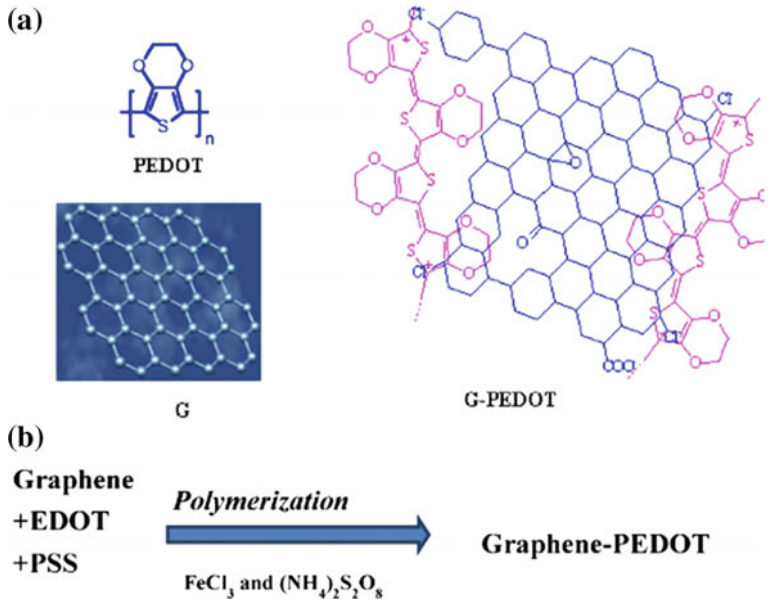

Fig. 10 **a** Schematic structures of graphene, PEDOT and G-PEDOT. **b** Schematic of synthesis of G-PEDOT [72] (Reprinted with permission from Ref. 72 Copyright (2011) by Elsevier)

High capacitive G–PEDOT nanocomposites material synthesized using chemical polymerization technique for supercapacitor application. G-PEDOT electrode shows the specific capacitance of 374 F/g (F/g)[72]. The schematic of the synthesis process of G-PEDOT nanomaterial is shown in Fig. 10.

The major advantage of PEDOT and PTh-based nanostructure is the flexible fabrication of electrode materials using screen printing. Cho et al. [71] have fabricated ternary screen-printed electrode based on PEDOT:PSS, G and RuO_2-based supercapacitor where PSS worked as binder and allowed to disperse graphene and RuO_2 in the solution as illustrated in Fig. 11. The $\sim$5 μm coated RuO_2/PEDOT:PSS/graphene electrode exhibited the specific capacitance of 820 F/g with a cyclic stability of 81.5 after 1000 cycles.

Another research on RGO/PEDOT nanostructure based supercapacitor was studied for its specific capacitance and stability by Yang et la. The PEDOT–poly (styrenesulfonate)/reduced graphene oxide (PSS/RGO) film-based electrode have shown 193.7 F/g of high specific capacitance at 0.5 A/g with capacity retention of 90.6 % after charging-recharging for 1000 cycles. The cyclic voltammetric study showed in Fig. 12a observed good capacitive properties of RGO–PEDOT–PSS nanocomposites than PEDOT–PSS and pure RGO films. Figure 12b shows a good reversibility of galvanostatic charge/discharge behavior at 0.5 A/g at a constant current density [72].

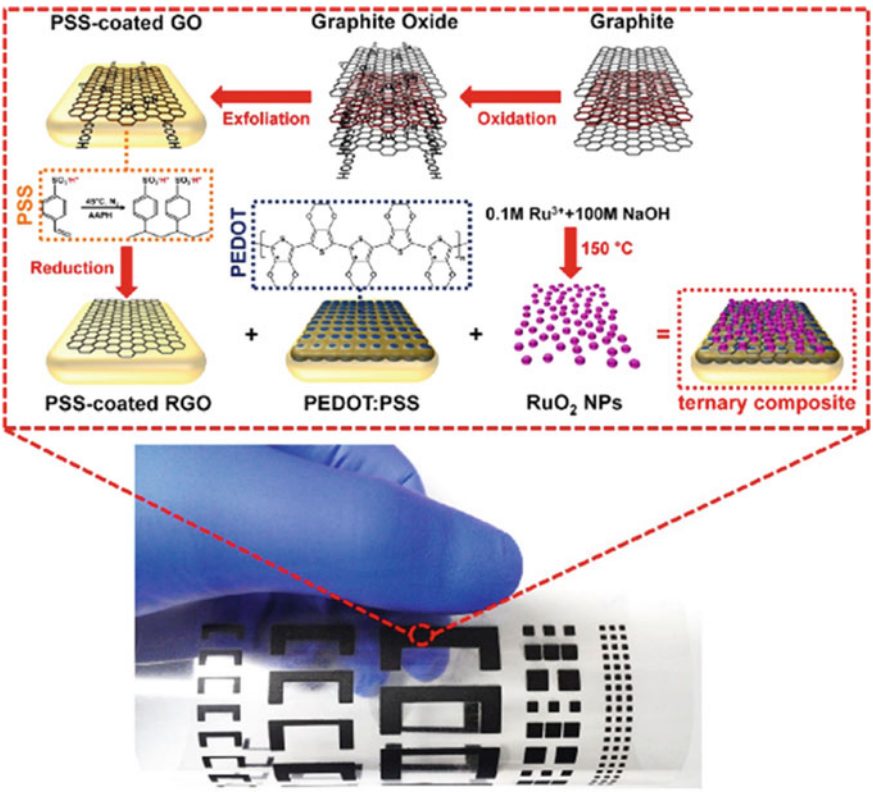

Fig. 11 Overall procedure for fabricating RuO_2/PEDOT:PSS/graphene screen-printed electrode and digital camera image of screen-printed electrode [71] (Reprinted with permission from Ref. [62] Copyright (2011) by ACS Publication)

A tertiary nanocomposite of graphene, SnO_2, and PANI was used to prepare supercapacitor, which revealed specific capacitances of 1012 Fg^{-1} at 4 Ag^{-1}, and 729 Fg^{-1} at 3.5 Ag^{-1}. The observed capacitance is considerably high compared with most of the G-CP-based supercapacitor cells, suggesting that the combination of major materials categories formed enhanced performance of next-generation supercapacitors, and direct the current research towards the research and development of tertiary nanocomposites. Figure 13 shows the DLC and pseudocapacitive capacitance for the tertianary film in 1 M Na_2SO_4 and 1 M H_2SO_4 [73]. The cellulose a nanocrystal (CNXLs) has been used to synthesize PANI/CNXL and PEDOT/PEDOT/CNXL nanocomposites-based supercapacitor electrodes. Liew et al. [74] showed the specific capacitances of 488 F/g for PANI/CNXL, and 69 F/g for PEDOT/CNXL based electrodes.

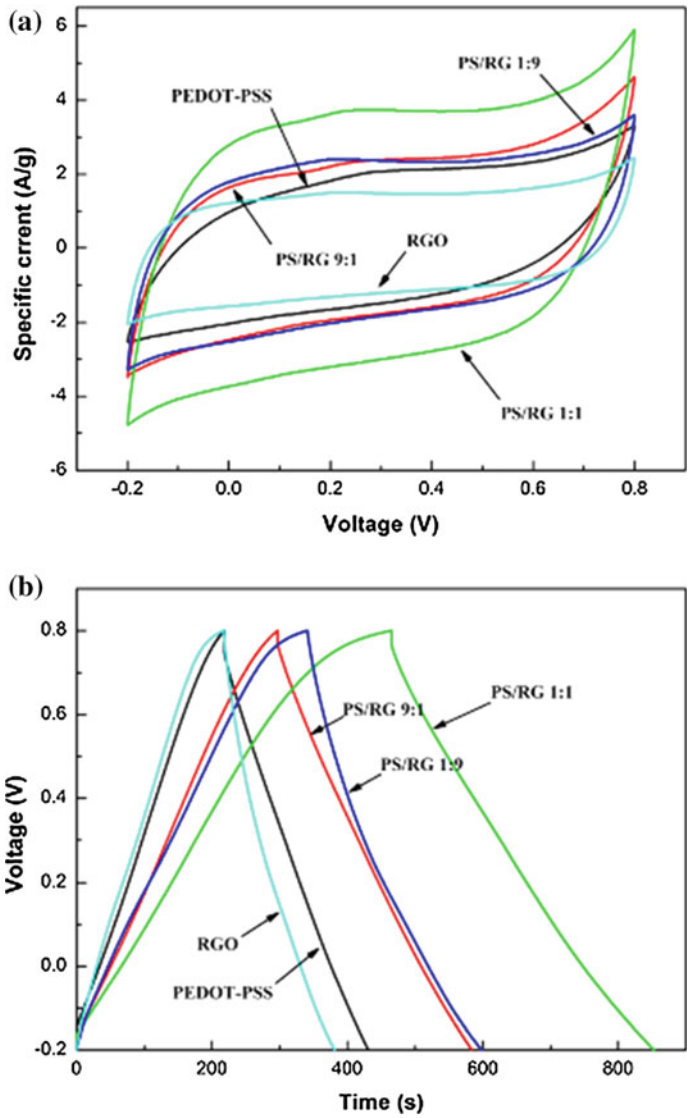

Fig. 12 **a** Cyclic voltammograms curves of varied films at a scanning speed of 20 mV/s; **b** galvanostatic charge to discharge curves of varied films at a current density of 500 mA/g [72] (Reprinted with permission from Ref. [72] Copyright (2015) by Springer)

Raj et al. have fabricated flexible supercapacitor by using flexible substrate of graphite nanoflakes and a thin layer PPY film for enhanced conductivity, and was observed stable capacitance of 6 mF/cm^2 in solid-state capacitor. Figure 14 shows the stability, charge–discharge and CV of the fabricated GF/PPy supercapacitor [75].

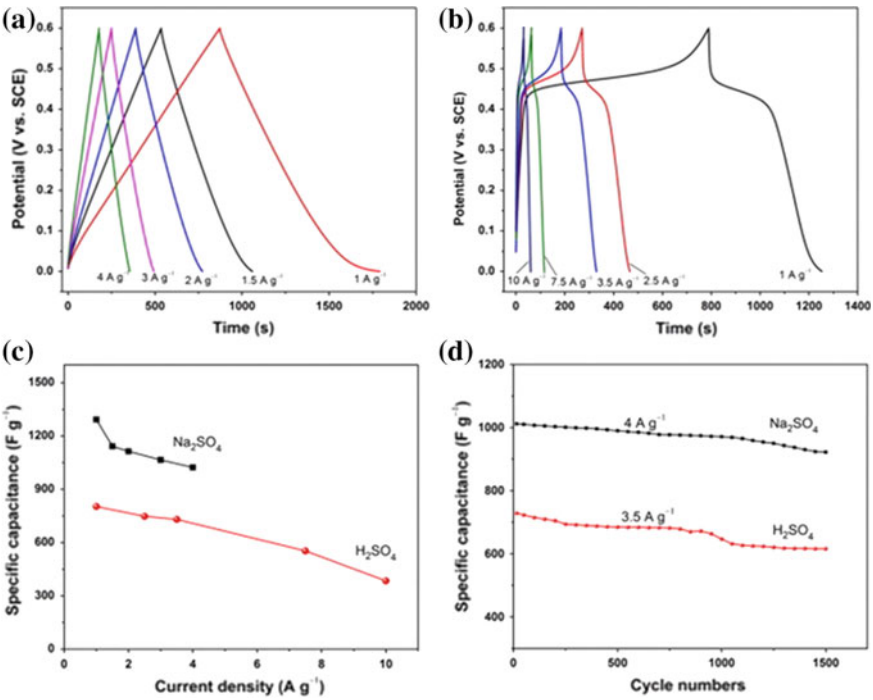

Fig. 13 **a** Galvanostatic discharge curves of the RGO@SnO_2@PANI electrode measured in **a** Na_2SO_4 and **b** H_2SO_4 at different current densities; **c** specific capacitance of the electrode tested in 1 M H_2SO_4 and Na_2SO_4 at different current densities; **d** variation of the specific capacitance as function of the cycle numbers in 1 M Na_2SO_4 at 4 Ag^{-1} and in 1 M H_2SO_4 at 3.5 Ag^{-1} [73] (Reprinted with permission from Ref. [73] Copyright (2015) by Elsevier)

4.4 CP Hybrids for Flexible Semisolid/Solid-State Supercapacitors

The solid-state flexible supercapacitors have been found appealing due to higher specific and volumetric energy density, reliable, small in size, ease in packaging, and light weight while matched with conventional capacitors [60, 76–82]. A solid-state supercapacitor was fabricated based on hybrid nanocomposite from PANI and polyoxometalate $H_3[PMo_{12}O_{40}]$, and the work demonstrates the usefulness of organic–inorganic hybrid materials for energy storage in electrochemical capacitor. [83].

A highly conductive PANI-nanofiber and graphene layered structure are fabricated by vacuum filtration process and observed a specific capacitance as 210 F/g at discharge current density 0.3 A/g. The fabricated flexible electrode is shown in Fig. 15 [84].

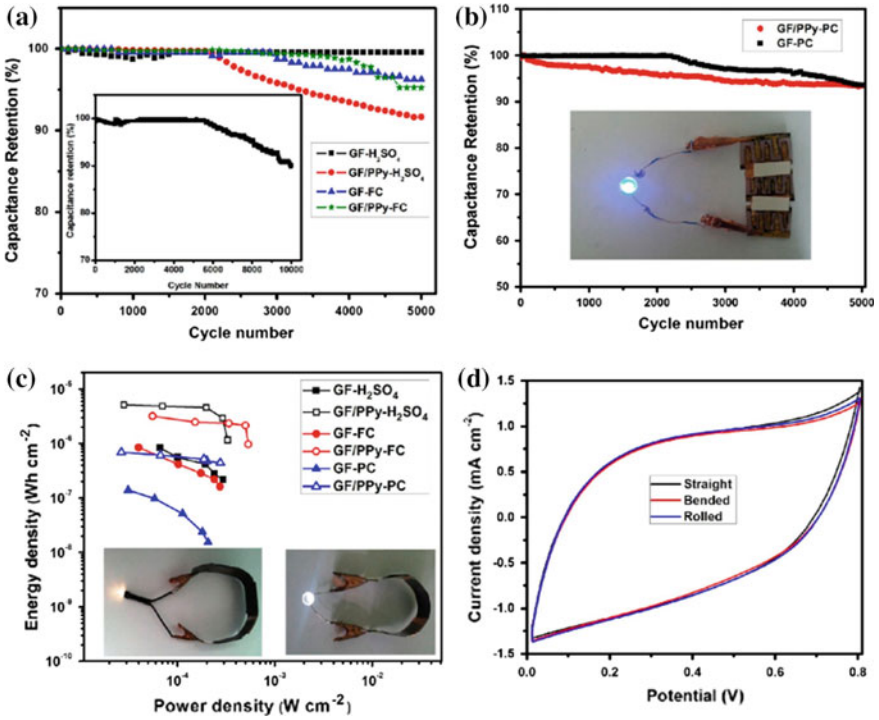

Fig. 14 **a** Cycling stability of the GF and GF/PPy in H_2SO_4 electrolyte and GF and GF/PPy full cells for 5000 cycles (*inset* shows the extended cyclic stability of GF in H_2SO_4 electrolyte for 10,000 cycles revealing the good stability of GF in 4000 grit polymer lapping film). **b** Cycling stability of the GF and GF/PPy planar cells for 5000 cycles [*inset* shows the demonstration of serially connect planar cells glowing a blue LED (2.2 V, 10–20 mA)]. **c** Ragone plot for GF and GF/PPy electrodes, full cells, and planar cells; the inset picture showing that three SCs in series can lighten up a warm and pure white LED (3 V, ~10–20 mA) powered by 30 s charged SCs. **d** CV curves of the flexible GF/PPy full cell at different measurement conditions like straight, bent, and rolled state at 100 mV/s scan rate [75] (Reprinted with permission from Ref. [72] Copyright (2015) by ACS Publications)

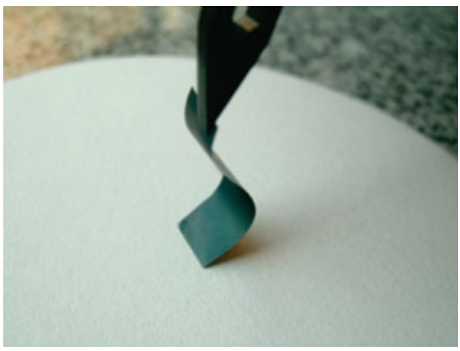

Fig. 15 A flexible Graphene–PANI–nanofiber film [55] (Reprinted with permission from Ref. [55] Copyright (2010) by American Chemical Society)

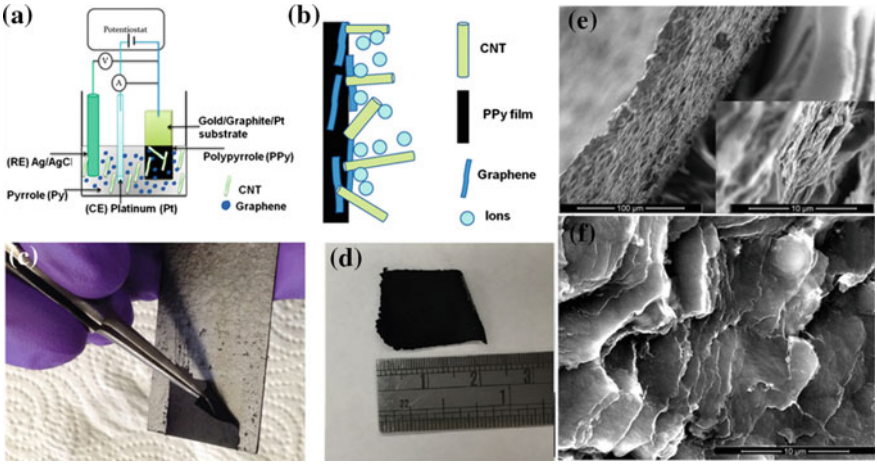

Fig. 16 **a** Schematic representing the fabrication process of the nanocomposite electrodes. **b** Illustration of hybrid nanocomposite film forming a unique interface where graphene and CNT are embedded in situ during polymerization of PPy. **c**, **d** Optical image of the actual freestanding film on the graphite substrate with ~2 cm × 2 cm area. **e** Cross-sectional SEM micrograph showing layered formation of the polypyrrole film. **f** Layers of graphene-CNT coated with PPy during polymerization forming a nanocomposite PCG film. Reprinted with the permission from ref [85] copyright (2015) by Nature Publishing Group [85]

Another solid-state polymer supercapacitor has been fabricated by a simple two-step process. The PANI/CNT nanocomposite electrodes were separated by solid gel polyvinyl alcohol (PVA)–H_2SO_4 electrolyte. The entire device showed six times of specific capacitance as 31.4 F/g compared to commercial supercapacitor [66]. Wei et al. [76] also have fabricated cloth-supported single-walled carbon nanotubes (SWCNTs) and PANI-based flexible supercapacitor and estimated the specific capacitance as 410 F/g along with high rate capability. Recently, graphene and carbon nanotubes (CNT) were made composite with pyrrole monomer and the electrode shows the specific capacitance of 453 F/g, the specific energy of 62.96 W h/kg and power density of 566.66 W kg^{-1} were obtained. Figure 16 shows the schematic representing the fabrication process with characterization of the composite film [85].

Similarly, graphene-PPy based flexible electrodes are also studied for supercapacitors. One study shows an application of pulse-electrochemical polymerization of PPy on flexible freestanding graphene film. The pulse polymerized PPy films showed the power densities as ~33 Wh/kg and ~1184 W/kg for a scan rate of 0.01 V/s [76]. Figure 17 shows an illustration of flexible supercapacitor device with a sandwich structure. Another recent research reported ternary nanostructured free standing flexible electrode based on titania–graphene–polypyrrole (TiO_2–G–PPy), and polypyrrole/graphene oxide/zinc oxide nanocomposite by claiming the higher stability with the incorporation of metal oxides into the nanostructure [77, 84]. The yarn of SWCNTs/PANINWs was fabricated using spinning process and obtained

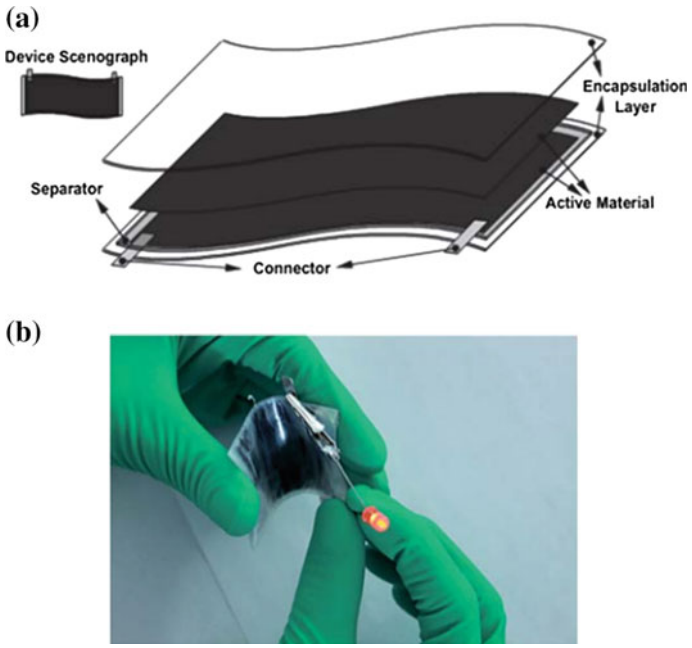

Fig. 17 **a** A schematic illustration of a flexible supercapacitor device with a sandwich structure. **b** The supercapacitor can light a red LED for several minutes [56] (Reprinted with permission from Ref. [69] Copyright (2011) by Royal Society of Chemistry)

capacitance of 6.23 mF cm^{-2} which is compared to be 18 times higher than the simple SWCTS-based yarn-based electrodes. [86].

Souze et al. have fabricated the solid electrolyte-based supercapacitor based on SWCNTs/PANI on polyethylene terephthalate-PET substrates. They have used H_2SO_4–PVA gel electrolyte and measured the pseudocapacitive properties and estimated the coulometric specific capacitance of 76.7 F cm^{-3} [87]. The poly (3,4-ethylenedioxypyrrole) and PEDOT wrapped Sb2S3 nanorods were synthesized hydrothermally by Reddy et al. [88] and 1008 F/g specific capacitance, 504 W/kg power density, and 88 % capacitance retention over 1000 cycles were estimated in the fabricated supercapacitor. Further, the supercapacitor was fabricated using semisolid electrolyte using PMMA in ionic liquid.

4.5 Equivalent Circuit Models

EIS is an electrochemical measurement tool that can be used to predict performance of electrochemical power electronic systems, such as supercapacitors and batteries [89–92]. EIS method is used to find the equivalent circuit models, where each lump parameter can be explained by physical phenomena occurring during

charging/discharging of electrochemical systems. EIS is used to verify the performances calculated by other alternative electrochemical methods such as CV and galvanostatic charging/discharging techniques. The charge transfer resistance, equivalent series resistance, interfacial capacitance, dielectric constants are among parameters estimated by the EIS measurements with a proper equivalent circuit models.

The equivalent series resistance is shown for high frequency starting point at real axis and charge transfer resistance is identified by small semicircle. At low frequency, nonideal interfacial capacitance is observed. As observed in Fig. 18, addition of graphene reduces the charge transfer resistance by fivefolds, which make supercapacitor cells high rate capable [93]. There are some equivalent models developed to describe the morphological structures of electrode surface like porosity by transmission model line circuit proposed by De Levie [93]. Several circuit models (they are combinations of resistors and capacitors connected parallel and series) used to describe the electrochemical behavior including the surface structure of carbon-based supercapacitors are used and describe the frequency response behavior given in Fig. 19.

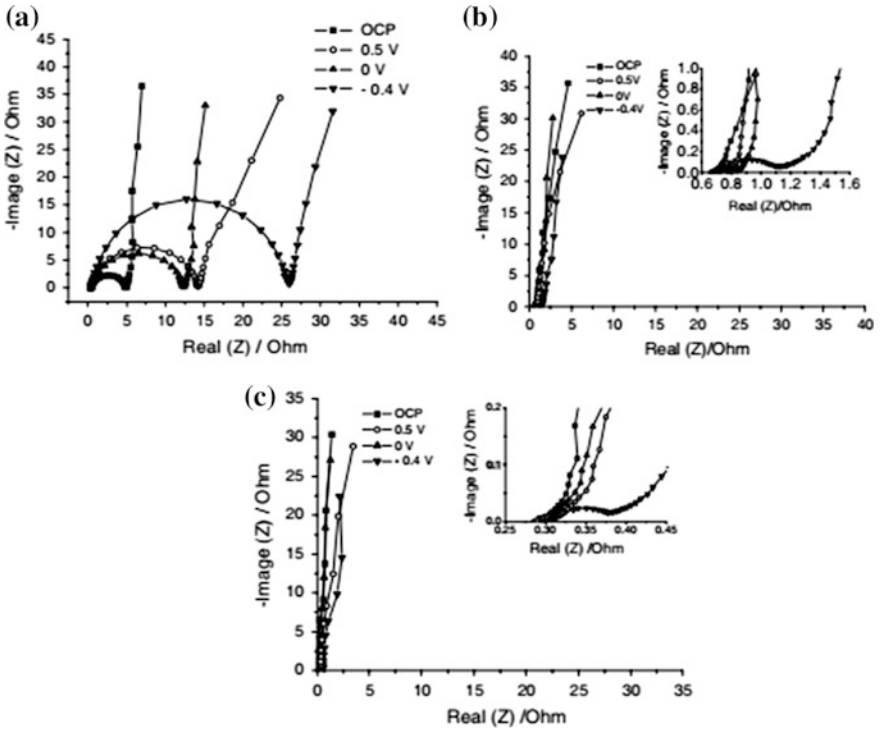

Fig. 18 EIS curves of pristine PPy (**a**), PPy/SWNTs (**b**) and PPy/functionalized SWNTs (**c**) composite films at OCP, 0.4 V (vs. SCE), 0 V (vs. SCE) and 0.5 V (vs. SCE) in 1 M KCl solution [92] (Reprinted with permission from Ref. [76] Copyright (2007) by Elsevier)

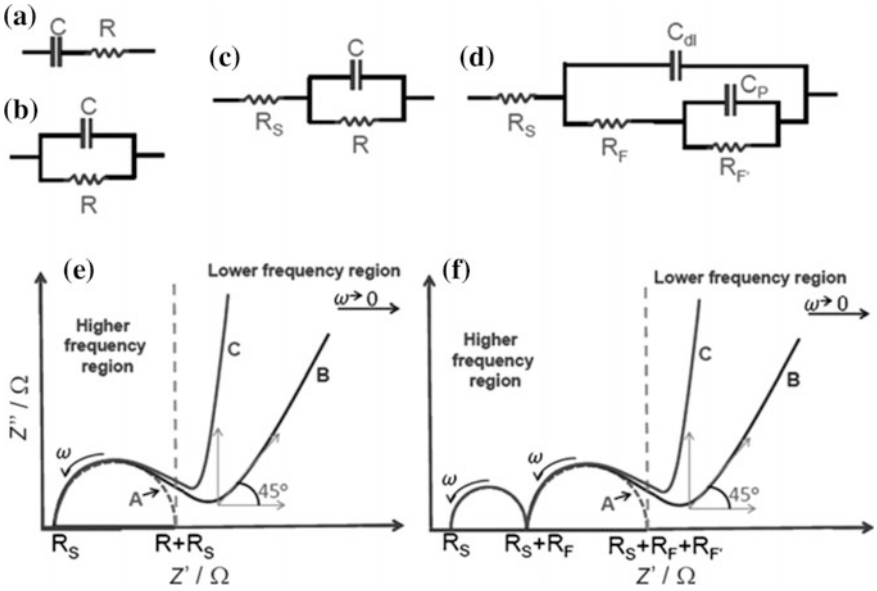

Fig. 19 Equivalent circuit models for carbon-based porous electrodes; RC circuits for **a** series and **b** parallel connections, representing an equivalent circuit (simplest) of a capacitor. *R* resistor, *C* capacitor. Equivalent circuits of only one capacitor (Cdl or CP) in parallel to a resistor *R* and in series to resistor RS (**c**) and considering both Cdl (in parallel to RF) and CP (in parallel to RF′) in series with RS (**d**) are also shown. The ac responses to the latter two circuits are shown in (**e**, **f**) [33] (Reprinted with permission from Ref. [33] Copyright (2012) by John Wiley and Sons)

The capacitance observed is not ideal capacitance as observed by the inclined line at low frequency in impedance and usually represented by constant phase angle element (CPE) shown in Fig. 20 [5, 7, 57, 63, 76, 93].

Recently, Fletcher et al. has proposed for carbon-based supercapacitors, a general equivalent circuit through the comprehensive and reasonably dependable explanation through open circuit voltage decay, capacitance loss at high frequency, and voltammetric distortions at high scan rate [94]. Table 4 shows the few selected conducting polymer nanocomposite supercapacitor performances.

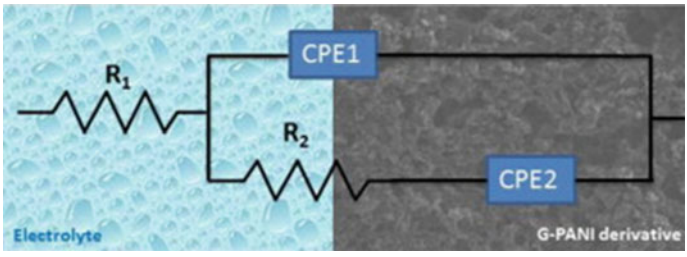

Fig. 20 Representation of nonideal interfacial capacitance of G/POANI nanhybrids in a circuit model [57] (Reprinted with permission from Ref. [57] Copyright (2013) by Elsevier)

Table 4 Supercapacitor performance of selected conducting polymer nanocomposite based supercapacitor

No	Electrode materials	Electrolyte (solid/liquid)	Specific capacitance	Voltage window	Cycles	Ref.
1	Polyaniline (conducting polymer) and $H_3[PMo_{12}O_{40}]$ (polyoxometalate)	(Polybenzimidazole) membrane with phosphoric acid (solid)	195 mF cm^{-2}	0–0.8 V	2000	[83]
2	Fibrillar polyaniline (PANI) doped with graphene oxide sheets	1 mol H_2SO_4 solution	531 F/g	Range from 0 to 0.45 V		[62]
3	(PANI) nanowire arrays grown vertically on graphene oxide sheets	11 M H_2SO_4	555 F/g	−0.2 to 0.8 V		[95]
4	Flexible GO–polyaniline (PANI) and graphene–PANI hybrid papers	1 M H_2SO_4	489 F/g	−0.2 to 1.0		[96]
5	Polyaniline-grafted reduced graphene oxide (PANi-g-rGO) composite	1 M H_2SO_4	250 F/g	−0.2 to 1.0 V	Good	[97]
6	G-PEDOT electrode	1 M HCl and	374 F/g		95 % for 800 cycles	[70]
7	PANI/, PPY and PEDOT, 20 wt% of CNTs	TEABF4 in acetonitrile and 1 M H_2SO_4	100–330 F/g			[23]
8	Polypyrrole/molybdenum disulfide (PPy/MoS_2)	1 M KCl	553.7 F/g	−0.8 to 0.4	90 % after 500 cycles	[98]
9	PANI/MoS_2	1 M H_2SO_4	575 F/g	−0.4 to 0.6 V	500 cycles	[99]
10	PEDOT/MoS_2	1 M $LiClO_4$ in acetonitrile		1.0–4.0 V versus Li		[100]
11	PEDOT/MoS_2	1.0 M H_2SO_4	405 F/g	−0.2 to 0.8 V	90 % after 1000	[101]
12	Bacterial cellulose nanofiber-supported PANI	1 M H_2SO_4	273 F/g	−0.2 to 0.8 V		[102]
13	PANI/Mesoporous Carbon Composite Electrode	1 M H_2SO_4	770 F/g	−0.2 to 0.8 V	5 % loss after 3000	[103]
14	GO-PPY	2 M H_2SO_4	500 F/g	−0.2 to 0.8 V	70 % after 1000 cycles	[104]
15	PPy NWs array and also PPy@LDH	PVA/KOH electrolyte	2034 F/g	0–0.5 V	90.7 % after 1000 cycles	[105]

5 Conclusion

Carbon and CP nanocomposite materials have shown great potential for supercapacitor application. The CP nanocomposite electrode materials have been fabricated using various metal oxides (MnO_2, RuO_2, etc.), carbon materials (graphene, carbon nanotubes, cellulose, activated carbon), and with the use of graphene-metal oxide/as tertiary nanocomposite. The electrodes materials of Carbon-CP have been reviewed advancement of supercapacitor technology by carbon-based CPs hybrid electrode is discussed interms of design, synthesize, fabrication of supercapacitor cells, performance evaluation and modeling of CP/carbon hybrid nanomaterials. The supercapacitor cells have been theoretically modeled and fabricated in achieving the high capacitance, wide potential window, high energy density. Improved energy storage has been achieved by designing electrode materials by combined EDL capacitance and highly reversible pseudocapacitance. The nanocomposite electrodes have revealed improved larger surface area, electrical conductivity, specific capacitance, energy and power density, and cycle stability.

However, the synthesis of precisely controlled nanocomposites is still challenging to exploit fully the nanocomposite material for energy applications. The nanocomposite electrode material can be synthesizing various techniques, and there is no one optimized technique to exploit the material properties fully. The little diversity in nanomaterial with monomer changes the properties of the nanocomposite completely. The method of preparation, condition of preparation (monomer to nanomaterial ratio), mixing or polymerization time, etc., significantly varies the chemical and physical properties of the nanocomposite, and hence affects the properties of the supercapacitor.

Further, the improvements in next-generation supercapacitor technology by solid-state flexible supercapacitor research using graphene and graphene/CPs flexible electrode are discussed. The researchers are making efforts in reducing cost involving synthesis and fabrication of electrode and cells of supercapacitors. It is believed that the nanocomposite materials have great future for commercial supercapacitor applications. The supercapacitors are projected to match batteries in several applications where higher power, sustainability, safety, and life cycles are required.

Acknowledgments The authors acknowledge Clean Energy Research Center at University of South Florida for their continued support for supercapacitor work.

References

1. Chen GZ (2013) Understanding supercapacitors based on nano-hybrid materials with interfacial conjugation. Prog Nat Sci Mater Int 23:245–255
2. Inagaki M, Konno H, Tanaike O (2010) Carbon materials for electrochemical capacitors. J Power Sources 195:7880–7903
3. Rolison DR, Nazar LF (2011) Electrochemical energy storage to power the 21st century. MRS Bull 36:486–493
4. Sun Y, Shi G (2013) Graphene/polymer composites for energy applications. J Polym Sci Part B Polym Phys 51:231–253
5. Wang G, Zhang L, Zhang J (2012) A review of electrode materials for electrochemical supercapacitors. Chem Soc Rev 41:797–828
6. Burke AF (2007) Batteries and ultracapacitors for electric, hybrid, and fuel cell vehicles. Proc IEEE 95:806–820
7. Conway BE (2013) Electrochemical supercapacitors: scientific fundamentals and technological applications. Springer, Berlin
8. Reisch MS (2015) Supercapacitor makers charge ahead: materials research advances promise to make the energy storage device a complement to batteries. C&EN 93:20–21
9. Huang Y, Liang J, Chen Y (2012) An overview of the applications of graphene-based materials in supercapacitors. Small 8:1805–1834
10. Snook GA, Kao P, Best AS (2011) Conducting-polymer-based supercapacitor devices and electrodes. J Power Sources 196:1–12
11. Tiwari JN, Tiwari RN, Kim KS (2012) Zero-dimensional, one-dimensional, two-dimensional and three-dimensional nanostructured materials for advanced electrochemical energy devices. Prog Mater Sci 57:724–803
12. Pan H, Li J, Feng YP (2010) Carbon nanotubes for supercapacitor. Nanoscale Res Lett 5:654–668
13. Vangari M, Pryor T, Jiang L (2012) Supercapacitors: review of materials and fabrication methods. J Energy Eng 2:72–79
14. Zhang Y, Feng H, Wu X, Wang L, Zhang A, Xia T et al (2009) Progress of electrochemical capacitor electrode materials: a review. Int J Hydrogen Energy 34:4889–4899
15. Lang X, Hirata A, Fujita T, Chen M (2011) Nanoporous metal/oxide hybrid electrodes for electrochemical supercapacitors. Nat Nanotechnol 6:232–236
16. Lu P, Xue D, Yang H, Liu Y (2013) Supercapacitor and nanoscale research towards electrochemical energy storage. Int J Smart Nano Mater 4:2–26
17. Long JW, Bélanger D, Brousse T, Sugimoto W, Sassin MB, Crosnier O (2011) Asymmetric electrochemical capacitors—stretching the limits of aqueous electrolytes. MRS Bull 36:513–522
18. Zhong C, Deng Y, Hu W, Qiao J, Zhang L, Zhang J (2015) A review of electrolyte materials and compositions for electrochemical supercapacitors. Chem Soc Rev 44:7484–7539
19. Nyholm L, Nyström G, Mihranyan A, Strømme M (2011) Toward flexible polymer and paper-based energy storage devices. Adv Mater 23:3751–3769
20. Mastragostino M, Arbizzani C, Soavi F (2001) Polymer-based supercapacitors. J Power Sources 97:812–815
21. Rudge A, Raistrick I, Gottesfeld S, Ferraris JP (1994) A study of the electrochemical properties of conducting polymers for application in electrochemical capacitors. Electrochim Acta 39:273–287
22. Khosrozadeh A, Xing M, Wang Q (2014) A high-capacitance solid-state supercapacitor based on free-standing film of polyaniline and carbon particles. Appl Energy 153:87–93
23. Frackowiak E, Khomenko V, Jurewicz K, Lota K, Beguin F (2006) Supercapacitors based on conducting polymers/nanotubes composites. J Power Sources 153:413–418
24. Shen H, Liu E, Xiang X, Huang Z, Tian Y, Wu Y et al (2012) A novel activated carbon for supercapacitors. Mater Res Bull 47:662–666

25. Gamby J, Taberna P, Simon P, Fauvarque J, Chesneau M (2001) Studies and characterisations of various activated carbons used for carbon/carbon supercapacitors. J Power Sources 101:109–116
26. Saliger R, Fischer U, Herta C, Fricke J (1998) High surface area carbon aerogels for supercapacitors. J Non-Cryst Solids 225:81–85
27. Kalinathan K, DesRoches DP, Liu X, Pickup PG (2008) Anthraquinone modified carbon fabric supercapacitors with improved energy and power densities. J Power Sources 181:182–185
28. Baughman RH, Zakhidov AA, de Heer WA (2002) Carbon nanotubes—the route toward applications. Science 297:787–792
29. Futaba DN, Hata K, Yamada T, Hiraoka T, Hayamizu Y, Kakudate Y et al (2006) Shape-engineerable and highly densely packed single-walled carbon nanotubes and their application as super-capacitor electrodes. Nat Mater 5:987–994
30. Kaempgen M, Chan CK, Ma J, Cui Y, Gruner G (2009) Printable thin film supercapacitors using single-walled carbon nanotubes. Nano Lett 9:1872–1876
31. Sun Y-P, Fu K, Lin Y, Huang W (2002) Functionalized carbon nanotubes: properties and applications. Acc Chem Res 35:1096–1104
32. Liu C, Yu Z, Neff D, Zhamu A, Jang BZ (2010) Graphene-based supercapacitor with an ultrahigh energy density. Nano Lett 10:4863–4868
33. Wang Y, Shi Z, Huang Y, Ma Y, Wang C, Chen M et al (2009) Supercapacitor devices based on graphene materials. J Phys Chem C 113:13103–13107
34. Ghosh A, Lee YH (2012) Carbon-based electrochemical capacitors. ChemSusChem 5:480–499
35. Davies A, Yu A (2011) Material advancements in supercapacitors: from activated carbon to carbon nanotube and graphene. Can J Chem Eng 89:1342–1357
36. Zhang LL, Zhou R, Zhao X (2010) Graphene-based materials as supercapacitor electrodes. J Mater Chem 20:5983–5992
37. Martín A, Escarpa A (2014) Graphene: the cutting–edge interaction between chemistry and electrochemistry. TrAC Trends Anal Chem 56:13–26
38. Wang H, Dai H (2013) Strongly coupled inorganic–nano-carbon hybrid materials for energy storage. Chem Soc Rev 42:3088–3113
39. Fialkov A (2000) Carbon application in chemical power sources. Russ J Electrochem 36:345–366
40. Markoulidis F, Lei C, Lekakou C, Figgemeier E, Duff D, Khalil S et al (2012) High-performance supercapacitor cells with activated carbon/MWNT nanocomposite electrodes. In: IOP conference series: materials science and engineering, p 012021
41. Pandolfo A, Hollenkamp A (2006) Carbon properties and their role in supercapacitors. J Power Sources 157:11–27
42. Selvakumar M, Krishna Bhat D (2008) Activated carbon-polyethylenedioxythiophene composite electrodes for symmetrical supercapacitors. J Appl Polym Sci 107:2165–2170
43. Sonia T, Mini P, Nandhini R, Sujith K, Avinash B, Nair S et al (2013) Composite supercapacitor electrodes made of activated carbon/PEDOT: PSS and activated carbon/doped PEDOT. Bull Mater Sci 36:547–551
44. Castellano RJ, Akin C, Giraldo G, Kim S, Fornasiero F, Shan JW (2015) Electrokinetics of scalable, electric-field-assisted fabrication of vertically aligned carbon-nanotube/polymer composites. J Appl Phys 117:214306
45. Khomenko V, Frackowiak E, Beguin F (2005) Determination of the specific capacitance of conducting polymer/nanotubes composite electrodes using different cell configurations. Electrochim Acta 50:2499–2506
46. Lee H, Kim H, Cho MS, Choi J, Lee Y (2011) Fabrication of polypyrrole (PPy)/carbon nanotube (CNT) composite electrode on ceramic fabric for supercapacitor applications. Electrochim Acta 56:7460–7466
47. Lota K, Khomenko V, Frackowiak E (2004) Capacitance properties of poly (3, 4-ethylenedioxythiophene)/carbon nanotubes composites. J Phys Chem Solids 65:295–301

48. Lu X, Dou H, Yuan C, Yang S, Hao L, Zhang F et al (2012) Polypyrrole/carbon nanotube nanocomposite enhanced the electrochemical capacitance of flexible graphene film for supercapacitors. J Power Sources 197:319–324
49. Peng C, Zhang S, Jewell D, Chen GZ (2008) Carbon nanotube and conducting polymer composites for supercapacitors. Prog Nat Sci 18:777–788
50. Wu M, Snook GA, Gupta V, Shaffer M, Fray DJ, Chen GZ (2005) Electrochemical fabrication and capacitance of composite films of carbon nanotubes and polyaniline. J Mater Chem 15:2297–2303
51. Branzoi V, Branzoi F, Pilan L (2010) Electrochemical fabrication and capacitance of composite films of carbon nanotubes and polyaniline. Surf Interface Anal 42:1266–1270
52. Murugan AV (2006) Novel organic–inorganic poly (3,4-ethylenedioxythiophene) based nanohybrid materials for rechargeable lithium batteries and supercapacitors. J Power Sources 159:312–318
53. Hou Y, Cheng Y, Hobson T, Liu J (2010) Design and synthesis of hierarchical MnO_2 nanospheres/carbon nanotubes/conducting polymer ternary composite for high performance electrochemical electrodes. Nano Lett 10:2727–2733
54. Yang X-F, Wang G-C, Wang R-Y, Li X-W (2010) A novel layered manganese oxide/poly (aniline-co-o-anisidine) nanocomposite and its application for electrochemical supercapacitor. Electrochim Acta 55:5414–5419
55. Mahore RP, Burghate DK, Kondawar SB (2014) Development of nanocomposites based on polypyrrole and carbon nanotubes for supercapacitors. Adv Mater Lett 5:400–405
56. Chen F, Liu P, Zhao Q (2012) Well-defined graphene/polyaniline flake composites for high performance supercapacitors. Electrochim Acta 76:62–68
57. Fan W, Zhang C, Tjiu WW, Pramoda KP, He C, Liu T (2013) Graphene-wrapped polyaniline hollow spheres as novel hybrid electrode materials for supercapacitor applications. ACS Appl Mater Interfaces 5:3382–3391
58. Gómez H, Ram MK, Alvi F, Villalba P, Stefanakos EL, Kumar A (2011) Graphene-conducting polymer nanocomposite as novel electrode for supercapacitors. J Power Sources 196:4102–4108
59. Ma B, Zhou X, Bao H, Li X, Wang G (2012) Hierarchical composites of sulfonated graphene-supported vertically aligned polyaniline nanorods for high-performance supercapacitors. J Power Sources 215:36–42
60. Wu Q, Xu Y, Yao Z, Liu A, Shi G (2010) Supercapacitors based on flexible graphene/polyaniline nanofiber composite films. ACS Nano 4:1963–1970
61. Zhang K, Zhang LL, Zhao X, Wu J (2010) Graphene/polyaniline nanofiber composites as supercapacitor electrodes. Chem Mater 22:1392–1401
62. Wang H, Hao Q, Yang X, Lu L, Wang X (2009) Graphene oxide doped polyaniline for supercapacitors. Electrochem Commun 11:1158–1161
63. Basnayaka PA, Ram MK, Stefanakos EK, Kumar A (2013) Supercapacitors based on graphene–polyaniline derivative nanocomposite electrode materials. Electrochim Acta 92:376–382
64. Basnayaka PA, Ram MK, Stefanakos L, Kumar A (2013) Graphene/polypyrrole nanocomposite as electrochemical supercapacitor electrode: electrochemical impedance studies graphene. 2:81–87
65. Bora C, Sharma J, Dolui S (2014) Polypyrrole/sulfonated graphene composite as electrode material for supercapacitor. J Phys Chem C 118:29688–29694
66. Bose S, Kim NH, Kuila T, Lau K-T, Lee JH (2011) Electrochemical performance of a graphene–polypyrrole nanocomposite as a supercapacitor electrode. Nanotechnology 22:295202
67. Chen Z, Yu D, Xiong W, Liu P, Liu Y, Dai L (2014) Graphene-based nanowire supercapacitors. Langmuir 30:3567–3571
68. Alvi F, Basnayaka PA, Ram MK, Gomez H, Stefanako E, Goswami Y et al (2011) Graphene-polythiophene nanocomposite as novel supercapacitor electrode material. J New Mater Electrochem Syst 15:89–95

69. Alvi F, Ram MK, Basnayaka P, Stefanakos E, Goswami Y, Hoff A et al (2011) Electrochemical supercapacitors based on graphene-conducting polythiophenes nanocomposite. ECS Trans 35:167–174
70. Alvi F, Ram MK, Basnayaka PA, Stefanakos E, Goswami Y, Kumar A (2011) Graphene–polyethylenedioxythiophene conducting polymer nanocomposite based supercapacitor. Electrochim Acta 56:9406–9412
71. Cho S, Kim M, Jang J (2015) Screen-printable and flexible RuO_2 nanoparticle-decorated PEDOT: PSS/graphene nanocomposite with enhanced electrical and electrochemical performances for high-capacity supercapacitor. ACS Appl Mater Interfaces 7:10213-10227
72. Yang W, Zhao Y, He X, Chen Y, Xu J, Li S et al (2015) Flexible conducting polymer/reduced graphene oxide films: synthesis, characterization, and electrochemical performance. Nanoscale Res Lett 10:1–7
73. Shim J-J (2015) Ultrasmall SnO_2 nanoparticle-intercalated graphene@ polyaniline composites as an active electrode material for supercapacitors in different electrolytes. Synth Met 207:110–115
74. Liew SY, Thielemans W, Walsh DA (2014) Polyaniline-and poly (ethylenedioxythiophene)-cellulose nanocomposite electrodes for supercapacitors. J Solid State Electrochem 18:3307–3315
75. Raj CJ, Kim BC, Cho W-J, Lee W, Jung S-D, Kim YH et al (2015) Highly flexible and planar supercapacitors using graphite flakes/polypyrrole in polymer lapping film. ACS Appl Mater Interfaces 7:13405-13414
76. Davies A, Audette P, Farrow B, Hassan F, Chen Z, Choi J-Y et al (2011) Graphene-based flexible supercapacitors: pulse-electropolymerization of polypyrrole on free-standing graphene films. J Phys Chem C 115:17612–17620
77. Jiang L-L, Lu X, Xie C-M, Wan G-J, Zhang H-P, Youhong T (2015) Flexible, free-standing TiO_2–graphene–polypyrrole composite films as electrodes for supercapacitors. J Phys Chem C 119:3903–3910
78. Meng C, Liu C, Chen L, Hu C, Fan S (2010) Highly flexible and all-solid-state paperlike polymer supercapacitors. Nano Lett 10:4025–4031
79. Shao Y, El-Kady MF, Wang LJ, Zhang Q, Li Y, Wang H et al (2015) Graphene-based materials for flexible supercapacitors. Chem Soc Rev 44:3639–3665
80. Wang K, Zhao P, Zhou X, Wu H, Wei Z (2011) Flexible supercapacitors based on cloth-supported electrodes of conducting polymer nanowire array/SWCNT composites. J Mater Chem 21:16373–16378
81. Yuan L, Lu X-H, Xiao X, Zhai T, Dai J, Zhang F et al (2011) Flexible solid-state supercapacitors based on carbon nanoparticles/MnO_2 nanorods hybrid structure. ACS Nano 6:656–661
82. Yuan L, Yao B, Hu B, Huo K, Chen W, Zhou J (2013) Polypyrrole-coated paper for flexible solid-state energy storage. Energy Environ Sci 6:470–476
83. Gómez-Romero P, Chojak M, Cuentas-Gallegos K, Asensio JA, Kulesza PJ, Casañ-Pastor N et al (2003) Hybrid organic–inorganic nanocomposite materials for application in solid state electrochemical supercapacitors. Electrochem Commun 5:149–153
84. Chee WK, Lim HN, Huang NM (2015) Electrochemical properties of free-standing polypyrrole/graphene oxide/zinc oxide flexible supercapacitor. Int J Energy Res 39:111–119
85. Aphale A, Maisuria K, Mahapatra MK, Santiago A, Singh P, Patra P (2015) Hybrid electrodes by in-situ integration of graphene and carbon-nanotubes in polypyrrole for supercapacitors. Sci Rep 5:14445
86. Meng Q, Wang K, Guo W, Fang J, Wei Z, She X (2014) Thread-like supercapacitors based on one-step spun nanocomposite yarns. Small 10:3187–3193
87. de Souza VHR, Oliveira MM, Zarbin AJG (2014) Thin and flexible all-solid supercapacitor prepared from novel single wall carbon nanotubes/polyaniline thin films obtained in liquid–liquid interfaces. J Power Sources 260:34–42

88. Reddy BN, Deepa M, Joshi AG (2014) Highly conductive poly (3, 4-ethylenedioxypyrrole) and poly (3, 4-ethylenedioxythiophene) enwrapped Sb 2 S 3 nanorods for flexible supercapacitors. Phys Chem Chem Phys 16:2062–2071
89. Barsoukov E, Macdonald JR (2005) Impedance spectroscopy: theory, experiment, and applications. Wiley, Hoboken
90. Basnayakaa PA, Ramb MK, Stefanakosb EK, Kumara A (2015) Nanostructured hybrid graphene-conducting polymers for electrochemical supercapacitor electrodes. Handbook of Nanoelectrochemistry. 1–19
91. Buller S, Thele M, De Doncker R, Karden E (2005) Impedance-based simulation models of supercapacitors and Li-ion batteries for power electronic applications. IEEE Trans Ind Appl 41:742–747
92. Wang J, Xu Y, Chen X, Sun X (2007) Capacitance properties of single wall carbon nanotube/polypyrrole composite films. Compos Sci Technol 67:2981–2985
93. De Levie R (1963) On porous electrodes in electrolyte solutions: I. Capacitance effects. Electrochim Acta 8:751–780
94. Fletcher S, Black VJ, Kirkpatrick I (2014) A universal equivalent circuit for carbon-based supercapacitors. J Solid State Electrochem 18:1377–1387
95. Xu J, Wang K, Zu S-Z, Han B-H, Wei Z (2010) Hierarchical nanocomposites of polyaniline nanowire arrays on graphene oxide sheets with synergistic effect for energy storage. ACS Nano 4:5019–5026
96. Yan X, Chen J, Yang J, Xue Q, Miele P (2010) Fabrication of free-standing, electrochemically active, and biocompatible graphene oxide–polyaniline and graphene–polyaniline hybrid papers. ACS Appl Mater Interfaces 2:2521–2529
97. Kumar NA, Choi H-J, Shin YR, Chang DW, Dai L, Baek J-B (2012) Polyaniline-grafted reduced graphene oxide for efficient electrochemical supercapacitors. ACS Nano 6:1715–1723
98. Ma G, Peng H, Mu J, Huang H, Zhou X, Lei Z (2013) In situ intercalative polymerization of pyrrole in graphene analogue of MoS_2 as advanced electrode material in supercapacitor. J Power Sources 229:72–78
99. Huang K-J, Wang L, Liu Y-J, Wang H-B, Liu Y-M, Wang L-L (2013) Synthesis of polyaniline/2-dimensional graphene analog MoS_2 composites for high-performance supercapacitor. Electrochim Acta 109:587–594
100. Murugan AV, Quintin M, Delville M-H, Campet G, Viswanath AK, Gopinath CS et al (2006) Synthesis and characterization of organic–inorganic poly (3, 4-ethylenedioxythiophene)/MoS 2 nanocomposite via in situ oxidative polymerization. J Mater Res 21:112–118
101. Wang J, Wu Z, Yin H, Li W, Jiang Y (2014) Poly (3, 4-ethylenedioxythiophene)/MoS_2 nanocomposites with enhanced electrochemical capacitance performance. RSC Adv 4:56926–56932
102. Wang H, Zhu E, Yang J, Zhou P, Sun D, Tang W (2012) Bacterial cellulose nanofiber-supported polyaniline nanocomposites with flake-shaped morphology as supercapacitor electrodes. J Phys Chem C 116:13013–13019
103. Wang YG, Li HQ, Xia YY (2006) Ordered whiskerlike polyaniline grown on the surface of mesoporous carbon and its electrochemical capacitance performance. Adv Mater 18:2619–2623
104. Zhang LL, Zhao S, Tian XN, Zhao X (2010) Layered graphene oxide nanostructures with sandwiched conducting polymers as supercapacitor electrodes. Langmuir 26:17624–17628
105. Shao M, Li Z, Zhang R, Ning F, Wei M, Evans DG et al (2015) Hierarchical conducting polymer@ clay core–shell arrays for flexible all solid state supercapacitor devices. Small 11:3530–3538

Conducting Polymer Hydrogels and Their Applications

Kashma Sharma, Vijay Kumar, B.S. Kaith, Susheel Kalia and Hendrik C. Swart

Abstract The industrial demand for novel and smart materials as well as the urge for basic understanding has led to a notable improvement in the area of polymer science. Recently, significant consideration has been given to the modifications of biodegradable hydrogels based on natural polymers with conducting polymers (CPs), because this extends a straightforward process to couple the better features of CPs with the highly cross-linked hydrogels. The final hydrogels have been developed to change mainly electrical and structural properties to a larger degree. Herein, we present a comprehensive survey of the existing and current literature on conducting hydrogels based on natural polymers. This chapter also highlights ample of methods used to synthesize conducting hydrogel, properties, and characterization techniques. Conducting hydrogels have been used in the removal of dyes from wastewater, drug delivery, fuel cells, supercapacitors, dye-sensitized solar cells, rechargeable lithium batteries, etc. All these justify the rising interest in both academia and industrial development. In this analysis, an overview of potential applications of these conducting hydrogels and current challenges in the field are discussed; some new and futuristic advances in this captivating area are also provided.

Keywords Hydrogels · Natural polymers · Conducting polymers · Drug delivery · Dye removal

K. Sharma (✉) · V. Kumar · H.C. Swart
Department of Physics, University of the Free State, P.O. Box 339, Bloemfontein 9300, South Africa
e-mail: shama2788@gmail.com

V. Kumar
Department of Applied Physics, Chandigarh University, Gharuan, Mohali, Punjab 140413, India

B.S. Kaith
Department of Chemistry, Dr. B.R. Ambedkar National Institute of Technology, Jalandhar, Punjab 144011, India

S. Kalia
Department of Chemistry, Army Cadet College Wing, Indian Military Academy, Dehradun 248007, India

V. Kumar et al. (eds.), *Conducting Polymer Hybrids*,
Springer Series on Polymer and Composite Materials,
DOI 10.1007/978-3-319-46458-9_7

Abbreviations

CP	Conducting Polymers
APS	Ammonium persulfate
P-HEMA	Poly(2-hydroxythyl methacrylate)
IPN	Interpenetrating Polymer Network
PSN	Poly(sulfur nitride)
PA	Poly (acetylene)
LB	Langmuir–Blodgett
SA	Self-assembly
PPy	Polypyrrole
SAPHs	Superabsorbent hydrogels
PANI	Polyaniline
PAMPS	Poly(2-acrylamide-2-methyl propane sulphonic acid)
PVP	Poly(*N*-vinyl pyrrolidone)
PVA	Poly(vinyl alcohol)
FTIR	Fourier transform Infrared Spectroscopy
ToF-SIMS	Time-of-Flight Secondary Ion Mass Spectra
ESDRDs	Electro-stimulated drug release devices
CMC	Carboxymethylcellulose
MG	Malachite green
MO	Methyl orange
MB	Methylene blue
FS	Fluorescent sodium
Rh	Rhodamine (Rh)
CNT	Carbon nanotube

1 Introduction

In recent years, noteworthy consideration has been given on the alterations of cross-linked hydrogels with conducting polymers (CPs) as this provides an easy way to couple the better characteristics of CPs with the highly modified gel networks. The final hydrogels have been demonstrated to change primarily electrical and structural properties to a larger degree [1–4]. They also have excellent processability, chemical stability toward dopants and solubility under readily open environments [5]. An extra consideration has been centered on the superabsorbent polymers for producing novel applications in wide range of areas [6–12]. The characteristics of these conducting hydrogels are directly proportional to the content and structure of the CP within the hydrogel. Though, the research on conducting hydrogel based on the cross-linked hydrogels and CPs is still few to see. On the different side, it is now important for researchers working in this sector to generate practical strategies to achieving intended structures of conducting hydrogels and to

further optimize the characteristics and roles for electronic applications. The interpenetrating hydrogels of CPs draw enough recognition from the history as various researchers listed materials that demonstrate both mechanical and swelling behavior of gels by the summation of the particular transport properties of CPs [13, 14]. The new conducting hydrogel materials have been synthesized by cross-linking the CP by chemical reaction or via crystallization and aggregation [15, 16]. This point to the formation of three-dimensional network structures which can contain an enormous quantity of water [17]. Nowadays, a straightforward and flexible approach has been developed for the production of conducting polymer hydrogels. This includes supramolecular self-assembly among polymer chains and multivalent cations [18]. The multivalent cations play an important twofold role to speed up the polymerization as the oxidant and also support in starting the gelation by performing the function of an ionic cross-linker. The researcher prepares a triple network system, double network composite hydrogels, and self-strengthened hydrogel by the addition of prepared hydrogels into the multiple networks showing both exceptional mechanical toughness and striking electrical behavior [19]. However, the CPs-based hydrogels are still inadequate which can be employed in a broad range of applications such as electro sensor, a capacitor to electromechanical actuator, and tissue engineering [20–22]. Till date, numerous researchers synthesized an electrical conducting gum-based polymer through the graft copolymerization reaction of various gums with aniline using ammonium persulfate as the initiator [23, 24]. Moreover, many natural polysaccharides such as starch, cellulose, chitosan, alginate, and their derivatives have been adopted to prepare conducting hydrogels in different conditions. This chapter gives a survey of the current state of conducting hydrogels based on natural polymers and conducting polymers. The purpose of the introductory section is to provide enough information to understand the origin of cross-linked hydrogels-based research and how to characterize these materials for various applications. The second part of the chapter will describe the discovery and properties of conducting polymers. The goal of this part is not to cover all the existing literature, but rather to present some of the most relevant achievements in this direction. In the third section, we will include some potential applications of conducting hydrogels. Finally, we end the chapter with conclusion and prospects for future development of cross-linked hydrogels with different materials. With this, we hope that the reader will get thte updated information on the conducting hydrogels that have arrived for plenty of applications and also new insights on this topic.

1.1 Hydrogels

Hydrogels are three-dimensional, hydrophilic, polymeric chains that can absorb, swell, and retain large quantities of water or aqueous fluids [25]. The overall properties of the hydrogels are reliant on numerous parameters such as the hydrophilicity of the polymer chains and the extent of cross-linking [26, 27]. The

water-absorbing behavior of the hydrogels occurs primarily due to the existence of hydrophilic groups, viz., –OH, –COOH, –CONH–, $–CONH_2$, and $–SO_3H$ groups, in the polymer chains. Hydrogels have obtained substantial interest in the past 30 years, owing to their unique properties to be utilized in biomaterial applications. The elevated-water-content within the hydrogel loads up the spongy surface of the polymer chains and permits selective diffusion of solutes through the polymeric hydrogel matrix. These properties make them be employed in a membrane separation process [28]. Hydrogels can be synthesized from a large number of materials (both natural and synthetic) and may present a broad spectrum of properties that are essential to drug delivery and medical devices. Hydrogels have been found in nature from the time when the evolution of life started. A range of naturally occurring polymers such as collagen, alginate, agarose, and gelatin was also discovered in near the beginning human history. Though, the current history of hydrogels as a group of materials developed for biomedical applications dates back to the late 1950s. DuPont scientists in 1936 synthesized first synthetic hydrogels named poly(2-hydroxythyl methacrylate) commonly known as P-HEMA [29]. In the year 1960, Wichterle and Lim recognized the significance of P-HEMA hydrogels as excellent materials for contact lens applications [30]. This invention directed to the contact lens industry and the new area of biomedical hydrogels. Some hydrogel transitions (volume changes) occur in response to changes in environmental conditions such as temperature, pH, solvent, composition, and electrical stimuli. These materials are also named "Smart hydrogels" [31]. Past research shows that hydrogels can be employed in some areas such as agriculture, pharmaceutics, and biotechnology [32–38]. In recent times, hydrogels have turn out to be quite exciting candidates to be used in the field of controlled drug delivery, tissue engineering as matrices for repairing and regenerating a large number of tissues and organs.

1.2 Classifications of Hydrogels

Depending upon their source, methods of preparation, ionic charge, or physical structure features, the hydrogel may be classified in several categories [25].

1.2.1 Classification Based on Source

A categorization of hydrogels based on their origin is displayed in Fig. 1 [39].

1.2.2 Classification According to Polymeric Composition

The method of preparation leads to formations of some important classes of hydrogels which may be the following:

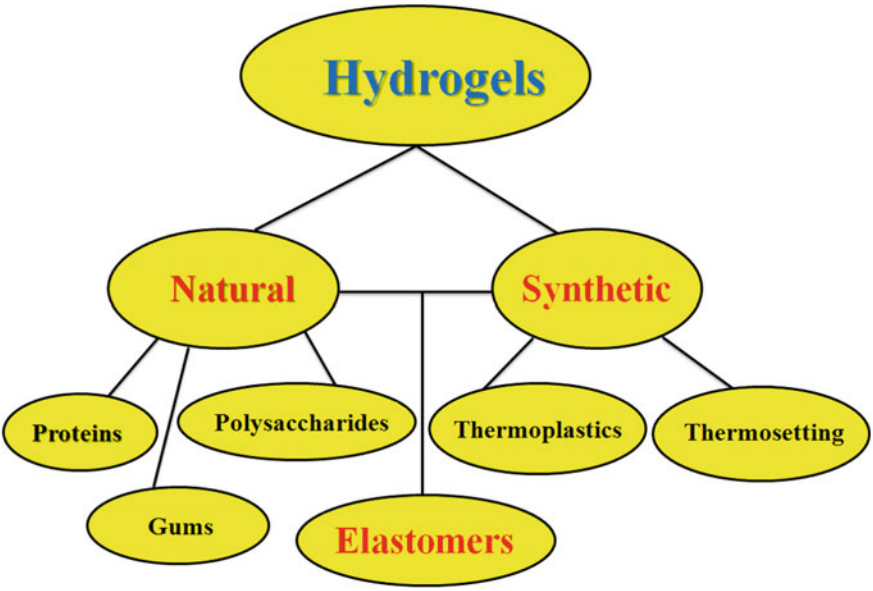

Fig. 1 Classification of hydrogels based on their origin

Homopolymeric Hydrogels: These referred to polymer networks derived from one type of hydrophilic monomer unit [39, 40]. Homopolymers may have a cross-linked skeletal structure based on the nature of the monomer and polymerization technique.
Copolymeric Hydrogels: These are composed of two or more different monomer species, at least one of which must be hydrophilic to render them swellable [39].
Multipolymer Hydrogels: These are produced from three or more commoners reacting together.
Interpenetrating Polymeric (IPN) Hydrogel: IPNs were initially reported in 1914 when Aylsworth developed the first synthetic IPN for the manufacturing of phonograph records [41] after that worker started to gain attention in these complex structures. The term "Interpenetrating Polymer Network" was founded by Millar in the year 1960 [42]. After that numbers of investigations have been directed to the synthesis and characterization of these networks for different applications using both synthetic and natural polymers [39, 43].

If only one element is cross-linked, the resulting system is defined as semi-IPN of which the IUPAC definition is the following: "a polymer consisting of one or more networks and one or more linear or branched polymers differentiated by the diffusion on a molecular scale" [39, 44]. Semi-IPNs are different from IPNs since the constituent linear or branched polymers can, in principle, be separated from the component polymer networks without breaking chemical bonds; they are polymer blends.

1.2.3 Classification Based on Structural Feature

The ranking of hydrogels depends on their physical structure, and their chemical composition can be classified as follows [25]:

(a) Amorphous (noncrystalline).
(b) Semi-crystalline: A complex mixture of amorphous and crystalline phases.
(c) Crystalline.

1.2.4 Classification Based on Physical Appearance

In general, hydrogels have appeared as a matrix, film, or microsphere which in terms depends on the synthesis technique used [25].

1.2.5 Classification Based on Ionic Charges

Hydrogels may be categorized into nonionic (neutral), ionic, an amphoteric electrolyte containing both acidic and basic groups and Zwitterionic containing both anionic and cationic groups in each structural repeating unit.

1.2.6 Classification Based on Type of Cross-Linking

Depending on the synthesis methods, the cross-linked hydrogels can be synthesized chemically or physically (Fig. 2) [39, 45]. Physical gels are cross-links by molecular entangled chains or secondary forces such as hydrogen bonding [39, 46, 47], hydrophobic interactions [45], and crystallite formation [48].

1.3 Synthesis of Graft Copolymers

Graft copolymerization is the used method for the modification of surfaces of polymeric materials, and it is a valuable tool to modify the physical and chemical properties of polymers [39, 49]. The active sites are generated on the polymeric backbone for the preparation of cross-linked hydrogels, either a free radical or a chemical group that can get entangled in an ionic polymerization or a condensation process [39, 50]. Typically, low molecular weight graft copolymers are obtained in ionic grafting, while in the case of free radical copolymerization high molecular weight copolymers could be synthesized [39, 50]. Till date, numbers of method have been employed for the creation of radical sites on the polymeric backbone and are broadly categorized as as follows:

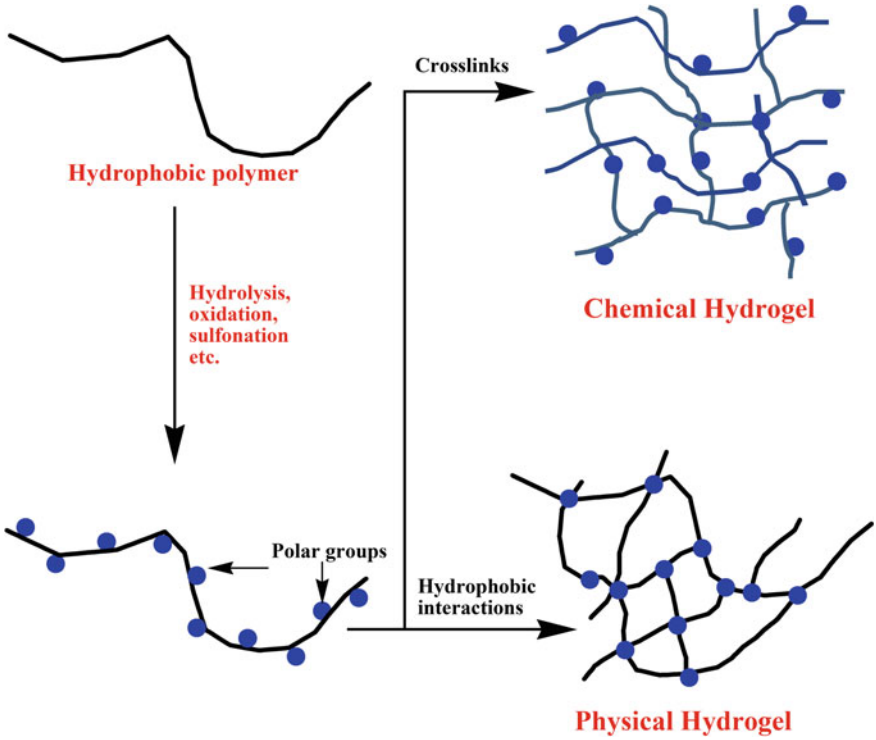

Fig. 2 Schematic of formation of hydrogels by chemical and physical method

- Physical methods
- Chemical methods
- Photochemical grafting
- Plasma radiation-induced grafting
- Enzymatic grafting.

1.4 Characteristics of Hydrogels

Hydrogels can be categorized into a large number of groups based on their stimuli-sensitivity. Stimuli-responsive hydrogels can adjust their volumes with outside environmental conditions such as temperature [51, 52], pH [53], solvent composition [54], salt concentration [55], photo irradiation [56], and electric field [57] (Fig. 3). These distinctive features are of keen concern in drug delivery, actuator, cell encapsulation, and tissue engineering [58]. The pH-sensitive hydrogels for these applications are typically loaded with enzymes that alter the pH of the neighborhood environment within the hydrogels (Fig. 3).

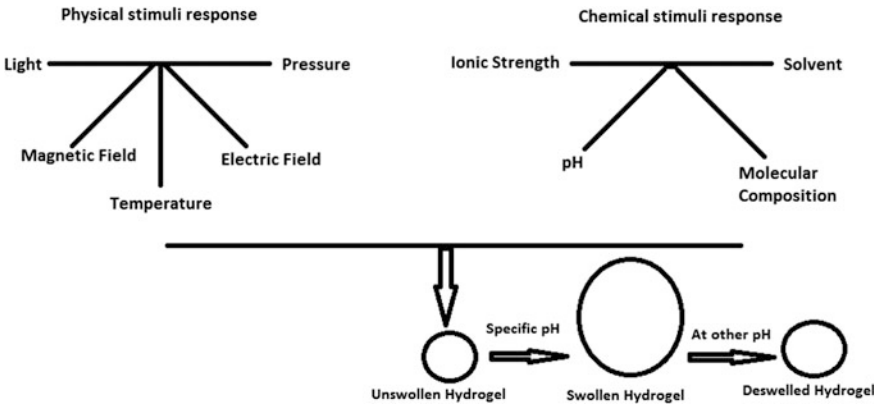

Fig. 3 Stimuli-responsive swelling hydrogels

2 Conducting Polymers

Conducting polymer (CPs) is sort of a polymer with spatially extended π–bonding system, which forms the delocalized charge carrier. The expansion of CPs did not gain ample scientific responsiveness until the mid-1970s, albeit they have been known for many years. The electrical conductivity of CP chains is higher than that of other polymeric materials although they are not metallic. On the other hand, the probability of fabricating polymers with conductivities near to metals was not recognized at that time. In 1973, Waltaka and co-workers observed that the inorganic polymer poly (sulfur nitride) is highly conducting [59]. Two years later, Greene et al. [60] found superconductivity nature of poly(sulfur nitride) (PSN) at a low temperature. These findings were of particular relevance as they evoked the prospect of producing highly CPs and aroused the great research spotlight and required venture for the exploration of other polymeric conductors. Later, it was noted that the room temperature conductivity of SNx could be improved by an order when reacting with bromine or other similar oxidizing agents [61], reveals that it was feasible to intensify the number of free radicals in the CP via doping. The polymer that brought the maximum recognition in the early evolution of CPs is poly (acetylene) (PA), which is a conjugated polymer with the alternating single- and double bond. It was initially prepared in the late 1950s, but for more than two decades scientists were engaged only in spectroscopic and theoretical investigations of PA as the final member of the polyene family. In 1977, MacDiarmid, Heeger, Shirakawa, and their groups revolutionized the development of electrically CPs by synthesizing PA as the simplest conjugated CPs [62, 63]. They found that when the insulating PA films are treated to iodine vapors at room temperature, a notable enhancement in the conductivity happened [63–65]. With the invention of CPs, a period of profound theoretical and experimental research started, and the struggles

of MacDiarmid, Heeger, and Shirakawa were acknowledged with the award of Nobel Prize in Chemistry in the year 2000 [65–67].

Active protonic acids, such as perchloric, sulfuric, or trifluoromethane sulfonic acids, function as "proton dopants," generating conductivities in the range of 103 Ω^{-1} cm^{-1}. In the case of these chemically doped polymers, the mobile charge carriers responsible for conductivity are produced by the oxidation–reduction mechanism. By removal of electrons or addition of electrons, the polymeric chain with appropriate chemical agents (dopants), charge defects are created along the polymer backbone which may then be available as free carriers. Hence, the reaction among the dopant and the polymeric chain is essentially the production of free electrons along the molecule. Once plenty of these conductive sites are created, percolation is reached, and high conductive materials are formed. However, many organic systems are known to carry free radicals or charged species and yet remain insulators. In order to become conductive, the polymeric system (or any system) must possess in addition to charge carriers, an overlapping set of orbital's, such as conjugated double bonds, which allows them to move along the polymer chain [68]. CPs has the electronic and optical properties that lie in between the semiconductors and the metals, also to the captivating mechanical properties owing to processing advantages of polymers.

CPs are well suited for many applications, including semiconductor devices, batteries, electronic and optoelectronics devices, electrochromic devices, optical switching devices, sensors, and so on [69–72]. Chemical and electrochemical methods are used to synthesize CP films. These preparations include spin-coating, dip coating, drop coating, thermal evaporation, Langmuir–Blodgett (LB), and self-assembly techniques (SA) belonging to chemical approach [73, 74]. While electrochemical method includes galvanostatic/potentiostat techniques such as cyclic voltammetry, chronopotentiometry, chronoamperometry, etc. [39].

3 Conducting Hydrogels

Conducting hydrogel is the name employed to define a hybrid network made from cross-linked hydrogels coupled with CPs. They have characteristics similar to conventional hydrogel but with the extra benefit of electrical conductivity. Gilmore et al. [75] synthesized first conducting hydrogel based on polypyrrole (PPy) which is directly electropolymerized on a preformed polyacrylamide hydrogel. Notwithstanding the incorporation of the hydrophobic PPy, the resultant hydrogel preserved its hydration/rehydration properties. This work has initiated a novel area in CP science. Due to the availability of a vast number of hydrogels and a series of CPs, there has been an increment in the number of articles detailing the synthesis of conducting hydrogels and their application in the biomedical field. Electrically conductive hydrogels are prepared by employing many methods such as adding conductive metallic nanoparticles to the hydrogels [76, 77], use of electrically conductive polymer nanoparticles [7], and by preparation of composite hydrogels

through the incorporation of electrically conductive polymers into the network structure of the hydrogel [78]. The final material is hydrogel network in which the CP chains are physically or chemically entangled inside the typical hydrogel matrix.

3.1 Conducting Hydrogel Based upon Conducting Polymer

Modification of superabsorbent hydrogels (SAPHs) with CPs may point to the development of multifunctional electrical conducting materials due to their compatibility with the environment and biological systems. It has been found in the literature that the addition of CPs into a flexible matrix of hydrogels appeared in good processability as well as the electrical conductivity, chemical stability toward dopants and thermal stability [5, 39, 79]. Currently, various natural polysaccharides such as starch, cellulose, chitosan, alginate, and their derivatives have been adopted to prepare conducting hydrogels in different conditions. The most studied synthetic method of forming a CP-hydrogel is polymerization of CPs by already made hydrogel matrices [80]. The synthesized hydrogel product is drained on a surface of the substrate and then again on swelled solution containing CP monomer. The various synthesis processes for the preparation of conducting hydrogels has been reported by Rylie and co-workers [80]. The synthesis of CP-hydrogel hybrid has been suggested as a way to overwhelm few of the deficiencies that CPs holds [81, 82]. Semi-interpenetrating hydrogel networks based on PANI and various biopolymers such as chitosan, gum arabic, cellulose acetate, etc., were also prepared by a large number of research groups [83–85]. Many methods have been used for the synthesis of conducting hydrogels that combine both CPs and hydrogel matrices. These hybrid materials have been synthesized by uniting two different phases generated by each group. The most-used methods are template CP-hydrogels, CPs deposited in a hydrogel matrix, and CP-hydrogels made from mixed precursor-either simultaneously or in a two-step process. Hydrogels networks based on acrylamide and acrylic acid doped with a polypyrrole/carbon black composite was synthesized, and their utilization as an artificial muscle was reported [86].

The synthesis of polyaniline–polyacrylamide composites was carried out using electropolymerization of the CP inside an insulating hydrogel matrix of various pore sizes [87]. The synthesis of a hydrogel composite in which polyaniline was impregnated within a cross-linked polyelectrolyte hydrogel, poly(2-acrylamide-2-methyl propane sulphonic acid) (PAMPS) was conducted [88]. Nikpour et al. [89] developed CP composites of PPy with poly (methyl methacrylate), confirming the synthesized hydrogels as a suitable candidate for controlled drug delivery devices. Park and Park [90] studied the electrical properties of the conducting composite poly (MMA-co-pyrrolmethylstyrene)-g-polypyrrole. The PMMAPMS-g-PPy was synthesized by the electrochemical reaction of PMMAPMS and pyrrole in an electrolyte solution comprising lithium perchlorate and a solution of acetonitrile and dichloromethane.

3.2 Conducting Hydrogel Based upon Metal/Nanoparticles

The polymer-metal nanocomposites material gives synergistic properties arising from both metal nanoparticles as well as from hydrogel matrix [91]. The stimuli-responsive hydrogel metal nanocomposite has been used in some applications such as artificial muscles, switches, memory devices; catalyst stands photographic materials [92, 93]. The graphene-based hydrogel materials were also manufactured by workers due to its excellent mechanical strength, electrical conductivity, thermal stability, and adsorption capability that can be utilized in various fields such as environmental protection, biomedicine, and energy sources [94]. Development of Gum ghatti and Fe_3O_4 magnetic nanoparticles-based nanocomposites for the efficient adsorption of rhodamine and methylene blue has been reported [95, 96]. Similarly, Dispenza et al. [97] synthesized the novel electrically conductive composite material, consisting of polyaniline nanoparticles dispersed in a polyvinyl pyrrolidone hydrogel, was prepared 'in situ' by water dispersion polymerization of aniline using PVP as a steric stabilizer through gamma radiation-induced cross-linking methods. The electrically conducting composite hydrogel materials composed of the polyaniline nanoparticles embedded in poly (vinyl alcohol) matrix was prepared by in situ polymerization of aniline monomer [98].

3.3 Method of Synthesis of Conducting Hydrogels

A plethora of routes has been employed for the preparation of conducting hydrogels. Some of the methods are explained as follows:

3.3.1 Chemically Cross-Linked Conductive Hydrogels

Lira and Torresi [87] synthesized the PANI/PAAM electrically conductive hydrogel by an electrochemical polymerization process that triggered by an electric pulse that will result in a drug release response and act as a controlled drug delivery device. Similarly, various authors prepared super absorbing poly(acrylate-aniline) and poly (acrylamide-aniline) conducting hydrogels by in situ polymerization procedure [1, 4]. The graft copolymerization of CP over the semi-interpenetrating network by the chemical cross-linking method under different reactions such as air, gamma radiation, vacuum, and microwave radiation conditions also give conducting hydrogels by further grafting with aniline monomer. These IPNs hydrogels are further doped with an acidic dopant to make them ohmic in nature [99–106]. The synthesis of semi-IPN, IPN, and conducting IPN based on Gum ghatti, acrylic acid, and aniline is shown in Fig. 4.

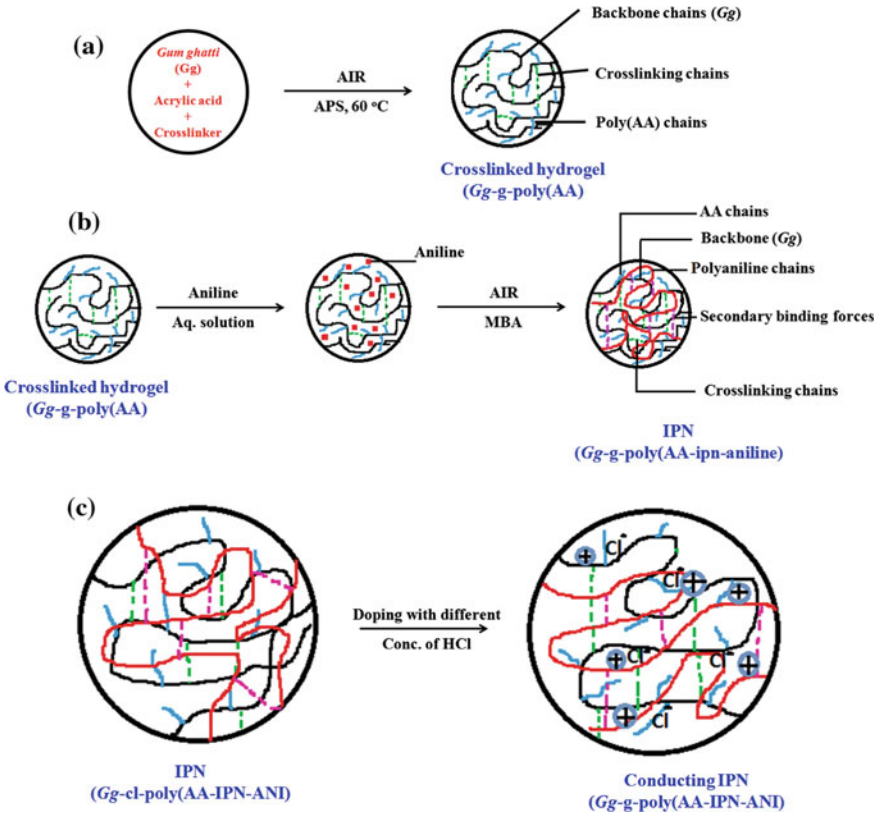

Fig. 4 Schematic representation of the synthesis of **a** semi-IPN, **b** IPN, and **c** conducting IPN. Reproduced from Ref. [105] with permission from the Royal Society of Chemistry

The CPs have an unstable backbone that results in the generation of alternate single and double bonds during polymerization of the monomer units. This delocalized pi-bond over the conjugated backbone, render an electrical pathway for free charge carriers which are offered conductivity in the whole polymer. Chemically synthesized CPs most commonly used as emeraldine salt of PANI, can be favorably made in a biocompatible form [107]. In recent times, most of the CPs are comprised of heterocyclic aromatics, such as derivatives of thiophene and pyrrole [108]. The electrochemical route is also commonly employed for synthesis. A typical electrochemical system includes aqueous electrolyte solution of monomer units and dopant ions in a three-electrode cell, containing a working, counter and reference electrode. During applying an electric potential, conducting polymer monomers start oxidizing to cation radical resulting in positively charged CP films with anionic doping on the working electrode. Additionally, many researchers incorporate biological entities such as silk-like protein fragments, hyaluronic acid, various laminin peptides, enzymes, polymeric amino acids, growth factors, and whole

cells in addition to conducting polymer [109–112]. Pan et al. [113] also synthesized nanostructured polymer hydrogel by an electrochemical route which gives good electronic activities which make it a useful material for bioelectronics and future-generation energy storage electrodes.

3.3.2 Radiation Cross-Linked Conductive Hydrogels

Radiation-based cross-linked hydrogel involve cross-linking by ionizing high energy radiation, like gamma rays and electron beams, has been employed as an initiator to synthesize the hydrogels of unsaturated compounds [114]. The irradiation of aqueous polymer solution leads to the generation of free charge carriers on the polymer chains. Moreover, radiolysis of water molecules ends in the formation of hydroxyl ions, which also strike the polymer chains, thereby leads to the production of macroradicals. Gum-ghatti-based conducting hydrogels of different monomers are synthesized under the influence of microwave radiation and used in moisture retention and biodegradation studies [115, 116]. Similarly, Gum-ghatti-based conducting hydrogel is also synthesized under the effect of gamma emissions. Gamma radiation is used to generate the free radicals on the backbone as well as on monomer without adding addition initiator [115–117]. Figure 5 displays the schematic representation of the formation of Gg-cl-poly(AAm-ipn-aniline) conducting IPN hydrogels.

Dispenza et al. [118] synthesized PANI-ES nanoparticles through a chemical oxidative dispersion polymerization process in the vicinity of either poly(N-vinyl pyrrolidone) (PVP) or poly(vinyl alcohol) (PVA) as steric stabilizers. This was the first of two active steps, the second being gamma irradiation of the stabilized PANI

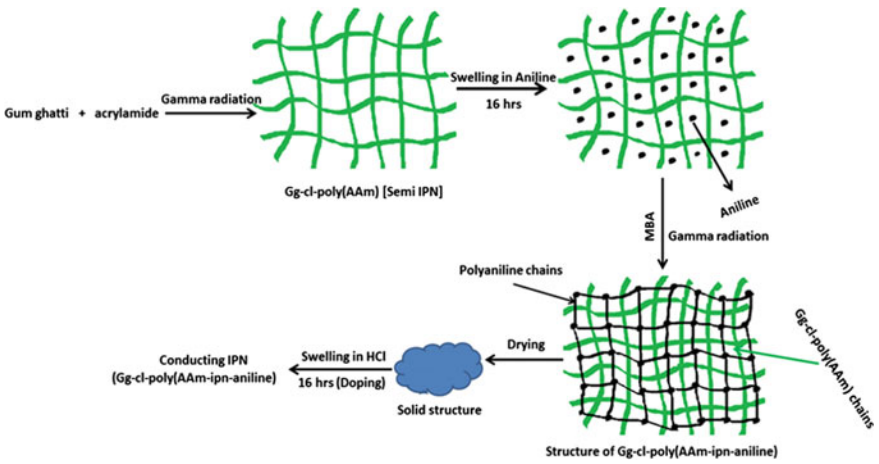

Fig. 5 Mechanism of radiation-induced polymerization process. Reproduced from Ref. [117] with permission from the Elsevier

dispersion to cross-link the polymeric surfactant, resulting to either PANI–PVP hydrogel or PANI–PVA hydrogel nanocomposites with appealing characteristics regarding electrochemical activity and conductivity (Fig. 6).

4 Characterization

Various characterization techniques have been used to study the cross-linked hydrogels (Fig. 7). The most-used techniques are FTIR (Fourier Transform Infrared Spectroscopy), XRD, SEM, TGA/DSCFTIR and ToF-SIMS (Time-of-Flight Secondary Ion Mass Spectra). Percentage grafting can also determine the functionalized polymer unit in the hydrogel.

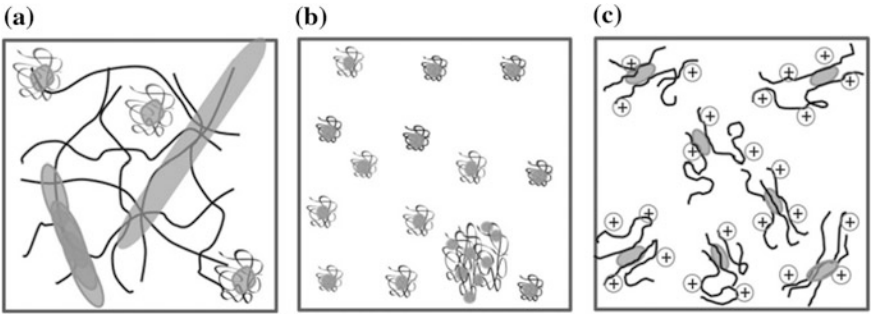

Fig. 6 **a** PVP–PANI; **b** PVA–PANI; **c** CT–PANI. Reproduced from Ref. [118] with permission from the Elsevier

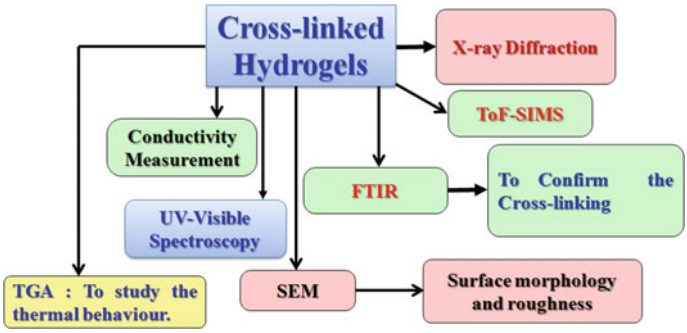

Fig. 7 Characterization techniques

5 Applications of Conducting Hydrogels

Hydrogels have found a broad range of applications in diverse areas as mentioned earlier such as in drug delivery, tissue engineering, barrier materials, and regenerative medicine to regulate biological adhesions, contact lenses, membrane separation, and adhesives (Fig. 8) [81, 119–123]. The discovery of hydrogels brings new transformations in the field of drug delivery because of their exciting properties, viz., porosity, resemblance to natural tissues, biocompatibility and high permeability rate for oxygen and essential nutrients, tunable viscoelasticity and high water holding capacity [124]. Similarly, conducting hydrogels also have various applications in electrical conductors, batteries, chemical and biological, sensors, corrosion protection, electro-optic and electrochromic devices, etc. [125]. Some of them are discussed briefly in this section.

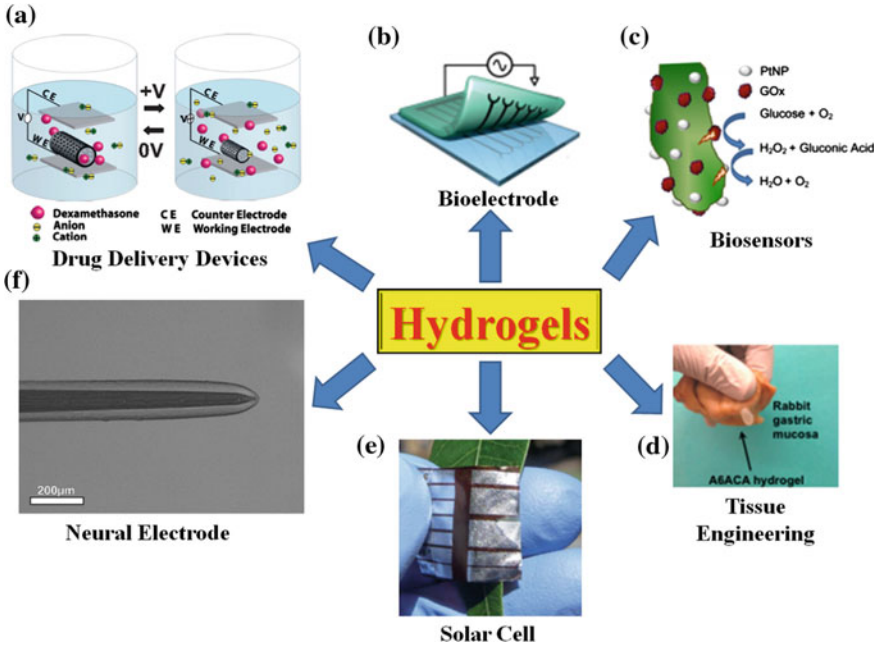

Fig. 8 Applications of hydrogels. **a** Drug delivery. Reproduced from Ref. [81] with permission from the Wiley-VCH. **b** Bioelectrode. Reproduced from Ref. [119] with permission from the American Chemical Society. **c** Biosensors. Reproduced from Ref. [120] with permission from the American Chemical Society. **d** Tissue engineering. Adapted with permission from Ref. [125]. National Academy of Sciences of the United States of America. **e** Solar cell. Reproduced from Ref. [122] with permission from the Royal Society of Chemistry. **f** Neural electrode. Reproduced from Ref. [123] with permission from the Wiley-VCH

5.1 Drug Delivery Devices

Drug delivery is the process of observing a pharmaceutical compound achieves a therapeutic effect in humans. Drug delivery method is a useful formulation technology which helps in the modification of drug-release profile, absorption and distribution for the patient convenience and safety along with improving product efficacy. The conventional routes of delivery include the noninvasive peroral, topical, transmucosal, and inhalation [126]. The medications like peptide and protein, antibody, vaccine and gene-based drugs, are generally not be transported by this method since they might be disposed by either enzymatic degradation or cannot be absorbed into the systemic circulation. This may be due to their high molecular size and charge issues. Nowadays, researchers are trying to develop devices for targeted delivery in which the drug is only working in the selected area of the body like in cancerous tissues. The further development also includes sustained drug-release formulations in which the drug is released over a period in a controlled manner from the drug device.

Hydrogels have a good porous network. The porosity of hydrogels can be modified by managing the density of cross-linkers used or by changing the swelling efficiency of hydrogels in the environment. This porosity of hydrogels helps in the release of drugs. The drug release from hydrogel can be controlled by controlling the diffusion coefficient of drugs through hydrogel matrix. We can also make a depot formulation of hydrogel drug. The depot formulation is a new technique where drugs were trapped in liposomes and incorporating liposomes in the hydrogel [127]. The electroconductive hydrogel of poly(hydroxyethyl methacrylate) and polypyrrole was studied for its application to clinically relevant biomedical diagnostic biosensors [128].

Amongst the different devices electroconductive hydrogel devices, are investigated as neural prosthetic and recording devices [129, 130] and electro-stimulated drug release devices (ESDRDs) [87]. The electro-stimulated drug release devices benefit from a high loading capacity and low voltage actuation. We have carried out the preparation of conducting hydrogels based on Gum ghatti, vinyl monomers, and aniline and to investigate their physio-chemical properties. The application of synthesized hydrogels as drug delivery devices have also been carried out [101, 104, 105, 131]. The release profile of the hydrogels networks were investigated through amoxicillin trihydrate and paracetamol as model drugs under different pH conditions at 37 °C [101, 104, 105, 131]. Hydrogels are involved in a different type of drug delivery systems are given Table 1.

Table 1 Drug delivery systems based on different hydrogels

Drug delivery system	Hydrogel	References
Self-regulated insulin delivery system	Cationic hydrogels	[132]
Colon-targeted drug delivery system	Chitosan hydrogel beads	[133]
Fluorescent drug delivery system	DNA hydrogel	[134]
'On" and "off" drug delivery system	Smart magnetic hydrogels	[135, 136]
Self-regulated insuline delivery system	Glucose sensitive hydrogel	[137]
Optical switches, ophthalmic drug delivery	Photo sensitive hydrogel	[138]
Buccal drug delivery	Mucoadhesive hydrogels	[139]
Oral drug delivery system	pH-sensitive hydrogel	[140, 141]

5.2 Biomedical Applications

During 1989 researchers find tremendous abilities of hydrogels to act as artificial muscles [142]. Many a detailed study of artificial muscles, allowing that the muscle is both a system and material has been recently done [143]. Jain and co-workers synthesized the agarose scaffold, used to replace the irregular spinal cord defect in adult rats [144]. Many workers used hydrogels for spinal cord injury repair through structure bridging method by delivering neurotrophic factors favoring regeneration of neural connections [145–147]. The physical properties of hydrogels such as biocompatibility, hydrophilicity, easy synthesis, and possible sterilization make them be used in blood compatible biomaterials [145–147]. Nonionic hydrogels used in blood contact applications prepared from poly(vinyl alcohol), polyacrylamides, PHEMA, and poly(ethylene oxide) [148]. Hydrogels are used in artificial muscles formation, wound-healing bioadhesives, and artificial organ preparation like kidney membrane preparation, articular cartilage, artificial skin, sexual organ reconstruction materials, and vocal cord replacement materials. The evolution of tissue engineering is shown in Fig. 8. Hydrogels have become a priority matrices for tissue engineering by many workers [26]. Hydrogels prepared for tissue engineering scaffolds are chosen to have pores big enough to hold living cells, or they may be created to dissolve or deteriorate away, releasing growth factors and forming pores into which living cells may enter and propagate [26]. The evolution of tissue engineering is shown in Fig. 9.

Hydrogel nanocomposites are also attracting attention for using them in various biomedical applications. The combination of polymers and nanocomposite results in an enhanced surface which can be used in different biomedical applications. Recently, Dvir et al. [149] synthesized conducting alginate hydrogel matrix by incorporating gold nanowires. The conducting scaffolds made up of this material can be used to engineer the tissues required for the propagation of electrical signals to facilitate the formation of functional tissues. The gold nanowire included to alginate hydrogel gives a higher expression of the cardiac marker in cardiac cells. Similarly, magnetic nanoparticles are covalently conjugated with biocompatible and thermoresponsive hydroxypropyl cellulose to obtain stimuli-responsive hydrogels

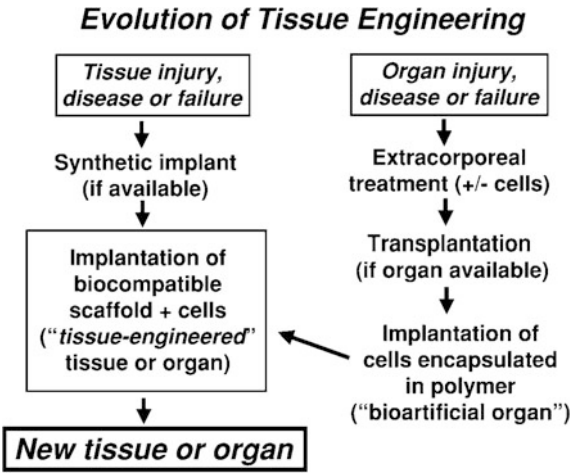

Fig. 9 Schematic showing the evolution of various therapeutic methods for treating injured of diseased tissues and organs, to tissue engineering. Reproduced from Ref. [26] with permission from the Elsevier

[150]. When stimuli-responsive hydrogels are subjected to external magnetic fields, the magnetic nanoparticles generate heat. The increase in the temperature of surrounding matrix above the lower critical solution temperature of the polymer results in a coil-to-globule transition of the polymer chains. Such triggers can be used to release therapeutic agents from the nanocomposite hydrogels [150]. Price and co-worker developed poly-(L-lactic-co-glycolic acid)-based hydrogel and incorporated alumina and titania in the hydrogel matrix result in increased osteoblast adhesion and proliferation [151]. In a similar effort, a multicomponent nanocomposite hydrogel of ferritin and PVA was synthesized by electrospinning method [152]. The produced nanocomposite when exposed to aqueous media, the electrospun fibrous mesh gives rise to the formation of nanocomposite hydrogels due to the swelling of polyvinyl alcohol. The synthesized ferritin-based nanocomposite PVA hydrogel is used to engineer scaffolds for tissue engineering applications, the stimuli-responsive matrix for drug release, or as actuators.

5.3 Agricultural and Horticultural

The deficiency of irrigation, drought, deforestation, and soil erosion are the main issues of agriculture across the world. The long-lasting phases of drought can cause environmental, agricultural, and socioeconomic troubles leading to societal disturbances and humanitarian calamity. The advancement of nontraditional new skills to preserve water is becoming significant for achieving a progressive economic growth, particularly in agricultural countries. The superabsorbent used as controlled release devices in agro industries having improved commercial possibility than the conventional synthetic polymers [153]. Fertilizers and water are vital elements in agriculture production, so it is very necessary to look up the water resources and

Fig. 10 Hydrophilic gels, commonly known as hydrogels, are dry crystals that can absorb many times their own weight in water. With permission from Ref. [156]. Rocky Mountain Research Station

fertilizer nutrients. Superabsorbents are directly cross-linked hydrophilic hydrogels that can absorb and retain an enormous amount of water (Fig. 10). Considered necessary qualities of superabsorbents are like its enough swelling capacity and good strength to hold water makes it suitable alternate for agricultural applications [154]. The superabsorbent polymers recover the plant nutrition, lower water evaporation loss, and reduce the need for irrigation. Carboxymethylcellulose (CMC) available as sodium salt NaCMC is a polyelectrolyte show good swelling capability and is used to improve soil quality through water retention [155].

Seed germination and creation are critical stages in plant growth and development. The agricultural growth of crops is restricted due to the low moisture content in soil and sometimes due to fewer irrigation facilities. The implementation of hydrogels to this type of soil leads to healthy practice to the promotion of plant growth by increased water retention in dry regions. The modification with hydrogel proves suitable for seed germination and seedling process in many species. The seedling development rate and biomass production found useful in lettuce, tobacco, and cotton in soil amended with the addition of hydrogel as compared to control sample [157]. Akhter et al. [158] studied the effects of different levels of a locally prepared hydrogel for moisture retention properties of sandy loam and loam soils and seedling growth of barley, wheat, and chickpea. Some researchers found varying degrees of improvement in the germination and establishment of different plant species. In some of the soil types and plant species have shown little or no benefit with hydrogel addition [159]. This reveals that the water-storing capacity depends on the texture of the soil, the type of hydrogel and particle size, the salinity of the soil solution, and the presence of ions. The cross-linked polyacrylamides hold up to 400 times their weight and release more than 95 % to plants [160]. We have synthesized conducting hydrogels with different monomer composition and found efficient for moisture retention in sandy, clay, and mixed type of soils [39]. Fertilizers are also one of the key parameters that inhibit or promote the production of agriculture, so it is of paramount to improve the utilization of manure nutrients. Most of the fertilizers result in leaching due to rain and cause contamination of

water resources. One way of reducing these deficiencies involves the utilization of controlled fertilizer-release devices. Many workers synthesized the hydrogel matrix for controlled release of fertilizers inside the soil [161–163]. Radiation-induced copolymerization is also used to synthesize hydrogel matrix for controlled fertilizer release devices [164].

5.4 Wastewater Treatment

Inorganic effluents discharged from the industries contain toxic metal ions and toxic dye release which contaminate food chain through the water system. These dye materials and toxic heavy metal ions show high solubility in the aquatic environment and is quickly taken up by marine lives. The metal ions and toxic dye molecules cause serious health hazards when ingested beyond the permitted concentration [99, 115, 165]. Some technologies and processes such as filtration, chemical precipitation, ion exchange, adsorption, electrodepositing and membrane systems have been urbanized to remove toxic metal ions, and dye molecules from water resources [166, 167]. Hydrogels interact through polar functional groups with dye molecules and heavy metal ions and bind them. The hydrogel is easy to handle and also their reusability makes them promising materials for water purification. Hydrogels are of two types, i.e., ionic and nonionic materials. The ionic form hydrogels involve the groups like $–CO_2–$, $–SO_3–$ (anionic) or $–NH^{3+}$ (cationic) and nonionic involves pendants. The presence of anionic and cationic group makes hydrogel useful for many potential applications like dye removal and metal-ion adsorption [39, 99, 115].

The natural polysaccharides like gum ghatti, guar gum, chitosan, and the deacetylated products of chitin, reflects a good adsorption capacity toward many types of dye due to its multiple functional groups, biocompatibility, and biodegradability [168]. Recent research articles stated that chitosan-based hydrogels that are usually used in the form of hydrogel beads have shown the high adsorption capacity for numerous dyes [169]. However, their little mechanical strength limits their use as a commercial adsorbent, so several chemical modification via chemical cross-linking, poly amination, and carboxy alkyl substitution have been employed to increase mechanical strength [170]. The natural polysaccharides are interpenetrated with suitable monomers to make them efficient absorbents. We have synthesized the gum ghatti-based Gg-cl-poly(AAm) semi-interpenetrating hydrogel, and Gg-cl-poly (AAm-ipn-aniline), Gg-cl-poly(MAA-ipn-aniline, Gg-cl-poly(Acrylic acid-aniline) interpenetrating hydrogel matrices and use them effectively for the removal of malachite green (MG), methyl orange (MO), methylene blue (MB), stilbene, fluorescent sodium (FS), and rhodamine (Rh) dye from water system [99, 115, 116]. To get the qualitative approximation of the dyes adsorption in the Gg-cl-poly(acrylic acid-aniline) based conductive hydrogels, % adsorption was calculated into the hydrogels and is shown in Fig. 11. The adsorption of the FS, (Rh), and stilbene dye was more or less same in the synthesized IPN [115]. The slight difference among these arises because molecular structures of these dye molecules are different.

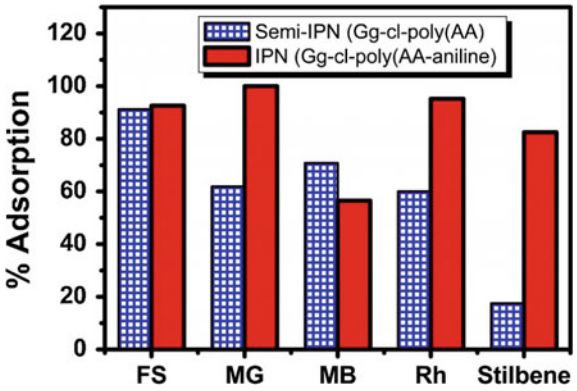

Fig. 11 Graphical representation of the percentage of adsorption of dyes into the cross-linked hydrogels. Reproduced from Ref. [115] with permission from the Elsevier

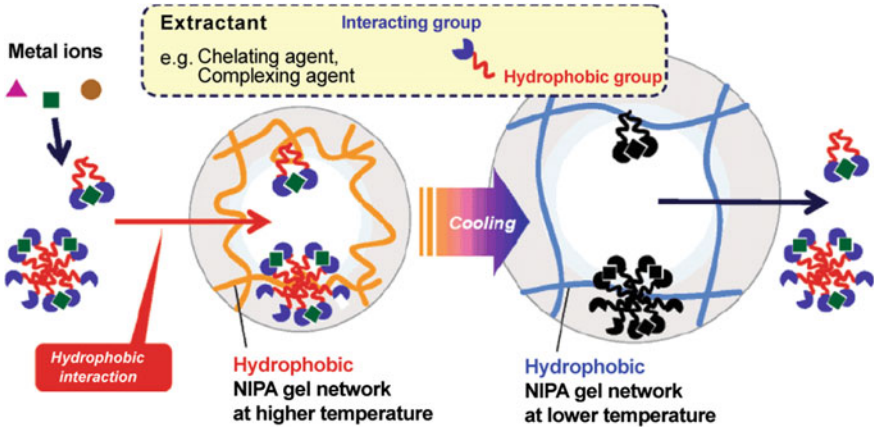

Fig. 12 Scheme of TS-SPE of a metal ion complexed with an extractant onto a NIPAM hydrogel. Reproduced from Ref. [174] with permission from the American Chemical Society

Similarly, chitosan mixed with different nanofillers such as clay nanoparticles and silica nanoparticles are used for dye removal purpose [171]. In recent carbon nanotube (CNT) appeared as a promising nanofiller for the preparation of chitosan–CNT nanocomposites because of its excellent mechanical, electrical, and thermal properties [171]. Several papers reflect CNT as a superb adsorbent for different material like dioxin removal and dye removal because of its hollow and layered nanosized structures that have a large specific surface area [171, 172]. A number of conventional methods like precipitation, membrane filtration, ion exchange treatment are used to remove metal ions from the water system, but hydrogel based adsorbents have attracted distinctive attention because of they are highly potential for efficient removal of heavy metals [173, 174] (Fig. 12).

Most of the hydrogels involve metal-ion adsorption process can develop negative charges to form complexes with positively charged metal ions. So a number of hydrogels having positive charge produced in a variety of shapes, such as bulk, and micro and nano size, have been prepared and utilized for environmental applications [167]. The presence of hydrophilic groups like –OH, –COOH, $–NH_2$, $–CONH_2$, SO_3H can be used for the removal of toxic metal ion [39, 99]. In the past few decades, a large number of cross-linked hydrogel and chemically modified biosorbents have been studied to be used as adsorbents for removal of lead ions from aqueous solutions. Zare et al. [175] synthesized the conducting nanocomposite based on polypyrrole and modified poly(styrene-alt-maleic anhydride) through emulsion polymerization and utilized for heavy metal sorbent activity. The stimuli-responsive IPN gel of poly(N-isopropyl acrylamide) (PNIPAm) and poly (sodium acrylate) (PNaAA) and diethyl aminoethyl dextran hydrogel have been synthesized for the removal of heavy metal ions and [176]. A series of CS-g-poly (acrylic acid)/APT/sodium humate(CS-g-PAA/APT/SH) hybrid hydrogels incorporated with various amounts of attapulgite have been synthesized, and their utilization as adsorbents for the removal of Pb^{2+} from water system has been studied [177, 178]. Tu and co-workers prepared poly(VI-co-HEA) hydrogels and review their performance for the adsorption of copper ions. They found that the content of 2-hydroxyethylacrylate (HEA) affected the features of hydrogel samples substantially [179]. Lu and fellow researcher examined the removal of lead ions by polyvinylpyrrolidone/acrylic acid-based hydrogel [180]. They found that the ion exchange between –COOH and metal ions played a significant role in Pb(II) adsorption and some researcher synthesized carboxyl groups into poly(2-(acrylamide)-2-methyl-1-propanesulfonicacid) through itaconic acid and concluded that it leads to a slight increase in the total removal capacity of the copolymer [180, 181]. So from reported literature, it is clear that interpenetrating hydrogels are effectively utilized in waste water treatment.

5.5 Bioelectrodes

Conducting hydrogel holds substantial secure as electrode coatings; on the other hand, they are considered by intrinsically weak mechanical properties. Hybrid or making layered CPs with other polymer forms, such as hydrogels, has been projected as a method of getting better these properties. Bioelectrodes are an important part of the delivery of charge and recording of neural activity in some neuroprosthetic devices. Electrodes are traditionally fabricated from platinum, platinum alloys, and gold. Surface modification of metallic electrodes has been done to increase the incorporation of biological tissue and minimizing foreign body encapsulation over the electrode interface [82, 182, 183]. The enhanced interface between the electrode

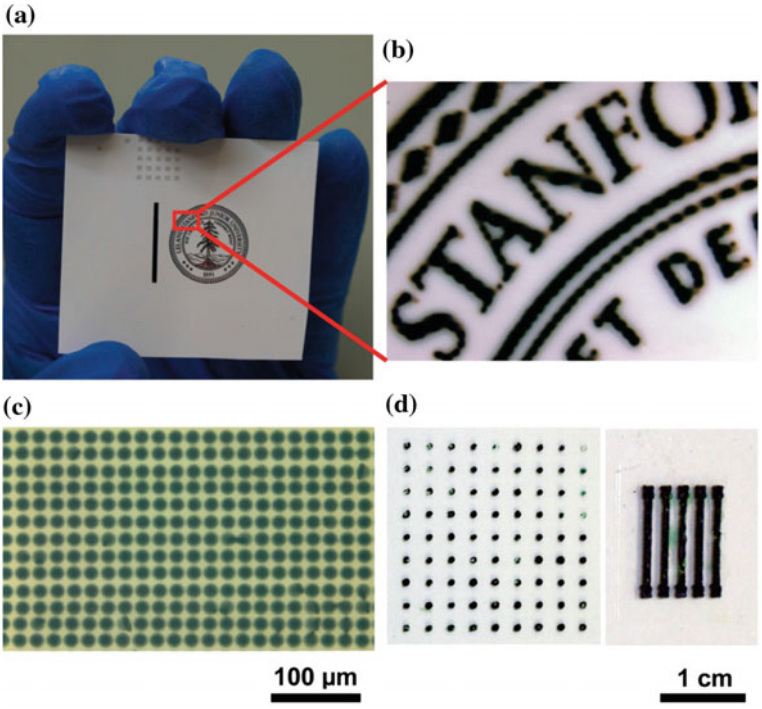

Fig. 13 Micropatterning of PANI hydrogel by ink-jet printing (**a**–**c**) and spray coating (**d**). Reproduced from Ref. [186] with permission from the PNAS

and biological systems will make the medical devices function more effectively by allowing the use of smaller charges to obtain a neural response [184]. Researchers synthesized the alginate hydrogels act as a bioelectrode for rendering a favorable mechanical match for neural tissue and able of tailoring fibrotic responses [185]. Pan et al. [186] synthesized scalable and versatile synthesis of multifunctional polyaniline hydrogel with excellent electronic conductivity and electrochemical properties which possess high surface area and three-dimensional porous nanostructures. The PANI hydrogels possess potential as a high-performance supercapacitor electrode with high specific capacitance, unprecedented rate capability, and cycling stability. The patterned PAni hydrogel in different solution is shown in Fig. 13. The PANI hydrogel also possesses credential for glucose sensing application and future-generation energy storage electrodes [186].

Dhand and co-workers also synthesized PANI hydrogels-based biosensor electrode. The working mechanism of the sensor relies on the redox properties of the glucose oxidase where the enzymatic reaction of glucose oxidase and glucose is monitored through electrochemical measurement of the glucose oxidase–PANI

hydrogel based electrode [187]. Abidian et al. [188] synthesized conducting polymer nanotubes which improve the electrical properties, mechanical adhesion, neural attachment and neurite outgrowth of the natural electrode.

6 Conclusion and Future Perspective

Hydrogels are polymeric networks, which consume and hold a significant quantity of water. In the polymeric network, hydrophilic groups or domains are presents which are hydrated in an aqueous environment thereby producing the hydrogel structure. Because of their water-absorbing ability, hydrogels are not only mattered of a study by scientific communities interested in essential features of swollen polymeric networks but have also encountered broad application in various technological sectors like biomedical, pharmaceutical, tissue engineering, and agriculture division. In this chapter, we have reviewed some relevant information regarding synthesis, characterization, and applications of conducting hydrogels based on different materials. In the today's situation of the go-green, all materials at the end of the day should be biodegradable so that it may not create any infliction to the atmosphere. Since in all living beings there exists some electrical impulse, therefore the need of present time is to produce a biomaterial with electroconductive properties that could be employed in biomedical applications with better biocompatibility and biodegradability. Therefore, there is a growing interest for biodegradable polymers as a replacement of the synthetic polymers and also a solution to the solid waste management.

References

1. Tang QW, Lin JM, Wu JH, Zhang CJ, Hao SC (2007) Carbohydr Polym 67:332
2. Tang Q, Wu J, Lin J (2008) Carbohydr Polym 73:315
3. Lin J, Tang Q, Hu D, Sun X, Li Q, Wu J (2009) Colloids Surf A 346:177
4. Tang QW, Wu JH, Sun H, Fan SJ, Hu D, Lin JM (2008) Carbohydr Polym 73:473
5. Tiwari A (2008) J Polym Res 15:337
6. Abd El-Rehim HA, Hegazy El-Sayed A, Abd El-Mohdy HL (2004) J Appl Polym Sci 93:1360
7. Dispenza C, Lo Presti C, Belfiore C, Spadaro G, Piazza S (2006) Polymer 47:961
8. Ito K, Chuang J (2003) Prog Polym Sci 28:1489
9. Omidian H, Rocca JG, Park K (2005) J Control Release 102:3
10. Richter A, Howitz S, Kuckling D (2004) Sens Actuators B 99:451
11. Siddhanta SK, Gangopadhyay R (2005) Polymer 46:2993
12. Wada H, Nohara HS, Iwakura C (2004) Electrochim Acta 49:4871
13. Forrest SR (2004) Nature 428:911
14. Pepin-Donat B, Viallat A, Blachot JF, Lombart C (2006) Adv Mater 18:1401

15. Chen L, Kim BS, Nishino M, Gong JP, Osada Y (2000) Macromolecules 33:1232
16. Vikki T, Ruokolainen J, Ikkala OT, Passiniemi P, Isotalo H, Torkkeli M (1997) Macromolecules 30:4064
17. Terech P, Weiss RG (1997) Chem Rev 97:3133
18. Dai T, Jiang X, Hua S, Wang X, Lu Y (2008) Chem Commun 36:4279
19. Dai T, Qing X, Zhou H, Shen C, Wang J, Lu Y (2010) Synth Met 160:791
20. Moschou EA, Peteu SF, Bachas LG, Madou MJ, Daunert S (2004) Chem Mater 16:2499
21. Liang SM, Weng LH, Xu SX, Tan J, Zhang XL, Zhang LN (2007) Appl Phys Lett 90:153506
22. Calvert P (2009) Adv Mater 21:743
23. Tiwari A, Singh SP (2008) J Appl Polym Sci 108:1169
24. Tiwari A, Singh V (2008) Carbohydr Polym 74:427
25. Ahmed EM (2013) J. Adv. Res. 6:105
26. Hoffman AS (2002) Adv Drug Deliv Rev 54:3
27. Sastry SK, Lakonishok M, Wu S, Truong TQ, Huttenlocher A, Turner CE, Horwitz AF (1999) J Cell Biol 144:1295
28. Bell CL, Peppas NA (1995) J Control Release 37:277
29. Nemours EIP (1936) Ind Eng Chem 28:1160
30. Wichterle O, Lim D (1960) Nature 185:117
31. Qiu Y, Park K (2001) Drug Deliv Rev 53:321
32. Pulapura S, Kohn J (1992) J Biomater Appl 6:216
33. Zhang X, Goosen FA, Wyss SP, Pichora D (1993) Polym Rev 33:81
34. Rehab A, Akelah A, Issa R, D'Antone S, Solaro R, Chiellini E (1991) J Bioact Compat Polym 6:52
35. Yoshida R, Sakai K, Okano T, Sakurai Y (1993) Adv Drug Deliv Rev 11:85
36. Kamath KR, Park K (1993) Adv Drug Deliv Rev 11:59
37. Heller J (1993) Adv Drug Deliv Rev 10:163
38. Daubresse C, Grandfils C, Jerome R, Teyssie P (1994) J Colloid Interfaces Sci 168:222
39. Sharma K (2015) Synthesis of conducting gum ghatti-PANI based interpenetrating networks and their applications as controlled drug delivery devices. A Thesis submitted to the Faculty of Basic Sciences Shoolini University of Biotechnology and Management Sciences, Solan (Himachal Pradesh), 173229 (India)
40. Takashi L, Hatsumi T, Makoto M, Takashi I, Takehiko G, Shuji S (2007) J Appl Polym Sci 104:842
41. Aylsworth JW (1914) US Patent 1111:284
42. Millar JRJ (1960) J Chem Soc 263:1311
43. Matricardi P, Meo CD, Coviello T, Hennink WE, Alhaique F (2013) Adv Drug Deliv Rev 65:1172
44. Jenkins AD, Kratochvìl P, Stepto RFT, Suter UW (1996) Pure Appl Chem 68:2287
45. Hennink WE, Nostrum CV (2002) Adv Drug Deliv Rev 54:13
46. Lin DC, Yurke B, Langrana NA (2005) J Mater Res 20:1456
47. Oh KS, Han SK, Choi YW, Lee JH, Lee JY, Yuk SH (2004) Biomaterials 25:2393
48. Stenekes RJH, Talsma H, Hennink WE (2001) Biomaterials 22:1891
49. Khan F (2004) Biomacromolecules 5:1078
50. Chauhan A, Chauhan P, Kaith BS (2004) J Chem Eng Process Technol 3:1
51. Ricka J, Tanaka T (1984) Macromolecules 17:2916
52. Li Y, Tanaka T (1990) J. Chem. Phy. 92:1365
53. Hoffman AS (1987) J Control Release 6:297
54. Hrouz J, Ilvasky M, Ulbrich K, Kopecek J (1981) Eur Polym J 17:361
55. Park TG, Hoffman AS (1993) Macromolecules 26:5045
56. Kungwatchakun D, Irie M (1988) Macromol Rapid Commun 9:243
57. Eisenberg SR, Grodzinski AJ (1984) J Memb Sci 19:173
58. Ishida K, Uno T, Itoh T, Kubo M (2012) Macromolecules 45:6136
59. Walatka VV, Labes MM, Perlstein JH (1973) Phys Rev Lett 31:1139

60. Greene RL, Street GB, Suter LJ (1975) Phys Rev Lett 34:577
61. Gill WD, Bludau W, Geiss RH, Grant PM, Greene RL, Mayerle JJ, Street GB (1977) Phys Rev Lett 38:1305
62. Chiang CK, Fincher CR, Park YW, Heeger AJ, Shirakawa H, Louis EJ, Gau SC, MacDiarmid AG (1977) Phys Rev Lett 39:1098
63. Shirakawa H, Louis EJ, MacDiarmid AG, Chiang CK, Heeger AJ (1977) J Chem Soc, Chem Commun 474:578
64. Bredas JL, Chance RR, Silbey R (1982) Phys Rev B 26:5843
65. Heeger AJ (2001) Rev Mod Phys 73:681
66. MacDiarmid AG (2001) Rev Mod Phys 73:701
67. Shirakawa H (2001) Rev Mod Phys 73:713
68. Dotrong M, Mehta R, Balchin GA, Tomlinson RC, Sinsky M, Lee CYC, Evers RC (1993) J Polym Sci, Part A: Polym Chem 31:723
69. Kakuda S, Momma T, Osaka T, Appetecchi GB, Scrosati B (1995) J Electrochem Soc 142: L1
70. Coskun Y, Cirpan A, Toppare L (2007) J Mater Sci 42:368
71. Katsumi Y, Keiichi K, Yoshio I (1983) Jpn J Appl Phys 22:L157
72. Shirakawa H (2001) Synth Met 125:3
73. Agbor NE, Petty MC, Monkman AP (1995) Sens Actuators B Chem 28:173
74. Xie D, Jiang Y, Pan W, Li D, Wu Z, Li Y (2002) Sens Actuators B Chem 81:158
75. Gilmore K, Hodgson AJ, Luan B, Small CJ, Wallace GG (1994) Polym Gels Netw 2:135
76. Xiang Y, Chen D (2007) Eur Polym J 43:4178
77. Devaki SJ, Narayanan RK, Sarojam S (2014) Mater Lett 116:135
78. Naficy S, Razal JM, Spinks GM, Wallace GG, Whitten PG (2012) Chem Mater 24:3425
79. Basavaraja C, Kim NR, Jo EA, Pierson R, Huh DS (2009) Bull Korean Chem Soc 30:1543
80. Rylie AG, Sungchul B, Laura AP, Penny JM (2010) Sci Technol Adv Mater 11:1
81. Abidian MR, Kim DH, Martin DC (2006) Adv Mater 18:405–409
82. Abidian MR, Martin DC (2009) Adv Funct Mater 19:573
83. Ahmed AA, Mohammada F, Rahman MZA (2004) Synth Met 144:29
84. Shin SR, Park SJ, Yoon SG, Spinks GM, Kim SI, Kim SJ (2005) Synth Met 154:213
85. Tiwari A (2007) J Macromol Sci Part A Pure Appl Chem 44:735
86. Moschou E, Madou MJ, Bachas LG, Daunert S (2006) Sens Actuators B Chem 115:379
87. Lira LM, Torresi CD (2005) Electrochem Commun 7:717
88. Kumar S, Gangopadhyay R (2005) Polymer 46:2993
89. Nikpour M, Chaouk H, Mau A, Chung DJ, Wallace G (1999) Synth Met 99:121
90. Park YH, Park SB (2002) Synth Met 128:229
91. Haraguchi K, Farnworth R, Ohbayashi A, Takehisa T (2003) Macromolecules 36:5732
92. El-Sherif H, El-Masry M, Kansoh A (2011) Macromol Res 19:1151
93. Varaprasad K, Mohan YM, Vimala K, Raju KM (2011) J Appl Polym Sci 121:784
94. Zhao Z, Wang X, Qiu J, Lin J, Xu D, Zhang C, Meijiao LV, Yang X (2014) Adv Mater Sci 36:137
95. Mittal H, Mishra SB (2014) Carbohydr Polym 101:1255
96. Mittal H, Ballav N, Mishra SB (2014) J Ind Eng Chem 20:2184
97. Dispenza C, Fiandaca G, Lo Presti C, Piazza S, Spadaro G (2007) Radiat Phys Chem 76:1371
98. Soni SN, Bajpai J, Bajpai AK (2012) Nanosci Methods 1:164
99. Sharma K, Kaith BS, Kumar V, Kumar V, Som S, Kalia S, Swart HC (2013) RSC Adv 3:25830
100. Sharma K, Kaith BS, Kumar V, Kalia S, Kumar V, Som S, Swart HC (2014) Express Polym Lett. 8:267
101. Sharma K, Kaith BS, Kalia S, Kumar V, Swart HC (2015) Colloid Polym Sci 293:293
102. Kaith BS, Sharma R, Kalia S, Bhatti MS (2014) RSC Adv. 4:40339
103. Kaith BS, Sharma R, Kalia S (2015) Int J Biol Macromol 75:266

104. Sharma K, Kumar V, Kaith BS, Som S, Kumar V, Pandey A, Kalia S, Swart HC (2015) Ind Eng Chem Res 54:1982
105. Sharma K, Kumar V, Kaith BS, Kumar V, Som S, Pandey A, Kalia S, Swart HC (2015) New J Chem 39:3021
106. Kaith BS, Sharma K, Kumar V, Kalia S, Swart HC (2014) Synth Met 187:61
107. Cogan SF (2008) Annu Rev Biomed Eng 10:275
108. Guimard NK, Gomez N, Schmidt CE (2007) Prog Polym Sci 32:876
109. Stauffer WR, Cui XT (2006) Biomaterials 27:2405
110. Brahim S, Narinesingh D, Guiseppi-Elie A (2002) Biosens Bioelectron 17:53
111. Brahim S, Narinesingh D, Guiseppi-Elie A (2002) Biosens Bioelectron 17:973
112. Brahim S, Wilson AM, Narinesingh D, Iwuoha E, Guiseppi-Elie A (2003) Microchim Acta 143:123
113. Pan L, Yu G, Zhai D, Lee HR, Zhao W, Liu N, Wang H, Tee BC-K, Shi Y, Cui Y, Bao Z (2012) PNAS 109:9287
114. Karadao E, Saraydin D, Guven O (2001) Macromol Mater Eng 286:34
115. Sharma K, Kaith BS, Kumar V, Kalia S, Kumar V, Swart HC (2014) Geoderma 232–234:45
116. Sharma K, Kumar V, Kaith BS, Kumar V, Som S, Kalia S, Swart HC (2015) Polym Degrad Stab 111:20
117. Sharma K, Kaith BS, Kumar V, Kalia S, Kumar V, Swart HC (2014) Polym Degrad Stab 107:166
118. Dispenza C, Sabatino MA, Chmielewska D, LoPresti C, Battaglia G (2012) React Funct Polym 72:185
119. Sekine S, Ido Y, Miyake T, Nagamine K, Nishizawa M (2010) J Am Chem Soc 132:13174–13175
120. Zhai D, Liu B, Shi Y, Pan L, Wang Y, Li B, Zhang R, Yu G (2013) ACS Nano 7:3540
121. Phadke A, Zhang C, Arman B, Hsu C-C, Mashelkar RA, Lele AK, Tauber MJ, Arya G, Varghese S (2012) Proc Natl Acad Sci USA 109:4383–4388
122. Hu L, Zheng G, Yao J, Liu N, Weil B, Eskilsson M, Karabulut E, Ruan Z, Fan S, Bloking JT, McGehee MD, Wagberg L, Cui Y (2013) Energy Environ Sci 6:513
123. Kim D-H, Abidian M, Martin DC (2004) J Biomed Mater Res, Part A 71:577–585
124. Jia X, Kiick KL (2009) Macromol Biosci 9:140
125. Beadle P, Armes SP, Gottesfeld S, Mombourquette C, Houlton R, Andrews WD, Agnew SF (1992) Electrically conductive polyaniline-copolymer latex composites. Macromolecules 25 (9):2526–2530
126. Tan X, Feldman SR, Chang JW, Balkrishnan R (2012) Exp Opin Drug Deliv 9:1263
127. Kopecek J (2009) J Polym Sci 47:5929
128. Guiseppi-Elie A, Brahim S, Narinesingh D (2001) J Macromol Sci Part A Pure Appl Chem 38:1575
129. Kim DH, Abidan M, Martin DC (2004) J Biomed Mater Res 71:577
130. Green RA, Lovell NH, Wallace GG, Poole-Warren LA (2008) Biomaterials 29:3393
131. Sharma K, Kumar V, Chaudhary B, Kaith BS, Kalia S, Swart HC (2016) Polym Degrad Stab 124:101
132. Peppas NA (2004) J Drug Deliv Sci Technol 14:247
133. Chourasia MK, Jain SK (2003) J Pharm Pharm Sci 6(1):33
134. Bertz A, Ehlers JE, Wöhl-Bruhn S, Bunjes H, Gericke KH, Menzel H (2013) Macromol Biosci 13(2):215
135. Liu TY, Hu SH, Liu KH, Liu DM, Chen SY (2006) J Mag Mag Mater 304:397
136. You JO, Almeda D, Ye GJC, Auguste DT (2010) J Biol Eng 4:15
137. Ravaine V, Ancla C, Catargi B (2008) J Control Release 132:2
138. Gupta AK, Siddiqui AW (2012) J Drug Deliv Ther 2(1):81–88
139. Xu J, Strandman S, Zhu JXX, Barralet J, Cerruti M (2015) Biomaterials 37:395
140. Qiu Y, Park K (2001) Adv. Drug Del. Rev 53:321
141. Kim B, Peppas NA (2002) J Biomater Sci Polym Ed 13:1271

142. Suzuki M (1989) Proceedings of the annual international conference of the IEEE engineering in medicine and biology society, 1989. Images of the Twenty-First Century
143. Bassil M, Davenas J, El Tahchi M (2008) Sens Actuators B 134:496
144. Jain A, Kim Y-T, McKeon RJ, Bellamkonda RV (2006) Biomaterials 27:497
145. Hejcl A, Lesny P, Pradny M, Michalek J, Jendelova P, Stulik J, Sykova E (2008) Physiol Res 57:121
146. Sykova E, Jendelova P, Urdzikova L, Lesny P, Hejc A (2006) Cell Mol Neurobiol 26:1111
147. Nisbet DR, Crompton KE, Horne MK, Finkelstein DI, Forsythe JS (2008) J Biomed Mater Res, Part B 87B(1):251
148. Peppas NA, Keys KB, Torres-Lugo M, Lowman AM (1999) J Control Release 62:81
149. Dvir T, Timko BP, Brigham MD, Naik SR, Karajanagi SS, Levy O, Jin H, Parker KK, Langer R, Kohane DS (2011) Nat Nanotechnol 6:720
150. Gaharwar AK, Wong JE, Muller-Schulte D, Bahadur D, Richtering W (2009) J Nanosci Nanotechnol 9:5355
151. Price RL, Gutwein LG, Kaledin L, Tepper F, Webster TJ (2003) J Biomed Mater Res A 67:1284
152. Shin MK, Spinks GM, Shin SR, Kim SI, Kim SJ (2009) Adv Mater 21:1712
153. Chen L, Xie Z, Zhuang X, Chen X, Jing X (2008) Carbohydr Polym 72:342
154. Kabiri K, Omidian H, Hashemi SA, Zohuriaan-Mehr MJ (2003) Eur Polym J 39:1341
155. Sannino A, Demitriemail C, Madaghiele M (2009) Materials 2:353
156. Landis TD, Haase DL (2012) USDA forest service proceedings, RMRS-P-68
157. Wallace A, Wallace GA (1986) Soil Sci 141:321
158. Akhter J, Mahmood K, Malik KA, Mardan A, Ahmad M, Iqbal MM (2004) Plant Soil Environ 50:463
159. James EA, Richards D (1986) Sci Hort 28:201
160. Huttermann A, Zommorodi M, Reise K (1999) Soil Tillage Res 50:295
161. Jiao Y, Liu Z, Ding S, Li L, Zhou C (2006) J Appl Polym Sci 101:1515
162. Zhao L, Xu L, Mitomo H, Yoshii F (2006) Carbohydr Polym 64:473
163. Nho YC, Park KR (2002) J Appl Polym Sci 85:1787
164. Singh B, Pal L (2011) Int J Biol Macromol 48:501
165. Dadhaniya PV, Patel AM, Patel MP, Patel RG (2009) J Macromol Sci Part A Pure Appl Chem 46:447
166. Solpan D, Torun M (2005) J Macromol Sci Part A Pure Appl Chem 42:1435
167. Sahiner N (2008) Turk J. Chem 32:113
168. Majeti NV, Kumar R (2000) React Funct Polym 46:1
169. Crini G, Badot PM (2008) Prog Polym Sci 33:399
170. Chiou MS, Ho PY, Li HY (2004) Dyes Pigments 60:69
171. Wang L, Wang A (2007) J Chem Technol Biotechnol 82:711
172. Wu CH (2007) J Hazard Mater 144:93
173. Charerntanyarak L (1999) Water Sci Technol 39:135
174. Tokuyama H, Iwama T (2007) Langmuir 23:13104
175. Zare EN, Lakouraj MM, Moghadam PN, Hasanzadeh R (2015) Polym Comp 34:732
176. Yamashita K, Nishimura T, Nango M (2003) Polym Adv Technol 14:189
177. Zhang JP, Wang AQ (2010) J Chem Eng Data 55:2379
178. Jing G, Wang L, Yu H, Amer WA, Zhang L (2013) Colloids Surf A Physicochem Eng Asp 416:86
179. Tu J, Zhou J, Wang CF, Zhang QA, Chen S (2010) J Polym Sci Pol Chem 48:4005–4012
180. Lu QF, Yu J, Gao JZ, Yang W, Li Y (2011) Plasma Process Polym 8:803
181. Cavus S, Gurdag G (2009) Ind Eng Chem Res 48:2652
182. Deen GR (2010) J Dispers Sci Technol 31:1673
183. Abidian MR, Martin DC (2008) Biomaterials 29:1273
184. Seymour J, Kipke DR (2006) Mater Res Soc Symp Proc 926:1
185. Kim DH, Wiler JA, Anderson DJ, Kipke DR, Martin DC (2010) Acta Biomater 6:57

186. Pan L, Yub G, Zhai D, Lee HR, Zhao W, Liu N, Wang H, Tee BC-K, Shi Y, Cui Y, Bao Z (2002) Proc Natl Acad Sci 109:9287
187. Dhand C, Das M, Datta M, Malhotra BD (2011) Biosens Bioelectron 26:2811
188. Abidian MR, Corey JM, Kipke DR, Martin DC (2010) Small 6:421

Conducting Polymer Nanocomposites for Sensor Applications

Subhash B. Kondawar and Pallavi T. Patil

Abstract Due to numerous potential applications of conducting polymers, these materials are now world wide studied since the discovery of first conducting polymer (polyacetylene) in 1977. Particularly for sensing concerned, conducting polymers are very sensitive to environmental conditions. The developments in nanostructure conducting polymers and conducting polymer nanocomposites have large impact on sensor research. Due to large surface-area-to-volume ratio of nanostructure conducting polymers, they show superior performance compared to conducting polymers in bulk form. However, the sensitivity and selectivity of nanostructure conducting polymer-based sensors still leave room for improvement. The conducting polymer nanocomposites have gained tremendous recognition in the field of sensors to improve the sensitivity and selectivity due to synergistic effect of size reduction for nanofiller and high electrical conductivity of conducting polymer in nanocomposites. Therefore, the sensitivity and selectivity of conducting polymer nanocomposites-based sensors have been enhanced compared to that of the classical materials-based sensors. This chapter provides the current research activities of the sensors/biosensors based on conducting polymer nanocomposites. The synthesis of nanostructure conducting polymers and conducting polymer nanocomposites, their application in sensors/biosensors are reviewed and discussed in this chapter.

Keywords Conducting polymers · Nanostructure conducting polymers · Nanofibers · Nanocomposites · Gas sensors · Biosensors

S.B. Kondawar (✉) · P.T. Patil
Polymer Nanotech Laboratory, Department of Physics, Rashtrasant Tukadoji Maharaj Nagpur University, Nagpur 440033, India
e-mail: sbkondawar@yahoo.co.in

V. Kumar et al. (eds.), *Conducting Polymer Hybrids*,
Springer Series on Polymer and Composite Materials,
DOI 10.1007/978-3-319-46458-9_8

1 Introduction to Sensors/Biosensors

It is well known that the sensors/biosensors provide physical, chemical, and biological environmental information. A chemical sensor is different from biosensor on the basis of whether sensor contains biological recognition agents. All biosensors contain biological recognition agent, on the other hand, chemical sensors do not contain such agents. Sensitivity, selectivity, and stability are the most important aspects of sensors. Materials like metal (gold, silver), carbon, and polymers (especially conducting polymers) at nanoscale are promising for chemical and biological sensors [1]. Tin oxide (SnO_2)-based commercial sensors was investigated as the first semiconducting devices for gas detection [2]. In case of semiconducting metal oxides (SMO)-based gas sensors for gas detection, the oxygen in air at temperature between 150 and 400 °C is adsorbed at the surface of the metal oxides by trapping electrons causing increase or decrease in resistance of the sensor for n-type or p-type materials, respectively. The occurrence of a target gas in the atmosphere reacts with the pre-adsorbed oxygen determines a change of the sensor resistance, which is recorded as a sensor signal and the magnitude of which is correlated to the concentration of the target gas. Thus, a sensor is divided into receptor for the surface reaction to occur between the semiconducting material and the gases and into the transducer for transduction of it into the corresponding changes of the electrical resistance of the sensor [3]. The conducting polymers are known to have considerable flexibility in chemical structures that can be modified. When such materials are used for chemical or biological sensing purpose, they easily interact with analytes leading to its change in resistance. Therefore, conducting polymers are suitable materials for the development of chemical sensors. The advent of nanotechnology made these materials most suitable for sensing purpose in the form of conducting polymer nanostructures which can be widely explored as chemical and biosensors. Conducting polymer nanostructure possesses very large surface-area-to-volume ratio than that of the bulk conducting polymers [4, 5].

A chemical sensor is based on the principle of transforming the chemical information originated by chemical reaction to a useful signal. The schematic representation of a chemical sensor is shown in Fig. 1. Chemical sensors usually contain chemical recognition system (receptor) and transducer. Due to interaction of receptor with analyte molecules, transducer gains an electrical signal. In chemical sensors the interaction processes are adsorption, ion exchange, and liquid–liquid extraction. Transducer transforms the actual concentration value, a nonelectric quantity into an electric quantity, voltage, current or resistance.

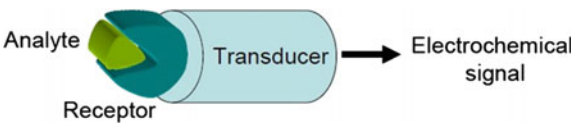

Fig. 1 Schematic representation of chemical sensor

Chemical sensors can be of gas, liquid, and solid particulate sensors based on the phases of the analyte. Depending on the operating principle of transducer in a chemical sensor, it can be used as optical, electrochemical, thermometric, and gravimetric sensor. Chemical sensors also include a special branch referred to as biosensors for the recognition of biochemicals and bio-reactions. The use of biological elements such as organisms, enzymes, antibodies, tissues, and cells as receptors differentiates biosensors from conventional chemical sensors.

A chemical sensor which detects gas consists of a sensing element that reacts with gaseous species and a transducer that translates the results of this reaction to a signal, is called as gas sensor [6]. The resistance of the gas sensor changes due to chemical reaction with gaseous species, and hence such sensor is called as chemiresistor-type gas sensor. This sensor contains interdigited electrode (IDE) geometry and a layer of sensing material. IDE may consist of finger type of metallic (cost effective Cu) electrode electrochemically patterned on an epoxy glass substrate as shown in Fig. 2 and the schematic representation of a chemiresistor-type gas sensing is shown in Fig. 3.

The gas sensing behavior of chemiresistor sensors can be studied by calculating change in the surface resistance of sensing film with time toward gas exposure. The schematic block diagram of gas sensing setup is shown in Fig. 4.

The resistance variation is measured by Keithley unit as shown. The chemiresistor-type sensor is mounted on hot plate (filament heater) which is coupled with ceramic base stand. The two leads of thin copper wires are attached to interdigited electrodes by silver paste for electrical connections. The electrical connections for gas sensing measurements, thermocouple and temperature variation are made using instrumentation feed through. The response of sensor is monitored in terms of the normalized resistance calculated by response = R_0/R_g and the sensitivity factor is monitored in terms of % sensitivity = $\partial R/R_0$. Where ∂R is the variation in resistance of sensing materials after exposure to gas, R_g is the resistance of the sensor in presence of gas and R_0 is the initial resistance with gas.

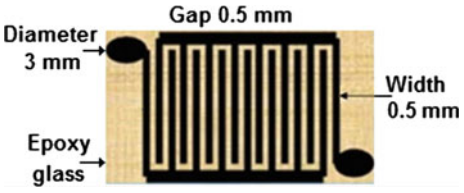

Fig. 2 Schematic diagram of IDE configuration on epoxy glass substrate

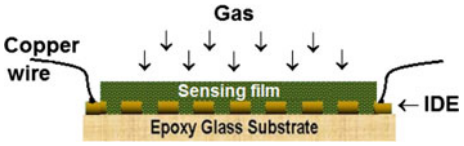

Fig. 3 Schematic representation of a chemiresistor-type gas sensing

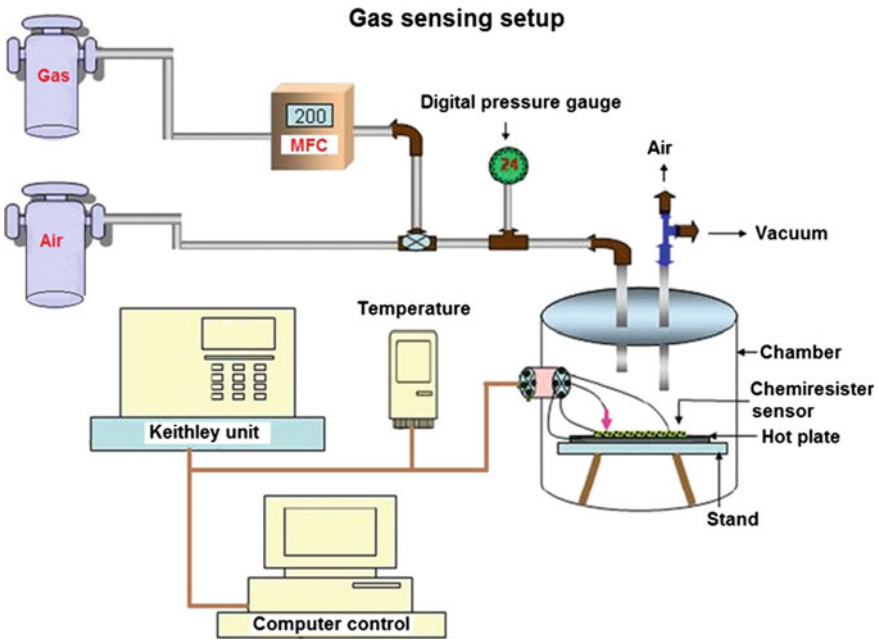

Fig. 4 Schematic block diagram of gas sensing setup

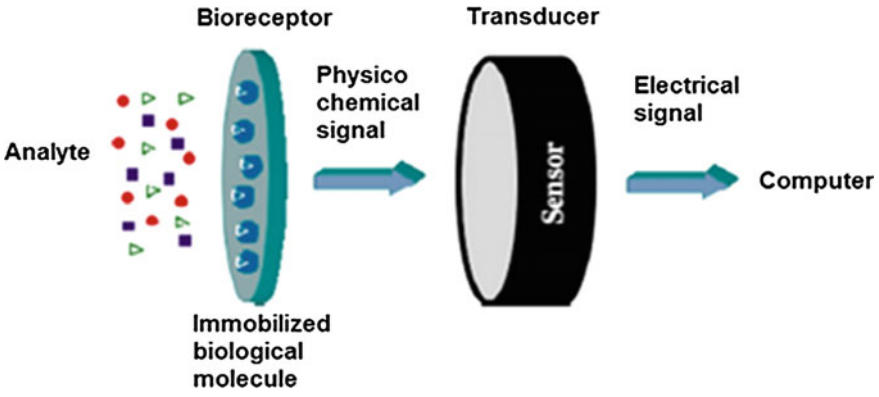

Fig. 5 Schematic of a biosensor

Biosensors have proved to be promising devices used in many areas of health care, food safety, environmental monitoring, and diagnosing disease [7]. A biosensor is a device composed of two intimately associated elements as shown in Fig. 5.

A biosensor consists of bioreactor and transducer. Bioreceptor is an immobilized sensitive biological element that recognizes the presence of an analyte. Transducer converts the interaction of the analyte with the bioreceptor into electrical signal. The

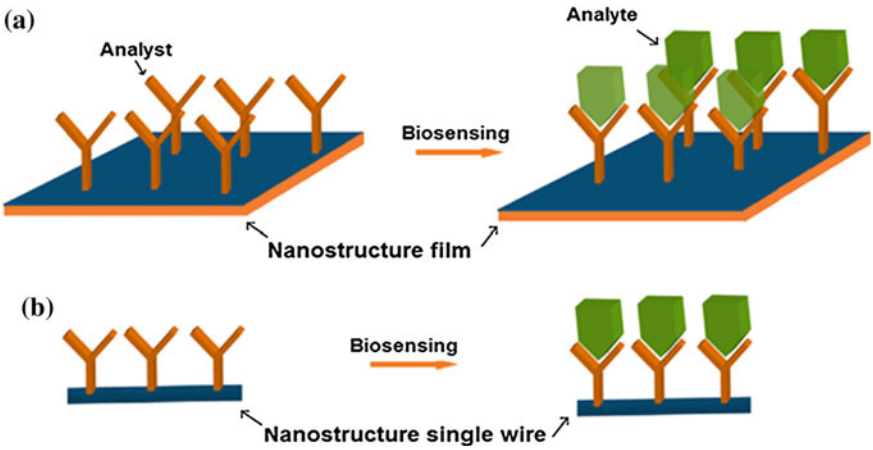

Fig. 6 Schematic of the application of **a** nanostructure film and **b** nanostructure single wire in biosensing

electrical signal is proportional to the analyte concentration. Biosensors can be based on gravimetric, calorimetric or optical detection. A numerous biosensors have been developed for determining various substances such as glucose, cholesterol or lactic in biological fluids (blood, serum, urine), toxicity analysis in environmental monitoring, food, and quality control and in the biomedical and drug sensing [8]. A biosensor couples an immobilized bio-specific recognition which then converts into a measurable electrical signal, pinpointing the presence of the target analyte [9]. Schematic of the application of different nanostructure film and wire in bio-sensing is shown in Fig. 6a and b respectively, for film and wire at nanoscale. The sensitivity of biosensor enhances due to high contact area between analysts and nanostructures of film or single wire.

Conducting polymer-based sensors have now been replacing nanostructure conducting polymer-based sensors due to the ability of having more surface area for adsorption of analytes. Conducting polymer nanostructures in the form of nanotubes, nanowires, and nanoparticles offer enhancement in the sensitivity of biosensor and provide sensing platforms for biological and environmental applications. Nanostructure conducting polymers are being widely used in the field of biological sensing, and have already made a major impact on the field of biosensors. Conducting polymer nanocomposites are functional advanced materials now replacing conducting polymer nanostructure in biosensors due to synergistic effect of two individual components with high conductivity and fine structure at nanoscale. Conducting polymer nanocomposites-based biosensors have shown improvement in sensitivity, selectivity, and reversibility. With the recent development in nanoscience and nanotechnology, conducting polymer nanocomposites have received an increasing attention for their potential applications in the field of sensors/biosensors.

2 Conducting Polymers

Saturated polymers are basically insulators, because all of the four valance electrons of carbon are used up in covalent bonds. But in some of the polymers, the electronic configuration is fundamentally different. Such polymers are called as conjugated polymers. In conjugated polymers, the unpaired electrons (π-electrons) per carbon atom lead to electron delocalization along the backbone of the polymers providing high charge mobility. Such polymer can exhibit semiconducting or even metallic properties due to chain symmetry decided by number of atoms and kind of atoms within the repeat units of the polymers. These conjugated polymers are called as conducting polymers because they show semiconducting nature with electrical conductivity as those of conductors. Conjugated polymers can become conducting only by the process of doping. The electrical properties of the conducting polymers can be fine-tuned using the methods of organic synthesis and by advanced dispersion techniques [10]. Although conducting polymers possess a relatively large number of delocalized π-bonded electrons, the energy band gap between the valence band and conduction band is greater than 1 eV. Therefore, conducting polymers are considered to be semiconducting materials with high electrical conductivity as that of metals. Heeger [11, 12], Alan G. MacDiarmid and Hideki Shirakawa were awarded the Nobel Prize in Chemistry in 2000 for the discovery of first conducting polymer (polyacetylene). Such conducting polymers must be doped by altering the number of π-electrons to produce the truly conducting polymers [13]. Conducting polymers are designated as the fourth generation of polymeric materials. The mechanism of conductivity in conducting polymer is based on the motion of charged defects within the conjugated framework. The charge carriers either positive or negative type in truly conducting polymers are due to oxidizing or reducing the polymer. The conductivity of these polymers varies as a function of charge incorporated in the polymer and for charges up to 20 % by weight of the polymers. The concentration of the charges (metallic powders) cannot be increased beyond this limit because then the charged polymers lose the mechanical properties of the host polymer and become less useful. By adjusting the level of doping, conductivity of the conducting polymers can be tuned between insulating to highly conducting form. Conducting polymers have the backbone of delocalized π-system in the doped state and conjugated backbone in the undoped state.

Doping with acceptor molecules causes a partial oxidation (p-doping) and with donor molecules causes a partial reduction (n-doping) of the polymer molecule. Thus, positively or negatively charged quasi-particles are created known as polarons. Due to continued doping, a pair of charged solitons is formed by the reaction of polarons called as bipolarons. Conducting polymers and their derivates as shown in Fig. 7, undergo redox doping by chemical or electrochemical processes during which the number of electrons associated with the polymer backbone changes. There are different types of redox doping of a conducting polymer. In chemical and electrochemical p-doping (partial oxidation of the backbone π-system) as well as chemical and electrochemical n-doping (partial reduction of

the backbone π-system), dopant ions are introduced which stabilize the charge on the polymer backbone by creating quasi-particles such as solitons, polarons, and bipolarons. In other types of doping in which dopant ions are not involved and these doping processes are called photo doping and charge injection doping in which transitory-doped species are produced such as solitons, polarons, and bipolarons which have similar spectroscopic signatures to polymers containing dopant ions [14].

On the other hand, the number of electrons associated with the polymer backbone does not change during non-redox doping process. The emeraldine base form of polyaniline was the first example of the non-redox doping. Highly conductive emeraldine salt form of polyaniline can be produced by treating emeraldine base with aqueous protonic acids as shown in Fig. 8.

In π-conjugated polymers with degenerate ground states, solitons are the important and dominant charge storage species. Polyacetylene, $(CH)_x$, is the only known polymer with a degenerate ground state due to its access to two possible configurations differing from each other by the position of carbon–carbon single and double bonds. While polyacetylene can exist in two isomeric forms: *cis* and

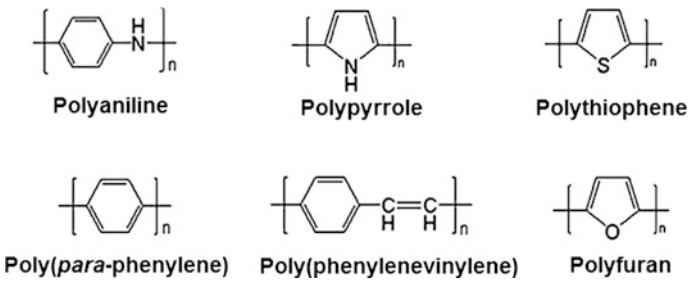

Fig. 7 Conducting polymers and their derivatives undergo redox doping

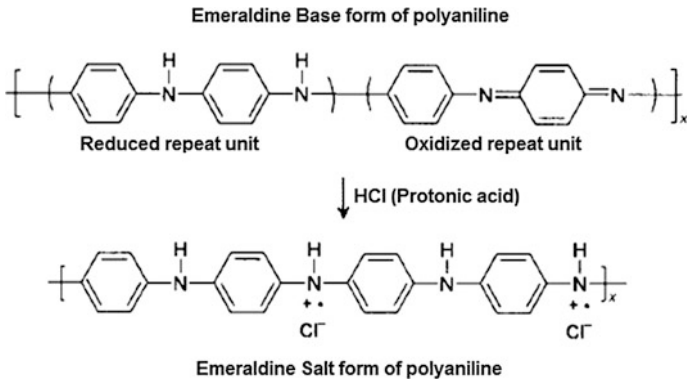

Fig. 8 Polyaniline (emeraldine) base is protonated in acidic medium to polyaniline (emeraldine) salt

trans polyacetylene, the *trans* acetylene form is thermodynamically more stable and the *cis–trans* isomerization is irreversible. In π-conjugated polymers with non-degenerate ground states such as poly(pyrrole), poly(thiophene), and poly (aniline), solitons as charge storage species do not support because the ground state energy of the quinoid form is substantially higher than the aromatic benzenoid structure. As a result, the charge defects on these polymers are different.

Conducting polymers are usually synthesized via oxidative coupling of monomers. For polymerization, the first step is the oxidation of the monomer, which results in the formation of a radical cation, which then reacts with another monomer or radical cation, forming a dimer. Hence, an obvious classification is the initiation process of polymerization. The three general initiation routes are chemical, electrochemical, and photo-induced polymerization, each having its own advantages and disadvantages. In chemical polymerization, chemical oxidants (such as ferric chloride or ammonium persulfate) are applied to oxidize the monomer. The morphology of the polymer synthesized by chemical route can be controlled by varying the parameters of the process such as monomer/oxidant concentration, temperature, pH, and reaction time. In electrochemical polymerization, an oxidant is not required, the monomers are oxidized electrochemically and conducting polymer deposited on the substrate. A high potential may lead to over oxidation of the polymer. In photo-induced polymerization, light is required to oxidize the monomer with a photoinitiator. Photo-induced route is designed to solve the over oxidation problem as of electrochemical process. This process can be controlled simply by light illumination.

3 Nanostructure Conducting Polymers

Conducting polymer nanostructures possess very large surface area and porous structure, due to which sensors based on such materials show very fast response to analyte. Conducting polymers can be synthesized in various sizes and morphologies, with a useful distinction to be drawn between bulk and nanostructure conducting polymer. The bulk, granular conducting polymer can be easily obtained through conventional processing methods, namely by dissolving the monomer in a strong acid and then polymerizing it through the addition of oxidant. Nanostructure conducting polymers can be prepared by physical approaches like electrospinning, chemical routes like hard physical template-guided synthesis and soft chemical template synthesis (e.g., interfacial polymerization, template-free method, dilute polymerization, reverse emulsion polymerization, etc.) and a variety of lithography techniques [15]. The actual synthesis of nanostructure conducting polymers is another issue currently limiting their application in sensors. Several novel synthesis approaches target to precisely control the nanostructures of conducting polymers have been studied. Electrospinning is an effective approach to fabricate nanofibers from polymers [16, 17].

3.1 Hard Template Synthesis

This is a powerful and controllable method to synthesize the nanostructure materials of inorganic semiconductors, metals, and polymers. In the hard template method, the growth of the nanostructures takes place within the pores or channel of template membrane by polymerization and then the template is removed after the polymerization. The porous membrane is the basic and most important part of the hard template method. Porous membrane such as polycarbonate and alumina can be used as the hard template to produce conducting polymer nanotubes and nanowires as shown in Fig. 9.

Nanofibers of various insulating polymer, metal, and inorganic semiconductor as prepared by electrospinning can be used as hard template to produce conducting polymer nanotubes. Nucleation and growth of conducting polymers take place on nanofiber templates during the polymerization process and then the nanofibers were dissolved or depolymerized to obtain the desired conducting polymer nanotubes as shown in Fig. 10.

Colloidal particles as the hard template can be used to produce conducting polymer nanoporous membranes. The monomers of conducting polymers are polymerized in the voids between colloidal particles. When colloidal particles were removed, a three-dimensional conducting polymer porous structure will be obtained as shown in Fig. 11.

Though the hard template method is most efficient approach for preparing well controlled and highly oriented nanostructures of conducting polymers, the removal of template is very difficult [18].

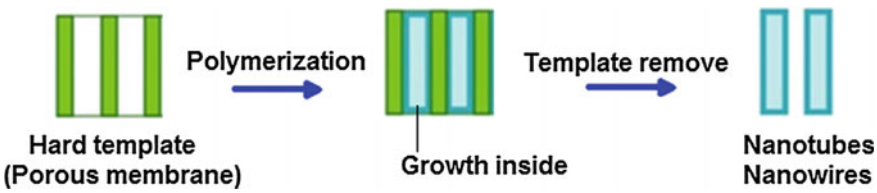

Fig. 9 Hard template synthesis for nanotubes and nanowires using porous membrane

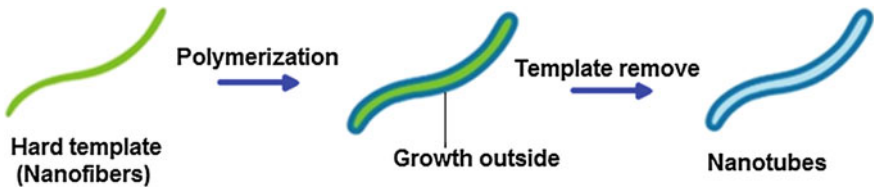

Fig. 10 Hard template synthesis for nanotubes using nanofibers as template

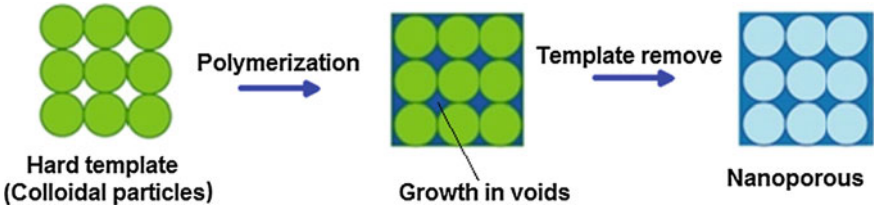

Fig. 11 Hard template synthesis for nanoporous using colloidal particles as template

3.2 Soft Template Synthesis

In order to circumvent the draw backs of the hard template method, the development of synthesis of conducting polymer nanostructure can be studied using a soft template method since it is a template-free or self-assembly method. Surfactants, colloidal particles, structure-directing molecules, oligomers, soap bubbles, and colloids as soft templates have been employed to synthesize conducting polymer nanostructures. Surfactant is a class of molecules that form thermodynamically stable aggregates of inherently nanoscale dimensions both in solution and at interfaces. The self-assembly ability of surfactants in a bulk solution creates the possibility of surfactant micelles serving as soft templates to form conducting polymer nanostructures. The mechanism of the soft-template synthesis of different conducting polymer nanostructures is shown in Fig. 12. When micelles acted as soft templates are formed by the self-assembly of dopants, and the polymerization is carried out on the surface of the micelles, the nanotubes of conducting polymers can be formed. When the polymerization is carried out inside the micelles, nanowires of conducting polymers can be formed by the protection of dopants. When monomer droplets acted as soft templates, nanosphere of conducting polymers can be formed.

Micelles are formed with the head groups floating in water, whereas tail group filling the cavity along with the organic liquid inside. Reverse is the case for inverse micelles. The most widely used surfactant to form reverse micelles is sodium bis (2-ethylhexyl) sulfosuccinate (AOT), which is an anionic surfactant with two hydrophobic tail groups. AOT molecules favorably form reverse micelles in the oil phase because of their bulky hydrophobic tail groups compared with the hydrophilic head groups. Several research groups have reported the chemical polymerization of conducting polymer nanostructures in the presence of AOT. Polypyrrole nanotubes with diameter 94 nm were synthesized by using AOT reverse cylindrical micelles as the soft templates [19, 20]. Soft template method is the simplest approach to fabricating conducting polymer nanostructures because it eliminates the post process of removal of the template as like in hard template method. Li et al. [21] developed a novel electrochemical soft template method to synthesize conducting polypyrrole nanofiber arrays. Ramanathan et al. [22] employed this technique to prepare conducting polymer nanowires.

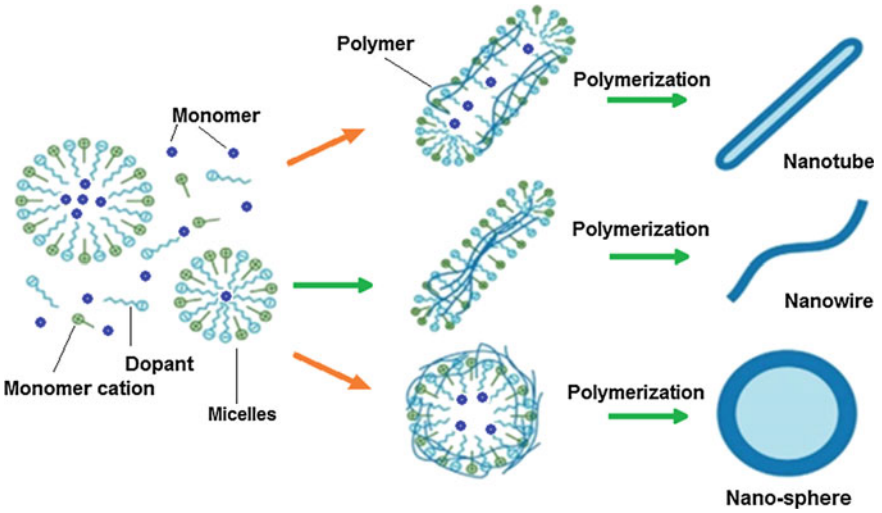

Fig. 12 Mechanism of the soft template synthesis of conducting polymer nanostructures

3.3 Electrospinning Method

Apart from hard and soft template methods, electrospinning is an effective approach to fabricate long polymer fibers with diameter from micrometers down to 100 nm or even a few nanometers by using strong electrostatic forces. Electrospinning is a simple and versatile technique for generating nanofibers of conducting polymer which are good candidates for sensor applications because of their large specific surface area and large aspect ratio. In electrospinning process, polymer solution is extruded from the tip of the needle of syringe to form a small droplet in the presence of strong electric field, and then the charged solution jets are extruded from the cone. The jet undergoes an instability and elongation process, which allows the jet to become very long and thin. The solvent evaporates, leaving behind a charged polymer fibers collected on grounded collector. The schematic of electrospinning process is shown in Fig. 13.

By using steady collector, randomly oriented polymer nanofibers can be fabricated. If rotating cylindrical collector is used instead of steady collector, aligned polymer nanofibers in proper direction can be obtained. Compared with other synthetic approaches, the electrospinning process seems to be the only method which is useful for mass production of polymer nanofibers. Though, electrospinning technique is very useful for the fabrication of polymer nanofibers, but unfortunately most of the conducting polymers pose low solubility problems, making them difficult to electrospun in diameters smaller than 100 nm. This can be overcome by utilizing a polymer blend and composites. Nanofibers of polyaniline [23] and polypyrrole [24, 25], poly(3-hexyl-thiophene)/PEO [26], polyaniline/PEO/carbon nanotubes [27], and polyaniline/ZnO [28] have been prepared by this technique.

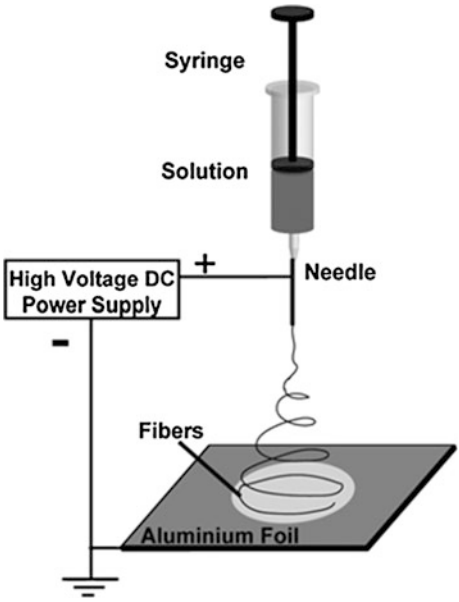

Fig. 13 Schematic of electrospinning process

Electrospun conducting polymer nanofibers have been studied for the possibility of developing attractive sensors whose electrical properties change upon interaction with the analytes. An early study at this field was the work of MacDiarmid et al. [29], who studied electrospun polyaniline-based chemical transducers with submicron dimensions. Chemical sensing of NH_3 with PMMA coaxial nanofibers was also reported in the studies of Dong et al. [30] and Huang et al. [31]. Further, PANI nanowires oriented by electrospinning were deposited on gold electrodes [32]. Nanofibers of conducting polymers were found to have superior performance relative to conventional materials because of their much greater exposed surface area. The sensitivity of the sensor film made of conducting polymer nanofibers does not depend on thickness of the film. Using the electrospinning technique, Aussawasathiena and coworkers prepared lithium perchlorate ($LiClO_4$)-doped PEO electrospun nanofibers for humidity sensing and camphosulfonic acid (HCSA)-doped PANI/PS electrospun nanofibers for sensing hydrogen peroxide (H_2O_2) and glucose [33–35]. Pinto and coworkers prepared electrospun nanowires of PANI with tunable conductivity and used them in the fabrication of gas sensors [36, 37]. Coaxial PMMA/PANI composite nanofibers have also been fabricated using the electrospinning technique and an in situ polymerization method and were then transferred to the surface of a gold interdigitated electrode to construct a gas sensor [38]. It was found that these nanofibers exhibited a high sensing magnitude toward triethylamine (TEA) vapors in the range 200–500 ppm. Use of nanostructure conducting polymers in biosensors allows the use of many new signal transduction technologies in their manufacture [39–44]. Nanoparticles, nanowires, and nanotubes have already made an impact on the field of electrochemical biosensors, ranging from glucose enzyme electrodes to

genoelectronic sensors. As conducting polymer nanomaterials are light weight, have large surface area, adjustable transport properties, chemical specificities, low cost, easy processing, and scalable productions, they are used for applications in nano-electric devices, chemical, and biological sensors [45].

4 Conducting Polymer Nanocomposites

A composite is a structural material which consists of combining two or more constituents. Composite is more efficient, possesses the advantages of the constituents and has improved strength, stiffness, thermal conductivity, corrosion resistance, etc. In the constituents, one of them is called reinforcing phase and the other in which it is embedded is called matrix phase. Composites are classified by the geometry of the reinforcement—particulate, flake, and fiber or by the types of matrix—polymer, metal, ceramic. In a composite even if one of the constituents is in nanosize then it is called as nanocomposite. If the nanosize particulate/flake/fiber is reinforced with the polymer matrix, it is called as polymer nanocomposites. If the polymer is conducting, it is called as conducting polymer nanocomposites. Conducting polymer binary nanocomposite is a structural material which consists of combining two constituents with one of them reinforcing phase (nanosize particulate/flake/fiber) and the other, in which reinforcing phase is embedded, conducting polymer matrix phase. Conducting polymer ternary nanocomposite is a structural material which consists of combining three constituents with two of them reinforcing phase (nanosize particulate/flake/fibre) embedded in conducting polymer matrix phase.

Nanocomposites can be of zero-dimensional, one-dimensional, two-dimensional, and three-dimensional [46]. Nanocomposites belong to special class of materials originating from suitable combinations of two or more nanosize components. Such materials have unique physico-chemical properties and wide potential applications [47, 48]. Mostly nanocomposites consist of one or more discontinuous phases of distributed in one continuous phase. Discontinuous phase is usually harder and with superior mechanical properties than continuous phase [49]. The continuous phase is called “matrix” and discontinuous phase is called “reinforcement.” The properties of nanocomposites materials depend on the properties of their individual components as well as their morphology [50].

Conducting polymer nanocomposites consist of a conducting polymer or copolymer having nanofillers in the form of particulate (0D) or fiber (1D) or flake (2D) dispersed in the conducting polymer matrix. These may be of different shape, but at least one dimension must be in the nanoscale. Nanocomposites of conducting polymers have been prepared by various methods such as colloidal dispersions, electrochemical encapsulation, coating of inorganic polymers, in situ polymerization with nanoparticles and have opened new avenues for material synthesis.

Conducting polymers have been composited with any one of these materials constituting binary nanocomposites and any two of these materials constituting ternary nanocomposites with which the sensing performances of such advanced functional and hybrid materials have been improved by the synergistic effects especially for sensor applications.

4.1 Synthesis of Conducting Polymer Nanocomposites

The properties of the conducting polymer nanocomposites depend on the their structure determined by the interfacial adhesion between conducting polymers and the secondary component as well as the aspect ratio. Therefore, the synthetic strategies for the preparation of conducting polymer nanocomposites are of great importance. A correct selection of the preparation techniques is critical to obtain nanocomposites with suitable properties. The top-down and bottom-up approaches can also be applied for the synthesis of polymer nanocomposites. Direct mixing of nanofiller into polymer matrix in solution for the preparation of polymer nanocomposites is a top-down approach as shown in Fig. 14, in which layered silicate is mixed with polymer. The in situ polymerization of monomer in the presence nanoparticles previously prepared or the in situ polymerization of monomer in the presence of precursor nanoparticles as shown in Fig. 15 are bottom-up approaches.

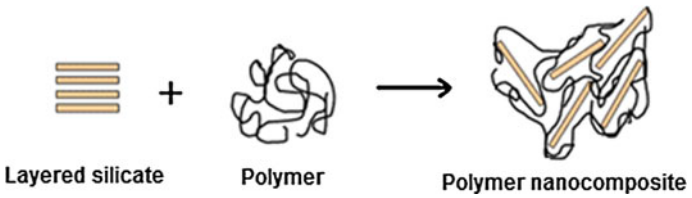

Fig. 14 *Top-down* approach for polymer nanocomposites

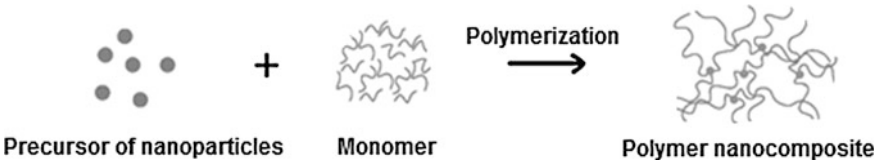

Fig. 15 *Bottom-up* approach for polymer nanocomposites

4.2 Particulate (0D)-Reinforced Nanocomposites

In conducting polymer nanocomposites, particulate refers to nanoparticles which are zero-dimensional (0D) nanomaterials in the matrix of conducting polymer. The examples of zero-dimensional nanomaterials are quantum dots, nanoparticles of metals, metal oxides, etc. Inorganic nanoparticles can be introduced into the matrix of a host-conducting polymer either by some suitable chemical route or by an electrochemical incorporation technique. Inorganic materials used for this purpose are generally of two types: nanoparticles and some nanostructure materials or templates. Depending upon the nature of association between the inorganic and organic components, nanocomposites are also classified into two categories: one in which the inorganic particle is embedded in organic matrix and the other where organic polymer is confined into inorganic template. However, in each case the composite formation demands some entrapment or encapsulation rather than simple blending or mixing.

Let us consider an example of preparation of polyaniline/nickel ferrite nanocomposites (PANI/$NiFe_2O_4$) prepared by an in situ polymerization of aniline (monomer) using ammonium persulphate (APS) as an oxidant in the presence of as-synthesized $NiFe_2O_4$ nanoparticles by reflux method at room temperature [51]. In a typical process, aniline (0.1 M) and APS (0.1 M) were dissolved separately in 1 M H_2SO_4 solution and stirred. As-synthesized $NiFe_2O_4$ nanoparticles were suspended separately in 1 M H_2SO_4 solution and sonicated to reduce aggregation of $NiFe_2O_4$ nanoparticles. Aniline solution and $NiFe_2O_4$ nanoparticles suspension were mixed and further sonicated. APS solution was then slowly added drop wise to well-dispersed suspension mixture with a continuous stirring. In this way conductive emeraldine salt (ES) form of PANI/$NiFe_2O_4$ nanocomposites was prepared. The schematic representation of formation of PANI/$NiFe_2O_4$ nanocomposites is shown in Fig. 16.

Kondawar et al. [52] compared two different ways to prepare polyaniline-tin oxide (PANI/SnO_2) nanocomposites. Sample A prepared by the usual in situ polymerization of aniline in the presence of as-synthesized SnO_2 nanoparticles, wherein sol–gel method was used for the synthesis of SnO_2 nanoparticles. Tin oxide-intercalated polyaniline nanocomposite (sample B) prepared using tin chloride ($SnCl_4{\cdot}5H_2O$) as precursor during polymerization of aniline. In this technique, formation of nanocomposite proceeds through an inorganic/organic interface reaction. The pH of $SnCl_4{\cdot}5H_2O$ solution was maintained less than 4 using HCl. Hydrogen peroxide (H_2O_2) was added to oxidize tin ions to tin oxide. When the solution turned into a white color suspension of SnO_2, aniline was added. For polymerization, ammonium persulphate was added and the color of the solution was turned to blue and then to green. In this way the conductive emeraldine salt (ES) form of PANI/SnO_2 nanocomposite (sample B) was obtained. PANI/SnO_2 nanocomposites were found to be good materials for ammonia sensing as compared to that of pure PANI. Ammonia sensing characteristics of these PANI/SnO_2 nanocomposites synthesized by different routes are explained in Sect. 5.

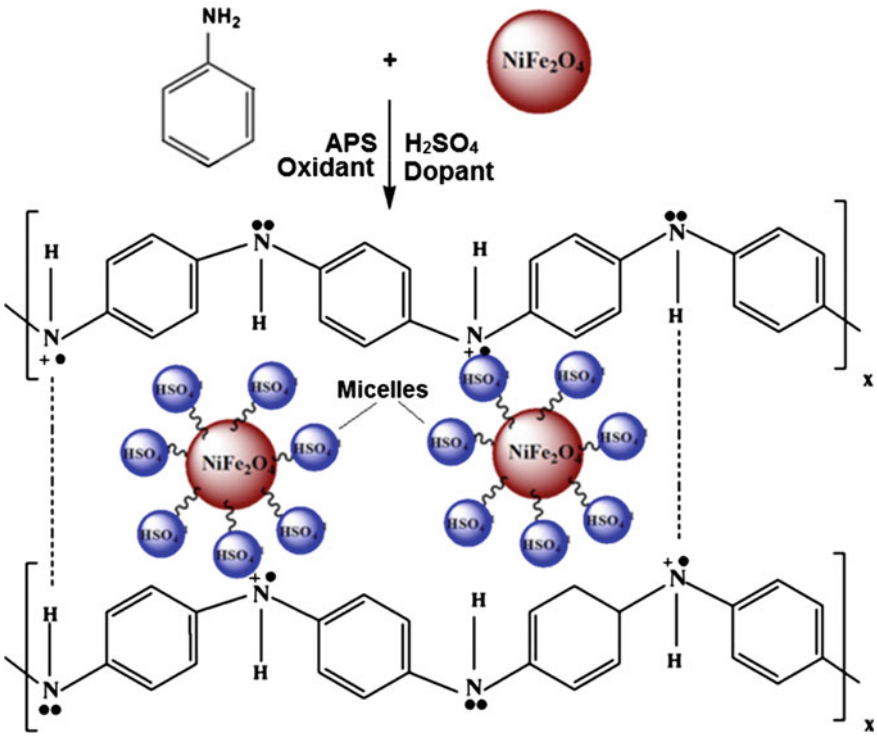

Fig. 16 Schematic of preparation and charge compensation of PANI–$NiFe_2O_4$ nanocomposite

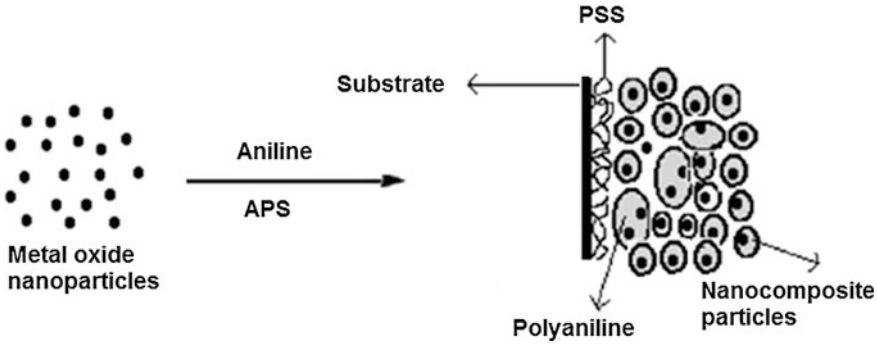

Fig. 17 PANI-nanocomposite film fabrication by in situ self-assembled process

Ram et al. [53] studied CO gas sensing from ultrathin nanocomposite conducting polymer film. They have prepared PANI–SnO_2 and PANI–TiO_2 nanocomposite films deposited on sulfonated polystyrene (PSS)-treated glass plate. Figure 17 shows the schematic of nanocomposite deposition of PANI–SnO_2 and PANI–TiO_2 films.

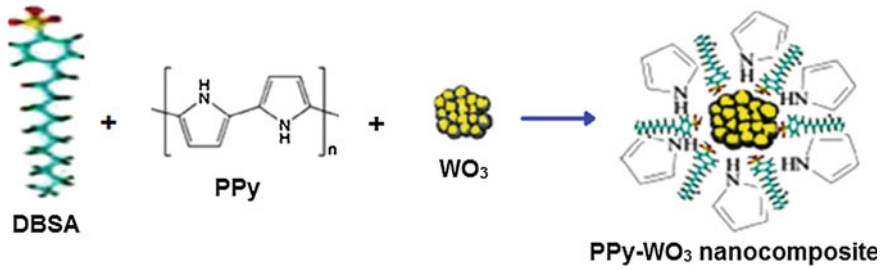

Fig. 18 Schematic of DBSA doped PPy–WO_3 hybrid nanocomposite film

Fig. 19 Schematic illustration of the processes involved to prepare nanofibers of PANI/Al–SnO_2 composites

DBSA doped PPy–WO_3 nanocomposites could be prepared by adding DBSA into PPy–WO_3 nanocomposites matrix by solid state synthesis method and studied for room temperature NO_2 gas sensing properties [54]. The prepared DBSA doped PPy–WO_3 hybrid nanocomposites powder was dissolved in m-cresol solvent and stirred at room temperature to get DBSA doped PPy–WO_3 casting solution. In order to prepare the films, the casting solution was deposited on glass substrate using drop casting method and dried at room temperature. Figure 18 shows schematic representation of formation of DBSA doped PPy–WO_3 hybrid nanocomposite film.

Nanofibers of semiconducting metal oxides have been widely utilized for applications in gas sensors due to high surface reaction between the metal oxides and adsorbed gas species but require the high operating temperature (200–400 °C). The conducting polymers have improved many aspects of the gas sensors especially in lowering the operating temperature to around room temperature. In addition to this, the ability to incorporate specific binding sites into conducting polymer promises it for the improvement of selectivity and sensitivity of material. Sharma et al. [55] reported the fabrication of electrospun SnO_2/polyaniline composite nanofibers using electrospinning technique for hydrogen gas sensing application. In a typical procedure, $SnCl_2 \cdot 2H_2O$ and CSA-doped PANI were dissolved in a solution mixture of DMF and ethanol under vigorous stirring. Subsequently, PVP was added to form a desired viscous solution. Then the solution was loaded into a glass syringe for electrospinning process. Nanofibers of SnO_2/polyaniline composite were collected

on aluminum foil wrapped on rotating collector. Nanofibers were then calcinated to remove the organic constituents of PVP and crystallize the SnO_2.

Kondawar and coworkers [56] fabricated electrospun nanofibers of conducting polyaniline/Al–SnO_2 composites for hydrogen sensing applications. Schematic illustration of the processes involved to prepare nanofibers of PANI/Al–SnO_2 composites is shown in Fig. 19. In a typical procedure for the synthesis of nanofibers of polyaniline/Al–SnO_2 composites, 1 % Al $(NO_3)_3 \cdot 9H_2O$ was added in the solution of $SnCl_2 \cdot 2H_2O$ and CSA-doped polyaniline before loading into syringe for electrospinning. Nanofibers of Al-doped SnO_2/polyaniline composite were collected on aluminum foil wrapped on rotating collector. Nanofibers were then calcinated to remove the organic constituents of PVP and crystallize Al–SnO_2. Hydrogen gas sensing characteristics of these nanocomposites are explained in Sect. 5.

4.3 Fiber (1D)-Reinforced Nanocomposites

Fibers are one-dimensional (1D) materials. Nanotubes, nanorods, nanowires, and nanofibers are examples of one-dimensional nanomaterials which possess very large aspect ratio apart from their surface-area-to-volume ratio, due to which such materials have high charge transfer rate along one direction. Hence fiber-reinforced conducting polymer nanocomposites can show better properties performance compared to other types of nanocomposites. Here, we report the preparation of carbon nanotubes (CNT)-reinforced conducting polymer nanocomposites due to one-dimensional characteristics of CNT. A carbon nanotube is a tubular structure made of carbon atoms, having diameter of nanometer order but length in micrometers. Due to its excellent mechanical characteristics, nanometer size, good electrical conductivity, and extremely accessible surface area, CNT can be used for the preparation of the multifunctional nanocomposites with outstanding mechanical and electronic properties. CNTs can be divided into two main categories: single-walled carbon nanotubes (SWNTs) and multiwalled carbon nanotubes (MWNTs). The first are formed by a single graphene sheet. The latter are formed by additional graphene sheets wrapped around the SWNT core. Many efforts have been made to combine CNTs and polymers to produce functional composite materials with superior properties. Composite materials based on the coupling of conducting polymers (CPs) and CNTs have shown that they possess properties of the individual components with a synergistic effect. The combination of CNTs with CPs offers an attractive route to reinforce the polymer as well as to introduce electronic properties based on morphological modification or electronic interaction between the two components. In CPs–CNTs composites, it has been suggested that either the polymer functionalizes the CNTs or the CPs are doped with CNTs, i.e., a charge transfer occurs between the two constituents. The main functionalization possibilities of CNTs reported until now are: (a) generation and functionalization of defect sites at the tube ends and side walls by oxidation and subsequent conversion

into derivatives; (b) covalent side wall functionalization using addition reactions and subsequent nucleophilic substitution; and (c) non-covalent exohedral functionalization with surfactant-type molecules. These are represented in Fig. 20.

Taking into account these functionalization types, three routes have been used to prepare CPs/CNs composites: (i) direct mixing of the CP with CNTs, (ii) chemical polymerization of the corresponding monomer in the presence of CNTs and (iii) electrochemical synthesis of CP on CNTs electrode. All these three routes are supposed to give similar compounds.

Carbon nanotubes (MWCNT or SWCNT) can be easily prepared by chemical vapor deposition (CVD) method. In this method, hydrocarbon (CNT precursor) vapor is allowed to pass through a tubular reactor in which a catalyst material is present at sufficiently high temperature (600–1200 °C) to decompose the hydrocarbon. CNTs grow on the catalyst in the reactor, which are collected upon cooling the system to room temperature. The growth of CNTs on the substrate can be of two types as shown in Fig. 21.

When the catalyst–substrate interaction is weak (metal has an acute contact angle with the substrate), hydrocarbon decomposes on the top surface of the metal, carbon diffuses down through the metal, and CNT precipitates out across the metal bottom, pushing the whole metal particle off the substrate. As long as the metal's top is open for fresh hydrocarbon decomposition (concentration gradient exists in the metal allowing carbon diffusion), CNT continues to grow longer and longer. Once the metal is fully covered with excess carbon, its catalytic activity ceases and the CNT

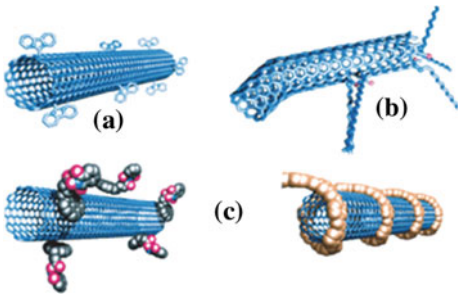

Fig. 20 Several possible functionalization mechanisms for SWNTs

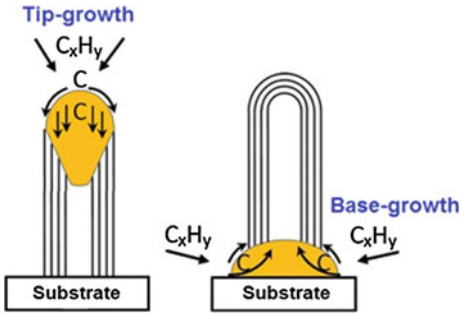

Fig. 21 Schematic diagram of tip-growth and base-growth mechanism

growth is stopped. This is known as tip-growth model. When the catalyst–substrate interaction is strong (metal has an obtuse contact angle with the substrate), initial hydrocarbon decomposition and carbon diffusion take place similar to that in the tip-growth case, but the CNT precipitation fails to push the metal particle up; so the precipitation is compelled to emerge out from the metal's apex (farthest from the substrate, having minimum interaction with the substrate). First, carbon crystallizes out as a hemispherical dome (the most favorable closed-carbon network on a spherical nanoparticle) which then extends up in the form of seamless graphitic cylinder. Subsequent hydrocarbon deposition takes place on the lower peripheral surface of the metal, and as dissolved carbon diffuses upward. Thus CNT grows up with the catalyst particle rooted on its base; this model is called as base-growth model. Formation of single- or multiwall CNT (SWCNT or MWCNT, respectively) is governed by the size of the catalyst particle. When the particle size is a few nm, SWCNT forms, whereas particle size is few tens nm favors the formation of MWCNT.

Kondawar et al. [57], synthesized methane sulfonic acid-doped PANI–MWCNT nanocomposites using in situ oxidative polymerisation. In a typical polymerization procedure, first CNTs mixed with the solution of CH_3SO_3H, de-ionized water and aniline. The resulting mixture was sonicated and stirred. APS as an oxidant was added during stirring. Figure 22 shows the schematic representation of protonated pernigraniline chains of PANI with the basal walls of unoxidised carbon nanotubes. The polymer chains simply wrapped up around CNTs with no strong interaction,

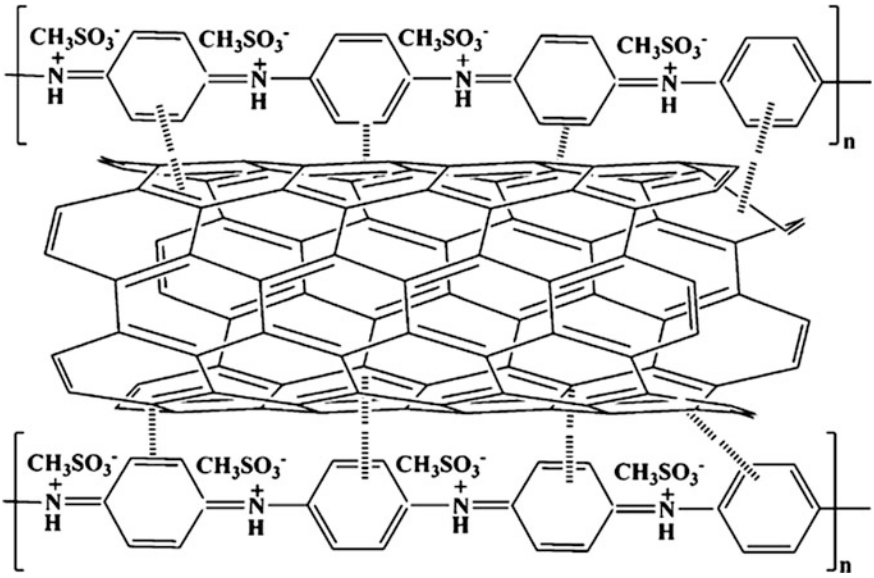

Fig. 22 Schematic of PANI/CNT nanocomposite doped with methane sulfonic acid

thus supporting the considerations related to the polymer chains growing process around the surface of CNTs.

Meshram et al. [58] prepared PPy/c-MWCNT/LOD nanobiocomposite film for lactate biosensor. In a typical process, MWCNTs were functionalized by sonication using 3:1 sulfuric acid/nitric acid mixture. Subsequently, the pretreated MWCNTs were washed with water, then with 0.1 M NaOH (to reach neutrality of pH 7.0), filtered, and dried overnight at 80 °C. The functionalized c-MWCNTs were dispersed in distilled water by sonication. The selected amount of lactate oxidase (LOD) in 0.1 M PBS (pH 7) was then added to the c-MWCNTs solution. In the end, pyrrole was added (at a concentration of 0.5 M) to the LOD-c-MWCNT mixture and this solution was again stirred. Nanobiocomposite film was electrochemically synthesized by electrolyzing this medium on the steel electrode in continuous stirring conditions by sweeping the potential on the working electrode, from −0.8 to +0.8 V versus a standard counter electrode, at room temperature with a scan rate 50 mV/s. PPy/c-MWCNT/LOD film thus obtained was washed repeatedly with double distilled water and then dried at room temperature under vacuum. Figure 23 shows the schematic diagram of electrodepositon of PPy, c-MWCNT and LOD simultaneously on steel electrode. During the electrodeposition the enzyme LOD gets incorporated into the PPy/c-MWCNT matrix. The incorporation of LOD includes the formation of an intermediate ester (the product of condensation of the free –COOH groups of PPy/c-MWCNT/LOD). The active ester intermediate reacts with the amide ($–NH_2$) groups on the surface of enzyme to yield the final amide bond, confirming the enzyme on the surface of PPy/c-MWCNT/LOD nanobiocomposite film.

Mahore et al. [59] prepared ternary nanocomposites of conducting polymer polyaniline/polypyrrole (PANI/PPy) with CNTs and MnO_2 by an in situ chemical oxidation polymerization using $KMnO_4$ oxidizing agent. To prepare PANI/CNT/MnO_2 ternary nanocomposites, monomer aniline 0.75 M was added in aqueous solution containing 0.25 M SDS and then 1 % (w/w) functionalized MWCNTs were suspended in this monomer solution. The solution containing CNTs and monomer was sonicated for 30 min to facilitate proper dispersion of

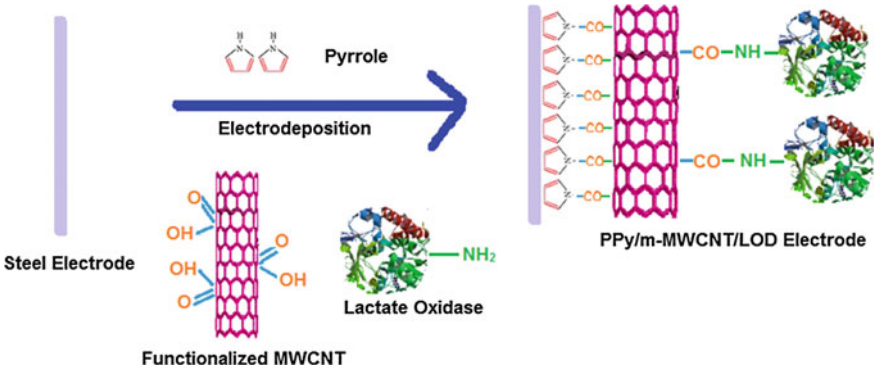

Fig. 23 Schematic diagram of the electrodeposition of PPy/c-MWCNT/LOD lactate biosensor

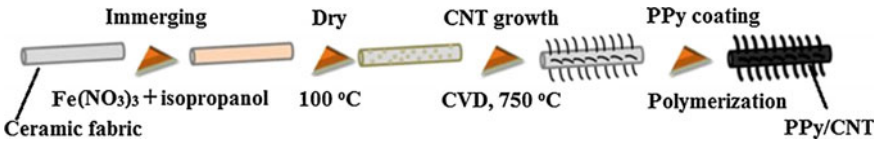

Fig. 24 Fabrication of the PPy–CNTs composite electrode on ceramic paper and fabric

CNTs and for more absorbance of monomer on walls of CNTs so that when oxidant is added drop wise it will provide a better polymerization and growth of polymer on the walls of CNTs. To this solution while stirring, 0.75 M $KMnO_4$ was drop wise added as an oxidant as well as to embed MnO_2 into polymer matrix along with CNTs.

Polypyrrole (PPy)/carbon nanotube (CNT) composite electrodes are fabricated by growing CNT on the ceramic fabrics by the chemical vapor deposition (CVD) method and PPy is subsequently coated on them by chemical polymerization [60]. The procedure used for the preparation of the PPy/CNT composite electrode on the ceramic fabrics is represented in Fig. 24. The CNT-ceramic fabric was prepared by thermal chemical vapor deposition. The unwoven ceramic fabric was used as a substrate for the growth of the CNTs. The original ceramic fabrics contain some polymer binder which was completely removed by dissolution in acetone, dichloromethane, and ethanol under sonication. Then, the ceramic fabric was immersed in 0.5 M Fe $(NO_3)_3 \cdot 6H_2O$ in isopropyl alcohol under sonication and dried. For the growth of the CNTs, the ceramic fabrics containing the Fe precursor were inserted in a quartz tube and then heated up to 750 °C with He flow. After reaching 750 °C, the sample was annealed in a gas mixture of He and H_2. Finally, the prepared the CNT/ceramic fabrics were rapidly cooled down to room temperature with He flow. CNT-ceramic fabric was immersed in 0.5 M pyrrole solution and then in 0.5 M $FeCl_3$ aqueous solution.

4.4 Flake (2D)-Reinforced Nanocomposites

The two-dimensional (2D) materials are flakes. The 2D honeycomb lattice structure of flake with thickness in nano-regime is an example of graphene which exhibited unusual and intriguing physical, chemical, and mechanical properties. Here, we report the preparation of graphene-reinforced conducting polymer nanocomposites. Graphene is an allotrope of carbon. The promising mechanical, electrical, optical, thermal, and magnetic properties of graphene have "led to the creation of a new and exciting "laboratory" for the study of fundamental science." Graphene is a single layer of carbon atoms packed densely in a honeycomb crystal lattice. Direct use of graphene materials is unsuitable for intercalation by polymer chains to produce polymer nanocomposites because graphene has tendency to agglomerate in a polymer matrix. The oxidation followed by chemical functionalization will

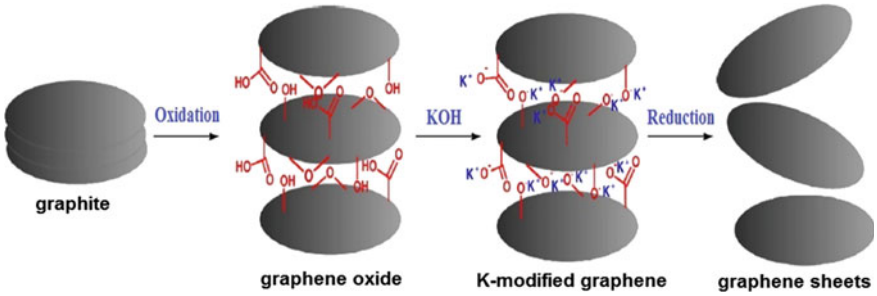

Fig. 25 Preparation of graphene sheets from graphite

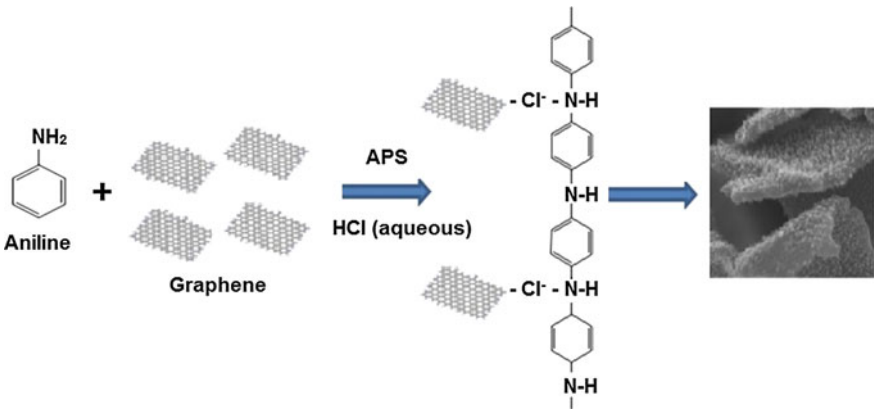

Fig. 26 Schematic of G–PANI nanocomposite synthesis

facilitate the dispersion and stabilize graphene to prevent agglomeration in polymer matrix. Graphene sheets can be prepared from graphite by oxidation and reduction as shown in Fig. 25. KOH confers a large negative charge through reactions with the carboxylic acid groups on the graphene oxide sheets with negative charges and K^+ ions. The addition of hydrazine monohydrate to K-modified graphene oxide produces a homogeneous suspension of graphene sheets.

Bai et al. [61] prepared graphene–polyaniline (G–PANI) nanocomposites by oxidative polymerization of aniline using ammonium peroxydisulfate under controlled conditions in an acidic medium. The schematic of synthesis process is shown in Fig. 26.

4.5 Multicomponents-Reinforced Nanocomposites

To achieve multifunctional materials, two or more than two nanocomponents are sometimes combined with conducting polymers to form nanocomposites. Among

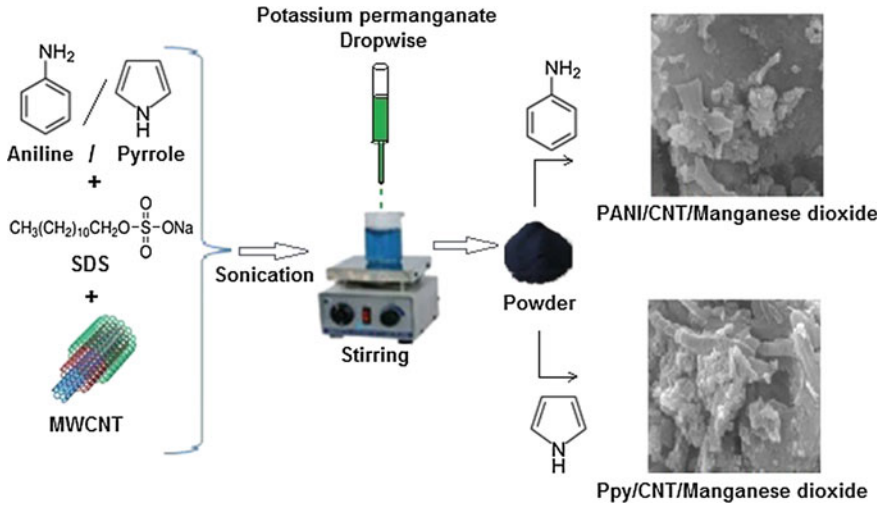

Fig. 27 Schematic illustration of preparation of PANI/CNT/MnO_2 and PPy/CNT/MnO_2 ternary nanocomposites

many kinds of multicomponent nanocomposites, CNTs/conducting polymers coaxial nanocables are often employed for loading other functional nanoparticles. For example, metal and Fe_3O_4 nanoparticles are common functional nanoparticles to combine with CNTs/conducting polymer coaxial nanocables for catalytic or biosensor applications. Lee and coworkers [62] prepared PANI/CNTs/Au nanocomposites through a one-pot synthesis in the presence of γ-irradiation. Reddy and coworkers [63] demonstrated the fabrication of CNT/PPy/Co nanocomposites via a multistep method. Kong and coworkers [64] demonstrated the fabrication of CNT/PANI/Fe_3O_4 composite nanotubes in two steps. Wu et al. [65] prepared CNT/PPy/Fe_3O_4 nanocomposites through a different synthetic strategy. Kondawar and coworkers [66] synthesized conducting polymer polyaniline/polypyrrole (PANI/PPy) with CNTs and MnO_2 nanocomposites using in situ polymerization. A schematic illustration of preparation of polyaniline/CNT/MnO_2 and polypyrrole/CNT/MnO_2 ternary nanocomposites by an in situ chemical oxidation polymerization is shown in Fig. 27.

To prepare PANI/CNT/MnO_2 ternary nanocomposites, monomer aniline 0.75 M was added in aqueous solution containing 0.25 M SDS (sodium dodecyl sulfate) and then 1 % (w/w) functionalized CNTs were suspended in this monomer solution. The solution containing CNTs and monomer was sonicated to facilitate proper dispersion of CNTs and for more absorbance of monomer on walls of CNTs so that when oxidant is added drop wise it will provide a better polymerization and growth of polymer on the walls of CNTs. To this solution while stirring, 0.75 M $KMnO_4$ was drop wise added as an oxidant as well as to embed MnO_2 into polymer matrix along with CNTs. To prepare the ternary nanocomposite PPy/CNT/MnO_2, same

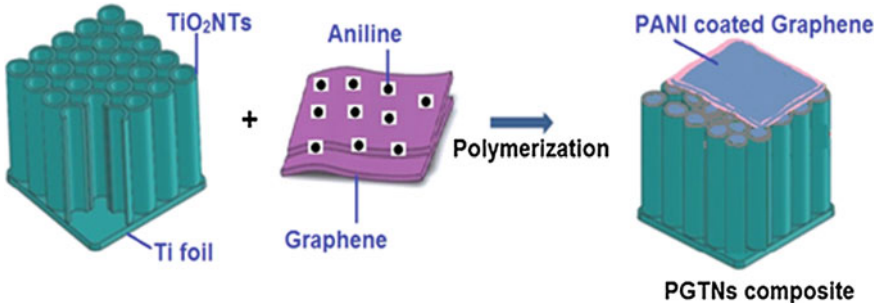

Fig. 28 Schematic illustration of the preparation process of PGTNs

process was adopted using pyrrole as monomer instead of aniline in the same condition to compare their results.

Polyaniline/graphene/titania nanotubes (PGTNs) ternary nanocomposites were fabricated by in situ polymerization [67]. PGTNs possesses a novel three-dimensional (3D) highly ordered hybrid nanostructure consisting of coaxial polyaniline (PANI)/TiO_2 nanotube arrays and graphene coated with PANI on the surface of TiO_2. The titania nanotubes were fabricated on titanium foils via potentiostatic anodization in an electrochemical cell. As-usual functionalised graphene sheets and aniline solution were sonicated and then polymerized in presence of as-prepared titania nanotubes grown on titanium foil was mixed with aniline solution. Figure 28 shows the schematic illustration of the preparation procedures of PGTNs composite.

5 Conducting Polymer Nanocomposites for Sensors/Biosensors

Although conducting polymers are good materials for chemical and biological sensing, their low sensitivity and poor selectivity are limitations and must be improved. By using conducting polymer nanostructures the response time could be significantly faster due to porous structure and large specific surface area of the nanostructure of conducting polymer. Nanofibers thin film of polyaniline (PANI) synthesized by an interfacial polymerization responded much more rapidly than that of conventional PANI thin film [68]. Conducting polymer nanostructures with large specific surface area and porous structure are therefore predicted to be excellent sensing materials. Their sensitivity, selectivity and response time can be further improved by using conducting polymer nanocomposites. Adding a nanocomponent, such as carbon nanotubes, metal, and metal oxide particles, metal salts, insulating polymers, and biological materials, into conducting polymer matrix is one of the best ways to address the above issues because the nanocomponent increases the

chain mobility of conducting polymers or change the affinity of the composite or even act as a catalyst. A large number of new nanocomposites with a synergetic behavior can be obtained with applications for electrochemical sensor and biosensor, because of the interaction between electron donor and acceptor.

5.1 Gas Sensing Application

Semiconducting metal oxide (SMO) nanomaterials have been demonstrated to be high efficient sensors owing to their large surface-to-volume ratio, which can convert the large surface chemical processes into electrical signals. Many metal oxide gas sensors based on SMO nanomaterials including SnO_2, GeO_2, ZnO, WO_3, indium tin oxide (ITO) and TiO_2 have been successfully prepared. Performance of these metal oxide nanostructures could be further enhanced by doping the surface of sensing materials by noble metals (Au, Pt, Pd or Al). Dopant used as a catalyst for improving the selectivity and sensitivity of gas sensors. However, even doped SMO needs high operating temperature (200–500 °C) and high power consumption for gas sensing application. Therefore, much effort has been focused on the development of gas sensors with low power consuming at low operating temperatures by new materials. Accordingly, the use of smart sensors with high sensitivity, fast regeneration, low cost, long-term response, and working ability at room temperature is necessary. The combination of conducting polymer with nanoscale semiconducting metal oxides with or without metal dopant, create p–n heterojunction between p-type polymer and n-type SMOs seems to be a suitable strategy for the improvement of gas sensor efficiency at room temperature.

A simple four-probe laboratory set-up for ammonia sensing is described in Fig. 29. The electrical resistivity of polyaniline-tin oxide (PANI/SnO_2) nanocomposites was

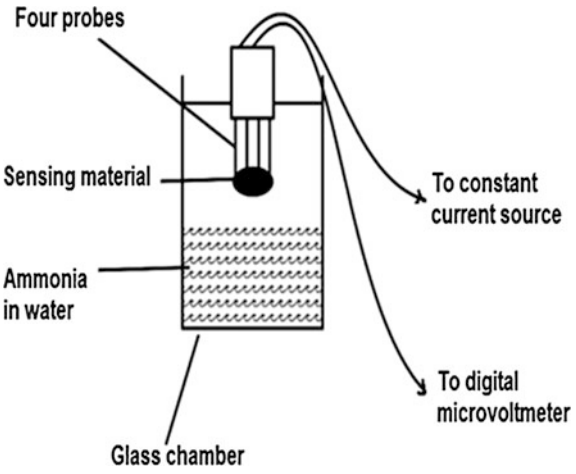

Fig. 29 Four-probe laboratory setup for ammonia sensing

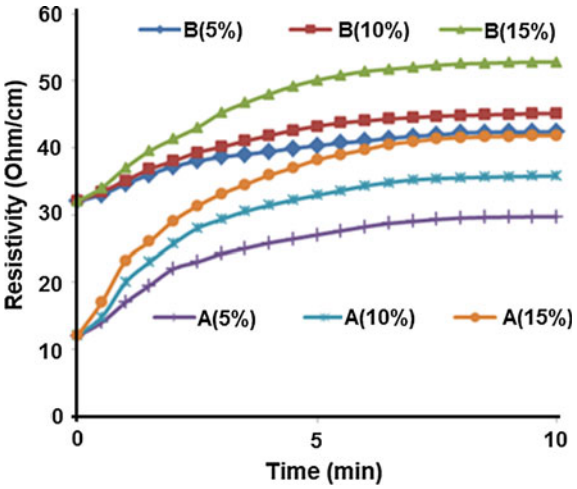

Fig. 30 Resistivity response of PANI/SnO_2 nanocomposites A and B at 5, 10, and 15 % concentration of ammonia

determined as a function of exposing time of the ammonia [52]. The sensing material was placed into the glass chamber and gently pressed by four probe to record the current–voltage. The distance between sensing material and ammonia was kept 3–4 cm at the time of exposure of different concentrations of aqueous ammonia on the sensing material at room temperature. The initial resistivity of sensing material was allowed to stabilize before the addition of ammonia. The sensing material was exposed to ammonia for appropriate time.

The electrical resistivity of PANI/SnO_2 nanocomposites A and B (refer Sect. 4 for their preparation) shows a remarkable change when exposed to different percent (5, 10, 15 %) of aqueous ammonia as shown in Fig. 30.

The sensing mechanism is governed by the protonation/deprotonation phenomena. It shows that resistivity of the material increases when it is exposed to increasing percentage 5, 10 and 15 % of aqueous ammonia. Both the samples A and B show similar response to the ammonia vapor. On high concentration of aqueous ammonia (15 %) the sensing material has shown the fast response. The resistivity of both the composites increases because of the reduction of charge carriers by adsorption of ammonia on the surface of material. The difference between resistivity variations with time for two samples A and B is due their method of preparation. Incorporation of SnO_2 nanoparticles in PANI matrix played a significant role by enhancement in the porosity and the surface activities of sample A as compared to that of sample B. Therefore, conductivity of sample A was found to be more than that of sample B. This result shows that the sensitivity of the sensor depends on the preparative technique of the nanostructure materials used in designing the sensor.

Nanofibers of PANI/ZnO nanocomposites were synthesized by an in situ polymerization and electrospinning for chemical vapor sensing [69]. The resistance of the composite nanofibers was determined as a function of exposing time of the ammonia and HCl vapors. The Cu-interdigited electrode coated by sensing material soldered at two points was placed inside the glass chamber and attached to high

sensitive digital multimeter to record the resistance of the material at different concentration of NH_3 and HCl vapors at room temperature. The resistance of sensing material showed a remarkable change when exposed to different percentages of aqueous ammonia as function of time. Resistance of the material increased when it is exposed to increasing percentage of aqueous ammonia. The resistance of sensor increased because of the reduction of charge carriers by adsorption of ammonia causing de-doping of polyaniline in the composite nanofibers. When these sensors were tested for HCl vapor, the resistance was found to be decreased due to increase in charge carriers by adsorption of HCl caused by the doping of PANI. The sensitivity and response time were found to be improved for nanofibers of PANI/ZnO nanocomposites as compared to that of PANI nanofibers for ammonia as well as HCl vapors. ZnO nanoparticles in PANI matrix played a significant role by enhancement in the porosity and the surface activities of nanofibers of PANI/ZnO as compared to that of PANI.

Ram et al. [53] studied CO gas sensing using PANI–SnO_2 and PANI–TiO_2 nanocomposite films. The change in resistance (ΔR) values obtained for nanocomposite films showed that there is a continuous change in the resistance value in PANI–SnO_2 films indicating that CO does not saturate the films till 1000 ppm exposed for the film. The PANI–TiO_2 showed the saturation after 800 ppm when exposed to CO gas. Mane et al. [54] studied room temperature gas sensing properties of PPy–WO_3 nanocomposite film for various gases NO_2, NH_3, H_2S, C_2H_5OH, and CH_3OH. PPy–WO_3 nanocomposite film showed highest response for NO_2 gas indicating film is more selective toward NO_2 gas.

High-efficiency hydrogen gas sensor based on SnO_2/polyaniline and Al-doped SnO_2/polyaniline composite nanofibers have been demonstrated via electrospinning technique and calcination procedure [55, 56]. The results proved that the gas performances are affected by the dopant, Al present in the host material. Excellent hydrogen sensing properties such as high sensitivity, fast response-recovery behavior, and good selectivity have been obtained. In order to systematically investigate the gas sensing properties of SnO_2/PANI and Al-doped SnO_2/PANI composite nanofibers, the study of gas sensing response with time and sensitivity with temperature was carried out toward different ppm from 1000 to 5000 ppm of H_2 gas. The sensing properties were measured using a dynamic flow system. Hydrogen gas was injected into a sealed glass test chamber by a syringe through a rubber plug. After fully mixed with air, the sensor was put into the test chamber. When the response reached to a constant value, the sensor was exposed in air to recover. The sensor response was measured between 25 and 100 °C, which is defined as the ratio of resistance of sensor in air to the resistance in gas. The optimal operating temperature of the sensors for detecting H_2 is an important issue, and it was obtained by performing the gas sensing experiments at different temperatures. Figure 31a, b represents sensitivity to H_2 gas for the SnO_2/PANI and Al-doped SnO_2/PANI composite nanofibers, respectively. For SnO_2/PANI composite nanofibers, the sensitivity increased up to 35 °C, then decreased rapidly. On the contrary, Al-doped SnO_2/PANI composite nanofibers show very high sensitivity value with respect to pure SnO_2/PANI at same temperature.

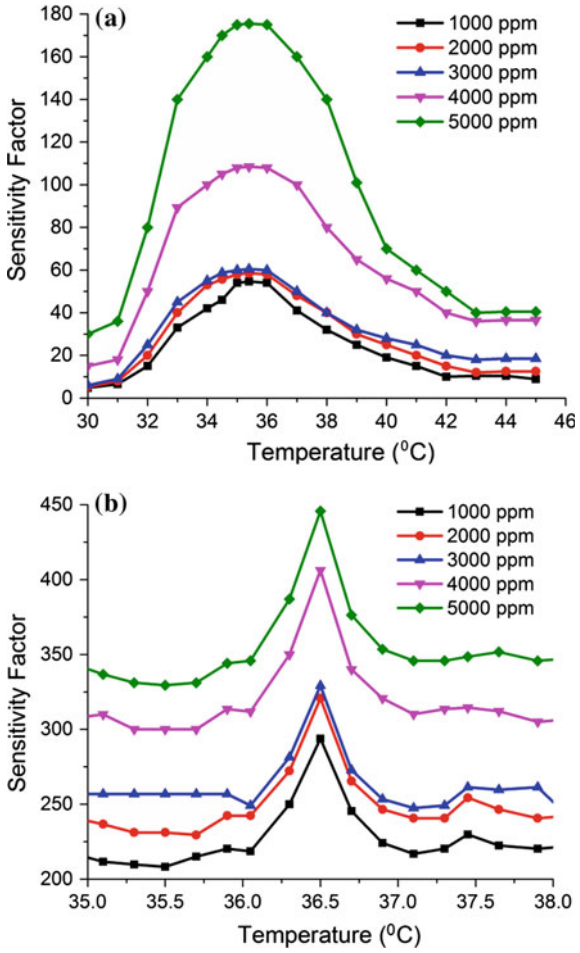

Fig. 31 **a** Sensitivity of SnO_2/PANI at different ppm of H_2, **b** sensitivity of Al-doped SnO_2/PANI at different ppm of H_2

It was found that Al-doped SnO_2/PANI composite nanofibers show good sensitivity to H_2 gas compared to SnO_2/PANI. Both composites are working at lower operating temperature than the reported working temperature of pristine SnO_2 and Al-doped SnO_2 (about 200–400 °C). From literature survey available in this regard, there is no appreciable change noticed in the nanofibers film resistance for the case of pure SnO_2 and Al-doped SnO_2, on exposure to different concentrations of H_2 gas and films remained insensitive to this gas near to room temperature. SnO_2/PANI and Al-doped SnO_2/PANI composite nanofibers showed appreciable sensitivity for H_2 gas. The sensitivity of composite nanofibers was found to be increased and reached its maximum around 35–36 °C for H_2 gas. The response of sensor was monitored in terms of the normalized resistance calculated by response = R_0/R_g and the sensitivity factor was monitored in terms of the % sensitivity calculated by %

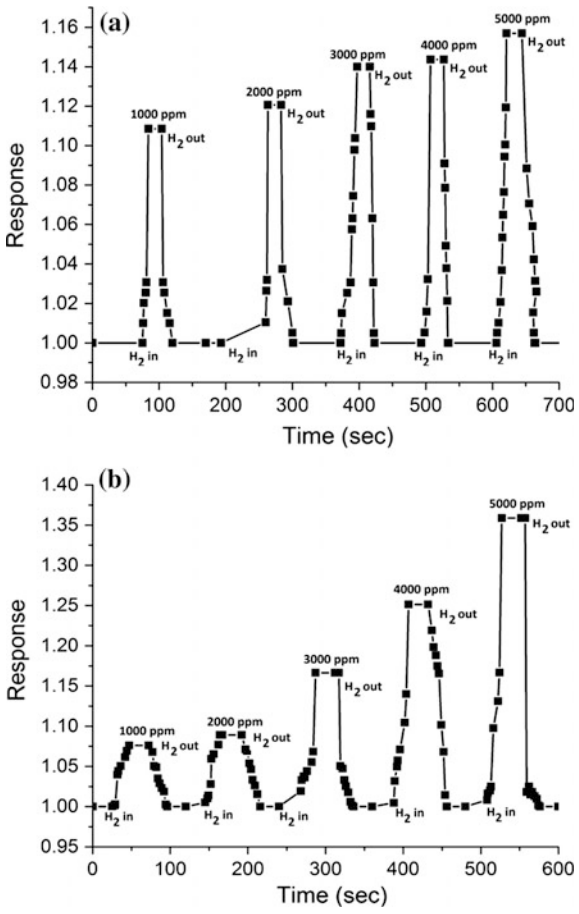

Fig. 32 **a** Response and recovery behavior of SnO_2/PANI nanofibers, **b** response and recovery behavior of Al-doped SnO_2/PANI nanofibers

sensitivity = $\Delta R/R_0$. Where ΔR is the variation in resistance of composite films from baseline after exposure to H_2 gas, R_g is the resistance of the sensor in presence of H_2 gas and R_0 is the initial baseline resistance of the sensor. As per the definitions of "Response time (R_P)" and "Recovery time (R_C)" for gas sensing, R_P and R_C for Al-doped SnO_2/PANI nanofibers were found to be less compared to that for SnO_2/PANI, i.e., less than 30 s. The response and recovery behavior of both the composites are compared as shown in Fig. 32a, b, respectively, for SnO_2/PANI and Al-doped SnO_2/PANI nanofibers. Response of the Al-doped SnO_2/PANI nanofibers was more as compared to that of SnO_2/PANI nanofibers. Response was observed during the gas for different ppm in the chamber whereas recovery was observed during air. In comparison to the pure SnO_2 and Al-doped SnO_2 nanofibers-based sensors reported elsewhere, the SnO_2/PANI and Al-doped SnO_2/PANI composite nanofibers exhibited the higher sensitivity for hydrogen gas near to room temperature and faster response and recovery.

For gas sensor fabrication, incorporation of carbon nanotubes (CNTs) into polymer has been employed these days since it offers further scope for improving their sensing characteristics, such as enhancing sensitivity and selectivity, lowering the detection limit, extending detection capacities to an ever-increasing number of gases, sensing at room temperature, etc. Reinforcement of CNTs in conducting polymer (CP) matrix represents a new class of material as some conducting polymers can behave like semiconductors due to their heterocyclic compounds which display physico-chemical characteristics. As a result, changes in conductivity of CNT–CP matrix composite can be detected upon polar chemicals adsorption on the surfaces at room temperature. The role of polymer is believed to facilitate only the charge transfer between gas molecules and CNTs. This mechanism suits the use of CNT–CP composite as highly sensitive and selective gas/chemical sensor and provides much room for tailoring the electronic properties of CNTs hence enhances gas sensing properties. Two types of conducting polymers like poly(3,4-ethylenedioxythiophene) polystyrene sulfonic acid (PEDOT:PSS) and polyaniline (PANI) were used and compared for their ammonia gas sensing properties at room temperature [70]. Both the sensors were found to exhibit excellent sensitivity and poor recovery for ammonia gas at room temperature, but as compared to PANI, PEDOT:PSS polymer composite was found to be more sensitive (with sensitivity of $\sim$16 %) with less response time ($\sim$15 min). Figure 33 shows the electrical response of the PEDOT:PSS polymer film after exposure to 100 ppm of ammonia gas at room temperature and no change in electrical resistance was observed, while a sharp increase in resistance hence sensitivity (%) was observed when MWCNT–PEDOT:PSS composite exposed to 30 ppm of ammonia. Similar behavior was observed in case of PANI film as shown in Fig. 34. Hence it is clearly concluded that both the polymers are almost insensitive to ammonia gas and it is the presence of MWCNT which makes both the composites highly sensitive toward ammonia.

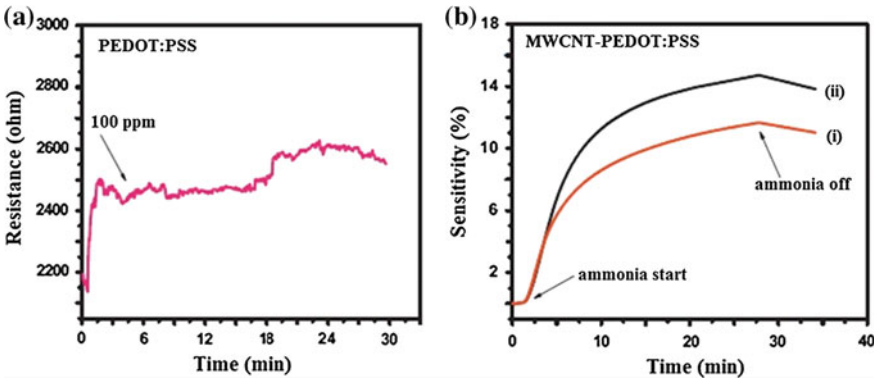

Fig. 33 Ammonia sensing response of **a** PEDOT:PSS polymer film, **b** MWCNT–PEDOT:PSS composite to (*i*) 20 ppm (*ii*) 30 ppm of ammonia gas at room temperature

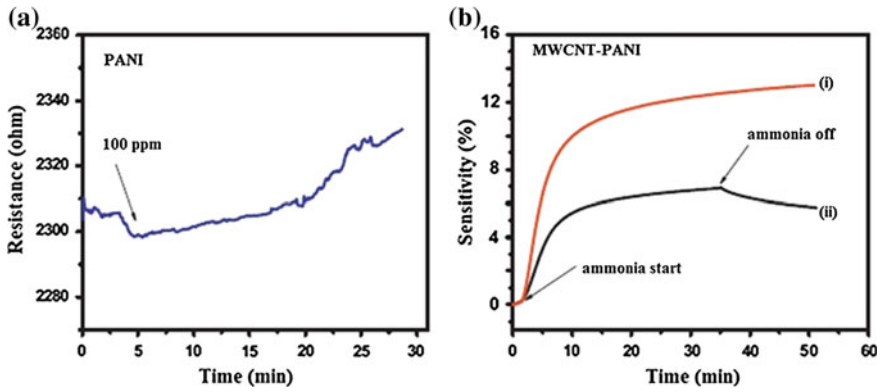

Fig. 34 Ammonia sensing response of **a** PANI and **b** MWCNT–PANI composite to (*i*) 20 ppm (*ii*) 30 ppm of ammonia gas at room temperature

To improve the sensing performance of graphene-based binary nanocomposites further, ternary graphene-based conducting polymer nanocomposites have been developed in which noble metal-conducting polymer or metal oxide-conducting polymer was hybridized with graphene to combine their advantages. Polyaniline/graphene/titania nanotube arrays (PGTNs) nanocomposites fabricated by in situ polymerization are found to good sensor [71]. The response and recovery time of the PANI–G compared with that of PGTNs nanocomposites for hydrogen gas. The response time, and the recovery time are defined as the time required for a material resistance to reach 90 % of its saturation value from the starting value on gas exposure, and on removal of the gas, respectively. PANI–G shows relatively faster response times $\sim$9 s, but as usual the recovery times were relatively larger, around 150 s. Notice that the larger recovery times are due to the slower out diffusion rate (concentration dependent) of the gas, which always decreases as time progresses. Furthermore, these diffusion rates are small at room temperature. PGTNs nanocomposite shows times of 14 s, and the recovery time around 80 s. It may be seen that the PGTNs showed faster recovery time as compared to the PANI-G. In Fig. 35a, b shows response of the PANI–G and PGTNs nanocomposites with respect to time, for repeated exposure and removal of hydrogen gas, and it may be seen that both the nanocomposites showed good reproducible resistance change for a number of cycles.

5.2 Biosensing Application

Conducting polymers are versatile materials for sensing application because they not only possess unique properties but also can be used as immobilization matrices, receptors and transducers (redox systems for the transport of electrical charge) in a

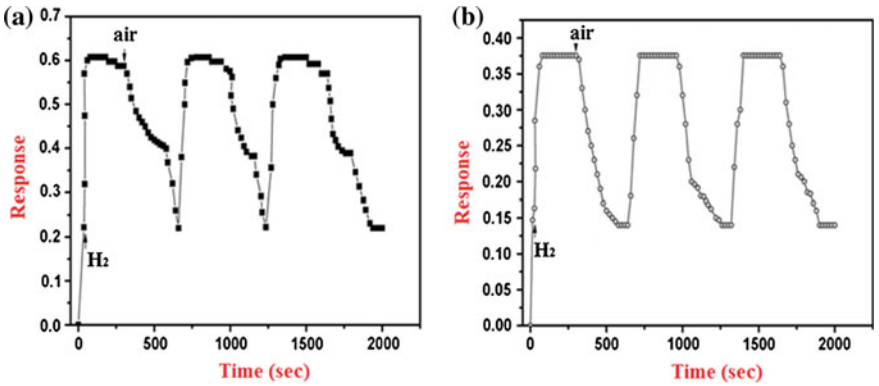

Fig. 35 Sensing curves for **a** PG and **b** PGTNs nanocomposites

biosensor. As a result the sensing mechanism of conducting polymers-based sensors has been formulated in a variety of schemes. In conductometric sensors, the change of electrical conductivity of conducting polymers upon interaction with analytes is measured. The conductivity change can be generated from doping/de-doping process, conformational change and redox process. In potentiometric sensors, the concerned changes in the system's chemical potential are mainly resulted from shifts in the anion equilibrium within the polymer film that is caused by doping/de-doping or redox processes. In recent years, studies of conducting polymer-based sensors have shown a trend toward the development of nanostructure conducting polymer-based sensors, owing the ability to tailor the sizes and structures, and hence the properties, of these nanomaterials. Conducting polymer nanostructures and nanocomposites, offers new opportunities as sensing platforms for biological and environmental applications. Actually, a desirable biosensor may take advantage of several enhance elements (composites, nanostructure, specific molecular design, etc.). On one hand, the nanostructures can be an enhance element for a nanocomposites-based sensor and vice versa. Moreover, the processability of conducting polymer materials is often important for the formation of specific nanostructures or nanocomposites.

Conducting polymer nanocomposites could greatly improve the efficiency of sensing characteristics since they have much greater exposed surface area, as well as much greater penetration depth compared to their bulk counterparts as a result the basic properties of a biosensor like detection limit get enhanced. The oriented microstructure and the high surface area also favors high enzyme loading and has potential for high sensitivity detection. Moreover, the relative stability is increased due to efficient bonding of enzyme on the transducer surface which gives it better reproducibility. Use of nanomaterials in biosensors allows the use of many new signal transduction technologies in their manufacture [72]. In molecular electronics and sensors, conducting polymer nanocomposites have been used as potential systems for the immobilization of enzymes. In these systems, there is a direct

transfer of electrons to and from the enzymes. The entrapment of enzymes in nanocomposites films provides a controlled method of localizing biologically active molecules in defined area on the electrodes. Also the use of conducting polymer nanocomposites in the area of bioanalytical sciences is of great interest since their biocompatibility opens up the possibility of using them in biosensors, for continuous monitoring of drugs or metabolites in biological fluids. The use of biological elements in biosensor construction comes with a challenge of preserving their biological integrity outside their natural environment. For this reasons these biological components of biosensors are generally immobilized onto supports by physical, covalent, or electrochemical methods.

In order to make a useful biosensor, enzyme has to be properly attached to the transducer with maintained enzyme activity. This process is known as enzyme immobilization. The choice of immobilization method depends on many factors such as the nature of the enzyme, the type of transducer used, the physiochemical properties of analyte, and the operating conditions [73]. The major requirement out of all these is its maximum activity in immobilized microenvironment. Enzyme-based electrodes provide a tool to combine selectivity of enzyme toward particular analyte and the analytical power of electrochemical devices. The amperometric transducers are highly compatible when enzymes such as urease, generating electro-oxidizable H^+ ions, are used [74]. The effective fabrication of enzyme biosensor based on how well the enzyme bounds to the transducer surface and remains there during use. The enzyme molecules dispersed in solutions will have a freedom of their movement randomly. Enzyme immobilization is a technique that prohibits this freedom of movement of enzyme molecules. There are four basic methods of immobilizing enzymes on support materials [75] and they are physical adsorption, entrapment, covalent bonding, and cross-linking, as shown in the Fig. 36.

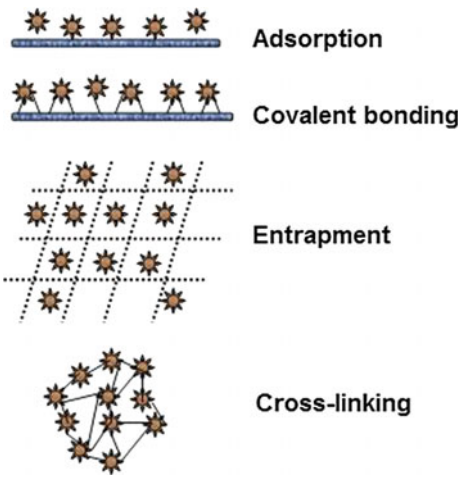

Fig. 36 Enzyme immobilization methods

The physical adsorption is the simplest one and more efficient as compared to others because it gives reversible surface interactions between enzyme and supporting matrix. This method utilizes surface chemistry between enzyme and support, so there is no need of activators or chemical modification for the bonding purpose, instead little beat damage are made to enzymes. The attachment of enzyme to the support is achieved with suitable conditions such as pH and ionic strength, for a period of incubation. This will result into immobilization of enzyme on the supporting matrix. The excessive non-bound enzyme molecules can be removed by washing with distilled water. The porosity must be controlled to ensure that the structure is tight enough to prevent enzyme leakage, but at the same time to allow free movement of substrates and products. This method is performed at low temperature and low pH range. In covalent bonding method, the actual covalent bond is formed between the nonactive site of an enzyme and the supporting matrix. The enzyme possesses chemical functional groups of amino acid residues on their surface. These groups are not taking any part in the activity of an enzyme. Hence these groups can be attached covalently to chemically activated supports such as glasses, cellulose, or synthetic polymers. The frequent groups involved in the covalent bonding are the amino group of lysine or argirine, the carboxyl group of aspartic, and glutamic acid, the hydroxyl group of serine and threonine, the sulfydril group of cysteine. In order to maintaining enzyme activity, the hydrophilic nature of the supporting matrix is the main requirement. Polysaccharide hydrophilic gel polymers are the examples fulfilling this requirement. Other supports for enzyme immobilization are porous glasses and silica. For the activation of functional group on the support, a specific reagent is required such as glutaraldehyde, carbodiimide, and silane compounds. These agents may interfere with the enzyme activity, especially at higher concentration of analyte [76, 77]. In the method of entrapment, the enzymes are free in solution, but limited by the lattice structure of the entrapment system to a certain domains. The different classes of entrapment are: Entrapment behind a membrane; Entrapment within self-assembled monolayers (SAMs) or bilayer lipid membranes (BLMs); Entrapment within a polymeric matrix membrane such as polyacrylonitrile, agar gel, polyurethane, or polyvinyl-alcohol. The most used technique is the entrapment in polymeric film, e.g., Polyaniline, Nafion through electropolymerization on the supporting transducer. [78]. Cross-linking method support-less procedure and involves interconnecting network between the enzymes with each other to form a large, three-dimensional complex structure. Cross-linking can be done using chemical or physical methods. Chemical method involves covalent bond formation between the enzymes by means reagent, such as glutaraldehyde. Physical cross-linking of cells by flocculation is well known in biotechnology industry and does lead to high cell densities. Flocculating agents, such as polyamines, poly-ethyleneimine, polystyrene sulfonates, phosphates, have been extensively used and well characterized. This method is rarely used because of less mechanical strength and poor stability of the resulting matrix [79].

Conducting polymer can be exploited as an excellent tool for the preparation of nanocomposites with entrapped nanoscale biomolecules, mainly proteins, enzymes,

and DNA oligomers. Recently, conducting polymer/CNTs composites have received significant interest because the incorporation of CNTs into conducting polymers can lead to new composite materials possessing the properties of each component with a synergistic effect that would be useful in particular application. CNT/polymer composites have been used for immobilization of metalloproteins and enzymes by either physical adsorption or covalent binding. Polypyrrole and polyaniline can be used for the fabrication of CNT/PPy and CNT/PANI nanocomposite electrodes due to the ease in the preparation through copolymerization by a chemical or electrochemical approach and the resulting nanocomposites exhibit high conductivity and stability [80]. PANI/CNTs composite modified electrode fabricated by galvanostatic electropolymerization of aniline on CNTs-modified gold electrode, exhibits enhanced electrolytic behavior to the reduction of nitrite and facilitates the detection of nitrite [81].

Amperometric response of the PPy/MWCNT/urease biosensor in the presence of urea was studied [82]. All the measurements were carried out in electrochemical cell, containing 20 ml of 0.1 M PBS (pH 7.2) with successive addition of 0.1 ml of 10 mM urea. Figure 37 shows the chronoamperometric curves of PPy/MWCNT/urease biosensor, with successive addition of 0.1 ml of 10 mM urea in 0.1 M PBS (pH 7.2) at potential of −0.6 V. It can be seen from figure that the current increased with the addition of urea which is due to the produced ammonium from the enzymatic reaction, then reached saturation. The results show that this biosensor exhibits an excellent response for urea at working potential of −0.6 V. The greater sensitivity was due to the incorporation of MWCNTs deposited PPy film of the electrode.

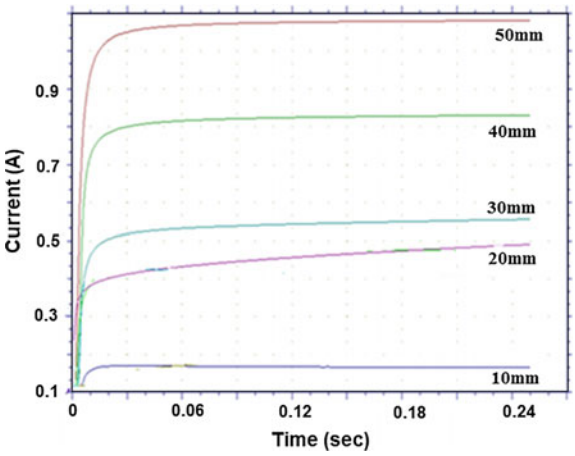

Fig. 37 Chronoamperometric curves of PPy/MWCNT/urease biosensor

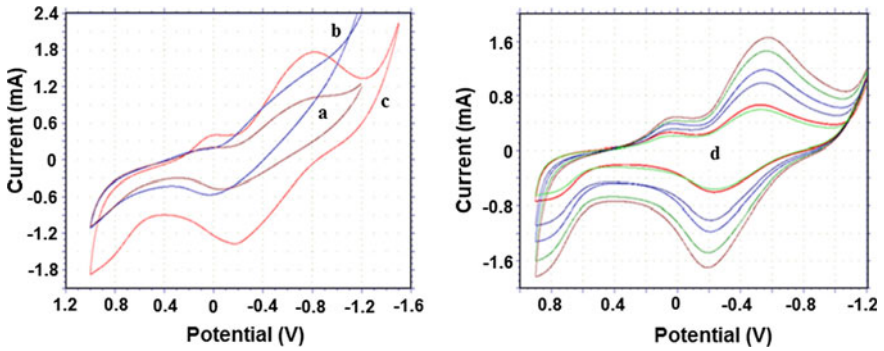

Fig. 38 Cyclic voltammograms of (*a*) bare steel electrode, (*b*) modified PPy/c-MWCNT electrode, (*c*) modified PPy/c-MWCNT/LOD electrode and (*d*) PPy/c-MWCNT/LOD electrode in PBS (0.1 M, pH 7) at a scan rate of 50 mV s^{-1} at different concentrations of Lactic acid

Cyclic voltammograms of PPy/c-MWCNT/LOD nanocomposite film prepared for lactate biosensor [83] as shown in Fig. 38 illustrates the bare steel electrode (curve a) has no redox peak. The functionalized carbon nanotubes are represented by c-MWCNT. It can be seen that a polymer growth, with increasing current is observed in the presence of c-MWCNT (curve b). The rise in the anodic current at −0.6 V potential range corresponds to the oxidation of the pyrrole monomer to form methylpyrrole radical cation, subsequent the radical reacts with another monomer to form dimerization of radical cation and coupling will result in the formation of an insoluble polymer, positively charged on the surface. In this case the growth of PPy/c-MWCNT is performed without additional other dopants. Thus, the CNTs acts as the counter ion incorporated within the polymer film to balance the cationic charge of the oxidized polymer. The PPy/c-MWCNT film also offers a more symmetrical voltammogram (curve c), with redox activity starting at a lower potential (−0.6 vs. −0.2 V), indicating that the presence of the CNT promotes the electron transfer of the oxidation–reduction process. The LOD incorporated to the PPy/c-MWCNT films by entrapment and then diffuse in the nanocomposite film leading to decrease the current density due to the negative charge on the film. The peak current increased from 0.9 to 1.8 by the introduction of LOD into the film, indicating the synergy effect between LOD and CNTs. In addition to this, the electrocatalytic sites placed in the active center of LOD would join into the PPy/c-MWCNT nanobiocomposite film. Curve (d) shows response of PPy/c-MWCNT/LOD biosensor, with successive addition of 0.1 ml of 1 μM Lactic acid in 0.1 M PBS (pH 7) at a scan rate of 50 mV s^{-1} and potential of −0.8 V. As soon as the lactate was introduced into the buffer, the lactate was converted into pyruvate and H_2O_2 by PPy/c-MWCNT/LOD. The electrons thus generated from H_2O_2 were detected at the applied potential utilizing PPy/c-MWCNT/LOD as electron transferring medium. The response current increased linearly with increasing concentration of lactate in the range 5–60 μM, which is due to the produced ammonium from the enzymatic reaction, then reached saturation.

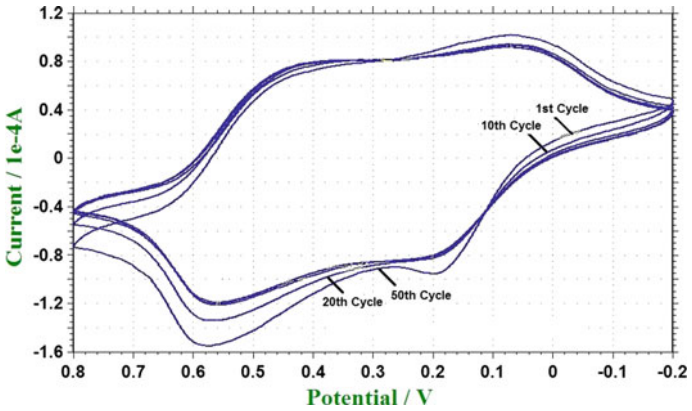

Fig. 39 Cyclic voltammograms of PANI/MnO_2 nanocomposite

PANI/MnO_2 nanocomposites were electrochemically synthesized by electrolyzing aniline [84]. Different weight percentages of nanostructure MnO_2 (5, 10, and 15 %) are used in 1 M H_2SO_4 containing of 0.4 M aniline on the steel electrode by sweeping the potential on the working electrode, from −0.2 to +0.8 V versus Ag/AgCl for 10 cycles with a scan rate of 50 mV/s to form PANI/MnO_2 nanocomposites. Figure 39 shows the cyclic voltammograms obtained during aniline polymerization in the presence of nanostructure MnO_2. A shifting of potential to more positive values occurs. The potential peak for aniline without MnO_2 shows significant difference which can be attributed to the incorporation of the anionic metal oxide into the polymer backbone, which favors the charge transference processes during the conducting polymer-metal oxide formation. Similarly, PANI/ZnO nanocomposites were also electrochemically synthesized by electrolyzing aniline. Figure 40 shows the cyclic voltammograms obtained during aniline polymerization in the presence of nanostructure ZnO. The PANI/ZnO film also offers a more symmetrical voltammogram, with oxidation starting at a lower potential (0.05–0.08 V) compared to pure PANI indicating that the presence of the ZnO promotes the electron transfer of the oxidation process.

Figure 41 shows the cyclic voltammograms of PANI/MnO_2/urease electrode with 5, 10, and 15 % compositions in phosphate buffer solution. Cyclic voltammograms were obtained by sweeping the potential on the working electrode, from −0.4 to 0.6 V versus Ag/AgCl at a scan rate 100 mV/s. The CV shows that the potential reversals at the potential limits are fast and instantaneous. This suggests that the adsorption/desorption process of the ions are very fast during cycling The oxidation current for PANI/MnO_2 nanocomposites was found to increase with an increase in concentration of MnO_2. Thus, conducting polyaniline having amine functional group can be utilized as a suitable matrix for the physical adsorption of urease [85]. Figure 42 shows the cyclic voltammograms of PANI/ZnO/urease electrode with 5, 10, and 15 % compositions in phosphate buffer solution. Cyclic voltammograms were obtained by sweeping the potential on the working electrode,

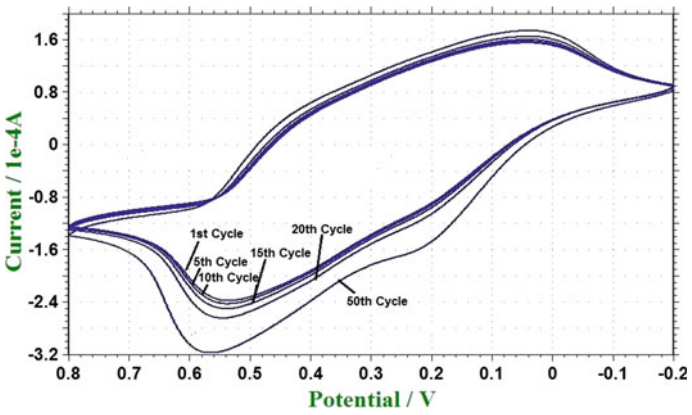

Fig. 40 Cyclic voltammograms of PANI/ZnO nanocomposites

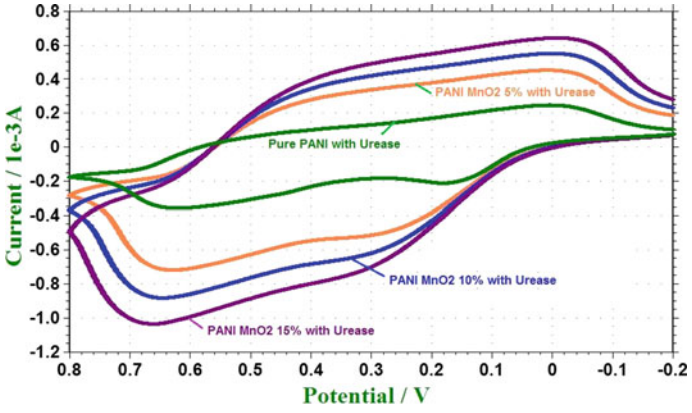

Fig. 41 Cyclic voltammograms of PANI/MnO_2/urease electrode

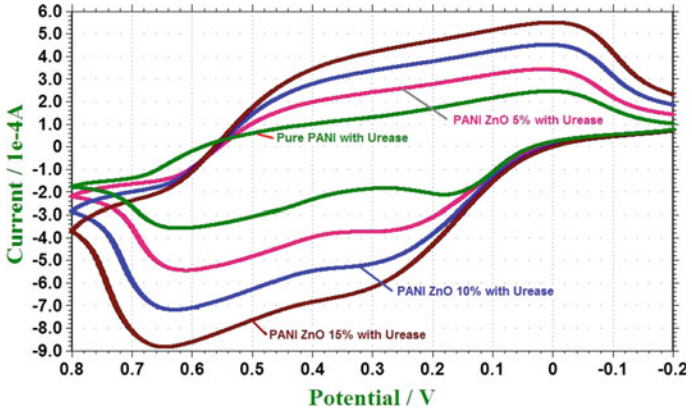

Fig. 42 Cyclic voltammograms of PANI/ZnO/urease electrode

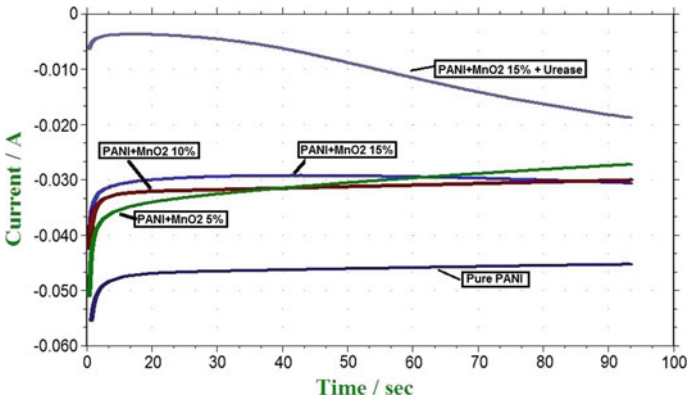

Fig. 43 Chronoamperometry of PANI/MnO_2/urease electrode

from −0.2 to 0.8 V versus Ag/AgCl at a scan rate 100 mV/s. The oxidation potential peaks occurring in CV of ZnO–PANI 15 % film depicts the oxidized potential at around 0.2 V, which is at higher potential as compared to other lower weight %, indicating larger surface area and larger potential window as compared to others. The magnitude of peak current gets increased with increasing concentration of ZnO, which ensures quick response time of the sensor.

Figure 43 illustrates the chronoamperometric response of the Pure PANI, PANI/MnO_2 (5, 10, and 15 %) and PANI/MnO_2/urease (15 %) electrodes in the potential range 0.2–0.6 V versus reference electrode for time interval of 100 s in PBS of pH 7. Chronoamperometry curve of PANI/MnO_2/urease (15 %) electrodes shows that the immobilization of urease on modified PANI/MnO_2 (15 %) film results in getting larger saturation current in the time of 10 s. But the curve obtained is not stable for long time. Thus the PANI/MnO_2 matrix shows degradation of the urease from the electrode surface. Figure 44 illustrates the chronoamperometric response of the PANI/ZnO (5, 10, and 15 %) and PANI/ZnO/urease (15 %) electrodes. The increase in the current suggests the predominance of the fast electron transfer over the degradation of enzyme layer into the electrolyte, whereas the decrease means the predominance of the degradation over the fast electron transfer. Chronoamperometry curve of PANI/ZnO/urease (15 %) electrode shows that the immobilization of urease on modified PANI/ZnO (15 %) film results in getting larger saturation current in the time of 10 s. This suggests that the immobilized enzyme by physical adsorption method is well entrapped into the PANI/ZnO matrix and it will not show degradation of the urease from the electrode surface [86].

Figures 45 and 46 shows response of PANI/MnO_2/urease and PANI/ZnO/urease biosensor, respectively, with successive addition of 0.1 ml of 10–50 mM urea in 0.1 M PBS (pH 7.2) at potential of −0.3–0.6 V and at a scan rate of 50 mV/s. Urease hydrolyzes urea to ammonium and hydrogen carbonate anions. Ammonium ion interacts with polymer to induce a decrease in conductivity of the polymer. Reversible deprotonation of the polymer structure takes place, while increase in the

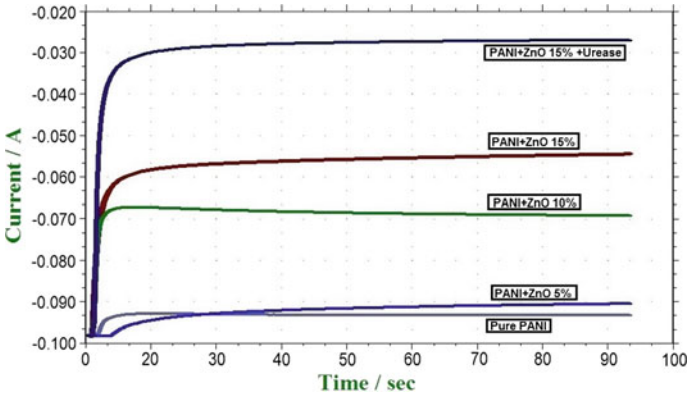

Fig. 44 Chronoamperometry of PANI/ZnO/urease electrode

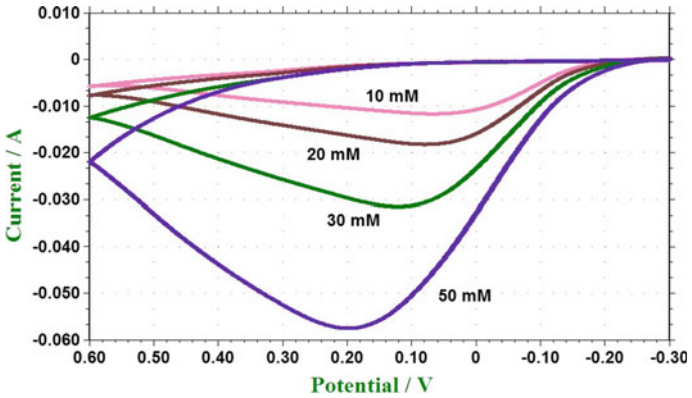

Fig. 45 Response of PANI/MnO_2/urease biosensor

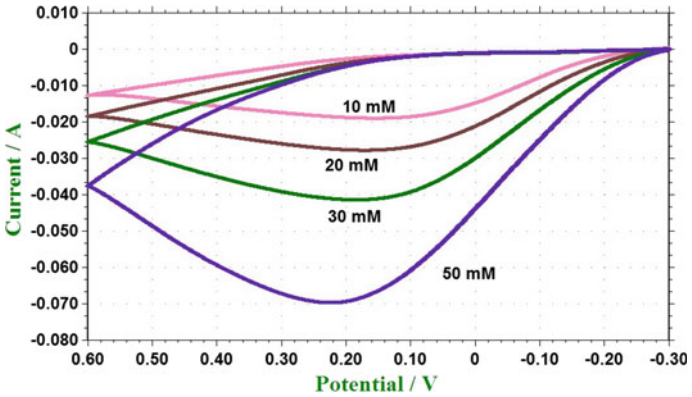

Fig. 46 Response of PANI/ZnO/urease biosensor

pH of the medium can be detected electrochemically at the applied potential utilizing PANI/ZnO/urease as electron transferring medium. The response current increased linearly with the addition of urea in the range of 10–50 mM which is due to the produced ammonium from the enzymatic reaction, then reached saturation. The results show that these biosensor exhibits an excellent response for urea at working potential of −0.3–0.6 V.

A functionalized single-wall CNTs/PPy composite served as amperometric glucose biosensors [87]. A polyaniline composite film was prepared through a chemical oxidation method by adding CNTs as nanofiber seeds and was used to examine gas response to trimethylamine [88]. Hydrogen peroxide sensors are extremely important since H_2O_2 has great importance in pharmaceutical, clinical, environmental, mining, textile, and food manufacturing applications, also being a product generated in biochemical reactions catalyzed by oxidase enzymes. Kum et al. [89] prepared biomolecules (horseradish peroxidise)-carbon nanotubes doped conducting polymer nanocomposites (PPy/SWNT–HRP) and their sensor application for H_2O_2 response. Ethanol has drawn attention as a biofuel since it can be produced by fermentation of biomass, its use in enzymatic fuel cells offers the possibility of small-scale power generators. CNT/polyphenazine-based biosensors, containing enzyme alcohol dehydrogenase (AlcDH) for the detection of ethanol have been reported [90].

Sensors/biosensors based on various conducting polymer nanocomposites for different analytes are summarized in Table 1.

Table 1 Conducting polymer nanocomposites for sensor/biosensor

Conducting polymer nanocomposites	Analyte	Refs.
PANI/SnO_2	NH_3, CO	[52, 53]
PANI/ZnO nanofibers	HCl, NH_3	[69]
PANI/TiO_2	CO	[53]
PPy–WO_3	NO_2	[54]
PANI/SnO_2 nanofibers	H_2	[55]
PEDOT/CNT	NH_3	[70]
PANI/CNT	NH_3, trimethylamine	[70, 88]
PPy/MWCNT/urease	Urea	[82]
PPy/MWCNT/LOD	Lactate	[83]
PANI/graphene/titania	H_2	[84]
PPy/SWNT-HRP	H_2O_2	[89]
PPy/CNT	Glucose	[87]
CNT/polyphenazine	Ethanol	[90]

6 Conclusion

The low sensitivity and selectivity of conducting polymers for chemical and biological sensing can be improved by fabricating conducting polymers in nanostructure form. Conducting polymer nanostructures with large specific surface area and porous structure are therefore predicted to be excellent sensing materials. Their sensitivity, selectivity, and response time can be further improved by using conducting polymer nanocomposites because the nanostructure component increases the chain mobility of conducting polymers or change the affinity of the composite or even act as a catalyst. Carbon nanotubes, metal and metal oxide particles, metal salts, insulating polymers, and biological materials can be incorporated into conducting polymer matrix to form good sensing materials. This chapter is a brief review on preparative strategy of nanostructure conducting polymers and conducting polymer nanocomposites for sensor/biosensor applications. However, more research in the field of conducting polymer nanocomposites-based sensor needs to be done in the form of new methods for the fabrication of advanced hybrid materials and understanding of sensing mechanism by nanocomposites.

References

1. Rajesh AT, Kumar D (2009) Sens Actuators B 136:275
2. Heiland G, Kohl D (1988) Chem Sensor Technol 1:15
3. Cabot A, Vila A, Morante JR (2002) Sens Actuators B 84:12
4. Dan YP, Cao YY, Mallouk TE, Evoy S, Johnson ATC (2009) Nanotechnology 20:434014
5. Cao Y, Kovalev AE, Xiao R, Kim J, Mayer TS, Mallouk TE (2008) Nano Lett 8:4653
6. Safidine Z, Ghebache Z, Lamouri S (2013) Polym J 45:946
7. Yang N, Chen X, Ren T, Zhang P, Yang D (2015) Sens Actuators B 207:690
8. Sassolas A, Blum LJ, Leca-Bouvier BD (2012) Biotechnol Adv 30:489
9. Cosnier S (2007) Anal Lett 40:1260
10. MacDiarmid AG (2001) Synth Met 125:11
11. Heeger A (2001) Rev Mod Phys 73:681
12. Heeger A (2002) Synth Met 125:23
13. Lu X, Zhang W, Wang C, Wen T, Wei Y (2011) Prog Polym Sci 36:671
14. MacDiarmid AG (2001) Synth Met 125:11
15. Long YZ, Li MM, Gu C, Wan M, Duvail J, Liu Z, Fan Z (2011) Prog Polym Sci 36:1415
16. Im JS, Park SJ, Lee YS (2009) Int J Hydrogen Energy 34:1423
17. Ding HJ, Long YJ, Shen JY, Wan MX (2010) J Phys Chem B 114:115
18. Wu CG, Bein T (1994) Science 264:1757
19. MacDiarmid AG, Jones WE Jr, Norris ID, Gao J, Johnson AT Jr, Pinto NJ, Hone J, Han B, Ko FK, Okuzaki H, Llaguno M (2001) Synth Met 119:27
20. Norris ID, Shaker MM, Ko FK, MacDiarmid AG (2000) Synth Met 114:109
21. Li M, Wei ZX, Jiang L (2008) J Mater Chem 18:2276
22. Ramanathan K, Bangar MA, Yun M, Chen W, Mulchandani A, Myung NV (2007) Electroanalysis 19:793
23. Cardenas JR, Vasconcelos EA, Azevedo WM, de Silva EF Jr (2007) J Phys D Appl Phys 40:1068
24. Kang TS, Lee SW, Joo J, Lee JY (2005) Synth Met 153:61–64

25. Chronakis IS, Grapenson S, Jakob A (2006) Polymer 47:1597
26. Laforgue A, Robitaille L (2008) Synth Met 158:577
27. Shin MK, Kim YJ, Kim SI, Kim SK, Lee H, Spinks GM, Kim SJ (2008) Sens Actuator B Chem 134:122
28. Patil PT, Anwane RS, Kondawar SB (2015) Proced Mater Sci 10:195
29. MacDiarmid AG, Norris ID, Jones WE Jr, El-Sherif MA, Yuan J, Han B, Ko FK (2000) Polym Mater Sci Eng 83:544
30. Dong H, Megalamane U, Jones W Jr (2003) Polym Mater Sci Eng 44(2):124
31. Huang J, Virji S, Weiller BH, Kaner RB (2004) Chem Eur J 10:1314
32. Liu H, Kameoka J, Czaplewski DA, Craighead HG (2004) Nanoletters 4:671
33. Aussawasathien D, Dong J-H, Dai L (2005) Synth Met 154:37
34. Haynes AS, Gouma PI (2008) IEEE Sens J 8:701
35. Haynes A, Gouma P (2007) Mater Manuf Proc 22:764
36. Pinto NJ, Ramos I, Rojas R, Wang P-C, Johnson AT Jr (2008) Sens Actuators B 129:621
37. Rojas R, Pinto NJ (2008) IEEE Sens J 8:951
38. Ji S, Li Y, Yang M (2008) Sens Actuators B 133:644
39. Jianrong C, Yuqing M, Nongyue H, Xiaohua W, Sijiao L (2004) Nanotechnol Biosens Biotechnol Adv 22:505
40. Rajesh, Takashima W, Kaneto K (2004) Sens Actuators B 102:271
41. Rajesh, Bisht V, Takashima W, Kaneto K (2005) Surf Coat Technol 198:231
42. Rajesh, Bisht V, Takashima W, Kaneto K (2005) Biomaterials 26:3683
43. Bisht V, Takashima W, Kaneto K (2005) React Funct Polym 62:51
44. Ahuja T, Mir IA, Kumar D, Rajesh (2007) Biomaterials 28:791
45. Geeta S, Roa CRK, Vijayan M, Trivedi DC (2006) Anal Chim Acta 568:119
46. Kamigaito O (1991) J Jpn Soc Powder Metal 38:315
47. Biercuk MJ, Llaguno MC, Radosvljevicm HJ (2002) Appl Phys Lett 80(15):2767
48. Ounaies Z, Park C, Wise KE, Siochi EJ, Harrison JS (2003) Compos Sci Technol 63(11):1637
49. Weisenberger MC, Grulke EA, Jacques D, Ramtell T, Andrews R (2003) J Nanosci Nanotechnol 3(6):535
50. Dalton AB, Coolins S, Muñoz E, Razal JM, Ebron VH, Ferraris JP (2003) Nature 423:703
51. Kondawar SB, Nandapure AI, Nandapure BI (2014) Adv Mater Lett 5(6):339
52. Kondawar SB, Agrawal SP, Nimkar SH, Sharma HJ, Patil PT (2012) Adv Mater Lett 3:393
53. Ram M, Yavuz O, Lahsangah V, Aldissi M (2005) Sens Actuators B 106:750
54. Mane AT, Navale ST, Patil VB (2015) Org Electron 19:15
55. Sharma HJ, Sonwane ND, Kondawar SB (2015) Fibers Polym 16:1527
56. Sharma HJ, Jamkar DV, Kondawar SB (2015) Proced Mater Sci 10:186
57. Kondawar SB, Deshpande MD, Agrawal SP (2012) Int J Compos Mater 2:32
58. Meshram BH, Mahore RP, Virutkar PD, Kondawar SB (2015) Proced Mater Sci 10:176
59. Mahore RP, Kondawar SB, Burghate DK, Meshram BH (2015) J Chin Adv Mater Soc 3:45
60. Lee H, Kim H, Cho MS, Choi J, Lee Y (2011) Electrochim Acta 56:7460
61. Bai C, Wang J, Jia S, Yang Y (2010) Appl Phys Lett 96:011102
62. Lee KP, Gopalan AY, Santhosh P, Lee SH, Nho YC (2007) Compos Sci Technol 67:811
63. Reddy ALM, Rajalakshmi N, Ramaprabhu S (2008) Carbon 46:2
64. Kong L, Lu X, Zhang W (2008) J Solid State Chem 181:628
65. Wu TM, Yen SJ, Chen EC, Chiang RK (2008) J Polym Sci, Part B: Polym Phys 46:727
66. Mahore RP, Kondawar SB, Burghate DK, Meshram BH (2015) J Chin Adv Mater Soc 3 (1):45
67. Huang H, Gan M, Ma L, Yu L, Hu H, Yang F, Li Y, Ge C (2015) J Alloy Compd 630:214
68. Huang JX, Virji S, Weiller BH, Kaner RB (2003) J Am Chem Soc 125:314
69. Kondawar SB, Patil PT, Agrawal SP (2014) Adv Mater Lett 5:389
70. Sharma S, Hussain S, Singh S, Islam SS (2014) Sens Actuators B 194:213
71. Radhakrishnan S, Rao CRK, Vijayan M (2009) J Appl Polym Sci 114:3125
72. Jianrong C, Yuqing M, Nongyue H, Xiaohua W, Sijiao L (2004) Nanotechnol Biosens Biotechnol Adv 22:505

73. Lakard B, Herlem G, Lakard L, Antoniou A, Fahys B (2004) Biosens Bioelectron 19:1641
74. Soares JC, Brisolari A, Cruz Rodrigues V, Sanches EA, Gonçalves D (2012) React Funct Polym 72:148
75. Sassolas A, Blum LJ, Leca-Bouvier BD (2012) Biotechnol Adv 30:489
76. Cosnier S (2003) Anal Bioanayl Chem 377:507
77. Tiwari A, Aryal S, Pilla S, Gong S (2009) Talanta 78:1401
78. Wolowacz S, YonHin B, Lowe C (1992) Anal Chem 64:1541
79. Cosnier S (1999) Biosens Bioelectron 14:443
80. Ghica ME, Brett MA (2005) Anal Chim Acta 532:145
81. Baibarac M, Baltog I, Lefrant S, Mevellec JY, Chauvet O (2003) Chem Mater 15:4149
82. Guo M, Chen J, Li J, Tao B, Yao S (2005) Anal Chim Acta 532:71
83. Meshram BH, Kondawar SB, Mahajan AP, Mahore RP, Burghate DK (2014) J Chin Adv Mater Soc 2:223
84. Mahajan AP, Kondawar SB, Mahore RP, Meshram BH, Virutkar PD (2015) Proced Mater Sci 10:699
85. Malhotra D, Chaubey A, Singh SP (2006) Anal Chim Acta 578:59
86. Moyo M, Okonkwo JO, Agyei NM (2012) Sensors 12:923
87. Callegari A, Cosnier S, Marcaccio M, Paolucci D, Paolucci F, Georgakilas V, Tagmatarchis N, Vazquez E, Prato M (2004) J Mater Chem 14:807
88. Ma X, Zhang X, Li Y, Li G, Wang M, Chen HZ, Mi Y (2006) Macromol Mater Eng 291:75
89. Kum MC, Joshi KA, Nosang WC, Myung V, Mulchandani A (2007) Talanta 74:370
90. Yang DW, Liu HH (2009) Biosens Bioelectron 25:733

Conducting Polymer Nanocomposite-Based Supercapacitors

Soon Yee Liew, Darren A. Walsh and George Z. Chen

Abstract The use of nanocomposites of electronically conducting polymers for supercapacitors has increased significantly over the past years, due to their high capacitances and abilities to withstand many charge-discharge cycles if properly structured. We have recently been investigating the use of nanocomposites of electronically conducting polymers containing conducting and nonconducting nanomaterials, such as carbon nanotubes and cellulose nanocrystals, for use in supercapacitors. In this contribution, we provide a summary of some of the key issues in this area of research. This discussion includes some history, fundamental concepts, the physical and chemical processes involved and the challenges that these nanocomposite materials must overcome in order to become technologically viable. Due to space limitations, this is not a complete review of all the work that has been done in this field and we have focussed on common themes that appear in the published work. Our aim is that this chapter will help readers to understand the advantages and challenges involved in the use of these materials in supercapacitors and to identify areas for further development.

Keywords Supercapacitors · Charge storage mechanisms · Conducting polymers · Carbons · Nanocomposites · Energy storage

S.Y. Liew · G.Z. Chen (✉)
Faculty of Engineering, Department of Chemical and Environmental Engineering, University of Nottingham, University Park, Nottingham NG7 2RD, UK
e-mail: george.chen@nottingham.ac.uk

D.A. Walsh (✉)
GSK Carbon Neutral Laboratory for Sustainable Chemistry, School of Chemistry, University of Nottingham, Jubilee Campus, Nottingham NG7 2TU, UK
e-mail: darren.walsh@nottingham.ac.uk

V. Kumar et al. (eds.), *Conducting Polymer Hybrids*,
Springer Series on Polymer and Composite Materials,
DOI 10.1007/978-3-319-46458-9_9

1 Introduction

Tackling the future global energy problem will require us to use a combination of renewable energy technologies, including solar, wind, hydroelectric energy, and etc. However, many of these technologies are intermittent in nature and methods for storing excess energy (for example, when abundant solar energy is available) and load levelling (when the Sun is not shining) will be required. Electrochemical energy storage and conversion devices have much to offer in this respect and can be used to store energy in the reactants within batteries or at the charged interface between an electrode and an electrolyte in supercapacitors [1–6]. Supercapacitors are most commonly described as devices that fit the gap between conventional batteries and conventional capacitors. They can store considerable amounts of energy (i.e., have high energy densities) but in principle they operate no different from conventional capacitors. As the charge can be stored and removed rapidly, supercapacitors are capable of delivering high power. The combination of high energy storage density and high power capability is thus the principal character of supercapacitors. The first supercapacitor patent appeared in 1957 and described a carbon–carbon capacitor [7]. Interest in supercapacitors, however, was rather limited until the late 1980s, when interest in supercapacitors increased with the development of new hybrid electric vehicles. Supercapacitors have since become a widely studied topic [7–9]. As well as use in hybrid electric vehicles, other applications of supercapacitors include distributed power generation, mechanical actuators, memory protection in computers, remote sensing, and etc [10]. A popular recent trend has been the development of paper-based supercapacitors [11], flexible supercapacitors [12–14] and even wearable supercapacitors [15, 16]. In the literature, supercapacitors are also called ultracapacitors, electrochemical capacitors, pseudocapacitors, electric double-layer capacitors (EDLC), and electrochemical double-layer capacitors (ECDLC). To avoid confusion, and for convenience, the term 'supercapacitor' will be used throughout this book chapter. In the following sections, we give a introduction to supercapacitor technology, the materials from which supercapacitors are constructed, the charge storage mechanisms, and etc. We then give a detailed description of the use of conducting polymers and their nanocomposites in supercapacitors. A discussion of the development of supercapacitor prototypes and devices containing these nanocomposites is then included, before we offer some perspectives on the area of research and suggest some areas for future development.

2 Energy and Power Characteristics of Supercapacitors

2.1 Capacitance of an Electrode

We first consider what happens when a surface of an ideally polarisable electrode is charged. The charging of the electrode happens when the electrolyte counterions balance the induced charge on the electrode surface. This accumulation of charge

on the electrode side of the interface and the counterions in the electrolyte on the opposite side of the interface is called double-layer charging. The amount of charge that can accumulate at an electrode/electrolyte interface depends on the relative permittivity of the electrolyte, ε_r, and the thickness of the double layer, d, according to $C/A = \varepsilon_r\varepsilon_0/d$, where C is capacitance in unit of farads (F), A is the interface area (m^2) and ε_0 is the permittivity of vacuum (8.85×10^{-12} F m^{-1}). Taking a typical interfacial area specific capacitance of 25 μF cm^{-2} and a porous electrode with a specific area of 1000 m^2 g^{-1} (typical for a porous carbon electrode), a mass capacitance of 250 F g^{-1} is expected, although much lower values are normally achieved due to poor accessibility of the internal surface of the porous electrode to the electrolyte [17]. This calculation allows the estimation of the mass-specific capacitance of materials based on double-layer capacitance. Conducting polymers, on the other hand, store charge not only by the double-layer mechanism, but rather and mainly due to redox reactions (pseudocapacitance, described in detail below). Thus, the capacitance does not depend only on the interfacial area. However, while capacitance estimates based on interfacial areas are not directly applicable to conducting polymers and any other pseudocapacitive materials, the concept of interfacial area specific capacitances is a very useful concept to note.

The capacitance, C, is related to charge, Q, in coulombs (C) and voltage, V, in volts (V), or joules per coulomb, by the following equation:

$$C = \frac{\mathrm{d}Q}{\mathrm{d}V} \tag{1}$$

When the charge and voltage are expressed in time derivatives:

$$C = \frac{\mathrm{d}Q/\mathrm{d}t}{\mathrm{d}V/\mathrm{d}t} \tag{2}$$

and since $\mathrm{d}Q/\mathrm{d}t$ is the current, i, in unit of amperes (A):

$$C = \frac{i}{\mathrm{d}V/\mathrm{d}t}, \tag{3}$$

where $\mathrm{d}V/\mathrm{d}t$ is the voltage scan rate, or the potential scan rate. This equation is the most common one used for the characterisation of capacitive materials. In the case of cyclic voltammetry, i is the capacitive current that flows when the capacitive material is subjected to a potential ramp at the rate $\mathrm{d}V/\mathrm{d}t$. In galvanostatic (constant current) methods, $\mathrm{d}V/\mathrm{d}t$ is the rate of potential change in response to a set charge/discharge i. When the capacitance is divided by the mass of the electrode material, the specific capacitance C_{sp} (F g^{-1}) is obtained. Likewise, when i is replaced with mass-specific current i_s (A g^{-1}) in Eq. 3, the capacitance is also specific to mass. Back calculation can also be performed using the C_{sp} to obtain i_s.

It should be noted that Eq. 3 implies that i is constant at any given $\mathrm{d}V/\mathrm{d}t$, and changes its polarity (positive or negative) when $\mathrm{d}V/\mathrm{d}t$ changes in polarity as well.

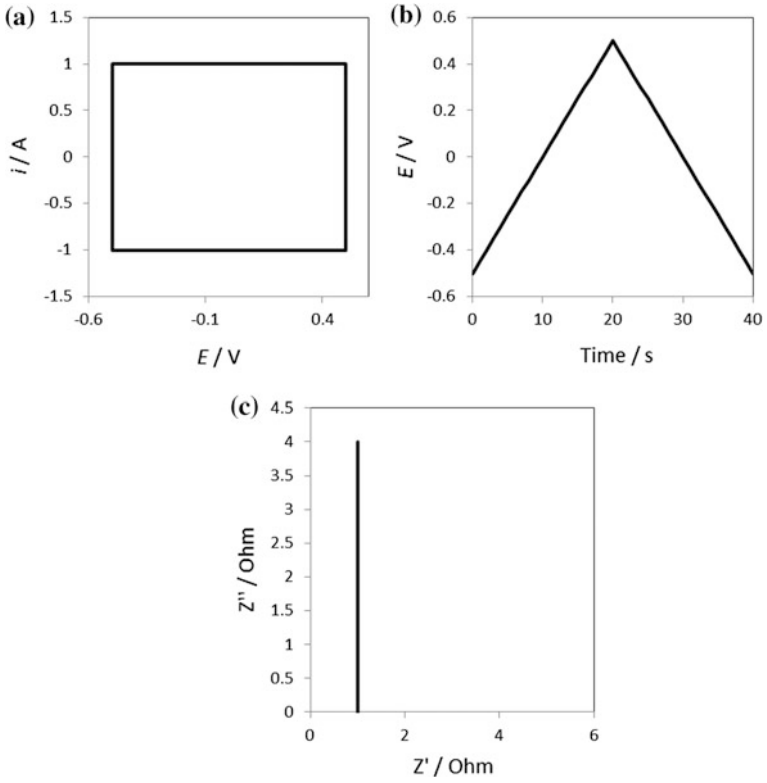

Fig. 1 The expected **a** CV, **b** GCD, and **c** EIS results for an ideally capacitive material. The potential values in **a** and **b** extending to negative values indicate that the characterisation was performed in three-electrode configuration and in which the potential was measured against a standard reference

This i - dV/dt correlation means that cyclic voltammograms (CVs) recorded for capacitive processes are rectangular in shape, while galvanostatic charge/discharge (GCD) plots are triangular in shape. While the shape of CVs or GCDs can be used to determine whether an electrode material is capacitive, measured CVs and GCD plots normally deviate slightly from this ideal shape, even for purely capacitive material. Typically this non-ideality appears when the potential scan direction switches at the limits of a CV, and also when current switches when the potential of a GCD reaches the set limit. These effects arise due to non-ideal transport of charge on the electrode side, and ions on the electrolyte side, of the electrode/electrolyte interface due to resistance within the electrode material and mass-transport limitations within the electrolyte. To account for non-ideal responses in CVs, the average current is usually determined from the integration of CV current over the potential range, while in GCD plots, the slope of the linear portions of the GCD plot can be used to determine the capacitance value. Figure 1 shows the expected results for an ideally capacitive material in a three-electrode cell.

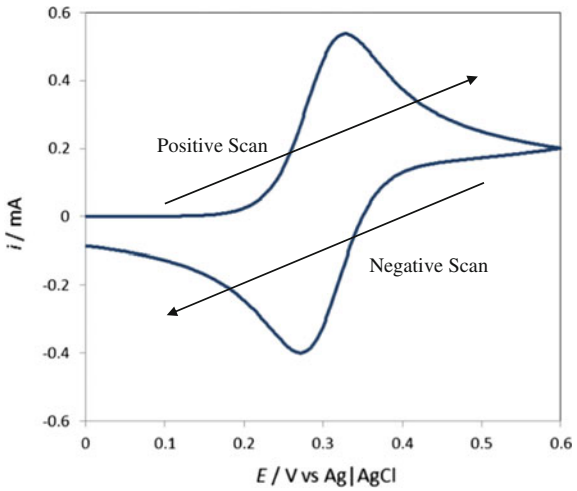

Fig. 2 A model CV of a redox mediator in a solution

When the shape of CVs deviates significantly from a rectangle and the shape of GCD plot deviates significantly from a symmetrical triangle, this can mean that the electrode material or the electrochemical system under examination is not capacitive. As an example, CVs that show characteristic current peaks can mean that there are redox reactions taking place across the electrode/electrolyte interface involving mobile redox species as in the case of the irreversible oxygen reduction on platinum surfaces or oxidation/reduction of the reversible ferrocene/ferrocenium redox couple over a glassy carbon electrode (Fig. 2 is a simulated CV that shows the oxidation and reduction of a redox couple with a formal potential of 0.3 V). When a reversible redox couple is immobilised on the surface of an electrode, the CV responses would similarly be peak shaped, although in the case of an immobilised redox couple, the potentials of the current peaks on the forward and backward scans would be identical. The materials from which rechargeable batteries are made are examples of immobilised redox couples. The GCD plots of a system which involve an immobilised redox couple would typically show a potential/voltage plateau both on the charging and discharging processes.

As well as CV and GCD analysis, another characterisation method that is often used to characterise supercapacitor materials is electrochemical impedance spectroscopy (EIS), or alternating current (AC) impedance spectroscopy. The following equation can be used to calculate the capacitance value from impedance measurements:

$$C = -\frac{1}{\omega Z''} = -\frac{1}{2\pi f Z''}, \tag{4}$$

where ω is the angular frequency of the driving AC potential waveform and the response, f is the frequency in hertz (Hz) and Z'' is the imaginary complex impedance in ohms (Ω) which is at a 90° (for an ideal case) phase angle relative to the driving AC potential waveform. Capacitive responses to an AC potential waveform are manifested in the complex Nyquist plots of EIS as a vertical line (Fig. 1c).

It is interesting that Eqs. 3 and 4 apply when electrode materials are characterised either in two-electrode systems or in three-electrode systems. A two-electrode system is one in which two electrodes are connected in series, so that the potential of one electrode is measured against the other electrode which at the same time conducts current in the closed circuit. The difference in potential between the electrodes is the cell voltage V. Electrochemical devices, including supercapacitors, are usually consisting of two electrodes in each cell for commercial purposes. The use of potentiostats, however, makes convenient the characterisation of electrode materials in the three-electrode systems. In the three-electrode systems, the potential of the working electrode, on which the electroactive material is immobilised, is measured against that of a reference electrode such as the "silver| silver chloride" electrode or the standard hydrogen electrode. The current in the three-electrode system travels through the auxiliary electrode (also called the counter electrode). The advantage of using a three-electrode system is that the potential of the reference electrode is insignificantly affected by passage of current through the cell, since the current is conducted through the auxiliary electrode. Therefore, measurements of potential are more accurate and the full potential window of the electrode material can be determined. In addition, the use of an auxiliary electrode means that the working electrode becomes the current limiting electrode, this allows more accurate determination of the capacitance of an electrode material. Such advantages, notwithstanding characterisation of capacitive materials using two-electrode systems, are also of interest because the results directly reflect the performance of real devices. This will be further discussed later.

2.2 Electrical Power and Energy of a Supercapacitor

Electrical power, P, in watts (W) or joules per second is given by:

$$P = Vi \tag{5}$$

It follows that for constant voltage and current, the energy, W, in joules (J) is a simple integration of P with respect to time. So:

$$W = \int_0^t P\mathrm{d}t = \int_0^t Vi\mathrm{d}t = Vit \tag{6}$$

Equation 6, however, can be used only if both V and i are constant, which occurs in batteries but not in capacitors. For capacitors, neither V nor i is constant in the same test. These two quantities are related by Eq. 3. By substituting the capacitive current into the power expression:

$$P = CV\frac{\mathrm{d}V}{\mathrm{d}t} \tag{7}$$

The time integral of power would be substituted for a voltage-integral, hence

$$W = \int_0^t CV\frac{dV}{dt}dt = \int_0^V CVdV = \frac{1}{2}CV^2 \tag{8}$$

Alternatively, W can also be derived from Eq. 1, by substituting $V = dW/dQ$,

$$C = \frac{Q}{dW}dQ \tag{9}$$

By separating the variables and integrating both sides,

$$\int_0^W dW = W = \int_0^Q \frac{Q}{C}dQ = \frac{Q^2}{2C} \tag{10}$$

This form of energy equation contains no information on the voltage. By replacing $Q = CV$, the equation becomes $W = \frac{1}{2}CV^2$. Equations 8 and 10 describes the energy stored in a capacitor for a given C and V. When the total mass-specific capacitance, C_{ssp} (F g^{-1}) is used, the specific energy, W_{sp} results, in units of J kg^{-1}, or more commonly expressed in units of Wh kg^{-1}, the conversion is 1 Wh equals 3600 J. For the calculation of W_{sp}, C_{ssp} has to be the capacitance recorded in a two-electrode configuration, divided by the sum of both electrodes' mass. In this way, the W_{sp} value reflects that of an operational supercapacitor device. The variation of W_{sp} for devices having different C_{ssp} and different operating voltage is plotted in Fig. 3.

The energy storage density and power delivery capability of various storage and conversion systems are summarized in a chart called the Ragone plot shown as Fig. 4. Typical commercial supercapacitors can store up to 10 Wh kg^{-1} of energy and deliver up to 10^5 W kg^{-1} of power. In the Ragone plot, the plot area covered by supercapacitors overlaps at both ends with that of capacitors (at the high power, low energy end) and that of batteries (at the high energy, low power end). In the Ragone plot we also find fuel cells and internal combustion engines, which are conversion systems that convert energy stored in other forms into electrical energy or mechanical work. Fuel cells convert energy stored in chemical bonds into electrical energy during

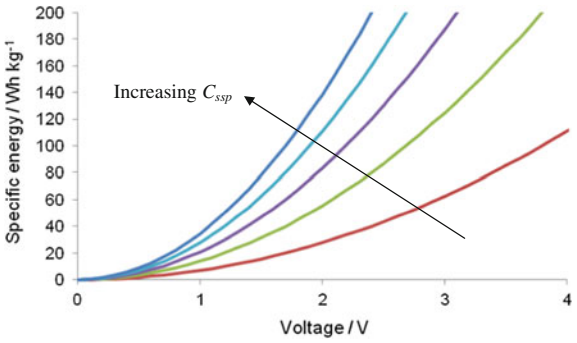

Fig. 3 Variation of W_{sp} for supercapacitor devices against operating voltages, for cells with different C_{ssp}. The increasing C_{ssp} is indicated with an *arrow*, starting with *bottom line* for 50, 100, 150, 200 and 250 F g^{-1}

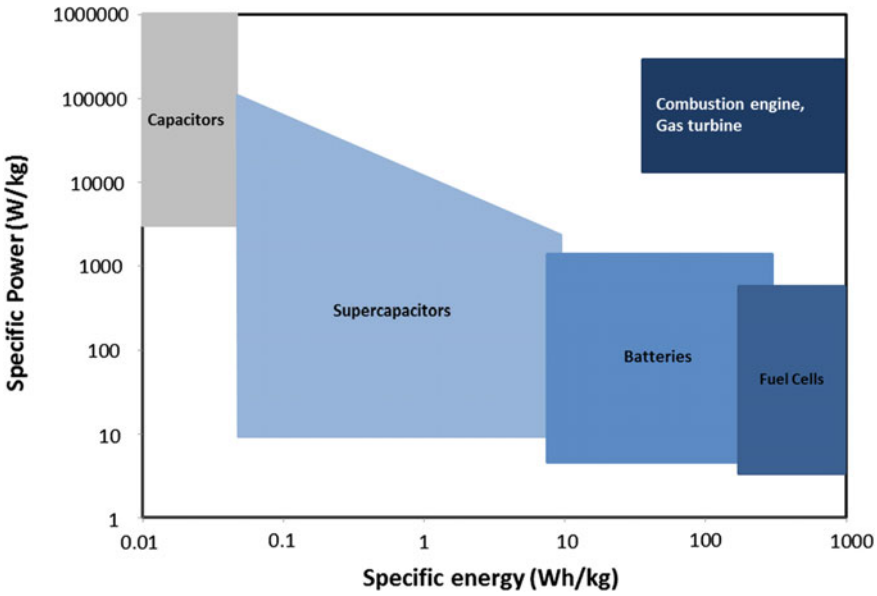

Fig. 4 Ragone plot of various energy storage and conversion devices. Adapted from Winter and Brodd [18]

controlled oxidation reaction while internal combustion engines release the energy stored in chemical bonds in uncontrolled oxidations. Notably, the characteristics of internal combustion engines are almost always present in Ragone plots because researchers often attempt to match performance data of other systems to those of combustion engines. It is also important to point out that none of the electrochemical devices shown in the Ragone plot matches the performance of combustion engines and so to utilise them would require hybrid systems made of combinations of these component systems [18]. More importantly, the information provided in Ragone plots for supercapacitors and batteries most often only refers to the capability of the active materials. Actual device performance may be significantly lower when the weight of the electrolyte, current collectors and device housing are considered.

In most cases, the relatively high power/low energy supercapacitors contain aqueous electrolytes, whereas the relatively high energy/low power supercapacitors contain organic electrolytes and/or ionic liquid electrolytes. The differences between these electrolytes are their conductivity, viscosity, diffusivity and electrochemical stability (voltage window), among others. Aqueous electrolytes have the highest conductivity of all electrolytes, due to the high dielectric constant of water. This gives rise to small sizes of hydrated ions which favoured high capacitance and high power capability. The disadvantage of aqueous electrolytes however, is the relatively low voltage window, limited by the potential window for the decomposition of water, i.e., 1.23 V. On the contrary, organic and ionic liquid electrolytes are generally less conductive, but permit much higher voltage window

(above 3.5 V and up to 6 V) [19, 20]. As the energy stored in supercapacitors scales with the square of the voltage (Eq. 8), the energy storage density in organic and ionic liquid electrolyte-based supercapacitors can be much higher compared to aqueous ones. However, it is worth mentioning that while most research work is performed on developing better electrode materials for supercapacitors, the choice of electrode materials can somewhat limit the choice of electrolytes. We will return to this discussion in a later section.

2.3 *Materials for Construction of Supercapacitors*

It is impossible to discuss the advancement of supercapacitor development as an independent subject, because a supercapacitor consists of two capacitive electrodes and a strong electrolyte. However, since the charge storage in supercapacitor devices is limited by the electrodes in most cases, we can say that the development of electrode materials can translate directly to the development in supercapacitors. Thus, a discussion first on the development of materials from which supercapacitors are constructed may be more useful as that is where some of the most fundamental issues are addressed. When both electrodes of a supercapacitor are made of the same material, the device is called a symmetrical supercapacitor. Otherwise the device is called an asymmetrical supercapacitor. In symmetrical supercapacitors, either electrode may be used as the positive or negative electrode. For asymmetrical supercapacitors, the electrode material which operates at the more positive potential region is used as the positive electrode, and the negative electrode is the electrode material which operates at the more negative potential region. The main advantages of symmetrical supercapacitors are the ease of making them since either electrode may be used as the positive or negative electrode. Asymmetrical supercapacitors, on the contrary, may be tailored to achieve a higher operating voltage and thus achieve higher energy storage density [21–24]. Common symmetrical supercapacitors are made of carbon [25–27] while asymmetrical supercapacitors are commonly made of carbon as the negative electrode whereas a wide range of materials are used for the positive electrode including metal oxides [25, 28, 29] and electronically conducting polymers (ECPs) [23, 30–34]. Asymmetrical supercapacitors that are made from two different metal oxides or two different ECPs are also common [32, 35–42]. The performance of most supercapacitors is usually reported as that of a single cell only. However, in application, they can be stacked to achieve a higher operational voltage [35, 43–45].

The types of materials used for making the supercapacitor electrodes can be put into the three main categories of carbons, metal oxides and ECPs. Carbon, in its various forms, is the most widely used commercial material for supercapacitors [7, 46, 47]. In fact, as mentioned above, the first supercapacitor was a carbon–carbon one [7, 18]. Carbon materials are popular as supercapacitor electrodes due to the relatively low cost, high conductivity, good corrosion resistance, high temperature stability, availability and established electrode production technologies

[7, 26]. However, the capacitance of carbon materials is significantly lower compared to the metal oxides and the ECPs. Thus, interest in metal oxides and ECP materials are primarily due to their significantly higher specific capacitance values. The higher specific capacitance of metal oxides and ECPs can be explained by the different charge storage mechanisms taking place in them compared to carbon.

2.4 Charge Storage Mechanisms

Energy in supercapacitors can be stored through the electric double-layer (termed double-layer capacitance), or as the result of a faradaic process (termed pseudocapacitance, or redox-capacitance), or a combination of both. For double-layer capacitance, charge storage occurs at the interface of a polarisable electrode and an ionic conductor which is often a solution. This is the predominant charge storage mechanism for carbon materials. The charging of the double-layer is ascribed to the effect of ionic and electronic charge separation at the electrode/electrolyte interface when the voltage between the two capacitor electrodes is varied. As the storage of charge in a double-layer is electrostatic in nature, i.e., cations accumulate at a negatively charged electrode and likewise anions at a positively charge electrode, [17, 48] the charging and discharging (or draining) processes can take place very rapidly and with high reversibility [17].

In contrast to double-layer capacitance, pseudocapacitance occurs as a result of an electron transfer process, i.e., a faradaic process. This is the predominant charge storage mechanism for metal oxides and ECP materials. Unlike double-layer capacitance, which only involves charging the surface of a material, pseudocapacitance occurs in materials that can be reversibly oxidised and reduced. The redox process is accompanied by either absorption or expulsion of counterions to maintain electroneutrality. In this case, the charge can be stored throughout the volume of the pseudocapacitive material provided there is sufficient electrolyte access for counterion diffusion. However, although the role of the counterions is to maintain electroneutrality of the charged material, the quick faradaic charge transfer process results in concentration or depletion of ions of a particular charge in the solution next to the electrode [17]. In this case it is similar to double-layer capacitance, and hence the birth of the term ‘pseudocapacitance’ [17]. The other uniqueness of pseudocapacitance lies in the charging characteristics; the capacitance can vary to a certain degree with potential for a pseudocapacitive material, [17, 48] but the variation should not be too far away from that of a true capacitor. In other words, when measured by cyclic voltammetry, the CV must be rectangular in shape, at least approximately. This is because for a peak-shaped CV, it is invalid to apply the simple relation $C = Q/V$ [49, 50]. On metal oxides and ECPs, pseudocapacitance occurs across a broad range of potentials, and hence, there is an associated potential

window with them. This is due to the close vicinity of individual redox sites in metal oxides and ECPs, close enough for them to interact with each other, i.e., they form bands [49]. The explanation of such behaviour for metal oxides and ECPs may be provided using the band theory and interested readers are directed to the articles by Chae et al. [50] and Chen [49].

For materials in which capacitance arises from purely double-layer charging, such as carbon, as the charging is purely electrostatic in nature, they can be used with any electrolytes, and so we can afford to choose the electrolyte based on the requirement of higher power, or higher energy. However, to utilise materials in which capacitance arises from pseudocapacitance, there is less freedom of choice, and they are more often used with aqueous electrolytes. Metal oxides and ECPs have associated potential windows (whereas double-layer charging would occur through an infinitely wide potential window, in theory) so it is not necessarily beneficial to charge the material outside the pseudocapacitive potential range, and in many cases doing so can even be damaging to the electrode material. Modes of failure of such materials include overoxidation of ECPs [51] and potential-dependent dissolution of metal oxides [52]. Fortunately, the pseudocapacitive potential range of most ECPs and metal oxides coincides with that of water. It is possible to use other types of electrolytes with these materials, but doing so may be disadvantageous because the highest capacitance is achieved when aqueous electrolytes are used. Moreover, the delicate chemical nature of some pseudocapacitive materials also needs to be taken into account. As an example, polyaniline requires protonation in order to become conductive so it has to be used with protic solvents such as aqueous acids [53].

Thus far, we have pointed out that the use of ECPs in supercapacitor applications is due to their high capacitance compared to carbon materials and this is due to the different charge storage mechanism of these materials. However, the same charge storage mechanism that takes place on ECPs also takes place on metal oxide materials and the result is that these two types of materials have comparable mass-specific capacitance [47]. To distinguish between these two classes of materials, considerations actually have to be taken beyond the metric of capacitance. The advantages of the use of ECP materials, in our opinion, are generally due to the non-hazardous nature of these polymeric materials, lower cost and ease of fabrication.

2.5 Electronically Conducting Polymer

ECPs are polymers which have a π-conjugated backbone, which consists of a regularly alternating single (C–C) and conjugated (e.g. C=C) bonds. The π-conjugated backbone is responsible for the generation and propagation of charge carriers, making the polymers intrinsically conducting. Thus all ECPs share the same π-conjugated structure [54]. The understanding of the electronic conductivity in ECPs was first developed by Heeger, MacDiarmid and Shirakawa in the 1970s,

based on the example of polyacetylene, which is the simplest form of any ECPs [55, 56]. Upon doping with bromine, the polyacetylene film showed a dramatic conductivity increase [55] The doping in that case corresponds to oxidation of the ECP (p-doping), and de-doping corresponds to the reduction of ECPs. Thus p-type ECPs are conducting in the oxidised state, while being largely insulating in the neutral state. Taking such behaviour into consideration, the name 'semiconducting polymers' is more accurate because it describes the nature of the material's conductivity. It is due to the semiconducting nature of ECPs that charge storage occurs in these materials [49, 50].

Charge storage in ECP materials arises from the possibility of reversibly oxidising and reducing these materials over a certain range of potential. Therefore, they are pseudocapacitive materials. When ECPs are placed or grown on electrodes, they can be electrochemically oxidised or reduced. This redox process is accompanied by either absorption or expulsion of counterions to maintain electroneutrality. ECPs are attractive materials for fabrication of supercapacitor electrodes because the redox processes in ECPs can proceed at very fast rates (if electrolyte access allow it), and therefore give rise to rapid charging and discharging, which translates to high capacitance and high power in the context of supercapacitor performance [51]. In most cases, the insulating-conducting switching potential in ECPs presents the negative potential limit for its application in supercapacitors, while the positive limit is set either by the potential at which the solvent becomes oxidised or the potential where the ECP undergoes irreversible oxidative degradation, termed "overoxidation". The most popular ECPs for supercapacitor applications are polypyrrole (PPy), polyaniline (PAn) and poly(ethylenedioxythiophene) (PEDOT) (Fig. 5). This is due to their high conductivity, ease of preparation, cost effectiveness and their relatively light weight, which translate to higher specific capacitance [47, 51, 57]. The three common ECPs mentioned above are all p-type ECPs. Although n-type ECPs also exist, such as certain polythiophene derivatives, they are far less popular in comparison [19]. The other exception is polyacetylene which although is lighter than any other ECPs, it is not commonly used in supercapacitors due to its relative instability [58, 59]. For all ECPs, their theoretical mass-specific capacitance (which can be compared with measurements from a three-electrode setting) can be conveniently estimated using $C_{\mathrm{tmsp}} = \frac{nF}{(\Delta V \times M_W)}$, where F is the Faraday constant (96,485 C mol^{-1}), n is the average number of electrons transferred per unit monomer of the ECP electrode material during the redox process, ΔV is the potential range across which the charging occurs and M_W is the relative molecular weight per monomer unit. For the ECPs that we will discuss, Table 1 shows a comparison of their theoretical mass-specific capacitances.

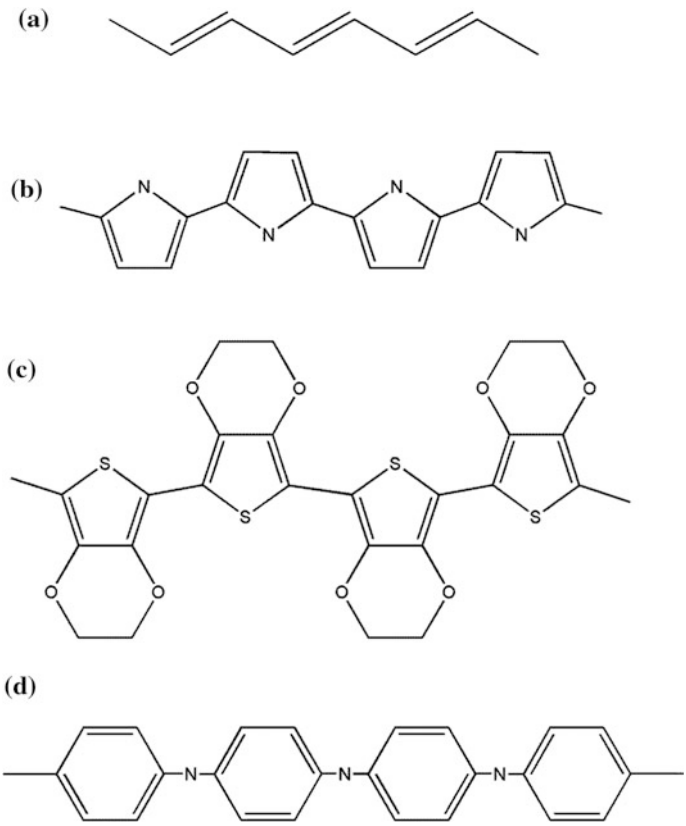

Fig. 5 Chemical structures of some most common ECPs in their neutral state, hydrogen atoms are omitted for clarity. **a** Trans-polyacetylene, **b** PPy, **c** PEDOT and **d** PAn

Table 1 Theoretical mass-specific capacitance, cited from Lota et al. [60]

ECP	n	ΔV	M_W	Theoretical mass-specific capacitance, C_{tmsp} (F g^{-1})
PPy	0.33	0.8	67	620
PAn	0.5	0.7	93	750
PEDOT	0.33	1.2	142	210

2.6 Polypyrrole (PPy)

After polyacetylene, PPy is one of the simplest ECPs. The π-conjugated backbone of a neutral PPy resembles that of cis-polyacetylene, except PPy has an additional nitrogen heteroatom every four carbon atoms, linking between the 1st and 4th carbon atoms (Fig. 5b) [56]. The nitrogen heteroatom and the ring structure of the repeating unit stabilise the polymer's molecular structure. PPy is very attractive for

supercapacitor applications due to the ease of processing as the pyrrole monomer is soluble in water, and the polymer has good conductivity and environment stability. The typical measured mass-specific capacitance values of PPy materials are in the range of 200–500 F g^{-1}.

2.7 Polyaniline (PAn)

Polyaniline (PAn) is an ECP discovered in 1934 as aniline black. PAn is a unique ECP as the transition from insulator to metallic conductivity not only depends on the oxidation state, but it is also induced by protonation [56]. Due to the requirement of protons for PAn to become conducting, and to enable proper charging and discharging, protic solvents are required. Aqueous acidic solutions are the most common electrolyte used for PAn material characterisation. While examples of PAn characterised in neutral [61] and alkaline [62] solutions exist and high specific capacitance values have been reported, the ill-defined shape of the CVs suggest that the Pan was non-capacitive. The main advantage of using PAn is its significantly higher capacitance (higher than 600 F g^{-1}) than other ECPs, because the reversible redox reaction of PAn can remove up to one electron for every two monomer units, compared to the maximum one electron every three monomer units in the case of PPy (Table 1).

2.8 Poly(3,4-Ethylenedioxythiophene) (PEDOT)

Next to PPy and PAn, PEDOT is the most commonly used ECP for supercapacitors. PEDOT was developed during the late 1980s, at the Bayer AG research laboratories in Germany [63]. The original intention was to produce a soluble conducting polymer that lacked the presence of undesired α-β and β–β coupling like those usually present in PPy [63]. The undesired couplings do not take place during polymerisation of PEDOT as both of the β positions are occupied by the ethylenedioxy functionalities. As a result, a higher conjugation length is achieved, giving rise to a higher intrinsic electronic conductivity. The ethylenedioxy functionalities also result in higher stability of the polymer in the oxidised state. PEDOT was initially found to be insoluble, but this was overcome by using poly(styrenesulfonate) (PSS) as the dopant during polymerisation. The latter is soluble in water, and the combination of PEDOT:PSS becomes soluble as well [63]. PEDOT:PSS is commercially available, known as BAYTRON P from the Bayer company [63]. The main advantage of PEDOT over the other ECPs is its wider potential range and higher stability. Typically, mass-specific capacitances of around 100–200 F g^{-1} are reported for PEDOT materials which is lower than for PPy or PAn. However, thick PEDOT films can be made by potentiostatic deposition and the electrode capacitance, normalised to electrode area, can reach 5 F cm^{-2} [64].

2.9 The Necessity for ECP Nanocomposites

The ECPs introduced above share a common weakness which limits their application alone in supercapacitors: their propensity do degrade during repeated charge/discharge cycles (or redox cycles). This happens because the associated ion and solvent transfer across the ECP/electrolyte interface causes swelling and shrinkage of the ECP [47, 51]. This weakness is very profound especially for PPy and PAn. Among the most commonly used ECPs, PPy has the worst redox cycling stability performance [51]. The relatively poor redox cycling stability is largely due to the structure of the PPy polymer aggregates which are non-porous structures and consist of 'large' micrometre-sized particles that are commonly visible on the surface as typical 'cauliflower-like' or 'muffin-like' structures (Fig. 6) [51]. These structures are not favourable for electrolyte access during the redox cycling as the electrolyte must penetrate thick layers of solid PPy to accomplish the redox processes. PAn (Fig. 7) is mechanically much weaker than PPy and PEDOT, and hence still suffers from poor redox cycling stability despite the fact that porous structures can be achieved easily using different fabrication methods [51, 65–68]. For PEDOT, the comparatively better redox cycling stability arises from a combination of at least two effects. First, PEDOT has a porous structure, made up of connected aggregates of nanoparticles, [51, 64] which favours electrolyte access. Second, the lower mass-specific capacitance of PEDOT means that, for any given

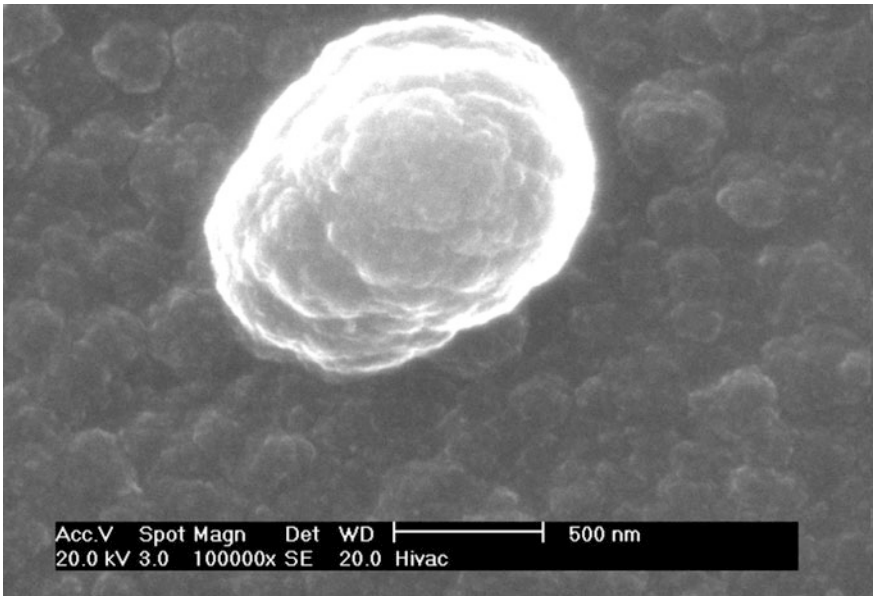

Fig. 6 Scanning electron microscopy image of electrodeposited PPy with chloride anions showing an example of what is called a 'cauliflower structure' or 'muffin structure'

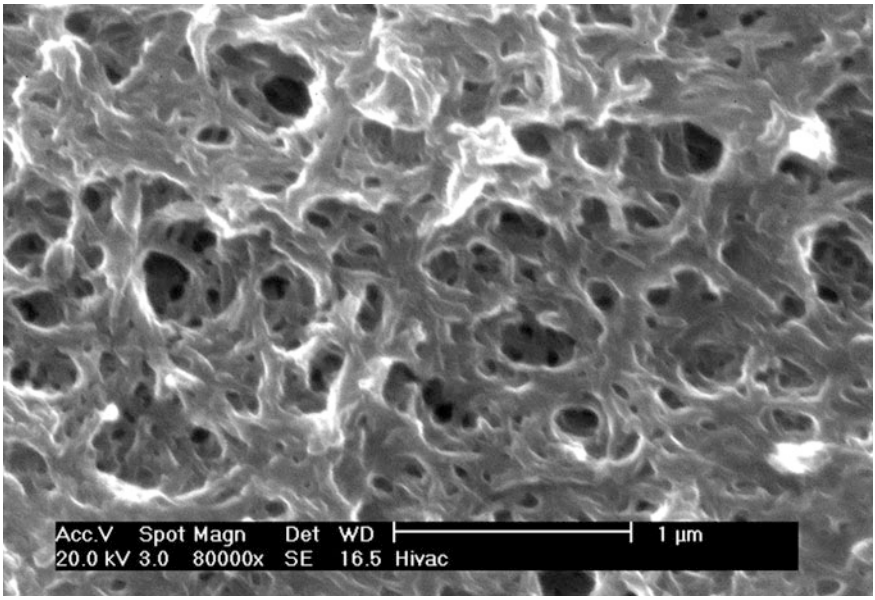

Fig. 7 Scanning electron microscopy image of electrodeposited PAn with chloride anions

mass of PEDOT, the amount and rate of counterion ingression and expulsion during redox cycling of PEDOT are lower than in PPy and PAn. Perhaps applying the same interpretation to the relatively high mass-specific capacitance value of PAn would also explain its relatively poor redox cycling stability.

The instability of PAn towards repeated redox cycling shows that just a porous structure alone is insufficient to make these materials into high performing electrode materials. To improve on the performance of ECP materials, materials also require mechanical strength. A range of ECP nanocomposites, containing nanoparticulate materials, has been developed to impart mechanical strength, as well as porosity to ECPs to improve the redox cycling stability and this approach is described in the following section [47, 51, 69–73].

2.10 The Formation of ECP Nanocomposites

ECPs and their composites can be formed using chemical and electrochemical methods. Each method involves oxidation of monomers in the presence of a counterion species (either small mobile ions such as Cl^- or large immobile species such as negatively charged [51, 74]). Chemical synthesis of ECPs is achieved by oxidation of the monomers using an oxidising agent such as iron chloride or ammonium persulfate, while electrochemical synthesis involves anodic polymerisation on electrode in presence of the counterion species. The chemical synthesis of ECP composites involves mixing the monomer of an ECP with the supporting

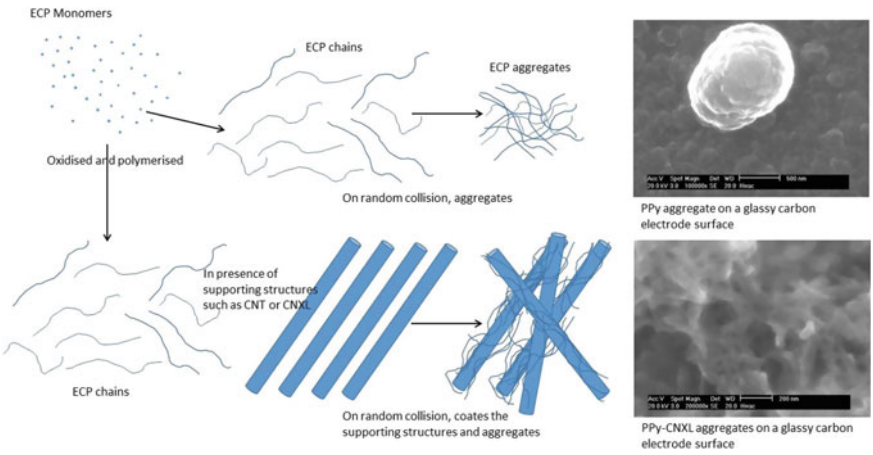

Fig. 8 The schematic of the formation of ECP and ECP nanocomposites

material (which can be charged or uncharged) prior to the oxidation step. When forming a composite with an uncharged supporting material, supporting electrolytes are also required in the reaction mixture. Electrochemical synthesis of ECP composites can proceed in two ways, either by polymerisation on a pre-formed layer of the support material on an electrode, or by co-electrodeposition in which the electrochemical deposition of the ECP and the adhesion of the supporting material to the deposited ECP occurs simultaneously. During ECP composite formation, chemical or electrochemical oxidation of the monomers leads to precipitation of the polymers from solution. In the presence of an additive supporting material, it becomes energetically favourable for the polymer to coat the additive material during the precipitation process (Fig. 8).

The main advantage of chemical synthesis of ECPs and their nanocomposites is the ease of mass production, but the final product is always present in powder form. Then, to make an electrode using such ECP products most of the time would require the use of a binder. The use of the binder material or the presence of reduction products of the oxidising agent may also affect the overall performance of the material [51]. On the contrary, as the ECPs and their nanocomposites are directly formed on the electrode surface during the electrochemical synthesis process, there is no need for a binder. The contact resistance within the ECP material and between the ECP and the current collector is also significantly reduced, as they grow on the electrode substrate directly [51]. However, the disadvantage of the electrochemical synthesis process in making ECP and their nanocomposites is the difficulty to produce at large scale with this method, because production in this case (assuming the monomers are of surplus) is limited by amount of charge (or current) supplied through the electrode. In the case of chemical synthesis, the production is limited by amount of charge supplied through the oxidant chemicals. By

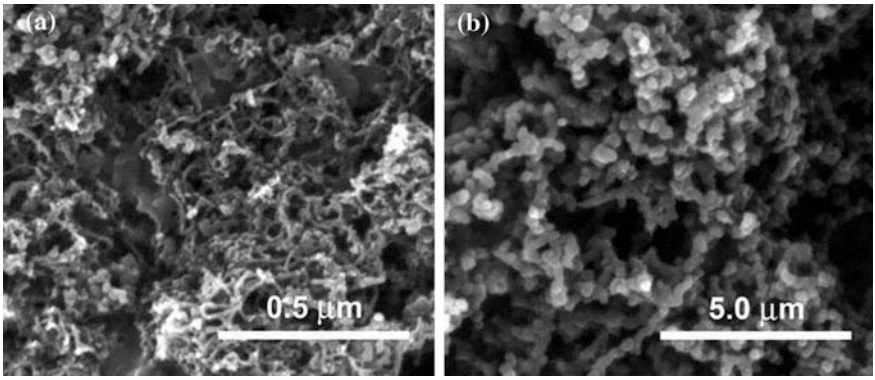

Fig. 9 Scanning electron micrographs showing the morphology of PPy-MWCNT, prepared by chemical oxidation. This figure was adapted from Zhou et al. [45]

comparison, it is much easier to supply a large amount of charge through the use of oxidant chemicals rather than through an electrode surface (Fig. 9).

2.11 ECP–CNT Nanocomposites

Among all nanocomposites of ECPs, the most common is nanocomposites of ECPs with CNTs. The properties of CNTs are quite amenable to making porous ECP composites, and as they are also extremely strong, the reinforcement of the composite is also remarkable. For example, pellet electrodes were made from chemically synthesised PPy-multiwalled carbon nanotube (MWCNT) nanocomposites by just pressing without any polymer binder and this composite had a specific capacitance of 495 F g^{-1} [69]. The strength of the nanocomposite provided by MWCNT is evident because the pellet composite electrodes pressed at 500 kg cm^{-2} retained their porous internal structure to allow fast ion diffusion and migration as a result of the strength contributed by the MWCNTs [69].

PPy-CNT composites with controlled pore sizes were fabricated for an investigation of how the performances of these composites are affected by the pore sizes [75]. It was found that the composite that had bigger pore sizes also achieved higher capacitance when tested electrochemically [75]. This behaviour was consistent when the composites were tested at a range of potential scan rate [75]. For co-electrodeposited PPy-MWCNT films, the capacitance of the composites was twice that of pristine PPy films for all deposition charges due to the significantly higher porosity and surface area (Figs. 10 and 11) [76]. The electrode capacitance, per unit area of the underlying electrode, for the composite reached 1 F cm^{-2}, while the mass averaged capacitance was 192 F g^{-1} [76]. Later studies also achieved electrode-specific capacitance of 2.35 F cm^{-2} using a co-electrodeposited PPy-CNT

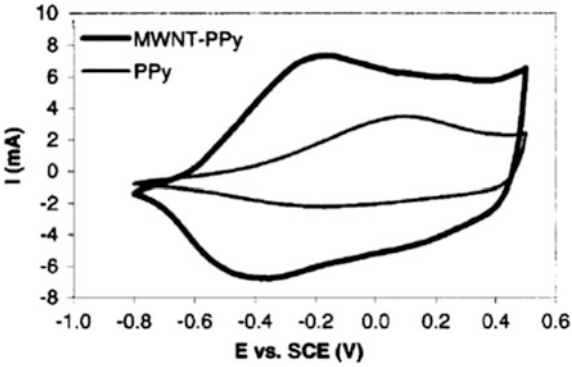

Fig. 10 CVs showing the comparison of MWCNT-PPy composite films and PPy films prepared using 1.8 C/cm^2 film formation charge. Scan rate was 50 mV/s. Figure adapted from Hughes et al. [76]

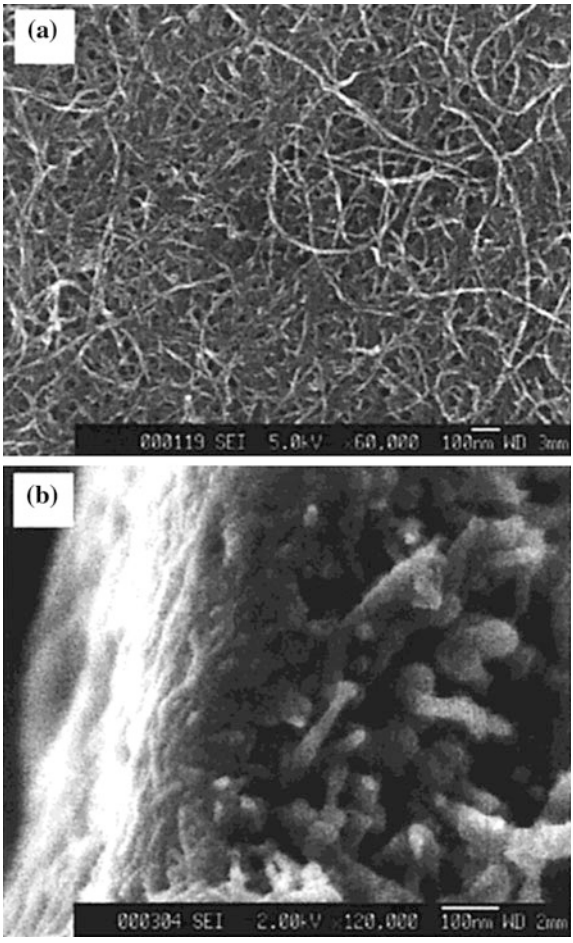

Fig. 11 Scanning electron micrograph showing the porous network of PPy-MWCNT composite films: **a** at the film surface and **b** the fractured film cross-section. Figure from Hughes et al. [76]

composite [51]. Without the CNT, the electrodeposited PPy only reached around 0.7 F cm^{-2} [76].

There are many ways by which the nanocomposites of PPy and CNT can offer improvement over the pristine PPy. Other than producing a porous structure with strength enhancement by the CNTs within the composite, if the CNTs have negative surface charge, there is an additional enhancement effect on the electrochemical performance. For an example, the presence of acid-treated CNTs within PPy-CNT nanocomposites, as a large negatively charged immobile species, means that electroneutrality of the composite material during redox cycling will also involve the cations of the electrolyte, rather than just anions for the case of pristine PPy [77]. Thus when an electrolyte such as aqueous KCl is used, K^+ ions will also be involved in the redox cycling of the PPy-CNT composite if the embedded CNTs are negatively charged, rather than just Cl^- ions otherwise. This effect is highly beneficial, because the transport of K^+ is easier than Cl^-, due to the smaller size of the hydrated K^+. Furthermore, in this case the oxidation of the PPy corresponds to releasing of K^+ ions, which is an entropically favourable process [78]. This transport behaviour of counterions has been studied using an electrochemical quartz crystal microbalance. When KCl was used as the electrolyte for the redox cycling of PPy-CNT, uptake of both K^+ and Cl^- have been observed, when tetrabutylammonium bromide was used, only uptake of Br^- was observed, this shows the transport of smaller ions is favoured during the redox process [79]. Thus, although the role of the negative charge on the CNTs has not yet been fully clarified on how the ECP–CNT composite form, as discussed in the above section, the improved performance of the resulting composite can be reasoned to the charge on the CNTs.

For PAn–CNT nanocomposites, it has been found that the capacitances of co-electrodeposited PAn–CNT nanocomposites were not significantly better than those of pristine PAn films because PAn films also have a very porous structure (Figs. 7 and 12) [51]. In PAn–CNT nanocomposites, the significance of the CNTs is in the redox cycling stability, as they alleviate stress generated by the electrolyte movements during redox cycling [51]. The strength of CNTs has another very significant effect that the use of CNTs allows the formation of stronger and thicker

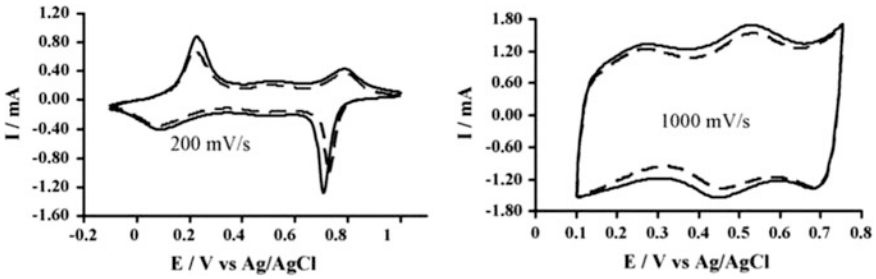

Fig. 12 CVs showing the comparison between PAn/CNT (*solid line*) and PAn (*dashed line*). The electrodes were formed using electrodeposition to a formation charge of 6.5 mC. Figure was adapted from Peng et al. [51]

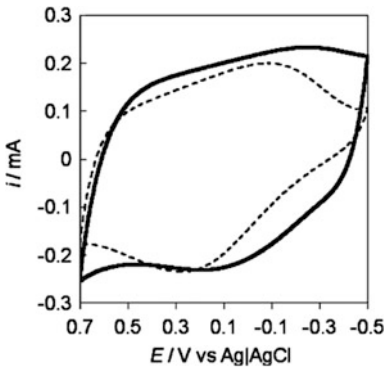

Fig. 13 CVs obtained at an electrodeposited PPy (*dashed line*) and PPy/CNXL (*solid line*) in 0.1 M KCl at a scan rate of 0.25 V/s. Each film was electrodeposited with a charge of 0.1 C cm^{-2}. Figure from Liew et al. [71]

films. For example, significantly higher electrode capacitances can be achieved for electrodeposited PAn–CNT (3.5 F cm^{-2}) composites than for pristine PAn (2.3 F cm^{-2}) [80]. By electrodepositing PAn on pre-formed CNT electrodes, the composite had a mass-specific capacitance of 485 F g^{-1}, whereas the pristine electrodeposited PAn had a specific capacitance of about 260 F g^{-1} [81]. Using a chemical synthesis method, PAn–CNT composites were also much more stable in response to redox cycling tests than the PAn [82]. Chemically synthesised PAn–CNT composites, pressed into a pellet formed without using any polymeric binder, exhibited a specific capacitance of 650 F g^{-1} [69]. When PAn–CNT nanocomposite was supported on cloth, flexible supercapacitor electrodes were made [83]. Using a simple dip coating method, CNTs were coated on nonwoven wiper cloth and PAn was subsequently deposited on the surface of this CNT-cloth composite through chemical polymerisation. This simple fabrication method produced a PAn–CNT-cloth composite which had a capacitance of 410 F g^{-1} and a very stable performance (Fig. 13) [83].

It was recently reported that PAn–CNT composite can also be made from enzymatic synthesis [84]. This is a non-conventional synthetic route (although essentially still a chemical synthetic route) for the making of such composites. However, as an enzymatic process, it has the merit of being environmentally friendly. Also., the PAn–CNT composites made from this method had comparable structure and morphology to those made of the conventional chemical oxidation method. The specific capacitance of this composite was 440 F g^{-1} [84].

It is interesting to recap on the process by which PAn–CNT form. As a reminder, the electronic conduction of PAn requires protonation and dispersions of CNTs in water require negative surface charges. The negative charge of CNTs is usually due to surface carboxylic groups, but in presence of high acid concentration in a monomer/CNT mixture (which is required to make conductive PAn), the surface carboxylic groups on the CNTs will be protonated. Hence, the surfaces of CNTs on which PAn deposit are uncharged and this is a demonstration that negative surface charge on CNTs are not necessary for the forming of ECP–CNT composite.

The capacitive performance of PEDOT was also highly improved by forming composites with CNTs electrochemically. The capacitance of an electrochemically synthesised PEDOT–CNT nanocomposite was more than twice that of pristine PEDOT synthesised using the same deposition charge [51, 85]. However, thicker films of PEDOT–CNT could not be made using electrochemical co-deposition due to the phase separation of the deposition solution, which consists of an aqueous/acetonitrile mixture, after long deposition times [51]. The oxidised CNTs are dispersed in the aqueous phase whereas the EDOT monomer is only soluble in acetonitrile [51]. The aqueous solubility issue is not present for chemical synthesis of PEDOT–CNT composites [60, 86]. For example, an asymmetrical supercapacitor built using the PEDOT-carbon composite as the cathode and activated carbon as the anode, containing organic electrolyte exhibited average mass-specific capacitance of 160 F g^{-1} over a voltage of 1.5 V, and a stable performance for over 20,000 cycles [60]. A ternary composite of MnO_2–CNT–PEDOT in which PEDOT was used as the conductive wrapping over the MnO_2–CNT composite for better conductivity had 427 F g^{-1} in capacitance [87].

2.12 ECP-Graphene Nanocomposite

Graphene has recently become a very popular choice as a material for the fabrication of ECP nanocomposites for use in supercapacitors. Graphene is similar to CNTs that it is very strong material and can have very good conductivity. The main difference between graphene and CNTs concerning their use for making ECP nanocomposites is geometry. Rather than the high aspect ratio rod form of CNTs, graphene take the form of sheets. However, like CNTs, graphene can provide very good surfaces for ECPs to deposit on and some of the developments on ECP-graphene materials have been very interesting.

Composite films of sulfonated graphene and PPy have been co-electrodeposited from aqueous solutions containing Py monomer, sulfonated graphene and dodecylbenzene sulfonic acid [88]. For a film formation charge of 2 C cm^{-2}, the film showed a specific capacitance of 285 F g^{-1} at a current density of 0.5 A g^{-1} [88]. When a higher film formation charge of 4 C cm^{-2} was employed, the specific capacitance of the PPy-graphene composite decreased to 215 F g^{-1} [88]. The geometry of graphene, as sheets, makes it difficult to form porous films when deposited on electrode surfaces. This is demonstrated when the specific capacitance of electrodeposited films of PPy-sulfonated graphene decreased significantly from 285 to 215 F g^{-1} when the deposition charge was increased from 2 to 4 C cm^{-2}. This shows the nonlinear increase of capacitance with the amount of material deposited, which begins at a rather low deposition charge. In other words, the high performance is limited to only a very thin film and not extendable to thicker films. Another example is electrodeposited composites of PPy-graphene oxide which had specific capacitance of 424 F g^{-1} but the film formation charge was relatively low, 0.13 C cm^{-2} [89]. On the contrary, when PPy-CNT nanocomposites were

synthesised with these deposition charges, the increase of capacitance with the amount deposited was linear [51, 76]. The main difference is that CNTs facilitate the formation of porous films easily due to its geometry, whereas graphene sheets have the tendency to stack on each other.

By forming 'sandwich' composites by utilising spacers, the stacking problem is addressed. Layered graphene oxide nanostructures with sandwiched PPy synthesised chemically in the presence of surfactant cetyltrimethylammonium bromide (CTAB), showed capacitance over 500 F g^{-1} when characterised at 0.3 A g^{-1} [90]. In this 'sandwich' composite, PPy fibers were synthesised between graphene oxide (GO) sheets assisted by CTAB, and acted as a spacer component between the GO sheets. Doing so, stacking of the graphene sheets is prevented, hence allowing the utilisation of double-layer capacitance of the graphene and pseudocapacitance of the PPy simultaneously [90]. Blending of PPy nanowires, made with CTAB as the counter ion, with graphene oxide also allowed the making of high stability nanocomposites [91]. In fact, CTAB has been used as a surfactant for stabilising graphene sheets in water for the making of PPy-graphene composite, and the resulting composite had a specific capacitance of 492 F g^{-1} at 0.2 A g^{-1} [92]. A free-standing film made of a ternary composite of PPy-CNT-graphene had capacitance of 211 F g^{-1} [93]. Similarly, the PPy-CNT was used as the spacer to prevent stacking of the graphene sheets [93]. When a similar ternary composite material was prepared in powder form and pressed onto a current collector for testing, the specific capacitance was 361 F g^{-1} under the optimal combination [94].

Like CNTs, graphene does not disperse in water. That is the reason for the widespread use of surfactants, such as CTAB, in preparation of nanocomposites of graphene with PPy, as we have discussed, Py monomers are water soluble. More often, GO is used as it often has a negatively charged surface, which allows dispersion in water [95]. The composite of PPy-GO can then chemically reduced to make PPy-graphene composite, and the effect of using different reduction chemicals, hydrazine and ethylene glycol, for this purpose has been investigated [95]. The use of GO allows the formation of PPy-GO nanocomposites by the co-electrodeposition method, whereby GO was incorporated as the charge balancing species [96]. The effect of incorporating GO as the immobile charge balancing species is similar to that with acid-treated CNTs. A spherical graphene-hollow PPy composite was constructed by mixing GO and polystyrene/PPy core-shell spheres followed by reduction of GO and etching of polystyrene [97]. This composite material had a specific capacitance of 500 F g^{-1} when tested at 5 A g^{-1} [97]. A PPy-GO hydrogel composite exhibited specific capacitance of 375 F g^{-1} and retained 87 % of capacitance after 4000 potential cycles [98].

To further improve the surface wettability of graphene for deposition of PPy, beyond GO, the effects of other graphene surface groups on the PPy-modified graphene composite have been investigated and it has been shown that the composite of PPy with nitrogen incorporated graphene had the best performance [99]. Similarly, when graphene with grafted surface aminophenyl groups were used to make composite with PPy, the apparent grafting of PPy on the modified graphene

took place and PPy-grafted graphene composite performed better electrochemically than the control PPy-GO composite [100].

PAn-sulfonated graphene composites fabricated in neutral aqueous solution have been shown to have a specific capacitance of 676 F g^{-1} [101]. The presence of the sulfonated graphene in the reaction mixture allowed nucleation of PAn on the graphene surface while at the same time protonating the PAn to make it conducting [101]. In the absence of the sulfonated graphene, the non-protonated PAn displayed a much less desirable electrochemical performance in neutral electrolyte, as PAn is nonconducting unless protonated. A PAn-graphene oxide (GO) composite made from chemical oxidation had a specific capacitance of 531 F g^{-1}, while PAn made using the same procedure had only 216 F g^{-1} [102]. It was possible to control the growth of vertically aligned PAn on graphene oxide nanosheets by varying the ratio of the monomer of An and graphene oxide [103]. This allowed the tailoring of the composite morphology for the making of supercapacitor electrode materials [103]. Similarly, by varying the mass ratios of PAn and graphene, an optimisation study has been performed for PAn-graphene and PAn-graphene oxide composites [104]. A free-standing film of sandwiched structured ternary composite of PAn–CNT-graphene, which had PAn–CNT composite acting as a spacer between graphene sheets, had specific capacitance of 569 F g^{-1} [105]. When high surface area graphene nanoribbons, made from treating multiwalled carbon nanotubes with a sodium potassium alloy was used for the making of composite with PAn, the PAn-graphene nanoribbon composite has capacitance of 340 F g^{-1} [106].

Reduced graphene oxide/PEDOT hybrid composites were fabricated by coating PEDOT onto reduced graphene oxide Langmuir–Blodgett films [107]. By using the Langmuir–Blodgett deposition method, the structure of the graphene oxide film was tunable and hence the templating of the PEDOT film was also tunable. Composites fabricated with this method achieved a specific capacitance of 213 F g^{-1} [107]. PEDOT/graphene and PEDOT/CNT composites synthesised from an in situ chemical vapour phase polymerization process had a specific capacitance of 156 and 137 F g^{-1}, respectively [108]. A ternary composite of PEDOT–CNT-graphene in which PEDOT functioned as the spacer between graphene sheets and CNTs as conductive additive to the composite had specific capacitance of 225 F g^{-1} [109].

2.13 ECP-Cellulose Nanocomposites

The use of nanocellulose for the fabrication of ECP nanocomposites is only very recent, due to the growing interest in using more environmental friendly materials. In our opinion, nanocomposites of ECP with cellulose are very interesting because the composite filler is non-conducting. Previously, it was generally believed that conductivity of the ECP composite filler was the key for their high performance, because ECP–CNT composites and ECP-graphene composites contained conducting fillers and showed very good performance. The development of PPy-cellulose nanocrystal (PPy-CNXL) nanocomposites showed that the conductivity of the ECP filler is not necessary, when the PPy-CNXL showed equally high

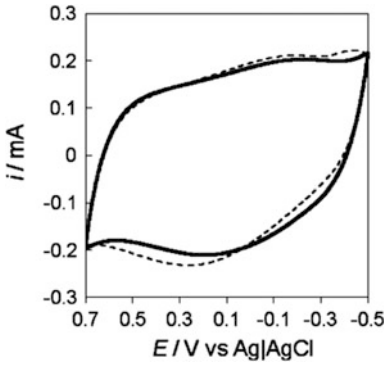

Fig. 14 CVs of electrodeposited PPy-CNT (*solid line*) and PPy-CNXL (*dashed line*) in 0.1 M KCl at a scan rate of 0.25 V s^{-1}. Each film was electrodeposited with a charge of 0.1 C cm^{-2}. Figure from Liew et al. [71]

performance when compared to a PPy-CNT nanocomposite in the same work (Fig. 14) [71]. The CNXLs were non-conducting but had negatively charged surface that allowed their incorporation into the PPy-CNXL nanocomposite during the co-electrodeposition process [71]. The performance of the PPy-CNXL nanocomposite was attributed to the porous structure of the composite and the negative charge on the CNXL surfaces [71]. Interestingly, it has also been pointed out from one of the recent PPy-GO work that the conductivity of GO was irrelevant towards the performance of the PPy-GO composites [96]. The examples of PPy-GO and the PPy-CNXL show that the performance of ECP composite is almost only influenced by the composite structure and morphology [71, 96]. More recently, good performance had also been reported for PPy-CNXL nanocomposites made by the chemical deposition method (Fig. 15) [73, 110].

As the CNXLs are also very strong materials, their use may facilitate the making of strong thick ECP–CNXL films. For example, thick PPy-CNXL films which had electrode capacitances above 1 F cm^{-2} can be made easily by electrodeposition, [72]. The high electrode capacitance of the thick PPy-CNXL films was a result of uniform growth of these porous films, which is supported by the strength of the CNXLs in the nanocomposite structure. Recently, nanocomposite films of PAn–CNXL (Fig. 16) and PEDOT-CNXL were also reported, on the premise that CNXLs can bring similar reinforcements on PAn and PEDOT as they did for PPy [111]. It was found that PAn–CNXL nanocomposites were particularly promising, similar to PPy-CNXL, as shown by the possibility of electrodepositing a thick PAn–CNXL film which had high electrode capacitance exceeding 2 F cm^{-2} [111]. The electrodeposition of thick PEDOT-CNXL film was unsuccessful, however, due to the same reasons that electrodeposition of thick PEDOT–CNT films were unsuccessful [51, 111].

The other form of cellulose used for the making of nanocomposite with PPy is the cellulose nanofibril. Compared to CNXLs, cellulose nanofibrils are longer and more flexible as they contain some amorphous structures. Paper-based supercapacitor has been made using nanocomposites of PPy and cellulose nanofibrils.

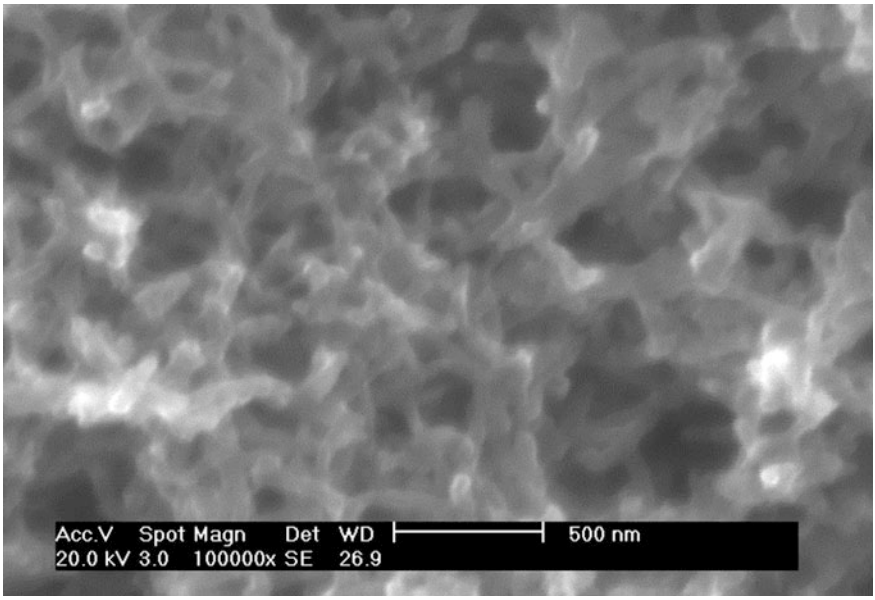

Fig. 15 Scanning electron micrograph of an electrochemically deposited PPy-CNXL film on glassy carbon electrode [73, 110]

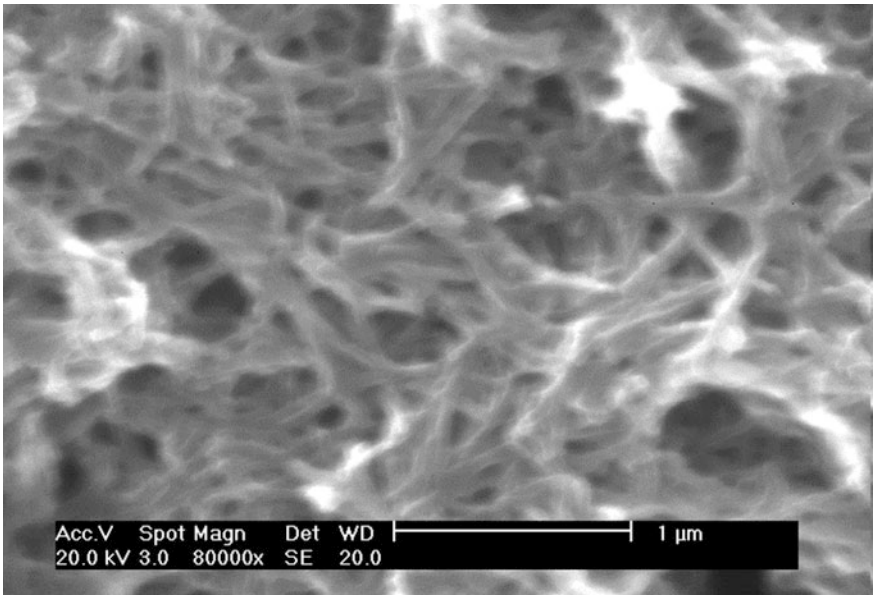

Fig. 16 Scanning electron micrograph of an electrochemically deposited PAn–CNXL on glassy carbon electrode [111]

A device specific capacitance of 32.4 F g^{-1} was achieved, based on dry weight of 20.8 mg of both electrodes [112]. The effect of paper substrates on the capacitive performance of PPy-cellulose nanofibrils has been investigated [113]. Similarly, there has been some investigations on cellulose nanofibril aerogel-PPy composites for use as supercapacitor electrodes [114]. In addition, cellulose nanofibrils derived from a bacterial source has been used for making of PAn composites [115, 116].

2.14 Prototypes and Devices

In this section, we will discuss the performance of conducting polymer nanocomposite-based supercapacitor prototypes and devices. In essence, a supercapacitor prototype is easily made with connecting 2 capacitive electrodes in series, separated by an electrolyte layer. A simple laboratory supercapacitor prototype is shown in Fig. 17, consisting of two electrodes connected in a tube which is then filled with electrolytes (called a tube cell). Otherwise, a more sophisticated assembly can be that as presented in Fig. 18, where a supercapacitor is assembled from titanium plates whose surfaces are coated with electrode materials.

In discussing the performance of supercapacitor prototypes or devices, the parameter that forms the basis for performance comparison is W_{sp} (Wh/kg) and the specific power, P_{sp} (W/kg). For packaged commercial supercapacitors, the typical range of the W_{sp} is 1–10 Wh/kg, and the typical range of P_{sp} is 100–4000 W/kg [118]. In the interest of energy storage, we have found that very frequently the W_{sp} is reported but not so often the P_{sp}. However, the P_{sp} is easily calculated just by dividing the W_{sp} by the discharging time in a GCD curve [38]. Otherwise, the maximum specific power P_{max} is calculated as $P_{max} = V^2/(4.m.ESR)$, where m is the total mass of the active materials on both positive and negative electrodes, and ESR is the equivalent series resistance which can be measured using EIS [45, 119].

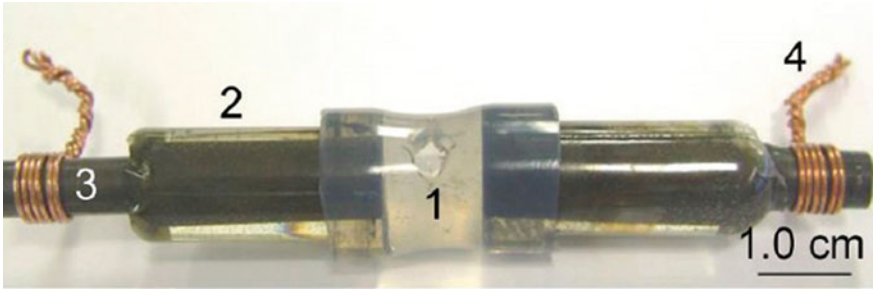

Fig. 17 A photograph image of a tube cell, an example of a supercapacitor prototype (*1*) silicone rubber tube with a hole for electrolyte addition, (*2*) epoxy resin sheath, (*3*) graphite rod as the current collector (*4*) copper wire connector. Figure adapted from Hu et al. [117]

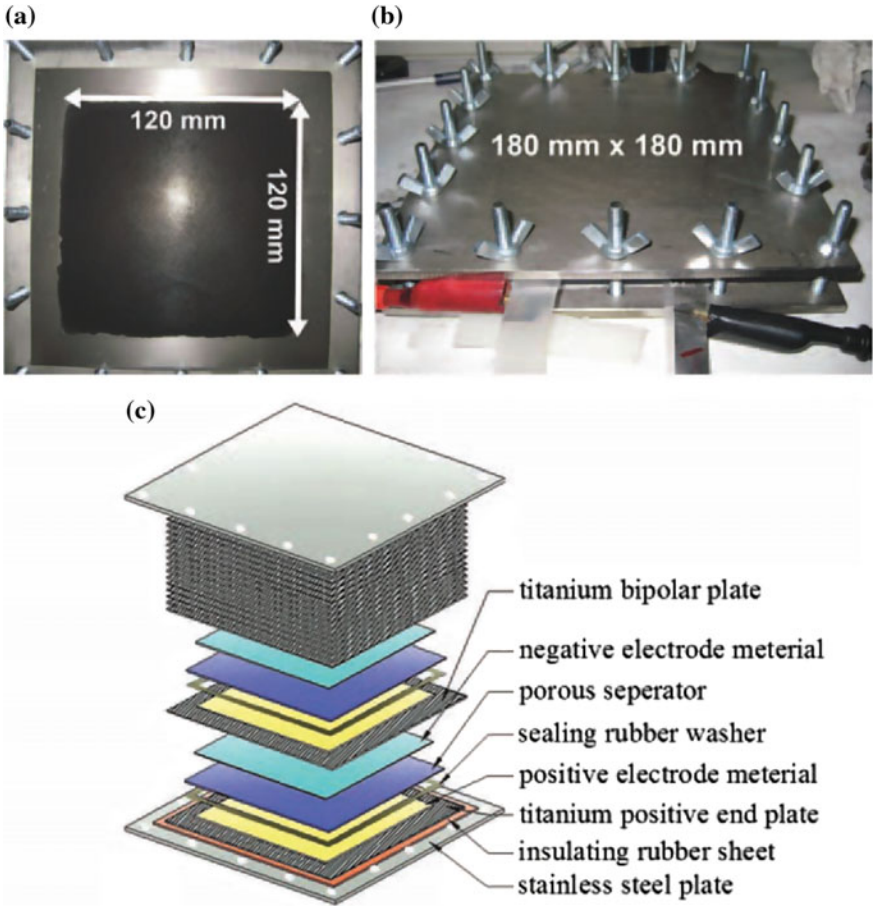

Fig. 18 Photographs of **a** a middle titanium bipolar plate in the stack loaded with the active material (PPy-CNT composite) and **b** the stack of 19 "PPy-CNT **a** | 3 mol/L KCl | CMPB (-)" supercapacitors connected through titanium bipolar plates. **c** The expanded schematic illustration of the bipolarly connected stack. Figure from Zhou et al. [45]

Using a symmetrical configuration, W_{sp} and P_{max} was determined for PAn–CNT, PPy-CNT and PEDOT–CNT nanocomposite-based supercapacitors. The W_{sp} values were 3.13, 2.38 and 1.13 Wh/kg, and the P_{max} values were 10.9, 19.7 and 23.8 kW/kg, respectively [23]. However, when carbon was used as the negative electrode in each case, making asymmetrical supercapacitors with the ECP nanocomposites, which allowed significantly higher operating voltages, both the W_{sp} and P_{max} increased significantly. For the asymmetrical supercapacitors, the W_{sp}

values were 11.46, 7.64 and 3.82 Wh/kg and P_{max} were 45.6, 48.3 and 54.1 kW/kg, respectively [23]. It is noteworthy that these values only take into account the electrode material weight and so tend to be higher than the value measured for a packaged supercapacitor. Nonetheless the above example shows clearly the benefit of employing the asymmetrical configuration in real application for both higher energy storage and power capability as shown by the examples listed in Table 2, which compares the performance of some supercapacitors, symmetrical and asymmetrical, based on ECP nanocomposites.

Table 2 Energy and power performance of some supercapacitors fabricated using ECP nanocomposites

Electrode and electrolyte			Supercapacitor Characteristics			Reference
Positive	Negative	Electrolyte	V (V)	W_{sp} (Wh/kg)	P_{sp} or P_{max} (kW/kg)	
PPy-CNT	PPy-CNT	Aq. 0.5 M Na_2SO_4	0.9	4.5	3.1	[120]
PPy-CNT	PPy-CNT	1 M $LiClO_4$/PC	2	21.22[a]		[121]
PAn–CNT	PAn–CNT	1 M $LiClO_4$ in 1:1:1 mixture of EC/DEC and DMC	2	131[b]	62.5[b]	[122]
PAn-graphene	PAn-graphene	Aq. 1 M H_2SO_4	0.8	9.6	3.47	[123]
PPy-CNT	PPy-CNT	Aq. 1 M KCl	0.6	8.25[a]		[124]
PPy-CNXL	PPy-CNXL	Aq. 2 M KCl	1	8.34		[72]
PAn–CNT	PAn–CNT	H_2SO_4-PVA gel electrolyte	0.8	2.79[c]		[125]
Graphene	PEDOT–CNT	2 M $BMIBF_4$ ionic liquid/PC	4	176.6	233	[126]
Polymethyl thiophene-CNT	Activated carbon	1 M $(C_2H_5)_4N(BF_4)$/PC	2.5	33.4		[34]
PPy-GO	Activated carbon	Aq. 1 M Na2SO4	1.6	21.4	2.1	[22]
MnO_2–RGO	PPy-RGO	LiCl-PVA gel electrolyte	1.8	16	7.4	[38]
PPy-CNT	Carbon black	3 M KCl	20[d]	3.64	25	[45]

[a]The value was determined by calculation from the data reported in the original papers
[b]The electrode is ultrathin film of 10 μg mass
[c]This is measured from a packaged prototype/device
[d]20 V is achieved by stacking 19 supercapacitors fabricated on titanium bipolar plates

3 Comments

As mentioned early in this book chapter, since the performance of supercapacitors depends highly on the electrode materials from which it is constructed, our discussion had mostly been on the materials rather than the prototypes/devices. However it is clear from Table 2 that different electrode materials can be combined to improve the performances of supercapacitor. On the characterisation of electrode materials for use in supercapacitors, we find too often that the only measurement provided to indicate the performance has been the mass-specific capacitance (F g^{-1}). While it is probably true that the mass-specific capacitance is the most basic and important measurement for supercapacitor electrode materials, over emphasizing on this single measurement can mean that much of the other important information may be ignored. First of all, the mass-specific capacitance is not linearly dependent on mass of the ECP material and hence cannot be an independent performance indicator. As we have discussed, the physical processes that are involved to give rise to capacitive behaviour of ECP materials involve diffusion of electrolyte species. In a diffusion process, the statistical average time required for molecules or ions to diffuse through a certain distance, scales as the square of the distance [127]. This implies that when the mass of an ECP material or ECP nanocomposite film is doubled, the statistical average time required for the whole electrode to become charged (as it is limited by diffusion) is increased fourfold. A corollary is that when measurements of capacitance are realised by voltammetry, potentiometry and so on, where often time is fixed by constant scan rate or constant current (rate of charge), the mass-specific capacitance of a material will decrease when more material is applied. Thus, it is not surprising that high mass-specific capacitance is only reported for a material when only a very small amount of the material is used for the characterisation. However, the only advantage that high mass-specific materials have over others is when they are applied in mobile applications, where the supercapacitor has to travel and extra mass becomes burden. There are also many applications where the supercapacitors would remain stationary. In these cases, when mass is irrelevant, there is no advantage having a lightweight supercapacitor and the redox cycling stability, low equivalent series resistance, and etc. become important. The fact that high mass-specific capacitance is often only reported when small amounts of materials are used, also has implications on the utilisation of the geometric area of an electrode. This can be illustrated with an electrode that has 0.01 mg cm^{-2} of an electrode material. If the material had mass-specific capacitance of 1000 F g^{-1}, which is very high, the capacitance normalised to the electrode geometric area (the electrode capacitance) will be 0.01 F cm^{-2}, which is too low for practical purposes. In supercapacitor development, a high electrode capacitance (F cm^{-2}) is necessary as it reflects the utilisation of the geometric electrode area and translates directly into the device capacitance [76]. This is especially important in the energy storage application, where electrodes need to be fully utilised to store as much charge as possible. High electrode capacitances can be achieved using many materials, including those

which have inherently low mass-specific capacitance. One example is PEDOT, which has relatively low theoretical mass-specific capacitance compared to other ECPs, but thick films of PEDOT with capacitances of 5 F cm^{-2} can be made [64]. In our opinion, for any high mass-specific capacitance materials to become of practical relevance, focus should also be placed on achieving high electrode capacitance, of the order of 1 F cm^{-2}. 1 F cm^{-2} corresponds to electrode loading of 10 mg cm^{-2}, for a material which has 100 F g^{-1} mass-specific capacitance. Methods to achieve high electrode capacitance have been discussed above, i.e., to form an extended porous structure (without losing too much conductivity), so that electrolyte access throughout the thickness of the film is unimpeded. That is the advantage offered by nanocomposites of ECP–CNT, and has also been shown with ECP-cellulose nanocomposites whereas graphene-based ECP nanocomposite material would offer less in this aspect, due to the less ideal geometry of graphene for making thick porous material. However, by no means are we suggesting that ECP-graphene nanocomposite materials are by any measurements less useful. As we have mentioned, there are applications where device capacitance need not be very high, but very fast response is required, so thin films of electrode material will be advantageous in meeting these requirements.

The depth and width of the current field makes offering our perspectives on future developments within the category of ECP nanocomposites for supercapacitor applications a very challenging task. In our opinion, since our work has targeted energy storage applications, we suggest taking into account the electrode capacitance per unit geometric area of the underlying current collector, when a new material is developed and characterised.

Although we have been unable to cover fully the mathematical basics of how capacitive materials are characterised electrochemically, there are a few issues that we felt necessary to point out. First, the calculation of specific energies is only valid when characterisation is performed in two-electrode system. In a three-electrode cell, the working electrode is connected in series with the counter electrode, which effectively has infinite capacitance, and thus the system does not reflect a real supercapacitor device in any way. The exception is when the same material analysed in the three-electrode cell is to be used to construct a symmetrical supercapacitor. We would also like to point out the invalidity of using a voltage window which is extended to negative values for the calculation of specific energy when characterisation is performed in two-electrode system. For example, 4 V has been employed for specific energy calculation, deduced from a voltage window from −2 to +2 V of a two-electrode cyclic voltammogram. That is wrong because voltage is the potential difference between two electrodes, and the notion of ‘potential difference’ means it cannot have a negative value. The way which the supercapacitors are characterised, with a potentiostat system however, allow the voltage to have negative values because it is measured with one of the two electrodes also connected as the reference. To illustrate with the example given above of 4 V voltage window from −2 to +2 V; if electrode A is connected as the reference electrode and B is connected as the working electrode, positive voltage of 2 V can be measured when B is positively charged with respect to A, and negative voltage of 2 V can be

measured when B is negatively charged with respect to A. However, the latter also means that A is positively charged respective to B, and hence if B is taken as the reference, the voltage of 2 V is positive! Irrespective of how they are measured, the potential difference (or voltage) between the two electrodes at any point of time has not been larger than 2 V, and thus the use of 4 V as the voltage window is clearly wrong. We have noticed that this mischaracterisation can occur for symmetric supercapacitors, because either electrode can be used as the positive or negative electrode. Fortunately, this mischaracterisation has not occurred when asymmetric supercapacitors are tested.

It is clear from Table 2 that the higher energy and power supercapacitor prototypes/devices tend to be those developed using a non-aqueous electrolyte, such as propylene carbonate and ionic liquids. These non-aqueous electrolytes offer a much higher voltage range for the supercapacitors as they do not electrolyse as easily as water does. These non-aqueous electrolytes, however, have the disadvantages of being less environmentally friendly, more flammable (for the case of organic electrolytes) and more difficult to manufacture and hence costly (especially the ionic liquids). Thus the practicality of these electrolytes depend on if these issues can be addressed, and this offers a huge opportunity for future developments not only at the fundamental level (for example, to design an ionic liquid that is more environmentally friendly) but also the engineering aspects of manufacturing them. However, it is probably most worth pointing out (perhaps as a gentle reminder), that when non-aqueous electrolytes are used, there is little advantage of using the ECP-based electrode materials in symmetrical supercapacitors compared to carbon-based electrode materials judging from the specific power and energy that they achieve. When the power and energy characteristics are comparable, carbon-based electrode materials will be more favourable due to their processing advantages and also their higher stability over long time use. The complexity that is involved in choosing between electrode materials and electrolytes is also a very interesting subject that we hope readers would appreciate. Such choices must take into account of all the fundamental principles and limits but to make impact at a large scale it also depends on the existence of favourable manufacturing technologies and cost.

4 Conclusions

In this chapter, the development of electronically conducting polymer nanocomposites for use in supercapacitors is discussed. This discussion began with some history of the supercapacitor development and how electronically conducting polymer was incorporated in this development in efforts to reach higher capacitance. However, there are weaknesses of electronically conducting polymer that would limit their use in supercapacitor applications, and these weaknesses are mainly mechanical. Nanocomposites of electronically conducting polymer with strong materials, such as carbon nanotubes, graphene and nanocellulose have been developed to improve the mechanical strength, and hence functionality of the composite materials. The mechanism by which these nanocomposites form is

discussed and we have described several types of electronically conducting polymer nanocomposites: carbon nanotube/polymer nanocomposites, graphene/polymer nanocomposites, and cellulose/polymer nanocomposites. The performances of some of the supercapacitor prototypes and devices based on ECP nanocomposites was discussed. We also offered our view on how reported information on capacitance of any materials should be assessed. Some perspectives on future developments have also been offered.

References

1. Fakham H, Di L, Francois B (2011) IEEE Trans Ind Electron 58:85
2. Hadjipaschalis I, Poullikkas A, Efthimiou V (2009) Renew Sustain Energ Rev 13:1513
3. Tao Z, Francois B (2011) IEEE Trans Ind Electron 58:95
4. Haihua Z, Bhattacharya T, Duong T, Siew TST, Khambadkone AM (2011) IEEE Trans Power Electron 26:923
5. Zahedi A (2011) Renew Sustain Energy Rev 15:866
6. Roberts BP, Sandberg C (2011) Proc IEEE 99:1139
7. Kotz R, Carlen M (2000) Electrochim Acta 45:2483
8. Khaligh A, Zhihao L (2010) IEEE Trans Veh Technol 59:2806
9. Ortuzar M, Moreno J, Dixon J (2007) IEEE Trans Ind Electron 54:2147
10. Mastragostino M, Arbizzani C, Soavi F (2001) J Power Sour 97–8:812
11. Razaq A, Nyholm L, Sjodin M, Stromme M, Mihranyan A (2012) Adv Energy Mater 2:445
12. Pushparaj VL, Shaijumon MM, Kumar A, Murugesan S, Ci L, Vajtai R, Linhardt RJ, Nalamasu O, Ajayan PM (2007) Proc Natl Acad Sci USA 104:13574
13. Lu X, Yu M, Wang G, Tong Y, Li Y (2014) Energy Environ Sci 7:2160
14. Babu KF, Subramanian SPS, Kulandainathan MA (2013) Carbohydr Polym 94:487
15. Meng Q, Wang K, Guo W, Fang J, Wei Z, She X (2014) Small 10:3187
16. Yue BB, Wang CY, Ding X, Wallace GG (2012) Electrochim Acta 68:18
17. Frackowiak E, Beguin F (2001) Carbon 39:937
18. Winter M, Brodd RJ (2004) Chem Rev 104:4245
19. Wang G, Zhang L, Zhang J (2012) Chem Soc Rev 41:797
20. Sato T, Masuda G, Takagi K (2004) Electrochim Acta 49:3603
21. Peng C, Zhang SW, Zhou XH, Chen GZ (2010) Energy Environ Sci 3:1499
22. Fan L-Q, Liu G-J, Wu J-H, Liu L, Lin J-M, Wei Y-L (2014) Electrochim Acta 137:26
23. Khomenko V, Raymundo-Pinero E, Frackowiak E, Beguin F (2006) Appl Phys A Mater Sci Process 82:567
24. Snook GA, Wilson GJ, Pandolfo AG (2009) J Power Sour 186:216
25. Khomenko V, Raymundo-Pinero E, Beguin F (2006) J Power Sour 153:183
26. Pandolfo AG, Hollenkamp AF (2006) J Power Sour 157:11
27. Wang M-X, Wang C-Y, Chen M-M, Wang Y-S, Sh Z-Q, Du X, Li T-Q, Hu Z-J (2010) New Carbon Mater 25:285
28. Cheng Q, Tang J, Ma J, Zhang H, Shinya N, Qin LC (2011) Carbon 49:2917
29. Brousse T, Taberna P-L, Crosnier O, Dugas R, Guillemet P, Scudeller Y, Zhou Y, Favier F, Belanger D, Simon P (2007) J Power Sour 173:633
30. Villers D, Jobin D, Soucy C, Cossement D, Chahine R, Breau L, Belanger D (2003) J Electrochem Soc 150:A747
31. Ryu KS, Lee YG, Hong YS, Park YJ, Wu XL, Kim KM, Kang MG, Park NG, Chang SH (2004) Electrochim Acta 50:843
32. Frackowiak E, Khomenko V, Jurewicz K, Lota K, Beguin F (2006) J Power Sour 153:413

33. Laforgue A, Simon P, Fauvarque JF, Mastragostino M, Soavi F, Sarrau JF, Lailler P, Conte M, Rossi E, Saguatti S (2003) J Electrochem Soc 150:A645
34. Sivaraman P, Bhattacharrya AR, Mishra SP, Thakur AP, Shashidhara K, Samui AB (2013) Electrochim Acta 94:182
35. Ng KC, Zhang SW, Peng C, Chen GZ (2009) J Electrochem Soc 156:A846
36. Brousse T, Belanger D (2003) Electrochem Solid State Lett 6:A244
37. Suppes GM, Cameron CG, Freund MS (2010) J Electrochem Soc 157:A1030
38. Khoh WH, Hong JD (2014) Colloids Surf A 456:26
39. Xiao QF, Zhou X (2003) Electrochim Acta 48:575
40. Mastragostino M, Paraventi R, Zanelli A (2000) J Electrochem Soc 147:3167
41. Ghenaatian HR, Mousavi MF, Rahmanifar MS (2012) Electrochim Acta 78:212
42. Mak WF, Wee G, Aravindan V, Gupta N, Mhaisalkar SG, Madhavi S (2012) J Electrochem Soc 159:A1481
43. Zhang S, Peng C, Ng KC, Chen GZ (2010) Electrochim Acta 55:7447
44. Zheng JP, Jow TR (1996) J Power Sour 62:155
45. Zhou XH, Peng C, Chen GZ (2012) AIChE J 58:974
46. Zhang LL, Zhao XS (2009) Chem Soc Rev 38:2520
47. Peng C, Zhang SW, Jewell D, Chen GZ (2008) Prog Nat Sci Mater Int 18:777
48. Conway BE, Birss V, Wojtowicz J (1997) J Power Sour 66:1
49. Chen GZ (2013) Prog Nat Sci Mater Int 23:245
50. Chae JH, Ng KC, Chen GZ (2010) Proc Inst Mech Eng Part A J Power Energy 224:479
51. Peng C, Jin J, Chen GZ (2007) Electrochim Acta 53:525
52. Zhang SW, Chen GZ (2008) Energy Mater 3:186
53. Malinauskas A (2001) Polymer 42:3957
54. Peng C (2007) PhD, The University of Nottingham
55. Park YW (2010) Chem Soc Rev 39:2428
56. Heeger AJ (2010) Chem Soc Rev 39:2354
57. Zhang JT, Zhao XS (2012) J Phys Chem C 116:5420
58. Lam JWY, Tang BZ (2005) Acc Chem Res 38:745
59. Huq R, Farrington GC (1984) J Electrochem Soc 131:819
60. Lota K, Khomenko V, Frackowiak E (2004) J Phys Chem Solids 65:295
61. Dhibar S, Sahoo S, Das CK (2013) Polym Compos 34:517
62. Yan J, Wei T, Shao B, Fan Z, Qian W, Zhang M, Wei F (2010) Carbon 48:487
63. Groenendaal BL, Jonas F, Freitag D, Pielartzik H, Reynolds JR (2000) Adv Mater 12:481
64. Snook GA, Peng C, Fray DJ, Chen GZ (2007) Electrochem Commun 9:83
65. Li H, Wang J, Chu Q, Wang Z, Zhang F, Wang S (2009) J Power Sour 190:578
66. Peng C, Hu D, Chen GZ (2011) Chem Commun 47:4105
67. Ran F, Tan YT, Liu J, Zhao L, Kong LB, Luo YC, Kang L (2012) Polym Adv Technol 23:1297
68. Chen W, Rakhi RB, Alshareef HN (2013) J Mater Chem A 1:3315
69. Khomenko V, Frackowiak E, Beguin F (2005) Electrochim Acta 50:2499
70. Li C, Shi GQ (2011) Electrochim Acta 56:10737
71. Liew SY, Thielemans W, Walsh DA (2010) J Phys Chem C 114:17926
72. Liew SY, Walsh DA, Thielemans W (2013) RSC Adv 3:9158
73. Wu X, Chabot VL, Kim BK, Yu A, Berry RM, Tam KC (2014) Electrochim Acta 138:139
74. Frackowiak E (2007) Phys Chem Chem Phys 9:1774
75. Kim JY, Kim KH, Kim KB (2008) J Power Sour 176:396
76. Hughes M, Chen GZ, Shaffer MSP, Fray DJ, Windle AH (2002) Chem Mater 14:1610
77. Chen GZ, Shaffer MSP, Coleby D, Dixon G, Zhou WZ, Fray DJ, Windle AH (2000) Adv Mater 12:522
78. Randriamahazaka H, Bonnotte T, Noel V, Martin P, Ghilane J, Asaka K, Lacroix JC (2011) J Phys Chem B 115:205
79. Snook GA, Chen GZ, Fray DJ, Hughes M, Shaffer M (2004) J Electroanal Chem 568:135
80. Wu MQ, Snook GA, Gupta V, Shaffer M, Fray DJ, Chen GZ (2005) J Mater Chem 15:2297

81. Gupta V, Miura N (2006) Electrochim Acta 52:1721
82. Sivakkumar SR, Kim WJ, Choi JA, MacFarlane DR, Forsyth M, Kim DW (2007) J Power Sour 171:1062
83. Wang K, Zhao P, Zhou XM, Wu HP, Wei ZX (2011) J Mater Chem 21:16373
84. Otrokhov G, Pankratov D, Shumakovich G, Khlupova M, Zeifman Y, Vasil'eva I, Morozova O, Yaropolov A (2014) Electrochim Acta 123:151
85. Peng C, Snook GA, Fray DJ, Shaffer MSP, Chen GZ (2006) Chem Commun 4629
86. Bai XX, Hu XJ, Zhou SY, Yan J, Sun CH, Chen P, Li LF (2013) Electrochim Acta 87:394
87. Hou Y, Cheng YW, Hobson T, Liu J (2010) Nano Lett 10:2727
88. Liu A, Li C, Bai H, Shi G (2010) J Phys Chem C 114:22783
89. Chang H-H, Chang C-K, Tsai Y-C, Liao C-S (2012) Carbon 50:2331
90. Zhang LL, Zhao SY, Tian XN, Zhao XS (2010) Langmuir 26:17624
91. Zhang JT, Chen P, Oh BHL, Chan-Park MB (2013) Nanoscale 5:9860
92. Mao L, Chan HSO, Wu JS (2012) RSC Adv 2:10610
93. Lu X, Dou H, Yuan C, Yang S, Hao L, Zhang F, Shen L, Zhang L, Zhang X (2012) J Power Sour 197:319
94. Lu X, Zhang F, Dou H, Yuan C, Yang S, Hao L, Shen L, Zhang L, Zhang X (2012) Electrochim Acta 69:160
95. Liu Y, Zhang Y, Ma GH, Wang Z, Liu KY, Liu HT (2013) Electrochim Acta 88:519
96. Zhu CZ, Zhai JF, Wen D, Dong SJ (2012) J Mater Chem 22:6300
97. Zhang J, Yu Y, Liu L, Wu Y (2013) Nanoscale 5:3052
98. Zhang F, Xiao F, Dong ZH, Shi W (2013) Electrochim Acta 114:125
99. Lai LF, Wang L, Yang HP, Sahoo NG, Tam QX, Liu JL, Poh CK, Lim SH, Shen ZX, Lin JY (2012) Nano Energy 1:723
100. Wang X, Wang TM, Yang C, Li HD, Liu P (2013) Appl Surf Sci 287:242
101. Feng W, Zhang QW, Li Y, Feng YY (2014) J Solid State Electrochem 18:1127
102. Wang H, Hao Q, Yang X, Lu L, Wang X (2009) Electrochem Commun 11:1158
103. Xu JJ, Wang K, Zu SZ, Han BH, Wei ZX (2010) ACS Nano 4:5019
104. Zhang K, Zhang LL, Zhao XS, Wu J (2010) Chem. Mat. 22:1392
105. Lu X, Dou H, Yang S, Hao L, Zhang L, Shen L, Zhang F, Zhang X (2011) Electrochim Acta 56:9224
106. Li L, Raji ARO, Fei HL, Yang Y, Samuel ELG, Tour JM (2013) ACS Appl Mater Interf 5:6622
107. Wen JF, Jiang YD, Yang YJ, Li SB (2014) J Mater Sci Mater El 25:1063
108. Yang YJ, Zhang LN, Li SB, Yang WY, Xu JH, Jiang YD, Wen JF (2013) J Mater Sci Mater El 24:2245
109. Chen J, Jia C, Wan Z (2014) Synth Met 189:69
110. Wu X, Tang J, Duan Y, Yu A, Berry RM, Tam KC (2014) J Mater Chem A 2:19268
111. Liew S, Thielemans W, Walsh D (2014) J Solid State Electrochem 18:3307
112. Olsson H, Nystrom G, Stromme M, Sjodin M, Nyholm L (2011) Electrochem Commun 13:869
113. Olsson H, Carlsson DO, Nystrom G, Sjodin M, Nyholm L, Stromme M (2012) J Mater Sci 47:5317
114. Carlsson DO, Nystrom G, Zhou Q, Berglund LA, Nyholm L, Stromme M (2012) J Mater Chem 22:19014
115. Wang H, Zhu E, Yang J, Zhou P, Sun D, Tang W (2012) J Phys Chem C 116:13013
116. Wang H, Bian L, Zhou P, Tang J, Tang W (2013) J Mater Chem A 1:578
117. Hu D, Peng C, Chen GZ (2010) ACS Nano 4:4274
118. Burke A (2000) J Power Sour 91:37
119. Chu A, Braatz P (2002) J Power Sour 112:236
120. Zhu YL, Shi KY, Zhitomirsky I (2014) J Power Sour 268:233
121. Lee H, Kim H, Cho MS, Choi J, Lee Y (2011) Electrochim Acta 56:7460
122. Niu ZQ, Luan PS, Shao Q, Dong HB, Li JZ, Chen J, Zhao D, Cai L, Zhou WY, Chen XD, Xie SS (2012) Energy Environ Sci 5:8726

123. Li Z-F, Zhang H, Liu Q, Liu Y, Stanciu L, Xie J (2014) Carbon 71:257
124. Paul S, Choi KS, Lee DJ, Sudhagar P, Kang YS (2012) Electrochim Acta 78:649
125. Meng C, Liu C, Chen L, Hu C, Fan S (2010) Nano Lett 10:4025
126. Zhou Y, Lachman N, Ghaffari M, Xu H, Bhattacharya D, Fattahi P, Abidian MR, Wu S, Gleason KK, Wardle BL, Zhang QM (2014) J Mater Chem A 2:9964
127. Bard AJ, Faulkner LR (2001) Electrochemical methods: fundamentals and applications. Wiley, New York

Composites Based on Conducting Polymers and Carbon Nanotubes for Supercapacitors

Paramjit Singh

Abstract The last decade has seen a significant interest in the composites of conducting polymers (CPs) and carbon nanotubes (CNTs). The CP–CNT composites present great interest for various applications due to the large surface area, high mechanical strength and high conductivity. The CP–CNT composites are used as actuators, fuel cells, electronic devices and 'supercapacitors'. The topic being very vast, particular emphasis has been given to polypyrrole (PPy) and polyaniline (PANi) based CNT composites for their use as supercapacitors. Polypyrrole and polyaniline have good conductivity and are cost effective for their use in electrical applications. Both the polymers have been a key interest for supercapacitive properties in the last decade. High specific capacitance (SC), high electrochemical stability and good cyclability are the main requirements for material to be used for energy storage properties. The present chapter provides an overview of past and current research on conducting polymer/carbon nanotube (CP–CNT) composite materials for use as supercapacitor electrodes. The various factors affecting the performance, cyclic stability and charge storage properties of CP–CNT composites, such as the method used for the synthesis of the composite, shape and size of polymer nanoparticles as well as the weight percentage of both the entities in the composite have been discussed in the present chapter. An overview of current research on PPy–CNT and PANi–CNT composites for their use as supercapacitor electrodes has been given in the chapter. The focus is given towards the various factors affecting their performance with relevant literature and description.

Keywords Carbon nanotubes · Supercapacitor · Conducting polymers · Polyaniline · Polypyrrole · Nanocomposites

P. Singh (✉)
Department of Applied Science,
Guru Nanak Dev Engineering College, Ludhiana 141006, India
e-mail: psd1985@gmail.com

V. Kumar et al. (eds.), *Conducting Polymer Hybrids*,
Springer Series on Polymer and Composite Materials,
DOI 10.1007/978-3-319-46458-9_10

Abbreviations

CP	Conducting polymer
CNT	Carbon nanotube
CNTA	Carbon nanotube arrays
SWCNT	Single walled carbon nanotube
MWCNT	Multi walled carbon nanotube
PPy	Polypyrrole
PANi	Polyaniline
PC	Pseudo capacitor
EDLS	Electrical double layer capacitor
SEM	Scanning electron microscope
TEM	Tunnelling electron microscope
SC	Specific capacitance
GN	Graphene
CV	Cyclic voltammetry
CELT	Charge energy limited model
SPADNS	Sulfanilic acid azochromatrop
CHR-BS	Sulfonazo III sodium salt
VACNT	Vertically aligned carbon nanotube
HC	Hybrid capacitor
P–CNT	Air plasma activated carbon nanotube
GNS	Graphene nanosheet

1 Introduction

Polymers are complex and giant molecules made up of smaller molecular repeating units called monomers. Intrinsically conducting polymers (CPs), also known as "synthetic metals" have been studied extensively for numerous applications in various fields since their discovery in the 1970s. Typically CPs include polyacetylene (PA), polyaniline (PANi), polypyrrole (PPy), polythiophene (PTh) and polyfurane (PF), etc. The conductivity of a conducting material is directly proportional to the number density of charge carriers and their mobility. Unlike semiconductors, the CPs have a large number of charge carriers due to the large degree of doping; but low mobility attributed to structural defects. The secondary treatments like doping or subjecting to chemical or electrochemical redox reactions, the electrical conductivity of these CPs increase several orders of magnitude. For example, the emeraldine base PANi (undoped form) is an insulator (conductivity in the range of $10^{-10} - 10^{-8}$ S/cm), after doping its conductivity can be increased to $10^{2} - 10^{3}$ S/cm [1]. The conductivity of these CPs is affected by many parameters, such as the chain structure and length, doping structure and degree of doping, polymerization conditions including the concentration of monomer, dopant and

oxidant, the molar ratio of dopant and oxidant to monomer as well as polymerization temperature and time [2]. Mainly, the electrical conductivity of these conjugated polymers can be modified by changing the level of doping and nature of dopants. The incorporation of secondary components into conducting polymers to form nanocomposite can improve the functionality of these conjugated conductive polymers.

Carbon nanotubes (CNTs), discovered by Sumio Lijima in 1991, have high mechanical strength, good electrical conductivity and chemical stability. CNTs can be divided into two main categories: single-walled carbon nanotubes (SWCNTs) and multi-walled carbon nanotubes (MWCNTs). SWCNT is formed by rolling of a single layer of graphene into a hollow cylinder. An MWCNT can similarly be considered to be a coaxial assembly of cylinders of SWCNTs. There are three types of nanotubes, armchair, zigzag and chiral. Carbon nanotubes can be either a metal or a semiconductor. They differ symmetrically and can vary in function due to the way they "roll up." The diameter of a CNT can be 50,000 times thinner than a human hair, yet a nanotube is stronger than steel per unit weight [3]. The interlayer spacing of MWCNTs ranges between 0.34 and 0.39 nm [4]. The lower range of the inner and outer diameter of MWCNTs starts from 0.2 to 2 nm respectively, but the upper range of both the diameters is not fixed; it may vary from 20 to 40 nm or more. Usually, both tips of MWCNT are closed, and the ends are capped by dome-shaped half-fullerene molecules (pentagonal defects) and axial size differs from 1 μm up to a few centimeters. The role of half-fullerene molecules (pentagonal ring defect) is to help in the closing of the tube at the two ends. On the other hand, SWCNT diameters differ from 0.4 to 2–3 nm and their length is typically of the micrometer range. SWCNTs usually can come together and form bundles (ropes) [5]. In a bundle structure, SWCNTs are hexagonally organized to form a crystal-like construction [6]. CNTs can be synthesized with either of the methods reported in literature such as chemical vapour deposition, vapour phase growth, arc discharge, laser ablation and thermal chemical vapour deposition, etc. [7]. Besides the synthesis method, the purification process is necessary to remove other molecules from the catalyst which are obtained together with CNT. Most of these additional molecules are graphite, amorphous carbon, fullerene and residuals of metals. The methods used for the purification process include chemical oxidation, liquid phase oxidation, filtration, centrifugation, ultrasonication, chromatography and high-temperature annealing [8]. The CNTs have a large range of applications including supercapacitors, actuators and lightweight electromagnetic shields [9]. The biomedical industry is using CNTs these days for drug delivery applications such as peptide delivery, cellular uptake and nucleic acid delivery, etc. [10]. However, the poor processability and some other drawbacks have limited their applications. These have been overcome by forming the composites of CNTs with other materials; one such is modifications of CNTs with polymers.

2 CNT Modifications with Polymers

The CNT–polymer composite involves two types of bonding between CNT and polymer: covalent or non-covalent. Non-covalent CNT modification concerns the physical adsorption and/or wrapping of polymers to the surface of the CNTs. Baskaran et al. [11] reported shear induced polymer wrapping over MWCNTs using solution dispersion and subsequent melt-mixing procedure. Figure 1 represents the graphical illustration of polymer wrapping over CNTs [11]. The graphitic sidewalls of CNTs provide the possibility for stacking interactions with conjugated polymers, as well as organic polymers containing hetero atoms with free electron pair [12]. Non-covalent bonding does not destroy the conjugated system of the CNT sidewalls and hence the structural properties remain unaffected. Covalent bonding involves strong chemical bonding between nanotubes and polymers called "grafting". The grafting is further divided into two categories: "grafting to" and "grafting from". In "grafting to" method, readymade polymer with reactive end groups is reacted with functional groups on the nanotubes surfaces. The steric hindrance of macromolecules hinders their diffusion to the CNT surface and hence this method is limited up to the polymers containing reactive functional groups. The "grafting from" approach involves growing of polymers from CNT surfaces via in-situ polymerization of monomers initiated by chemical species immobilized on the CNT sidewalls and CNT edges. The advantage of this method is that the high reactivity of monomers makes efficient, controllable, designable and tailored grafting feasible [12].

The basic route of CP–CNT composite offers two paths, either the polymer functionalizes the CNTs or the CPs are doped with CNTs, i.e., a charge transfer occurs between the two constituents [13]. The main functionalization possibilities of CNTs are: (A) generation and functionalization of defect sites at the tube ends and side walls by oxidation and subsequent conversion into derivatives; (B) covalent sidewall functionalization using addition reactions and subsequent

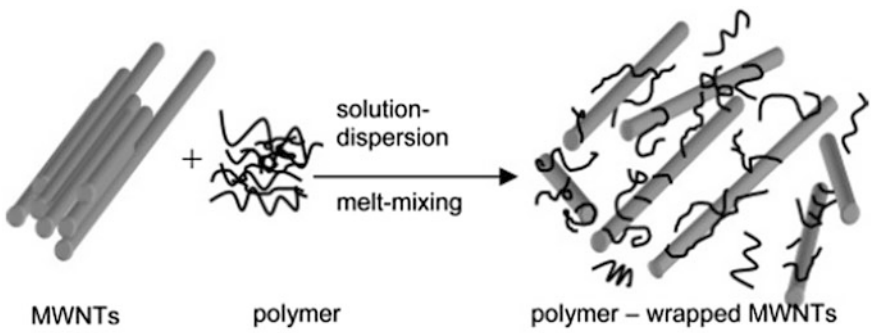

Fig. 1 Illsutration of polymer wrapping over CNTs (Reproduced with permission from [11])

nucleophilic substitution; (C) non-covalent exohedral functionalization with surfactant-type molecules and (D) endohedral functionalization with C_{60} [14]. These are represented in Fig. 2.

The electrical conductivity of polymer–CNT composites can be explained by percolation theory. The conductivity depends upon the filler concentration (commonly named as percolation threshold). The choice of polymer, nanotube type and solvent used during synthesis; all affect the percolation threshold. In addition to it; the processing technique, mixing stresses applied during preparation, as well as the shaping procedure play imperative roles [15].

Composite materials based on the coupling of CPs and CNTs have shown potential applications such as supercapacitors, sensors, solar cells, transistors, photovoltaic cells, photodiods and electromagnetic absorbers, etc. The nanotubes-polymer composite was first reported by Ajayan et al. [16]. The addition of CNTs to conducting polymers was demonstrated by Zhang et al. [17] to enhance the electrical properties. They synthesized PPy–CNT nanocables (by in-situ chemical oxidative polymerization method) having improved electrical properties and a negative temperature coefficient of resistance at 77–300 K as well as a negative magnetoresistance at 10–200 K.

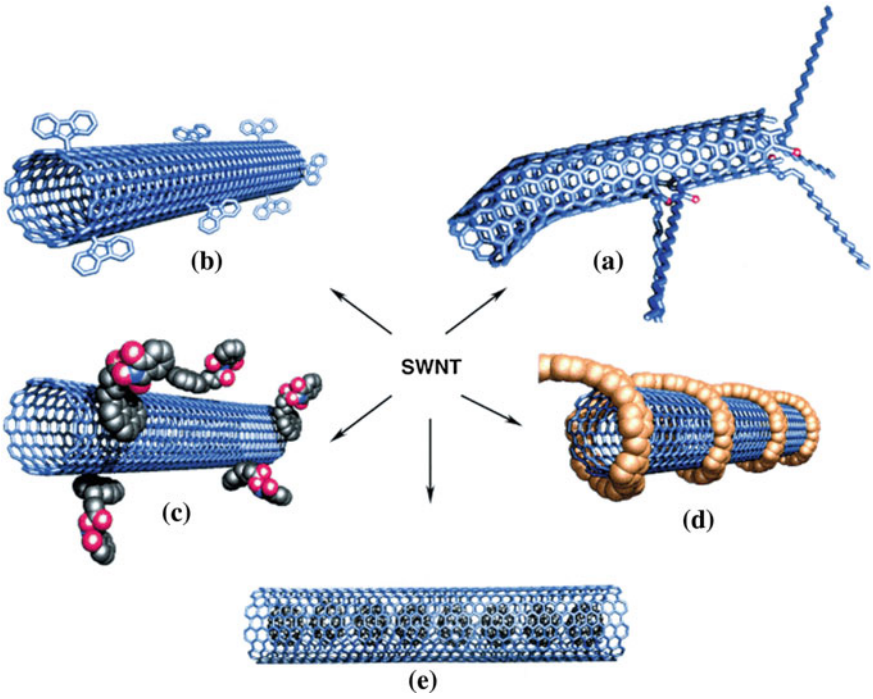

Fig. 2 Functionalization possibilities for SWCNTs (Reproduced with permission from [14])

3 Composites Based on CNTs and CPs for Supercapacitors

A supercapacitor consists of two electrodes immersed in the electrolyte solution, with a potential across current collector. A dielectric separator between the two electrodes prevents charge propagation between the electrodes [18]. Scheme 1 represents a supercapacitor cell. Based on the energy storage mechanism and electrode material used for the device fabrication, supercapacitors are classified into electrical double-layer capacitors (EDLC) and pseudo-capacitors (PC) or redox capacitors [19]. The former constitutes high surface area carbon materials whereas the latter constitutes metal oxides and conducting polymers [20–22]. In EDLC materials, charge separation takes place at the electrode/electrolyte interface, and charge storage mechanism is electrostatic in nature [23]. In PC materials, fast reversible faradic redox reaction takes place at the electroactive material's surfaces, and the reaction involves the whole active material [24, 18]. This makes pseudocapacitors achieve greater capacitance and energy densities than EDLC [25]. The high specific capacitance (SC), good electrical conductivity, fast charge–discharge process and low cost make conducting polymers attractive materials for PC. But, the main drawback is the poor cycling stability during the charge–discharge process of the conducting polymers due to swelling and shrinking of the polymer backbone [26, 23]. In addition to it, the high resistance and low power density also make PC-less useful than EDLC. The performance of supercapacitor depends upon the following factors [18]:

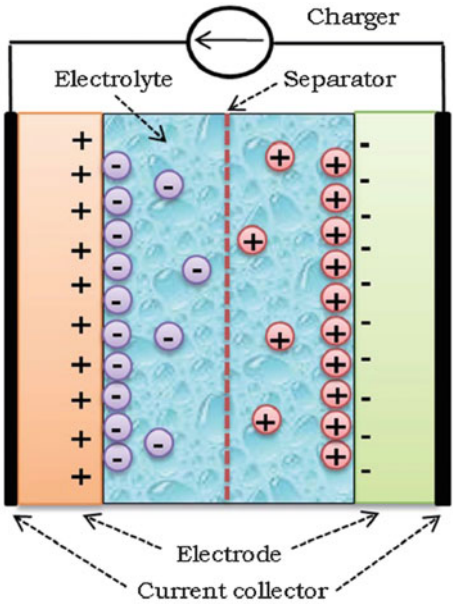

Scheme 1 Representation of a supercapacitor (Reproduced with permission from [18])

- High power density
- High electrochemical stability
- Fast charge–discharge phenomenon
- Reasonably low self-discharging.

The above-discussed factors can be incorporated in CPs by adding nanofillers (such as CNT or graphene) to CPs [27]. The CP–CNT composites (particularly PPy–CNT and PANi–CNT) have been reported to be used for supercapacitve properties to fulfil the requirements mentioned above. To achieve the goal, the composites have been optimized by using improved synthesis techniques, controlling the nano thickness of the fillers, uniform distribution of the nano-film, etc.

3.1 PPy–CNT Composites

Polypyrrole (PPy) is intrinsically conducting polymer with conjugated double bonds. PPy and its composites are used as biosensors, gas sensors, wires, micro-actuators, anti-electrostatic coatings, electrolyte capacitors, electronic devices and functional membranes, etc. [28]. PPy can be synthesized by any of the chemical techniques reported in the literature (such as change of solvent, oxidant, dopant, the ratio of oxidant to pyrrole, reaction temperature, reaction time, etc.) [29, 30]. The room temperature conductivity of PPy is of the order of 10^{-3} S/cm [31]. The preparation technique affects the electrical conductivity of PPy and it is reported to be enhanced up to 90 S/cm prepared by chemical oxidative polymerization method [32]. The doping of PPy with a suitable dopant such as LiF may increase its conductivity to 4.56×10^4 S/cm [33].

Wang et al. [34] reported polypyrrole/ carbon nanotube (PPy-CNT) composite nano-wires (prepared by template directed electrochemical synthetic route) of 200 nm pore size and having smoothed surface (as observed in TEM image, Fig. 3). The composites were reported to show metallic behavior as per V-I curve reports (Fig. 4), which follows Ohm's law (straight line in V-I curve). Cyclic voltammetry was used for probing the growth pattern of the electropolymerized PPy–CNT nanowires. The entrapped CNTs enhanced the electron flow within the composite as the CNTs acted as conducting bridges connecting the conducting domains of PPy.

Zhang et al. [17] controlled the size of PPy–CNT nanocables using in-situ chemical oxidative polymerization directed by different surfactants to overcome the difficulty of dispersing CNT into insoluble and infusible polymer matrix. They reported that 'cable like' structures showed the enhanced electrical properties. The average diameter of the nanocables was controlled by changing the pyrrole/CNT mass ratio. The poor solubility and process ability of CNTs in polymer matrices were overcome by the use of surfactants by the same group in another reported work [35]. They synthesized the co-axial nanowires of SWCNT–PPy using the similar technique of 'template directed synthesis' using cationic and anionic surfactants, of which the outer layers were composed of the conducting PPy polymers

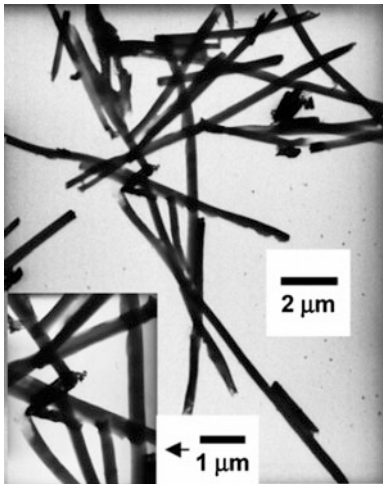

Fig. 3 TEM images of PPy–CNT (Reproduced with permission from [34])

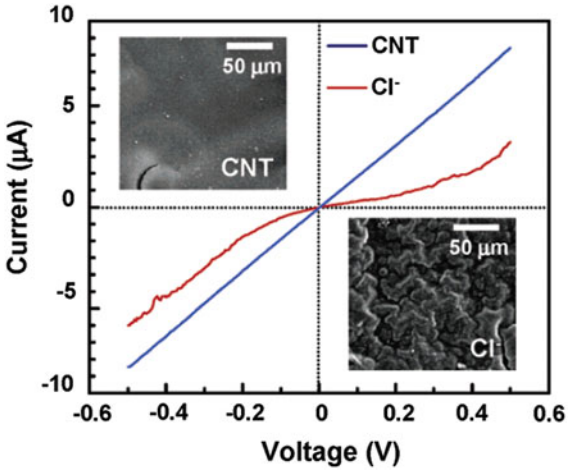

Fig. 4 Current–voltage curve of CNT doped PPy. The *blue straight line* indicates the metallic behaviour of the PPy–CNT composite as it follows Ohm's law (Reproduced with permission from [34])

and the inner layers were consisting of either the individual SWCNT or their small bundles as per shown in the high-resolution SEM and TEM images in Fig. 5. The diameter of individual SWCNTs was reported to be in the range of 0.9–1.3 nm. The wire-like structures of the diameter of several tens of nanometers and lengths up to several micrometers were obtained. The conductivity was found to decrease with increase of temperature. This behavior can be explained using charge-energy-limited tunneling (CELT) model which describes the charge transport in a system of metallic particles embedded in a dielectric matrix [36]. In their earlier studies, the same group synthesized the multi-walled carbon nanotube/polypyrrole (MWCNT–PPy) nanocomposites with cable-like morphology using an in-situ chemical oxidative polymerization method [31]. The conductivity of the synthesized

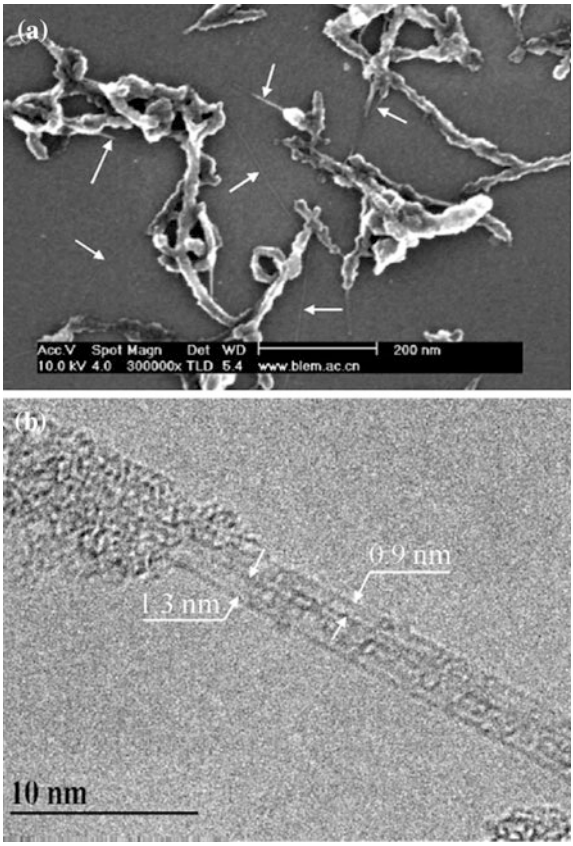

Fig. 5 **a** SEM and **b** TEM images of the nanostructures as thin as single-wall CNT bundles appeared within the PPy–SWCNT composites by applying the micelle/CNT hybrid template directed synthesis (Reproduced with permission from [35])

composite enhanced up to 100 times (0.23 S/cm) from the conductivity of pure PPy (7.3×10^{-3} S/cm) and it was temperature dependent. The conductivity was found to increase with increase of weight percentage of nanotube and it was indicative of percolative character. The MWCNT–PPy composite films offer an exciting combination of exceptional charge storage capacities (several times larger than that of either CNT or PPy) and have potential applications in supercapacitors and secondary batteries. The interfacial interactions between CNT and polymer matrix attribute to the enhanced properties [31]. The capacitive properties of PPy–CNT composite films can be influenced by applying the alternating electric field during their electrochemical synthesis [37].

In earlier studies, the charge storage properties of PPy were improved by growing the thin films of the polymer on different substrates, such as graphite, gold, nickel and titanium etc. using acidic and basic electrolytes [38–41]. In one such example, Shi and Zhitomirsky, [42] deposited PPy films on Ni substrate using Tiron as an anionic dopant. Tiron offered a higher charge to mass ratio which increased the charge transfer efficiency, and Ni provided a significant improvement in capacitance

retention at high scan rates. They reported that for pure PPy electrodes the mass normalized SC of 339–451 Fg^{-1} and area normalized SC of 0.4–0.95 F cm^{-2} could be achieved for material loadings of 0.84–2.80 mg cm^{-2}. However thin films of PPy showed poor cyclic stability which resulted in the poor capacitive behaviour and lack of durability [43]. These limitations can be improved using composites of PPy with CNTs and graphenes. The charge storage properties of PPy–CNT composite have been enhanced in the last decade using different routes of synthesis. The intrinsic properties of CNTs such as high surface area, high environmental stability, low electrical resistance and low mass density are responsible for their super capacitive nature. The stability in the capacitance requires control over the film thickness, composite composition and good contact with the current collectors. The insolubility, poor dispersibility and poor compatibility of CNTs hinder their incorporation with CPs. So, it is important to enhance the interaction between CNTs and CPs. These drawbacks can be overcome by using inorganic acid treated (such as HNO_3 and H_2SO_4) CNTs to generate carboxylic group capped CNTs (as shown in Scheme 2) followed by their association with CPs [44]. In the same line, Mi et al. [45] reported acid treated composites of CNTs and PPy in which the organometallic compound with methyl orange and iron (III) chloride (MO–$FeCl_3$) served as responsive seed template. They reported the SC of 304 Fg^{-1} for synthesized composite.

Fang et al. [46] synthesized the self-supported supercapacitor electrodes by coating PPy homogeneously on MWCNT membranes. The advantage of self-supported electrodes over the use of metal backing foils and binders is that the extra mass of these supporters is not added to composite, and it does not alter charge storage capacity of the composite. They used the pulsed potentio-amperometric

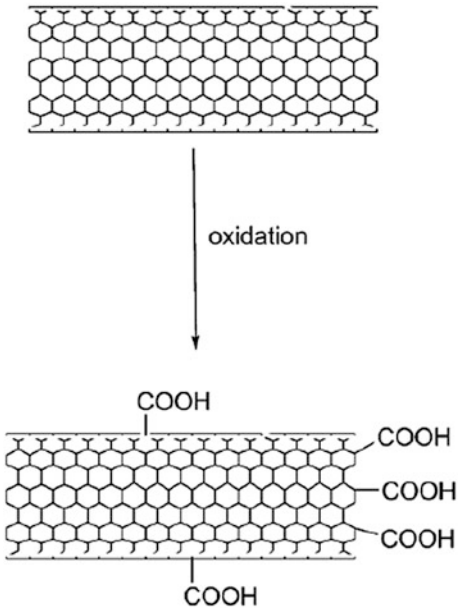

Scheme 2 Oxidation of CNT to generate carboxylic group capped CNTs (Reproduced with permission from [12])

method to deposit PPy on MWCNT electrochemically. They obtained the homogeneous coating by controlling the deposition time and current. The outer diameter of pure MWCNT (Fig. 6a) was modified from 13.62 ± 2.87 to 18.28 ± 6.06 nm after coating with PPy (Fig. 6b). The SEM images in Fig. 6c show the *top* surface of the MWCNT membrane after PPy deposition, which conforms to the nanotubes structure. The SC of so synthesized composite was reported to be 427 Fg^{-1}.

Paul et al. [47] used the different route (chemical oxidative polymerization method) of synthesis and reported the SC in the range of 146.3–167.2 Fg^{-1}, which was quite small as compared to the above-discussed reports. Lee et al. [48] synthesized PPy–CNT composites using thermally stable and porous nonwoven ceramic fabrics as the substrates. The CNTs on the ceramic fabrics were prepared by thermal vapour deposition process, and PPy was subsequently coated on the surface of CNTs onto the ceramic fabrics by chemical polymerization. Figure 7a represents the schematic of the synthesis process. CNTs provided a high surface area, and PPy enhanced the adhesion between CNTs and ceramic fabrics by working as conducting binder for connecting individual CNTs. Figure 7a, b shows the SEM, and TEM images of CNTs and PPy coated CNTs on the ceramic fabric respectively. The performance of PPy-CNT electrode was improved by the uniform and thin coating of PPy, which increased the diffusion and migration of ions in the polymer. Although the SC of PPy-CNTs on the ceramic fabrics was reported to be merely 152.78 Fg^{-1}(as compared to other reports), but its stability was well retained even after 5000 redox cycles as per reported in Fig. 8. The strong π–π stacking between PPy conjugated backbone and the graphitic sidewall of CNTs provided the enhanced stability of PPy-CNT composites [48].

Lu and his co-workers [49] synthesized the ternary composites of graphene (GN), PPy and CNTs in a particular ratio (GN: CNT = 8:1) via in-situ polymerization and compared the results with those of pure PPy, binary composites of CNT/PPy and GN/PPy. The negatively charged poly (sodium 4-styrene sulfonate) was used for dispersing graphene (GN) and CNT in the aqueous phase and tethering pyrrole monomer to facilitate the formation of uniform PPy coating. Morphology analyses

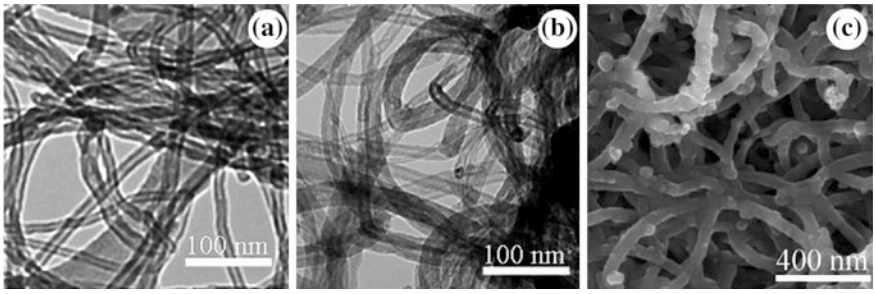

Fig. 6 **a** TEM image of pure MWCNT, **b** TEM image of MWCNT after PPy deposition, **c** SEM image of the *top surface* of the MWCNT membrane after PPy deposition (Reproduced with permission from [46])

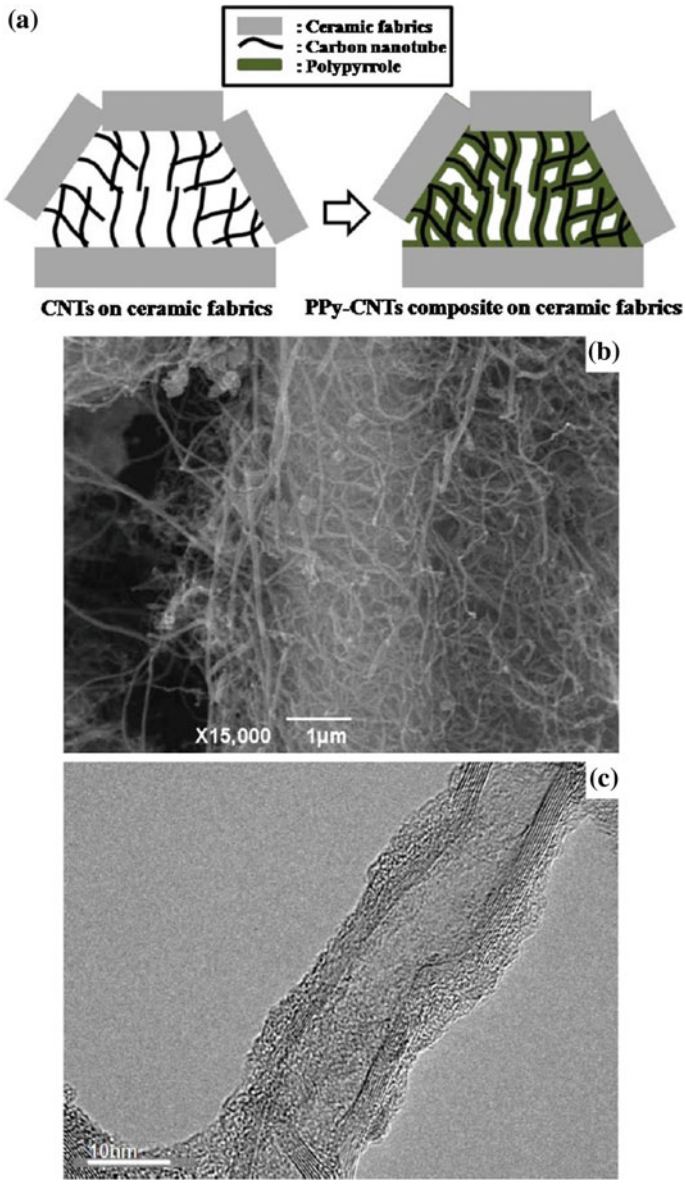

Fig. 7 **a** Schematic, **b** SEM image, **c** TEM image of PPy–CNT composite on ceramic fabric (Reproduced with permission from [48])

showed that stacking of laminated PPy/GN composite was inhibited by introducing one-dimensional CNT to form GN/PPy/CNT composite with three-dimensional hierarchical structure. The PPy particles of thickness 30 nm were wrapped uniformly around the CNT (Fig. 9a, b). The 8GCPPy (GN/PPy/CNT composite with GN:

CNT = 8:1) composite exhibited the largest SC of 361 Fg^{-1} at a current density of 0.2 A g^{-1}, higher than that of pure PPy (176 Fg^{-1}) and binary composites of CNT/PPy (253 Fg^{-1}) and GN/PPy (265 Fg^{-1}). The cycling stability tests of pure PPy, CNT/PPy, GN/PPy and 8GCPPy were investigated at a current density of 6 A g^{-1} and the results are shown in Fig. 10. After 2000 charge/discharge cycles, the SC degradation of pure PPy, CNT/PPy and GN/PPy was about 66, 24 and 33 %, respectively, while the SC decreased only 4 % of initial capacitance for 8GCPPy [49]. The degradation in capacitance is ascribed to the swelling and shrinkage of PPy chains during the doping/dedoping processes, leading to the mechanical degradation of the polymer and deteriorating the charge distribution of π conjugated PPy chains [49].

In another work by the same group, the flexible films with polypyrrole/carbon nanotube (PPy–CNT) composite homogeneously distributed between GN sheets were prepared by flow assembly of the mixture dispersion of GN and PPy–CNT. The thickness of GN–PPy–CNT composite film was ≈39.7 μm. The SCs of GN–PPy–CNT (52 wt% PPy–CNT) were reported to be 211 Fg^{-1} and 122 F cm^{-3} at a current density of 0.2 A g^{-1}, which was higher than those of the GN films (73 Fg^{-1} and 79 F cm^{-3}) and PPy–CNT (164 Fg^{-1} and 67 F cm^{-3}) composites respectively. Significantly the GN–PPy–CNT electrode showed excellent cycling stability (5 % capacity loss after 5000 cycles) [19].

The charge storage properties of PPy can be improved by doping it with the redox-active dopants. The stability and conductivity of the PPy films can be enhanced by the use of polycharged aromatic anionic dopants since the structure of anionic dopants influence the shape and size of PPy particles and increases the interchain mobility of charge carriers [43, 50–53]. The increase in the size of dopant molecules and charge to mass ratio results in reduced size of the PPy particles and increased capacitance [50]. However poor capacitance retention was observed at high charge-discharge rates for electrodes with high PPy mass loading [50]. Zhu and his group synthesized the PPy coated CNTs for supercapacitive properties with high mass loading, good cycling stability and good capacitance retention at high

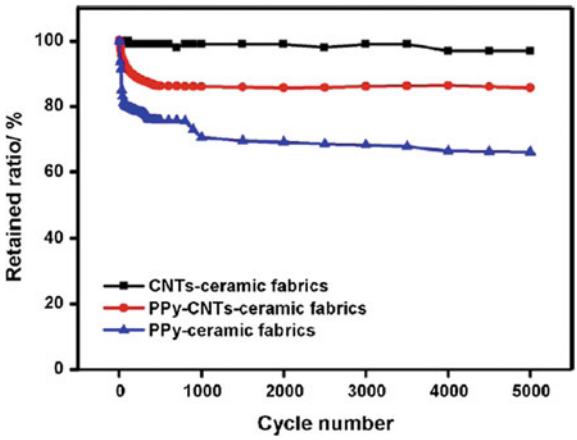

Fig. 8 Change of capacitance of CNTs, PPy and PPy–CNTs composite electrode on ceramic fabric as a function of the number of charge–discharge cycles at current density of 1 mA cm^{-2} (Reproduced with permission from [48])

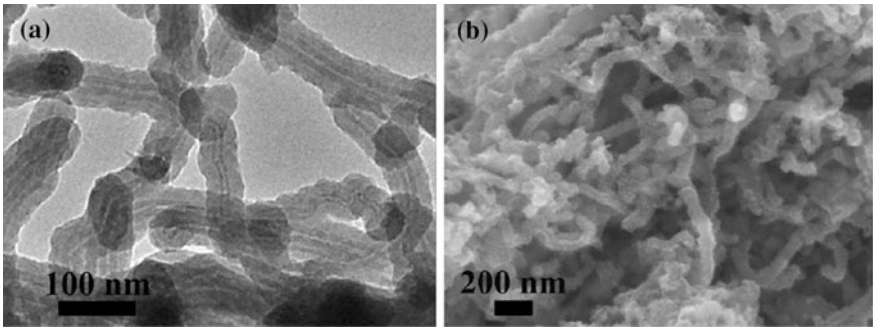

Fig. 9 **a** TEM image and **b** SEM image of PPy–CNT composite (Reproduced with permission from [49])

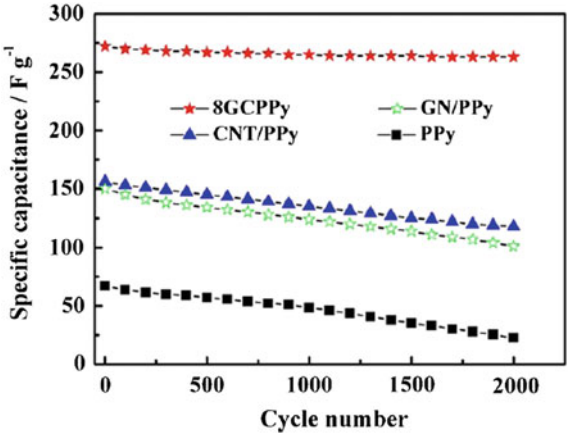

Fig. 10 SC of CNT/PPy, GN/PPy and 8GCPPy as a function of cycle number at a current density of 6 A g^{-1} (Reproduced with permission from [49])

charge–discharge rates [43]. As pointed above, they used amaranth dye as a redox-active anionic dopant for the chemical polymerization of PPy. In this investigation, a composite of PPy–MWCNT powders was prepared for the fabrication of electrochemical supercapacitor electrodes using amaranth as an anionic dopant for the chemical polymerization of PPy. Figure 11 compares SEM images of synthesized PPy and composite powders. The use of amaranth allowed the formation of PPy powders (Fig. 11a) with relatively small primary particle size in the range of 30–50 nm. However, the primary particles formed agglomerates. The formation of fine size of PPy primary particles in the presence of amaranth resulted to uniform coating of PPy on MWCNT (as observed in SEM image in Fig. 11b). The good dispersion of MWCNT and π–π interaction of MWCNT and PPy promoted the formation of PPy coated MWCNT. The formation of PPy coated MWCNT was confirmed by TEM investigations (Fig. 11c). The TEM image of PPy coated MWCNT (Fig. 11c) indicated that the thickness of the PPy layer was about 10 nm. They reported that PPy–MWCNT electrodes with MWCNT/PPy mass ratio of 1:9 and 2:8 showed high capacitance at low scan rates and improved

capacitance retention at higher scan rates, especially at scan rates above 10 mVs^{-1} (Fig. 12). The electrochemical supercapacitor cells, based on PPy coated MWCNT showed SC of 1.3–1.6 F cm^{-2} at discharge current densities of 1–33 mA cm^{-2} and good cycling stability.

In another report presented by Su and Zhitomirsky [54], PPy–MWCNT composites were synthesized using sulfanilic acid azochromotrop (SPADNS) and sulfonazo III sodium salt (CHR-BS) as anionic dopants for the chemical polymerization of PPy. The advantage of using CHR-BS was that it got adsorbed on the MWCNT's surface, allowed MWCNT dispersion and promoted the PPy polymerization on the MWCNT surface. The formation of PPy coated MWCNT

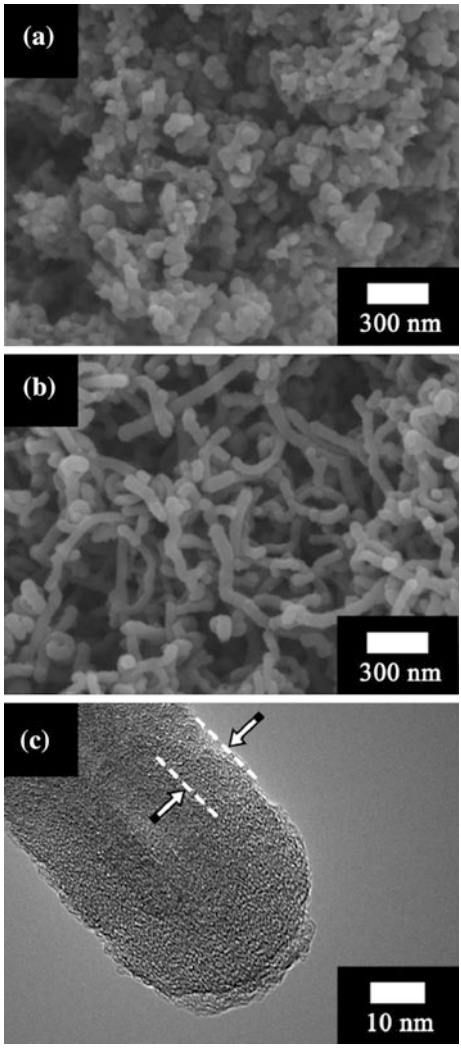

Fig. 11 **a** SEM image of PPy powder, **b** SEM and **c** TEM images of PPy coated MWCNT with MWCNT/PPy mass ratio of 3:7, *arrows* in **c** show a PPy layer (Reproduced with permission from [43])

using CHR-BS for MWCNT dispersion and PPy doping while polymerization was confirmed by TEM (Fig. 13). The formation of uniform coating and good contact of PPy and MWCNT was observed in TEM image which provided high conductivity of MWCNT, high capacitance of PPy, good cyclic stability and good electrical contact of both the materials.

Warren et al. [55] synthesized the vertically aligned carbon nanotube (VACNT)-PPy nanocomposites as a "hybrid supercapacitor (HC)" material directly integrated on silicon-based electrodes. The SEM images of the PPy-coated VACNT composite are shown in Fig. 14. They reported that total capacitance of the synthesized HC increased by five times as compared to its individual components due to its expanded operating voltage and current ranges. The enhanced energy storage in the VACNT–PPy nanocomposite is attributed primarily to fast surface redox reaction on PPy, a surface phenomenon that is unaffected by the thickness and hence the volume of deposited PPy. The cyclic voltammograms (CV) of pure PPy (three different thicknesses, 50, 100 and 200 nm) (Fig. 15a), CNT and CNT–PPy composite (Fig. 15b) were compared with the CV from VACNT forest coated with PPy under 0.5, 1, 1.5, and 2 min of PPy electroplating process (Fig. 15c). The following observations were drawn by authors from these graphs: The CV graphs of each of the three films, the thickness of as-deposited PPy film appears to have negligible influence on the total capacitance of the pure PPy film. Figure 15b shows that measured SC of the VACNT–PPy is 5 mF/cm^2, which is 500 % higher than that of as-grown VACNT or pure PPy film. Figure 15c shows that there is an optimal duration for PPy deposition that maximizes the total capacitance of a VACNT–PPy nanocomposite. They reported that optimal energy storage of the supercapacitor with low leakage current could be achieved with a PPy electrodeposition time of 1 min and thickness as low as 50 nm. This maximizes both the electrochemical double layer capacitance on VACNT and the pseudocapacitance on PPy, which yields an enhanced total capacitance.

The incorporation of titanium dioxide (TiO_2) nanoparticles in CNTs improves spatial confinement of TiO_2 and provides high surface area combined with faster

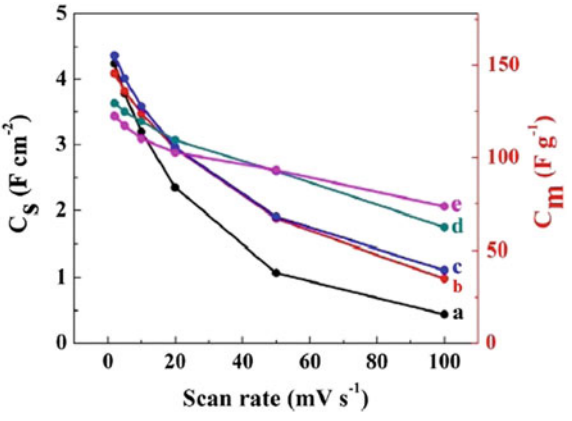

Fig. 12 C_s and C_m versus scan rate for 29 mg cm^{-2} electrodes of (*a*) pure PPy and (*b–e*) PPy coated MWCNT with MWCNT/PPy mass ratio of (*b*) 1:9, (*c*) 2:8, (*d*) 3:7 and (*e*) 4:6 (Reproduced with permission from [43])

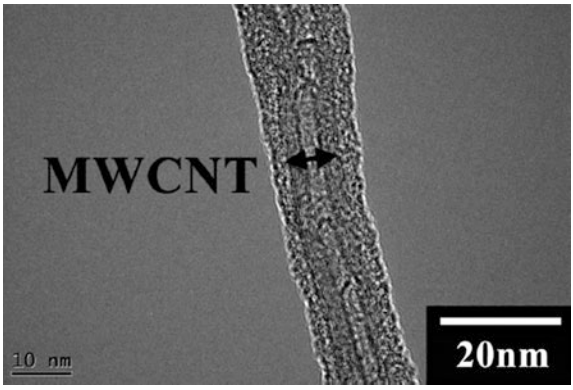

Fig. 13 TEM image of PPy–MWCNT prepared using CHR-BS, the *double arrow* shows MWCNT (Reproduced with permission from [54])

redox reactions. The SC of 282 Fg^{-1} of the CNT–PPy nanofibers core-shell composites decorated with TiO_2 nanoparticles has been reported in the literature [56]. The poor solubility of CNT films in solvents can be overcome by modifying the surface of CNTs with oxygen-containing groups (hydrophilic group) which act as nucleation sites for the coating of CPs on the CNT surface and allow CNTs to

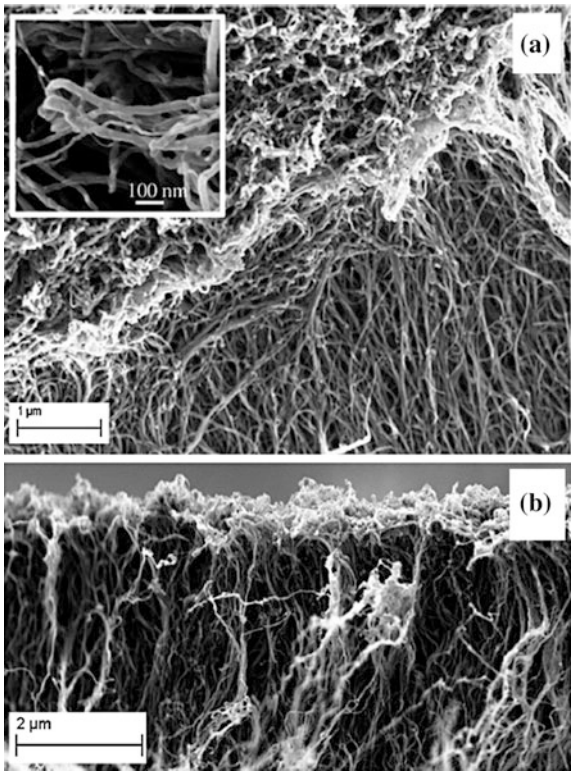

Fig. 14 SEM images of the PPY-coated VACNT forest **a** plan view with close-up image of the PPY-coated CNTs (*inset*). **b** Cross-sectional view of the VACNT–PPY supercapacitor (Reproduced with permission from [55])

disperse readily in aqueous solutions. One of the methods to produce oxygen containing CNT surfaces has been previously discussed that is to treat CNTs with acids such as HNO_3, H_2SO_4 or a mixture of HNO_3 and H_2SO_4, thus generating carboxylic group-capped CNTs before combining CNTs with PPy [44]. Similarly as reported by Wang et al. [57] the acid (sulfuric acid, nitric acid and thionyl chloride) treated MWCNTs were composited with graphene oxide and PPy by in-situ polymerization to synthesize graphene oxide/polypyrrole/multi-walled carbon nanotubes composites (PCMG). They reported the SC of PCMG composite to be 406.7 Fg^{-1} (at the current density of 0.5 A g^{-1}) and the retention capacitance of 92 % after 1000 cycles at a current density of 2 A g^{-1}.

The other method reported in literature is the air plasma treatment of CNT surfaces which is prominent up to few nanometers of the surface of the material and does not destroy structure of material which may otherwise, be caused by the acid treatment methods [58–60]. Yang et al. [61] synthesized the PPy bonded CNT composites directly using air plasma activated CNTs (P–CNT), via in-situ chemical oxidative polymerization with improved thermal stability and conductivity. Their SEM images (Fig. 16a, b) showed the tight coating of PPy on the plasma activated CNTs due to the π bonding between PPy and CNT as well as

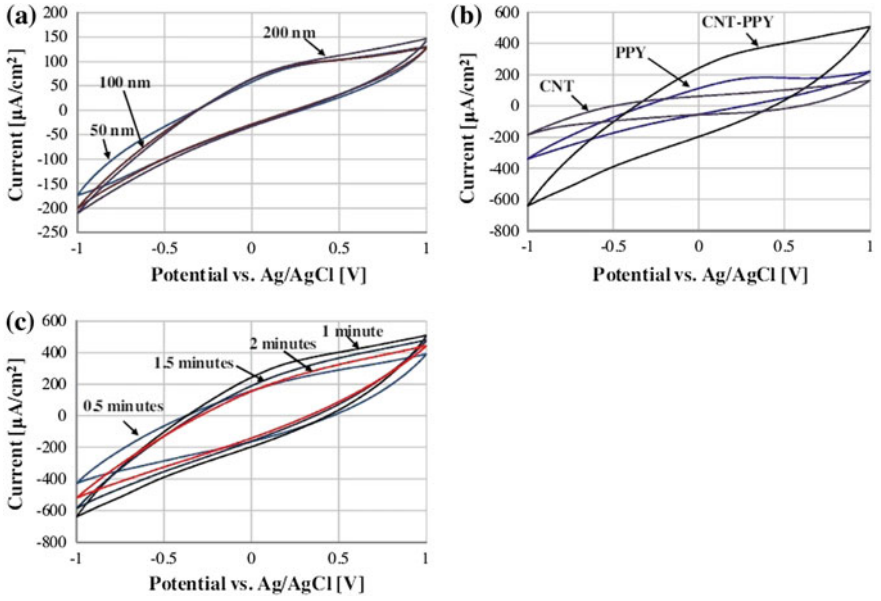

Fig. 15 **a** Cyclic voltammograms of a pure PPY film with a thickness of 50, 100, and 200 nm, respectively. **b** Cyclic voltammograms measured from: (*1*) VACNT forest electrode, (*2*) DBS-doped PPY electrode, and (*3*) VACNT coated with DBS-doped PPY electrode. Electrode made of VACNT–PPY has achieved 500 % higher capacitance than pure VACNT or pure PPY. **c** Cyclic voltammograms from VACNT forest coated with PPY under 0.5, 1, 1.5, and 2 min of PPY electroplating process (Reproduced with permission from [55])

oxygen-containing groups and pyrrolic nitrogen created via plasma activation on the surface of the P–CNTs. The plasma formed oxygen-containing groups and pyrrolic nitrogen groups supplied more active nucleation sites which could facilitate binding between P–CNT and PPy to form the P–CNT–PPy (Fig. 16b). The cyclic voltammetry showed the SCs of the PPy, CNT/PPy and P–CNT–PPy electrodes to be 130, 148 and 188 Fg^{-1} respectively. After charge-discharge tests for 1000 cycles at a current density of 5 mA/cm^2, the P–CNT–PPy electrode retained 89 % of its initial capacitance while the CNT/PPy retained 76 %. Thus P–CNT–PPy demonstrated as a promising electrode material for high-performance supercapacitors.

3.2 PANi–CNT Composites

Polyaniline (PANi) polymer has wide range of applications in electromagnetic interference, sensors, light emitting diodes and secondary batteries. Its thermal stability up to the temperature of 250 °C is advantageous over other conducting polymers. The general formula of PANi is $[(–B–NH–B–NH–)_n(–B–N=Q=N–)_{1-n}]_m$ in which B and Q denote the rings in the benzenoid and quinonoid forms respectively. PANi exists in three stable oxidation states: first is leucoemeraldine $[(C_6H_4NH)_n]$, which is white in colour, second is emeraldine $([C_6H_4NH]_2[C_6H_4N]_2)_n$, which is green for the emeraldine salt and blue for the emeraldine base. Third is pernigraniline $[(C_6H_4N)_n]$, which is blue/violet in colour. None of the above-described states are conducting unless in the oxidized states, in particular the emeraldine base, are protonated and charge carriers are generated. It is this process, (generally called 'protonic acid doping') which makes polyaniline so unique; no electrons have to be added to or removed from the insulating material to make it conducting [62]. The conductivity is affected by the water content; completely dry samples are five times less conductive than samples containing some water [62]. Further utilisation of PANi for making its composites with other materials requires its solubility; lack of solubility is one of the

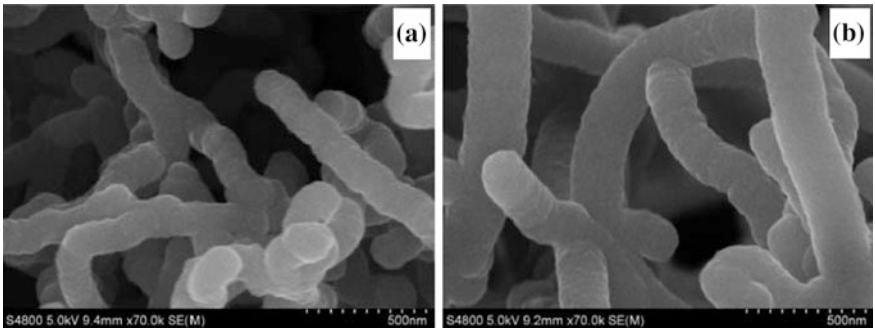

Fig. 16 SEM images of **a** PPy–CNT and P–CNT–PPy composites respectively (Reproduced with permission from Yang et al. [61])

major drawbacks of PANi. Emeraldine base is soluble in some polar organic solvents such as N-methylpyrrolidone (NMP) and dimethylsulfoxide (DMSO), but is an insulator, whereas emeraldine salts (ES) are conductive but usually insoluble and non-processable [63]. There are various methods reported in literature to increase the solubility of PANi. Some of the methods suggested in the literature are (a) the protonation of PANi, (b) incorporation of polar functional groups, polymeric chains or long and flexible alkyl chains in the PANi backbone to make it soluble in water or organic solvents, (c) homopolymerization, a derivative of aniline (e.g., ring or N-substituted anilines) or their copolymerization with aniline resulting in improved solubility of the polymers obtained and (d) incorporation of polar functional groups, polymeric chains or long and flexible alkyl chains in the PANi backbone [63–77].

By integrating CNTs with PANi nanofibers, high density and high-surface areas are possible that can lead to improvements in the conductivity and the development of electronic devices with superior properties [78]. The composites of PANi–CNT can be synthesized by various methods such as electrochemical processing, surfactant free aqueous polymerization, micelle–CNT hybrid template directed synthesis, inverse emulsion pathways, interfacial polymerization, plasma polymerization, "in-situ" and "ex-situ" polymerization. The details of these methods have been discussed by Oueiny et al. [8]. In-situ polymerization is one of the most important methods developed so far to integrate CNTs and polyaniline. Polymerization methods include stirring, static placement, sonication and emulsion polymerization [78].

Cochet et al. [79] synthesized the PANi–MWCNT composites by in-situ polymerization process using 10, 20, 30 and 50 wt% of MWCNTs (by weight of monomer). These composites were compared with the ex- situ polymerised composites prepared by mixing the doped PANi with 30 wt% of MWCNTs as well as with the ex-situ 30 wt% PMMA/MWCNTs composite. They measured the temperature dependence resistivity of PANi and the composites as shown in Fig. 17. PANi showed a typical room temperature resistivity of 0.3 Ω cm. It increased by 7 orders of magnitude following a $T^{-1/4}$ hopping law upon cooling to 1.7 K. The resistivity of MWCNT was 2 Ω cm at room temperature and increased up to 15 Ω cm at low temperature. At room temperature, the resistivity of composite was low as compared to PANi and it decreased further with the decrease of the temperature. The resistivity for the 50 and 30 wt% was lower than that of the ex-situ PANi–MWCNT composite. Wei et al. [80] reported the use of sulfonated MWCNTs [MWCNT–$(OSO_3H)_n$] as the self assembled templates for the syntheses of PANi-coated MWCNT–$(OSO_3H)_n$ and PANi nanotubes doped with MWCNT–$(OSO_3H)_n$. The morphological structures of the composites were reported to be dependent upon the weight ratio of aniline to MWCNT–$(OSO_3H)_n$.

Feng et al. [81] reported the PANi–MWCNT films synthesized by in-situ polymerization method. The MWCNT films were encapsulated in the cores of growing polymer chains resulting in the formation of PANi–MWCNT hybrid material of 90–100 nm diameters. They measured the temperature dependence conductivity of PANi, MWCNT and PANi–MWCNT composite. The conductivity of MWCNT was much larger as compared to the PANi polymer. It decreased for the PANi–MWCNT composite as compared to the pure MWCNT. The conductivity

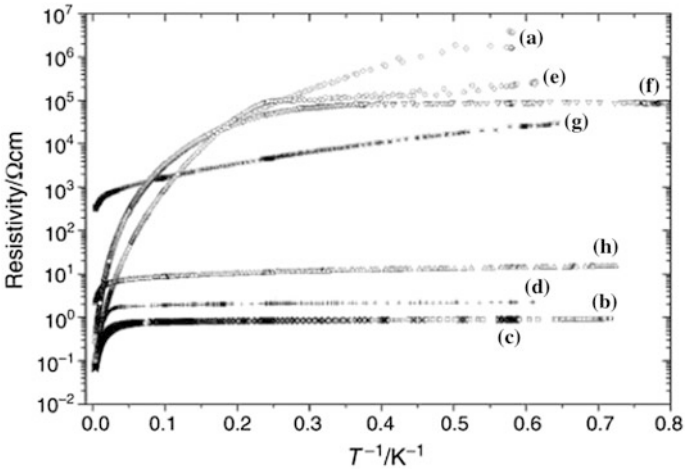

Fig. 17 Temperature dependence of the resistivity in polymer/MWCNTs composite: (*a*) PANi, in-situ PANi–MWCNTs composites with (*b*) 50, (*c*) 30, (*d*) 20 and (*e*) 10 wt% of MWCNTs, (*f*) the ex- situ 30 wt% PANi–MWCNTs composite, (*g*) the ex-situ 30 wt% PMMA/MWCNTs composite and (*h*) MWCNTs (Reproduced with permission from [79])

of MWCNT and PANi–MWCNT composite remained almost constant with a decrease of temperature while it dropped for pure PANi. These observations concluded that conductivity depends upon the doping level, chain length as well as compactness and orientation of the microparticles.

By introducing an aromatic additive into the in-situ polymerization method, the reaction rate can be increased. Liao et al. [78] used aniline dimer (N-phenyl-p-phenylenediamine) to create bulk 1D nanofibers of SWCNT/PANi composites possessing widely tunable conductivities (10^{-4}–10^2 S/cm) with low CNT loadings (≤ 5.0 wt%). Their SEM and TEM images in Fig. 18 showed the diameter of PANi nanofibers in the range of 30–60 nm, SWCNTs in the range of 1–2 nm and SWCNT–PANi nanofibers in the range of 20–50 nm. The active coating of PANi nanofibers on SWCNTs led to an extended conjugated network. Nanofibrillar composite materials exhibited enhanced conductivities with values up to 95 and 0.3 S/cm in their doped and dedoped states, respectively, compared to 1.7 and $<10^{-10}$ S/cm for PANi nanofibers by themselves as shown in Fig. 19.

PANi itself has a good electrical conductivity and can be used for supercapacitive properties, but the drawback is the poor cycleability of the PANi electrode. This disadvantage can be reduced by synthesizing the PANi–CNT composite. As per the previous discussion, the type of synthesis method adopted for the composite affects the SC as well as the redox cycleability of the PANi–CNT composite. The supercapacitive properties of PANi–CNT composites have been tested in the last decade. Numerous publications were produced predicting the SC and good cyclic voltammetry of the composite. The attention has been paid to synthesize the composites of PANi–CNT by optimizing the conditions and methods for their

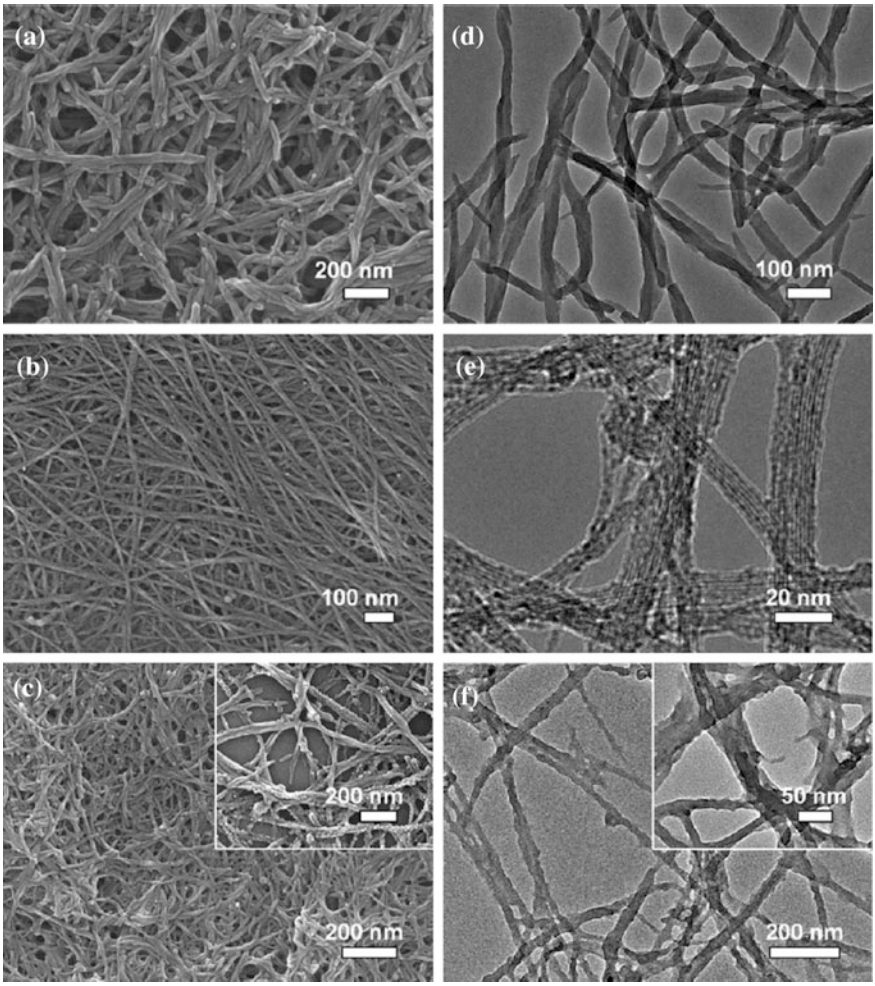

Fig. 18 **a**–**c** SEM and **d**–**f** TEM images of **a**, **d** polyaniline nanofibers, **b**, **e** SWCNTs, and **c**, **f** SWCNT/polyaniline composite nanofibers. The *insets* in (**c**, **f**) show a magnified view. (Reproduced with permission from [78])

preparation, which affect the morphology, size and distribution of CNTs into the polymer matrix and hence alter the conductive and capacitive nature of the final composite. The factors influencing the performance of the composite are the dispersion of CNTs in the polymer matrix and interfacial interaction between CNTs and PANi. The improvement in dispersion of MWCNTs in the polymer matrix through surface chemical modification of CNTs, can generally be achieved by the oxidation of MWCNTs, i.e., refluxing in a mixture of nitric acid and concentrated sulphuric acid for varying lengths of time to deliberately introduce functional groups [82] as per the previous discussion. The relatively high conductivity of

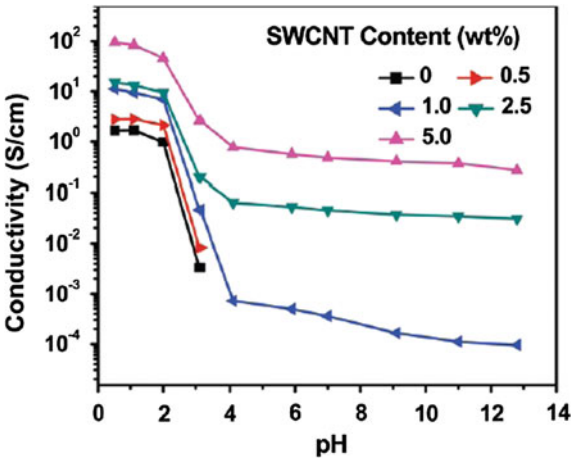

Fig. 19 Influence of pH and SWCNT loadings on the electrical conductivity of thin films of SWCNT/polyaniline composite nanofibers (Reproduced with permission from [78])

composites prepared using acid-treated nanotubes renders them more processable without diminishing the conductivity and is critical for effectively achieving their properties [82]. Another factor which is connected to the capacitance of composite is the nature and surface of the electrode/electrolyte interface, which provides the electrical transport and diffusion of anions and cations.

Dong et al. [83] reported the SC of 328 Fg^{-1} of the PANi-CNT composites synthesized by in-situ chemical oxidative polymerization method. It has been observed that the weight percentage of PANi and CNT in the composite plays a vital role for the good SC. Gupta and Miura [84] used the electrochemical polymerization of polyaniline onto SWCNTs, and their capacitive performance was evaluated using cyclic voltammetry and charge–discharge cycling in 1 M H_2SO_4 electrolyte. The single electrode of PANi-SWCNT composites showed much higher SC, specific energy and specific power than pure PANi and SWCNTs. The highest SC, specific power and specific energy values of 485 Fg^{-1}, 228 Wh/kg and 2250 W/kg were observed for 73 wt% PANi deposited onto SWCNTs. The PANi–SWCNT composites also showed long cyclic stability. The high surface area of the composite helps in improving the charge storage ability and is effective in the accession of the electrolyte to the electrode in the redox mechanism. Multi-walled carbon nanotube (MWCNT)/polyaniline (PANi) composite films were prepared by in-situ electrochemical polymerization of an aniline solution containing different MWCNT contents by Zhang et al. [85] and obtained the SC value of 500 Fg^{-1} for the MWCNT/PANi composite film containing MWCNT of 0.8 wt%. Sivakkumar et al. [86] synthesized polyaniline nanofibres with high surface area and have evaluated their electrochemical performances as electrode materials in an aqueous redox supercapacitor. They compared the results with the PANi–CNT composites synthesized by in-situ chemical polymerization. The initial SC of the cell based upon PANi nanofiber (diameter 90 nm and length 420 nm) was observed to be 554 Fg^{-1} at a constant current of 1.0 A g^{-1}, but this value rapidly decreased on

continuous cycling. The cell assembled with PANi–CNT composite electrodes showed a high initial SC of 606 Fg^{-1} and good capacitance retention in the voltage range of 0–0.4 V.

The ratio of PANi in the PANi–CNT composite affects the capacitive properties of the composite. Zhou et al. [82] synthesized the PANi–MWCNT composite by in-situ polymerization method and controlled the thickness of PANi layer in the PANi–MWCNT composites by changing the CNTs and aniline monomer ratios. Changing the thickness of PANi changed the SC of the resulting composites with core–shell structures. By increasing the polyaniline content from 0 to 80 wt%, the thickness of the polyaniline layer increased from 0 nm to about 60 nm. The optimized thickness of the PANi layer was found to be approximately 50 nm, where maximum SC of 177 Fg^{-1} was achieved for 66 wt% PANi. The highest SC for the composite with 66 wt% polyaniline content was observed to be 560 Fg^{-1} at a scan rate of 1 mV/s and 177 Fg^{-1} at a scan rate of 5 mV/s as shown in Fig. 20. The reduction in the SC was only 29.1 % after 700 cycles, and then remained stable after further cycles.

Zhang et al. [87] reported the tube-covering-tube nanostructured polyaniline–CNTs array (PANi–CNTA) composites synthesized by electrodeposition method. A uniform and compact PANi nanolayer, forming a tube-covering-tube unique microstructure of PANi nanolayer (of thickness 7 nm) was observed in the SEM and TEM images (Fig. 21a, b), which is very desirable for the supercapacitive properties. The TEM images in Fig. 21b shows that PANi nanolayer is composed of numerous nanoclusters with diameters of about 0.5 nm. Figure 21c shows the charge–discharge curves of the PANi–CNT composite at different current densities (current/the mass of composite). The discharge capacitance of the PANi–CNTA

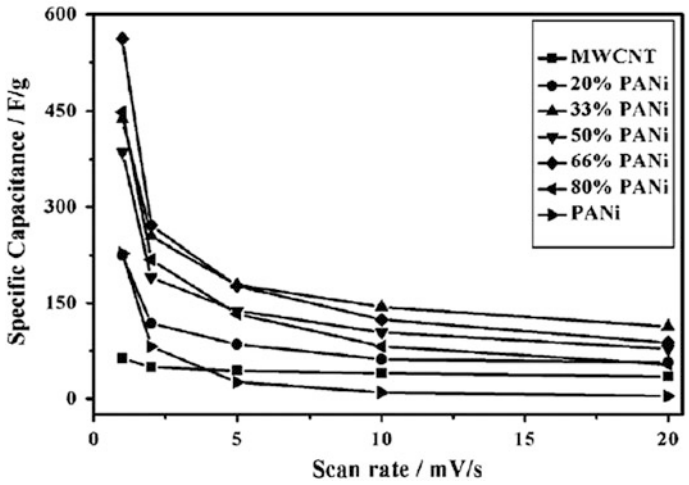

Fig. 20 Specific capacitance as a function of potential sweep rate for the resulting composites with various polyaniline contents (Reproduced with permission from [82])

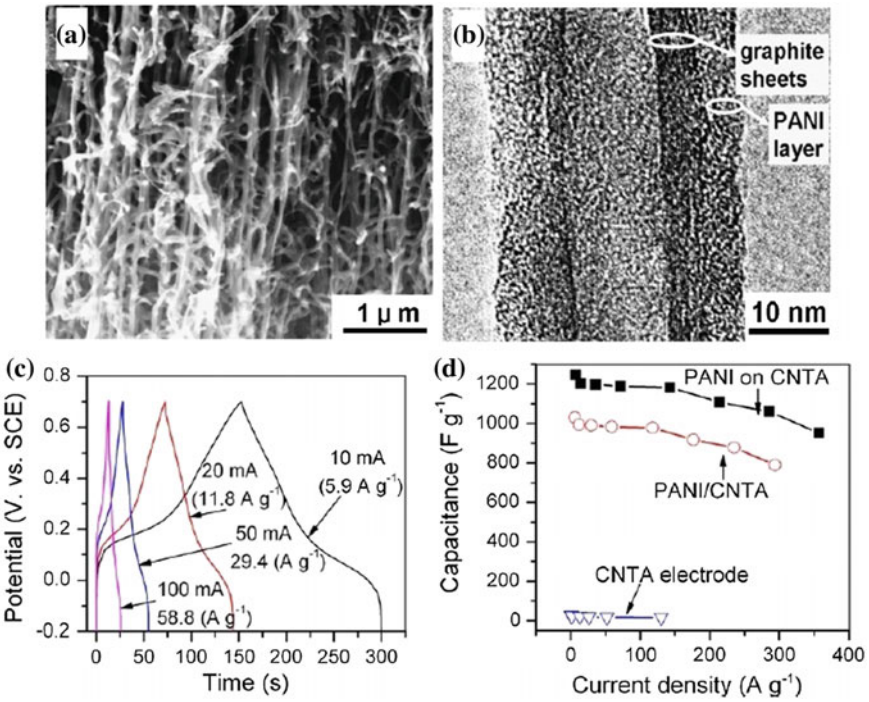

Fig. 21 **a** SEM image of the PANi–CNT composite, **b** TEM image of a PANi-covered CNT, **c** Charge–discharge curves at different current densities, **d** Specific capacitance of PANi on CNTA, PANi–CNTA (based on the mass of PANi on CNTA and PANi–CNTA composite respectively), and original CNTA versus discharge current density (Reproduced with permission from [87])

composite at a current density of 5.9 Ag^{-1} was reported to be 1030 Fg^{-1} which was much higher as compared to original CNT array electrodes (Fig. 21d).

In another study by the same group, PANi–CNTA composites were prepared by the same technique for 100–500 cyclic voltammetry (CV) cycles [88]. The SC was found to decrease with the increase of the CV cycles due to increasing in the thickness of PANi layer in the electrode. TEM images in Fig. 22 showed that the thickness of the PANi layer in the electrode prepared by 100 and 300 cycles was around 10 nm and 30 nm respectively. The composite prepared by 100 CV cycles showed the highest SC of 1030 Fg^{-1} at a current density of 5.9 Ag^{-1}. This composite retained 77 % capacity at a current density of as high as 294 Ag^{-1}. The PANi–CNTA electrode prepared by 300 CV cycles showed much lower SC and worse rate capability. The Smaller size of PANi layer (10 nm in 100 CV as compared to 30 nm in 300 CV) reduced the diffusion length of ions within the electrode during the charge–discharge process, which is reported to be one of the reasons for good SC [89]. The increment in SC is inversely dependent on PANi coating thickness. Potphode et al. [23] reported similar results. They synthesized PANi–MWCNT composites via in-situ polymerization method. The PANi to

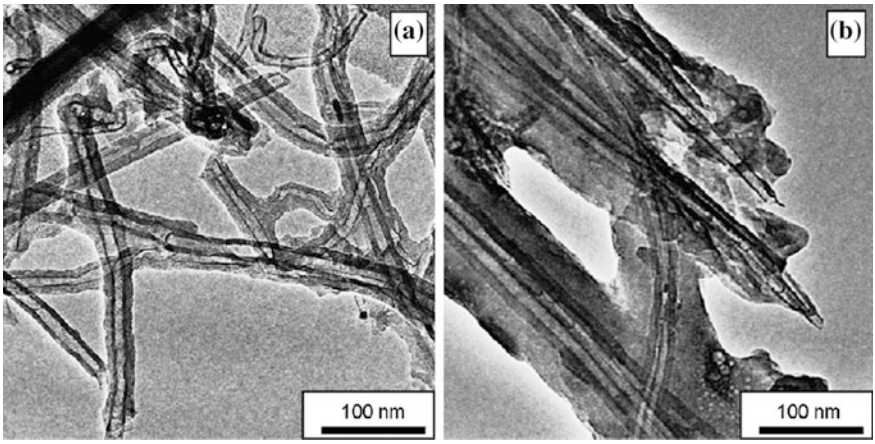

Fig. 22 TEM images of the PANi covered CNTs synthesized by **a** 100 and **b** 300 CV cycles at 100 mV s^{-1} between −0.2 and 0.8 V (Reproduced with permission from [88])

Table 1 Diffusion coefficient and diffusion length of PANi–Px–MWCNT nanocomposites [Reproduced with permission from [23]

Supercapacitor cell	Diffusion coefficient (cm^2 s^{-1})	Diffusion length (nm)
PANi-25	1.18×10^{-9}	116
PANi-50	5.70×10^{-9}	257
PANi-75	9.53×10^{-9}	445
PANi	12.7×10^{-9}	599

Px-MWCNT ratios were maintained as 0.75:0.25 (PANi-75), 0.50:0.50 (PANi-50) and 0.25:0.75 (PANi-25). PANi-50 and PANi-25 nanocomposites based supercapacitors exhibited 91 % and 93 % capacitive retention after 2000 charge-discharge cycle while pure PANi showed only 67 % capacitance retention for the same number of cycles. The diffusion length decreased with a decrease in PANi content in the nanocomposites as shown in Table 1. The enhancement of the charge-discharge rate capability of supercapacitors is attributed to the diffusion length of the nanocomposites [23].

Meng et al. [90] reported a novel method to prepare the interesting paper-like PANi–CNT composites by using the CNT network as the template. Compared to the conventional brittle PANi–CNT composites, these paper-like composites were much thin and flexible. The paper-like films can be rolled up, bent or twisted easily as compared to the brittle pellets of PANi–CNT composites (Fig. 23). The same group synthesized the PANi–CNT nanocomposite electrodes well solidified in the H_2SO_4-polyvinyl alcohol (PVA) gel electrolyte composites (of the thickness of the order of A4 size) by a two-step approach [91]. They synthesized the flexible PANi–CNT nanocomposite thin film electrodes by in-situ chemical solution method and then soaked them in the H_2SO_4-PVA gel electrolyte followed by solidification. They

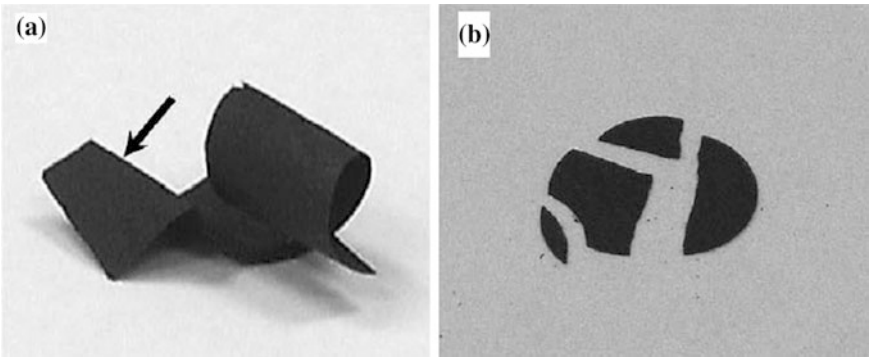

Fig. 23 **a**, **b** are digital macrographs of the flexible Buckypaper/PANi composite and the brittle CNT/PANi tablet, respectively (Reproduced with permission from [91])

reported the SC of 350 Fg^{-1} for the electrode materials, good cycle stability after 1000 cycles and a leakage current of as small as 17.2 μA. The introduction of graphene nanosheet (GNS) in the PANi–CNT composite increases the SC and cycleability of the composite electrode due to the large current density as well as the dispersion of nanoscale PANi particles on GNS reduces the diffusion and migration length of the electrolyte ions during the fast charge/discharge process and increases the electrochemical utilization of PANi [92]. Yan et al. [92] reported the synthesis of Graphene nanosheet/carbon nanotube/polyaniline (GNS/CNT/PANi) composite via in-situ polymerization method. The 2 nm thick PANi nano-particles were observed to be coated on the GNS surface. With 1 wt% of CNTs into GNS, the cyclic stability was reported to be improved due to the maintenance of highly conductive path as well as mechanical strength of the electrode during doping/dedoping processes. They reported the maximum SC of 1035 Fg^{-1} at a scan rate of 1 mVs^{-1} in 6 M KOH of the GNS/CNT/PANi composite as compared to 780 Fg-1 value of PANi–CNT as shown in Fig. 24. After 1000 cycles, the capacitance of the GNS/CNT/PANi composite decreased only 6 % of initial capacitance compared to 52 and 67 % for GNS/PANi and CNT/PANi composites.

Zhang and his team reported ternary composite of carbon nanotube/ethylvinylacetate/polyaniline (PANi/CNT/EVA) with a 3D co-continuous phase structure with excellent SC and magnificent cycleability, which is by far the highest performance of a PANi based electrode reported to till date [93]. In brief description, they synthesized carbon nanotubes–ethylvinylacetate (CNT/EVA) composite with a 3D co-continuous phase structure from EVA filled with 40 wt% CNT. The CNT/EVA composite had low cost, high conductivity (19.6 S cm^{-1}), great flexibility and excellent mechanical properties (tensile strength of 22.5 MPa). The CNT/EVA composite was dipped into the ethyl alcohol solution containing aniline hydrochloride and then taken out to volatilize the ethyl alcohol completely. Therefore the aniline hydrochloride remained inside the CNT/EVA composite to act as a working electrode. Finally, the continuous PANi network around the CNTs (denoted as PANi/CNT/EVA) was obtained by

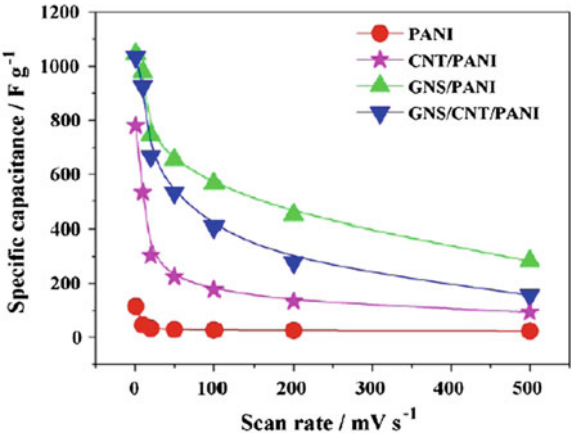

Fig. 24 Specific capacitance of PANi and PANi based composites at different scan. Rates (Reproduced with permission from [93])

incorporating the working electrode in a conventional three-electrode cell using cyclic voltammetry techniques. The 0.3 mm-PANi/CNT/EVA electrode achieved a high areal capacitance of 575 mF cm^{-2} and a SC of 1105 Fg^{-1} at a scan rate of 5 mV s^{-1}. More importantly, continuous PANi inside a 40 wt% CNT/EVA composite displayed excellent cycling performance maintained over 45, 000 cycles and the capacitance of the PANi/CNT/EVA composite depended on the thickness of the 40 wt% CNT/EVA composite [93].

4 Summary, Conclusive Remarks and Future Perspectives

The composites based on conducting polymers (CPs) and carbon nanotubes (CNTs) have been a key focus in the last decade for their unique properties such as large surface area, high mechanical strength and high conductivity. The CP–CNT composites are used as actuators, fuel cells, electronic devices and 'supercapacitors'. Polypyrrole (PPy) and polyaniline (PANi) have good conductivity and are cost effective for their use in electrical applications. The charge storage properties of these CPs can be improved by doping it with the redox-active dopants. The stability and conductivity of the CP films can be enhanced by the use of polycharged aromatic anionic dopants since the structure of anionic dopants influence the shape and size of CPs particles and increases the interchain mobility of charge carriers. The increase in the size of dopant molecules and charge to mass ratio results in reduced size of the PPy particles and increased capacitance. But in addition to it, the major challenge in this field is to achieve good cyclic stability and durability of the material to be used as a supercapacitor, which is poor in case of doped CPs and/or

CNTs independently. The reports are present to achieve the excellent cyclic stability by using different substrates such as graphite, carbon, nickel, and gold, etc. in acidic and basic electrolytes. The supercapacitance (SC) could be improved up to 339–451 Fg^{-1} but at the cost of poor cyclic stability; which can be achieved by intermixing CPs into CNTs to make a nano-composite.

The key requirements for CP/CNT composites to be used as supercapacitors are high specific capacitance (SC), high electrochemical stability and good cycleabilty. The CP–CNT composites (particularly PPy–CNT and PANi–CNT) have been reported to be used for supercapacitve properties to fulfill the above-mentioned requirements. The attention has been paid to synthesize the composites of CP–CNT by optimizing the conditions and methods for their preparation, which affect the morphology, size and distribution of CNTs into the polymer matrix and hence alter the conductive and capacitive nature of the final composite. The charge storage properties can be improved by optimizing the thickness and surface area of the fillers, uniform distribution of the nano-films, etc. But optimizing the parameters and controlling the cyclic stability is not an easy task. The insolubility, poor dispersibility and poor compatibility of CNTs hinder their incorporation with CPs. The interaction between CNTs and CPs can be increased by modifying CNT surface with oxygen containing groups which act as nucleation sites and allow dispersion of CNTs readily in aqueous solution. One of the easier and cheapest methods is the acid treatment (such as HNO_3, H_2SO_4, etc.) of CNTs. It generates carboxylic group capped CNTs which associates easily with CPs. This method is not suitable always, as the acid treatment may destroy the structure of material. The alternative method reported in the literature is air plasma treatment of CNT surfaces.

The degradation in capacitance is ascribed to the swelling and shrinking of CP chains during doping/de-doping process leading to the mechanical degradation of the polymer. The charge storage capacity/SC of CP–CNT composite can be increased by controlling the diameter of nano particles; it can be achieved by controlling the CP/CNT mass ratio by using different surfactants. The homogeneous coating of CPs on CNT surfaces may further increase the SC of the composite. Zhang et al. [17] controlled diameter of nano-cables by optimizing the PPy/CNT mass ratio. Lee et al. [48] used ceramic fibre as substrate and PPy was coated on CNT uniformly, with this they achieved 85 % of capacitance after 5000 cycles. The high surface area of the composite helps in improving the cyclic stability and is effective in accession of the electrolyte to the electrode in the redox mechanism. Sivakkumar et al. [86] synthesized high surface area PANi-MWCNT composite and reported SC of 606 Fg^{-1} with good cyclic stability.

The ternary composites of graphene, CNTs and CPs are the solution of discussed problems in the present research field and future perspectives. Zhang et al. [93] reported composites of CNT, ethyl-vinyl-acetate and PANI with a 3D co-continuous phase structure having SC of 1105 Fg^{-1} and excellent cycling performance over 45,000 cycles. The future perspective of the nano composites with high surface area lies in the ternary composites of graphene, CNTs and CPs which can have high cyclic stability as well as effective in accession of the electrolyte to the electrode in the redox mechanism.

References

1. Lu X, Zhang W, Wang C, Wen T, Wei Y (2011) Prog Polym Sci 36:671–712
2. Wan M (2008) Conducting polymers with Micro or Nanometer Structure. Springer, New York
3. Ganesh EN (2013) Int J Innov Technol Explor Eng 2:311–320
4. Ajayan PM, Ebbesen TW (1997) Rep Prog Phys 60:1025
5. Eatemadi A, Daraee H, Karimkhanloo H, Kouhi M, Zarghami N, Akbarzadeh A, Abasi M, Hanifehpour Y, Joo SW (2014) Nanoscale Res Lett 9(393):13
6. Chico L, Crespi VH, Benedict LX, Louie SG, Cohen ML (1996) Phys Rev Lett 76(6):971–974
7. Rao CNR, FRS, Govindraj A (2005) Nanotubes and Nanowires. RSC Publishing, Cambridge, UK
8. Oueiny C, Berlioz S, Perrin FX (2014) Prog Polym Sci 39:707–748
9. Volder MFL, Tawfick SH, Baughman RH, Hart AJ (2013) Science 339:535–539
10. Bianco A, Kostarelos K, Prato M (2005) Curr Opin Chem Biol 9:674–679
11. Baskaran D, Mays JW, Bratcher MS (2005) Chem Mater 17:3389–3397
12. Spitalsky Z, Tasis D, Papagelis K, Galiotis C (2010) Prog Polym Sci 35:357–401
13. Baibarac M, Gómez-Romero P (2006) J Nanosci Nanotechnol 6:1–14
14. Hirsch A (2002) Angew Chem Int Ed 41:1853–1859
15. Byrne MT, Gunko YK (2010) Adv Mater 22:1672–1688
16. Ajayan PM, Stephan O, Colliex C, Trauth D (1994) Science 265:1212–1214
17. Zhang X, Zhang J, Wang R, Zhu T, Liu Z (2004) Chem Phys Chem 5:998–1002
18. Bose S, Taoas K, Mishra AK, Rajashekar R, Kim NH, Lee JH (2012) J Mater Chem 22:767–784
19. Lu X, Dou H, Yuan C, Yang S, Hao L, Zhang F, Shen L, Zhang L, Zhang X (2012) J Power Sources 197:319–324
20. Pandolfo AG, Hollenkamp AF (2006) J Power Sources 157:11–27
21. Ghenaatian HR, Mousavi MF, Kazemi SH, Shamsipur M (2009) Synth Met 159:1717–1722
22. Kotz R, Carlen M (2000) Electrochim Acta 45:2483–2498
23. Potphode DD, Sivaraman P, Mishra SP, Patri M (2015) Electrochim Acta 155:402–410
24. Frackowiak E, Beguin F (2001) Carbon 39:937–950
25. Jiahua Z, Hongbo G, Zhiping L, Neel H, David PY, Suying W, Zhanhu G (2012) Langmuir 28:10246–10255
26. Li J, Xie H, Li Y, Liu J, Li Z (2011) J Power Sources 196:10775–10781
27. Arico AS, Bruce P, Scrosati B, Tarascon JM, Schalkwijk W (2005) Nat Mater 4:366–377
28. Wang LX, Li XG, Yang YL (2001) React Funct Polym 47:125–139
29. Mandal BM, Banerjee P, Bhattacharyya SN (1996) In: Salamone JC (ed) Polypyrrole (processable dispersions), in polymeric materialsencyclopedia. CRC Press, Boca Raton, 6670–6678
30. Rodriguez J, Grande HJ, Otero TF (1997) Handbook of organic conductive molecules and polymers, vol 2. Wiley, Chichester, pp 415–468
31. Long Y, Chen Z, Zhang X, Zhang J, Liu Z (2004) J Phys D Appl Phys 37:1965–1969
32. Kang HC, Geckeler KE (2000) Polymer 41:6931–6934
33. Puanglek N, Sittatrakul A, Lerdwijitjarud W (2010) Sci J UBU 1:35-42
34. Wang J, Dai J, Yarlagadda T (2005) Langmuir 21:9–12
35. Zhang X, Lu Z, Wen M, Liang H, Zhang J, Liu Z (2005) J Phys Chem B 109:1101–1107
36. Abeles B, Sheng P, Coutts MD, Arie Y (1975) Adv Phys 24:407
37. Zhang X, Song W (2009) Front Mater Sci China 3(2):194–200
38. Liu J, An J, Ma Y, Li M, Ma R (2012) J Electrochem Soc 159:A828–A833
39. Zhang D, Zhang X, Chen Y, Yu P, Wang C, Ma Y (2011) J Power Sources 196:5990–5996

40. Sharma R, Rastogi A, Desu S (2008) Electrochem Commun 10:268–272
41. Chang HH, Chang CK, Tsai YC, Liao CS (2012) Carbon 50:2331–2336
42. Shi K, Zhitomirsky I (2013) J Power Sources 240:42–49
43. Zhu Y, Shi K, Zhitomirsky I (2014) J Power Sources 268:233–239
44. Silva AMT, Machado BF, Figueiredo JL, Faria JL (2009) Carbon 47:1670–1679
45. Mi H, Zhang X, Xu Y, Xiao F (2010) Appl Surf Sci 256:2284–2288
46. Fang Y, Liu J, Yu DJ, Wicksted JP, Kalkan K, Topal CO, Flanders BN, Wu J, Li J (2010) J Power Sources 195:674–679
47. Paul S, Lee YS, Choi JA, Kang YC, Kim DW (2010) Bull Korean Chem Soc 31:1228–1232
48. Lee H, Kim H, Cho MS, Choi J, Lee Y (2011) Electrochim Acta 56:7460–7466
49. Lu X, Zhang F, Dou H, Yuan C, Yang S, Hao L, Shen L, Zhang L, Zhang X (2012) Electrochim Acta 69:160–166
50. Zhu Y, Zhitomirsky I (2013) Synth Met 185:126–132
51. Weng B, Shepherd R, Chen J, Wallace GG (2011) J Mater Chem 21:1918–1924
52. Han M, Chu Y, Han D, Liu Y (2006) J Colloid Interface Sci 296:110–117
53. Qie L, Yuan LX, Zhang WX, Chen WM, Huang YH (2012) J Electrochem Soc 159:A1624–A1629
54. Su Y, Zhitomirsky I (2015) Appl Energy 153:48–55
55. Warren R, Sammoura F, Teh KS, Kozinda A, Zang X, Lin L (2014) Sens Actuators A: Physical 231:65–73
56. Oliveira AHP, de Oliveira HP (2014) J Power Sources 268:45–49
57. Wang B, Qiu J, Feng H, Sakai E (2015) Electrochim Acta 151:230–239
58. Naseh MV, Khodadadi AA, Mortazavi Y, Pourfayaz F, Alizadeh O, Maghrebi M (2010) Carbon 48:1369
59. Tseng W, Tseng C, Chuang P, Lo A, Kuo C (2008) J Phys Chem B 112:18431
60. Yang L, Shi Z, Hao W (2014) Surf Coat Technol 251:122
61. Yang L, Shi Z, Yang W (2015) Electrochim Acta 153:76–82
62. Feast WJ, Tsibouklis J, Pouwer KL, Groenendaal L, Meijer EW (1996) Polymer 37:5017–5047
63. Jaymand M (2013) Prog Polym Sci 38:1287–1306
64. Saroop M, Ghosh AK, Mathur GN (2003) Intern J Plastics Technol 7:41–61
65. Levon K, Ho KH, Zheng WY, Karna T, Taka T, Osterholm JE (1995) Polymer 36:2733–2738
66. Athawale AA, Kulkarni MV, Chabukswar VV (2002) Mater Chem Phys 73:106–110
67. Kulkarni VG, Campbell JC, Mathew WR (1993) Synth Met 57:3780–3785
68. Paul RK, Pillai CKS (2000) Synth Met 114:27–35
69. Pron A, Rannou P (2002) Prog Polym Sci 27:135–190
70. Massoumi B, Abdollahi M, Jahed-Shabestari S, Entezami AA (2013) J Appl Polym Sci 128:47–53
71. Saini P, Choudhary V (2013) J Mater Sci 48:797–804
72. Mu S (2008) J Phys Chem B 112:6344–6349
73. Kulkarni MV, Viswanath AK (2004) Eur Polym J 40:379–384
74. Grigoras M, Catargiu AM, Tudorache F, Dobromir M (2012) Iranian Polym J 21:131–141
75. Teh CH, Rozaidi R, Rusli D, Sahrim HA (2009) Polym Plastics Technol Eng 48:17–24
76. Yasuda T, Yamaguchi I, Yamamoto T (2003) J Mater Chem 13:2138–2144
77. Zheng WY, Levon K, Laakso J, Oesterholm JE (1994) Macromol 27:7754–7768
78. Liao Y, Zhang C, Zhang Y, Strong V, Tang J, Li XG, Kalantar-zadeh K, Hoek EMV, Wang KL, Kaner RB (2011) Nano Lett 11:954–959
79. Cochet M, Maser WK, Benito AM, Callejas MA, Martínez MT, Benoit JM, Schreiber J, Chauvet O (2001) Chem Commun 1450–1451
80. Wei Z, Wan M, Lin T, Dai L (2003) Adv Mater 15:136–139
81. Feng W, Bai XD, Lian YQ, Liang J, Wang XG, Yoshino K (2003) Carbon 41:1551–1557
82. Zhou Y, Qin ZY, Li L, Zhang Y, Wei YL, Wang LF, Zhu MF (2010) Electrochim Acta 55:3904–3908
83. Dong B, He BL, Xu CL, Li HL (2007) Mater Sci Eng B 143:7–13

84. Gupta V, Miura N (2006) Electrochim Acta 52:1721–1726
85. Zhang J, Kong LB, Wang B, Luo YC, Kang L (2009) Synth Met 159:260–266
86. Sivakkumar SR, Kim WJ, Choi JA, MacFarlane DR, Forsyth M, Kim DW (2007) J Power Sources 171:1062–1068
87. Zhang H, Cao G, Wang Z, Yang Y, Shi Z, Gu Z (2008) Electrochem Commun 10:1056–1059
88. Zhang H, Cao G, Wang W, Yuan K, Xu B, Zhang W, Cheng J, Yang Y (2009) Electrochim Acta 54:1153–1159
89. Wang YG, Li HQ, Xia YY (2006) Adv Mater 18:2619–2623
90. Meng C, Liu C, Fan S (2009) Electrochem Commun 11:186–189
91. Meng C, Liu C, Chen L, Hu C, Fan S (2010) Nano Lett 10:4025–4031
92. Yan J, Wei T, Fan Z, Qian W, Zhang M, Shen X, Wei F (2010) J Power Sources 195:3041–3045
93. Zhang Z, Zhang Y, Yang K, Yi K, Zhou Z, Huang A, Mai K, Lu X (2015) J Mater Chem A 03:1884–1889